Developing, characterising, and testing a humanised 3D *in vitro* bone model, capable of long-term osteocyte culture

By Melissa Finlay

A thesis submitted to the University of Birmingham for the degree of

DOCTOR OF PHILOSOPHY

Institute of Inflammation and Ageing

College of Medical and Dental Sciences

The University of Birmingham

July 2023



UNIVERSITY OF BIRMINGHAM

UNIVERSITY OF
BIRMINGHAM

University of Birmingham Research Archive

e-theses repository

This unpublished thesis/dissertation is copyright of the author and/or third parties. The intellectual property rights of the author or third parties in respect of this work are as defined by The Copyright Designs and Patents Act 1988 or as modified by any successor legislation.

Any use made of information contained in this thesis/dissertation must be in accordance with that legislation and must be properly acknowledged. Further distribution or reproduction in any format is prohibited without the permission of the copyright holder.

Abstract

Introduction: Bone research, particularly into bone drug therapeutics, requires large-scale animal studies because complete *in vitro* bone models do not exist; primarily due to the complex and dynamic nature of bone tissue and the inability to culture osteocytes, (the main cell responsible for bone health maintenance). With an aging population, the number of people at risk and living with debilitating and enduring bone conditions, chiefly osteoporosis, is expected to rise. An ensuing increased pressure for effective therapies, along with the movement to replace animals in research, warrants greater effort to develop *in vitro* models that successfully recapitulate the cellular and extracellular complexities of bone tissue. Recent developments in 3D cell culture methods have enabled the creation of a self-structuring bone model (SSBM) that possesses physiochemical characteristics comparable to native bone, furthermore, it is the first model of its kind to house osteocytes long-term. However, this method used freshly isolated rat periosteal cells for production of each batch and the high variability in the resulting cell populations decreases reproducibility and reliability.

Aim: The aim of this project was to adapt and develop this SSBM culture method to utilise a secondary human osteoblast cell line to improve the reproducibility and relevance to human disease. Resulting constructs were structurally and biologically characterised, then their feasibility as a novel bone drug screening platform was investigated.

Methods: The human osteoblast cell line, hFOB 1.19, was seeded on a fibrin hydrogel, cast between two calcium phosphate anchors. Resulting SSBM constructs were cultured and analysed after 4-, 8- and 12-weeks post-cell seeding. Methods traditionally used for 2D cell culture and whole tissue analysis were adapted and

developed specifically for SSBM construct analysis. These methods were then used to structurally and biologically characterise SSBM constructs, as well as measure their responsivity after exposure to bone formation modulators (BFMs): vitamin D, parathyroid hormone and Betulin.

Results: The hFOB 1.19 cell line successfully produced bone model constructs composed of a collagen-containing matrix that mineralised over time. Structural analysis using alizarin red and picrosirius red staining approaches along with x-ray fluorescence revealed heterogenous distribution and maturation of this mineralising matrix; demonstrative of osteoid production, and its subsequent mineralisation to bone-like tissue. Polymerase chain reaction (qPCR) analysis showed distinct changes in gene expression over a 12-week culture period, indicative of maturing osteoblasts and osteocytogenesis. Immunofluorescent (IF) staining and ELISAs further supported these findings, confirming the presence of podoplanin (PDPN) (an early osteocytic marker), as well as prolonged cell viability and activity. qPCR, ELISAs and IF staining analysis also showed that SSBM cultures were responsive to the presence to each individual BFM.

Summary: A versatile, simple, and humanised osteocyte 3D culture method, with an optimised analytical pipeline, has been established. Confirmation of their responsivity to BFMs endorses the feasibility of using the method as a high-throughput assayable platform for bone research and drug development. Preliminary steps have been taken to assess the potential of 3D bioprinting to produce such a platform and its development has the potential to make a significant impact on how bone research is approached, as well as significantly reducing and replacing the reliance and use of animals in this research field.

Acknowledgements

I would like to thank the National Centre for the Replacement, Reduction and Refinement of Animals in Research (NC3Rs) for funding this PhD project. You are a fantastic organisation with so many engaging, kind and dedicated individuals. Thank you for all your help, advice, enthusiasm and making this rewarding research possible!

To my supervisors, Amy Naylor and Liam Grover, I don't know where to begin to show my gratitude to you both! The time I had during my PhD exceeded all my expectations and I cannot thank you both enough for giving me this tremendous experience, for the continuous support and encouragement, and for your commendable guidance.

I want to thank all the members of the Naylor group past and present. To Miruna Chipara, Kathryn Frost, Laurence Hill, Jonny Lewis, Georgiana Neag, Ellie Northall and Kieran Patrick. I am so grateful to you all for always making light of the difficult and trying times, for the in-depth (and not so in-depth) discussions, and for all the times I foisted cell culture work on to you! Your contributions and friendships are priceless.

It is difficult not to mention every member of the RRG. This is by far the best group of colleagues I have had the pleasure to work alongside, and I want to thank you all for welcoming me and making the RRG a joyful place to work (along with enlightening me on all possible methods of making cheese on toast!). Particular mentions must be given to Holly Adams, Em Powell and Charlotte Smith for being the driving forces that keep the labs afloat! Also, to Ladi Abudu, Lucy Jayne Marsh, Julia Manning, Triin Major for never failing to boost morale. And to John O'Neil for the early morning pep talks!

I am very grateful to all of those in the HTI laboratories, as well as the contributors and collaborators of this project for the invaluable technical support and insights; Scott

Dillon, James Edwards, Lisa Hill, Erik Hughes, Simon Jones, Hannah Lamont, Adam McGuinness, Tom Nicholson and Corinna Wehmeyer. Thank you!

I want to thank all the members of staff at Cilantro for the exceptional care, patience and support I have received. A particular mention goes to Karolina Wutke, whose enduring tolerance, empathy and guidance is admirable. And to Marketa Skorepova, for your wonderfully relaxed and encouraging demeanour.

I wouldn't be here if it wasn't for my family. To my mum, Lesley Finlay, my dad Ali Finlay, my sister, Megan Finlay and my most beloved friend, Rachael Murray. It has been a long journey and you have all stood beside me through thick and thin. I am beyond grateful, and I only hope I can repay you all for the time given, the miles travelled and the love I have felt.

And to my boyfriend, Matt Green. An acknowledgement for you in my thesis doesn't do justice to the amount of happiness and love you have brought me, for the relentless patience and comfort, nor for helping me find strength during my most stressful moments. Thank you, a googolplex times over (and then some!)

Contents

Abstract ..... **ii**
Acknowledgements ..... **iv**
Contents ..... **vi**
Figures ..... **xi**
Tables ..... **xvi**
Abbreviations ..... **xvii**
Research dissemination ..... **xix**
i. Publications and Collaborations xix
ii. Presentations xx
Chapter 1 Introduction **1**
1.1 Down to the bone **2**
1.1.1 Bone: structure equals function 2
1.1.2 Importance of bone 4
1.2 Maintaining bone health and metabolism **4**
1.2.1 Bone remodelling 4
1.2.2 Regulating bone metabolism 10
1.2.3 Stimulating bone formation and resorption 13
1.3 Bone disease **15**
1.3.1 Bone metabolism dysregulation 15
1.3.2 The aging skeleton 16
1.3.3 An aging population 20
1.4 Bone research and drug discovery **21**
1.4.1 Research and discovery 21
1.4.2 In vivo models 22
1.4.3 Ex vivo models 25
1.4.4 In vitro models 26
1.5 Issues hindering *in vitro* bone model development **28**
1.5.1 Problem 1: Bone tissue composition and structure 28
1.5.2 Problem 2: Osteocyte culture 34
1.6 Advances in cell culture **39**
1.6.1 2D vs 3D culture 39
1.6.2 3D culture approaches 43

1.6.3 Scaffolds for bone organoids 44
1.6.4 An assayable bone model 48
1.7 Birmingham Self-structuring bone model 51
1.7.1 Concept 51
1.7.2 Method 52
1.7.3 Adaptions and findings 53
1.7.4 Conclusion 55
1.7.5 Aims 56
Chapter 2 Methods and materials 58
2.1 hFOB 1.19 selection and culture 59
2.1.1 General cell culture and aseptic technique 59
2.1.2 Receipt of Human foetal osteoblast (hFOB) 1.19 cell line 59
2.1.3 Growth curves 61
2.1.4 Differentiation media investigation 62
2.1.5 Long-term culture and differentiation regime 63
2.2 Establishing SSBMs 63
2.3 Characterising hFOB 1.19 SSBMs – Biological analysis 64
2.3.1 Construct isolation 64
2.3.2 Conditioned Media analysis 65
2.3.3 Live-dead imaging 66
2.3.4 Gene expression analysis 68
2.3.5 Immunofluorescence (IF) analysis 74
2.4 Characterising hFOB 1.19 SSBMs – Structural analysis 78
2.4.1 Picrosirius red (PSR) staining 78
2.4.2 Alizarin red (AZ) staining 79
2.4.3 X-ray fluorescence (XRF) 80
2.5 SSBM Responsivity investigations 81
2.5.1 Treatment formulation 81
2.5.2 Determining treatment regimes 82
2.5.3 hFOB 1.19 responsivity – 2D 82
2.5.4 hFOB 1.19 responsivity – 3D 83
2.6 Bioprinting 83
2.6.1 Reagent preparation 84
2.6.1.1 0.6% Agarose solution 84

2.6.2 Bioprinting 84
2.6.3 Analysis of bioprinted constructs 85
Chapter 3 Creating humanised self-structuring bone models 86
3.1 Introduction 87
3.1.1 Arguments for creating a humanised in vitro bone model 87
3.1.2 Identification of an appropriate human cell line 88
3.1.3 Chapter aims 92
3.2 SSBM method repeatability 92
3.3 Characterising hFOB 1.19 growth in 2D 95
3.4 SSBM method adaptability to hFOB 1.19 cells 103
3.5 SSBM compositional and structural analysis 106
3.6 Discussion 112
3.6.1 hFOB 1.19 growth patterns in 2D showed significant batch-batch variation 112
3.6.2 Selecting the most appropriate hFOB 1.19 osteogenic media 114
3.6.3 The SSBM method is repeatable and shows adaptability 116
3.6.4 Collagen content of hFOB SSBM constructs increased through long-term culture 119
3.6.5 Mineralisation of hFOB 1.19 SSBM constructs occurs and matures with long-term culture 120
3.6.6 Optimising XRF preparation and analysis 121
3.6.7 Conclusions 124
Chapter 4 Biological characterisation of hFOB 1.19 SSBM constructs 125
4.1 Introduction 126
4.2 Gene expression analysis 129
4.2.1 Optimising RNA extraction 129
4.2.2 Housekeeper selection 130
4.2.3 hFOB 1.19 SSBM construct gene expression characterisation 132
4.2.4 2D vs 3D gene expression 136
4.3 Conditioned media analysis 140
4.3.1 SSBM construct isolation 140
4.3.2 hFOB 1.19 SSBM construct conditioned media analysis 142
4.3.3 2D vs 3D conditioned media analysis 143
4.4 Immunofluorescence staining and imaging 146

4.4.1 Immunofluorescence staining 146
4.4.2 Non-destructive viability staining 149
4.5 Discussion 150
4.5.1 Optimising RNA extraction and qPCR analysis 150
4.5.2 The SSBM culture system supports long-term osteoblast differentiation and matrix maturation 153
4.5.3 Enzyme-linked immunosorbent assays quantified the presence of soluble markers over prolonged culture of hFOB 1.19 constructs 159
4.5.4 IF approaches were used to confirm the presence of insoluble markers and assess cell viability 163
4.5.5 Conclusions 165
Chapter 5 Exploring the feasibility of hFOB 1.19 SSBM as a screening and assayable platform 167
5.1 Introduction 168
5.1.1 Vitamin D 169
5.1.2 Parathyroid hormone 170
5.1.3 Betulin 171
5.1.4 Chapter aims and approaches 172
5.2 Vitamin D 173
5.2.1 2D investigations 173
5.2.2 SSBM Vit D treatment: qPCR analysis 178
5.2.3 SSBM Vit D treatment: ELISA analysis 182
5.2.4 SSBM Vit D treatment: IF analysis 183
5.3 PTH 186
5.3.1 2D investigations 186
5.3.2 SSBM PTH treatment: qPCR analysis 188
5.3.3 SSBM PTH treatment: ELISA analysis 195
5.3.4 SSBM PTH treatment: IF analysis 197
5.4 Betulin 200
5.4.1 2D Betulin investigations 200
5.4.2 SSBM Betulin treatment: qPCR analysis 204
5.4.3 SSBM Betulin treatment: ELISA analysis 209
5.4.4 SSBM Betulin treatment: IF analysis 210
5.5 Bioprinting 213
5.5.1 Bioprinting observations 213

5.6 Discussion 214
5.6.1 2D investigations showed hFOB 1.19 were responsive to BFM treatments 214
5.6.2 hFOB 1.19 SSBM constructs had measurable responses to BFM treatments 221
5.6.3 Miniaturisation of hFOB 1.19 SSBM constructs is possible 233
5.6.4 Conclusion 235
Chapter 6 General discussion 237
6.1 Summary of findings 238
6.2 Cell differentiation in the 3D organotypic microenvironment 240
6.3 3Rs Impact 243
6.4 Practical limitations 245
6.5 Additional scope and future work 246
6.5.1 Further method development and optimisations 247
6.5.2 Potential applications of the SSBM culture system 249
6.6 Conclusion 250
Chapter 7 Bibliography 252
Chapter 8 Appendix 8-1
8.1 Published method 8-2
8.2 Chapter 3 & 4 appendix 8-26
8.3 Chapter 5 appendix 8-33
8.4 Adaptability – Dissemination and Collaborations 8-39
8.5 Analytical method development 8-42
8.5.1 Delaying CaP cement setting 8-42
8.5.2 Micro-computed tomography and Scanning electron microscopy 8-43
8.5.3 Mineral staining 8-47
8.5.4 Conclusions 8-48

Figures

Figure 1.1 - Physiological roles of the skeleton.. 3

Figure 1.2 – The bone remodelling cycle. 5

Figure 1.3 - Mesenchymal stem cell (MSC) differentiation and osteoblast lineage commitment......8

Figure 1.4 - Drug discovery process: From bench to bedside. 21

Figure 1.5 - ex vivo models commonly used in bone research......25

Figure 1.6 - in vitro co-culture systems used in bone research......27

Figure 1.7 - Bone tissue macroscopic arrangement and matrix microarchitecture.. 29

Figure 1.8 - Non-collagen proteins present in bone matrix. 32

Figure 1.9 - Morphological and gene expression changes between osteoblasts and osteocytes. 36

Figure 1.10 - The Birmingham self-structuring bone model.. 54

Figure 2.1 - Isolation of SSBM constructs......64

Figure 2.2 - Disruption and homogenisation of SSBM constructs for efficient RNA extraction. 68

Figure 3.1 - Assessing repeatability of the SSBM method using cells isolated from rat femoral periosteum......94

Figure 3.2 - Significant differences in growth rate exists between different batches of hFOB 1.19 cells at a similar passage number when cultured in 2D.. 97

Figure 3.3 - During short-term 2D culture (>1 week), % viability of hFOB 1.19 was relatively maintained throughout the culture duration......98

Figure 3.4 - Assessing hFOB 1.19 cell proliferation and viability when cultured with different osteogenic medias in 2D. 100

Figure 3.5 - Investigating osteogenic activity of hFOB 1.19 cells when cultured in 2D with different osteogenic medias.. 101

Figure 3.6 - Investigating hFOB 1.19 proliferation and viability in 2D when cultured at 37 °C with the selected osteogenic media.. 103

Figure 3.7 - Fibrin rearrangement occurs upon cell seeding.. 104

Figure 3.8 - Initial observations upon adapting the SSBM method to accommodate hFOB 1.19 cells......105

Figure 3.9 - Analysing collagen content of hFOB 1.19 SSBM constructs, after a culture period of 4-, 8-, and 12-weeks post cell seeding, through whole mount staining with Picrosirius red (PSR)......107

Figure 3.10 - Mineral content visibly and quantifiably increases within hFOB 1.19 SSBM constructs when cultured up to at least 12-weeks......108

Figure 3.11 - Heterogeneously-distributed mineral, containing calcium and phosphorous, develops on hFOB 1.19 SSBM constructs over time......110

Figure 3.12 – Analysis of mineral maturation over time in hFOB 1.19 SSBM constructs using Ca:P signal ratios obtained from XRF. 111

Figure 4.1 - Improving and characterising RNA extraction yields from hFOB 1.19 SSBM constructs......131

Figure 4.2 - Assessing suitability of housekeeping gene expression for quantitative polymerase chain reaction (qPCR) analysis.. 132

Figure 4.3 - qPCR analysis of bone matrix and mineralisation gene expression over time in hFOB 1.19 SSBM constructs......134

Figure 4.4 - qPCR analysis of osteoblast-specific gene expression over time in hFOB 1.19 SSBM constructs.. 135

Figure 4.5 - qPCR analysis of gene expression relating to other bone cell types over time in hFOB 1.19 SSBM constructs......136

Figure 4.6 - Comparison of gene between hFOB 1.19 cells cultured long-term in 2D or 3D (Part i). 138

Figure 4.7 - Comparison of gene between hFOB 1.19 cells cultured long-term in 2D or 3D (Part ii). 139

Figure 4.8 - Comparison of gene expression relating to bone resorption regulation between hFOB 1.19 cells cultured long-term in 2D or 3D......140

Figure 4.9 - **Assessing the effects of construct isolation on ELISA analysis of conditioned media.**.....141

Figure 4.10 - Assessment of hFOB 1.19 SSBM construct conditioned media by ELISA.....143

Figure 4.11 - Comparing assessment of conditioned media between hFOB 1.19 cells cultured in 2D and 3D......145

Figure 4.12 -Whole mount immunofluorescence staining of cells within SSBM constructs......146

Figure 4.13 - Adaption of established protocol for bone embedding, sectioning and staining enables high-resolution immunofluorescence (IF) imaging of SSBM constructs......148

Figure 4.14 - Cell proliferation within constructs can be analysed using non-destructive staining for up to 12-weeks of culture. 149

Figure 5.1 - Cell count and viability assessment of hFOB 1.19 cells cultured in 2D with Vitamin D (Vit D) treatment.. 174

Figure 5.2 - qPCR analysis of matrix and mineralisation, and chondrocyte related gene expression for 2D hFOB 1.19 treatment with Vit D......175

Figure 5.3 - qPCR analysis of osteoblast-specific gene expression for 2D hFOB 1.19 treatment with Vit D......176

Figure 5.4 - Vit D and VC had an inhibitory effect on the expression of certain osteoblast and osteocyte-specific genes in 2D hFOB 1.19 cells. 177

Figure 5.5 - qPCR analysis of matrix and mineralisation, and chondrocyte related gene expression for hFOB 1.19 SSBM construct treatment with Vit D. 179

Figure 5.6 - qPCR analysis of osteoblast-specific gene expression for hFOB 1.19 SSBM construct treatment with Vit D.. 180

Figure 5.7 - qPCR analysis of podoplanin (PDPN) expression for hFOB 1.19 treatment SSBM construct with Vit D.. 181

Figure 5.8 - Assessment of hFOB 1.19 SSBM construct conditioned media by ELISA after treatment with Vit D......183

Figure 5.9 - Immunofluorescence (IF) staining detected a notable increase in podoplanin presence after Vit D treatment across all analytical time points. .185

Figure 5.10 -Determining Parathyroid hormone Fragment 1-34 human (PTH) treatment concentration and duration......187

Figure 5.11 - qPCR analysis of matrix and mineralisation, and chondrocyte related gene expression for 2D hFOB 1.19 treatment with PTH.. 189

Figure 5.12 - qPCR analysis of osteoblast-specific gene expression for 2D hFOB 1.19 treatment with PTH. 190

Figure 5.13 - A suggestive inhibitory effect on the expression of certain osteoblast and osteocyte-specific genes in 2D hFOB 1.19 cells by PTH vehicle, d.H_2O.. 191

Figure 5.14 - qPCR analysis of matrix and mineralisation, osteoblast lineage commitment, and chondrocyte related gene expression for hFOB 1.19 SSBM construct treatment with PTH.....192

Figure 5.15 - qPCR analysis of formation and resorption regulation related gene expression for hFOB 1.19 SSBM construct treatment with PTH.. 194

Figure 5.16 - qPCR analysis of podoplanin (PDPN) expression for hFOB 1.19 treatment SSBM construct with PTH. 195

Figure 5.17 - Assessment of hFOB 1.19 SSBM construct conditioned media by ELISA after treatment with PTH......197

Figure 5.18 - IF staining detected a notable increase in podoplanin presence after PTH treatment across all analytical time points. 199

Figure 5.19 - Determining Betulin treatment concentration and duration......201

Figure 5.20 - qPCR analysis of matrix and mineralisation, and chondrocyte related gene expression for 2D hFOB 1.19 treatment with Betulin......202

Figure 5.21 - qPCR analysis of osteoblast-specific gene expression for 2D hFOB 1.19 treatment with Betulin. 203

Figure 5.22 - qPCR analysis of resorption and formation regulation, osteocyte and chondrocyte related gene expression for 2D hFOB 1.19 treatment with Betulin. 204

Figure 5.23 - qPCR analysis of matrix and mineralisation related gene expression for hFOB 1.19 SSBM construct treatment with Betulin.....206

Figure 5.24 - qPCR analysis of osteoblast-specific and chondrocyte related gene expression for hFOB 1.19 SSBM construct treatment with Betulin.....207

Figure 5.25 - qPCR analysis of podoplanin (PDPN) expression for hFOB 1.19 treatment SSBM construct with Betulin. 208

Figure 5.26 - Assessment of hFOB 1.19 SSBM construct conditioned media by ELISA after treatment with Betulin.. 210

Figure 5.27 - IF staining detected a notable increase in podoplanin presence after Betulin treatment across all analytical time points.. 212

Figure 5.28 - Bioprinting enabled miniaturisation of hFOB 1.19 SSBM constructs.. 214

Tables

Table 1.1 - Key stimuli known to dysregulate bone metabolism......15

Table 1.2 - Osteoporosis pharmacological treatments. 19

Table 1.3 - Established and commonly used rodent in vivo bone models......23

Table 1.4 - Details of each 3R principles. 24

Table 1.5 - Comparison of 2D and 3D in vitro cell culture conditions and requirements......40

Table 1.6 - Scaffolds used for 3D bone cell culture in vitro and in vivo. 45

Table 1.7– Critical features for an assayable bone model.. 50

Table 2.1 - hFOB 1.19 cell culture media recipes. 60

Table 2.2 - Osteogenic media tested for hFOB 1.19 cell culture media. 62

Table 2.3 - TaqMan™ primers used for qPCR analysis.. 71

Table 2.4 - Ingredient and concentration details for reagents prepared for construct embedding and sectioning.. 75

Table 2.5 - Ingredient and concentration details for reagents prepared for sectioned construct IF staining.. 76

Table 2.6 - Ingredient and concentration details for reagents prepared for Whole-mount construct IF staining.. 77

Abbreviations

ALP	Alkaline phosphatase
ATCC	American Type Culture Collection
ATP	Adenosine triphosphate
AZ	Alizarin red
BFM	Bone formation modulator
BMP	Bone morphogenic protein
BMU	Basic multicellular unit
BSP	Bone sialoprotein
CaP	Calcium phosphate
CT	Cycle threshold
d.H_2O	Distilled water
DAPI	4′,6-Diamidino-2-phenylindole
DMP1	Dentin matrix protein 1
DMSO	Dimethylsulfoxide
ECM	Extracellular matrix
ELISA	Enzyme-linked immunosorbent assay
EtOH	Ethanol
Gla	Gamma-carboxyglutamic acid
hFOB	Human foetal osteoblast
IF	Immunofluorescence
LN_2	Liquid nitrogen
LSD	Least significant difference
M-CSF	Macrophage colony-stimulating factor
MSC	Mesenchymal stem cells
OD	Optical density
OPC1	Osteoblastic Precursor Cell line 1
OPG	Osteoprotegrin
OPN	Osteopontin
P1NP	Amino-terminal propeptide of type 1 procollagen
PBS	Phosphate buffered saline
PDPN	Human podoplanin
PHEX	Phosphate-regulating neutral endopeptidase chromosome X
pNPP	Alkaline phosphatase yellow
PPi	Inorganic pyrophosphate
PSR	Picosirius red
PTH	Parathyroid Hormone Fragment 1-34 human
qPCR	Polymerase chain reaction
RANKL	Receptor activator of nuclear factor kappa-B ligand
RT	Room temperature
RUNX2	Runt-related transcription factor 2

SEM	Scanning electron microscopy
SLAM	Suspended layer additive manufacturing
SSBM	Self-structuring bone model
TGF-β	Transforming growth factor-β
TMB	Tetramethylbenzidine
VC	Vehicle control
Vit D	Vitamin D
XO	Xylenol orange
XRF	X-ray fluorescence
β-TCP	Beta-tricalcium phosphate
µCT	Micro-computed tomography

Research dissemination

i. Publications and Collaborations

(Chronological order)

April 2023 – University of Swansea, UK; Collaboration
Collaborator: Dr Laurence Hill (Biomedical sciences)
Dr Hill prepared and printed bone model constructs discussed in this thesis. *In vitro* bone model bioprinting concept development

March 2023 – Method Article (First author)
Finlay M, Hill LA, Neag G, Patel B, Chipara M, Lamont HC, et al. A detailed methodology for the long-term in vitro culture and analysis of three-dimensional, self-structuring bone models generated from cell lines or primary osteoblastic cell populations. F1000Research 2023 12:357. F1000 Research Limited; 2023;12:357. DOI: 10.12688/f1000research.130779.1

January 2023 – Robinson College, University of Cambridge, UK
Collaborator: Dr Scott Dillon (Yusuf Hamied Department of Chemistry)
In vitro bone model method dissemination and scanning electron microscopy (SEM) analysis.

September 7th-9th, 2022 – University Hospital Munster, Germany
Collaborator: Dr Corinna Wehmeyer (Institute of Musculoskeletal Medicine)
Travelled to Munster to present, demonstrate and set-up self-structuring bone model method.

July 2022 - Healthcare Technologies Institute, University of Birmingham, UK
Collaborator: Dr Kenny Mann
In vitro bone models used to investigate matrix vesicle secretion from hFOB 1.19 cells when cultured in 3D. Construct set up and maintenance, and media collection performed by Melissa Finlay. Media analysis performed by Dr Mann

July 2021 – Literature review (Second author)
Neag G, Finlay M, Naylor AJ. The cellular choreography of osteoblast angiotropism in bone development and homeostasis. Int. J. Mol. Sci. 2021, 22(14), 7253. DOI: 10.3390/ijms22147253

June 2021 – Healthcare Technologies Institute, University of Birmingham, UK
Collaborator: Mr Adam McGuinness
In vitro bone model method adaption to accommodate MC3T3 cell line. Construct preparation and maintenance performed by Melissa Finlay. Analysis performed by Mr Adam McGuinness.

March 2021 – Institute of Inflammation and Ageing, University of Birmingham
Collaborator: Professor Simon Jones & Dr Thomas Nicholson
In vitro bone model method adaption to accommodate primary osteoblastic cells isolated from scoliosis spine chips. Cell isolation and maintenance performed by Dr Nicholson. Construct preparation and maintenance performed by Melissa Finlay.

ii. Presentations
(Chronological order)

April 13-15th, 2023: Bone Research Society Annual Meeting (Liverpool, UK)
10-minute presentation. Category: Experimental models in MSK research.
"Optimisation and characterisation of an adaptable and humanised *in vitro* 3D self-structuring bone model, capable of long-term osteocyte culture."

December 1st, 2022: Institute of Inflammation and Ageing away day (Birmingham, UK). Poster presentation. Poster award: 1st prize.
"Method development and optimisation for an *in vitro* 3D self-structuring bone model capable of long-term osteocyte culture."

November 25th, 2022: Healthcare Technologies Institute Winter Symposium (Birmingham, UK). 3-minute flash talk.
"A humanised in vitro 3D self-structuring bone model, capable of long-term osteocyte culture"

November 23rd, 2022: Laboratory Animal Science Association Annual Meeting (Birmingham, UK). 25-minute presentation. Category: 3Rs. Best presentation award.
"Development of a humanised 3D *in vitro* bone model method for the replacement of animals."

July 8th, 2022: NC3Rs Midland's Symposium (Nottingham, UK). Poster presentation and 3-minute flash talk. Best poster award.
"An *in vitro* 3D self-structuring bone model of human origin, capable of long-term osteocyte culture."

May 7-10th, 2022: European Calcified Tissue Society Congress (Helsinki, Finland)
Poster presentation.
"An *in vitro* 3D self-structuring bone model capable of long-term osteocyte culture."

September 28-30th, 2021: Wellcome Organoids: Advances and applications conference (Online). Poster presentation.
"A simple 3D *in vitro* method to produce a bone model capable of long-term osteocyte culture using either primary or immortalised cell lines."

July 1-9th, 2021: NC3Rs PhD Summer School (Online). Poster and 3-minute flash talk. Best poster and presentation award.
"An organotypic model of the bone remodelling process."

June 28-30th, 2021: Bone Research Society Annual Meeting (Online). 5-minute presentation.
"A simple and robust *in vitro* method for long-term osteocyte 3D culture using either primary or immortalised cell lines."

Chapter 1
Introduction

1.1 Down to the bone

The average adult human skeleton is composed of 206 bones (1), which collectively provide a supportive and protective scaffold that enables movement, posture and shape. The unique chemical composition, highly organised structure and dynamic nature of bone are properties that are fundamental to its numerous and diverse functions, which must be maintained throughout an individual's lifetime [Figure 1.1].

1.1.1 Bone: structure equals function

More details of bone composition and structure are discussed in [Section 1.5].

Briefly, bone tissue is a composite material. It is a mineralised organic tissue that is differentially arranged to give rise to two distinct subtypes – compact and solid cortical bone, and porous and spongy cancellous bone. Each is organised within the whole bone in such a way as to provide optimal protection, support and strength. For example, cortical bone is present on the exterior surfaces of every bone in the body, which gives bone its distinct stiffness and strength. However, it is more brittle than cancellous bone. Cancellous bone has more sporadic molecular arrangement (responsible for giving rise to the spongy texture), which means it can carry greater mechanical loads (2). Hence, why trabecular bone is present on the inner-facing surfaces of cortical bone in skeletal areas that experience greater compression and tension (e.g., long bones, vertebral) (3). Furthermore, the arrangement of cortical bone and trabecular bone in long bones, results in a cavity within the diaphysis region which provides storage space and protection for bone marrow (4).

The organic phase of bone is a collagen-based matrix produced by osteoblasts - one of the three major bone cell types that resides within the bone. This matrix is also

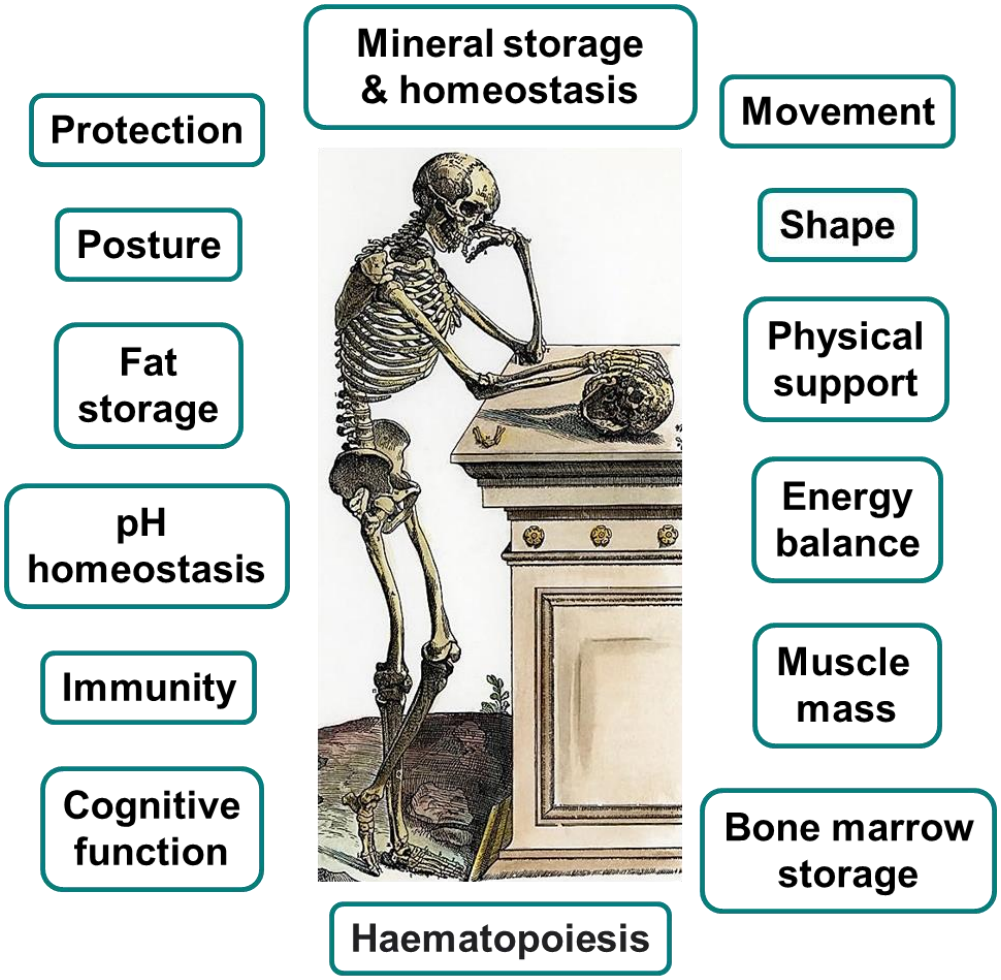


Figure 1.1 - Physiological roles of the skeleton. From artwork produced by Andreas Vesalius, the skeleton is clearly depicted as the framework of the body that is designed to provide posture and shape. However, there are many other physiological roles of bone tissue that lies within its ability to heal and regenerate, the organisation of its basic chemical compounds as well as the arrangement of its multiple, physically distinct niches. Bone contributes to the maintenance and actions of many organ systems primarily through the release of bone derived factors from the cells that reside within the bone compartments.

composed of multiple non-collagenous proteins that are essential for maintaining bone health, as well as contributing to extraskeletal functions. For example, bone cell derived osteocalcin contributes to energy balance by promoting the synthesis and release of insulin and increasing insulin sensitivity (5). The inorganic component of bone is composed of calcium phosphate (CaP) minerals, chiefly in the form of hydroxyapatite (6,7). As the main reservoir of the body's calcium and phosphate,

holding approximately 99% and 90% of the body's total content respectively (8), bone has a central role in maintaining mineral homeostasis. Calcium in particular must be tightly regulated to ensure meticulous neurotransmission and neurotransmitter release (9) and blood clotting (10).

1.1.2 Importance of bone

The functions of the skeleton, bone and bone cells are implicated across many physiological systems and thus it is imperative to maintain adequate bone health. This is achieved by adopting a number of lifestyle behaviours and habits including, but not limited to, regular weight-bearing exercise (11,12), adequate dietary calcium intake (13,14) and sunlight exposure to obtain vitamin D (14,15). These habits set in motion a sequence of highly regulated cellular processes which contribute to the repair, reinforcement and maintenance of bone tissue to ensure that it can fulfil these life-long demands.

1.2 Maintaining bone health and metabolism

1.2.1 Bone remodelling

Maintenance of bone health throughout life is achieved through the process of bone remodelling - a cyclic and tightly regulated metabolic activity of the three major bone cells (osteoclasts, osteoblasts and osteocytes) whose distinct roles cause bone resorption and bone formation (16). There are five phases of the bone remodelling cycle - activation, resorption, reversal, formation and termination [Figure 1.2] - and the transition between each relies on the tightly controlled communication and interaction between the bone cells (16). It is estimated that there are about $1x10^6$ sites of active bone remodelling at any given time (17), resulting in whole skeletal renewal every 10 years (18).

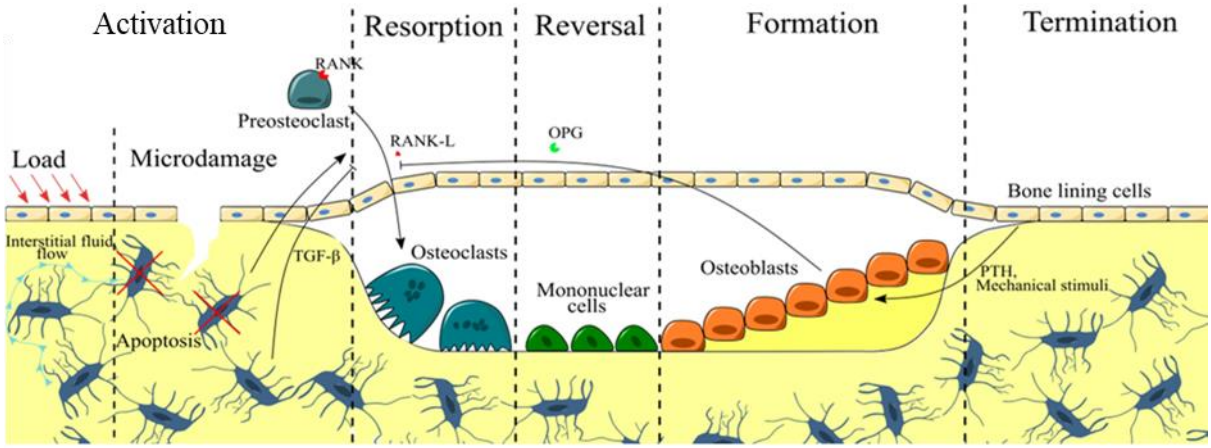


Figure 1.2 – The bone remodelling cycle. A tightly regulated process of bone cell metabolic activity which results in both resorption and formation of bone in order to fulfil its many physiological roles. There are five distinct and overlapping phases; activation, resorption, reversal, Formation and Termination/Quiescence which can be initiated by a number of endogenous and exogenous cues. Resorption and formation must be balanced in order to maintain adequate bone health; a number of regulatory mechanisms are in place to ensure this is met and prevent the onset of debilitating bone conditions such as osteoporosis and osteopetrosis. Figure adapted from Gudde, 2018 (19).

1.2.1.1 Activation phase

The activation phase of bone remodelling begins with the self-assembly of temporary basic multicellular units (BMU), which confine remodelling activity to specific sites on the bone tissue (16,20,21) and recruit pre-osteoclastic cells to these sites through the upregulation of osteoblastic factors, receptor activator of nuclear factor kappa-B ligand (RANKL) and macrophage colony-stimulating factor M-CSF (22–25). RANKL and M-CSF activate their respective membrane bound receptors, RANK and CSF1R, on pre-osteoclastic cells to induce osteoclastogenesis (26,27) - the RANKL-RANK interaction in particular is essential for mature cell survival (23,28,29).

1.2.1.2 Osteoclasts and resorption phase

Osteoclasts are large multinucleated cells, resulting from the activation and fusion of 10-20 pre-osteoclastic cells of the macrophage haematopoietic lineage (30) and are

responsible for bone resorption. The resorptive activity of mature osteoclasts is reserved at their distinctly convoluted ruffled border membrane, which is contained within a sealing zone upon attachment to bone that is also responsible for cell movement across the bone surface, due to the high density of cytoskeletal rings present (31–33). Osteoclasts adhere to the bone surface through $\alpha v\beta 3$-integrin binding to osteopontin (OPN) present within the bone matrix (34), which aids in the regulation of resorption activity and osteoclast survival (35,36).

Osteoclasts resorb bone through the secretion of chloride and hydrogen ions into the resorptive compartment, to create an acidic condition for dissolution of the alkaline hydroxyapatite mineral (37), as well as secretion of lysosomal enzymes, matrix metalloproteinases and cathepsin K, to digest collagen (29). Degradation products and released calcium and phosphate ions in the sealing zone are endocytosed at the ruffled border, transcytosed through the osteoclast and released into the extracellular space (38,39). This maintains the ionic gradients required for efficient resorptive activity (40) and increases calcium and phosphate serum concentrations.

On average, bone resorption lasts for 2-weeks and results in the formation of a pit called Howship's lacunae (41), which permits bone formation preparation steps carried out in the reversal phase.

1.2.1.3 Reversal phase

Prior to bone formation, the newly formed resorption pit is prepared for the deposition of the immature bone matrix, osteoid. The exact mechanisms that take place are still unknown, although the overall agreement is that undigested collagen remnants are removed and an osteopontin-rich matrix deposited by osteoblast lineage cells (42–45),

creating the cement line. The newly laid cement line has been suggested to promote osteoblast maturation and adhesion, act as a molecular glue to enable the newly secreted osteoid to adhere to the resorbed surface, as well as minimise the risk of future damage to the bone (46).

Coupling of bone resorption and formation occurs during this phase. Again, the exact mechanisms of this transition are unknown but there is evidence of direct cell-cell contact between osteoclasts and pre-osteoblasts (47,48), as well as paracrine (49–51) and endocrine (29,52,53) signalling events occurring.

During the reversal phase, osteoclasts undergo apoptosis, which signifies the end of the resorptive phase.

1.2.1.4 Osteoblasts and formation phase

Mesenchymal stem cells (MSC) are capable of multilineage differentiation, including generation of osteoblasts - the cells responsible for osteogenesis [Figure 1.3 A]. Osteoblasts arise from the specific upregulation of transcription factors bone morphogenic protein (BMP) 2 and 4 (54), SOX9, runt-related transcription factor 2 (RUNX2) (55–57) and osterix (58), as well as expression and activity of beta-catenin (59). Continuous expression of RUNX2 from the progenitor cells to the mature osteoblast is essential to maintain lineage commitment and osteogenesis (56).

Small, rounded, condensed osteoprogenitor cells (60) become cuboidal, polarised cells (61) which adhere to the bone and work as a cellular unit by forming a cellular network between adjacent osteoblasts via a series of tight, gap and adherens junctions. Respectively, these junctions allow osteoblasts to maintain their polarity,

enable cellular synchronisation, facilitate ionic transport, and regulate further osteoblast differentiation and fate (35).

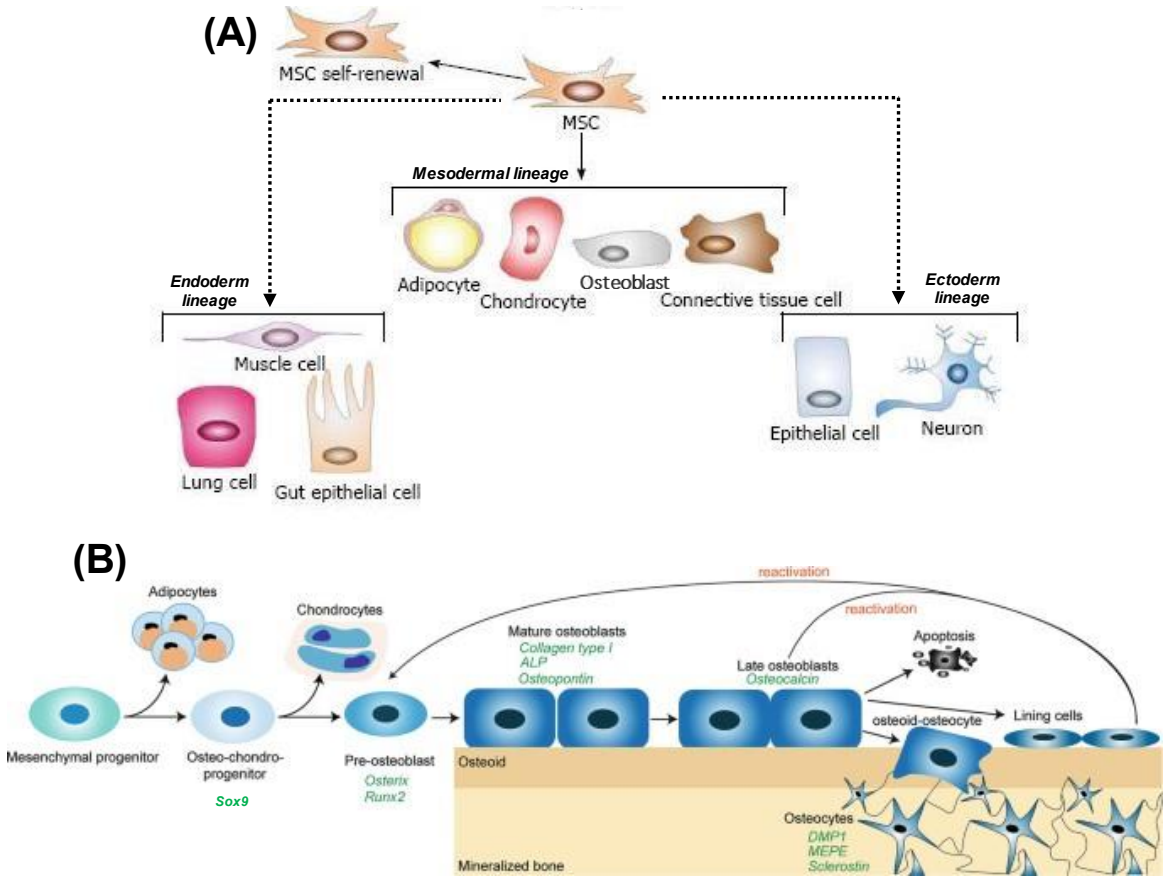


Figure 1.3 - Mesenchymal stem cell (MSC) differentiation and osteoblast commitment. MSCs are a heterogenous group of self-renewing multipotent stem cells found in the bone marrow. MSCs have the potential to differentiate into many different cell types which are grouped into three lineages: endoderm, ectoderm and mesoderm **(A)**, the latter of which includes osteoblasts. What determines osteoblast lineage from the other cells of the mesoderm lineage (i.e, adipocytes, chondrocytes and connective tissue cells) is the expression of specific transcription factors. Both osteoblasts and chondrocytes express transcription factor SOX9, however expression of osterix and RUNX2 are crucial for osteoblast commitment. Osteoblasts continue to differentiate once adhered to the bone surface and produce osteoid, and eventually undergo one of three fates: apoptosis, differentiate to dormant bone lining cells or become entombed within the mineralising bone to differentiate into osteocytes **(B)**. Adapted from Glenn and Whartenby, 2014 (62) **(A)** Vrahnas and Sims, 2020 (63)**(B)**.

Osteoblasts produce and deposit immature bone matrix, termed osteoid. A non-mineralised type I collagen-rich organic matrix, osteoid contains a mixture of non-collagenous proteins including, glycoproteins, proteoglycans and gamma-

carboxyglutamic acid (Gla)-containing proteins (64). These proteins are required for subsequent collagen mineralisation, to maintain cell attachment, as well as storage for future remodelling events (65,66). Osteoid and bone composition is discussed in detail in [Section 1.5].

Once an adequate amount of matrix has been deposited (approximately 4 months (67)), most osteoblasts undergo apoptosis (20,68) and the remaining further differentiate into either bone lining cells or osteocytes [Figure 1.3 B]. Osteoblast differentiation and osteocytes are discussed further in [Section 1.5].

1.2.1.5 Mineralisation and termination phases

Osteoid is an immature bone matrix and must be amalgamated with inorganic CaP mineral to give bone tissue its distinct rigidity and robustness. This occurs over two separate stages. During osteoid formation and deposition, primary mineralisation occurs within 5-10 days of the matrix being deposited, then lasting up to 3-4 months (41,69,70) and results in 50-70% of maximal mineralisation (70–72). Primary mineralisation begins with the formation of apatite crystals in the gap regions between newly deposited adjacent collagen fibrils (73).

The secondary mineralisation stage completes the mineralisation of osteoid, however the duration of which is dependent on numerous factors (particularly species and age) – it can be as short as weeks or up to several years (74,75). As the remodelling cycle only has a life span of 120-200 days (67), secondary mineralisation continues after termination of the remodelling cycle, signified by osteoblast apoptosis and differentiation. Secondary mineralisation occurs on the extrafibrillar collagen surfaces (i.e., on the surface of collagen fibrils) and intrafibrillar collagen surfaces (i.e.,

incorporated within collagen fibrils), as well as the overlap regions between collagen fibrils (76,77). During this phase, the majority of mature hydroxyapatite crystal nucleation occurs, as well as an increase in crystal size and number (74). As the amount of hydroxyapatite increases, the collagen fibres also become more compact and cross-linked, thus enhancing the tensile strength and viscoelasticity of bone (78). Mineral composition is discussed in more detail in [Section 1.5].

1.2.2 Regulating bone metabolism

Individually, resorption and formation are carried out to fulfil the physiological functions and roles of bone, however their overall activity must be matched to maintain bone health and prevent the incidence of debilitating bone conditions occurring. Thus, there are a number of regulatory mechanisms in place to ensure a balance is kept.

1.2.2.1 Paracrine signalling

Osteocytes are the main regulatory body of bone metabolism. More detail on osteocytes and their regulatory roles are discussed in [Section 1.2 and 1.5] and throughout this section. Briefly, osteocytes are of osteoblast lineage and are the most abundant bone cell type (79). They are uniquely positioned within mineralised bone matrix in fluid-filled lacunae and their highly dendritic phenotype is used to create an extensive lacunar-canalicular network throughout the bone (80). It is through this network that osteocytes regulate bone resorption, formation and mineralisation, by means of mechanotransduction, paracrine signalling and direct cell-cell contact with osteoclasts, osteoblasts and other osteocytes (81).

The main paracrine determinant of resorption regulation, (and bone formation by consequence) is the ratio of RANK:RANKL:osteoprotegerin (OPG) (28,82), where

osteoblasts and osteocytes are the key directing bodies in controlling this ratio. As discussed, initiation and promotion of osteoclast differentiation, survival and resorptive activity relies on the interaction of membrane-bound RANK with osteoblast- and osteocyte-derived RANKL (23,28,29). However, inhibition of further osteoclastogenesis, and thus resorptive activity, occurs as a result of osteoblast- and osteocyte-derived OPG (41,83). OPG is a soluble dimeric glycoprotein that binds to RANKL as an inert decoy receptor to reduce RANKL availability to interact with RANK-expressing osteoclasts and progenitors. In turn, a reduction in mature osteoclasts reduces resorption and therefore resorption pits for the reversal phase, subsequent osteoblastogenesis and bone formation (84).

1.2.2.2 Endocrine signalling

Calcitropic hormones, estrogen and parathyroid hormone (PTH), also have a role in regulating bone remodelling (67), plus, recent evidence suggests gastrointestinal hormone, leptin, also has a regulatory role (85).

Estrogen regulates bone remodelling in both women and men (86) by directly and indirectly inhibiting resorption. Binding to estrogen receptor α-expressing osteoclasts, estrogen promotes osteoclast apoptosis (87) and prevents differentiation through inhibition of the RANKL- and M-CSF-mediated signalling pathways (88). Furthermore, estrogen indirectly inhibits resorption by stimulating osteoblast- and osteocyte-derived OPG (89), RANKL, and pro-resorptive cytokine (TNFα, IL-1 and M-CSF) production (90).

PTH is produced by the parathyroid gland and its release is controlled by the calcium-sensing receptors present in response to changes in serum calcium levels, to ensure

it is kept within a tight range (~2.2-2.7 mmol/L) (91). More information on PTH and its activity is given in [Section 5.1.2]. Briefly, PTH has multiple modes of action (i.e., indirect and direct) which can promote bone formation with intermittent exposure as well as promote resorption through prolonged exposure. Indirectly, PTH increases renal absorption of calcium, as well as promoting vitamin D activation to calcitriol, another regulator of bone formation discussed in more detail in [Section 5.1.1]. Directly, activation of PTH receptor-expressing osteoblasts and osteocytes increases the production of RANKL and M-CSF and reduces OPG production (92–94), which increases osteoclastogenesis and thus resorption. However, intermittent exposure to PTH can also stimulate osteoblastogenesis, pre-osteoblast proliferation and cell survival via RUNX2 stimulation (95,96), thus promoting bone formation activity.

1.2.2.3 Mechanical loading

In bone, mechanical loading is the static and dynamic physical stress exerted on the tissue, which is experienced through everyday use, and its influence in skeletal structure was first noted by Julius Wolff in 1892. The Mechanostat theorem (97) states that regular periods of loading and unloading promote a balance between bone formation and resorption, whereas excessive periods of unloading (caused by injury, for example) will result in atrophy by increased bone resorption. Although, increased loading initially causes bone modelling (i.e., the formation of additional bone), pathological overloading drives the production of woven bone (98); a structurally weaker bone matrix produced rapidly by osteoblasts that carries a high risk of fracture.

It is now recognised that osteocytes are responsible for regulating these changes in bone formation and resorption in response to changes in loading. Evidence indicates that this occurs from the tether-like projections lining the osteocytes' dendritic

processes responding to changes in fluid flow shear stress; caused by the movement of interstitial fluid in the canalicular network when placed under mechanical strain (99–101). A variety of osteocyte-derived factors are influenced by changes in mechanical load and subsequently influence the rates of bone resorption and formation. Greater and more frequent loading results in increased expression of pro-anabolic factors nitric oxide (102), cyclooxygenase-2 (103) and prostaglandin E2 (104,105), as well as a marked reduction in pro-resorptive factors, sclerostin and dickkopf-1 (106). Greater production of these factors, most notably sclerostin, seen with unloading (106–108). These factors have roles within the canonical Wnt/β-Catenin signalling pathway; a key osteoblast signalling system necessary for regulating bone formation and mineralisation as well as indirectly regulating osteoclast bone resorption (83,109,110).

1.2.3 Stimulating bone formation and resorption

Damaged bone is the most recognisable stimulus that activates the bone remodelling process (111). Bone can become weakened and damaged through traumatic injury but can also occur through repetitive, everyday use. Apoptotic osteocytes at the site of damage initiate osteoclastogenesis by stimulating adjacent, surviving osteocytes to increase expression of RANKL and M-CSF, as well as downregulating OPG expression (112,113). This is a further example of the role osteocytes have in orchestrating bone remodelling, as apoptotic osteoblasts alone do not evoke the same response (114). The result of remodelling in this case is to remove the damaged, weakened bone, and allow it to be replaced with new, stronger bone.

An imbalance in serum calcium levels is also another notable driver in activating the bone remodelling processes, which is determined by the release of PTH as discussed in [Section 1.2]. These changes in calcium demands occur most notably during

pregnancy (115) and nutrient deficiencies from prolonged periods of starvation and/or intestinal malabsorption – such as poverty (116), eating disorders (117) and metabolic conditions (118,119). As the main reservoir of calcium (storing approximately 99% of body's total content (8), resorption and formation of bone is initiated to meet the increased demands for calcium or restore calcium serum levels to the physiological range, respectively. This coincides with changes in renal and intestinal reabsorption of calcium as a further result of PTH activity (120).

As discussed [Section 1.2], regular periods of loading and unloading maintains balanced bone remodelling, and more sudden changes to the frequency and amount of loading is closely followed by proportional and direct changes in bone density and strength (i.e., changes in bone metabolism are initiated rapidly) (121–124). Increasing the frequency of regular weight-bearing exercise (e.g., walking, running and strength training) is universally recommended in individuals at risk of fragility fractures to lower due to the immediate benefits gained in bone strength (125,126). Long (127,128) and short (129) periods of bedrest, resulting from injury and illness, and the prolonged weightlessness experienced by astronauts (130) also clearly exemplify the rapid response of bone metabolism to sudden changes mechanical loading.

Although the balanced activity between resorption and formation in remodelling is highly regulated, several factors can cause it to become unbalanced and, as a result, leads to the development of bone disorders.

1.3 Bone disease

1.3.1 Bone metabolism dysregulation

Loss of bone metabolism regulation causes an imbalance in resorption and formation, which leads to tissue structure weakness and the emergence of bone disease. Many stimuli have been found to cause dysregulation, the more established of those are summarised in [Table 1.1].

Table 1.1 - Key stimuli known to dysregulate bone metabolism. Each stimulus is categorised into a primary source and their effects on the bone are listed.

	Stimulus	Effect(s)	Ref.
Age	Menopause	Reduced estrogen production increases bone resorption	(131)
	Impaired MSC differentiation	Reduced osteoblast activity and thus osteoclastogenesis regulation	(132–135)
	Sedentary	Long periods of immobility and lack of sunlight causes bone atrophy	(136)
Prolonged unloading	Injury and bedrest	Immobility causes bone atrophy and illtreated bone injury can lead to ectopic bone formation	(127,129)
	Space flight	Little gravity causes rapid calcium release from bones leading to bone atrophy and kidney stones	(137,138)
Genetics	Sclerosteosis & van Buchem's	Reduced sclerostin production increases bone thickness and density	(139,140)
	Osteopetrosis	Defective osteoclast differentiation and function reduces resorption	(141)
	Fibrodysplasia ossificans progressive	Spontaneous flare-ups cause bone formation of inflamed soft tissues	(142)
Trauma	Blast injury	Dislodged bone causes ectopic bone formation into surrounding muscle	(143)
Primary Cancer	Ewing sarcoma, chondrosarcoma, osteosarcoma	Causes rapid, simultaneous formation and resorption	(144)

Previously existing conditions /factors	Hyper- /hypoparathyroidism	Increased/decreased PTH activity which causes calcium and phosphate imbalances, thus changes in remodelling rates.	(145–147)
	Medications	Various mechanisms of action causing bone weakness and fragility. Examples: Proton pump inhibitors, barbiturates, glucocorticoids, Warfarin, Loop diuretics, anti-convulsants	(86,148–150)
	Malnourishment	Malnutrition, starvation, inflammatory bowel conditions, diabetes, eating disorders cause calcium and phosphate imbalances thus changes in remodelling rates.	(116–119)
	Secondary Cancer	Metastatic tumour growth - particularly common from breast, prostate cancers and myeloma	(151)
	Rheumatic disease	Dysregulation of Wnt signalling factors that affect osteoblast- and osteoclastogenesis leading to imbalanced bone remodelling and thus bone fragility	(152)
	Diabetes	Differential effects between type 1 and 2 diabetes; both lead to increased risk of fractures	(153)

Typically, scenarios of bone dysregulation see the metabolic imbalance to favour osteoclastogenesis and resorption, and/or reduced osteoblast differentiation, resulting in weaker, more brittle and fragile bone (3). In the cases where bone formation is greater than resorption (e.g., Osteopetrosis), there is overproduction of bone, causing skeletal thickening and increased bone mass, which is also weak and at high risk of fractures (141).

1.3.2 The aging skeleton

Bone disease is most prevalent in older individuals (>50 years) due to changes in lifestyle, metabolism and the increased risk of developing conditions that can affect

bone health (e.g., rheumatic disease, diabetes, cancer) [Table 1.1] (154). There is also a predisposition to developing age-related bone conditions depending on an individual's bone health history prior to 30 years of age (11,150,155).

Globally, osteoporosis is the most common bone conditions (156) and is most prevalent in elderly individuals (21.7% of those 50-85 years old) (154). It is characterised by a reduced bone mass and mineral density (T-score <-2.5), resulting in a porous structure that is at a significantly greater risk of fracture (157–159).

Primary osteoporosis is the most common form and is caused by a pathological imbalance in bone metabolism (i.e., decline in estrogen, age-related increase in cellular senescence) (150). Secondary osteoporosis occurs as a comorbidity to many conditions that also have a greater prevalence in elderly individuals [Table 1.1] (160).

Elderly women are at the greatest risk of osteoporosis, with women >50 years old having a 5-fold greater chance of developing the condition than the general population, and the current estimation is 35.3% of elderly women globally are osteoporotic – almost 3-fold greater than elderly men where 12.5% are believed to have osteoporosis (154). This is due to the rapid decline in estrogen after menopause (161), which as discussed [Section 1.2] regulates osteoclastogenesis and resorption and increases the risk of experiencing a fragility fracture by 8% every year after onset (162). Men are more likely to experience a fracture later in life due to the slower decline in testosterone which has protective effects owing to its aromatisation to estrogen (85,163).

1.3.2.1 Osteoporosis treatment

Most treatments available for osteoporosis aim to reduce the rate of resorption by targeting osteoclast activity or differentiation, with very few anabolic agents available – see [Table 1.2] for the most commonly prescribed osteoporosis treatments.

The majority of anti-resorptive treatments lead to suppressed bone turnover due to the lack of osteoclast-dependent osteoblast differentiation. In addition, they can have many debilitating adverse effects that reduce quality of life. This leads to low therapeutic compliance and a consequential exacerbation to the patient's condition upon cessation of treatment. A number of prophylactic measures and recommendations, such as regular weight-bearing exercise (11,12), Vitamin D and calcium supplementation (13–15), are given to those within high-risk categories, have osteopenia (T-score -2.5<x<-1) or are in the early stages of the condition. Introducing pharmacological treatment is considered on a case-by-case basis, but it is generally recommended only in older individuals to prevent fractures and relieve symptoms associated with pre-existing fractures (156).

There is a clear need for more tolerable osteoporosis medications, particularly for more efficacious anabolic therapeutics that do not subsequently increase resorption through increased osteoclastogenesis (164,165). There is an ever-growing pressure to perform this research, optimise therapeutic approaches and diagnose osteoporosis earlier (with most diagnoses made after experiencing a fragility fracture) (166) due to the rapidly aging global population.

Table 1.2 - Osteoporosis pharmacological treatments.

Therapy	Examples *(Admin. route)*	Mechanism of action	Adverse effects	Ref.
Bisphos-phonate	Alendronate (*Or*), Risedronate (*Or*), Zoledronic acid (*IV*)	Incorporated and retained in bone mineral, released through resorption and endocytosed by osteoclasts. Inhibits cytoskeletal changes and causes apoptosis.	- Upper GI irritation (higher risk of cancer of oesophagus) - Osteonecrosis of the jaw (ONJ) - Severe joint and muscle pain (*IV primarily)* - Hypocalcaemia	(167–171)
Anti-resorptive monoclonal antibody	Denosumab (*SC*)	Binds to RANKL and thus inhibits binding to RANK on osteoclasts. Inhibits osteoclast differentiation and resorption	- Severe joint and muscle pain - Skin reactions - Rapid resorption after cessation - ONJ *(Denosumab)* - Greater risk of cardiovascular event *(Romosozumab only)*	(169,172–174)
	Romosozumab *(SC)* Blosozumab *(SC)*	Neutralises sclerostin to promote bone formation through increased osteoblast Wnt signalling		(175–177)
Selective estrogen receptor modulators (SERM)	Raloxifene, Bazedoxifene, Tamoxifen, Lasofoxifene (*All Or*)	Partial estrogen receptor agonist eliciting protective estrogen-associated effects on bone	- Increased risk of cancers (drug dependent) - Venous thromboembolism - Only effective against spinal fractures	(178–180)
Parathyroid hormone analogue	Teriparatide (*SC*), Abaloparatide (*SC*)	Recombinant human PTH (1–34) analogue stimulating osteoblast activity	- Mild general adverse effects - Time limited use (<2 years total) - Hypercalcemia	(181–183)

Or = Oral administration; IV = Intravenous administration; GI = Gastrointestinal; SC = Subcutaneous injection

1.3.3 An aging population

The latest statistics from the World Health Organisation reported that global life expectancy between 2000 and 2019 has increased from 67 to 73 years (184). It is estimated that 1 in 2 women and 1 in 5 men over the age of 50 will experience a fragility fracture (185) and the lifetime risks of these fractures are greater than that of experiencing strokes or developing cardiovascular disease (156,186).

With an aging population, the prevalence of osteoporosis, other detrimental bone conditions (e.g., Paget's disease), and age-related conditions that impact bone health are set to increase. This is validated by the most recent findings published in The Lancet (187) where a significant increase was found in new fracture incidents (33.4%) and fracture prevalence (70.1%) reported in 2019 when compared to those recorded in 1990. Despite a marginal decrease once corrected for age-standardisation, the number of patients living with the repercussions after experiencing fracture(s), as well as those at risk of fragility fractures will increase with time. It is estimated that by 2030 the annual number of fragility fractures that occur will increase by 23.3% from those in 2017 and the annual fracture-related costs will increase by 27% (186).

With more patients expected to have a reduced quality of life caused by deteriorating bone health, and consequently a greater financial and resource burden on the healthcare services globally, there is a clear urgency to prevent and treat fragility fractures. Regular screening and monitoring strategies, as well as greater endorsement of prophylactic measures are strongly advised to prevent the incidence of fractures (166,186,187). However, current pharmacological therapeutics are substandard in efficacy and tolerability and thus there is a greater drive in developing and creating bone drug therapeutics.

1.4 Bone research and drug discovery

1.4.1 Research and discovery

The drug discovery process, from bench to bedside, takes an average duration of 12-15 years and cost $2.87 billion dollars for a single therapeutic (188) [Figure 1.4]. Drug candidates are meticulously characterised, screened and tested using different platforms, including *in silico*, *in vitro*, *ex vivo* and *in vivo* systems, before reaching clinical trials (i.e., first administration to humans). However, it is at this point in the discovery process that many drug candidates fail, typically due to toxicity and/or insufficient efficacy (189,190). Selecting the most appropriate research models prior to clinical trials reduces the risk of these failings occurring, saving time, money and improving clinical translational (191).

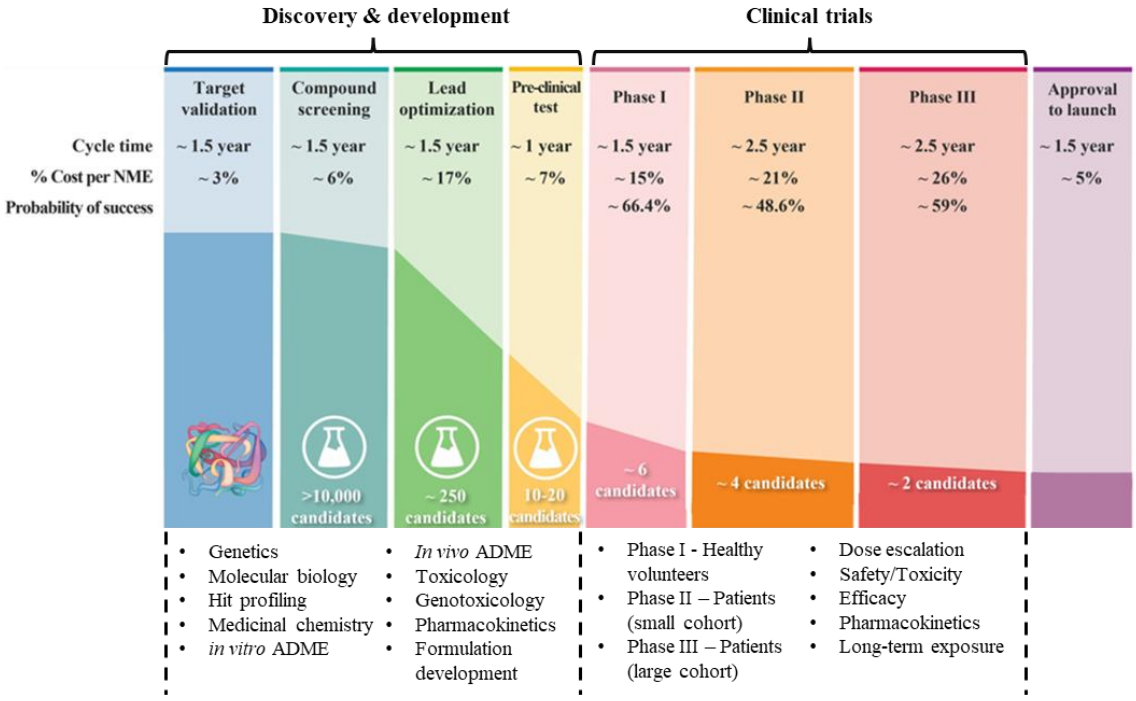


Figure 1.4 - Drug discovery process: From bench to bedside. The multidisciplinary process comprises of several stages of rigorous testing to shortlist the number of drug candidates to a final drug product that has shown to be effective and safe. It is a cost- and time-consuming process with a high risk of failure, which can be improved with selecting the correct testing platforms, models and tests. Adapted from Sun *et al.*, 2022 (191).

There are a number of models established in bone research. The advantages and drawbacks of each are discussed briefly here

1.4.2 In vivo models

Currently, the use of animals in the preclinical stages of the drug development process is essential to test drug efficacy, pharmacokinetics and safety pharmacology of potential drug candidates, before proceeding to clinical trials. The advantages of *in vivo* models are that all cell types and physiological features (i.e., vascularisation, cell-cell and matrix-cell interactions) are present; genetic manipulation (primarily in the case of rodent models) is possible; and, in bone research, smaller *in vivo* models often have faster bone turnover (192). In many cases, particularly in bone research (the reasons for which will be discussed in [Section 1.5]), *in vivo* models, often mimicking the disease phenotype, are valuable research tools for target identification and validation in the earliest phases of the drug discovery process (193). A number of *in vivo* bone models have been established, predominantly using rodents, and are outlined in [Table 1.3].

In vivo models have the fundamental limitation of species difference between the model organism and the intended end-user. This may be important in both target expression and function, speed of the bone remodelling/healing process in the model organism, inability to accurately reproduce the disease phenotype in an *in vivo* model etc. This is a major intrinsic factor that has been found to negatively impact scientific data, in addition to approaches in animal welfare and husbandry, resulting in poor predictions of clinical translation (194). The clinical studies of Alendronate [Table 1.2] provides a real-world example of this.

Table 1.3 - Established and commonly used rodent *in vivo* bone models.

Model	Procedure and purpose	Severity	Ref.
Bone labelling	Fluorochromes are administered intravenously, -peritoneally, -muscularly or subcutaneously, which bind to calcium and are incorporated into the skeleton to study osteogenesis and bone remodelling dynamics.	Mild	(195)
Calvarial defect	Defect made to calvaria via trephination or steroidal injections and used to assess bone development and regeneration, as well as a platform to assess compatibility and synergistic effects of novel scaffolds	Moderate	(196,197)
Ovariectomy	Ovaries are surgically removed to cause estrogen deficiency to mimic osteoporosis caused by the onset of the menopause.	Moderate	(198,199)
Osteotomy	Surgical creation of a fracture gap where the two remaining ends are held apart using a fixation system. Used to investigate delayed healing and non-union bone formation.	Moderate	(200,201)
Fracture healing	Insertion of an intermedullary pin followed by fracturing with a dropped weight. Used to investigate closed fracture healing.	Moderate - Severe	(202,203)

The slower turnover of bone in humans in comparison to the rodent *in vivo* models (204,205) used prior to clinical trials meant that an optimal dose in humans was not found until late into phase III clinical trials, where patients were initially receiving a dose four times greater than that of the effective dose. This caused an overwhelming number of patients and volunteers to develop oesophageal sores and upper gastrointestinal irritation that risked undermining the successful progression of the drug into clinic (206,207). The use of more physiologically relevant *in vitro* models earlier in the drug discovery process would provide an additional tool to demonstrate efficacy preclinically and as such prevent errors in dosing during clinical studies. Furthermore, using more physiologically relevant *in vitro* models support the reduction of *in vivo* research, which is in line with the principles of the 3Rs.

1.4.2.1 The principles of the 3Rs

In 1959, William Russell and Rex Burch published, “The Principles of Humane Experimental Technique”, in which they describe the 3R principles, in order to promote the humane care of animals in research and improve the reliability and value of the experiments performed (208). Each of the 3Rs are detailed in [Table 1.4].

In the UK, all scientific research using animals must adhere to the Animal (Scientific Procedures) Act 2013 (originally passed in 1986), which was described by the UK Select Committee on Animals in scientific procedures as, “the tightest system of regulation in the world”, for protecting animals in research (209). The act outlines the legal regulations implementing the principles of the 3Rs that must be met to authorise and licence the use of animals in scientific research. (210–212)

Table 1.4 - Details of each 3R principles. (210–212)

“R”	Definition	Real life examples
Replacement	Where possible, utilise models and technologies that can replace or avoid the use of animals to answer the scientific aims of an experiment.	- Organ-on-a-chip models - *in silico* models - Tissue engineering - Alternative animal models (e.g., Zebrafish)
Reduction	Use the minimum number of animals required for every experiment, but without compromising on the scientific validity. Adhere to ARRIVE guidelines	- Data sharing - Resource sharing - Use of non-animal reagents - Optimising reproducible and robust animal experiments (i.e., ARRIVE guidelines)
Refinement	Employ methods and take measures that will reduce any potential pain, suffering or distress to the animals.	- Improved housing and husbandry - Gentler handling techniques (e.g., tickling, handling tunnels) - Optimal analgesics and anaesthesia selection

ARRIVE = Animal research: reporting of in vivo experiments (213)

The National Centre for the 3Rs (NC3Rs) was established in 2004 under the recommendation of the Select Committee on Animals in scientific procedures to form a central hub that supports the implementation of the principles into scientific research. The organisation awards funding to UK-based groups whose research is intended to positively contribute to the 3Rs principles, as well as providing the necessary training, networking and engagement to support and drive changing attitudes towards the use of research animals (214).

1.4.3 Ex vivo models

After *in vivo* models, *ex vivo* models provide the closest recapitulation of the *in vivo* environment, whilst reducing the harm and suffering experienced by model organisms. A number of *ex vivo* models are used in bone research and the more commonly used approaches are detailed in [Figure 1.5]. The majority of *ex vivo* models used are long bone/limb organ cultures, as they provide a complete set of all bone cell types, which

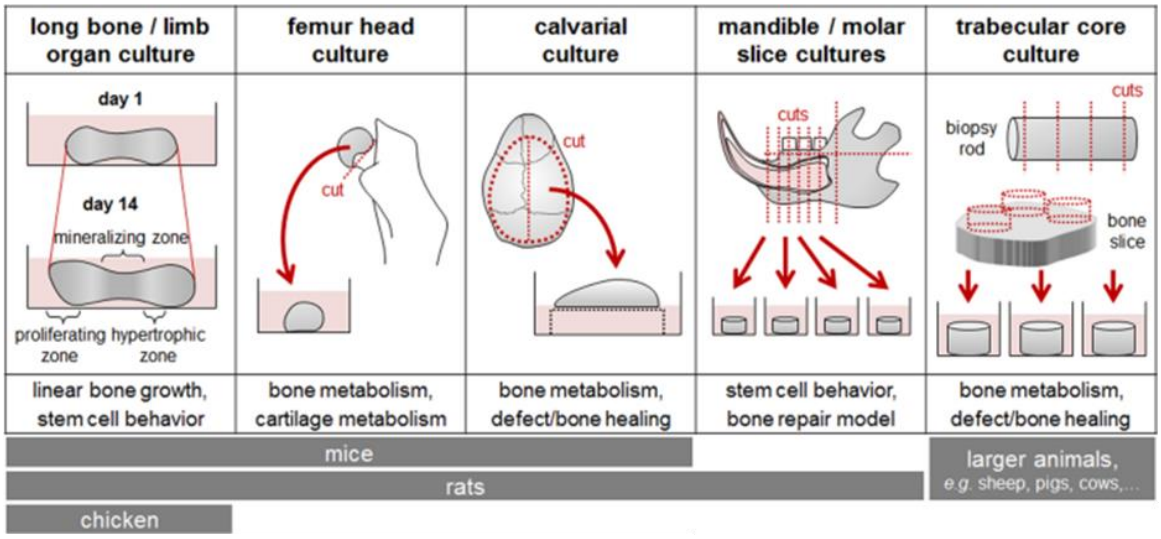


Figure 1.5 - *ex vivo* models commonly used in bone research. The appropriate model required depends on the research interest, with rodent tissue being the most commonly used. Multiple cuts of tissue samples, as shown in mandible/molar slices and trabecular core culture, are carried out to make efficient use of larger samples (i.e., multiple replicates) – an example of implementing the 3Rs principles. However, this has previously shown large variability in the individual cell types present, which is not representative of normal bone. Adapted from Ehnert *et al.,* 2020 (192).

enables the study of stem cell behaviour and bone metabolism (215), although the usefulness of each *ex vivo* model is dependent on the specific research interests concerned.

The most prominent limitation to using *ex vivo* models is the lack of perfusion through the tissue (192,216,217). This creates a hypoxic environment within the tissue and accumulation of waste and lactic acid, which exacerbates cell death, cell migration out of the tissue, and necrosis of the bone sample (216,218). The lack of perfusion and short-term culture period has been improved with the development of bioreactors, which aid nutritional transportation and distribution into the tissue, as well as waste removal, and as a result prolong the viability of the model (218–220). Despite these efforts, the use of *ex vivo* models are limited to tissue availability, human tissue in particular is difficult to obtain (221–223). So, while *ex vivo* cultures are beneficial research tools in place of using *in vivo* models, and as an intermediate model prior to *in vivo* testing, their limited lifespan in culture and limited tissue availability means they are not readily accessible, nor can they be completely relied upon for bone research.

1.4.4 In vitro models

In vitro models in drug discovery and development provide valuable tools for the preliminary high-throughput testing of potential drug candidates, as well as target identification and characterisation (224). This enables inexpensive and rapid screening, without the use of animals or human tissues, and with biological materials (i.e., cell lines) that do not have the same supply limitations as *ex vivo* and *in vivo* models (225).

Advances have been made to enable co-culturing of multiple cell types that are present within the *in vivo* and *ex vivo* tissue – refer to [Figure 1.6] for commonly used *in vitro* co-culture systems used in bone research. Traditional *in vitro* systems use different adaptations of 2D platforms, but there are differential effects in cell behaviour from cells within a 3D environment (i.e., *in vivo* and *ex vivo*) (226,227). More detail on the comparison between 2D and 3D culture systems will be discussed in [Section 1.6]. Briefly, 2D culture systems lacks the extracellular matrices that are essential for cell differentiation, activity and survival, and the means to create a scaffold that closely recapitulates these environments has been limited (228,229). This means fewer complex *in vitro* models exist and drives the use of *in vivo* models.

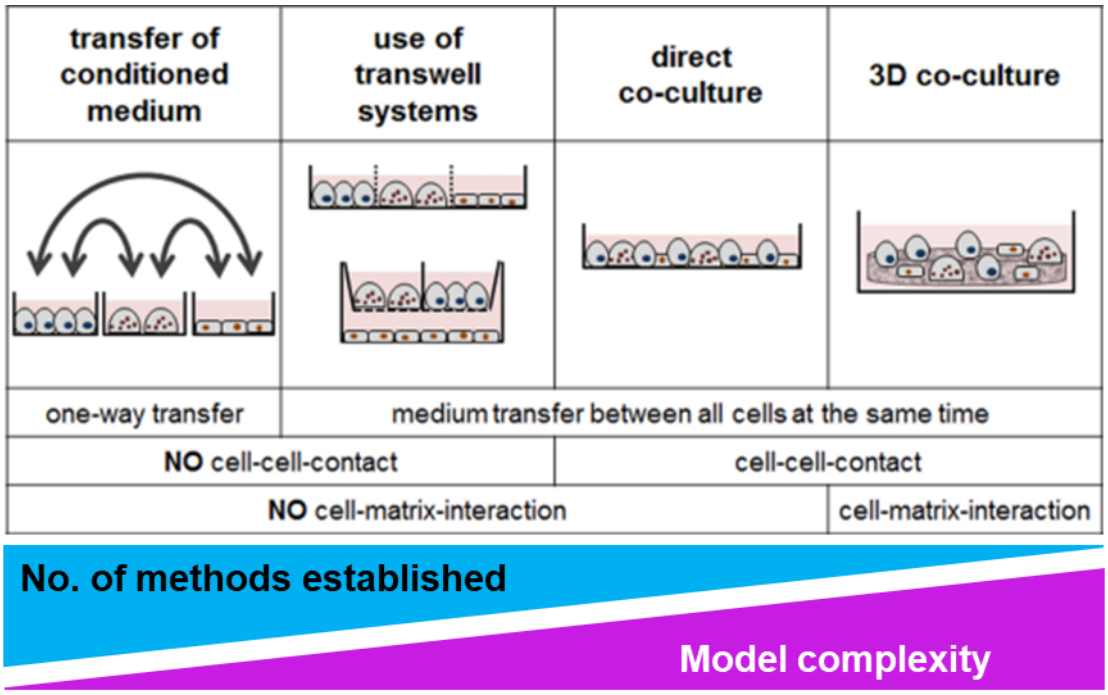


Figure 1.6 - *in vitro* co-culture systems used in bone research. Bone is a multicellular organ and as such the use of *in vitro* co-culture systems are important in the drug discovery and development process. Standard in vitro culture systems can be used to answer many research questions (e.g., cellular interactions, media transfer), however the development of more complex models of bone has been hindered by the multifaceted structural and biological nature of bone tissue. Adapted from Ehnert *et al*., 2020 (192).

With the number of limitations *ex vivo* and *in vitro* models display, it is no surprise that a great reliance on *in vivo* models still exists. Although, by using these other model types, the number of animals required is reduced, and this only continues with the use of more advanced and complex *ex vivo* and *in vitro* systems. Yet, a balance between technique simplicity and model complexity must be struck for greater uptake. Creating complex models of bone has been hindered by two main factors, the intricate and unique composition and architecture of bone tissue and the complex nature of the main regulatory bone cell, osteocytes.

1.5 Issues hindering *in vitro* bone model development

1.5.1 Problem 1: Bone tissue composition and structure

Bone is a unique combination of an organic tissue amalgamated with an inorganic mineral composed of calcium and phosphate. The hierarchical organisation of this tissue at the microarchitecture level up to that of the whole bone is responsible for its distinct enduring strength, rigidity and elasticity (230,231) [Figure 1.7].

There are two main forms of bone tissue present within whole bones – cancellous (trabecular) and cortical bone – of which the proportions vary between different skeletal sites (232) [Figure 1.7 A]. Cancellous bone has a honeycomb-like arrangement, giving rise to a sponge-like texture and a large porous surface area (67,233) which is filled with marrow, fat and vasculature (234). Cancellous bone is surrounded by cortical bone which accounts for 80% of total bone mass and has a lower surface to volume ratio than cancellous bone. The arrangement of the two bone types provides mechanical strength by the cortical bone and shock absorbance as well as load transmission by the cancellous bone (233).

Cancellous and cortical bone share the same chemical composition however, the different arrangement of these compounds gives rise to the two bone types [Figure 1.7 B].

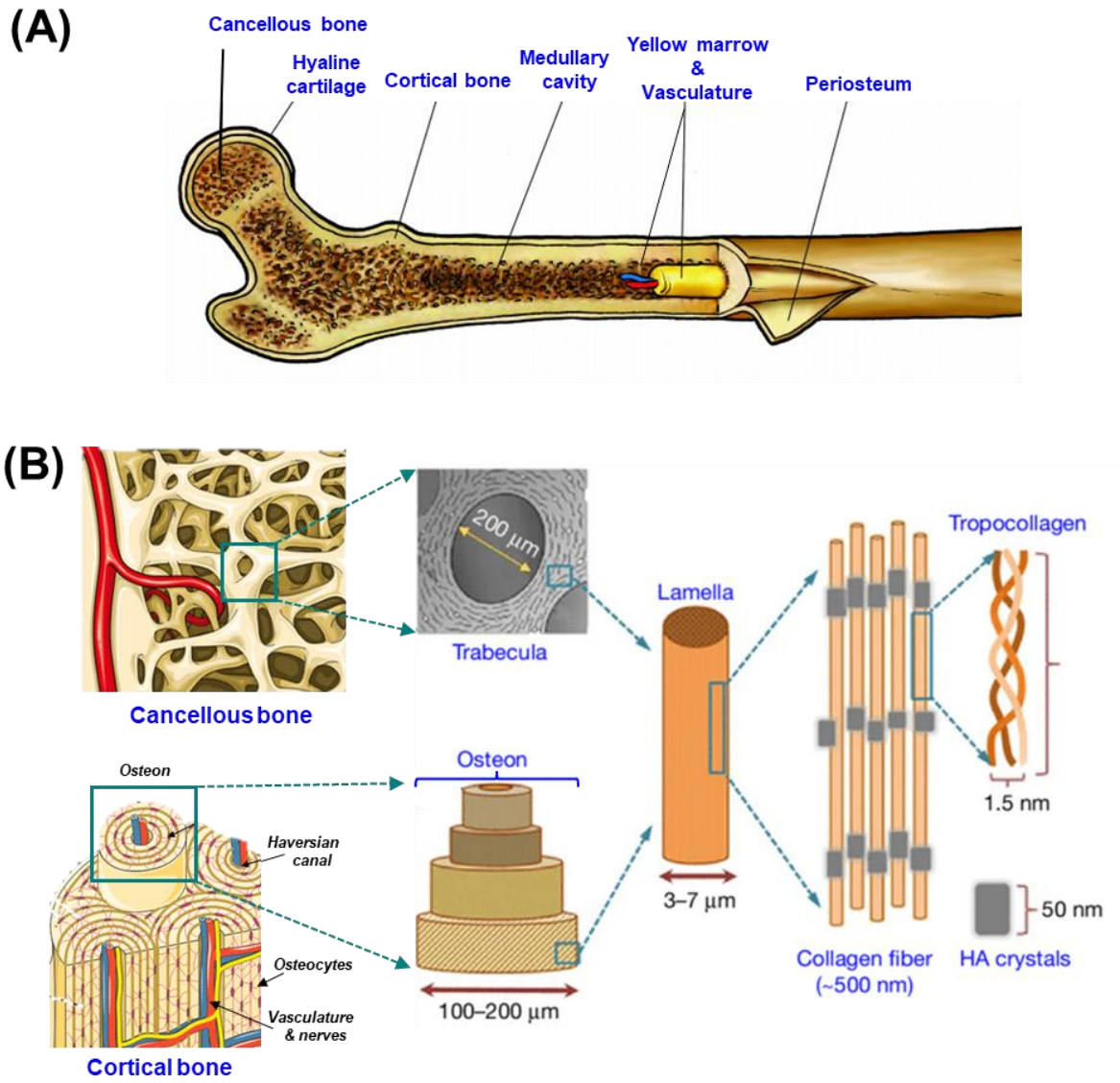


Figure 1.7 - Bone tissue macroscopic arrangement and matrix microarchitecture. (A) Bone is a highly organised tissue, the arrangement of which creates a structure with a high load tolerance and high resistance to breakage. Adapted from Nigerian Scholars, 2023 (235). **(B)** The differential arrangement of bone matrix gives rise to two distinct microarchitectures – porous, sponge-like cancellous bone and densely-packed, rigid cortical bone. Adapted from Gao *et al.* 2017 and Chabanon, 2015 (236,237).

Mineralised collagen fibrils are packed together to form fibres, which are further organised into concentric lamellae. In cortical bone, lamellae are arranged perpendicularly and concentrically around a vascular space (i.e., Haversian canal) to create a distinct unit, an osteon. These units are tightly compacted together to give rise to the dense cortical (21). However, when lamellae are arranged as interspersed rods and plates, this generates the cancellous bone (238). This hierarchical organisation of the bone matrix is lost when bone is formed rapidly (e.g., during embryonic development, fracture healing, osteopetrosis, bone cancer). The fast production of osteoid creates woven bone, which is characterised by a haphazard arrangement of the bone matrix, delayed calcification and the presence of many large osteocytes (239,240). Over time, this mechanically weak osteoid serves as a scaffold that is replaced by lamellar bone (241).

Recapitulation of bone *in vitro* is hindered by the dynamic nature of the bone microarchitecture by the bone remodelling process, along with a unique and highly organised macroscopic structure; the complex composition of the organic and inorganic phases only adds to this challenge.

1.5.1.1 Organic phase

The organic phase of bone is a proteinaceous matrix which, prior to mineralisation, is produced by osteoblasts and called osteoid. Type I collagen is the primary protein found in this matrix, accounting for 90% of the organic phase (242). There are 28 types of collagen identified in humans, with type I collagen making up 90% of the total collagen content in the human body (243).

In bone, type I collagen is a heterotrimeric molecule composed of two polypeptide α1 chains and a single α2 chain arranged into a triple helix (244). The precursor, procollagen, has three distinct domains; a long central helical domain capped with short C-terminal and N-terminal peptide domains (245). Respectively, these two end domains are cleaved during bone formation by osteoblast-derived bone morphogenetic protein 1 (BMP1) (246) and a disintegrin and metalloproteinase with thrombospondin motifs (ADAMTS) (245,247). This cleavage gives rise to the cleaved end terminals, carboxy-terminal propeptide of procollagen type I (P1CP) and amino-terminal propeptide of procollagen type I (P1NP), along with tropocollagen fibrils (i.e., the basic structural collagen unit in bone matrix). Clinically, P1NP is used as marker of bone turnover, with significantly increased levels seen in the blood after bone anabolic therapy (248,249).

The remaining 10% of osteoid composition is made up of a mixture of non-collagenous proteins (64) [Figure 1.8]. The roles of these protein families and its members has been reviewed by Carvalho *et al.* (250). Often multifunctional, their roles in the bone are extensive, contributing to cell attachment (i.e., glycoproteins) (251), mineralisation regulation (i.e., Gla-containing proteins) (252) and maintaining the interface between the organic and inorganic phases (i.e., proteoglycans) (253). Furthermore, trace amounts of other proteins, both bone- and non-bone derived, are found within bone matrix, including growth factors and cytokines, and their roles contribute to mineralisation of bone and regulating bone metabolism (254,255).

The inclusion of non-collagenous proteins requires as much consideration in novel biomaterials for fabricating *in vitro* scaffolds as the structural unit (e.g., collagen, fibrin, ceramic). They have already shown to be beneficial in recapitulating the extracellular

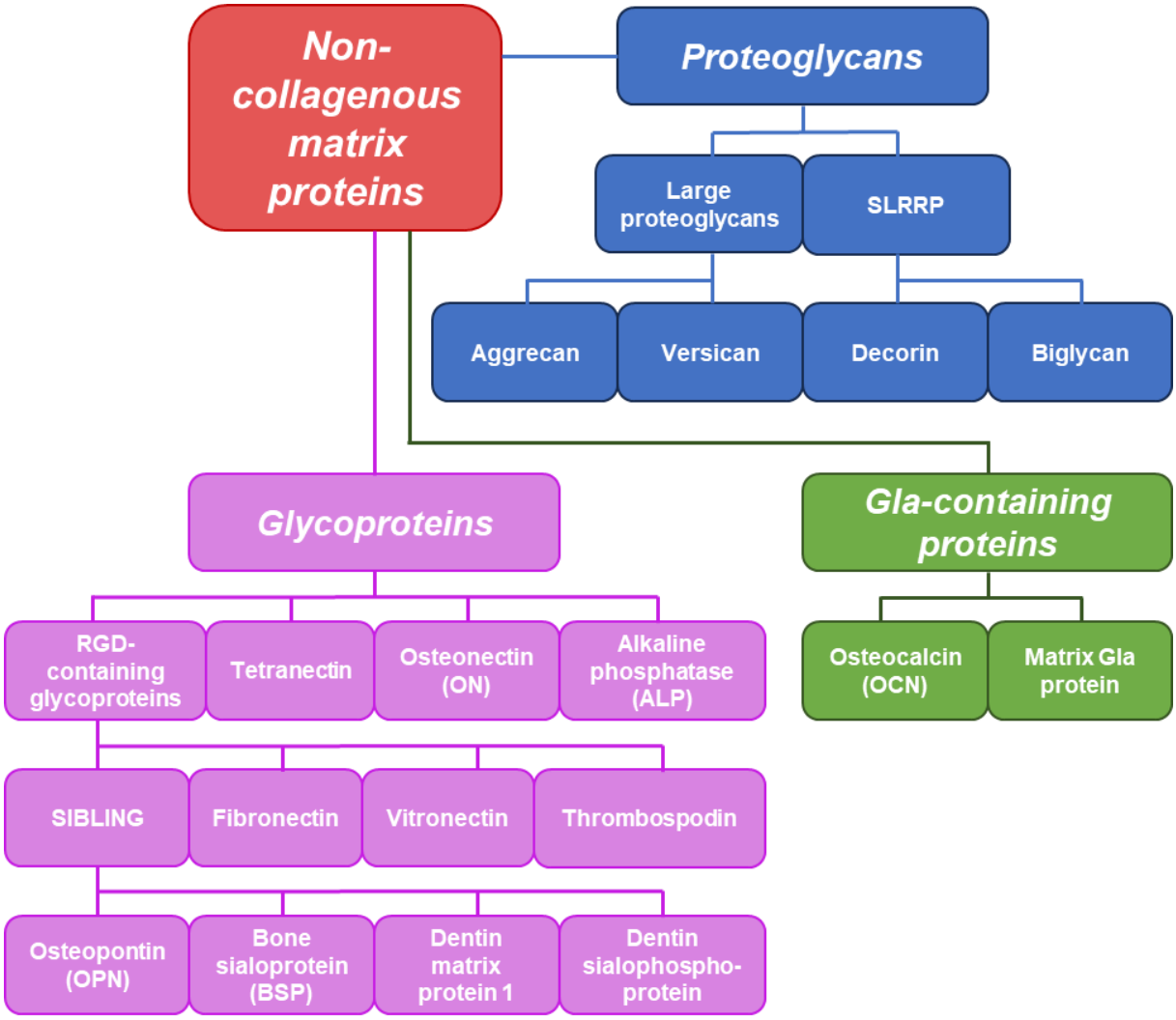


Figure 1.8 - Non-collagen proteins present in bone matrix. There are three major non-collagenous proteins present in osteoid and bone matrix; proteoglycans, glycoproteins and Gla-containing proteins; each with several members that have an array of roles within bone metabolism regulation, mineralisation and maintaining structural integrity. SLRRP – small leucine-rich repeat proteoglycans. SIBLING – small integrin-binding ligand, N-linked glycoproteins. Adapted from Carvalho *et al*., 2021 (250).

matrix for supporting long-term viability and migration of cells, osteogenesis and mineralisation – reviewed by Carvalho *et al.* (250) - which highlights their importance in normal bone formation and maturation, as well as the challenge of creating optimal scaffolds for *in vitro* bone models.

1.5.1.2 Inorganic phase

The inorganic phase of bone constitutes about 70% of the total bone tissue composition and is in the form of carbonated hydroxyapatite mineral (6,7). The precipitation and nucleation of calcium and phosphate crystals to produce hydroxyapatite mineralises the collagen (19), giving rise to a matrix which provides bone with its distinct stiffness.

During mineralisation, the deposited mineral matures over time through changes in crystal volume, calcium and phosphate ion ratios and water content. Initially, the mineral is less organised and stable, and becomes a modified hydroxyapatite that contains additional carbonate and phosphate ions – resulting in a less crystalline mineral (256). As such, due to the dynamic nature of bone tissue, the inorganic phase of bone is heterogenous and contains varying proportions of immature and mature minerals at any given time and between different skeletal sites. Thus, the heterogeneity of bone mineral and its osteoinductive and osteoconductive properties must be considered during *in vitro* bone model development.

The incorporation of hydroxyapatite relies on adequate extracellular concentrations of calcium and phosphate, which are regulated through the cooperative actions of alkaline phosphatase (ALP), non-collagenous osteoid proteins and activated vitamin D, calcitriol (232,257).

ALP is an enzyme present on the extracellular surface of osteoblasts that hydrolyses inorganic pyrophosphate (PPi), an inhibitor of mineralisation. PPi is produced from the hydrolysis of extracellular adenosine triphosphate (ATP) and inhibits calcium and phosphate ion crystallisation, as well as binding strongly to hydroxyapatite to prevent

further crystal growth (258). Hydrolysis of PPi by ALP to inorganic phosphate removes this inhibitory action and provides a source of phosphate for hydroxyapatite crystal formation (259,260).

Osteonectin and bone sialoprotein (BSP) are two non-collagenous proteins present in osteoid, produced at the later stages of bone formation just prior to mineralisation (261) and have prominent roles in mineralisation. Osteonectin binds to hydroxyapatite crystals through its high affinity for calcium and it is required in the growth and maintenance of deposited crystals (262–264). BSP also has a high affinity for calcium and has found to act as a nucleator of hydroxyapatite to collagen, with *in vitro* studies showing that overexpression caused enhanced mineralisation (265) and anti-BSP antibodies reduced mineralisation (266).

Calcitriol is the activated form of vitamin D, which controls and regulates serum calcium and phosphate levels, by stimulating their absorption through the intestine. Furthermore, serum calcitriol has also shown to be a promoter of osteoblast differentiation and enhance expression of ALP and the other proteins involved in bone mineralisation, including osteocalcin (232,267).

1.5.2 Problem 2: Osteocyte culture

Osteocytes are the most abundant bone cell in the body, accounting for 90-95% of the total bone cell population (79). However, their challenging culture condition requirements have made them difficult to study - with their roles in bone metabolism regulation only being elucidated in the last 20 years. As described in [Section 1.2], osteocytes are considered the main regulatory unit in bone metabolism through their mechanosensation and mechanotransduction capabilities, paracrine signalling and

direct cell-cell contacts with other cells. These regulatory actions warrant their inclusion in *in vitro* bone models as their absence would be an incomplete recapitulation of natural bone and an inaccurate reflection of *in vivo* bone metabolic activity.

1.5.2.1 Osteocytogenesis and osteocyte connectivity

Osteocytes are of osteoblast lineage, with about 20% of osteoblasts undergoing osteocytogenesis after osteoid production (268), although the determining factors remain unknown. These osteoblasts become embedded within the newly produced non-mineralised osteoid during bone remodelling and differentiate during the mineralisation process. Subsequently, mature osteocytes remain within the mature mineralised bone, potentially for over 25 years (269). The transition from osteoblast to osteocyte involves a series of significant changes gene expression and in morphology [Figure 1.9].

Bonewald (270) have reviewed the gene and protein expression patterns that occur during their differentiation, with reference to their morphological changes at each phase of osteocytogenesis [Figure 1.9 A]. Youlten *et al.* (271) also mapped the osteocyte transcriptome which revealed a high level of conservation between skeletal sites and was distinct from their ancestoral cells in the bone marrow. This is exemplified by the declining expression of osteoblasts genes (e.g., RUNX2) which is initially retained in early osteocytes and then becomes downregulated as the cell matures (272).

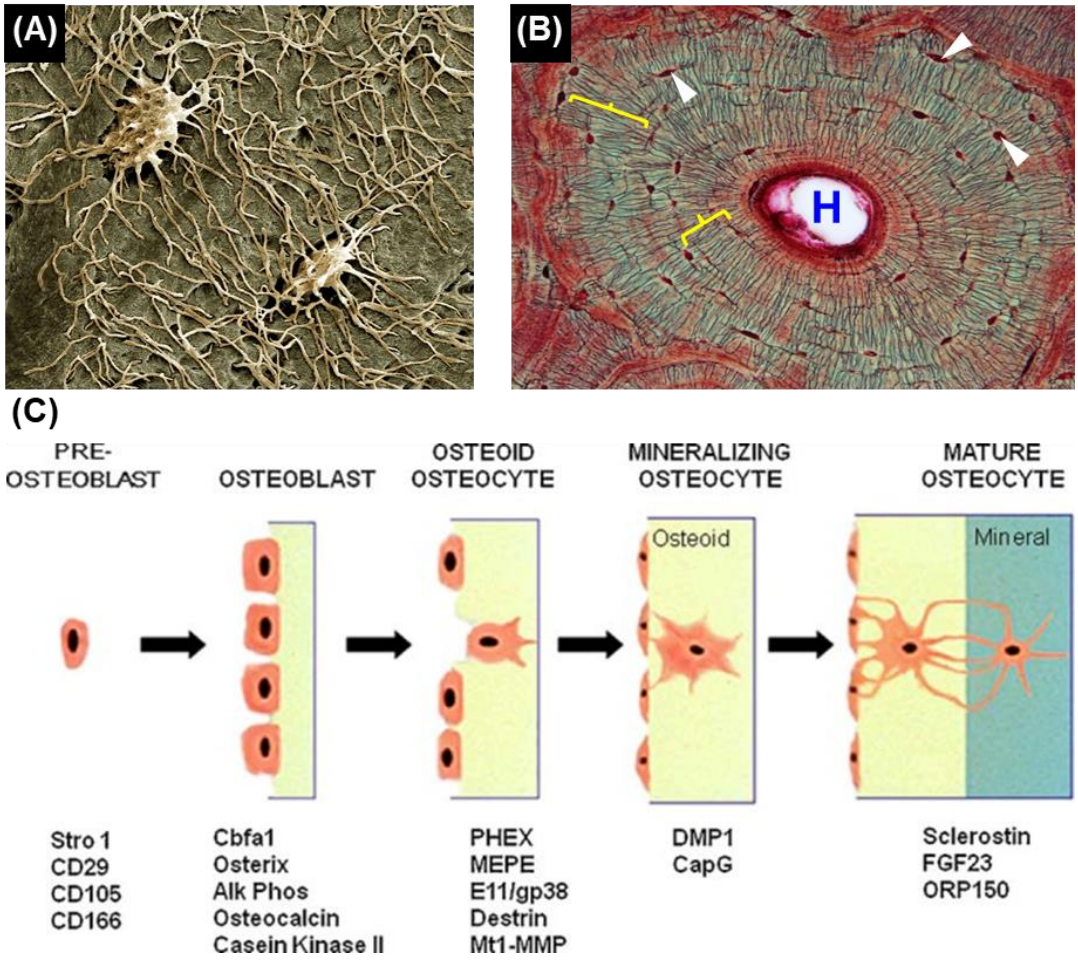


Figure 1.9 - Morphological and gene expression changes between osteoblasts and osteocytes. (A) Osteocytes are highly dendritic cells that reside in lacunae within mineralised bone. Taken from MacKenzie 2018 **(B)** An osteon showing the extensive lacunar-canalicular network created by osteocytes and their dendrites to make direct cell-cell contact and intra-lacunar fluid flow between other osteocytes, as well as other bone cells. White arrows = lacunae; yellow bars = canaliculi between lacunae; blue 'H' = haversian canal. Adapted from Embryology UNSW Sydney, 2020 **(C)** Expression of specific genes and proteins appears or increases at specific points during osteoblast differentiation towards osteocytes. Taken from Bonewald 2011 (270,273,274)

The earliest marker of osteocytogenesis is indicated by an increased transcription and expression of podoplanin, which is responsible for development and elongation of the osteocyte dendritic processes (275,276), and is also implicated in regulating osteocyte bone remodelling activity (277,278) for mature osteocyte As osteocytes mature, their gene and protein expression indicate declining bone formation activity, but increased

activity that is associated with phosphate metabolism and osteoid mineralisation (e.g., phosphate-regulating neutral endopeptidase chromosome X (PHEX) and dentin matrix protein 1 (DMP1) (279,280). Once mature, although many of the genes involved in regulating osteoclast resorption are retained (e.g., RANKL) expression of formation regulation genes specific to mature osteocytes appear (e.g., sclerostin, dikkopf-1, fibroblast growth factor 23 (FGF23)) to govern osteoblast activity (281–283). There is also evidence indicative of bone resorptive activity by osteocytes through increased expression of cathepsin K, however it is negligible in comparison to osteoclasts (284) and believed to be utilised for maintaining their extracellular space within the bone (285).

The formation of the osteocyte network requires radical morphological changes of the polygonal osteoblasts on the bone surface to become stellate, dendritic osteocytes [Figure 1.9 B]. The cell body of the osteocyte resides within fluid-filled spaces in the bone called lacunae, and their dendritic projections travel along tunnels (i.e., canaliculi) throughout the bone to create a creating a 3D, lacunar-canalicular network between other osteocytes and bone cells [Figure 1.9 C] (109,270,286,287). The formation of dendrites relies on the expression of E11/gp38 and podoplanin, which has been shown to occur in response to increased fluid sheer-stress (288). Furthermore, it also depends on the expression of specific matrix metalloproteinases which remodel the newly deposited osteoid, through collagenolytic activity, to accommodate the differentiating cell (289).

The number of canalicular connections that connect each osteocyte differs between species and skeletal sites, with an average of 41 for humans (290). A high degree of connectivity provides network resilience in the event of connection interruptions and is

also indicative of more active remodelling sites for rapid communication (291). The degree of connectivity of the osteocytic network is comparable to that of neuronal connections in the brain, with an estimated 3.7 trillion dendritic projections in the average human skeleton, and furthermore an estimated 9.1 million osteocytes replaced daily highlights the dynamic nature of bone at the cellular level (80).

1.5.2.2 Culture requirements and osteocyte cell lines

Despite being the most abundant bone cell, osteocytes have been extremely difficult to study and the technology with which to analyse them in greater depth has only been made possible due to significant developments and advances in the last 30 years. This is due to their unique position within the bone that is responsible for their phenotype and survival. Isolation of osteocytes from bone causes them to rapidly dedifferentiate (i.e., >3-days) - losing their dendritic morphology and expression of osteocyte markers (e.g., sclerostin DMP1 and FGF23) (292,293).

Several immortalised osteocytic cell lines have been created to survive outside of the bone matrix. They are primarily of murine origin - (8-murine only and 4-murine/rat according to Cellosaurus search [15/07/2023]), with MLO-Y4 (294) and IDG-SW3 (295) being the most commonly used – with only one of human origin, HOB-01-C1 (296). MLO-Y4 share similar characteristics to primary osteocytes, including low ALP activity and high production of osteocalcin (294), however they have a low expression of sclerostin (297), which is counter to the primary phenotype. The IDG-SW3 cell line was produced to create an osteocytic cell line capable of sclerostin production, although there has been limited use of these cells in the bone research community, perhaps due to their requirement for interferon-gamma stimulation to maintain their conditionally immortalised state (298).

In order to investigate osteocyte function, they must be studied in a mineralised 3D matrix (275) as primary osteocytes and their network cannot mature in 2D *in vitro* culture conditions, nor can osteocytic cell lines fully recapitulate the characteristics of primary osteocytes under 2D conditions. This has driven the use of *in vivo* and *ex vivo* models as a source of cells and bone tissue, however, recent developments in 3D *in vitro* culture technology have provided promising results in osteocyte culture, prolonging their survival and encouraging activity not unlike that of primary osteocytes. Brady, Brian and Hoey (298) showed that by culturing MLO-Y4 in 3D they become capable of producing sclerostin and Sawa *et al.* (292) showed primary osteoblasts and the murine osteoblast cell line MC3T3-E1 when cultured in 3D *in vitro* conditions differentiate into an osteocytic phenotype.

These recent developments of 3D *in vitro* culture systems demonstrate that solutions to the issues that currently hinder the development of *in vitro* bone research models and assay platforms for bone drug research and development are within reach. Furthermore, they warrant further research into creating *in vitro* bone models of human origin.

1.6 Advances in cell culture

1.6.1 2D vs 3D culture

Cell culture is a laboratory technique that has been practised since 1907, when frog embryonic tissue was successfully cultured *in vitro* on lymph-treated coverslips (299). The traditional method of culturing cells on treated 2D surfaces has prevailed, and culture conditions and approaches have been established and optimised, giving rise to one of the most applicable, adaptable and powerful tools in medical research and development.

The extracellular matrix (ECM) is the dynamic non-cellular component of tissues, and it has important influences on cell metabolism and survival through chemical (e.g., growth factors and proteoglycans) (300) and physical cues (e.g., adhesion proteins) (301). In recent years, new cell culture techniques are being developed in which cells are cultured under 3D conditions, particularly as more is learned about the critical relationship that exists between cells and their extracellular environment (226). The ECM is largely absent from 2D cell culture approaches, but is an intrinsic part of most 3D *in vitro* culture systems, supporting these key regulatory influences.

A comparison between 2D and 3D culture approaches is summarised in [Table 1.5]. Each approach has their advantages and disadvantages, with the hesitation to utilise 3D *in vitro* culture systems being predominantly caused by the practicality (i.e., low running costs, shorter culture periods, easy reproducibility) and familiarity (i.e., well-established culture and analytical methods) of using 2D culture systems (302).

Table 1.5 - Comparison of 2D and 3D *in vitro* cell culture conditions and requirements. (303,304)

Factor/aspect	2D	3D
Culture methods	Well-established	Novel; not as refined
Analytical methods	Well-established	Novel; not as refined
Financial cost	Low	Often high
Culture time	Fast turnover	Slower turnover
Reproducibility	High	Lower/not as refined
Cell conformation	Unnatural	Natural
Cell behaviour	Changed gene expression and metabolic activity	Gene expression and metabolic activity more comparable to *in vivo*
Cell interactions	Loss of some direct cell-cell and cell-ECM contact	Preservation of more cell-cell and cell-ECM interactions
Drug sensitivity	Less resistance, poor metabolism	Accurately reflects *in vivo* responses
Cellular senescence	High	Low

However, there are particular aspects of adopting 3D cell culture systems being overlooked which will provide benefits to the research and drug discovery process that outweighs the time and financial costs for their development and utilisation. These include the following:

- **Cells are cultured in a natural conformation**: *In vivo*, cells are within a 3D environment; surrounded by the presence of other cells and ECM components. However, by using established 2D *in vitro* culture approaches, cells grow into a monolayer on a flat surface. As such they adopt a flatter and stretched morphology, due to adherence with the growth surface on only one side of the cell, and thus do not accurately reflect those found in the *in vivo* environment. This unnatural morphology has been shown to negatively affect the proliferation, differentiation, and viability of cells (305,306). Whereas 3D culture approaches achieve an *in vitro* culture condition reminiscent of the *in vivo* environment; **restoring the enveloped cell-cell and cell-ECM interactions** that are key to holding cells in a natural conformation and largely lacking in the 2D culture conditions.
- **Transcription and protein expression reminiscent of *in vivo*:** The transcriptome and proteome of cells can differ considerably when they are cultured under 2D and 3D conditions, with those of 3D cultured cells more reminiscent of cells *in vivo* (307,308). As such, resultant **cell behaviour, metabolic activity, and drug sensitivity within 3D cell culture assays** have been better predictors of the *in vivo* response in comparison to 2D cell culture assays (309).

- **Greater adaptability:** 3D culture scaffolds and approaches can be **readily and easily fine-tuned and modified** to ensure optimal growth conditions for specific cell types as well as create multicellular platforms. With focus on bone models, as discussed in [Section 1.5.2], the osteocyte phenotype cannot be retained in 2D *in vitro* cell culture following isolation from bone. Thus, to culture osteocytes *in vitro*, they require a mineralised 3D matrix (275), scaffolds of which have been, and continue to be created (more detailed discussion in [Sections 1.6.2 and 1.6.3]). In order to create a clinically relevant *in vitro* bone model reminiscent of *in vivo* bone, osteocytes must be present, therefore, developing 3D bone cell culture approaches is necessary.

Overall, the altered morphology and behaviour of cells when cultured under 2D conditions are unlikely to be the best predictors of *in vivo* responses, which can be detrimental within the drug discovery process and increases the risk of drug candidates failing at clinical testing stages. The benefits of developing and using a 3D platform to prevent such an event outweighs the financial cost and time required, as failure of the drug, which may otherwise have been successful with more appropriate pre-clinical testing platforms, is itself costly (310) [Figure 1.4]. As with any developing technology, further advancements are made with greater uptake. 3D assay methods, construction, maintenance, and analysis will become more refined and established, and as a result financial costs and costs will reduce considerably. For example, the cost to decode a single human genome between September 2001 and May 2022 has reduced from $95,263,072 to $525 (USD), due to the advancements made with increased uptake of genome sequencing technology (311).

1.6.2 3D culture approaches

Culturing cells in 3D was first used for embryogenesis and developmental biology studies in the 1940s. Since the 1970's, which saw pioneering work in creating self-assembling multicellular 3D tumour models (312) there has been exponential growth in the number of developed and optimised 3D *in vitro* cell culture approaches. These spheroid culture models have been instrumental in understanding cancer biology and treatment development, as well as understanding the significance of the relationships between cells and with their extracellular matrix (226,313). This increase in novel 3D culture strategies over the last 50 years, including technological advances in tissue engineering, has led to the next generation of experimental platforms, including organoids and organ-on-chip models (314).

Organoids and organ-on-chip models are 3D platforms designed to replicate the *in vivo* environment with *in vitro* applications as research models in drug discovery and development (228). However, organ-on-chip models are simplified recapitulations of the *in vivo* environment lacking stem cells, thus they do not undergo tissue remodelling. As such, organoids are believed to have greater physiological relevance and can be used to more accurately reflect normal *in vivo* conditions as well as disease states (315,316). It follows, therefore, that organoids are also more likely to be most useful in drug research and development (317).

Fundamental properties that are required for ideal bone cell culture are biocompatibility, like-for-like mechanical properties, pore size of at least 100 μm for adequate diffusion, and biodegradability to allow the scaffold to be remodelled by the cells (318). For the purposes of this project, the additional critical properties that the bone model must possess is the ability to support osteocytogenesis and long-term

osteocyte culture. This requires an environment with a close recapitulation of the *in vivo* environment (i.e., one that can mineralise, promote osteoblast differentiation, and can be mechanically stimulated (275,319,320)). Furthermore, accessibility to the resultant model is a fundamental requirement of 3Rs research, of which this project is funded. Therefore, simplicity and use of materials that can be obtained and maintained by other research laboratories is essential. Organoid bone models show the most promise in creating a bone model that fulfils the necessary requirements for the scope of this project. Despite organ-on-chip models having a simple set up and maintenance, as well as providing adequate perfusion (and with that, mechanical shear-stress), there is a lack of tissue remodelling, which is a key process that links the differentiation of mature osteoblasts into osteocytes (79). Organoids on the other hand are simple and have demonstrated successful cell culture, as well as having the capacity to be adapted to enable bone tissue remodelling and introduce mechanical stimuli.

1.6.3 Scaffolds for bone organoids

The development of bone organoids is still a new branch of research, which has been reviewed in detail recently by Chen *et al.* (321). Briefly, the basis of creating a bone organoid begins with selecting the appropriate cell origin and scaffold approach, then optimising culture conditions to create one of the many niches bone contains (i.e., bone marrow, cortical and trabecular bone, woven bone). The type of model created (and therefore cell type and scaffold) depends on the research interest, as the properties of the resultant organoid must reflect those of the ECM found *in vivo* (226,322). Refer to [Table 1.6] for a list of scaffold types commonly used in 3D bone cell culture.

Many of the materials mentioned in [Table 1.6] have been derived from surgical scaffolds used for bone repair (i.e., ceramics, metals and synthetic polymers), as well

as major structural components of the ECM that are commonly used in other areas of research for fabricating 3D scaffolds (i.e., fibrin, collagen).

Table 1.6 - Scaffolds used for 3D bone cell culture *in vitro* and *in vivo*.

Class	Examples	Features	Ref.
ECM – Natural	Collagen	- Close resemblance to *in vivo* - High cell survival and adaption - High batch-to-batch variation - Prone to contamination	(323–327)
	Fibrin		
	Alginate		
	Matrigel™		
	Cellulose		
ECM – Synthetic	Poly(ethylene oxide)	- Controllable physical and chemical properties - Cost effective - Lower contamination risk - Possible cytotoxicity - No biochemical stimuli	(328–331)
	Poly(vinyl alcohol)		
	Polycaprolactone		
	Poly(ethylene glycol oxide)		
ECM – Natural-synthetic hybrid	Hydroxyapatite-gelatin	- A combination of Features for ECM-Natural and ECM-Synthetic scaffolds (see above)	(332–334)
	CaP-fibrin/collagen		
	Silk/polycaprolactone		
	Chitosan/ poly(lactic acid-co-glycolic acid)		
Metal	Cobalt-chromium	- Biocompatible - Strong - Poor biodegradability - Potentially cytotoxic - Susceptible to corrosion	(335–337)
	Zirconium		
	Titanium		
	Tantalum		
Ceramics	Hydroxyapatite	- Similar composition to *in vivo* bone - Osteoinductive - Osteoconductive - Brittle - lack of protein content - Greater use in clinical orthopaedics rather than cell culture	(338–340)
	Tricalcium phosphate		
	Biphasic calcium phosphate		

Whilst ceramics and metals are primarily reserved for clinical applications, incorporating them with ECM derivates to make a composite scaffold has been used in cell culture techniques to improve their functionality (341,342). Creating different

combinations of these materials means bespoke scaffolds can be created to fit the research purpose specifically, which is an added advantage to using organoids in research and drug development. However, these scaffolds can also be used alone, which at times is preferred due to the drawbacks of the other biomaterials (e.g., presence of unnatural materials) (343).

ECM-based biomaterials are the most commonly used 3D *in vitro* scaffolds, due to having the closest representation of the *in vivo* environment. Owing to their physical and chemical properties, many of these ECM-derived biomaterials are classed as hydrogels (344) which are becoming increasingly applied within medical research, as well as many other industries, such as agriculture (345), cosmetics (346) and food (347).

In 1960, Wichterle and Lím first recorded the use of hydrogels as a versatile biomaterial capable of mimicking *in vivo* matrices due to their high water content and soft, flexible, porous structures (348,349). Hydrogels are cross-linked networks of polymers with a water totalling for at least 10% of its weight (344). As shown in [Table 1.6], the polymers within hydrogels can be naturally derived or synthetically fabricated. They have hydrophilic backbones and cross-linked network chains, which mean they have a high resistance to dissolving and are capable of swelling and retaining a large volume of water without affecting their structure (350). An additional advantage of hydrogels is their readily modifiable physiochemical properties (e.g., porosity, degradation rate, rigidity, cell adherence), allowing the creation of bespoke *in vitro* scaffolds through the addition of functional groups combining with other hydrogels and different preparation approaches (351). The fundamental physiochemical properties of *in vitro* hydrogel scaffolds also fulfil the criteria desired for *in vivo* tissue repair and regeneration

scaffolds, which are currently under development in surgical bone and dental implants to improve biocompatibility and reduce immunogenicity (236,322,352–355).

Natural hydrogels are derived from components of the ECM and are categorised into 3 groups: protein-based (e.g., collagen, fibrin), polysaccharide-based (e.g., alginate) and decellularised tissue (356). They have low cytotoxicity, produce non-toxic metabolites when degraded and innately encourage cell adhesion, differentiation and proliferation, unlike synthetic hydrogels which require further modifications to have the same properties [Table 1.6]. As such, the use of natural hydrogels, or hybrids containing natural hydrogels, are preferred over synthetic ones.

Amongst the natural scaffolds, the use of fibrin has proven to be one of the most promising biomaterials in bone organoid development. In response to tissue injury, haematomas (i.e., blood clots) are formed as a temporary scaffold to guide and support the tissue repair process through the attachment of cells that create the new tissue. A haematoma is composed of a cross-linked fibrin network; a product resulting from the enzymatic cleavage of the liver glycoprotein, fibrinogen, by thrombin (357,358). The fibrin network is considered as a natural hydrogel; up to 80% water composition (359), a porous polymer network stabilised with crosslinks, supports cell attachment and encourages the deposition of new tissue as itself is degraded by serum protease, plasmin (323,360). The formation of fibrin networks has an important role in the bone healing process with the physiochemical properties of fibrin showing the greatest osteoinductive potential (361–363). As such, the properties of fibrin scaffolds have led to their successful use in clinical applications, as well as *in vitro* research (364,365).

As well as fibrin, collagen is a popular and commonly used scaffold for creating bone organoids, however it often requires additional biomaterials – such as bioceramics and additional bone ECM components (e.g., glycosaminoglycans) – to improve its low mechanical strength and osteoinductivity (366). For simplicity, a key and desired feature for developing a novel bone model [Table 1.7], collagen would not be an ideal biomaterial for the scaffold. Furthermore, fibrin has shown to promote greater osteoblast survival, proliferation and differentiation (367,368), as well as promote greater bone formation (369), when compared against collagen scaffolds. Prolonged cell survival in particular is another key property to feature in novel bone models [Table 1.7], and for the purpose of this project [Section 1.7].

1.6.4 An assayable bone model

The need for appropriate bone models in drug research and development, along with the exponential growth in 3D cell culture technologies, has driven an increase in the creation of many *in vitro* bone model methods and approaches that display the characteristics of bone at the cellular and structural level, as well as some also successfully culturing osteocytes.

Static organoid models were created using primary human bone cell cultures cultured on biphasic calcium phosphate ceramic particles – a bone mineral mimetic – by Boukhechba *et al.*(370), which resulted in their successful differentiation to osteocytes. Similar models were also successfully created using primary human bone cell cultures seeded on collagen hydrogels by Bernhardt *et al.* (371,372) as part of a co-culture system with other bone cells, and also by Nasello *et al.* (373), which investigated the effects of miniaturisation on osteocytogenesis capabilities.

Other *in vitro* osteocyte culture models employ bioreactors which enable equal distribution of nutrients, mechanical stimulation through shear-stress and as a result cells remain viable for longer periods (217). Such models include one used by Munir *et al.* (374) where primary human osteoblasts incubated in a rotary culture system for 3-weeks generated mineralising collagen-containing spheroids with embedded osteocytes. And another by Akiva *et al.* (324) who displayed the successful culture of primary human bone marrow stromal cells in silk fibroin scaffolds – a natural, fibrous and insoluble protein produced by silk-spinning insects, such as Bombyx mori silk worms – in a spinner-flask bioreactor and differentiated into osteocytes with the presence of a network within a mineralised matrix.

However, there is still an unmet need for a bone model with a scope for assay development which encompasses all the features and criteria listed in [Table 1.7]. It is a great achievement that 3D *in vitro* systems enabling osteocyte culture have been created, as this has been one of the main hinderances of developing novel bone drug therapeutics [Section 1.5.2]. However, these models require further refinement before they can be considered for assay development. For example, those that use primary human cells would require adaption to accommodate a secondary cell line as healthy primary tissue is not available to other laboratories, and also limits the scalability of the platform with reduced availability of the tissue. Plus, using a primary cell source is associated with a higher risk of impacting on the reproducibility and reliability of the data attained from these models, due to the heterogenous nature of the cell population between batches of primary cells (375).

Table 1.7– Critical features for an assayable bone model. Based on the key findings from the literature discussed throughout this introduction. Features not limited to those listed below.

Criteria	Reason
Supports all bone cell types (Osteocytes particularly)	- Bone is a multicellular organ that is maintained through the cooperative actions of osteoclasts, osteoblasts and osteocytes. - Osteocytes are the main regulators of bone metabolism and must be included for accurate recapitulation of osteoblast and osteoclast activity
Similar chemical composition to bone	- Resorption of bone by cathepsin K requires the presence of mineral and cross-linked collagen
3D culture	- Osteocytes are only viable in 3D cultures - Cell behaviour and characteristics are more accurate of the in vivo environment when cultured under 3D conditions
Human derived	- More physiologically relevant; circumvents interspecies differences - Implements the 3Rs
Prolonged culture	- Bone therapeutics are taken over a prolonged period. Prolonged culture enables investigations into long-term effects of therapeutics on bone cells and bone structure.
Homogeneity	- Assay platforms require tight intra- and inter-assay precision and accuracy. - Improves reliability. Variation will result in unreliable data
Reproducible	- Accessible to all users - Improves reliability. Variation will result in unreliable data
Simplicity	- Cheaper to set up and maintain - Greater uptake and dissemination of the culture method.

To summarise, there is currently no 3D *in vitro* bone model that fulfils the basic criteria [Table 1.7] to enable it to be developed into an assayable platform as those that currently exist do not possess the mechanical stimulation, a readily available cell source or require complex apparatus. However, the properties of a bone model system created at the University of Birmingham show promise as a foundation in which to develop an assayable bone model due to its simple set up and maintenance, as well as a unique in-built strain which provides mechanical stimulation to the culture system.

1.7 Birmingham Self-structuring bone model

1.7.1 Concept

In response to trauma where bone becomes damaged, there are four defined stages of tissue repair: inflammatory phase, soft callus phase, hard callus phase and bone remodelling (376,377). The immediate event following trauma is the formation of a haematoma at the site of injury and subsequently leads to the release of cytokines and inflammatory cell infiltration; thus begins the aptly named inflammatory phase of bone repair. The haematoma scaffold enables adherence of a mixed population of inflammatory cells - such as macrophages and lymphocytes – as well as mesenchymal stem cells (MSCs). The recruitment and differentiation of MSCs to early-stage chondrocytes and osteoblasts is greatly promoted through the temporal and time-sensitive release of haematoma-, inflammatory cell- and bone tissue-derived cytokines and growth factors, particularly members of the transforming growth factor-beta (TGF-β) superfamily (378).

MSC differentiation stimulates the production of collagen-rich ECMs to replace the haematoma with a soft callus, bridging the gaps between the broken bone fragments, which gradually mineralises to form a hard callus composed of woven bone (379). Woven bone is typified by a haphazard organisation of the collagen fibres, rendering it a weaker and immature form of bone, and it arises during events where osteoid has been produced rapidly, such as embryonic bone development and healing (239). Mineralisation of the woven bone, like the arrangement of its collagen fibres, also occurs arbitrarily, favouring more collagen-dense regions (380). Believed to be driven by BMP signalling (381,382), callus mineralisation requires high concentrations of calcium (Ca^{2+}) and phosphate (PO_4^{3-}) ions, for the precipitation and amalgamation of

hydroxyapatite (HA) crystals to the collagen fibres, which are provided by membrane-bound matrix vesicles released by the osteoblastic and chondrocyte cells present (383)

The woven bone making up the hard callus provides the foundation for the deposition of a more organised, and thus stronger, lamellar bone through remodelling – the final stage of bone fracture repair (240,384,385). This final phase sees the sculpting and reinforcement of the hard callus into a shape and strength resembling that of the original bone before injury (386). The woven bone is initially broken down by osteoclasts arriving to the callus site via blood vessel invasion during angiogenesis (387,388), followed by slower and organised osteoblast osteoid production and its subsequent mineralisation to form the newly repaired bone tissue.

The biological process of bone fracture healing meets many of the desirable and required criteria for a model of bone formation - i.e. it begins with a biocompatible scaffold for cells to remain in a natural conformation, then encourages cell differentiation and bone matrix production to produce a bony foundation that can be remodelled by the coupled activity of osteoclasts and osteoblasts. It is this process that has provided a biological and physical basis to create a novel *in vitro* model of bone, in particular the use of fibrin-based scaffolds *in vitro* as the basis for bone formation is something that we have used to generate a self-structuring model of bone (SSBM).

1.7.2 Method

The original basis of the SSBM, was work by Paxton, Grover and Barr (389) who aimed to create a novel method of engineering ligament tissue by recapitulating the interface between ligament tissue and bone. Like bone, ligaments are a fibrous and collagenous tissue, of which 85% is type I collagen (390), however they do not become mineralised

under normal conditions. Their approach involved casting a fibrin hydrogel between two brushite ($CaHPO_4 \cdot 2H_2O$) anchors and seeding it with chick tendon fibroblasts. In this set-up, the brushite anchors represent the two bone ends which a ligament would normally connect, and the fibrin hydrogel acts as the naturally occurring haematoma scaffold occurring at the site of injury. This resulted in subsequent self-reorganisation and contraction of the fibrin hydrogel, driven by the seeded cells, around the anchors which formed a cylindrical structure [Figure 1.10 A]. The presence of the brushite anchors was responsible for long-term retention of the cylindrical structure (391), along with simultaneously providing a passive tension that forces alignment and elongation of the seeded cells and consequently inducing changes in their metabolic activity (392,393). The combination of tension-mediated metabolic manipulation and supplementation with ascorbic acid, proline and transforming growth factor-β (TGF-β), enhanced collagen production and deposition to replace the initial fibrin matrix with a new ligament-like tissue matrix that had comparable tensile strength to that of embryonic ligaments (389,394).

This initial body of work by Paxton, Grover and Barr (389) provided a platform in which the fracture repair process could be recapitulated *in vitro*, enabling cells to adhere and replace the matrix with a new collagenous one, and under the correct conditions lead to the creation of *in vitro* bone tissue.

1.7.3 Adaptions and findings

Iordachescu *et al*. (395) adapted the Paxton, Grover and Barr (389) *in vitro* ligament method by replacing the use of fibroblasts with primary cells isolated from rat femoral periosteal tissue [Figure 1.10 B], which are one of the key sources of MSCs with osteoblastic potential that are recruited in the bone fracture healing process (396).

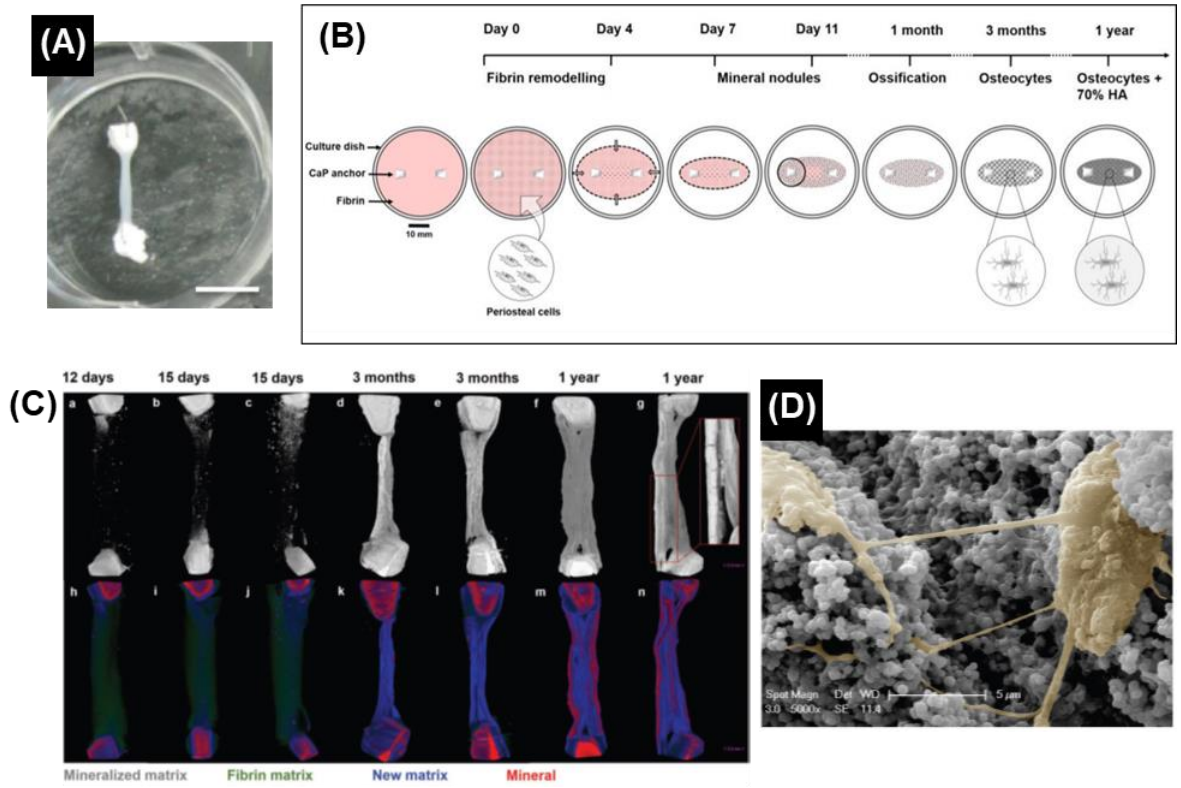


Figure 1.10 - The Birmingham self-structuring bone model. **(A)** Seeding cells onto a fibrin hydrogel causes contraction of the matrix to form a defined cylindrical structure. Taken from Wudebwe *et al*., 2015 (392) **(B)** A schematic of the SSBM method timeline outlining the milestones observed when seeded with rat femoral periosteal cells. Taken from Iordachescu thesis (397). **(C)** Overtime, the fibrin matrix of the SSBM culture system is replaced with a collagenous-matrix which mineralises from the anchors towards the centre of the construct. Taken from Iordachescu *et al*. (395). **(D)** After 1 year of culture, dendritic cells can be observed within the SSBM matrix using scanning electron microscopy (SEM). Taken from Iordachescu *et al.* (395).

Iordachescu *et al*. (395) showed the same fibrin matrix contraction seen previously (389), forming a cylindrical structure held between the two brushite anchors. The constructs were cultured under normal growth conditions, to encourage cell proliferation, for up to a month, after which they were cultured long-term (up to a year), under osteogenic conditions to promote osteoblastic differentiation and ossification.(397)

Structural analysis using second-harmonic imaging, Sirius red staining and Raman spectroscopy revealed a gradual deposition and maturation of a new collagen-containing ECM originating from the anchor regions towards the central region of the constructs [Figure 1.10 C]. Also, micro-computed tomography (μCT), x-ray fluorescence (XRF) and Raman spectroscopy also showed the same progressive appearance of mineral, co-localising with the new ECM, originating from the anchors and furthermore, revealed the presence of hydroxyapatite after 3 months of culture [Figure 1.10 C].

At the biological level, the constructs supported long-term survival of the seeded cells, with evidence of cells with dendritic-like projections imaged using scanning electron microscopy (SEM) and synchrotron radiation computed tomography (SR-CT) after one year of culture [Figure 1.10 D]. The presence of dendrites suggests this construct model provides a culture system encouraging osteocytogenesis, which is also seen in woven bone during the fracture healing process, as the presence of many large, dendritic osteocytes has been observed in the hard callus (239).

The prolonged cell survival, differentiation and matrix production within the constructs, along with the development of the organic and inorganic phases of the new ECM, was concluded to be reminiscent to that of haematoma maturation seen during bone fracture repair into a soft callus and mineralising into a hard callus, or in other words, bone tissue.

1.7.4 Conclusion

This novel method successfully creates *in vitro* self-structuring bone models (SSBMs) that have comparable chemical and biological properties to that of the woven bone

created in response to bone fracturing. The mineralised collagen matrix provides the fundamental 3D platform for bone remodelling by osteoclasts and osteoblasts - the process defining the final stage of fracture healing, as well as in maintaining adequate bone health.

Furthermore, under osteogenic culture conditions, these models support osteoblast differentiation and then house the subsequent viable osteocytic cells, for a prolonged time period. As discussed previously, the existence of a model that accommodates osteocytes long-term, without the need for less than reliable or representative osteocytic cell lines or the use of animals, does not exist and yet is under growing demand. Harnessing and utilising the recent advances made in 3D cell culture approaches, this model is the first of its kind to show that the limitations of recapitulating bone *in vitro* can be overcome.

1.7.5 Aims

The Birmingham SSBM method laid the foundation for the aims of this project, which are:

1. Adapt, develop and optimise the SSBM method to accommodate a secondary cell line of human origin, with the goal to creating a method that can be easily adapted, replicated and repeated.

2. Introducing homogeneity amongst the cell culture population and producing SSBMs that are more clinically relevant to humans.

3. Fully analyse and characterise the resultant constructs at the biological and structural level.

4. Map the significant stages of the SSBM development and maturation, to aid experimental design for future studies, as key stages of bone development, remodelling and repair heavily rely on the presence and/or absence of specific time-sensitive bone structure and cellular cues, features and characteristics.

This aim has required the development and optimisation of analytical approaches specific to these constructs by adapting methods that are currently used for bone cell cultures and bone tissue explants.

5. Assess the responsivity of the SSBM constructs to known bone formation modulators (BFM) to investigate their potential as a drug testing platform.

6. Explore the possibilities of miniaturising and bioprinting SSBM constructs, to create a high-throughput drug screening platform.

Overall, the objective of this project is to create a versatile and simple physiologically relevant *in vitro* bone model, complete with osteocytes and mineralised matrix that has the potential to become an assayable platform, which implements the 3Rs into many areas of bone research.

Chapter 2

Methods and materials

2.1 hFOB 1.19 selection and culture

2.1.1 General cell culture and aseptic technique

All cell work adhered to aseptic technique to prevent and reduce the risk of contamination to the cultures. Cell work was conducted inside class II laminar flow hoods of which all inner surfaces were cleaned before and after all work was performed. Hood surfaces were first cleaned with Chemgene HLD_4L laboratory surface disinfectant (cat no.: XTM309; supplier: Medimark Scientific Ltd, Kent) at a 5% dilution using distilled water ($d.H_2O$), followed by ethanol absolute ≥99.8% (cat no.: 20821.365DP; supplier: VWR Chemicals, Leicestershire) at a 70% dilution using $d.H_2O$. All consumables and equipment used within the hoods were sterilised prior to entering the hoods and commencing work.

2.1.2 Receipt of Human foetal osteoblast (hFOB) 1.19 cell line

Over the duration of this project, the Human foetal osteoblast (hFOB) 1.19 cell line (RRID: CVCL_3708) was obtained from NDORMS Laboratory (University of Oxford, UK) in October 2019, as well as from American Type Culture Collection (ATCC, USA) in October 2021 and January 2022. When received, vials were kept in liquid nitrogen (LN2) storage until required.

2.1.2.1 hFOB 1.19 LN2 recovery and culture

Vials were completely thawed in a water bath at 37 °C with continuous and gentle agitation, then the total cell suspension was added dropwise to a falcon tube containing 9 mL of cold complete media [Table 2.1]. Cells were centrifuged (250 rcf, 5 minutes), the supernatant discarded and resuspended in 3 mL warm complete media. The whole cell resuspension volume was transferred to a T25 flask and incubated at 33.5 °C, 5%

CO_2. Media was renewed after 48 hours and then again every 3-4 days thereafter, until reaching 80-90% confluence.

Table 2.1 - hFOB 1.19 cell culture media recipes.

Media	Ingredient	Concentration	Cat no.; Supplier
Complete	DMEM/F-12, no phenol red	Base	21041025; Fisher Scientific
	FBS	10%	FB-1001; BioSera, France
	G418	0.3 mg/mL	4727878001; Sigma
Freezing	***Complete media***	72%	See ***Complete media*** above
	FBS	20%	FB-1001; BioSera
	DMSO	8%	D8418; Sigma
Osteogenic	***Complete media***	Base	See ***Complete media*** above
	Menadione	10^{-8} M	M5625; Sigma
	Ascorbic acid	100 µg/mL	A92902; Sigma

2.1.2.2 hFOB 1.19 passaging

Cultures were passaged according to ATCC guidelines once reaching 80-90% confluence. Cell culture media was removed and discarded, followed by a brief rinse in phosphate buffered saline solution (PBS) – prepared by dissolving a Gibco PBS tablet (1X) (cat no.: 18912014; supplier: Fisher Scientific, Loughborough, UK) per 500 mL d.H_2O. Cells were dissociated with Trypsin-EDTA solution (cat no.: T4171-100ML; supplier: Sigma, USA) (diluted from 10x to 2x using PBS) for 5 minutes at 33.5 °C, 5% CO_2, which was ceased with the addition of complete media. The cell suspension was centrifuged (250 rcf, 5 minutes), and the resultant cell pellet resuspended in complete media, then seeded at a 1:4 split ratio.

2.1.2.3 hFOB 1.19 cell viability and cryopreservation

Following trypsinisation and subsequent centrifugation as outlined in [Section 2.1.2.2], cells were resuspended in 3 mL freezing media [Table 2.1] and a viability cell count was performed using 0.4% trypan blue (cat no.: T8154-100ML; supplier: Sigma), at a 1:1 dilution, and using a Fast-Read® 102 counting chamber (cat no.: 630-1893; supplier: VWR Chemicals).

The remaining cell suspension was further diluted with freezing media to a concentration of 1.0 x 10^6 cells/mL then aliquoted into cryotubes at 1mL/tube. Tubes were stored at -80 °C in a CoolCell Freezing container (cat no.: 432000; supplier: Corning Inc., USA) freezing at a rate of 1.0 °C/minute, which were then moved to LN2 storage at least 2 hours later.

2.1.2.4 hFOB 1.19 mycoplasma testing

Mycoplasma testing was carried out for every new line of hFOB 1.19 received from NDORMS and ATCC once recovered and cultured from cryopreservation, as well as on occasions when cell proliferation was slower than expected. Mycoplasma testing was carried out using and following the steps outlined in the MycoAlert™ mycoplasma detection kit (cat no.:LT07-318; supplier: Lonza, Switzerland).

2.1.3 Growth curves

Cells were seeded at 25 x10^4 cells/well into 6-well culture plates with the appropriate media [Table 2.1] and cultured under the appropriate conditions, with media renewal every 3-4 days. At the chosen analytical time points, cells were harvested following trypsinisation and centrifugation. A trypan blue viability cell count was performed [Section 2.1.2.3] for each individual well.

2.1.4 Differentiation media investigation

Cells were seeded at 6.25 x10^4 cells/well into two 24-well culture plates and incubated (33.5 °C, 5% CO_2) for 3-4 days, reaching 80-90% confluence. Each differentiation media tested [Table 2.2] was added to six wells per plate and incubated for 1 or 2 weeks, with media renewal every 3-4 days. After 1 and 2 weeks of culture, cells were harvested from three of the six wells per differentiation media and used for trypan blue viability cell counting [Section 2.1.2.3]. The remaining wells for each media tested was used for alkaline phosphatase (ALP) analysis as outlined in [Section 2.3.2.4].

Table 2.2 - Osteogenic media tested for hFOB 1.19 cell culture. Composition details and information for potential hFOB 1.19 osteogenic medias. Tested on 2D cultures.

Medium	Ingredient	Concentration	Cat no.; Supplier
Medium 1 *(Final Complete medium)*	DMEM/F-12, no phenol red	Base	21041025; Fisher Scientific
	FBS	10%	FB-1001; BioSera, France
	G418	0.3 mg/mL	4727878001; Sigma
Medium 2 *(Final osteogenic medium)*	***Medium 1***	Base	See ***Medium 1*** above
	Menadione	10^{-8} M	M5625; Sigma
	Ascorbic acid	100 µg/mL	A92902; Sigma
Medium 3	***Medium 2***	Base	See ***Medium 2*** above
	β-glycerophosphate	5 mM	G9422; Sigma
Medium 4	DMEM/F-12, no phenol red	Base	21041025; Fisher Scientific
	FBS	0.2%	FB-1001; BioSera
	G418	0.3 mg/mL	4727878001; Scientific Laboratory Supplies
	Menadione	10^{-8} M	M5625; Sigma
	Ascorbic acid	100 µg/mL	A92902; Sigma

2.1.5 Long-term culture and differentiation regime

Cells were seeded at 25 x10^4 cells/well into two 6-well culture plates and maintained in culture under permissive conditions (33.5 °C, 5% CO_2), with media renewed every 3-4 days. After 4 weeks of incubation, conditioned media was collected and stored at -80 °C, cells were harvested following trypsinisation and centrifugation from a single 6-well. Cells were used for trypan blue viability cell counting and quantitative polymerase chain reaction (qPCR) analysis [Section 2.3.4]. The remaining 6-well plate was cultured under osteogenic conditions (osteogenic media [Table 2.1] at 37 °C, 5% CO_2) for a further 4 weeks, with media renewal every 3-4 days. After culturing for a total of 8 weeks, cells were processed as outlined above after 4 weeks of culture.

2.2 Establishing SSBMs

All the steps involved in preparing setting up and maintaining primary rat SSBM construct cultures were followed as outlined in the original protocol (398). All the steps involved in preparing, setting up and maintaining hFOB 1.19 SSBM construct cultures have been published (325). Refer to [Appendix 8.1].

In brief, the method objective is to provide a detailed protocol for an *in vitro* 3D cell culture system which gives rise to SSBM constructs. The method outlined is not specific to creating hFOB 1.19 SSBM constructs, as it can accommodate other cell types. To create hFOB 1.19 SSBM constructs, a cell seeding density of 0.25x10^6 cells/construct was used. All other details required for hFOB 1.19 SSBM construct preparation, set up, maintenance and analysis are outlined in the published method (325) and within the Methods of this thesis.

2.3 Characterising hFOB 1.19 SSBMs – Biological analysis

hFOB 1.19 SSBM constructs were incubated for 4 weeks under normal growth conditions (i.e., 33.5 °C, 5% CO_2; complete media [Section 2.1]), then a further 4- or 8-weeks (i.e., 8- and 12-weeks post cell seeding, respectively) under osteogenic conditions (i.e., 37.0 °C, 5% CO_2; osteogenic media [Section 2.1]). SSBM constructs were analysed at 4-, 8- and 12-weeks post cell seeding.

2.3.1 Construct isolation

SSBM constructs were isolated from the original culture wells 3-4 days prior to the analytical timepoint. Using a disposable sterile scalpel (cat no.: 0511; supplier: Swann-Morton, Sheffield, UK), a rectangular strip of the elastomer base, in close proximity (3-5 mm) to the constructs and both their calcium phosphate (CaP) anchors, was dissected, removed and then placed into a fresh well of a 6-well plate [Figure 2.1]. 3.5 mL/well of the appropriate, naïve media was added to the isolated construct wells and incubated at the appropriate culture conditions (i.e., normal or osteogenic) up to the analytical timepoint.

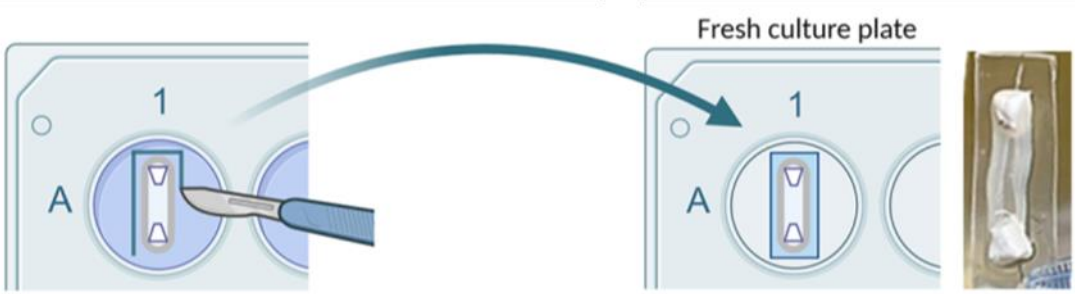


Figure 2.1 - Isolation of SSBM constructs. Prior to analysis, and during responsivity treatment regimes, SSBM constructs would be removed from their original culture plate and moved into a fresh plate. This was required to isolate the cell population within the SSBM construct from any cell populations growing on the elastomer base or in suspension. To retain the shape, and the presence of the anchors, the elastomer was dissected around the SSBM construct and the attached anchors. Figure adapted from Finlay *et al.* 2023 (325).

On the day of the timepoint, the total media volume (i.e., 3.5 mL) from the isolated constructs' wells were collected into separate aliquots and stored at -80 °C. The constructs were then processed accordingly, depending on the analytical approach.

2.3.2 Conditioned Media analysis

Prior to Enzyme-linked immunosorbent assay (ELISA) ALP analysis, collected conditioned media samples were centrifuged (20 minutes; 1000 rcf) and the resultant supernatant separated into 300 µL aliquots and stored at -80 °C until required. Estimated dilutions for media samples were also determined prior to analysis by running the assay using a single sample from each analytical timepoint/condition diluted 5-, 30- and 50-fold.

For every assay occasion, all samples, standards and blanks were ran in duplicate wells.

2.3.2.1 Osteoprotegrin (OPG) ELISA

OPG ELISA analysis was carried out using the RayBio® Human Osteoprotegerin (OPG) sandwich ELISA kit (cat no.: ELH-OPG; supplier: RayBiotech, USA) and following the instructions provided. Media samples required a 30-fold dilution prior to analysis.

2.3.2.2 Osteopontin (OPN) ELISA

OPN sandwich ELISA analysis was carried out using the RayBio® Human Osteopontin (OPN) ELISA kit (cat no.: ELH-OPN; supplier: RayBiotech) and following the instructions provided. Media samples were run neat – no prior dilution required.

2.3.2.3 Procollagen of type 1 propeptide (P1NP) ELISA

P1NP ELISA analysis was carried out using the Human P1NP Sandwich ELISA kit (cat no.: STJE0002042; supplier: St John's Laboratory, London, UK) and following the instructions provided. Prior to analysis, 3D media samples required a 10-fold dilution and 2D media samples required a 20-fold dilution.

2.3.2.4 ALP assay

Where 2D cell culture ALP activity was assessed, media was discarded, and cells washed in PBS. Cells were lysed using RIPA buffer (cat no.: R0278; supplier: Sigma) at 100 µL/well (for 48-well plates; adjusted accordingly for other well sizes) and incubated on ice for 30 minutes. A cell scraper was used to Cells were harvested using a scraper, transferred to Eppendorf tubes and centrifuged (10 minutes, 13000 rcf). Resultant cell lysis supernatants were then isolated and processed immediately or stored at -80 °C until required.

Cell lysis supernatant samples, and conditioned media [Section 2.3.2], were added neat and in triplicate to a flat-bottomed 96-well plate at 40 µL/well, followed by addition of 10 µL/well alkaline phosphatase yellow (pNPP) liquid substrate (cat no.: P7998; supplier: Sigma). The plate was wrapped in foil and incubated on an incubator shaker (SciQuip, Shropshire, UK) maintained at 37 °C for 30 minutes. Absorbance values were read immediately on a plate reader (Synergy H1 plate reader; supplier: BioTek, USA) at wavelengths of 405- and 570 nm – the latter used as a background control.

2.3.3 Live-dead imaging

Cell counts and %viability of cells within SSBM constructs was analysed using ReadyProbes™ Cell Viability Imaging Kit (Blue/Green) (cat no.: R37609; supplier:

Fisher Scientific) and the provided protocol. At any given analytical timepoint, after media was removed from the wells of isolated constructs [Section 2.3.1], 3.5 mL of fresh complete media was added, followed by the addition of 7 drops each of NucBlue® Live reagent and NucGreen® Dead reagent. Constructs were incubated for 30 minutes at 37 °C before being imaged using the EVOS™ M5000 Imaging System (Software version: C1819-225A-0151; cat no.: AMF5000; supplier: Fisher Scientific).

NucBlue® Live reagent was detected with the DAPI channel (excitation/emission maxima = 360/460 nm) and the NucGreen® Dead reagent detected with the GFP channel (excitation/emission maxima = 504/523 nm). At 10x objective, z-stacks were taken at 3 random and separate areas of the constructs near the anchors, as well as within the main body of the constructs, with a mean step size of 11.3 µm. Resultant z-stack images were projected into a single image for the DAPI and GFP channels.

Using ImageJ (National Institutes of Health, USA), the brightness and contrast of acquired DAPI and GFP projection images were adjusted, then the two images were merged to obtain a single image showing both the live and dead cells. A grid overlay was added to this live-dead image; centrally positioned with a grid area of 0.0625 mm^2. The total number of live and dead cells were manually counted in three randomly selected, non-adjacent grids, then the estimated cell density (cells/mm^3) and % viability was calculated using the mean counts of the three grids within 0.0625 mm^2 and the depth of the z-stack.

2.3.4 Gene expression analysis

2.3.4.1 RNA Extraction

Prior to beginning RNA extraction, all surfaces were cleaned with RNaseZap (cat no.: AM9780; Invitrogen, Hertford, UK). RNA extraction protocols were followed as provided by the QIAGEN Mini RNEasy kit (cat no.: 74104; supplier: QIAGEN, Germany) used, except for the following disruption and homogenisation steps which were developed and optimised specifically for the SSBM constructs.

At any given analytical timepoint, isolated constructs [Section 2.3.1] that were to undergo qPCR analysis on a later date were unhooked from their anchors and immediately stored in RNAse-free eppendorf tubes containing 600 µL RNA*later*™ Stabilization Solution (cat no.: AM7020; supplier: Fisher Scientific), at 4 °C, then moved to -80 °C after 24 hours.

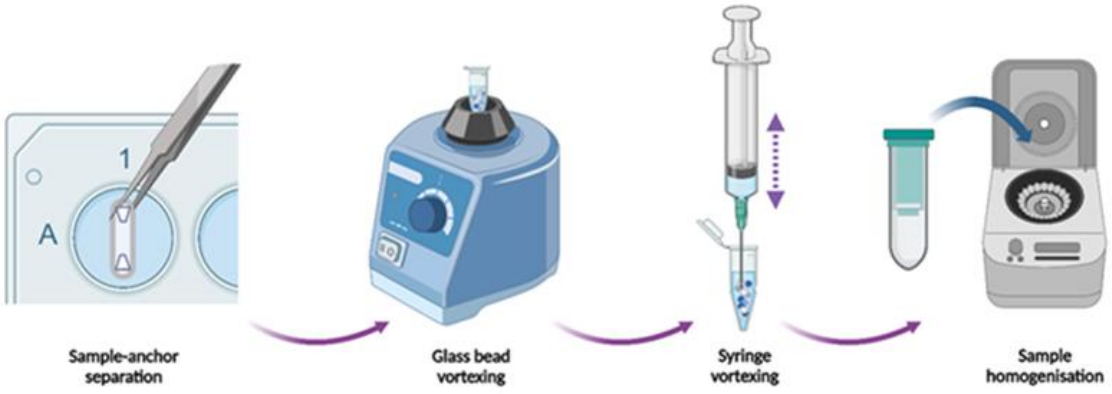


Figure 2.2 - Disruption and homogenisation of SSBM constructs for efficient RNA extraction. A process was developed specifically for SSBM constructs in order to extract a sufficient quantity of good quality RNA which was then analysed through qPCR. Samples were removed from their culture plates , followed by rigorous vortexing with glass beads and then with repeated syringe aspiration. Finally, the resultant suspension was homogenised using QIAshredder spin columns (QIAGEN). Figure adapted from Finlay *et al.* 2023 (325).

If they were to be analysed immediately, unhooked constructs were placed in 2.0 mL RNAse-free eppendorf tubes containing 10-15 3 mm diameter glass beads (cat no.:

Z143928-1EA; supplier: Sigma, USA) and 600 µL of buffer RLT containing 10% β-mercaptoethanol (v/v) (cat no.: M6250; supplier: Sigma). Each sample was vortexed (bench top vortex) for 1-2 minutes, then shredded to a fine powder in suspension by repeated aspiration, using a disposable 5.0 mL syringe (cat no.: 15295083; supplier: Fisher Scientific) along with, initially, a 16G needle (cat no.: 11532445; supplier: Fisher Scientific), followed by a 19G needle (cat no.: 15341537; supplier: Fisher scientific). These suspensions were transferred to QIAshredder spin columns (cat no.: 79654; supplier: QIAGEN) and centrifuged (2 minutes; 13000 rcf). The spin columns were removed and the collection tubes containing the sample supernatants were capped, then centrifuged further (3 minutes; 13000 rcf). Refer to [Figure 2.2] for a schematic overview of the above disruption and homogenisation steps.

The resultant supernatants from the second centrifugation step were transferred to new microcentrifuge tubes and 70% ethanol (EtOH) added at a 1:1 volume ratio, then mixed immediately by pipetting. Samples were added to RNEasy spin columns, then centrifuged (1 minute; 13000 rcf) and the resultant supernatants discarded. 350 µl Buffer RW1 was added to the RNeasy spin columns, then centrifuged (1 minute; 13000 rcf) and the resultant supernatants discarded. DNase I stock solution was prepared in advance, using the RNase-Free DNase I kit (cat no.: 79254; supplier: QIAGEN), by dissolving lyophilized DNase I in 550 µL RNAse-free water, then storing as 50 µL aliquots at -20 °C. DNAse I working solution was prepared by diluting DNAse I stock solution aliquots with Buffer RDD at a 1:7 volume ratio, respectively. Per sample, 80 µL DNase I working solution was added directly to the spin column membrane and incubated at RT for 15 minutes, followed by addition of 350 µl Buffer RW1, centrifugation (1 minute; 13000 rcf) and the resultant supernatant discarded. 500 µl

Buffer RPE was added to the spin columns, then centrifuged (1 minute; 13000 rcf) and the resultant supernatants discarded, followed by a further 500 µl Buffer RPE addition and centrifugation (2 minutes; 13000 rcf). The supernatants and collections tubes were discarded, then the spin columns were placed in new 2 mL collection tubes, centrifuged (1 minute; 13000 rcf) and again, supernatants and collection tubes discarded. Spin columns were placed in new 1.5 ml collection tubes, then 20 µL RNAse-free water added directly to the spin column membranes and left at RT for 10 minutes. Spin columns were centrifuged (1 minute; 13000 rcf) and the supernatants collected, then placed back into the spin columns, followed by centrifugation (1 minute; 13000 rcf) and the spin columns discarded. These RNA samples were stored at 2-4 °C if using the same day, and/or at -80 °C long-term.

2.3.4.2 cDNA reverse transcriptase

The RNA concentration (ng/µL) of RNA extraction samples was determined using the NanoDrop™ One Microvolume UV-Vis Spectrophotometer (cat no.: ND-ONE-W; supplier: Fisher Scientific) with the quality of the extracted RNA meeting acceptance with a 260/280 ratio of 2 ± 0.15. Furthermore, the calculated volume of RNA extraction sample containing 500 ng RNA must be <14.2 µL to meet acceptance. Samples that met both acceptable requirements were converted to cDNA using Applied Biosystems High Capacity cDNA Reverse Transcriptase kit (cat no.: 4368814; supplier: Scientific, Loughborough, UK) and following the instructions provided.

A reverse transcription master mix was prepared with RT Buffer (10x) and Random primers (10x) at 2 µL/RNA sample each, dNTPs mix (100 mM) at 0.8 µL/RNA sample and 1 µL/RNA sample Transcriptase enzyme. The calculated volume of RNA extraction sample containing 500 ng RNA was added to individual PCR tubes (cat:

I1402-6700; supplier: STARLAB, Germany), along with 5.8 µL of reverse transcription master mix, and the total reaction volume made up to 20 µL with RNAse-free water.

Samples were converted to cDNA using the Mastercycler Nexus GSX1 (cat no.: 6333000049; supplier: Eppendorf, Germany) using the following program, set up as per the guidelines provided by the Applied Biosystems High Capacity cDNA Reverse Transcriptase kit (Fisher Scientific). An initial 10 minutes incubation at 25 °C was followed by a 2 hour incubation at 37 °C and then at 85 °C for 5 minutes. Once completed, samples were held at 4 °C until collected and then were used immediately for quantitative qPCR, and/or stored at -20 °C until required.

2.3.4.3 qPCR

qPCR was carried out following the recommended protocol provided by Fisher Scientific, USA, and using Applied Biosystems TaqMan Gene Expression Assay primers (Fisher Scientific), of which are listed in [Table 2.3]. Primers and samples were kept on ice throughout the dilution and plating steps of the protocol.

Table 2.3 - TaqMan™ primers used for qPCR analysis. Gene product, function(s), and associated bone cell type information included. Primers from Fisher Scientific.

Gene (TaqMan™ primer cat no.)	**Gene product**	**Function**	**Cell type**
B2M (Hs99999907)	β2 microglobulin	Component of MHC class I and class I-like molecules	N/A (Housekeeper)
GAPDH (Hs02786624)	Glyceraldehyde 3-phosphate dehydrogenase	Part of the glycolytic chain to convert glucose to pyruvic acid	
ALPL (Hs01029144)	Alkaline phosphatase	Dephosphorylating enzyme with elevated levels indicative of high bone metabolism	Osteoblast
BMP2 (Hs00165814)	Bone morphogenetic protein 2	Growth factor required for expression of Smad	

		regulated genes that promote bone formation and maintenance	
RUNX2 (Hs00231692)	RUNX family transcription factor 2	Key transcription factor that commits preosteoblasts to the osteoblast lineage	
SP7 (Hs01866874)	Osterix	Transcription factor essential for osteoblast differentiation	
SPARC (Hs00234160)	Osteonectin	Calcium-binding protein found in osteoid, promoting mineralisation	
BGLAP (Hs01587814)	Osteocalcin	Calcium-binding protein found in osteoid, Vit K dependent production. Major non-collagenous protein (~1% of bone matrix composition)	Osteoblast-Osteocyte
COL1A1 (Hs00164004)	Type I collagen	Major structural component of bone tissue	
PHEX (Hs01011689)	Phosphate Regulating Endopeptidase X-Linked	Endopeptidase promoting bone mineralisation through OPN degradation	
SPP1 (Hs00959010)	Osteopontin (OPN)	Organic component found in bone, calcium-binding protein involved in inhibiting mineralisation	
TNFSF11 (Hs00243522)	RANK ligand (RANKL)	Ligand for RANK; promoting osteoclast proliferation and differentiation	
TNFRSF11B (Hs00900358)	Osteoprotegerin (OPG)	Decoy receptor for RANKL; inhibits osteoclast proliferation and differentiation	
DMP1 (Hs01009391)	Dentin matrix acidic phosphoprotein 1	Extracellular matrix protein critical for bone and dentin mineralisation	Osteocyte
FGF23 (Hs00221003)	Fibroblast growth factor 23	Phosphate and vitamin D metabolism regulation	
MEPE (Hs00220237)	Matrix extracellular phosphoglycoprotein	SIBLING protein involved in	

		mineralisation and phosphate homeostasis	
PDPN (Hs00366764)	Podoplanin	Mucin-type glycoprotein ubiquitously expressed in multiple tissues	
SOST (Hs00228830)	Sclerostin	Produced in response to mechanical stress. inhibiting formation and consequently promotes resorption	
SOX9 (Hs00165814)	Transcription factor SOX-9	Transcription factor essential for chondrocyte differentiation and commitment	Chondrocyte

Primers were diluted 1:10 with TaqMan Gene Expression Master Mix (cat no.: 4369016; supplier: Fisher Scientific), then cDNA samples were diluted 1:4 with RNAse-free water. Using the E1-ClipTip™ Electronic pipettor (cat no.: 4672060BT; supplier: Fisher Scientific), 2.3 µL/well of diluted cDNA samples were added to the appropriate wells of 384-Well Skirted PCR Plates (cat no.: E1042-9909; supplier: STARLAB), followed by the addition of 2.7 µL/well of diluted primer to triplicate wells of cDNA sample. Plates were sealed with adhesive PCR film seals (cat no.: 391-1254P; supplier: VWR Chemicals), centrifuged (2 minutes; 1200 rcf) and loaded into the CFX384 Touch Real-Time PCR System (cat no.: 1855484; supplier: Bio-Rad Laboratories, USA). The thermal protocol followed begins with an incubation at 50 °C for 2 minutes to activate uracil-N glycosylase, then an incubation at 95 °C for 10 minutes for polymerase activation. The protocol then enters 40 cycles of denaturing and annealing incubations (95 °C for 15 seconds and 60 °C for 1 minute, respectively).

qPCR data was analysed firstly by calculating a mean cycle threshold (CT) value from the three primer replicates for each gene of interest, providing the individual replicate values were <35 and within 1 CT of each other. 2 replicates within 1 CT were also

accepted, with the third replicate removed from calculations. ΔCT values were then calculated by subtracting the housekeeper mean CT value from that of the gene of interest. B2M was the housekeeper used for all the qPCR data provided in this thesis. Finally, ΔCT values were used to calculate $2^{-\Delta CT}$ values, which were plotted graphically.

2.3.5 Immunofluorescence (IF) analysis

2.3.5.1 Construct preparation, embedding and sectioning

The subsequent steps for IF analysis in this section were developed following the protocol outlined by Kusumbe *et al.* (399) with specifications mentioned being different from the original protocol.

At any given analytical timepoint, isolated constructs [Section 2.3.1] were fixed in 10% formalin (cat no.: 1004965000; supplier: Sigma) for 4 hours at 4 °C, on a gentle shaker plate, followed by three PBS washes, and then stored at 4 °C in PBS. Prior to embedding, constructs were unhooked from their anchors – taking care to avoid tearing and ensuring they retained their shape – and incubated in decalcification solution [Table 2.4] for 24 hours at 4 °C, followed by the same incubation conditions in a cryoprotective solution [Table 2.4].

Embedding solution [Table 2.4] was freshly prepared on every embedding occasion. Briefly, constructs were incubated in 5 mL embedding solution aliquots, that was precooled to 45 °C from 60 °C, and incubated for 90 minutes in a water bath set to 45 °C. Constructs were then incubated at room temperature in 2 mL embedding solution in Tissue-Tek Cryomold moulds (25 x 20 x 5 mm; cat no.: AGG4580; supplier: Agar Scientific, Essex, UK) for at least 30 minutes, before storing long-term at -80 °C.

Table 2.4 - Ingredient and concentration details for reagents prepared for construct embedding and sectioning. Prepared as outlined by Kusumbe *et al.*, 2015 (399).

Reagent	Ingredients (final concentration)	Catalogue number	Supplier
Decalcification solution	EDTA, pH 7.4-7.6 (0.5 M)	EDS-1KG	Sigma
	Sodium hydroxide pellets	567530-500GM	Sigma
	$d.H_2O$	NA	NA
Cryoprotective solution	Sucrose (0.58 M)	S0387-1KG	Sigma
	Polyvinylpyrrolidone (0.17 M)	P5288-500G	Sigma
	$d.H_2O$	NA	NA
Embedding solution	Sucrose (0.58 M)	S0387-1KG	Sigma
	Polyvinylpyrrolidone (0.17 M)	P5288-500G	Sigma
	Gelatin (8%)	G1890-500G	Sigma
	$d.H_2O$	NA	NA

Embedded samples were cut into 50 µm longitudinal sections using a Leica CM1950 cryostat (Leica Biosystems, Germany) (chamber temperature = -23 °C; specimen head temperature = -21 °C), with two successive sections per slide (cat: 3800200E; supplier: Leica Biosystems). After air drying, sections were stored at -20 °C.

2.3.5.2 Podoplanin (PDPN) staining and imaging

Briefly, slides were thawed and sections on the slides margined using a Super PAP liquid blocker pen (cat no.: N71310-N; supplier: Science Services Ltd., Germany). Each section was rehydrated for 10-15 minutes with 500 µL PBS, which was then removed by carefully applying paper towels in the margins. 200 µL of freshly prepared permeabilization solution [Table 2.5] was added to each section and incubated at RT for 45 minutes, which was removed, then followed by a 200 µL addition of freshly prepared blocking solution [Table 2.5] and incubated at RT for 30 minutes. After removing the blocking solution, anti-PDPN primary antibody [Table 2.5] was added to one of the sections on the slides, with PBS added to the other section, and then incubated at 4 °C overnight. Primary antibody solution and PBS was removed, followed

by three PBS washes, then addition and 2-hour incubation of secondary antibody solution [Table 2.5] to both sections on the slides.

Table 2.5 - Ingredient and concentration details for reagents prepared for sectioned construct IF staining. Prepared fresh at each staining occasion.

Reagent	Ingredients (final concentration)	Catalogue number	Supplier
Permeabilisation solution	TritonX-100 (0.03%)	X100-5ML	Sigma
	PBS (1X)	18912014	Gibco
Blocking solution	Horse serum blocking solution (5%)	NC9328247	Fisher Scientific
	PBS (1X)	18912014	Gibco
Anti-hPDPN primary antibody solution	Podoplanin (D9D7) Rabbit mAb (1:200)	9047S	Cell Signalling Technology, The Netherlands
	PBS (1X)	18912014	Gibco
Secondary antibody solution	Hoechst 3342 (1:400)	62249	Fisher Scientific
	Alexa Fluor™ 488 phalloidin (1:100)	A12379	Fisher Scientific
	Alexa Fluor™ 647 AffiniPure Donkey Anti-Rabbit IgG (1:200)	711-605-152	Jackson ImmunoResearch, USA
	PBS (1X)	18912014	Gibco

After removing the secondary antibody solution, sections were washed thrice with PBS and cover slipped (cat no.: D102460; supplier: Deltalab, Spain) using ProLong™ Diamond Antifade Mountant (cat no.: P36961; supplier: Fisher Scientific). Slides were left to dry overnight at 4 °C, then imaged, or stored at -20 °C long-term.

Images were acquired using the Zeiss LSM 880 with Airyscan Fast confocal microscope (ZEISS, Germany) and then processed using the Zen Black (version: 2.3 SP1; supplier: ZEISS) and Zen Blue (version: 3.2; supplier: ZEISS) software packages.

2.3.5.3 Whole-mount IF staining

The following protocol was developed initially for paraffin-embedded and sectioned collagen-based matrices, with volumes adjusted to accommodate the whole and intact SSBM constructs.

Briefly, SSBM constructs were prepared, decalcified and cryoprotected as described in [Section 2.3.5.1]. Constructs were incubated in 3 mL/well blocking buffer solution (1 hour; RT) [Table 2.6] then washed in PBS twice. When a primary antibody was required, primary antibody was diluted accordingly using antibody buffer solution [Table 2.6] and constructs were then incubated in primary antibody solution (2 hours; RT), followed by three washes with PBS. Secondary antibody (if required) was diluted accordingly in antibody buffer solution, along with Hoechst 3342 (cat no.: 62249; supplier: Fisher Scientific) and Alexa Fluor™ 488 phalloidin (cat no.: A12379; supplier: Fisher Scientific) at 1:400 and 1:100 dilution, respectively. Constructs were incubated in secondary antibody solution (2 hours; RT; covered) followed by three washes with PBS.

Table 2.6 - Ingredient and concentration details for reagents prepared for Whole-mount construct IF staining. Prepared fresh at each staining occasion.

Reagent	Ingredients (final concentration)	Catalogue number	Supplier
Blocking buffer solution	PBS (1X)	18912014	Gibco
	TritonX-100 (0.1%)	X100-5ML	Sigma
	BSA (30 mg/mL)	A8806-5g	Sigma
Antibody buffer solution	PBS (1X)	18912014	Gibco
	Tween 20 (0.5%)	P1379-25ML	Sigma
	BSA (30 mg/mL)	A8806-5g	Sigma

Images were acquired as previously described [Section 2.3.5.2] with the whole construct placed on a glass-bottomed imaging disk (170±5 µm thickness) (cat no.: 80137; supplier: Ibidi, Germany).

2.4 Characterising hFOB 1.19 SSBMs – Structural analysis

All isolated constructs [Section 2.3.1] to be structurally analysed were fixed in 10% formalin solution (containing 4% formaldehyde) (cat no.: HT501128; supplier: Sigma), still attached to the anchors and elastomer, immediately after removing media, then stored at 4 °C for at least 4 hours. The fixative was removed, and constructs were washed thrice with PBS before being stored in PBS at 4 °C until required for analysis.

2.4.1 Picrosirius red (PSR) staining

Fixed constructs [Section 2.4] were washed thrice in d.H_2O and then they were unhooked from their anchors. Constructs were then placed in separate wells of 12-well plates. Picrosirius red (PSR) solution was prepared by dissolving Sirius red (cat no.: 365548; supplier: Sigma) in saturated aqueous solution of picric acid (cat no.: P6744; supplier: Sigma) to a concentration of 0.18 M, then 1.5 mL PSR solution was added to each well and incubated at RT for 1 hour. Each well was washed twice with acidified water (i.e., 87 mM glacial acetic acid (cat no.: 36289; supplier: VWR Chemicals)) and stored in d.H_2O at 4 °C until required for PSR extraction.

Prior to PSR extraction, each stained construct was cut into several pieces and placed in a fresh well of a 12-well plate, then incubated in 1.5 mL/well of 0.5 M sodium hydroxide at RT on a shaker plate for 30 minutes. The resultant solution was added to a flat-bottomed 96-well plate in triplicate at 80 µL/well. Absorbance values were read

immediately on a plate reader (Synergy H1 plate reader; supplier: BioTek) at 490 nm wavelength.

2.4.2 Alizarin red (AZ) staining

Fixed constructs [Section 2.4] were washed thrice in d.H_2O and then they were unhooked from their anchors. Constructs were then placed in separate wells of 12-well plates. AZ staining and analysis was performed using the Alizarin Red S Staining Quantification Assay (cat no.: 8678; supplier: ScienCell Research Laboratories, Canada) and following the instructions provided. Volumes specified for 6-well plates were used, with any following specifications mentioned indicating a deviation from the instructions.

Briefly, constructs were stained with 40 mM AZ stain for 24 hours at RT, then the stain was removed, and constructs washed in d.H_2O. Constructs were then dissected into small (~3-5 mm long) fragments and incubated in 10% acetic acid for 2 hours. The stain was extracted by collecting the sample solutions and construct fragments into 2 mL centrifuge tubes, briefly heating at 85 °C, quickly cooling on ice, then centrifuging. The resultant supernatant was neutralised with 10% ammonium hydroxide and then diluted further with the provided standard dilution solution, if required. Samples were plated on flat-bottomed 96-well plates (cat no: 10695951; supplier: Fisher Scientific) in triplicate along with AZ standards and blank. Absorbance values were read immediately on a plate reader (Synergy H1 plate reader; supplier: BioTek) at 405 nm wavelength. AZ concentrations were determined for samples after plotting the resultant standard curve using Microsoft Excel (Microsoft Office 365), then normalised to construct mass, and graphed using GraphPad Prism.

For cell culture plates (prepared as described in [Section 2.1.4]), AZ staining and analysis was performed using the same instructions provided with Alizarin Red S Staining Quantification Assay used for the constructs. However, prior to dye extraction, culture plates were imaged using a Cytation 5 microscope (Biotek) and preloaded Gen5 software (Biotek). Multiple images taken at 4x magnification ensured imaging of the whole well, which were then stitched and forming one complete image per well. ImageJ was used to determine the proportion of well surface area stained, by adjusting the colour threshold to exclude non-stained areas of the selected region of interest.

2.4.3 X-ray fluorescence (XRF)

2.4.3.1 Freeze drying

Prior to freeze drying, constructs were snap frozen using isopentane solution (cat no.: PHR1661; supplier: Sigma). A dry ice bath with a half-submerged 100 mL glass beaker containing 50-75 mL isopentane solution was set-up in a fume cupboard. Still attached to the elastomer strip, fixed constructs [Section 2.4] were washed at least twice in d.H_2O, then placed in individual 5 mL Eppendorf tubes with the cap closed. Dry ice pellets were added to the isopentane solution until bubbling and the closed Eppendorf tubes submerged in the solution (ensuring the cap was above the solution, but above the top of the construct) for at least 5 minutes. If processing more one construct at a time, frozen construct Eppendorfs were buried in the dry ice bath until all constructs were processed. Once frozen, constructs were placed in the Lablyo mini freeze drier (Frozen in Time Ltd., York, UK) with the Eppendorf caps open and freeze dried at -52 °C under vacuum overnight.

2.4.3.2 XRF Scanning

Freeze-dried constructs attached to the elastomer strip were adhered to a plastic dish with Blu tack and placed in the M4 Tornado XRF (Bruker Nano Gmbh, Germany) under a 20 mBar vacuum. After focussing and outlining the region of interest, constructs were scanned at ~1000 spots/10 mm (spot size = 25 µm) (ensuring overlap of the spots) and 5 ms/pixel exposure time. Rhodium µ-focus X-Ray tube and a polycapillary lens used at 50 kV, 400 µA.

Image analysis of elemental maps was performed using the provided M4 Tornado XRF software. The region of interest was outlined and isolated, and the spectrum obtained and used for elemental signal analysis.

2.5 SSBM Responsivity investigations

2.5.1 Treatment formulation

Vitamin D (Vit D) (cat no.: B22524.06; supplier: Alfa Aesar, USA) was dissolved initially in EtOH (cat no.: 51976; supplier: Sigma) to make a stock concentration of 40 mM, stored at 4 °C for up to a week. Vit D stock solution was further diluted using osteogenic media [Table 2.1] to working concentrations of $1x10^{-7}$, $3x10^{-7}$, and $5x10^{-7}$ M (375). These were stored at 4 °C for up to a week.

Parathyroid Hormone Fragment 1-34 human (PTH) (cat no.: P3796-1MG; supplier: Sigma) was initially dissolved in sterile d.H_2O to make a stock concentration of 0.12 mM, which was aliquoted (50 µL) and stored at -20 °C. PTH stock was further diluted using osteogenic media [Table 2.1] to working concentrations of $1x10^{-7}$ and $1x10^{-8}$ M (375). These were stored at 4 °C for up to a week.

Betulin (cat no.: B9757; supplier: Sigma) was initially dissolved in sterile dimethylsulfoxide (DMSO) (cat no.: D8418; supplier: Sigma) to make a stock concentration of 5 mM, which was aliquoted (500 µL) and stored at 4 °C. Betulin stock was further diluted using osteogenic media [Table 2.1] to working concentrations of $5x10^{-7}$, $3x10^{-7}$, and $1x10^{-7}$ M (400). These were stored at 4 °C for up to a week.

2.5.2 Determining treatment regimes

For PTH and Betulin, two 48-well plates were seeded with hFOB 1.19 cells at 21 $x10^3$ cells/well. Cells were cultured to confluence under passive culture conditions (33.5 °C, 5% CO_2), then the media was replaced with normal osteogenic media, or osteogenic media containing PTH ($1x10^{-7}$ or $1x10^{-8}$ M) or Betulin ($5x10^{-7}$, $3x10^{-7}$, or $1x10^{-7}$ M). Plates were cultured under osteogenic conditions (37 °C, 5% CO_2) for 7- and 11-days, then their ALP activity analysed [Section 2.3.2.4]. Vit D treatment regime (i.e., $5x10^{-7}$ M, 7 days) was determined prior to this investigation through preliminary investigations using the 3D hFOB 1.19 SSBM constructs.

2.5.3 hFOB 1.19 responsivity – 2D

For each treatment, two 12-well plates were seeded with hFOB 1.19 cells at 21 $x10^3$ cells/well. Cells were cultured to confluence under passive culture conditions (33.5 °C, 5% CO_2), then the media was replaced with normal osteogenic media (3 wells/plate), osteogenic media containing the predetermined treatment concentration (i.e., Vit D = $5x10^{-7}$ M; PTH = $1x10^{-7}$ M; Betulin = $1x10^{-7}$ M) (3 wells/plate) or osteogenic media containing the relevant vehicle control (i.e., Vit D = EtOH; PTH = $d.H_2O$; Betulin = DMSO). Plates were cultured under osteogenic conditions (37 °C, 5% CO_2) for 7-days (Vit D and PTH) or 11-days (Betulin), with media and treatment renewal every 3-4

days. One plate per treatment was used for analysing cell viability with trypan blue [Section 2.1.2] and the other plate used for qPCR analysis [Section 2.3.4].

2.5.4 hFOB 1.19 responsivity – 3D

For each treatment, three 3D hFOB 1.19 SSBM plates were prepared [Appendix 8.1 and 8.2] over five separate occasions, containing six constructs each (i.e., nine plates prepared, and a total of 54 constructs). Plates were cultured under passive culture conditions (33.5 °C, 5% CO_2) for four weeks, with media renewal every 3-4 days.

After four weeks of culture, two constructs per plate were isolated - as outlined in [Section 2.3.1] – and the remaining constructs moved to osteogenic culture conditions (37 °C, 5% CO_2) with osteogenic media [Table 2.1]. This was repeated after another 4- and 8 weeks of culture under osteogenic conditions (i.e., 8- and 12-weeks post-cell seeding).

The isolated constructs were treated with the predetermined treatment concentration and duration, and cultured under osteogenic conditions (37 °C, 5% CO_2). Furthermore, 3 days prior to treatment completion, constructs were moved to a fresh well with fresh treatment media added. After completion of the treatment regime, the conditioned media was collected and stored at -80 °C, then one of the two constructs per treatment was fixed [Section 2.4], whilst the other processed for qPCR analysis.

2.6 Bioprinting

Bioprinting was carried out by Dr L. Hill (Research fellow, University of Swansea, UK) at the Healthcare Technologies Institute (University of Birmingham, UK).

2.6.1 Reagent preparation

2.6.1.1 0.6% Agarose solution

Under constant stirring on a stirring plate, Agarose (cat no.: BP1356; supplier: FisherScientific) was dissolved in d.H_2O, to a concentration of 0.6% (w/v). Once dissolved, the agarose solution was then autoclaved at 121 °C for 15 mins, then allowed to cool to room temperature, whilst under constant stirring. 0.6% Agarose solution was stored at room temperature and kept sterile.

2.6.1.2 Cell suspension

Prepared immediately before commencing bioprinting, hFOB 1.19 cells were harvested as outlined in [Section 2.1.2], however, the resultant cell pellet after centrifuging was resuspended in 20 mg/mL Fibrinogen solution (prepared as outlined in [Appendix 8.1]) to a concentration of $0.63x10^6$ cells/mL.

2.6.2 Bioprinting

Using the RegenHU BioCAD software (RegenHU, Switzerland), an autocad file was created to print a hollow cylinder into three sequential wells of a 12-well plate. Each cylinder was composed of five stacked rings (diameter = 10 mm) with a total height of 3.25 mm.

Suspended layer additive manufacturing (SLAM) solution was prepared by adding thrombin solution (prepared as outlined in [Appendix 81]) to 0.6% agarose solution at a ratio of 1.25 µL:1 mL. SLAM solution was added to the three prescheduled wells of a 12-well plate at 2 mL/well.

Fibrinogen-cell suspension was loaded into a 3 mL autoclaved syringe (cat no.: 7012074; supplier: Nordson EFD, USA) with a 21 G needle. Fibrinogen-cell

suspension was printed into the SLAM solution under an extrusion pressure of 4 kPa, extrusion thickness of 650 µm and 30 mm/s feed rate.

Bioprinting was carried out using the RegenHU Discovery 3D bioprinter (RegenHU). Printed constructs were incubated at 37 °C for 30 minutes, then the polymerised construct was removed from the SLAM solution and washed four times in PBS. Constructs were then incubated under passive conditions (33.5 °C, 5% CO_2), with media changes every 3-4 days.

2.6.3 Analysis of bioprinted constructs

Printed constructs were prepared and stained for IF analysis (nuclei and actin stains only) [Section 2.3.5] after 2 weeks of culture.

Chapter 3

Creating humanised self-structuring bone models

3.1 Introduction

3.1.1 Arguments for creating a humanised in vitro bone model

The original protocol for creating self-structuring bone models (SSBM)(395,398) was developed and optimised using primary femoral periosteal cells isolated from Wistar rats. However, with the intention to use this model in bone research and as a potential drug-testing platform, the use of rat cells would be inadvisable, for reasons which will now be discussed.

Rodent models have desirable properties as bone research platforms. For example, rat Mesenchymal stem cells (MSC), which give rise to the skeletal stem cell population (401), have significantly higher rates of proliferation and differentiation in comparison to human MSCs (402), whilst also possessing a genetic expression profile with a high degree of similarity to that of human MSCs (403). These data indicate that using rat MSCs provides a cell source that has similar markers of metabolic activity to humans, that can produce results at a faster rate, and therefore be relied upon as analytical readouts.

However, there are considerable interspecies differences that will impact the reliability of using rodent models. These include the genetic instability of rodent MSCs(404), and, in spite of a similar genetic expression profile to humans, it has been demonstrated previously - both *in vivo* (405) and *in vitro* (406) - that significant differences in metabolic responses between human and rodent cells occur when exposed to the same conditions. Interspecies differences increase the risk of obtaining false positive data and reducing the chance of achieving reliable and robust clinical translation (407). Furthermore, the principles of the 3Rs - to reduce, replace and refine the use of laboratory animals - warrants the development and optimisation of novel research

strategies and approaches with as little inclusion of animals and animal-derived products as possible.

Following the original protocol (398), isolation and culture of primary cells from rat femoral periosteum is subject to higher risk of failure as it heavily relies upon the experience of the operator to cleanly and efficiently excise the tissue required. Also, it incurs higher running costs and greater animal use, as obtaining primary cells requires multiple rats on each occasion (estimated 2-3 rats per SSBM 6-well plate) and as such is accompanied by husbandry costs and the requirement for adequate facilities to house rats, which is not possible or readily available to some research institutes.

With the lack of translation between different species, and the 3Rs movement at the forefront of this project, the first objective was to identify a suitable human osteoblastic cell source to replace the need for primary rat cells.

3.1.2 Identification of an appropriate human cell line

Osteosarcomas cell lines and primary cells are commonly used in *in vitro* culture systems due to their immortality (408) and close recapitulation to the *in vivo* cell (409), respectively. However, osteosarcoma cell lines present abnormal genotypes, karyotypes and phenotypes, making their proliferation rates and differentiation potential unpredictable (410), nor are they a true representation of healthy cells found *in vivo* (411). Primary cells on the other hand have a slower and variable proliferative rate, due to the varied heterogeneity between cell isolations, plus a further disadvantage that they are not as readily available, particularly in the case of healthy human tissue.

Using The Cellosaurus (412), a free online resource for knowledge on cell lines (with the exception plant cell lines), a search was conducted in October 2019 to seek a cell line that fits the criteria of "*Human*", "*Osteoblast*", and "*Non-cancerous*". Two cell lines fitting the required criteria resulted from the search; the human foetal osteoblast (hFOB) cell line, hFOB 1.19 (375) and Osteoblastic Precursor Cell line 1 (OPC1) (413). Both cell lines have desirable properties that make them suitable for creating human-derived SSBM constructs. OPC1 demonstrated detectable levels of alkaline phosphatase (ALP) activity over multiple passages (>30), with up regulation of osteoblastic and matrix gene expression - osteonectin (ON) (*SPARC*), osteopontin (OPN) (*SPP1*) and procollagen type 1 (*COL1A1*) – as well as evidence of osteoid production, when cultured with osteogenic supplementation (413). Similar findings were found with the hFOB 1.19 cell line, with increased production of ON, bone sialoprotein (BSP) and type 1 collagen at the protein level, in addition to mineral nodule formation once post-confluent (375). Out of these two cell lines, the hFOB 1.19 cell line was explored further as the OPC1 cell line was not available to purchase at the time, although both cell lines would have been investigated if it was possible.

3.1.2.1 Human foetal osteoblast (hFOB) 1.19 cell line

The hFOB 1.19 cell line is derived from primary cultures transfected with a mutant SV40 large T antigen gene which encodes for the temperature-sensitive tsA58 protein. SV40 is a DNA tumour virus found to inactivate retinoblastoma proteins which is associated with subsequent tumour development by encouraging S-phase entry in G1-arrested cells (414,415). The effect of the tsA58 protein is seen when the cells are cultured at temperatures below 39 °C; optimally at 33.5 °C. At these lower culture temperatures, the tsA58 protein inhibits retinoblastoma protein; the main regulator of

the cell cycle by supressing cell cycle G1/S transition under normal conditions (416). Therefore, when inhibited, cells are free to continually proliferate, effectively immortalising the hFOB 1.19 cell cells by preventing their differentiation to mature, non-proliferative osteoblasts. However, inhibition of the retinoblastoma protein can be reversed at incubation temperatures above 33.5 °C; proliferation rate is reduced and the cells begin to differentiate into a more mature osteoblast phenotype, then the inhibitory action of the tsA58 protein is completely ceased at an incubation temperature of 39 °C (410,417). As such, the hFOB 1.19 cell line is described as being a conditionally immortalised cell line.

Transfection of the SV40 large T antigen gene caused minimal chromosomal alterations, whilst retaining the vital osteoblast characteristics, such as the ability to produce bone-like tissue *in vivo* when seeded in Matrigel, and an extracellular matrix (ECM) when cultured *in vitro* that was ultrastructurally similar to the matrix produced by primary osteoblasts (410). As a result of the hFOB 1.19 cell line's osteogenic potential and stable karyotype, they have been used in bone and dental research in 2D culture systems (417,418) and more recently in 3D culture systems (419–421). The hFOB 1.19 cell line is therefore considered as a non-transformed cell line; even over multiple passages the karyotype stability and characteristics attained from SV40 large T antigen gene transfection are maintained (410).

To summarise, the use of the hFOB 1.19 cell line as an appropriate replacement of primary rat cells to create a humanised SSBM culture was justified due to meeting the following criteria and possessing the following features:

- **Is of human origin:** Successful adaption of the SSBM culture system to accommodate the hFOB 1.19 cell line would make it more clinically relevant and translatable, as well as replace the need for primary rat cells – compliance with the 3Rs movement.
- **Is a secondary cell line:** Provides a homogenous culture, unlike primary cells where the cell types present will vary between batches and risks producing large variations in data. Furthermore, secondary cell lines are universally more readily available than primary tissues, thus a successful hFOB 1.19 SSBM culture system would be accessible to other laboratories.
- **Possess a stable karyotype:** Fewer karyotype alterations after transfection (i.e., a partial additional chromosome 16), which is not unlike primary cells (410), thus have closer representation of primary cells, unlike osteosarcoma cell lines (e.g., MG63, SaOS-2) which have multiple, complex and dynamic alterations in their karyotype. This hFOB 1.19 karyotype is stable and maintained over multiple passages, thus less risk of erroneous data arising between different SSBM constructs that have been created with hFOB 1.19 cells using different passages.
- **Produce ECM components with ultrastructure similarity to those produced by primary cells:** Primary osteoblast cell phenotype is retained and thus the hFOB 1.19 cell line is a close recapitulation of the *in vivo* cell.
- **Successfully cultured in 3D previously:** Rejection and failure to adapt to the SSBM culture system is less likely to occur since the hFOB 1.19 cell line has successfully adapted to different 3D culture systems in the past, both *in vivo* (410) and *in vitro* (419–421).

- **Possess ability to differentiate:** Unlike commonly used cell lines for osteocyte research (e.g. MLO-Y4) which are unable to differentiate beyond certain stages of maturation (297), hFOB 1.19 are able to differentiate into other MSC-derived cell types (e.g. chondrocytes) (422), early-, mid- and late-stage osteoblast maturity, as well as evidence of osteocytogenesis (423). Thus, hFOB 1.19 cells have the capability to differentiate into cells that create bone-like tissue as well as become embedded osteocytes.

3.1.3 Chapter aims

The aims of this chapter were to establish optimal hFOB 1.19 cell proliferation and differentiation conditions in 2D, followed by SSBM method adaption to accommodate the human cell line, based on the findings from the 2D culture investigations. The final aim was to evaluate the success of creating SSBM constructs using hFOB 1.19 cells by comparing and identifying the structural and compositional changes with those discovered during development of the original method (398). This was achieved using similar analytical methods as those used previously by Iordachescu *et al.* (395) - such as x-ray fluorescence (XRF) and scanning electron microscopy (SEM) - as well as using adjusted analytical methods currently used in standard 2D cell and bone tissue culture research (e.g., Picosirius red (PSR) and Alizarin red (AZ) staining).

3.2 SSBM method repeatability

Prior to adapting and creating hFOB 1.19 SSBM cultures, it was also beneficial to attempt to follow the published SSBM protocol (398) precisely (i.e., using the same reagents, quantities, culture conditions and cell source) to ensure the culture method is repeatable given that, at the time of the beginning of this project (October 2019), Iordachescu *et al*. (395) was the only publicised occasion in which the protocol was

successfully created. By successfully repeating the method, during which the same changes and events outlined by Iordachescu *et al*. (395) were observed, a better insight into understanding the purpose and aim of each step was gained, thus enabling appropriate adaptions for creating hFOB 1.19 SSBM constructs to be made. Only once the rat SSBM method was successfully repeated, understood and simplified, was its adaptability tested.

Repeating the SSBM method (398) was achieved by first grouping and organising the steps into the five main aspects now shown in Finlay *et al*. (325) [Appendix 8.1], then estimating the preparation durations and shelf-life timings to improve the time and cost efficiency of the method. Then, all reagents and components were acquired, including a primary rat cell source – whole male Sprague-Dawley rat legs (x12 legs in total) received from Prof. Lisa Hill (School of Biomedical Sciences, University of Birmingham). All preparation steps were carried out whilst culturing the primary rat periosteal cells to confluence, at which point the rat SSBM constructs were created. The original method (398) did not specify a seeding density (i.e., cells/well), therefore, based on the information provided, SSBM constructs were set up using three seeding densities; $0.25x10^6$, $0.50x10^6$, and $0.75x10^6$ cells/well [Figure 3.1] (n=8/seeding density).

All three seeding densities tested showed contraction of the fibrin matrix - gathering and folding at the edges, drawing inwards and around the CaP anchors [Figure 3.1 A.i] - after 1-day post-cell seeding, with a defined construct arising within 5-days post-cell seeding. This aligns with the initial macroscopic changes observed by Iordachescu *et al*. (395). However, there was no obvious difference between the seeding densities observed at the macroscopic level. On the other hand, looking at the gathering edges

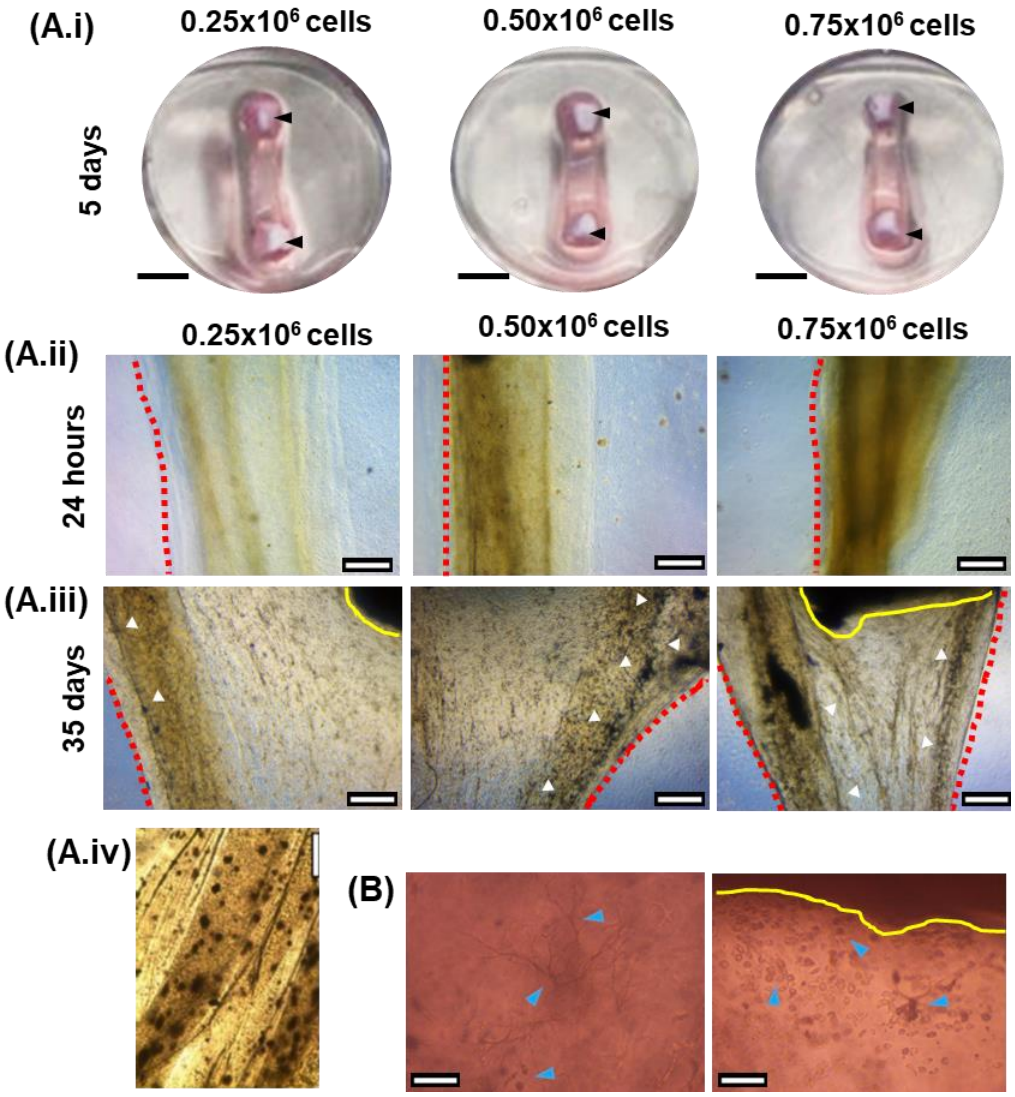


Figure 3.1 - Assessing repeatability of the SSBM method using cells isolated from rat femoral periosteum. (A) SSBM constructs were created following the original protocol using three cell seeding densities, with observable contraction at both the macroscopic **(i)** (scale bar = 7.5 mm) and microscopic **(ii)** (scale bar = 125 μm) level less than one week after seeding, as well as the establishment of black mineral nodules **(iii)** (white arrows) similar to those seen previously **(iv)** (figure taken from Iordachescu *et al.* 2018 (395) after a longer culture period. **(B)** Appearance of dendritic branching - similar to that of osteocytic protrusions or a vascular network - as well as cuboidal bodies (blue arrows) in rat SSBM cultures at 48 days post-cell seeding was indicative of the presence of a mixed cell population that was either a result of differentiation or during cell harvesting (Scale bar = 500 μm). Key: Black arrows = CaP anchors; Red dotted lines = SSBM outer edge; Yellow lines = CaP anchor edge.

of the fibrin matrix at the microscopic level [Figure 3.1 A.ii – the area immediately right of the red dotted line], there is an increase in matrix density as the seeding density increases. After a longer period of culture [Figure 3.1 A.iii], the fibrin matrix showed

continued inward contraction, which was greater with increasing seeding densities, as displayed with both outer edges of the construct capable of fitting within the same-sized frame. Furthermore, the presence of mineral nodules, reminiscent of those observed previously (395) [Figure 3.1 A.iv] developed over the culture period with markedly increased presence and size with increasing seeding densities.

Further culture of the rat SSBM constructs lead to newly arising and changing cellular features [Figure 3.1 B], observed after 48-days post-cell seeding. Clusters of densely coloured and cuboidal-shaped cells, as well as cells with dendritic projections with branching were seen emerging using brightfield microscopy, particularly within close proximity to the CaP anchors.

Having made the same observations along a similar time scale to those made previously (395), it was concluded that the method was indeed repeatable and testing its adaptability proceeded.

3.3 Characterising hFOB 1.19 growth in 2D

Prior to introducing hFOB 1.19 cells to a 3D culture system, it was essential to gain an insight into the culture conditions that can affect the cells ability to proliferate and differentiate, and, importantly, their osteogenic potential, whilst cultured under 2D conditions. This knowledge was beneficial in making the appropriate adaptions to the original SSBM method (398) to accommodate the cell line, as well as make considered decisions and assumptions when troubleshooting any technical issues that arose or justifying deviations in the data during their analysis. All of which went towards achieving optimal SSBM culture preparation and maintenance using hFOB 1.19. To attain this understanding of hFOB 1.19 cells, firstly, their proliferation rate was

assessed under permissive conditions (i.e., 33.5 °C, 5% CO_2) by determining their normal growth curves.

During this project, three separate batches of hFOB 1.19 cells were used, named according to the year in which they were obtained; the first (Batch 2019) was a single passage 9 vial gifted by Professor James Edwards, NDORMS Laboratory (University of Oxford, UK), and the remaining (i.e., Batches 2021 and 2022) were single vials purchased from ATCC (USA). Growth curves in complete media were set up [Section 2.1.3] for each batch once they reached passage 14.

Live cell count results between the three batches [Figure 3.2 i-iii] showed no difference in live cell counts after 2-days of culture. At 4-days of culture, Batch 2021 displayed a significantly greater mean live cell count ($1.41\pm0.18x10^6$ cells/well) than Batch 2019 ($0.75\pm0.21x10^6$ cells/well; p=0.004), as well as 2022 ($0.91\pm0.07x10^6$ cells/well; p=0.0145). After 6-days of culture, Batch 2022 and Batch 2021 had similar mean live cell counts ($2.27x10^6$ vs $2.91x10^6$ cells/well; p=0.316), whereas Batch 2019 on the other hand had a statistically smaller live cell count ($0.74\pm0.07x10^6$ cells/well) than Batch 2021 (p=0.046) and Batch 2022 (p=0.005). Live cell count results for each individual batch [Figure 3.2 iv-vi], showed a significant increase in live cell number between 2- and 4-days of culture (Batch 2019, -2021, -2022, respectively: $3.0x10^5$ vs $7.5x10^5$; p=0.05; $5.9x10^5$ vs $14.1x10^5$; p=0.006; $2.5x10^5$ vs $9.1x10^5$; p=0.005). However, Batch 2022 was the only batch to show a statistically significant increase in live cell count between 4- and 6-days of culture ($0.91x10^6$ vs $2.27x10^6$ cells/well; p=0.003).

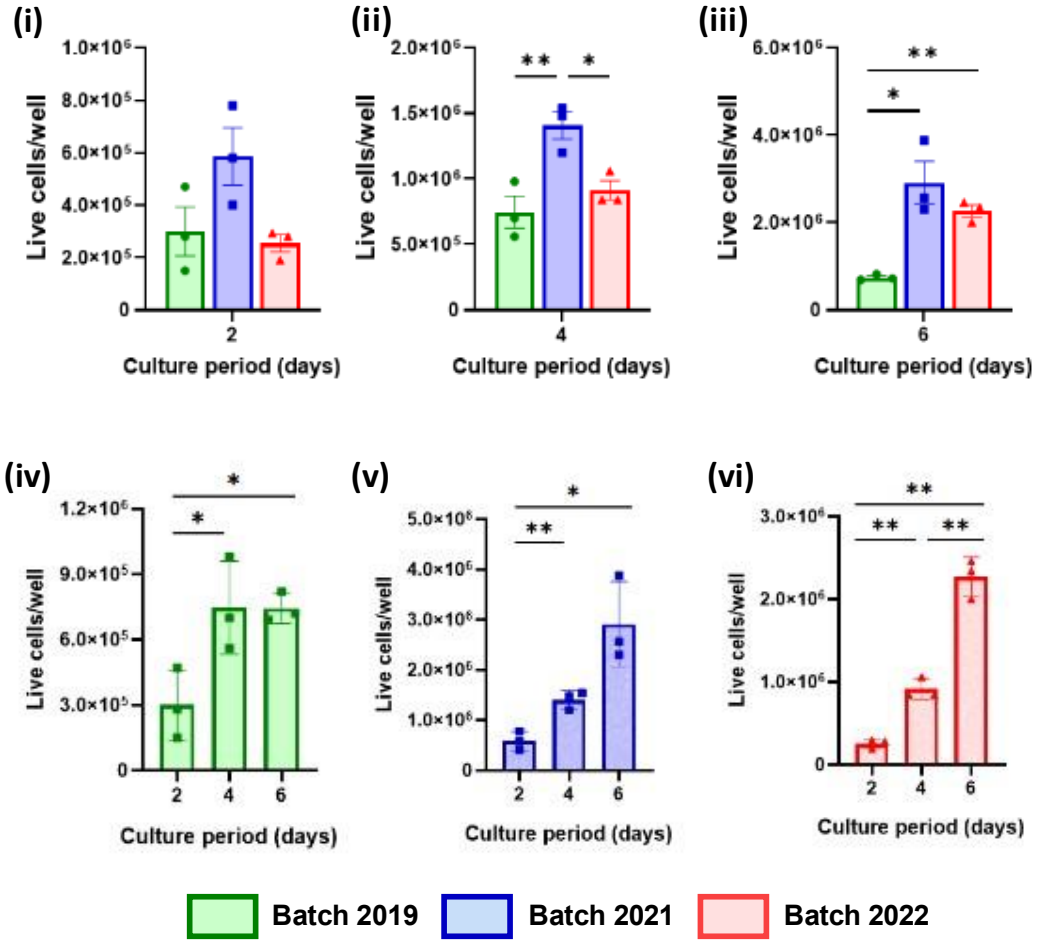


Figure 3.2 - Significant differences in growth rate exists between different batches of hFOB 1.19 cells at a similar passage number when cultured in 2D. Using trypan blue viability testing, resultant 6-day growth curves were obtained and analysed between each of the three batches of hFOB 1.19 cells received during this project **(i-iii)**, as well as assessed individually **(iv-vi)**. Data plotted as Mean±SD (n=3), then analysed with ordinary one-way ANOVA and Fisher least significant difference (LSD) test, or Brown-Forsythe and Welch ANOVA, based on SD ratio between batches. Multiple comparison outcome shown. * = $p<0.05$; ** = $p<0.01$, ns = not significant.

The % viability results from the same growth curves performed [Figure 3.3 i-iii] reveals that there was no significant changes within or between the three batches after 2- and 4-days of culture. However, after 6-days of culture, Batch 2022 had a significantly higher mean % viability (97.8±1%) than Batch 2019 (91.8%; p=0.002) and 2021 (92.4%; p=0.004). Yet, when comparing the baches individually [Figure 3.3 iv-vi], their mean % viability remained relatively unchanged across the whole duration of the

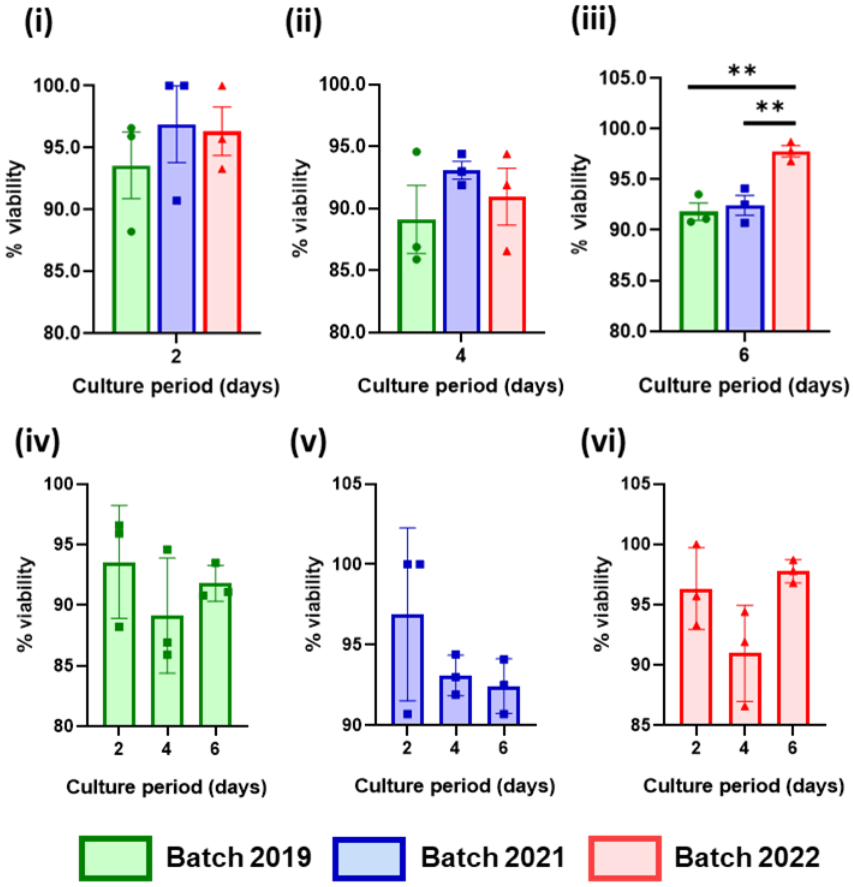


Figure 3.3 - During short-term 2D culture (>1 week), % viability of hFOB 1.19 was relatively maintained throughout the culture duration. Whilst obtaining growth curves for the three hFOB 1.19 batches used during this project, % viability was also assessed between **(i-iii)** and within individual the batches **(iv-vi)**. Data shown plotted as Mean±SD (n=3) then analysed with an ordinary one-way ANOVA and Fisher LSD, or Brown-Forsythe and Welch ANOVA, based on SD ratio between batches. ** = $p<0.01$. Absence of statistical result on the graph indicates no significant difference.

growth curve assessment (Batch 2019 = 91.5±3.9%; 2021 = 94.14±3.6%; 2022 = 95.02±4.1%).

After establishing typical growth patterns of hFOB 1.19 batches under permissive proliferation conditions, the next step was to establish an osteogenic medium that will maintain adequate cell proliferation and viability over a prolonged period of culture, as well as induce notable osteogenic activity at 33.5 °C, 5% CO_2. Osteogenic media that were used and reported previously (375,424–426) – and whose information can be

found in [Table 2.2] were tested on hFOB 1.19 cells acquired from Batch 2019 and Batch 2021. To evaluate proliferation and viability of hFOB 1.19 cultured in these potential osteogenic media, long-term growth curves as described in [Sections 2.1.4] were set up.

Live cell count and viability results showed no difference between the different media after 1-week of culture [Figure 3.4 A.i & B.i]. However, after a 2-week culture period, Medium 3 had a significantly lower live cell count ($0.19\pm0.05x10^6$ cells/well) than Medium 2 ($0.46\pm0.09x10^6$ cells/well) and 4 ($0.44\pm0.1x10^6$ cells/well) [Figure 3.4 A.ii], as well as a significantly lower viability than Medium 2 (62.5% vs 50.63%; p=0.045) [Figure 3.4 B.ii]. For each individual media, when comparing the differences in live cell count [Figure 3.4 C.i-iv] and viability [Figure 3.4 D.i-ii] between 1- and 2-weeks of culture, Medium 2 was the only medium that showed continued proliferation ($0.21x10^6$ vs $0.46x10^6$ cells/well; p=0.022) [Figure 3.4 C.i], however all media maintained their % viability [Figure 3.4 D.i-iv].

Next, to investigate the osteoinductive potential of Media 1, 2 and 4, the ALP activity of hFOB 1.19 cells and the presence of mineral after 1- and 2-weeks of culture was assessed following the steps outlined in [Sections 2.3.2.4 and 2.4.2], respectively.

Absorbance values obtained from the ALP activity assay were normalised to $/10^6$ cells using the corresponding mean live cell counts plotted in [Figure 3.4] (cells cultured on the same plate for both analyses). There was no significant difference in normalised ALP activity between Media 1, 2 and 4 after 1- and 2-weeks of culture (respectively, 1-week: 1.21 vs 1.05 vs 1.06; p=0.68. 2-weeks: 0.87 vs 0.47 vs 0.55; p=0.35) [Figure 3.5

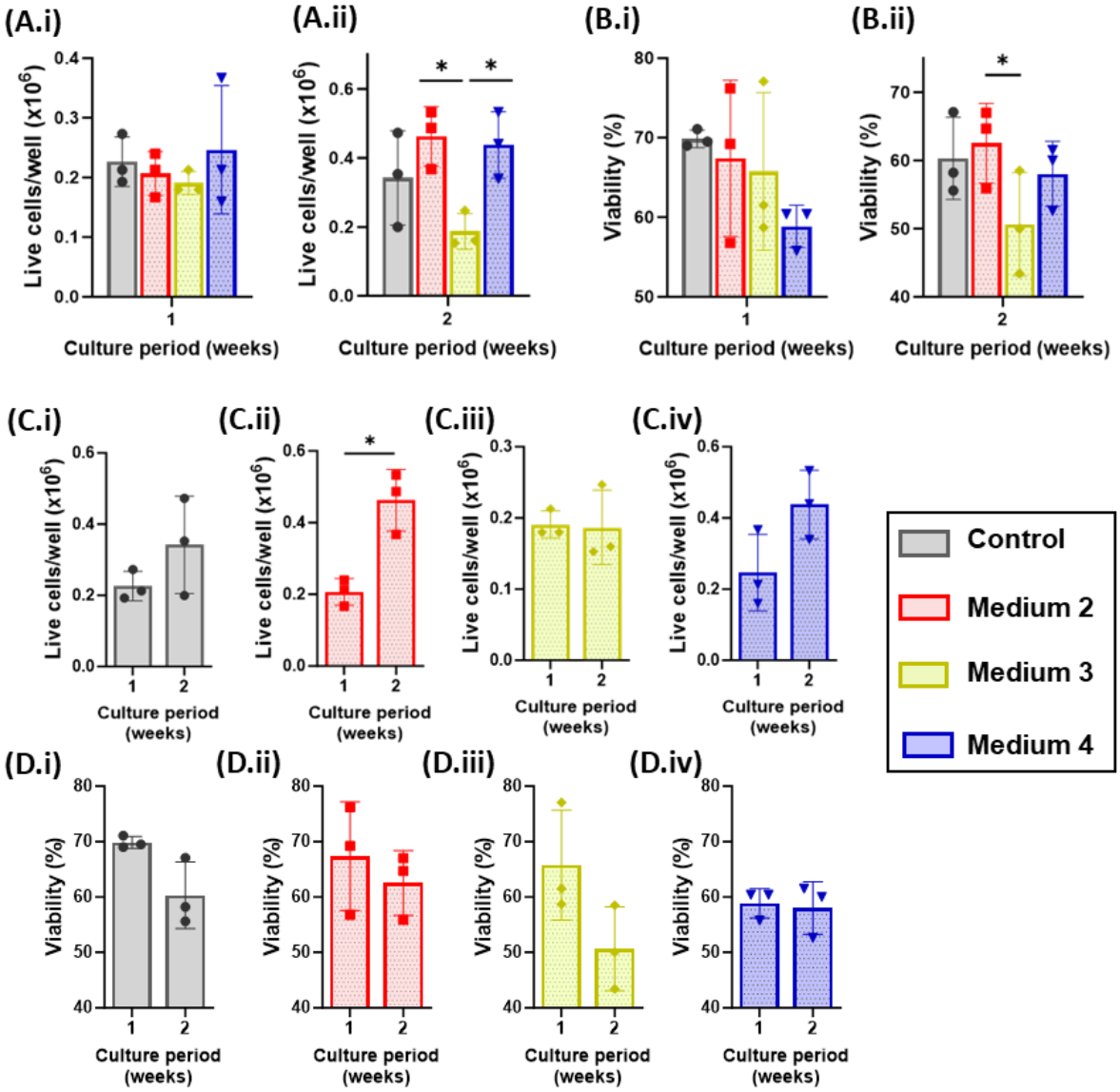


Figure 3.4 - Assessing hFOB 1.19 cell proliferation and viability when cultured with different osteogenic media in 2D. Proliferation **(A)** and viability **(B)** of hFOB 1.19 cells cultured with four potential osteogenic media was assessed over the period of 1- and 2-weeks under 2D permissive culture conditions (i.e. 33.5 °C, 5% CO_2). Data shown is Mean±SD (n=3) then analysed with an ordinary one-way ANOVA and Fisher LSD, or Brown-Forsythe and Welch ANOVA, based on SD ratios. Multiple comparison outcomes shown. Proliferation **(C)** and viability **(D)** was also assessed over time for each media, individually. Media information can be found in [Table 2.2]. Data shown is Mean±SD (n=3) then analysed with unpaired t test (with or without Welch correction, depending on SD ratio). * = $p<0.05$. Absence of statistical result on the graph indicates no significant difference.

A]. Comparison of the medias individually over time [Figure 3.5 B] showed Medium 2 had a significant decrease in normalised ALP activity from 1-week to 2-weeks (1.05 vs

0.47; p=0.022), whilst normalised ALP activity was maintained in Media 1 (1.21 vs 0.87; p=0.27) and 4 (1.06 vs 0.55; p=0.15).

Results from AZ staining [Figure 3.5 C] showed the presence of mineral in all steogenic media tested after 2-weeks of culture, as all wells visibly show red AZ staining. However, Medium 2 showed the greatest well area stained (25.2±3.3%) which was

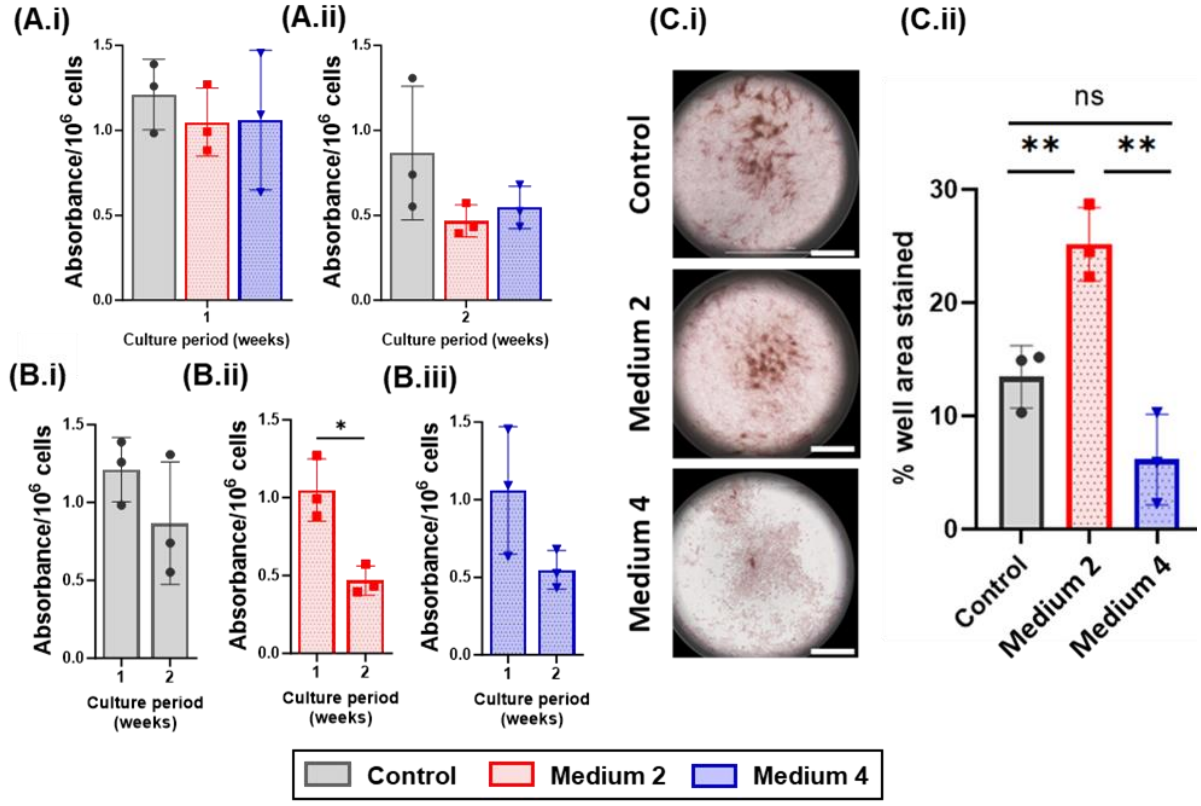


Figure 3.5 - Investigating osteogenic activity of hFOB 1.19 cells when cultured in 2D with different osteogenic media. ALP activity of hFOB 1.19 cells were determined and normalised, then assessed between the different media after 1- **(A.i)** and 2-weeks of culture **(A.ii)**. Normalised ALP activity was also assessed over time for each medium individually **(B.i-iii).** Images of AZ-stained culture wells where hFOB 1.19 cells were cultured with potential osteogenic medias under permissive conditions (33.5 °C) for 2-weeks **(C.i)**. Scale bar = 5 mm. Images were used to quantify the total surface area of the wells stained to indicate the amount of mineral present in the culture **(C.ii)**. Data shown Mean±SD (n=3) then analysed with Brown-Forsythe and Welch ANOVA **(A)** and unpaired t test (with or without Welch correction, depending on SD ratio) **(B.i-iii & C.ii)**. * = p <0.05; ** = p<0.01, ns = no significance. Absence of statistical result on the graph indicates no significant difference.

also significantly greater than Media 1 (13.5±2.7%; p=0.0095) and 4 (6.2±4.0%; p=0.0036) [Figure 3.5 C.ii].

The final step in characterising expected hFOB 1.19 cell growth in 2D, was to culture them at a higher temperature of 37 °C in the chosen osteogenic medium, Medium 2 (Table 2.2), which was selected based on the previous findings [Figures 3.4-3.5]. As previously discussed [Section 3.1.3], hFOB 1.19 cells cultured at temperatures closer to 39 °C renders the tsA58 protein (responsible for immortalising the cell line) inactive and as a result reduces proliferation and encourages differentiation (375). hFOB 1.19 cells were prepared as outlined in [Section 2.1.3] to obtain a growth curve.

Results from the growth curve showed no significant change in live cell number between any of the timepoints across the duration of the 4-day culture period (1-, 2-, 3-, 4-days, respectively: 0.98±0.42 vs 1.29±0.55 vs 0.95±0.26 vs 1.02±0.40; p=0.49) [Figure 3.6 i]. Furthermore, % viability showed no significant change between the beginning (i.e., 1-day) and the end (i.e., 4-days) of the culture period (74.1% vs 73.5%; p=0.93), although there was a slight decrease observed between 2-days and 3-days (78.3 vs 71.8; p=0.02) [Figure 3.6 ii].

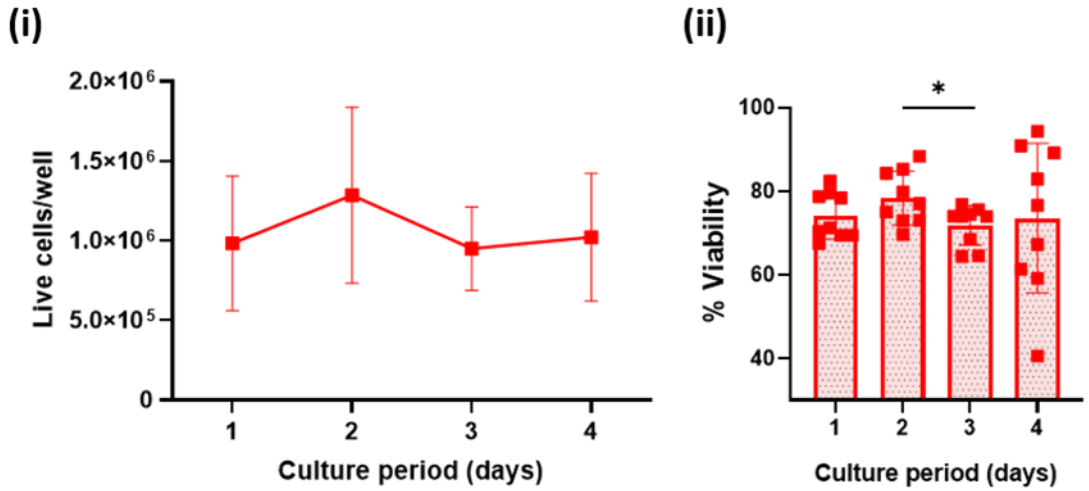


Figure 3.6 - Investigating hFOB 1.19 proliferation and viability in 2D when cultured at 37 °C with the selected osteogenic medium. Using trypan blue viability staining, hFOB 1.19 proliferation **(i)** and % viability **(ii)** was evaluated over a 4-day culture period when cultured in Medium 2 [Table 2.2]. Data shown are Mean±SD (n=9) and each time point analysed with an ordinary one-way ANOVA and Fisher LSD, or Brown-Forsythe and Welch ANOVA, based on SD ratios. Multiple comparison outcomes shown. * = $p<0.05$. Assume no significance in the absence of statistical result.

3.4 SSBM method adaptability to hFOB 1.19 cells

In order to accommodate the hFOB 1.19 cell line, the immediate adaptions included substituting the rat complete medium - used for preparing thrombin solution and maintaining the cultures – with hFOB 1.19 complete media [Table 2.2] as well as the culture conditions, to 33.5 °C instead of 37 °C. Cells were seeded initially at $0.50x10^6$ cells/well and cultured under hFOB 1.19 permissive conditions for 4-weeks.

On comparison to the initial contraction of the fibrin matrix seen previously [Figure 3.7 i], hFOB 1.19 cultures did show contraction, although at a slower rate; with minimal contraction occurring within 2-days of culture (vs 1-day) and achieving a defined construct between 2-3-weeks post-cell seeding (vs 1-week) [Figure 3.7 ii]. After 4-

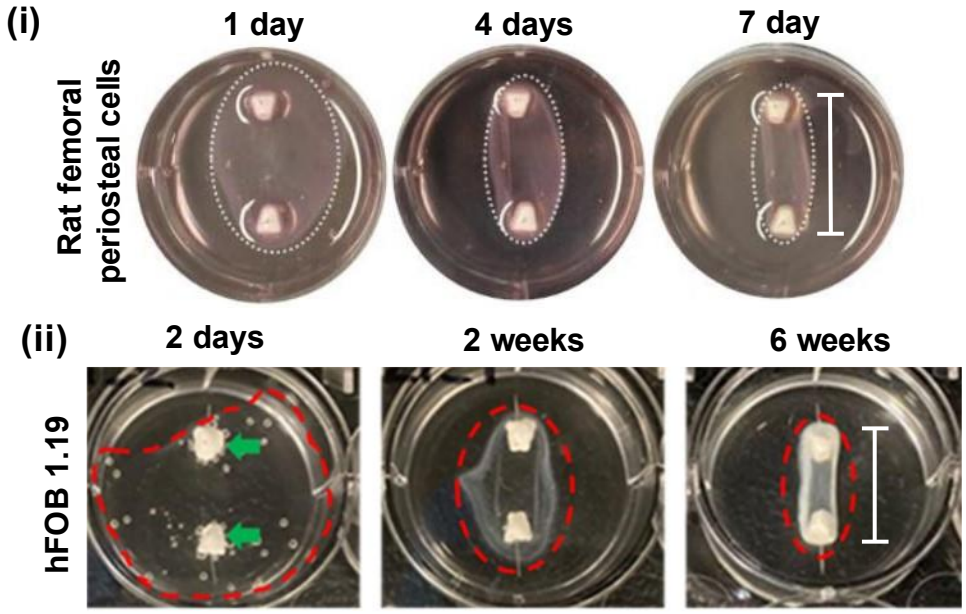


Figure 3.7 - Fibrin rearrangement occurs upon cell seeding. Progressive contraction of the fibrin matrix around the CaP anchors occurs upon seeding with primary rat cells **(i)** (taken from Iordachescu *et al.* 2018 (395)), as shown by the white dotted outline, and also occurs with hFOB 1.19 seeding **(ii)** (adapted from Finlay *et al*. 2023 (325)) as shown by the red dotted outline. Scale bars = 15 mm.

weeks post-cell seeding, osteogenic conditions were introduced (i.e., 37 °C; osteogenic media [Table 2.1]).

Beyond this point, contraction of the fibrin matrix ceased and became more opaque in appearance with continued osteogenic culture [Figure 3.7 ii].

Having made very few adaptions to accommodate the hFOB 1.19 cell line, the adapted method was repeated using three different seeding densities (i.e.,$0.25x10^6$, $0.50x10^6$, $0.75x10^6$ cells/well) to determine an optimal and suitable cell seeding density to successfully create hFOB 1.19 SSBM constructs, repeatedly. Like the rat SSBM constructs prepared [Figure 3.1 A.i], all three seeding densities tested successfully caused matrix contraction [Figure 3.8 i]. However, no visible structural differences at the macroscopic level were observed between the seeding densities of the hFOB 1.19 constructs up to the time of introducing osteogenic culture conditions. Although, at the

microscopic level [Figure 3.8 ii], it was observed that greater cell clustering occurred with larger seeding densities, which continued to develop with all seeding densities whilst cultured under permissive conditions, as shown by the growing cloudy appearance after 23-days post-cell seeding [Figure 3.8 iii]. At this same time point, black mineral nodules, like those seen previously [Figure 3.1 A.iii-iv] were visible between all three seeding densities, with $0.25x10^6$ and $0.50x10^6$ cells/well having nodules of a similar size and number, whereas those within $0.75x10^6$ cells/well were notably smaller.

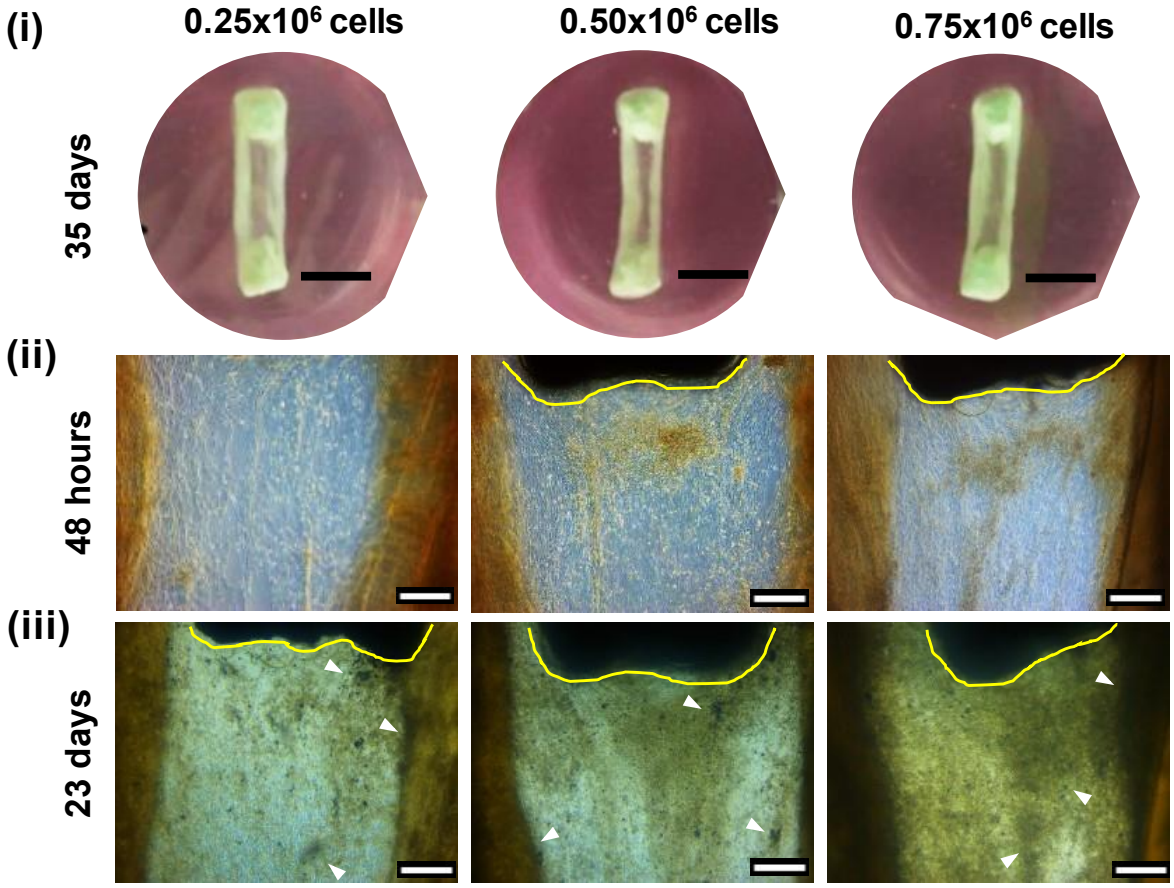


Figure 3.8 - Initial observations upon adapting the SSBM method to accommodate hFOB 1.19 cells. SSBM constructs were created after making adaptations to the original protocol (398) the same three cell seeding densities as previously, with similar observable results at both the macroscopic **(i)** (scale bar = 5 mm) and microscopic **(ii)** (scale bar = 500 µm) level after seeding, as well as the development of black mineral nodules and patches **(iii)** (white arrows) after a longer culture period. Key: Red arrows = cell clustering. Yellow lines = CaP anchor edge.

3.5 SSBM compositional and structural analysis

Iordachescu *et al.* (395) reported a detailed evaluation of the compositional and structural changes and milestones rat SSBM constructs occurring with prolonged culture (up to 1 year). It was decided early in this project that a culture period of up to 3-months as a more favourable time scale for those interested in utilising the model, as well as from a manufacturing point of view. Therefore, compositional and structural analysis of the hFOB 1.19 SSBM constructs was carried out at three analytical timepoints; 4-, 8- and 12-weeks post cell seeding (to clarify, these timepoints included an initial 4-week culture period at permissive conditions, with the remaining time being under osteogenic culture conditions; therefore, these time points signify 0-, 4- and 8-weeks of culture under osteogenic conditions, respectively). Previous findings (395,398) were used as a reference for the expected pattern of events, which primarily focussed on a rise in collagen production, as well as and mineral development and distribution.

To evaluate collagen content over time, hFOB 1.19 SSBM constructs were stained with PSR as outlined in [Section 2.4.1] after 4-, 8- or 12-weeks of culture. Successful staining was attained for all constructs treated with PSR, as seen by the white/clear to red colour change [Figure 3.9 A], although more mature constructs (i.e., some of those at 8- and 12-weeks of culture) displayed inconsistent staining, with yellow/white patches appearing after PSR incubation [Figure 3.9 B]. PSR was then eluted from the stained constructs following the steps outlined in [Section 2.4.1] to quantify the amount of stain and subsequently used as an indicator of the amount of collagen present [Figure 3.9 C]. Mean absorbance results (i.e., the quantity of dye present) showed a steady increase over time, with statistical significance present between each timepoint

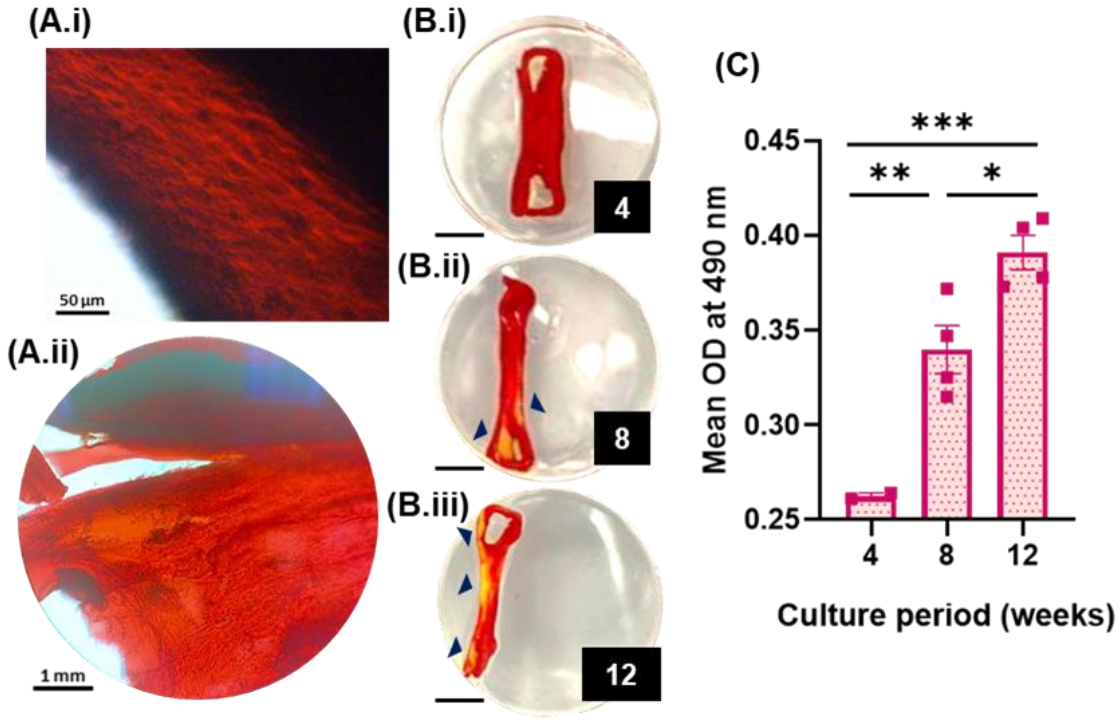


Figure 3.9 - Analysing collagen content of hFOB 1.19 SSBM constructs, after a culture period of 4-, 8-, and 12-weeks post cell seeding, through whole mount staining with Picrosirius red (PSR). Red colouration shows successful staining of collagen present within SSBM constructs (**Ai-ii**; scale bar = 50 um and 1 mm, respectively). **(B.i-iii)** Visible PSR staining is affected (black arrows) with constructs cultured for a longer period of time. Scale bars = 5 mm. **(C)** Resultant absorption at 490 nm of eluted PSR from stained constructs can be used to quantitively assess their collagen content. Data shown is Mean±SEM (n=2 at 4-weeks; =4 at 8- and 12-weeks) then analysed with Brown-Forsythe and Welch ANOVA. * = $p<0.05$; ** = $p<0.01$; *** = $p<0.001$.

(i.e., 4-weeks (0.26±0.002) vs 8-weeks (0.34±0.025) p=0.0083; 8-weeks vs 12-weeks (0.39±0.018) p=0.0192; 4-weeks vs 12-weeks p=0.0006).

Next, the mineralisation process as well as mineral content and properties of the SSBM cultures were evaluated. As noted previously, small mineral nodules were appearing during the first 4-weeks of culture under permissive conditions at all seeding densities. From 4-weeks of culture onwards under osteogenic conditions, mineral appeared as dense patches throughout the length of the folded matrix edges, as well as within the less fold inner area of the SSBM constructs. Darkening of these patches was visibly

seen using standard light microscopy from 4-, to 8-, to 12-weeks of culture [Figure 3.10 A.i-iii].To quantify the mineral within SSBM constructs, the AZ staining protocol [Section 2.4.2] was adapted to enable whole mount staining of constructs, then quantify the

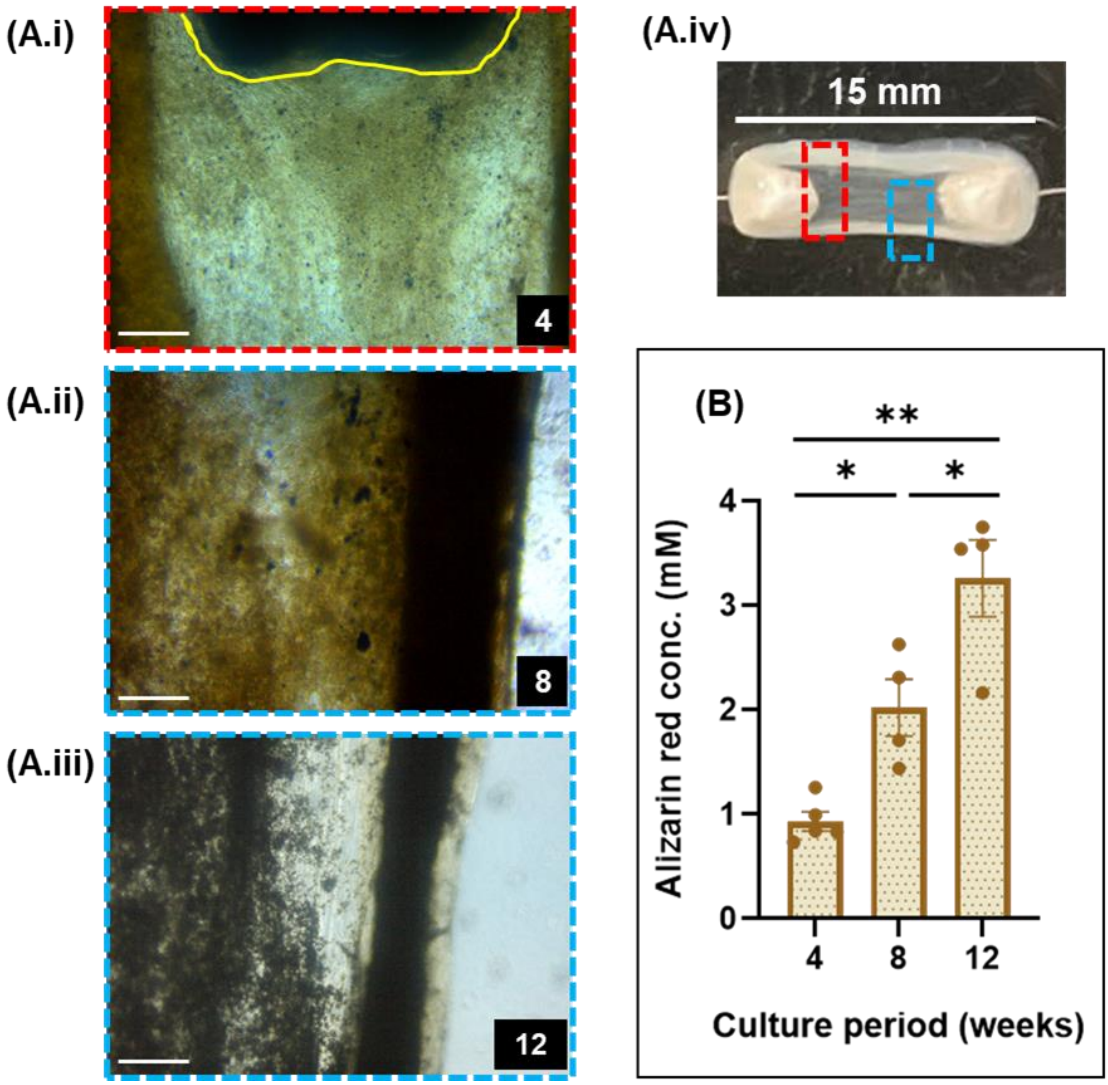


Figure 3.10 - Mineral content visibly and quantifiably increases within hFOB 1.19 SSBM constructs when cultured up to at least 12-weeks. (A) Images are of a single hFOB 1.19 SSBM construct, taken using a standard light microscope, after a culture period of 4-weeks **(i)**, 8- **(ii)** and 12-weeks **(iii)** post-cell seeding. They reveal the development of maturing mineral over time, seen as progressively darkening and dense nodules and patches. Scale bars = 250µm **(i)** and 500 µm **(ii-iii)**. **(A.iv)** represents areas of SSBM construct pertaining to images **(i-iii)**. **(B)** Whole mount AZ staining of hFOB 1.19 SSBM constructs and subsequent dye extraction enabled quantification of mineral present at analytical periods of 4-, 8- and 12-weeks post-cell seeding. Data shown as Mean±SEM (n= 5 (4-weeks) and 4 (8- and 12-weeks)) then analysed with Brown-Forsythe and Welch ANOVA. * = $p<0.05$; ** = $p<0.01$.

concentration of AZ stain retained as a measure of the amount of mineral present. There was a direct relationship between mean AZ concentration retained and the culture period duration [Figure 3.10 B], with a marked significant increase between the first and last analytical time points (i.e., 4-weeks vs 12-weeks: 0.93 vs 3.26 mM: p=0.0061) and significant increases between each subsequent time point (i.e., 4-weeks vs 8-weeks: 0.93 vs 2.00 mM; p=0.022. 8-weeks vs 12-weeks: 2.00 vs 3.26 mM; p=0.038)

In addition to quantifying mineral deposition within the SSBM constructs, x-ray fluorescence (XRF) was used to observe the mineralisation process in terms of distribution and timescale, as well as investigating the mineral composition, at the elemental level. The resultant XRF elemental maps from SSBM constructs scanned after 4-, 8- or 12-weeks of culture [Figure 3.11] visibly showed no or very little presence of calcium after 4- and 8-weeks of culture, with the exception of the CaP anchor, yet obviously present and prolific across the SSBM construct area after 12-weeks of culture. Phosphorous was visibly present across all three time points, across the entire surface area of the SSBM constructs. An overlay of the calcium and phosphorous elemental maps resulted in a yellow colouration where the presence of the two elements co-localise, as exemplified by the CaP anchors. Due to the low presence of calcium at 4- and 8-weeks, co-localisation was not visibly obvious, but where it was visible, appeared as small nodules (as indicated by the white arrows). In SSBM constructs cultured for 12-weeks, co-localisation was visible as a collection of nodules as well as covering large areas - particularly along the outer edges of the construct – and furthermore, there were areas of calcium and phosphorous alone present.

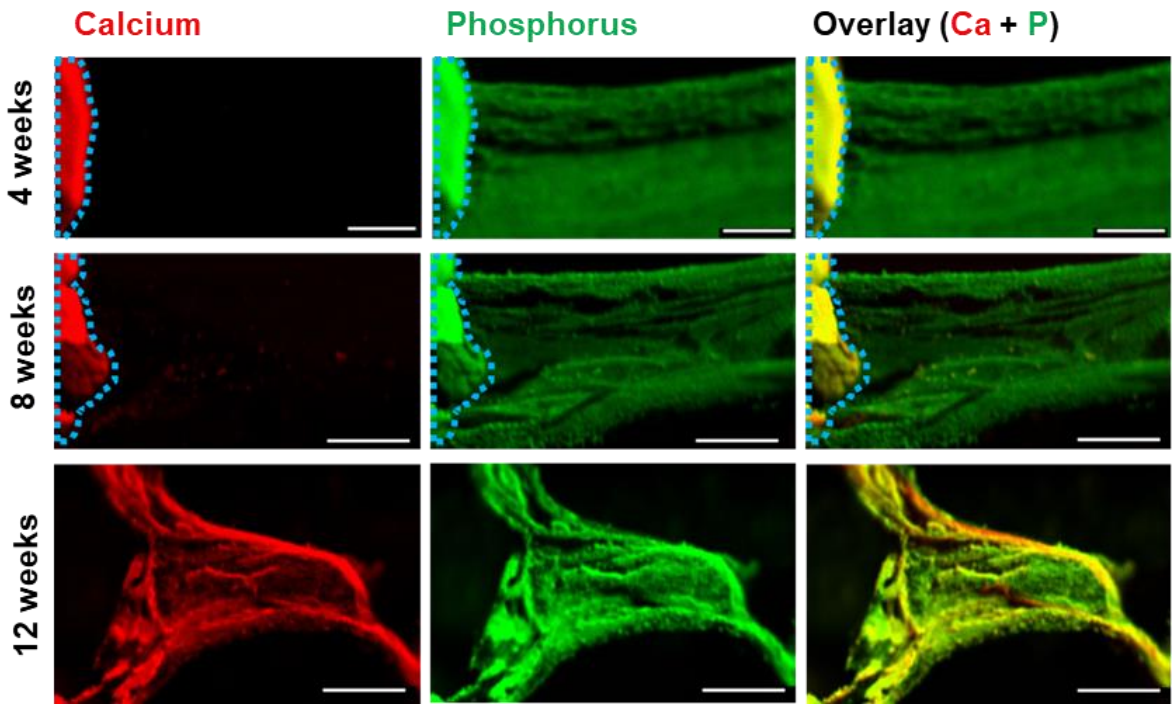


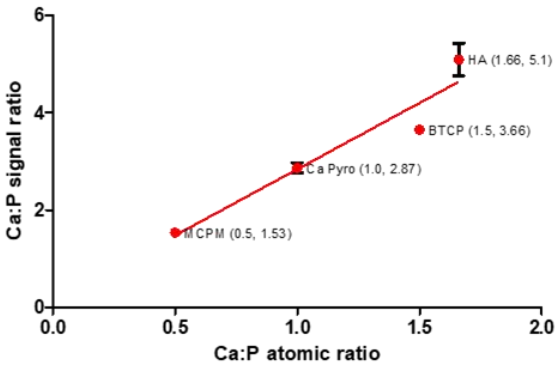
Figure 3.11 - Heterogeneously-distributed mineral, containing calcium and phosphorous, develops on hFOB 1.19 SSBM constructs over time. Using x-ray fluorescence (XRF), the presence of calcium and phosphorous atoms on freeze-dried constructs can be detected and located to create elemental maps. Maps on the left column indicates calcium in red, and the central column shows phosphorous in green. The right column overlays these separate elemental maps to reveal co-localisation of calcium and phosphorous in yellow (as a result of mixing the two primary colours), with the presence of a β-TCP anchor (area within blue dotted rings at 4 and 8 weeks) as a control. White arrows = colocalised nodules difficult to see on page. Scale bars = 1 mm (4wks), 2mm (8 &12 wks).

Previous work carried out by A. McGuinness (PhD, unpublished) [Figure 3.12 A] showed the CaP mineral within XRF scanned samples can be determined based on the ratio between the resultant calcium and phosphorous signal counts. From this, spectral analysis of the isolated SSBM matrices [Figure 3.12 B] was used to determine the mean Ca:P signal ratio and used against the standard curve provided by McGuinness (PhD, unpublished).

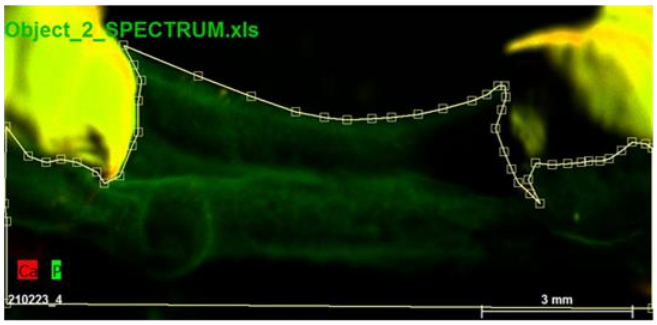
(A)

CaP Mineral	Ca:P atomic ratio	Ca:P signal ratio
Monocalcium phosphate monohydrate (MCPM)	0.50	1.53
Calcium pyrophosphate (Ca Pyro)	1.00	2.87
B-tricalcium phosphate (BTCP)	1.50	3.66
Hydroxyapatite (HA)	1.66	5.10

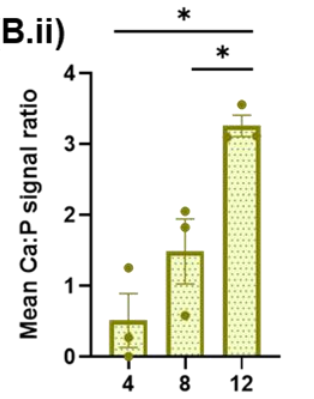
McGuinness, unpublished



(B.i)



(B.ii)



(B.iii)

Culture period (weeks)	Mean Ca:P signal ratio	Ca:P Mineral
4	0.514	na
8	1.489	MCPM
12	3.26	BTCP

Figure 3.12 – Analysis of mineral maturation over time in hFOB 1.19 SSBM constructs using Ca:P signal ratios obtained from XRF. Previous work carried out by McGuinness (unpublished, PhD work) **(A)** showed that CaP minerals of increasing maturity (i.e. increasing Ca:P atomic ratio) present in bone have increasing Ca:P signal ratios and can be used as a standard curve. **(B)** Regions of interest were drawn out on resultant XRF elemental maps of hFOB 1.19 SSBM construct scans (as demonstrated in **(i)**) to isolate the calcium and phosphorous signals from the matrix only and determine their Ca:P signal ratio. Determined for hFOB 1.19 constructs after 4-, 8- and 12-weeks post-cell seeding (**ii**; data shown is Mean±SD (n=3 at every time point) and analysed using Brown-Forsythe and Welch ANOVA. * = $p<0.05$), then compared against the standard curve to determine likely mineral present **(iii)**.

The mean Ca:P signal ratio of hFOB 1.19 SSBM constructs showed a significant increase from 4- to 12-weeks of culture (0.51 vs 3.26; $p=0.0103$) [Figure 3.12 B.ii]. A

significant increase in mean Ca:P signal ratiobetween each subsequent week was not found between 4- and 8- weeks (0.51 vs 1.49; p=0.18), although was present between 8- and 12-weeks (1.49 vs 3.26: p=0.049). Using the calibration curve and the mean values found for each time point [Figure 3.12 B.iii], hFOB SSBM constructs cultured after 4-weeks had a mean outside of the curve range, whereas 8- and 12-weeks showed means ranging in close proximity to monocalcium phosphate monohydrate (MCPM) and β-tricalcium phosphate (β-TCP), respectively.

3.6 Discussion

3.6.1 hFOB 1.19 growth patterns in 2D showed significant batch-batch variation

Growth curves provide useful information on cell proliferation as a means to monitor cell health, to be used as guides for expected growth characteristics under normal conditions, and as experimental read outs under varying conditions. Cell population growth can be affected by a number of factors, so natural variation exists, including between batches of the same cell line (427,428), thus growth curve analysis was carried out for all three batches of hFOB 1.19 cells obtained during the course of this project. Previous evidence has shown that proliferation of the hFOB 1.19 cell line was unaffected when cultured either under 2D or 3D conditions (429), therefore performing growth curve analysis of this cell line under 2D conditions provided a simpler and inexpensive means of analysis whilst strongly inferring expected proliferation patterns whilst cultured under 3D conditions.

Growth curves were performed at the same passage number (i.e., passage 14), which was selected as it was the lowest passage number that Batch 2019 could achieve an adequate number of cells for setting up a growth curve, as well as a median passage number within the designated “working” range (i.e., passages 8-20). Although hFOB

1.19 is an immortalised cell line, it is universally known that all cell lines, whether primary or secondary, are not infinitely robust. As passage numbers become too high, selective pressures will cause cell health to decline and/or elicit morphological and genetic changes (430–432). This will ultimately affect cell behaviour and thus produce erroneous experimental outcomes and data (433,434).

Despite the standardisation of passage number, variation still existed between the three batches. Batch 2019 showed the most notable difference in growth curve size and shape [Figure 3.2], to an extent greater than that expected from natural variations in culture conditions, such as imprecise seeding numbers, media renewal volumes, cell dissociation and harvesting. The main difference between the batches of cells was the source in which they were purchased; Batch 2019 was obtained from a collaborator, unlike Batch 2021 and -2022 which were purchased through ATCC.

Purchasing cells directly from a reputable source, such as ATCC, provides quality assurance that validates the identity of the cell line received, whereas cells from colleagues and other research facilities runs the risk of receiving the incorrect cell line, misnumbered passages and cross-contamination with other cell lines (435–438) as well as the risk of mycoplasma contamination (although this was screened and monitored as described in [Section 2.1.2.4]). It has been insisted that regular screening through gene profiling approaches, such as comparative genomic hybridisation and short tandem repeat polymorphism profiling, be introduced to revaluate and ensure authenticity of a working cell line (436,438–440) as is now routinely employed for murine strains. These data demonstrate the importance of performing in-depth assessment of proliferation, viability and osteogenic activity for all cell lines prior to their inclusion in the SSBM. These additional cell line assessments will be beneficial

for further optimisation work for creating SSBM construct platforms and the subsequent experimental data, as well as meeting regulations during assay development.

Results from the Batch 2019 growth curves also provided may be enough justification for the omission of outlying data points that arose during the analyses in this project, providing they were from cells of Batch 2019. However, the complete omission of all the data obtained from Batch 2019 cannot be justified as despite a lack of proliferation, the osteogenic potential of this batch may still be equal to, or greater than, Batch 2021 and 2022. Batch assessment of osteogenic potential was not performed, due to the interruptions by COVID 19.

hFOB 1.19 have demonstrated previously proliferation is inhibited upon cell-cell contact (410). Whilst results suggest Batch 2021 reached this point (i.e., no significant changes in live cell count at 6-days of culture), the live cell count value was significantly greater than that of Batch 2019, which also showed no significant change at 6-days of culture. This shows that the arrest in proliferation of Batch 2019 is not through cell-cell contact, as Batch 2021 had a greater population on the same surface area size. Instead, this indicates there was a possible issue with Batch 2019, or with this particular growth curve occasion.

3.6.2 Selecting the most appropriate hFOB 1.19 osteogenic media

There are a set of compounds that can be added to osteoblastic cell media which are known to induce their differentiation and osteogenic activity; these are dexamethasone, ascorbic acid and β-glycerophophate. Park (441) investigated osteoblastic cell proliferation, differentiation and osteogenic activity when cultured under different combinations of these three osteogenic compounds. They found that

ascorbic acid displayed no negative/inhibitory actions in terms of proliferation and viability, differentiation or osteogenic activity, either alone or in combination with either dexamethasone and/or β-glycerophophate. However, it was found that dexamethasone and β-glycerophophate negatively impacted on the cell cultures in all parameters measured when cultured alone. The authors concluded that the inclusion of ascorbic acid is beneficial for osteogenic media recipes, but care must be taken when using dexamethasone and/or β-glycerophophate - particularly dexamethasone which shows benefits for mineralisation in the short-term, but displays inhibitory effects long-term.

Amongst studies using hFOB 1.19, there is no generally accepted differentiation media recipe. Taking the findings by Park (441), into account, it was decided that the inclusion of ascorbic acid was essential, and dexamethasone excluded due to its long-term inhibitory effects on mineralisation - not a desirable effect in a long-term culture system. One compound that was ubiquitously used across hFOB 1.19 differentiation media (375,424–426) was menadione (i.e., Vitamin K_3), a precursor that is converted to menaquinone (i.e., Vitamin K_2) which promotes differentiation (442,443) and has beneficial effects on bone mineral density (444). Furthermore, low serum concentrations have been found to be preferential for osteocyte culture (371) and was also used by the authors that created the hFOB 1.19 cell line (375). With this information, three recipes were created for the differentiation investigations and tested alongside hFOB 1.19 complete media (i.e., Medium 1) as another potential differentiation media.

Medium 2 showed the most potential, primarily due to the significantly greater amount of mineral coverage after 2-weeks of culture [Figure 3.5], in comparison to Medium 1

and 4. Although there was a reduction in ALP activity after 2-weeks of culture, this was likely to be a result from the limitations of long-term 2D culture (i.e., reduced matrix production and greater mineralisation activity). The marked proliferation [Figure 3.4] and mineralisation [Figure 3.4] after 2-weeks, in comparison to Media 1 and 4, suggests greater metabolic activity, thus reaching peak activity and plateau phase sooner, at which point in 2D, cell activity and integrity will begin to decline.

The intention with long-term culture of the 3D system was to have an initial proliferation period followed by an osteogenic period. As previously shown (375,410), hFOB 1.19 show minimal osteogenic potential at 33.5 °C and require to be cultured at temperatures closer to 39 °C. For ease of use, and thus adding to the appeal of using this culture system by other users, culture conditions of 37 °C in osteogenic media was decided on. However, hFOB 1.19 proliferation ceases at temperatures over 33.5 °C because the inhibitory effect of tsA58 protein that is responsible for immortalising the hFOB 1.19 cells is removed (375). Therefore, hFOB 1.19 cells were cultured under osteogenic conditions in 2D to determine whether proliferation continues at 37 °C and ensure cultures remained viable. The results showed that these osteogenic conditions ceased the proliferation of hFOB 1.19 proliferation 1-day post-cell seeding and their viability over the total culture duration remained stable [Figure 3.6]. In the case of the 3D culture system, no to little proliferation is preferred, which will be discussed in [Section 3.6.3].

3.6.3 The SSBM method is repeatable and shows adaptability

The original method published by Iordachescu *et al*. (398) was replicated to fully understand the methodology and its reproducibility. This method was repeated on three separate occasions – using 6 rats in total – and a total of 12x 6-well plates prepared.

Although a seeding density was provided (i.e., $0.1x10^6$ cells/mL), the precise volume of cell suspension required per cell was not disclosed in the original method. According to ThermoFisher Scientific, for a typical 6-well plate, a seeding density of $0.3x10^6$ cells/well and a total working volume of 3mL is recommended (445). However, with the inclusion of a hydrogel, the total surface area increases and requires more cells to achieve a similar seeding density as per the recommendation. Therefore, three seeding densities were chosen; one similar to the recommended seeding density (i.e.,, $0.25x10^6$ cells/well), and two higher seeding densities ($0.50x10^6$ and $0.75x10^6$ cells/well).

Iordachesu *et al.* (395,398) noted that high seeding densities prevented the hydrogels being digested too quickly, despite the presence of antifibrinolytics. Although all three seeding densities used here successfully created SSBM constructs, there was evidence of extensive contraction of the matrix occurring in $0.75x10^6$ SSBM constructs after 35 days [Figure 3.1 A.iii].

After 48-days of culture, rat SSBM cultures contained cells close to the CaP anchors which displayed a range of different morphologies: cuboidal-shaped bodies (typical of mature, osteoid-producing osteoblasts) and others with branched, dendritic projections, observed using brightfield microscopy [Figure 3.1 B]. This was not a surprising observation as primary cultures display heterogeneity amongst the cell culture population (446), furthermore, the periosteum is a rich source of cells with multilineage capacity – they hold the ability to differentiate into osteoblasts, chondrocytes and adipocytes (447,448). However, the emergence of dendrites is the most distinguishing morphological change that occurs during osteocytogenesis, of which an average of 88 projections can be found on a single osteocyte – based on

calculations by Buenzli and Sims (80). Additional analyses of rat SSBM constructs containing dendritic cells – such as qPCR, western blotting and flow cytometry - would be necessary to establish whether these are osteocytic.

The use of primary cells in this culture system does not mean it cannot be a useful research platform, however, the lack of homogeneity makes it less desirable as an assay platform. Although, removing this heterogeneity and replacing it with a homogenous cell line ran the risk of failure to develop a mature SSBM construct as there is evidence of multicellular cooperation *in vivo* during fracture repair and bone formation (449). However, this was not to be the case as hFOB 1.19 SSBM constructs achieved the same developmental milestones as the rat SSBM constructs (i.e., fibrin reorganisation, collagen and mineral production), although, these important stages were achieved at later time points in the hFOB 1.19 SSBM constructs. For example, contraction of the fibrin matrix to produce a defined structure occurred 5-days post-cell seeding with the rat cultures but took more than 2-weeks post-cell seeding for the hFOB 1.19 cultures. Again, this was expected given the higher metabolic rate of rat cells compared to human cells (450,451).

The same seeding densities used for the rat constructs were used for establishing the hFOB 1.19 SSBM constructs and, again, all seeding densities succeeded in making SSBM constructs [Figure 3.8]. Unlike the rat cultures, over-contraction of the fibrin matrix didn't occur with any of the seeding densities, which coincides with the slower proliferation rates of human cells. However, mineral development in the $0.75x10^6$ cells/well constructs appeared as smaller nodules in comparison to $0.25x10^6$ and $0.50x10^6$ cells/well constructs, which were comparatively similar in size. The higher seeding density may result in greater cell death, or contact inhibition, which has been

found in 2D previously for hFOB 1.19 (410). A seeding density of $0.25x10^6$ cells/well was chosen due to comparatively similar observations with $0.50x10^6$ cells/well and furthermore, using fewer cells, enables more constructs to be prepared from each passage.

3.6.4 Collagen content of hFOB SSBM constructs increased through long-term culture

One of the first events in bone formation is the production of collagen-rich osteoid by osteoblasts. Iordachescu *et al.* (395) showed that the SSBM culture system supported rat periosteal cells to produce a collagen-containing matrix during prolonged culture whilst under normal and osteogenic conditions through a number of analytical techniques, including Raman spectroscopy, second harmonic imaging and PSR staining.

PSR is a polyazo dye, originally used as a textile dye, but is now a commonly used histological stain in research relating to connective tissue and extracellular matrices, as well as bone and musculoskeletal research, as it stains collagen within tissue samples when dissolved in saturated aqueous picric acid (452). Qualitative and quantitative assessment of collagen through PSR staining of collagen is achieved by using cross-polarised light, which forces alignment of the PSR elongated azo chain in parallel to that of the collagen fibres it has attached to, resulting in enhancing the natural birefringement of collagen (453). Although more commonly used on paraffin-embedded tissue sections, it was previously used by Iordachescu (395) to visualise collagen within whole, intact rat SSBM construct matrices, and was present just 1-week post cell seeding, however quantification was not performed.

As mentioned above, collagen content can be quantified using cross-polarised light, however access to a microscope with this capability was not possible. Although, PSR dye can be quantified by elution with 0.5 M sodium hydroxide (454–457). The results of this analysis [Figure 3.9 C] suggests that collagen content within hFOB 1.19 SSBM constructs is present from at least 4-weeks post-cell seeding and increases throughout long-term culture up to 12-weeks. This was despite the presence of unstained areas on more mature constructs [Figure 3.9 B], which may be explained by the rising presence of mineral that was either interfering with dye attachment or visualisation of attached dye. Further evidence indicating that patchy staining was caused by mineral can be seen in the regions that were adjacent to the anchors, where a slight excess of CaP remained after unhooking constructs.

3.6.5 Mineralisation of hFOB 1.19 SSBM constructs occurs and matures with long-term culture

Following the deposition of osteoid, it is then mineralised. Again, Iordachescu *et al*. (395) utilised an assortment of analytical approaches – from histochemical analysis to x-ray-based approaches - to show that the rat SSBM culture system also supported this process (with mineralisation continually progressing from 10-days of culture onwards) and furthermore confirmed that the mineralisation of the collagen fibres was reminiscent to that of *in vivo* bone. Assessment of mineralisation in hFOB 1.19 SSBM constructs over the 12-week culture period was achieved using AZ staining and XRF - also used by Iordachescu *et al*. (395).

Imaging mineral would not be straightforward, and furthermore, there was no certainty that the stain would have been completely absorbed and/or penetrated through the constructs. Both were due to the 3D nature of the SSBM constructs, where the

thickness of the matrix and density of the mineral limits penetration of light from standard brightfield microscopes, as well as dyes which must rely on passive absorption in the lack of a vascular network. Normally, these difficulties can be overcome by histological preparation of the tissues - fixing and embedding the tissue, followed by sectioning on to slides for staining. However, in the case of bone, preparation of undecalcified bone requires specialised equipment to reduce the risk of shattering (458,459). Also, during sectioning, sample architecture and sample block residue can become displaced, resulting in non-specific staining and erroneous data (460). AZ staining, whilst able to be quantified through image analysis, can provide quantitative analysis of mineralisation through its extraction. Additionally, to aid complete absorption/penetration, SSBM constructs were cut into smaller pieces and incubated in AZ stain overnight instead of 30 minutes. The results [Figure 3.10 B] show that the mean concentration of AZ stain extracted from hFOB 1.19 SSBM constructs increased with each subsequent analytical period, demonstrating that mineralisation was progressive (coinciding with the mineral development observed [Figure 3.10 A.i-iii]), which began after at least 4-weeks of culture and shows that the SSBM culture system supports subsequent mineralisation of the newly deposited matrix.

3.6.6 Optimising XRF preparation and analysis

XRF was used to attain a more in-depth analysis of the mineral present within the hFOB 1.19 SSBM constructs, however, prior to XRF analysis, samples must be dehydrated. Retaining the matrix architecture of the constructs following dehydration was challenging, given that hydrogels are >30% water by weight (355) due to their high water retention capabilities (348). To maintain the microscopic and chemical structure, freeze-drying was used as it has been shown previously (461–463) to maintain

samples better than alternative approaches such as oven-drying. Freeze-drying (lyophilisation) removes water by sublimination – water within pre-frozen samples is transformed from its solid state, directly to its gaseous state, which is removed by vacuum. However, the method in which samples are pre-frozen greatly influences the success of freeze-drying, with many constructs cracking, snapping and curling, during the process.

A number of different strategies were attempted to improve the lyophilisation process (e.g., removing the anchors, removing the elastomer, pre-drying steps etc.) for optimal pre-freezing and subsequent freeze-drying of samples. Although freeze-drying performs better wh(464), thus causing SSBM distortion and rendering them unusable for XRF. Large ice crystals are the result of slow freezing, therefore rapid, snap freezing of the constructs was performed using an isopentane bath setup [Section 2.4.3.1], rather than liquid nitrogen which has a slightly slower freezing rate, due to the presence of a nitrogen gas layer surrounding the sample, and thus does not preserve sample morphology to the same extent (465).

XRF is an inexpensive, non-destructive, and rapid analytical approach to investigate the elemental composition of samples. A commonly used material science method, it is also commonly utilised across a range of disciplines. These include the social sciences (e.g., art restoration and aging archaeological artefacts (466,467)), agriculture (e.g., determining soil composition and quality (468)), as well as medicine (e.g., heavy metal accumulation in tissues (469)). XRF uses the basic principle of eliciting the emission of secondary x-rays from atoms that have been ionised by a high-energy incident x-ray. Each element in the periodic table produces an x-ray of a unique and specific energy level, that is detected, located and measured by the XRF. This in

turn enables the XRF to produce a spectrum of energy signals with their corresponding intensity – the greater the intensity of a particular energy signal, the greater the amount of that corresponding element present in the sample. Furthermore, the high precision and accuracy of the technique in the temporal detection of the elements creates elemental maps [Figure 3.11].

Visually, XRF results [Figure 3.11] showed phosphorus was present across all three analytical time points, however the presence of calcium was not as prominent until 12-weeks post-cell seeding, although it was observed in 8-week cultured constructs as small nodules. When overlayed, the calcium and phosphorus co-localised, which strongly implies the presence of a calcium phosphate mineral. The results for the mean Ca:P signal ratios [Figure 3.12 B.ii] agree with the visual findings, that the significant increase in calcium - thus driving up the Ca:P signal ratio – is most noticeable between 4- and 12-weeks of culture and 8- and 12-weeks, but not between 4- and 8 weeks. In comparison to the AZ results obtained [Figure 3.10 B], the overall increasing trend in AZ concentration extracted (and thus assumed mineral concentration present) over time coincides with these XRF results. However, unlike the XRF results, AZ results showed a significant increase between 4- and 8-weeks. The most likely explanation for this result is XRF is a non-penetrative analytical approach (i.e., XRF only detects elemental signals on sample surfaces). This suggests mineralisation initially occurred within the SSBM constructs. Evidence of this can be seen within the densely folded edges of the SSBM constructs of which are noticeably darker than the inner, exposed regions [Figure 3.10 Ai-iii], and therefore these regions would not have been detectable by XRF.

3.6.7 Conclusions

The overall aim of this chapter was to adapt an established method for creating SSBM constructs to accommodate the secondary human osteoblastic cell line, hFOB 1.19, replacing the need for primary rat femoral periosteal cells. This was achieved by first characterising the expected growth and differentiation trends of hFOB 1.19 whilst under 2D culture conditions, followed by testing the repeatability of the original SSBM method (398) using rat periosteal cells. Then, appropriate adaptions were identified and made to create hFOB 1.19 SSBM constructs. Finally, to confirm the success of creating these humanised bone models, the structural and compositional properties of resultant constructs were analysed over time and compared against those previously reported during development of the original method (398).

Overall, these investigations found that the original protocol by Iordachescu *et al*. (398) was indeed replicable and repeatable using primary rat periosteal cells, and furthermore the method was also adaptable and accommodates the long-term culture of the hFOB 1.19 cell line. The results from the investigations into the collagen content and mineralisation process of hFOB 1.19 SSBM constructs are indicative of the seeded cells producing a new collagen containing matrix, potentially osteoid. This is subsequently followed by the primary mineralisation phase, where the newly produced and unmineralised bone tissue mineralises rapidly, primarily consisting of an immature form of CaP, which aligns with the XRF results. Together, these initial findings showed that successful long-term culture of hFOB 1.19 SSBM cultures results in the creation of a matrix reminiscent of early *in vivo* bone tissue at the chemical and structural level.

Chapter 4

Biological characterisation of hFOB 1.19 SSBM constructs

4.1 Introduction

During the drug research and development timeline, and prior to beginning drug candidate selection, extensive research is carried out to compare and contrast the changes that occur with disease at the microscopic and macroscopic level; during which potential drug targets are identified. At the cellular and molecular level, this is achieved through assays assessing a variety of biological readouts, including changes in gene and protein expression and activity. Whilst the use of *ex vivo* and *in vivo* models are currently unavoidable in the later stages of drug research (e.g., to assess toxicity and pharmacokinetics), having an *in vitro* platform that closely recapitulates the *in vivo* tissue prior to these investigations will reduce the need for *ex vivo* and *in vivo* models in the early stages of the drug discovery process (303).

Cells cultured under 2D conditions are unlikely to act and respond as they would *in vivo*, primarily due to the unnatural, polar conformation they acquire when cultured on a planar surface, which has great influence on cell behaviour through physical cues (i.e., adhesion molecules and polar arrangement of cytoskeleton and organelles), as well as the lack of chemical cues (i.e., a reservoir of bioactive molecules such as growth factors and cytokines) that are provided by the *in vivo* extracellular matrix (ECM) (470–472)). These limitations drive a reliance on *ex vivo* and *in vivo* models, which are both time and cost consuming, are opposed to the principles of the 3Rs, and despite this, remain poor predictors of human responses (194). 3D cell culture systems provide a solution to many of the limitations associated with 2D cell culture, and have shown a recent growth in development, optimisation and availability in a number of research areas (303,304).

Further development and optimisation of the SSBM method is with the intention to create a versatile bone research model capable of normal and disease modelling, co-culture with other cell types, and future adaptation into a 3D high-throughput assay platform for bone drug candidate testing. Before this can be achieved, three fundamental questions must be addressed to determine feasibility.

1. How can responsivity to bone formation modulators (BFM) be measured in the SSBM?
2. What are the baseline model characteristics against which responsivity is assessed?
3. Are SSBM constructs responsive to known BFMs?

The overall aim of this chapter is to answer the first two questions – identify, develop and optimise analytical methods in order to establish a baseline of normal hFOB 1.19 cell behaviour in the 3D environment that can then be used as a control.

Previous work by Iordachescu *et al.* (395,398) gives a detailed account of rat SSBM construct chemical and structural changes that occurs over prolonged culture, of which the previous chapter of this thesis has confirmed similar changes also occur with hFOB 1.19 SSBM constructs, although at a slower rate. However, by comparison, only a small amount of work was carried out to examine the concurrent biological changes that occurred during rat SSBM construct culture.

Optimisation of preparatory methods is critical to achieving accurate and reliable data (473–475). Therefore, a considerable focus and aim of this project was to adapt, develop and optimise analytical methods and preparatory techniques to accommodate SSBM constructs.

Gene expression analysis through real time polymerase chain reaction (qPCR); a powerful analytical method; highly sensitive, accommodates a number of sample media and has high-throughput capabilities (476,477). However, it is a fragile assay that heavily relies on user experience (474,478). There are several stages throughout this process that can hinder and affect qPCR analysis; the following of which occur more often: inappropriate disruption and homogenisation method, inappropriate sample/RNA/cDNA storage, RNAse contamination, and converting different amounts of RNA to cDNA for each sample (398).

IF staining and imaging is another valuable analytical tool for a variety of tissues and matrices that can both confirm biological marker expression and provide topographical information with high specificity and accuracy. However, like qPCR, it relies on optimised methods of preparation and storage, reagent selection and dilutions, along with user experience in these methods and imaging. Samples must be fixed to preserve tissue morphology and maintain antigenicity, and the most commonly used fixative is formalin solution. Permeabilization after fixation is also recommended, particularly when staining for intracellular markers (479). Unfortunately, there is no universal method of fixation and permeabilization, thus they must be optimised for different types of tissue (480). Improper fixation leads to a staining error called edge effect where the edges of the tissue matrix has been stained, rather than around the cellular features (481).

Fixed samples are then embedded into a solid block (commonly composed of paraffin) for ease of sectioning. In the case of bone and other mineralised tissues, particularly without prior decalcification of the mineral, the most commonly used approach is plastic- and resin-based embedding to match the solidity of the undecalcified bone.

But, it is a very time and cost consuming process (482). Issues also arise with demineralisation of bone; another lengthy process that can affect tissue architecture and protein antigenicity (483).

Adapting, developing and optimising analytical methods specifically for the SSBM constructs enabled their biological characterisation and identification of key developmental stages after 4-, 8- and 12-weeks of culture; the same analytical timepoints as those used for structural analysis to enable direct comparison of the biological characteristics against the structural changes observed.

The analytical techniques used by Iordachescu *et al.* (395) (i.e., qPCR and IF) were used as a starting point where the “pinch points” within the approaches were identified and altered accordingly. Furthermore, during method development, great consideration was taken to achieve efficient analysis of the SSBM constructs to enable multiple analytical approaches from a single construct, by correctly planning the sequence of analytical approaches to be taken. Great attention was also taken to ensure analytical methods were simplified for ease of repeatability and repetition, as well as accessibility and availability, for future users; further enhancing the appeal and uptake of this cell culture system.

4.2 Gene expression analysis

4.2.1 Optimising RNA extraction

Reliable qPCR analysis requires high-quality RNA to be extracted from samples of interest. As such, two extraction methods were tested and compared to extract RNA from hFOB 1.19 SSBM constructs; snap freezing and grinding with liquid nitrogen (LN_2), or repetitive vortexing needle aspiration [Figure 2.2].

When comparing all RNA yields from 12-week cultured hFOB 1.19 samples after extraction via the 'LN_2' or 'needle' methods [Figure 4.1 A.i], there was a significant increase in RNA yield when using the needle method (1.35 vs 73.71 ng/µL; p=0.0013). By comparing hFOB 1.19 SSBM constructs of the same batches at 4-, 8- and 12-weeks of culture [Figure 4.1 A.ii-iv], the results were inclined to confirm the greater yield obtained by the needle method was not caused by batch-batch variation (4-weeks = 38.1 vs 565.5; 8-weeks = 18.6 vs 153.0; 12-weeks = 0.8 vs 37.4) but the n number was too low for statistical testing.

To ascertain the expected RNA yields and purity from hFOB 1.19 SSBM constructs at the three analytical timepoints, using the needle method, RNA yields and 260/280 values were recorded and plotted [Figure 4.1 B.i-ii, respectively]. There was an overall significant decline in RNA yield between 4- and 12-weeks of culture (457.1 vs 151.5 ng/ µL; p=0.0059), although none between the sequential time points (i.e., 4- vs 8-weeks (457.1 vs 399.2 ng/ µL; p=0.69); and 8- vs 12-weeks (399.2 vs 151.5 ng/µL; p=0.076)). The same trends were observed for the 260/280 values, although not to the same degree as the RNA yield (i.e., 4- vs 12-weeks (2.101 vs 2.075; p=0.04); 4- vs 8-weeks (2.101 vs 2.100; p=0.94) and 8- vs 12-weeks (2.100 vs 2.075; p=0.19).

4.2.2 Housekeeper selection

Primers for two housekeeper genes, *B2M* and *GAPDH*, were included with every qPCR analyses. To determine the most appropriate gene to use as an internal control for overall qPCR analysis in this project, the mean Ct values (obtained from triplicate wells per sample) of both housekeeper genes for each hFOB 1.19 SSBM construct processed was compared between the 4-, 8- and 12-week culture periods [Figure 4.2A]. There was no significant difference found between any of the culture periods for

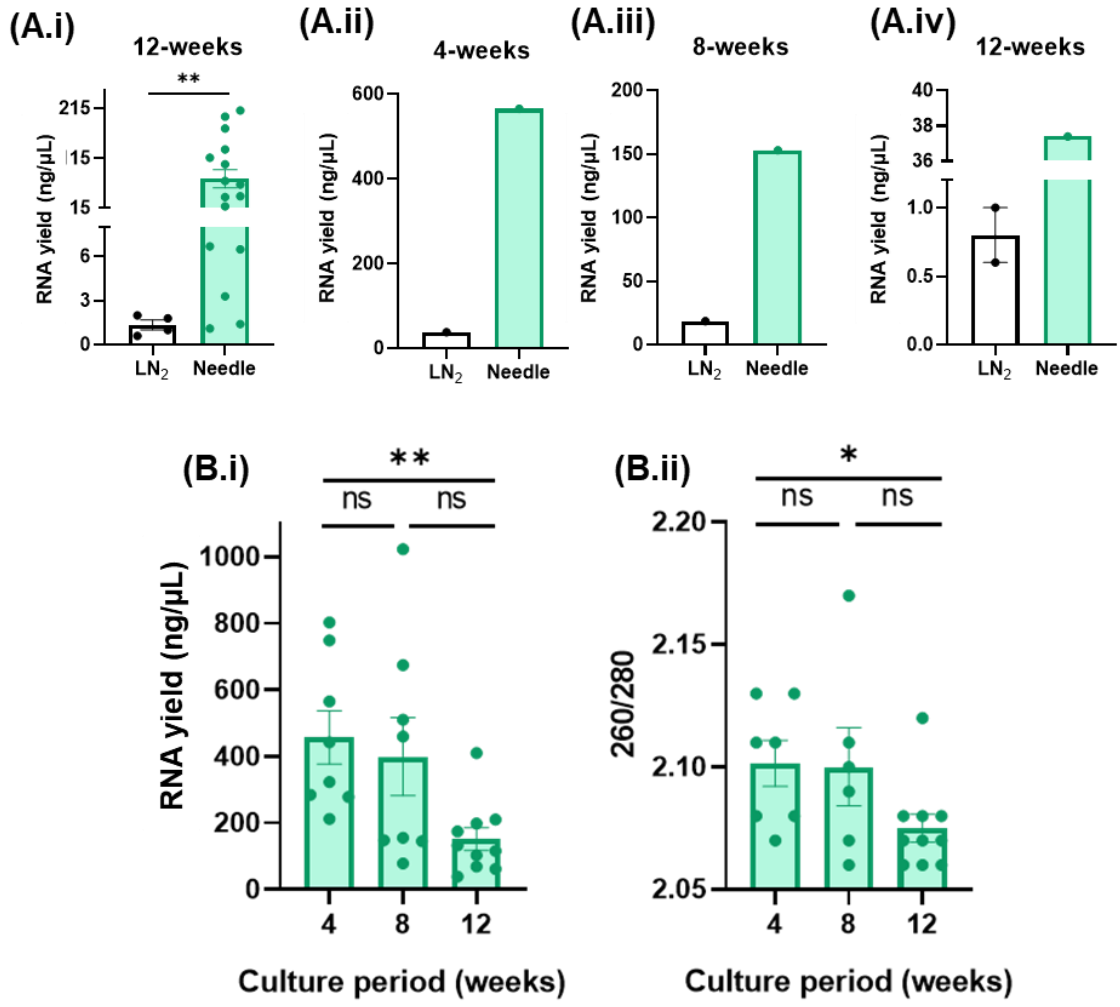


Figure 4.1 - Improving and characterising RNA extraction yields from hFOB 1.19 SSBM constructs. (A) Comparing mean RNA extraction yields between all 12-week samples **(i)**(n=4 (LN_2), 16(Needle)) and samples of the same SSBM batches after 4- **(ii)**(n=1), 8- **(iii)**(n=1) and 12-weeks **(iv)**(n=2 and 1, respectively) of culture, after disrupting and homogenising with either liquid nitrogen (LN_2) or the needle aspiration method [Section 2.3.4.1]. Data shown is Mean±SEM and analysed using unpaired t-test. ** = p<0.01; cannot analyse **(i-iv)** due to low n values. **(B)** Determining expected RNA yields at each analytical timepoint, after disrupting and homogenising hFOB 1.19 SSBM constructs using the needle aspiration method. Data shown is Mean±SEM (n=8, 8, 16, respectively) and analysed using Brown-Forsyth and Welch ANOVA with individual comparison results shown. * = p<0.05; ** = p<0.01; ns = no significance.

B2M (i.e., 4- vs 8- vs 12-weeks: 17.81 vs 18.51 vs 18.32; p=0.60) or *GAPDH* (i.e., 4- vs 8- vs 12-weeks: 20.08 vs 19.38 vs 19.41; p=0.68). The mean Ct values for each housekeeper gene were then accumulated to compare their distribution and variation

between *B2M* and *GAPDH* [Figure 4.2B]. Results showed *B2M* had less dispersion ($Q_3 – Q_1$ = 1.91) and spread (Max – Min = 5.34) than *GAPDH* ($Q_3 – Q_1$ = 2.56; Max – Min = 7.92). Furthermore, *B2M* had a significantly lower overall mean Ct value than *GAPDH* (18.23 vs 19.63; p=0.0016). Therefore, *B2M* was chosen as the housekeeper gene for qPCR analysis throughout the duration of this project.

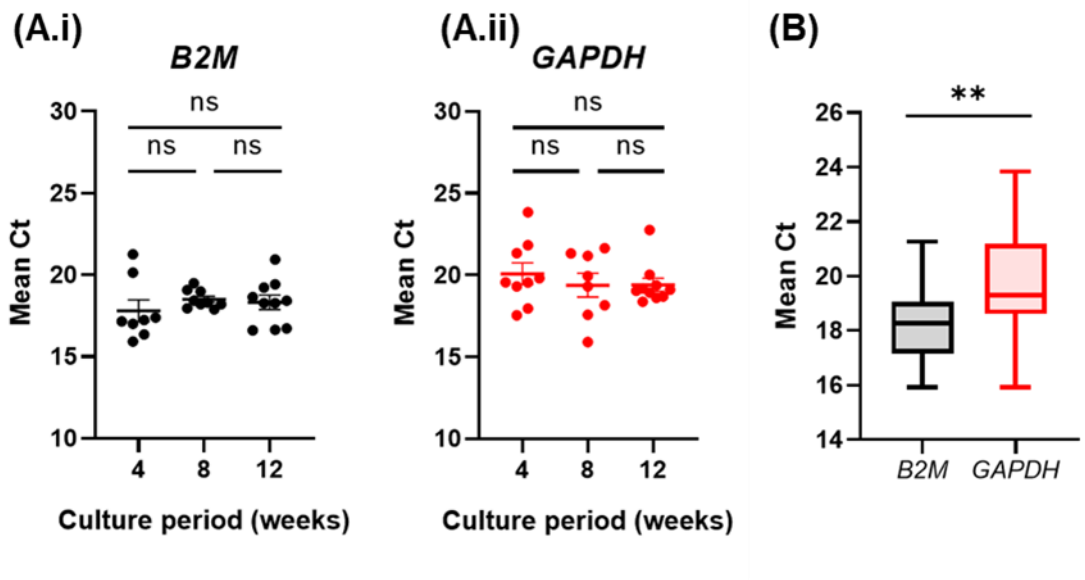


Figure 4.2 - Assessing suitability of housekeeping gene expression for quantitative polymerase chain reaction (qPCR) analysis. (A) Mean cycle threshold (Ct) values obtained for housekeeper genes, B2M **(i)** and GAPDH **(ii)**, of each sample used for qPCR analysis; displayed for each analytical timepoint. Data shown as mean±SEM (n=8, 9,10, respectively) and analysed using Brown-Forsythe and Welch ANOVA. ns = no significance. **(B)** The same mean Ct values obtained for housekeeper genes accumulated and a box plot created then compared for each housekeeper gene. Max-min. with upper and lower quartiles, and median values shown. N = 27. Overall mean analysed using unpaired t-test. ** = p<0.01.

4.2.3 hFOB 1.19 SSBM construct gene expression characterisation

qPCR was used to ascertain the expected gene expression profile of hFOB 1.19 SSBM constructs after 4-, 8- and 12-weeks of culture, with a total of 16 genes relating to osteoblasts, osteocytes and chondrocytes, as well as matrix deposition and maturation. Using the results from RNA extraction [Section 4.2.1] and housekeeper selection investigations [Sections 4.2.2], RNA was obtained via needle method

extraction and *B2M* used as the housekeeper gene. Expression was numerically quantified and displayed as resultant $2^{-\Delta Ct}$ values.

Genes relating to bone matrix composition and mineralisation were analysed and plotted as shown in [Figure 4.3]. Expression of *ALPL*, *SPARC* and *SPP1* (i.e., the genes encoding for ALP, osteonectin, and osteopontin, respectively), all showed to significantly increase between the first and last analytical time points (*ALPL*: $6.4x10^{-4}$ vs $52.0x10^{-4}$; p=0.0002. *SPARC*: $9.4x10^{-2}$ vs $26.4x10^{-2}$; p=0.009. *SPP1*: $2.1x10^{-4}$ vs $234.4x10^{-4}$; p=0.002). However, BGLAP (i.e., gene encoding for osteocalcin) only showed a significant increase in expression between 4- and 8-weeks of culture ($7.14x10^{-6}$ vs $27.3x10^{-6}$; p=0.0058), and *COL1A1* (i.e., gene encoding for alpha-1 chains of type I collagen) expression was consistent over time with no significant changes between 4-, 8- and 12-weeks of culture (0.15 vs 0.09 vs 0.15; p=0.31, respectively).

Genes relating to osteoblast activity and differentiation were analysed and plotted as shown in [Figure 4.4]. *BMP2* and *RUNX2* both showed significantly increased expression between the first and last analytical timepoints (*BMP2*: $1.57x10^{-5}$ vs $119.7x10^{-5}$; p=0.004. *RUNX2*: $2.1x10^{-3}$ vs $5.7x10^{-3}$; p=0.008). However, *PHEX*, *TNFSF11* (i.e., the gene encoding for RANKL) and *OPG* expression showed no significant changes in expression between any of the time points (ANOVA results – *PHEX*: p=0.55; *TNFSF11*: p=0.29; *OPG*: p=0.12).

The expression of genes relating specifically to osteocytes were analysed and included *DMP1*, *FGF23*, *MEPE*, *PDPN* and *SOST*. However, with the exception of podoplanin (*PDPN)* (i.e., gene encoding for podoplanin), there were no or very high (i.e., >35) Ct

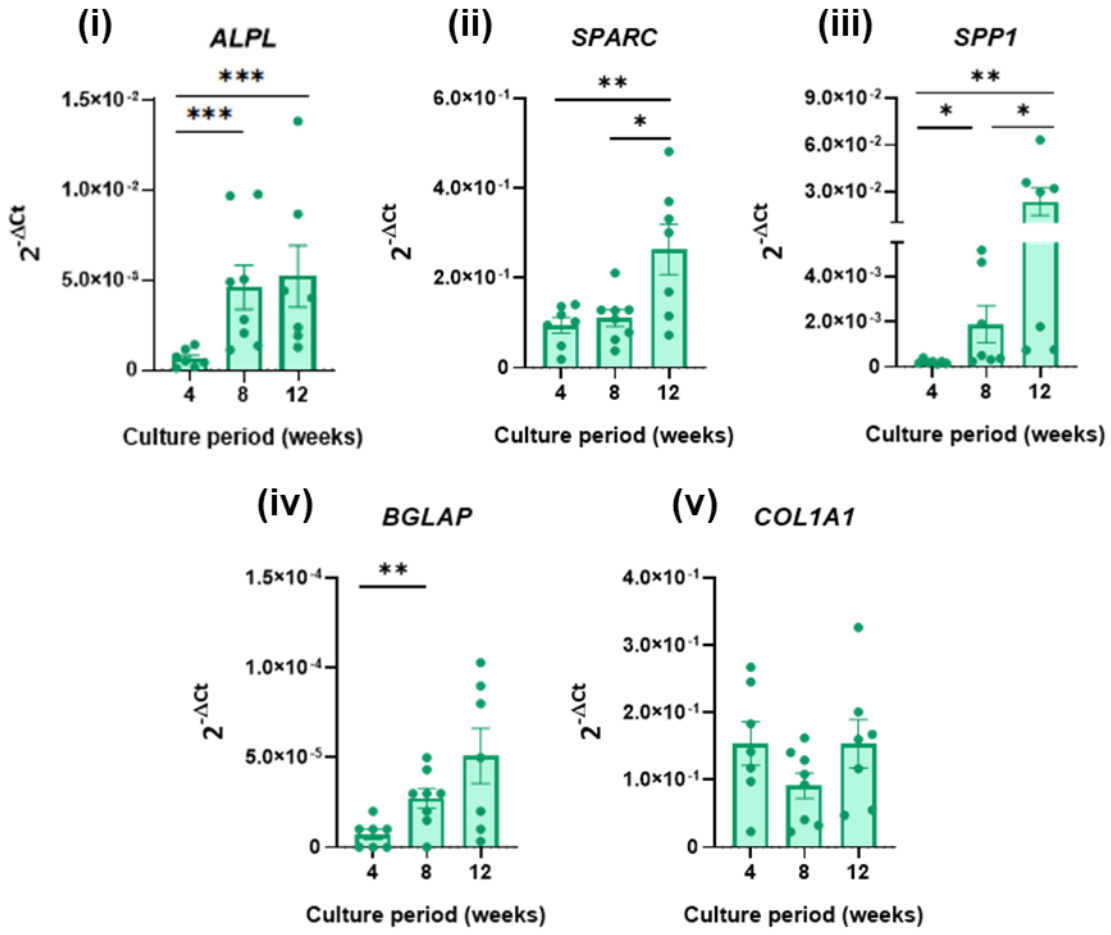


Figure 4.3 - qPCR analysis of bone matrix and mineralisation gene expression over time in hFOB 1.19 SSBM constructs. Expression of genes relating to matrix production and mineralisation were analysed in hFOB 1.19 SSBM constructs, cultured for 4-, 8-, and 12-weeks post-cell seeding. ALPL = Alkaline phosphatase **(i)**; SPARC = Osteonectin **(ii)**; SPP1 = Osteopontin **(iii)**; BGLAP = Osteocalcin **(iv)**; COL1A1 = alpha-1 chain of type I collagen **(v)**. Compared to housekeeper gene B2M. Results are mean ± SEM (n=6-8, inclusive). Raw Ct values analysed using ordinary one-way ANOVA with Fisher's LSD, or Brown-Forsythe and Welch ANOVA when SD ratio = >2. Multiple comparison results shown. * = p<0.05; ** = p<0.01; *** = p<0.001. Absence of statistical result on the graph indicates no significant difference.

values obtained. *PDPN* expression [Figure 4.5 i] had a very significant increase over the total culture period (i.e., 4- vs 12-weeks: $4.0x10^{-5}$ vs $100.5x10^{-5}$; p=<0.0001), as well as between each subsequent time point (i.e., 4- vs 8-weeks: $4.0x10^{-5}$ vs $37.5x10^{-5}$; p=<0.0001. 8- vs 12-weeks: $3.75x10^{-4}$ vs $10.1x10^{-4}$; p=0.0162).

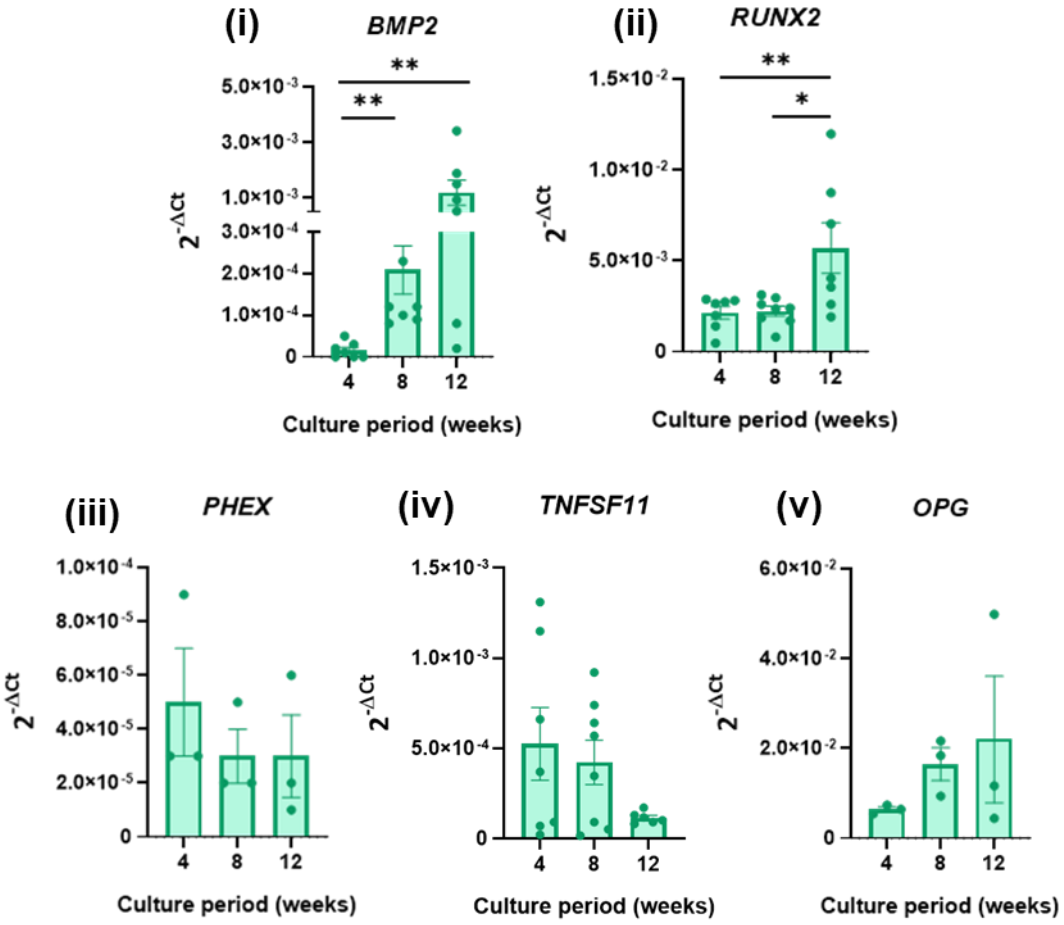


Figure 4.4 - qPCR analysis of osteoblast-specific gene expression over time in hFOB 1.19 SSBM constructs. Expression of genes relating to osteoblasts specifically were analysed in hFOB 1.19 SSBM constructs, cultured for 4-, 8-, and 12-weeks post-cell seeding. Compared to housekeeper gene B2M. Results are mean ± SEM (n = 6-8, inclusive). Raw Ct values analysed using ordinary one-way ANOVA with Fisher's LSD, or Brown-Forsythe and Welch ANOVA when SD ratio = >2. Multiple comparison results shown. * = $p<0.05$; ** = $p<0.01$. Absence of statistical result on the graph indicates no significant difference.

To determine the possibility of whether chondrocytes were present within the hFOB 1.19 SSBM cultures, the expression of the gene relating to chondrocyte lineage commitment, *SOX9*, was analysed [Figure 4.5 ii]. Results showed there was *SOX9* expression at 4- ($30.0\times10^{-6} \pm 5.77\times10^{-6}$), 8- ($6.67\times10^{-5} \pm 1.76\times10^{-5}$) and 12-weeks ($14.67\times10^{-5} \pm 7.17\times10^{-5}$) of culture, however, there was no significant difference in the mean expression found between any of the time points ($p=0.10$).

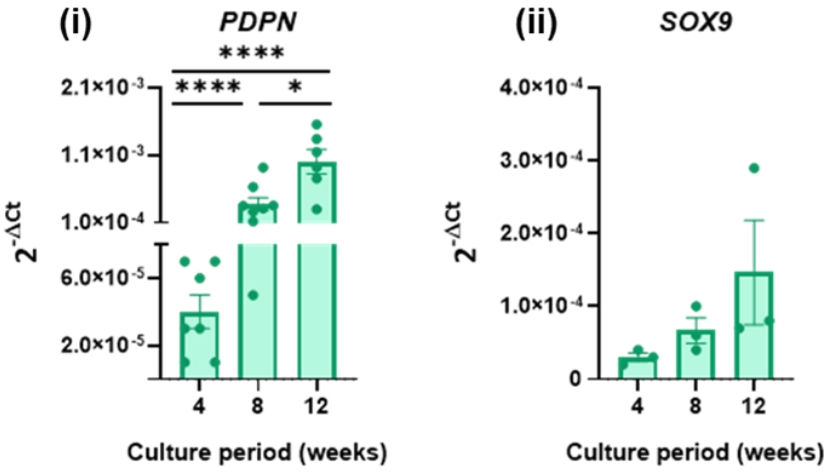


Figure 4.5 - qPCR analysis of gene expression relating to other bone cell types over time in hFOB 1.19 SSBM constructs. Expression of genes relating to early osteocytes **(i)** (n=7-8) and commitment to the chondrocyte lineage **(ii)** (n=3) were analysed in hFOB 1.19 SSBM constructs, cultured for 4-, 8-, and 12-weeks post-cell seeding. Compared to housekeeper gene B2M. Results are mean±SEM. Raw Ct values analysed using ordinary one-way ANOVA with Fisher's LSD **(i)**, or Brown-Forsythe and Welch ANOVA **(ii)**. Multiple comparison results shown. * = $p<0.05$; **** = $p<0.0001$. Absence of statistical result on the graph indicates no significant difference.

4.2.4 2D vs 3D gene expression

hFOB 1.19 cells were cultured in 2D for 4-weeks under permissive conditions, followed by a further 4-weeks (i.e., 8-weeks total culture period) under osteogenic conditions (Cells cultured under 2D conditions could only achieve a total culture period of 8-weeks). Gene expression after 4 and 8-weeks or culture was then analysed using qPCR to compare against the data obtained for the 3D culture system. The same genes assessed previously for the hFOB 1.19 SSBM cultures were also analysed in these 2D investigations [Table 2.3]. *B2M* was used as the housekeeping gene again.

Of the osteoblastic genes investigated, the expression of *PHEX* and *BMP2* had significantly different trends when compared against the results obtained from SSBM

constructs. *RUNX2* [Appendix 8.2] showed no overall significant difference in expression over time between the two culture systems. 2D cultures showed a significant decline in *PHEX* expression between 4- and 8-weeks ($2.75x10^{-5}$ vs 0; p=<0.0001) [Figure 4.6 A.i&iii], whereas the SSBM construct culture, although had a similar mean $2^{-\Delta Ct}$ at 4-weeks as the 2D cultured cells, this level of expression was maintained at 8-weeks ($5.0x10^{-5}$ vs $3.0x10^{-5}$; p=0.39) [Figure 4.6 A.ii-iii]. *BMP2* expression [Figure 4.6 B] in 2D cultured cells showed no significant change between 4- and 8- weeks of culture with little or no detectable expression (0 vs $1.0x10^{-5}$; p=<0.0001), whereas there was a significant increase in *BMP2* expression in hFOB 1.19 SSBM constructs over time ($1.57x10^{-5}$ vs $20.9x10^{-5}$; p=0.0031) and expression was considerably greater than 2D cells at 4- and 8-weeks.

Like the SSBM cultures, with the exception of *PDPN*, no expression was detected for the osteocyte-specific genes investigated were obtained. However, PDPN expression was found to be statistically similar by 8-weeks of expression [Appendix 8.2,].

For genes relating to matrix and mineralisation, very little (i.e., *ALPL* and *SPP1)* or no significant change (i.e., *BGLAP* and *COL1A1)* in expression was observed between the two culture conditions [Appendix 8.2]. However, *SPARC* expression was significantly greater in the 3D culture system than 2D after 8-weeks of culture (2D vs 3D: 0.04 vs 0.11; p=0.017) despite no significant change in expression between 4- and 8-weeks of culture when comparing 3D and 2D individually [Figure 4.7 A].

To determine the possibility of chondrocytes being present within the cultures, *SOX9* expression of the 2D cultured cells was analysed [Figure 4.7 B]. *SOX9* expression of the 2D cell cultures significantly decreased to undetectable expression between 4- and

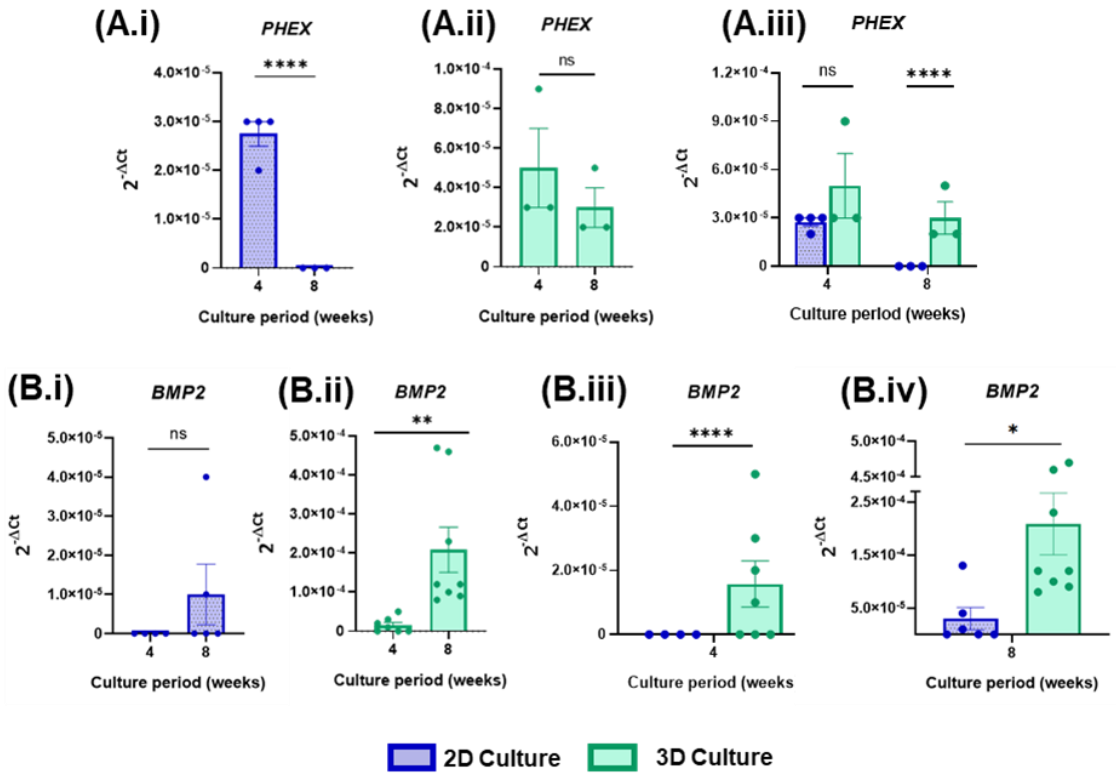


Figure 4.6 - Comparison of gene between hFOB 1.19 cells cultured long-term in 2D or 3D (Part i). qPCR analysis of PHEX **(A)** BMP2 **(B)** expression in hFOB 1.19 cells cultured in 2D (n=4-6) or 3D (n=7-8) for 4- and 8-weeks post cell seeding were compared over time individually **(i-ii)** and between the two culture conditions **(iii-iv)**. Compared to housekeeper gene B2M. Results are mean±SEM. Raw Ct values analysed using unpaired t-test, with Welsh correction if SD ratio = >2. * = p<0.05; ** = p<0.01; **** = p<0.0001; ns= no significance.

8-weeks of culture ($2.33x10^{-5}$ vs 0; p=<0.0001), whereas expression was maintained in the SSBM (i.e., no statistical difference found) after 8-weeks of culture ($3.0x10^{-5}$ vs $6.67x10^{-5}$; p=0.087).

The osteoblastic and osteocytic genes that are involved in the regulation of bone remodelling through the RANK/RANKL/OPG balance (i.e., *TNFSF11* (RANKL) and *OPG*) were also assessed in cells cultured in 2D. Expression of *TNFSF11* [Figure 4.8 A] significantly increased between 4- and 8- weeks of cells cultured in 2D ($7.25x10^{-5}$ vs $76.3x10^{-5}$; p=0.027), which did not significantly change over the same time period

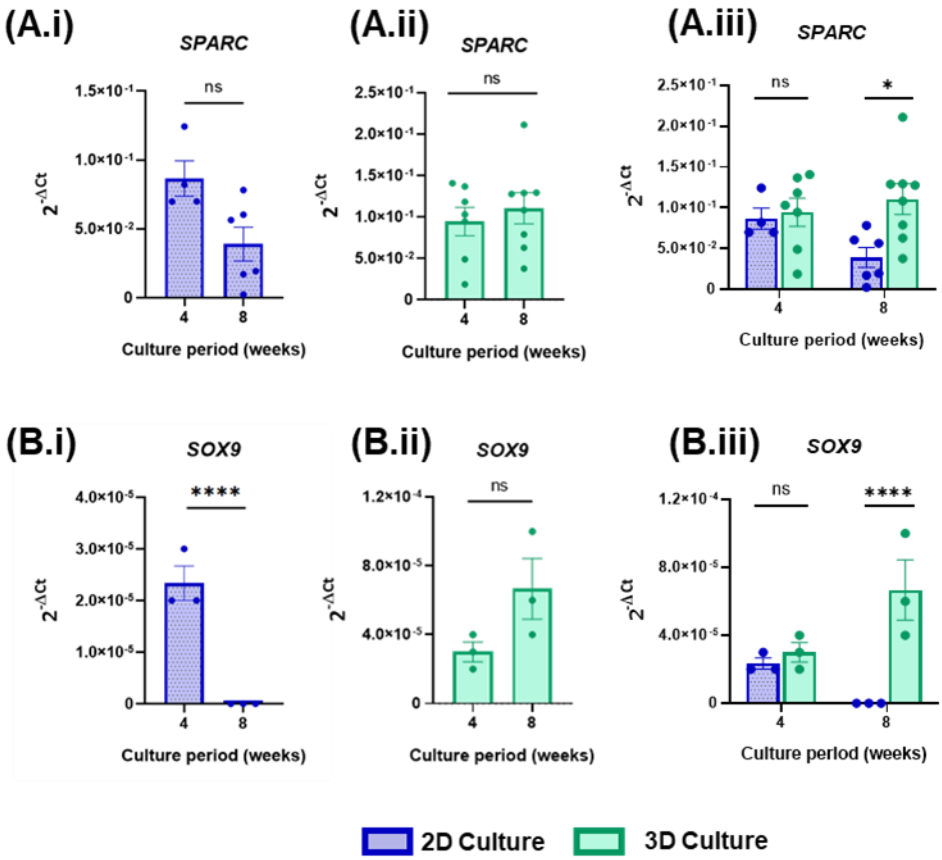


Figure 4.7 - Comparison of gene between hFOB 1.19 cells cultured long-term in 2D or 3D (Part ii). qPCR analysis of SPARC **(A)** and SOX9 **(B)** expression in hFOB 1.19 cells cultured in 2D (n=3-6) or 3D (n=3-8) for 4- and 8-weeks post cell seeding were compared over time individually **(i-ii)** and between the two culture conditions **(iii)**. Compared to housekeeping gene B2M. Results are mean±SEM. Raw Ct values analysed using unpaired t-test, with Welch correction if SD ratio = >2. * = p<0.05; ** = p<0.01; **** = p<0.0001; ns= no significance.

for the SSBM cultures. The culture conditions were not statistically different at 4-weeks, with an expected significantly greater magnitude of expression in the 2D cultures at 8-weeks of culture (2D vs 3D: $76.3x10^{-5}$ vs $42.2x10^{-5}$; p=0.044). Like *TNFSF11*, Expression of *OPG* [Figure 4.8 B] significantly increased between 4- and 8- weeks of cells cultured in 2D (p=0.041) which did not significantly change over the same time period for the SSBM cultures. However, hFOB 1.19 SSBM cultures had significantly higher expression of *OPG* at 4-weeks of culture than the cells cultured in 2D (2D vs

3D: 1.7x10^{-3} vs 6.4x10^{-3}; p=<0.0001), yet at 8-weeks of culture, 2D cultures had significantly greater expression of *OPG* (2D vs 3D: 0.158 vs 0.016; p=0.006).

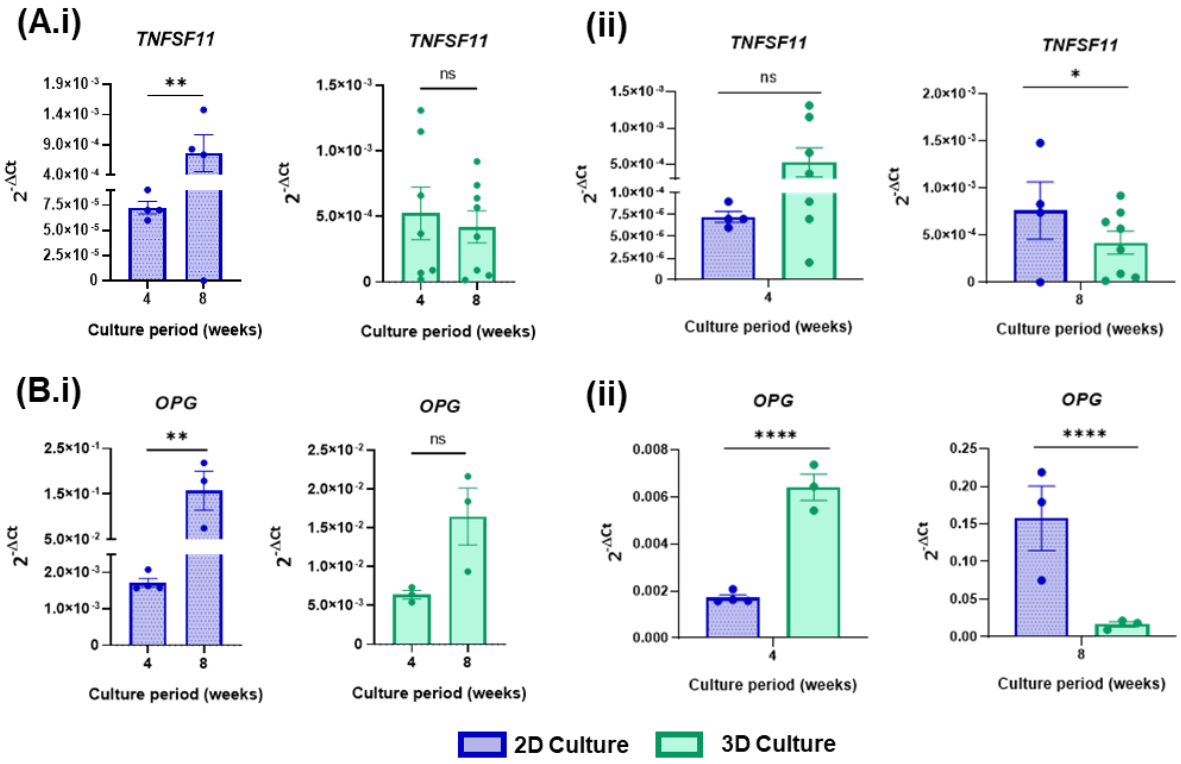


Figure 4.8 - Comparison of gene expression relating to bone resorption regulation between hFOB 1.19 cells cultured long-term in 2D or 3D. qPCR analysis of TNFSF11 **(A)** (i.e. the gene encoding for RANKL) and OPG **(B)** expression in hFOB 1.19 cells cultured in 2D (n=3-4) or 3D (n=7-8 (TNFSF11), 3 (OPG)) for 4- and 8-weeks post cell seeding were compared over time individually **(i)** and between the two culture conditions **(ii)**. Compared to housekeeping gene B2M. Results are mean±SEM. Raw Ct values analysed using unpaired t-test, with Welsh correction if SD ratio = >2. * = p<0.05; ** = p<0.01; **** = p<0.0001; ns= no significance.

4.3 Conditioned media analysis

4.3.1 SSBM construct isolation

Over prolonged culture, cells were found to be accumulating on the elastomer base (i.e., outside of the SSBM constructs) [Figure 4.9 A]. Therefore, analytes within the conditioned media of these cultures are the cumulative product of both the cells within

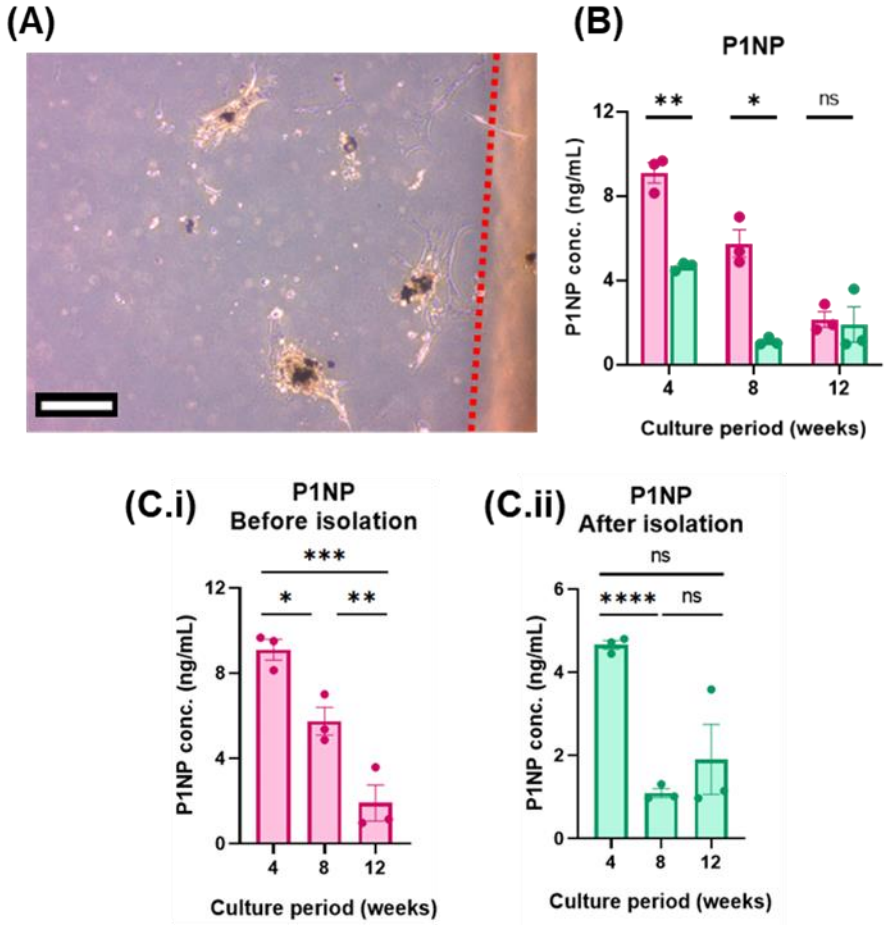


Figure 4.9 - **Assessing the effects of construct isolation on ELISA analysis of conditioned media. (A)** Cells accumulate into distinct populations on the elastomer base with prolonged culture. Image shows hFOB 1.19 SSBM culture 6-weeks after cell seeding. Red dotted line = SSBM construct outer edge. Scale bar = 200 µm. **(B)** The concentration of P1NP measured was compared between conditioned media before and after isolation at each of the analytical timepoints. Data shown is mean±SEM and analysed using unpaired t-test, with Welch correction if SD ratio = >2. * = $p<0.05$; ** = $p<0.01$; ns = no significance. **(C)** The P1NP concentration trend was also assessed over time for the conditioned media before **(i)** and after isolation individually. Data shown is mean±SEM and analysed using rdinary one-way ANOVA with Fisher's LSD, or Brown-Forsythe and Welch ANOVA when SD ratio = >2. Multiple comparison results shown. * = $p<0.05$; ** = $p<0.01$; *** = $p<0.001$; **** = $P<0.0001$. Absence of statistical result on the graph indicates no significant difference.

the SSBM constructs, as well as the elastomer cell populations, which could lead to inaccurate assumptions and interpretations of the results. To circumvent this issue, 3 days prior to the analytical time point, constructs were removed from the original culture

well and placed into a fresh one, along with fresh media [Section 2.3.1] to isolate the cells within the SSBM constructs from the elastomer cells.

Following the steps outlined in [Section 2.3.2.3], the difference in mean P1NP concentration measured before and after construct isolation was compared for each analytical time point [Figure 4.9 B]. There was a significant decrease in mean P1NP concentration after construct isolation for media samples collected after 4- (9.10 ng/mL vs 4.66 ng/mL; p=0.009) and 8-weeks of culture (5.74 ng/mL vs 1.10 ng/mL; p=0.017), but no difference found with samples collected at 12-weeks of culture (1.90 ng/mL vs 1.90 ng/mL; p=0.82). The trend in P1NP concentration was determined for media samples collected before and after isolation individually over 4-, 8- and 12-weeks of culture [Figure 4.9 C]. Prior to construct isolation, P1NP concentration showed a significant decline over the total culture period of 4- to 12-weeks (p=0.0003) as well as between each subsequent time point (i.e., 4- vs 8-weeks: p=0.013. 8- vs 12-weeks: p=0.007). After construct isolation, the media collected showed no significant difference in P1NP concentration over the total culture period (p=0.08) and only showed a significant decline between 4- and 8- weeks of culture (p=<0.0001).

4.3.2 hFOB 1.19 SSBM construct conditioned media analysis

Conditioned media from hFOB 1.19 SSBM cultures were further analysed for the presence and concentration of OPG and ALP activity after 4-, 8- and 12-weeks of culture. The media samples analysed were taken from SSBM cultures that were isolated 3-days prior to the analytical time point [Section 2.3.1] and following the steps outlined in [Section 2.3.2.1 and 2.3.2.4], respectively.

There was no significant increase in mean OPG concentration between 4- and 12-weeks (0.49 ng/mL vs 2.52 ng/mL; p=0.074), or between 8- and 12-weeks (2.00 ng/mL vs 2.52 ng/mL; p=0.47), yet there was a significant increase from 4- to 8- weeks of culture (p=0.011) [Figure 4.10 i].

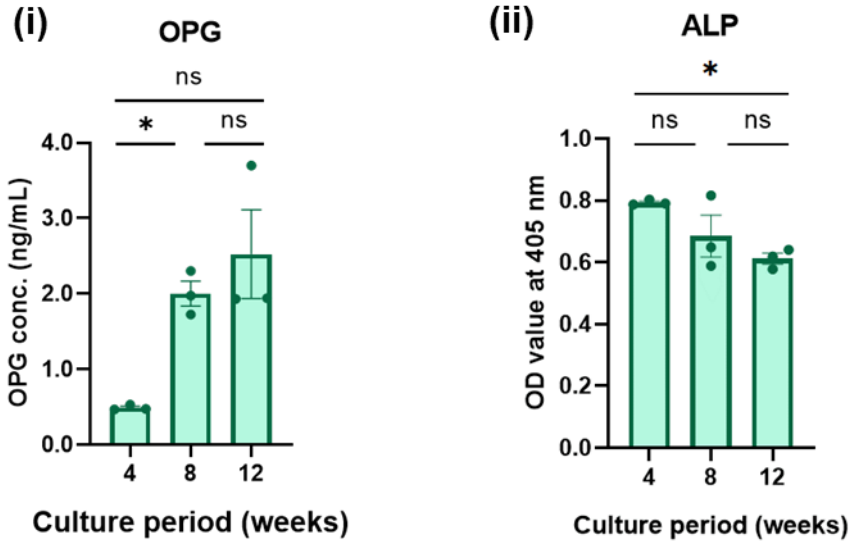


Figure 4.10 - Assessment of hFOB 1.19 SSBM construct conditioned media by ELISA. Media collected from isolated hFOB 1.19 SSBM constructs after 4-, 8- and 12-weeks post-cell seeding were analysed by ELISA to measure the concentration of OPG **(i)** and examine ALP activity **(ii)** over time. Results are mean±SEM (n=3) and analysed using Brown-Forsythe and Welch ANOVA. Multiple comparison results shown. * = $p<0.05$; ns = no significance.

Results from the ALP activity assessment showed a significant decline in mean optical density (OD) (i.e., measure of ALP activity) across the total culture period (i.e., 4- vs 12-weeks: 0.79 vs 0.61; p=0.013), although there was no significant difference seen between the subsequent time points of that culture period (4- vs 8-weeks: 0.79 vs 0.68; p=0.42. 8- vs 12-weeks: 0.68 vs 0.61; p=0.62) [Figure 4.10 ii].

4.3.3 2D vs 3D conditioned media analysis

Media was collected from cells cultured in 2D and under the same culture regime as the hFOB 1.19 SSBM cultures (i.e., 4-week culture under non-osteogenic conditions (33.5 °C, complete media), followed by osteogenic culture (37 °C, osteogenic media

[Table 2.1]), to assess and compare whether the two culture conditions differed in their secretion of markers of bone formation. Conditioned media from 2D cultures was collected and assessed for P1NP concentration and ALP activity by enzyme-linked immunosorbent assay (ELISA), as outlined in [Sections 2.3.2]. Cells cultured under 2D conditions could only achieve a total culture period after cell seeding of 8-weeks, therefore comparisons could only be made between the 4- and 8-week time points.

Results from assessment of P1NP concentration in conditioned media from 2D cultures [Figure 4.11 A] showed that there was a significant decline in mean P1NP concentration between 4- and 8-weeks of culture (7.64 ng/mL vs 2.81 ng/mL; p=<0.0001), which was also seen during assessment of SSBM construct media (after isolation) analysis between the same time period (4.66 ng/mL vs 1.10 ng/mL; p=<0.0001). When comparing against the two culture conditions at the individual time points, mean P1NP concentrations of 2D-conditioned media samples were significantly greater than the hFOB 1.19 SSBM construct conditioned media samples at both 4- (p=0.0013) and 8-weeks after cell seeding (p=0.015).

Results from assessment of ALP activity in conditioned media from 2D cultures [Figure 4.11 B] showed that there was a significant decline in mean OD (i.e., measure of ALP activity) between 4- and 8-weeks of culture (0.39 vs 0.34; p=0.013), whereas no significant change was seen during assessment of SSBM construct media (after isolation) analysis between the same time period (0.79 vs 0.68; p=0.42). When comparing against the two culture conditions at the individual time points, mean OD values of 2D-conditioned media samples were significantly lower than the hFOB 1.19 SSBM construct conditioned media samples at both 4- (p=<0.0001) and 8-weeks after cell seeding (p=0.036).

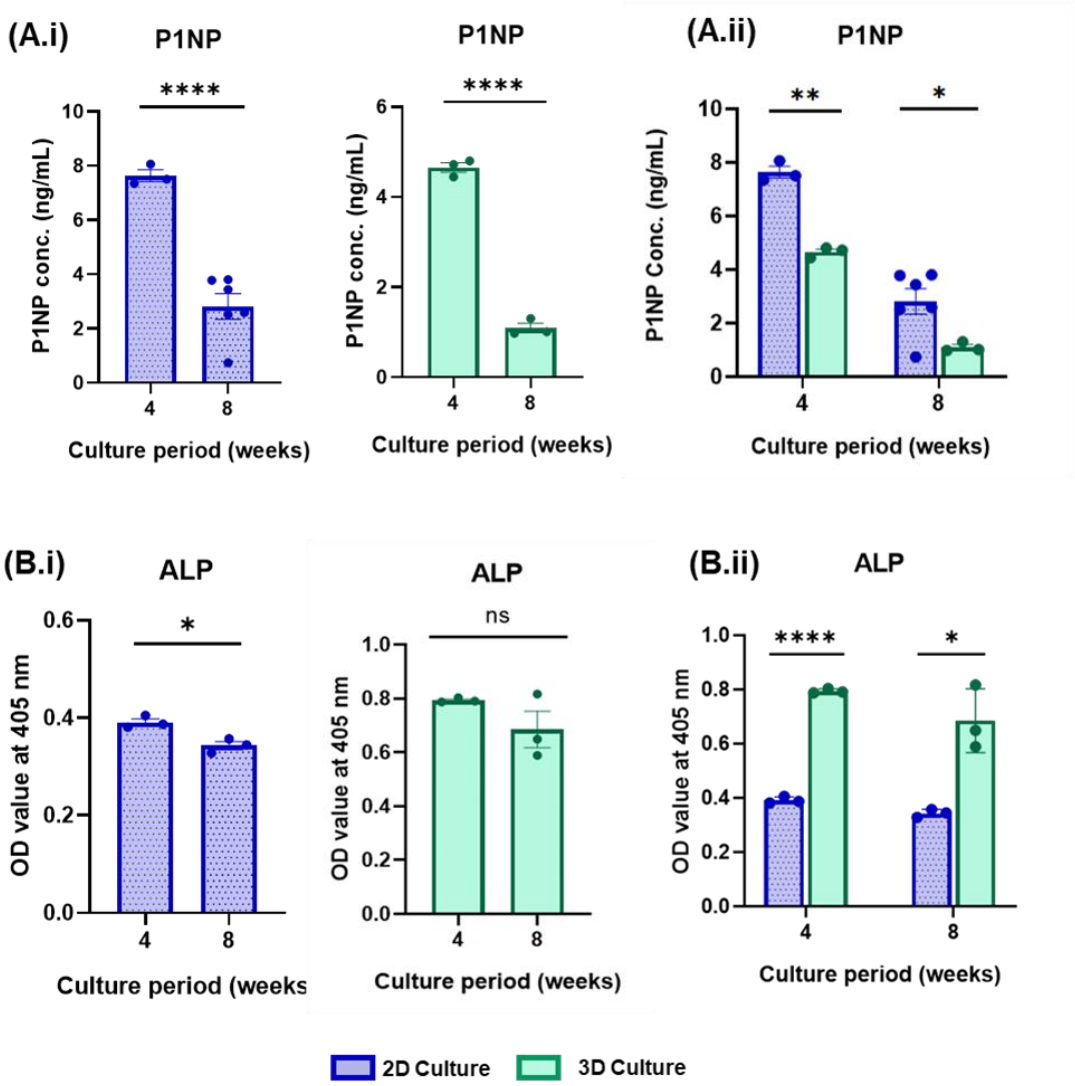


Figure 4.11 - Comparing assessment of conditioned media between hFOB 1.19 cells cultured in 2D and 3D. Conditioned media collected from hFOB 1.19 cells cultured in 2D (n=3-6) and isolated SSBM constructs (n=3) was analysed with ELISA to determine P1NP concentration **(A)** and examine ALP activity **(B)**. Individual culture conditions were compared over time **(A- & B.i)** as well as between the two culture conditions after 4- and 8-weeks of culture **(A- & B.ii)**. Results are mean±SEM and analysed using unpaired t-test, with Welch's correction if SD ratio = >2. * = $p<0.05$; ** = $p<0.01$; **** = $p<0.0001$; ns= no significance.

4.4 Immunofluorescence staining and imaging

4.4.1 Immunofluorescence staining

Immunofluorescence staining was carried out previously by Iordachescu *et al*. (395) [Figure 4.12 i]. Using 4′,6-Diamidino-2-phenylindole (DAPI) for nuclear/DNA staining and Phalloidin Alexa Fluor 594 for cytoskeleton stains, cells within the rat SSBM constructs were imaged to show their elongated, striated and parallel organisation, caused by the tensile forces of the fibrin matrix between the two CaP anchors. Whole, intact hFOB 1.19 SSBM constructs were also stained as outlined in [Section 2.3.5.3], the actin showed the cells had a similar conformation as those seen previously with the rat SSBM constructs [Figure 4.12 ii].

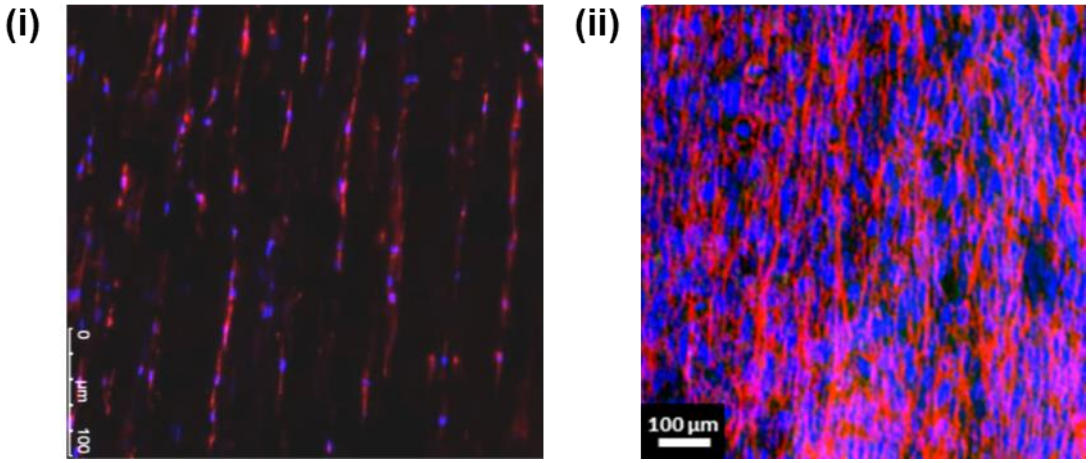


Figure 4.12 -Whole mount immunofluorescence staining of cells within SSBM constructs. Nuclear (blue) and actin (red) stains enabled visualisation and comparison of the parallel cell alignment and organisation within rat (**i**; taken from Iordachescu Thesis (397)) and hFOB 1.19 SSBM constructs **(ii)**. Scale bars = 100 µm.

This investigation showed that whole, intact SSBM constructs can be analysed using immunofluorescent staining, however to reduce the volume of reagents required, gain higher-resolution images and be less wasteful of SSBM constructs, a construct sectioning technique was optimised. This was achieved by adapting a protocol

specifically developed for preparing whole mouse bone for immunofluorescent staining and imaging to accommodate the SSBM constructs.

Following the steps outlined in [Section 2.3.5], high-resolution images and z-stacks of hFOB 1.19 SSBM constructs cultured for a period of 4-, 8- and 12-weeks were obtained to enable visualisation of cell organisation and expression of podoplanin (PDPN) at the protein level. PDPN was expressed in hFOB 1.19 SSBM constructs at 4-, 8- and 12-weeks of culture, with increasing expression between each subsequent time point [Figure 4.13]. Constructs from 4-weeks of culture showed very little or no positive PDPN staining. For example, the PDPN seen in the images in [Figure 4.13] at that timepoint was the only area within the whole section to positively express PDPN. However, the number of areas with positive PDPN staining increased in SSBM constructs after 8-weeks of culture, and after 12-weeks of culture, the majority of the hFOB 1.19 construct sections stained positive for PDPN – although some areas more strongly than others. Furthermore, it was noted that positive PDPN staining occurred initially in areas adjacent to the CaP anchors, then into the densely folded edges of the matrix, with minimal positive PDPN staining within the central inner surface of the matrix; the latter primarily found in hFOB 1.19 SSBM constructs cultured for 12-weeks.

Negative controls were performed and imaged for all samples. Equivalent negative controls for those in [Figure 4.13] found in [Appendix 8.2].

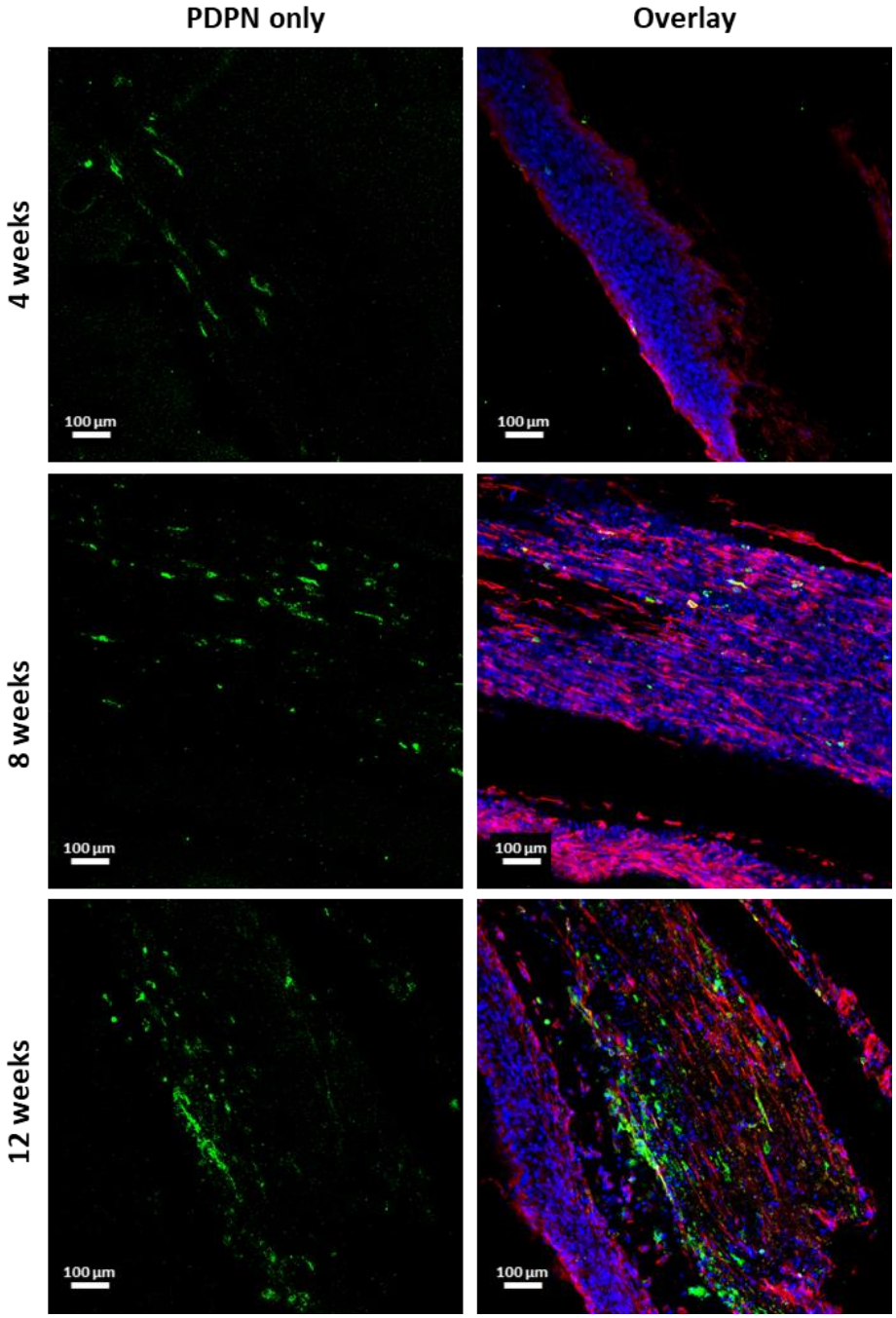


Figure 4.13 - Adaption of established protocol for bone embedding, sectioning and staining enables high-resolution immunofluorescence (IF) imaging of SSBM constructs. A method optimised for mouse bone IF analysis (399) was adapted to accommodate hFOB 1.19 SSBM constructs after 4-, 8- and 12-weeks of culture. Shown were 50 µm sections with an actin (phalloidin; red) and nuclear stain (Hoechst; blue) and an anti-human podoplanin (PDPN) antibody (green). Scale bars = 100 µm. 10x magnification. PDPN images = maximum intensity projection z-stacks (Step size = 2.1 µm). Overlay images = single plane snap shot.

4.4.2 Non-destructive viability staining

Assessment of cell proliferation and viability in the hFOB 1.19 SSBM was achieved with the Invitrogen™ ReadyProbes™ Cell Viability Imaging kit [Section 2.3.3]. This was only achievable in SSBM constructs cultured for a period of 4- and 8-weeks due to the obstruction caused by the mineral present. Using the images obtained, represented in [Figure 4.14 A], the live and dead cell densities were determined, as well as the % cell viability, for hFOB 1.19 SSBM constructs and compared at each time point [Figure 4.14 B.i-iii].

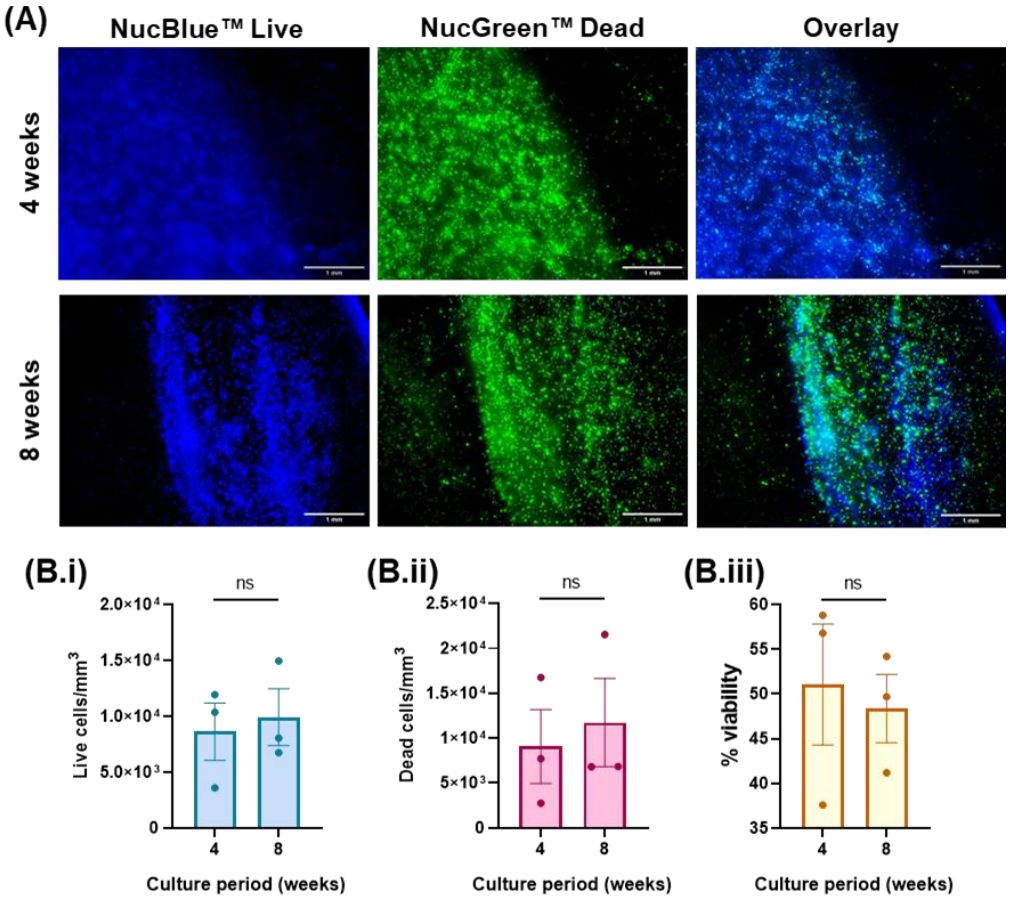


Figure 4.14 - Cell proliferation within constructs can be analysed using non-destructive staining for up to 12-weeks of culture. (A) The Invitrogen™ ReadyProbes™ Cell Viability Imaging kit [Section 2.3.3] was used to stain all cells (blue) and dead cells (green) within whole, intact constructs, by adding and incubating the ready-to-use probes to the culture media. Scale bar = 1 mm. Using the images obtained, live **(B.i)** and dead cell density **(ii)** were determined and then the culture viability **(iii)** calculated. Data shown is mean±SEM (n=3) and analysed using unpaired t-test. ns = no significance.

Between the 4- and 8-week culture period, there was no significant change in mean live ($8.6x10^3$ cells/mm^3 vs $9.9x10^3$ cells/mm^3; p=0.74) or dead cell density ($9.1x10^3$ cells/mm^3 vs 11.7 cells/mm^3; p=0.70); nor was there a significant change in mean %viability (51.1% vs 48.4%; p=0.75).

4.5 Discussion

4.5.1 Optimising RNA extraction and qPCR analysis

qPCR is a technique that can quantitively and qualitatively measure gene expression with high accuracy. This is achieved by cyclic amplification (up to 40 cycles) of transformed RNA transcripts into cDNA with fluorophore-tagged primers; detection of the fluorescent signal is deemed positive once surpassing a set threshold and the cycle at which this occurs (i.e., Ct value) is used to quantify the expression of the gene of interest. It is a versatile technique and thus has a vast number of applications, including as a routine analytical approach in cell and tissue cultures, as a health and safety measure in the identification of foodborne pathogens in contaminated foodstuffs (475,484), and has more recently gained recognition as the recommended COVID-19 diagnostic tool for the detection of SARS-CoV-2 in nasopharyngeal/oropharyngeal swabs (485–487). In the case of this project, it was used to serve as a readout for quantitative assessment of changes in gene expression with prolonged culture of hFOB 1.19 SSBM constructs.

The success of gene expression analysis by qPCR relies on choosing and correctly performing the appropriate preparation and data handling methods (473–475). Initially, sample preparation for RNA extraction was repeated with hFOB 1.19 SSBM constructs following the steps previously carried out (395) which used LN_2 to snap-freeze constructs, followed by grinding to a fine powder with a mortar and pestle. During this

process, it became evident that constructs thawed rapidly and required frequent refreezing with LN_2. Furthermore, substantial amounts of material were lost during the grinding process, with thawed material sticking to the surfaces of the mortar and pestle. Due to the high value of the hFOB 1.19 SSBM constructs, this approach was performed with very few repeats from 4-, 8- and 12-week culture periods (n=1, 1 and 4, respectively) and all returned low RNA yields [Figure 4.1 A.i-iv]. In terms of ease of use and RNA abundancy, it was concluded that extraction preparation by LN_2 was neither simple, nor efficient and that another method was required.

Other possible preparation approaches for RNA extraction included TRIzol solubilisation (488), pretreatment with collagenases (489) and rotor-stator homogenisers (490). The combination of needle aspiration and QIAshredders (with brief prior bead mill disruption), known here as the “needle” method, was identified as the safest, most time and cost effective, and simplest approach for disrupting and homogenising samples in preparation for RNA extraction. In comparison to the LN_2 method, using the 12-week culture samples due to the greater number of repeats [Figure 4.1 A.i], the needle method resulted in greater RNA yields after RNA extraction, although there were a small number of samples that resulted in a similar RNA yield to those using LN_2 preparation. This can be caused by any number of systemic (e.g., pipetting, contamination, user experience) or random errors (e.g., biological variation, subsampling) – reviewed by Taylor *et al*. (474). In order to reduce the risk of random errors, erroneous samples were measured twice using the nanodrop (to reduce the risk of subsampling errors), and RNA yields obtained from SSBM constructs created with the same cell batch and prepared with either LN2 or Needle were compared at the three time points [Figure 4.1 A.ii-iv]. Although statistical analysis was not possible,

results showed 14.8- (4-weeks), 8.2- (8-weeks) and 46.8-fold (12-weeks) increases in RNA yield when using the needle method, which strongly suggests that the lower values achieved in with the LN_2 method were not due to a bad hFOB 1.19 batch. Furthermore, RNA yields and purity were characterised over the prolonged culture period of hFOB 1.19 SSBM constructs, again using the needle disruption and homogenisation method, and showed a time dependent decline in both yield and purity, with expected variations at each time point [Figure 4.1 B.i-ii], although mean values were still within the acceptable boundaries for qPCR analysis [Section 2.3.4.2]. This further suggests that RNA yield and purity obtained by Iordachescu *et al*. (395) were likely to have been impacted upon by the longer culture period of 5-months and 1-year. See [Appendix 8.2] for all RNA yields and sample information.

During qPCR analysis, internal controls in the form of housekeeping genes are included for each sample being analysed, and for every qPCR run they are assessed, by normalising the expression of the other genes of interest to account for biological variations, such as tissue mass, cell numbers and RNA extraction efficiency (491). Housekeeping genes are those that are involved in ubiquitous and basic cellular functions (e.g., cell cycle regulation). To be useful as housekeeping genes, they must be constitutively and stably expressed across sample and treatments groups (492) and this can vary in different tissue types and different experimental treatments (493,494). To determine the most reliable housekeeping gene for qPCR analysis, the expression of two commonly used genes in qPCR analysis of osteoblastic cells, *B2M* and *GAPDH* was investigated. *B2M* and *GAPDH* were included within qPCR analyses of hFOB 1.19 SSBM constructs at each time point and their resultant Ct values compared [Figure 4.2 A.i-ii]. Both genes showed stable expression over the total culture period. However,

upon comparison between *B2M* and *GAPDH* [Figure 4.2 B] *GAPDH* showed variability spanning a greater range of measured mean Ct values, as well as a larger mean and median mean Ct value. Furthermore, between individual qPCR runs, *GAPDH* would fail more often (i.e., not meet acceptance criteria [Section 2.3.4.3]) where *B2M* would be unaffected (data not shown). *GAPDH* has shown to be a more unstable housekeeping gene and also easily affected in osteoblasts (495–497), and across other tissue types (473,498), although this is not to say that it isn't universally suitable (499). Therefore, it was necessary to ascertain its stability in hFOB 1.19 cells prior to qPCR analysis and as a result, *B2M* was found to be the more reliable housekeeping gene for hFOB 1.19 qPCR analysis.

4.5.2 The SSBM culture system supports long-term osteoblast differentiation and matrix maturation

During bone formation and osteoblast differentiation towards osteocytes, there are distinct and time-dependent changes in gene expression - Bonewald *et al*. (270) describes and reviews this. As such, genes that with more profound activity in osteoblasts were selected [Table 2.3] and categorised based on their notable roles: bone matrix maturation and mineralisation, osteoblast maturation and osteocyte maturation. Due to the multilineage differentiation potential of preosteoblastic cells, as well as previous reports of hFOB 1.19 cells being capable of chondrocytogenesis (420,422,429), *SOX9*, the gene encoding for the transcription factor, SOX9, that is essential to chondrocyte lineage commitment, was also assessed.

4.5.2.1 Matrix and mineralisation genes

Results from qPCR analysis of bone matrix and mineralisation genes [Figure 4.3] showed gene expression patterns in hFOB 1.19 SSBM constructs to be reminiscent of those reported *in vivo*.

Osteonectin and osteopontin, the respective protein products of *SPARC* and *SPP1*, are glycoproteins found within the bone matrix and are multifunctional proteins with important roles in regulating the collagen-mineral interface (262,264) as well as osteoblast and osteoclast adherence, migration and differentiation (500). Both arise later in bone formation (501,502), and although present at earlier time points, show significantly greater expression by 12-weeks of culture.

BGLAP is a late marker of bone expression (503,504) and is specifically expressed by osteoblasts (505). The protein product of *BGLAP*, osteocalcin, one of the major non-collagenous proteins in bone (1% of osteoid) (239,250). Measured here, expression significantly increases between 4- and 8-weeks of culture and despite another increase between 8- and 12-weeks, this was not statistically significant. This is most likely to have been caused by the large variations at 12-weeks, however it is possible that with longer culture (>12 weeks), a larger, more significant increase in expression would be detected. *In vivo*, increased expression of *BGLAP* coincides with decreased *ALPL* expression (260,503), and here qPCR results showed a plateau in *ALPL* expression at 8- to 12-weeks of culture although its expression was previously increasing, which may be indicative of a subsequent reduction. Thus, it is assumed prolonged culture of the hFOB 1.19 SSBM constructs will show a decline in *ALPL* expression along with an increased expression in *BGLAP*; mirroring the *in vivo* findings.

COL1A1 had a steadily high expression that was maintained over the entire culture period. This result for *COL1A1* suggests that, in the absence of any collagenases, collagen content increases over time, which was confirmed with the results obtained from PSR staining [Figure 3.9]. This pattern and level of *COL1A1* expression mirrors that seen during bone formation; arising early and having continuous expression throughout (504), not surprisingly as 94% of osteoid composition is collagen (506).

4.5.2.2 Osteoblast differentiation and bone remodelling genes

There was a mixed result for expression of genes relating to osteoblast differentiation when compared to those previously reported *in vivo* [Figure 4.4]. Expression of *BMP2* and *RUNX2* arise early in bone formation and are indicative of osteoblast differentiation and commitment (507). hFOB 1.19 SSBM culture showed that these markers had early expression and increased up to at least 12-weeks of culture, which is a strong indication that the culture system supports prolonged differentiation of hFOB 1.19 cells.

PHEX is expressed by osteoblasts and increases during osteocytogenesis, with promotional roles in mineralisation through degradation of osteopontin (508), and osteocytogenesis by inhibiting MEPE degradation, although is itself inhibited by sclerostin (509). However, with no detectable results for *SOST* (i.e., sclerostin) expression within the SSBM cultures (data not shown), it can be assumed *PHEX*-mediated mineralisation and differentiation is unaffected. *PHEX* is expressed consistently throughout the entire culture period, thus strengthening the evidence that the SSBM culture system promotes osteoblast differentiation over prolonged culture.

The expression of genes related to bone remodelling regulation, *TNFSF11* and *OPG*, (encoding for RANKL and OPG, respectively) *TNFSF11* expression decreased, while

OPG increased over time – although these trends were not found to be statistically significant over time individually. Mentioned previously [Section 1.2.2], the ratio between RANKL and OPG expression determines the whether the osteoblast activity is pro-resorptive (i.e., high RANKL:OPG) or pro-formation of bone (i.e., low RANKL:OPG). Unfortunately, as the OPG primer was purchased later in the project, the SSBM samples used were not analysed for *TNFSF11* expression (i.e., RANKL) at any time. Thus, the *TNFSF11:OPG* ratio cannot be calculated for individual constructs and then used to determine if a statistical change in the resorption/formation activity of osteoblasts occurs over the culture period. However, analysis of the RANKL:OPG ratio will be used in future investigations for a more in-depth analysis of osteoblast activity over time. Taking the trends in *TNFSF11* and *OPG* expression displayed here, a continual decrease in *TNSFS11* and increase in *OPG* expression [Figure 4.4 iv & v] signifies osteoblast activity over time within the hFOB 1.19 SSBM constructs progresses to a state of pro-formation of bone, although this has yet to be confirmed with statistical analysis.

4.5.2.3 Osteocytes and chondrocyte genes

No expression was detected for the mature osteocyte-specific genes (raw Ct readings were not given or were >35). However, *PDPN* - the gene encoding for Podoplanin – significantly increased over the total culture period [Figure 4.5 i]. Podoplanin is the earliest known marker of osteocytes (270,276,510) which is essential for the development of the osteocyte dendrites, as well as regulating osteocytic bone remodelling activity (275–277). Thus suggesting that after 12-weeks of culture, there was an increasing proportion of cells at the cusp of entering osteocytogenesis.

Assessing the expression of *SOX9* [Figure 4.5 ii] to provide an indication of potential chondrocytogenesis, revealed that whilst expression was present across all time points and showed an increasing trend over time, this was not significant. Although hFOB 1.19 cells have displayed multilineage capabilities, chondrocytes have shown to not be terminally differentiated and are capable of osteocytogenesis during bone formation and repair (511). As the basic concept of the SSBM model was based on recreation of the fracture callus, the presence of *PDPN*, *SOX9* and osteoblast-specific gene expression demonstrates that the SSBM culture system is an accurate reflection of the fracture callus, which *in vivo* contains a mixed cell population of osteoblasts, chondrocytes and osteocytes.

4.5.2.4 2D vs 3D gene expression

qPCR analysis of hFOB 1.19 cells cultured under 2D conditions for a prolonged period was carried out to compare gene expression between the two culture conditions. Many of the genes investigated showed expression pattern to those of the SSBM cultures, or SSBM cultures had greater and significant expression at 4-weeks, only for 2D cultures to match 3D expression at 8-weeks of culture [Appendix 8.2]. The remaining genes will be discussed here.

Expression of *PHEX* in 2D cultures ceased between 4- to 8-weeks of culture and *BMP2* expression was consistently low, with no change over time [Figure 4.6]. Without the expression of these genes, long-term promotion of osteoblast differentiation and *PHEX*-mediated mineralisation is compromised, as well as osteocytogenesis.

SOX9 expression, like *PHEX*, ceases between 4- and 8-weeks of culture in both 2D and 3D [Figure 4.7 B], and assuming this is true, may be indicative of a culture environment unsuitable for chondrocyte survival and differentiation.

In terms of matrix and mineralisation genes, *SPARC* (gene encoding osteonectin) expression was the only gene that showed significant difference in expression pattern in comparison to 3D; 2D showed a possible decline in expression after 8-weeks of expression [Figure 4.7 A]. A reduction in osteonectin further compromises bone formation and osteoblast differentiation, as demonstrated *in vivo* in SPARC-KO mice (264).

Finally, cells cultured in 2D showed a significant increase in expression of both *TNFSF11* and *OPG* (i.e., RANKL and OPG, respectively) [Figure 4.8], which contradicts the indirect relationship that occurs *in vivo,* as well as within the SSBM cultures. This finding indicates that the 2D cell culture environment favours neither bone formation nor bone resorption and as such highlights the limitations of using 2D *in vitro* cultures as research platforms, particularly where bone remodelling is the primary focus. It is this lack of an *in vitro* bone remodelling system that drives reliance and use on *in vivo* models.

Overall, qPCR analysis of hFOB 1.19 SSBM constructs has revealed that the 3D culture system supports the formation of new bone matrix and its subsequent mineralisation, as well as long-term osteoblast differentiation. Although there was no detection of mature osteocyte markers, the expression of a specific set of osteoblast markers - *BGLAP*, *COL1A1, PHEX* and *SPP1* – which demonstrate the presence of mature osteoblasts with potential to become osteocytes (512), are present within the

SSBM cultures at 12-weeks of culture. Therefore, we conclude that the 3D culture system provides the appropriate and adequate conditions to differentiate cells to the point of osteocytogenesis and support their prolonged survival *in vitro*.

4.5.3 Enzyme-linked immunosorbent assays quantified the presence of soluble markers over prolonged culture of hFOB 1.19 constructs

Expression of genes does not signify successful translation of the RNA to produce the protein product. As well as analysis at the genetic level, findings must also be confirmed at the protein level using other analytical methods.

The conditioned media of these culture systems provides another source of readouts that can be used for biological characterisation, using non-destructive and efficient methods. Enzyme-linked immunosorbent assays (ELISA) are one of the most accessible, simple and versatile approaches for detecting and quantifying soluble analytes in biological samples; this includes antigens, peptides, proteins and antibodies within serum, plasma, blood, cell lysates and conditioned media samples (513). The basic principle of ELISA takes advantage of the high affinity and specificity antibodies have for their antigens, to create complexes that can then be used to accurately measure the presence and/or quantity of the antigen present within a sample (514). There are many different types of ELISA (e.g., direct, indirect, competitive), however, in the case of this project (i.e., for the detection of analytes in conditioned media), sandwich ELISAs offer the best approach in terms of sensitivity and specificity (515). Typically, sandwich ELISAs use secondary antibodies conjugated with an enzymatic probe (e.g., Horseradish peroxidase) that is cleaved to produce a colour change; the intensity of which directly correlates with the amount of antigen present (516,517).

One of the major drawbacks of analysing the conditioned media of hFOB 1.19 SSBM constructs was the presence of cells on the elastomer outside of the SSBM matrix [Figure 4.9 A]. As these cells were not growing within the SSBM system, they represent a distinct subpopulation, growing under 2D conditions, that contaminate the media they were sharing with the SSBM cell populations, rendering it unsuitable for analysis. Preventative measures were attempted to reduce this cell adherence, such as coating the well and elastomer surfaces prior to construct set up with Pluronic F68 – a non-ionic and non-cytotoxic surfactant used to reduce cell attachment in microfluidic devices (518). However, this was found to affect fibrinogenesis and fibrin contraction. Regular trypsinisation of the elastomer base was found to be most effective, but only up to 4-weeks of SSBM culture where regular trypsin-EDTA treatments resulted in the inability of SSBM constructs to mineralise. To resolve this, constructs were removed, intact, from their original wells and be placed in a fresh well with naïve media. Conditioned media was collected from these constructs over 3-days. To retain the shape, consequential strain and maintain the same level of passive perfusion, a thin strip of elastomer holding the anchors in position was dissected out of the wells and remained with the construct.

Upon moving the constructs, it was predicted that the collected conditioned media would have a reduced concentration of the analyte compared to that within the conditioned media collected before construct isolation., at each timepoint, due to a reduction in cell number. Furthermore, this measure also risked the analyte concentration being below the range of detection and resulting in a false-negative conclusion. P1NP analysis by ELISA [Figure 4.9 B] showed that although the concentration of P1NP decreased significantly after construct isolation (with the

exception of the 12-week culture period) as predicted, the concentration was still within the range of detection.

Individual analysis of P1NP concentrations in media samples collected before and after isolation over the culture period [Figure 4.9 C.i-ii] showed that there was a significant difference in concentration pattern between the two conditions; before isolation, the concentration of P1NP declines over time, whilst after isolation, no overall change was calculated. Variation in results have a lot to answer for, nonetheless, these results strongly suggest that cells attached to the elastomer will negatively affect analytical measurements and overall assumptions, thus isolation of constructs prior to analysis was necessary.

P1NP and ALP concentrations are used clinically as markers of bone turnover (519,520); higher concentrations of P1NP and/or ALP are indicative of greater bone formation activity. As previously discussed, the mean P1NP concentration in conditioned media from isolated hFOB 1.19 SSBM constructs declines over the culture period, although this has shown to not be a significant change due to the minimum number of repeats and large variation in the results between those repeats [Figure 4.9 C.ii]. If this decline were found to be true, these results suggest that there were lower bone formation rates at the later stages of culture. However, this is not an indication that the culture system has limited support in matrix deposition, as structural analysis showed continual production and maturation of the matrix. Rather, it is indicative of a transition of the osteoblasts from a bone formation status to a more mature differentiation stage at the beginning of osteocytogenesis. Another possibility is that the P1NP ELISA kit used detected only one of the two isoforms (i.e., trimeric and monomeric) that P1NP exists in; the trimeric form is temperature sensitive and has

shown to transition to the monomeric form when incubated at 37 °C (521). ALP activity also showed a decline in activity over time [Figure 4.10 ii], which coincides with the P1NP ELISA results, however this contradicts the qPCR results which showed a significantly increased *ALPL* expression [Figure 4.3 i]. This is a clear example where gene expression does not equate to the amount of protein present and it can be a result of any number of causes, such as upregulation of post-translational modifications, delayed or saturation of the free enzyme. Although, it has also been noted previously that the pNPP-based assay used here [Section 2.3.2.4] is affected by culture media pH, with more acidic pH values lowering ALP activity (522,523).

The concentration of OPG measured [Figure 4.10 i] was a close reflection of the qPCR results for *OPG* expression [Figure 4.4]; an increase in concentration/expression over the whole culture period measured, but statistical significance was not achieved due to a lower number of repeats with great variation at the 12-week timepoint. Despite this, it can be confirmed that the assessment of OPG production by cells within the hFOB 1.19 SSBM constructs at the protein level over time reflected the results obtained from assessment of OPG at the genetic level, which assumed the SSBM culture system had growing favouritism for bone formation with prolonged culture.

Like qPCR analysis, conditioned media collected from long-term 2D hFOB 1.19 culture was assessed by ELISA and compared against the findings of the SSBM cultured media, again only after 4- and 8-weeks of culture. P1NP concentration in 2D cultured media showed the same trend as that found in 3D, although mean concentrations at both 4- and 8-weeks were greater in 2D media [Figure 4.11 A]. This was expected as 2D cell cultures did not require an isolation period prior to the analytical timepoint, thus media was a measure from greater cell numbers and media that was not completely

refreshed prior to collection, thus resulting in a greater concentration of analyte. However, ALP activity measured in the 2D conditioned media [Figure 4.11 B] whilst decreasing over time (like that seen in 3D, but over a longer culture period) was lower than the 3D culture conditions. This could also have been caused by a lower pH in the culture period; with sampling from a potentially larger cell population, the accumulation of waste and higher metabolic activity would drive the pH of the culture media towards acidic conditions, thus rendering the enzymatic activity of ALP. These ELISA results together further indicate that the 2D culture system does not support the long-term culture of osteoblasts, or recapitulation of the bone matrix *in vitro*.

4.5.4 IF approaches were used to confirm the presence of insoluble markers and assess cell viability

Visualising hFOB 1.19 cell orientation within the SSBM construct was achieved by whole-mount staining of intact constructs, using a method previously developed in the Healthcare Technologies Institute labs for staining collagen gels. This enabled further confirmation that findings from Iordachescu *et al*. (395) were also found in hFOB 1.19 SSBM constructs; cells were aligned in parallel to each other, elongated and pulled in the direction towards the two CaP anchors, resulting in an in-built strain. This staining approach required large volumes of reagents, was not efficient in the use of SSBM constructs (i.e., one whole construct per analyte) and the images produced were not high-resolution due to the density of the cellular staining and construct thickness, which impacted on thorough analysis.

There have been long-standing difficulties with immunofluorescence (IF) staining of bone and bone-like samples due to the nature of bone tissue. A protocol developed by Kusumbe *et al*. (399) enabled preparation of mouse bone tissue for high-resolution

confocal imaging, improved antigen retrieval and analysis of bone vasculature. This method was repeated successfully by individuals within the Naylor group using mouse tissue and provided a starting point for optimisation for SSBM construct IF imaging. The steps outlined in [Section 2.3.5] include the adaptions made to the original protocol, the most notable of which is an increased incubation period of the constructs within the embedding solution at a lower temperature due to a heightened fragility when in comparison to mouse bone tissue. Using this adapted protocol led to successful sectioning and IF staining of hFOB 1.19 SSBM constructs. qPCR results showed a very significant increase in *PDPN* expression between each analytical time point of the 12-week culture period [Figure 4.5 i]. Results from IF staining for PDPN showed notably increased positive PDPN staining between each time point, as exemplified in the images retrieved in [Figure 4.13]. As well as successfully adapting the protocol for efficient and accurate IF preparation, staining and analysis of hFOB 1.19 SSBM constructs, PDPN staining confirms the assumptions made from the qPCR results at the protein level; that there is an increase in PDPN expression and presence over time, providing further evidence that the SSBM culture system supports differentiation of osteoblasts towards osteocytogenesis. Due to the time constraints of this project, no further proteins were analysed using this method, but the positive and striking PDPN result provides evidence of the validity of using this approach in future for other markers.

Many methods used to assess cell viability, such as MTT assay (524) and Calcein AM (525), were viewed as unsuitable for analysis of cell viability within the SSBM constructs, primarily due to being an endpoint analytical approach, often requiring cell lysis and/or protein digestion, which limits further analysis of SSBM constructs (i.e.,

destruction of SSBM constructs impacts on efficient analytical potential). AlamarBlue offers a non-toxic solution to measuring cell viability (526), however, as the analyte is secreted into the media, constructs must be isolated repeatedly to prevent the accumulation of cells external to the SSBM construct, which may impact on cell viability. This requires long-term investigations prior to using alamarBlue routinely and furthermore, this added measure of continual moving of constructs adds to the labour intensity of the method; adding more complexity. An IF approach (the ReadyProbes™ Cell Viability Imaging Kit [Section 2.3.3]) was found to permeate through the SSBM matrix and provide a fast and simple approach to measuring cell viability. The density of the cell population within the SSBM constructs allowed for easy distinction from those accumulating out with the construct matrix. However, due to the presence of increasing mineral content between 8- and 12-weeks of culture, reliable analysis was only possible at 4- and 8-weeks of culture [Appendix 8.2]. Results showed [Figure 4.14] that between the two time points, there was no significant change in cell number, death or viability, which was expected as constructs were incubated under osteogenic conditions and had previously shown similar results [Figure 3.5]. It was noted that the measured %viability at both time points was low, however was not unexpected as one of the limitations of 3D cell culture is the inability to remove dead cells from the matrix (527). In future studies using the SSBM model, further investigation into measuring viability through metabolic output-based assays is required.

4.5.5 Conclusions

The overall aims of this chapter were to adapt, develop and optimise analytical approaches for biological assessment of hFOB 1.19 SSBM constructs for up to 12-weeks of culture. Here, the methods described have been optimised specifically for

these constructs and characterised in hFOB 1.19 cells cultured under 2D conditions, at time points of up to 12-weeks of culture at the gene transcription and translation level.

The main findings from this chapter are that the SSBM culture system supports long-term hFOB 1.19 cell differentiation, cell viability, and activity (up to 12-weeks), which is not possible in 2D culture. Furthermore, outcomes from biological analysis of markers relating to matrix development and mineralisation aligned with results found from structural analysis of the hFOB 1.19 SSBM constructs.

The main outcomes that has resulted from this chapter was that the optimised analytical methods were able to be used for the detection of changes at the genetic and protein level when investigating the responsivity potential of the SSBM construct cultures in the presence of known BFMs. The second outcome was the characterisation of the expected expression profile and activity of the hFOB 1.19 SSBM constructs over time under normal SSBM culture conditions can be used as a control when comparing the responses of the constructs to these BFMs. Finally, optimisation of analytical approaches and characterisation of the hFOB 1.19 SSBM constructs has simplified, whilst improving, the accuracy of the analysis of this culture system whilst, thus making it more accessible and a more attractive approach for other research groups.

Chapter 5

Exploring the feasibility of hFOB 1.19 SSBM as a screening and assayable platform

5.1 Introduction

As discussed previously in chapter 4, “Biological characterisation of hFOB 1.19 SSBM constructs”, in order to create a novel bone drug research platform using the SSBM approach, there were three questions that must be addressed first:

1. How can responsivity to bone formation modulators (BFM) be measured in the SSBM?
2. What are the baseline model characteristics against which responsivity is assessed?
3. Are SSBM constructs responsive to known BFMs?

Chapter 4 of this thesis addressed questions 1 and 2 by developing and adapting a range of analytical approaches specifically for SSBM constructs, using those approaches to characterise their development over time and establishing expected biological and structural outputs under osteogenic culture conditions. This chapter addresses the final question remaining, determining the responsivity of SSBM constructs.

The mechanism of action of the majority of bone therapeutics available is to inhibit bone catabolism. This is achieved by directly (e.g., Bisphosphonates) or indirectly (e.g., Denosumab) reducing osteoclast activity or differentiation to reduce resorption. These drugs lack bone anabolic activity, which limited the number of substances that could be used to assess SSBM construct responsivity capabilities, given the absence of osteoclasts within the current SSBM culture system. However, three BFMs, with evidence of direct action on osteoblast differentiation and/or activity were identified; Vitamin D (Vit D), Parathyroid hormone Fragment 1-34 human (PTH) and Betulin.

5.1.1 Vitamin D

Vit D are a group of fat-soluble seco-sterols (i.e., steroids with an open ring) with many essential roles for maintaining cardiovascular and bone health, as well as immunity (528). Vit D_2 (i.e., Ergocalciferol) and Vit D_3 (i.e., Cholecalciferol) are the two major forms, can be obtained through fortified foods and dietary supplements, although the majority of Vit D in the form of cholecalciferol (~90%) (529), is synthesised by photochemical conversion of 7-dehydrocholesterol in the skin when exposed to solar ultraviolet-B radiation. Vit D is metabolised by CYP enzymes to its active form, 25-hydroxyvitamin D (i.e., Calcitriol), which is upregulated by PTH (530) and inhibited by FGF23 (531,532); a growth factor primarily expressed by osteocytes. Ergocalciferol and cholecalciferol share a metabolic pathway and their specific roles depends on the organ system in question; however in terms of raising serum calcitriol levels, cholecalciferol has been found to be more efficacious (533–535).

The beneficial properties of Vit D on bone health have long been known; with a lack of Vit D from little sunlight exposure and/or poor nutrition causing bone deformities such as rickets (osteomalacia in adults) (528,536) and Vit D supplementation through cod liver oil to restore and maintain good bone health being recorded as early as the 1700s (537) – although elucidation of the responsible compounds wasn't until the 1900s. The beneficial actions of active Vit D, calcitriol on bone occur directly: osteoblasts express nuclear Vit D receptors and their activation in human and rat osteoblasts results in increased expression of genes relating to osteoblast differentiation, and bone matrix formation and maturation (538). And indirectly: calcitriol is one of the main regulators of calcium and phosphorous homeostasis by activating intestinal absorption of calcium

and phosphorous, along with stimulating osteoclast-mediated bone resorption and increasing renal reabsorption which also requires PTH (539).

Due to the direct effects of Vit D on osteoblast differentiation and matrix formation, as well as previous experimental work by Harris *et al.* (375) demonstrating the positive effects of Vit D supplementation on hFOB 1.19 cell ALP activity, Vit D was selected as one of the BFMs to examine the responsivity of hFOB 1.19 SSBM cultures. The intention was to use the active form of Vit D, calcitriol, for this investigation, however the inactive form of Vit D, cholecalciferol, was mistakenly used, rather than the active form. Repetition of this investigation would ensure that calcitriol is used, with appropriate titration analysis carried out prior to determine the new treatment concentration and duration.

5.1.2 Parathyroid hormone

PTH is a polypeptide; endogenously synthesised and activated by chief cells of the parathyroid gland. The primary role of PTH is to regulate serum calcium levels; activation and release of PTH occurs rapidly (within seconds) in response to low serum calcium concentration (120). It acts directly and indirectly within the kidney, intestine and bones to restore it to physiological levels. Briefly, within the kidney, PTH increases the reabsorption of calcium as well as reducing phosphate reabsorption to prevent insoluble salt formation with calcium (540). Within the intestine, PTH stimulates the synthesis of calcitriol, as discussed previously [Section 5.1.3].

Regarding its role within bone health and metabolism, PTH is a double-edged sword. When restoring serum calcium levels, prolonged PTH activity indirectly stimulates osteoclast recruitment, activation and resorption (thus releasing the stored calcium) by downregulating osteoblast OPG expression and upregulating osteoblast RANKL (541).

However, intermittent PTH activity has an anabolic effect on bone by promoting preosteoblast proliferation and differentiation (542), and inhibiting osteoblast apoptosis (543), then also indirectly through stimulation of calcitriol synthesis.

Synthetic PTH – known as Teriparatide (i.e., PTH 1-34) – is given as a daily injection at low doses in the treatment of osteoporosis (544,545) [Section 1.3]. However, due to its catabolic effect on bones, and an associated increased risk of osteosarcoma identified in rats, teriparatide can only be given for a maximum of 2 years (546–548). Nonetheless, due to its anabolic effects on osteoblasts and previous work carried out by Harris *et al*. (375) demonstrating a rise in bone formation promoter, cyclic-AMP, concentration following treatment, PTH is another obvious candidate to test hFOB 1.19 SSBM construct responsivity to BMFs.

5.1.3 Betulin

Betulin is a pentacyclic triterpene which can be extracted from over 200 plant species, although the greatest source are members of the Birch tree family - *Betula*, Betulaceae – (549) where Betulin accounts for ~34% of its dry weight (550). Isolation of Betulin and its derivatives dates back as early as the 1700s (549) and was traditional used in the treatment of a number of common ailments, including arthritis, gout, parasitic worms and baldness. The potential medicinal benefits of Betulin and its derivatives has expanded, showing *in vitro* and *in vivo* pharmacological responses as a potential anti-cancer (551), anti-inflammatory (552), anti-viral (553), anti-diabetic (554) and burn wound healing agent (555), amongst others.

Recently, Betulin and Betulinic acid have shown potential as candidates for treatment of osteoporosis through their inhibitory actions on RANKL-induced osteoclastogenesis,

via attenuation of downstream signalling upon RANK-RANKL binding and production of reactive oxygen species, which together downregulate osteoclast differentiation (556,557) to reduce resorption in ovariectomised rat models (558). Mizerska-Kowalska *et al.* (400) investigated the response of hFOB 1.19 to Betulin *in vitro* and additionally found an increase in osteoblast differentiation, osteoinductive activity and increased mineral production. These data indicate that Betulin possesses bone anabolic activity as well as inhibitory action on resorption. The next obvious step is to test hFOB 1.19 3D culture responses to Betulin treatment, therefore Betulin was chosen as the third BFM in the SSBM responsivity investigations.

5.1.4 Chapter aims and approaches

The overall aim of this chapter was to determine the feasibility of creating an assayable *in vitro* bone model using the hFOB 1.19 SSBM method developed – and discussed over chapters 3 and 4 of this thesis. This was achieved by treating 4, 8- and 12-week cultured hFOB 1.19 SSBM constructs with the BFMs discussed above, then measuring their biological outputs against the established non-treated outputs using the same analytical methods developed in chapter 4.

Once SSBM responsivity to BFMs was established, further adaptions to the size of the SSBM culture system would be necessary to create an assayable platform. SSBM constructs are large structures (i.e., 15 mm long) making them costly (i.e., large reagent volumes and consumable usage), impractical (i.e., incubation space, time consuming maintenance) and therefore undesirable. Therefore, miniaturising the SSBM constructs without compromising on their biological or structural integrity is necessary for assay optimisation. Bioprinting offers a solution.

Bioprinting is an automated manufacturing platform combining biomaterials science with 3D printing to create bespoke, biocompatible structures. Bioprinting techniques have been used previously to create small structures (<1 mm thickness), such as blood vessels (559) with repeated accuracy, precision and success. The use of bioprinting to create SSBM constructs introduces another level of homogeneity by eliminating possible human error and variability during construct set up. Therefore, another aim of this chapter was to use bioprinting to determine whether miniaturised SSBM fibrin matrices containing hFOB 1.19 cells could polymerise and form in an additive manufacturing system developed at the University of Birmingham - Suspended Layer Additive Manufacturing (SLAM) (560).

5.2 Vitamin D

5.2.1 2D investigations

Using data obtained by Harris *et al*. (375), as well as through preliminary investigations using hFOB 1.19 SSBM constructs [Appendix 8.3], the treatment concentration (i.e., $5x10^{-7}$ M) and duration (i.e., 1-week) was used for all of the following Vit D investigations.

Potential effects by exposure to $5x10^{-7}$ M Vit D, or its vehicle, ethanol (EtOH) were assessed by monitoring hFOB 1.19 cell proliferation and viability after the 1-week treatment period in 2D, under osteogenic culture conditions. Results showed that neither the vehicle control (VC) or Vit D affected hFOB 1.19 proliferation [Figure 5.1 A]. However, the VC showed a significant increase in cell viability (respectively, 22.9±1.8%; p=0.002), but no significance found between the VC and Vit D (p=0.89) [Figure 5.1 B].

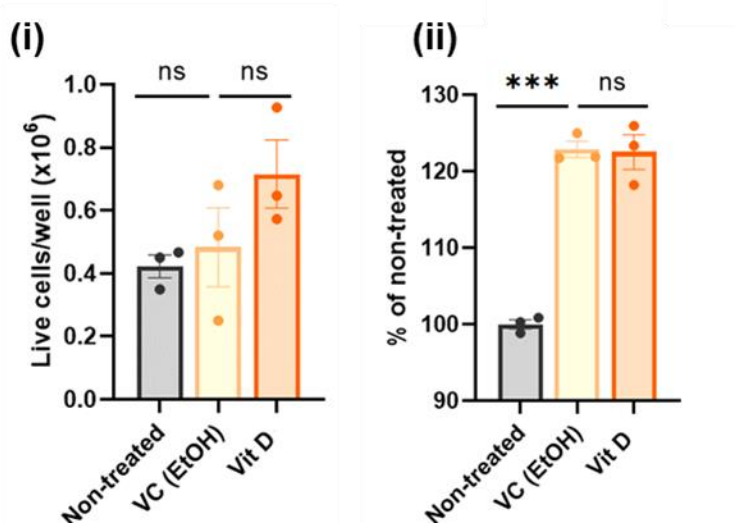


Figure 5.1 - Cell count and viability assessment of hFOB 1.19 cells cultured in 2D with Vitamin D (Vit D) treatment. Live cell counts **(i)** and %viability **(ii)** was assessed for hFOB 1.19 cells cultured with $5x10^{-7}$ M Vit D, or vehicle control (VC)(ethanol (EtOH)), as well as non-treated, for 1 week in 2D. Results are Mean % of non-treated±SD (n=3) and analysed using unpaired t-test, with Welch correction if SD ratio = >2. Multiple comparison results shown. ** = p<0.01; *** = p<0.001; ns = no significance.

To gain an insight into if and how hFOB 1.19 cells respond to Vit D at the gene expression level, qPCR was used to analyse gene expression of hFOB 1.19 cells treated for 1-week with $5x10^{-7}$ M Vit D, or its vehicle, EtOH, under osteogenic conditions in 2D. Refer to Table 2.3 for gene and TaqMan primer information. B2M was used as the housekeeper gene for the following qPCR analysis.

Briefly, results for genes associated with matrix formation, and its subsequent mineralisation [Figure 5.2 A], in this case *ALPL, COL1A1* and *SPARC*, showed no significant changes in expression when treated with the VC or Vit D, except for *ALPL*, where Vit D treatment showed a slight increase in expression, in comparison to the VC (VC vs Vit D: 0.008 vs 0.015; p=0.021) [Figure 5.2 A.i]. As with the matrix formation and mineralisation-associated genes, *SOX9* (i.e., chondrocyte lineage commitment) also showed no change in expression after Vit D or VC treatment [Figure 5.2 B].

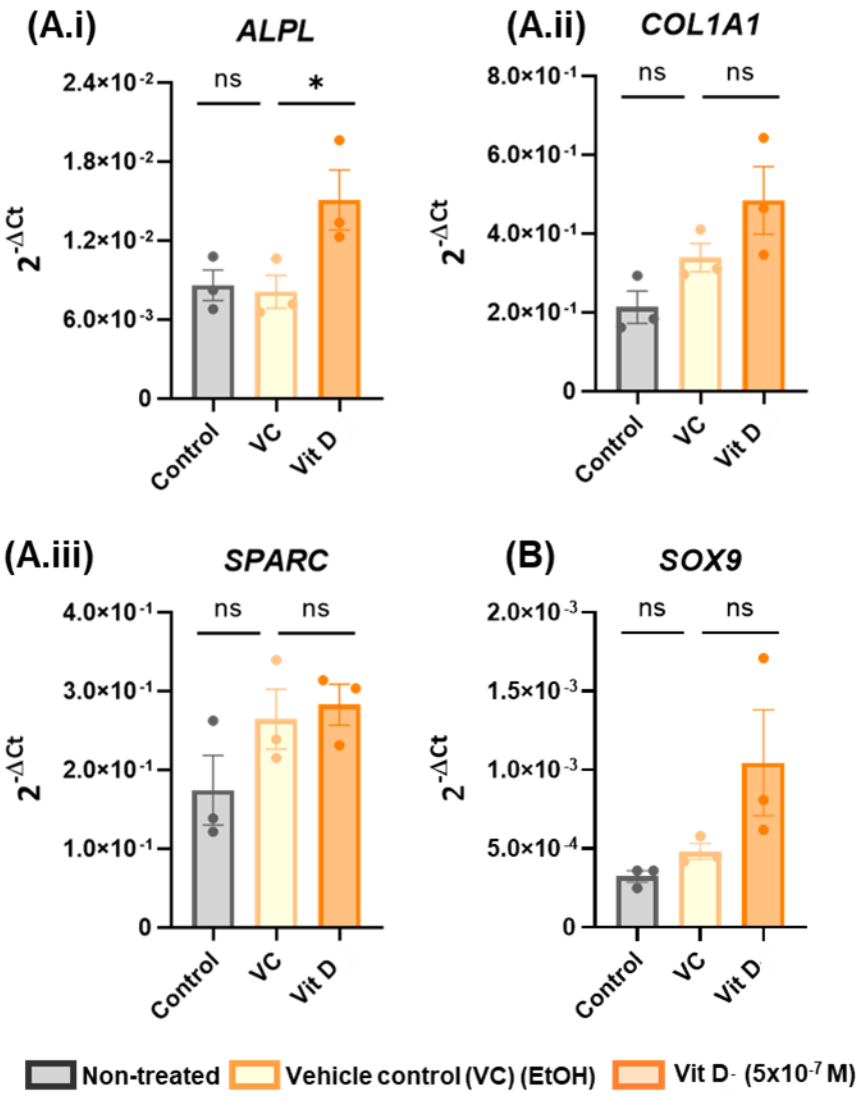


Figure 5.2 - qPCR analysis of matrix and mineralisation, and chondrocyte related gene expression for 2D hFOB 1.19 treatment with Vit D. The expression of genes relating to matrix and mineral formation and maturation (A) and chondrocyte lineage commitment (B) was assessed in hFOB 1.19 cells cultured for 1-week with $5x10^{-7}$ M Vit D, vehicle control (VC) (EtOH), and non-treated. Results are mean±SEM (n=3). Raw Ct values analysed using unpaired t-test, with Welch correction if SD ratio = >2. * = $p<0.05$; ns = no significance.

Osteoblast genes that are associated with the lineage commitment (i.e., *RUNX2*) and their differentiation (i.e., *PHEX*) [Figure 5.3 A], showed a reduced expression in response to Vit D in comparison to the VC (VC vs Vit D: $5.0x10^{-3}$ vs $2.0x10^{-3}$; p=0.027) and in response to the VC in comparison to the non-treated (non-treat. vs VC: $42.6x10^{-3}$ vs $6.3x10^{-5}$; p=0.007). The genes that encodes for a key regulator of bone resorption,

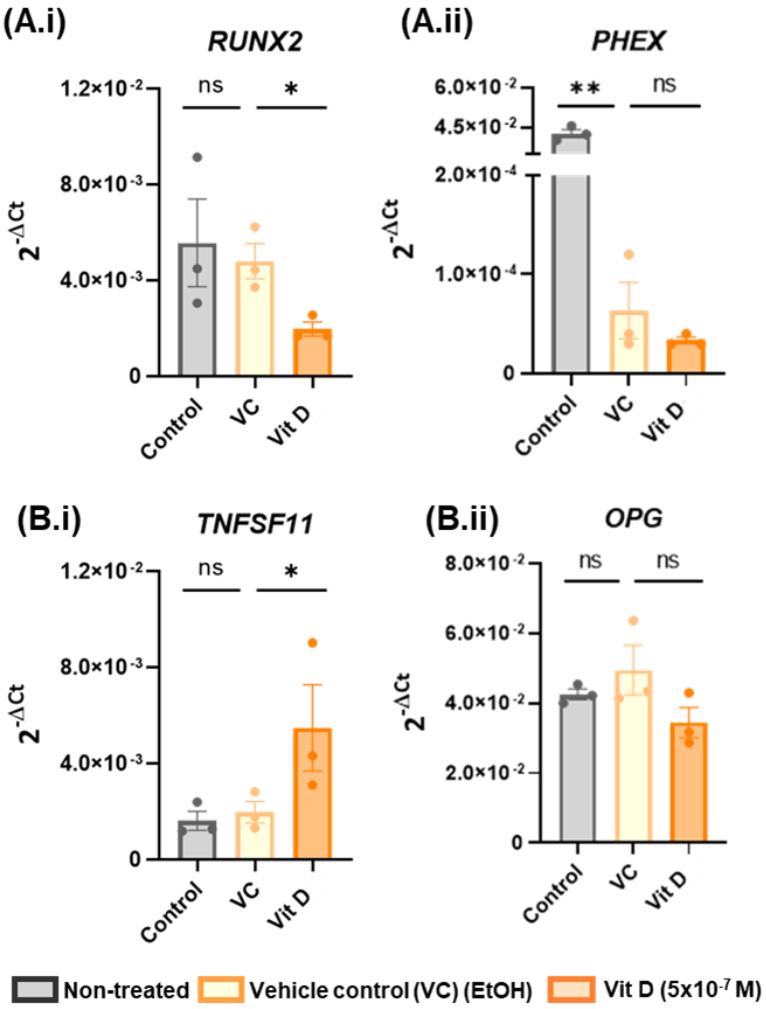


Figure 5.3 - qPCR analysis of osteoblast-specific gene expression for 2D hFOB 1.19 treatment with Vit D. The expression of genes relating to osteoblast differentiation **(A)** and bone resorption and formation regulation **(B)** was assessed in hFOB 1.19 cells cultured for 1-week with $5x10^{-7}$ M Vit D, vehicle control (VC) (EtOH), and non-treated. Results are mean±SEM (n=3). Raw Ct values analysed using unpaired t-test, with Welch correction if SD ratio = >2. * = $p<0.05$; ** = $p<0.01$; ns = no significance.

RANKL (*TNFSF11*), showed increased expression with Vit D in comparison to the VC (VC vs Vit D: $2.0x10^{-3}$ vs $5.5x10^{-3}$; p=0.037) [Figure 5.3 B.i]. However, for the gene that encodes for a key regulator of bone formation, *OPG*, no significant change occurred with either VC or Vit D treatment [Figure 5.3 B.ii].

There were four genes analysed whose expression was undetectable once treated with Vit D or its VC [Figure 5.4]. *BMP2* showed no detectable expression once treated

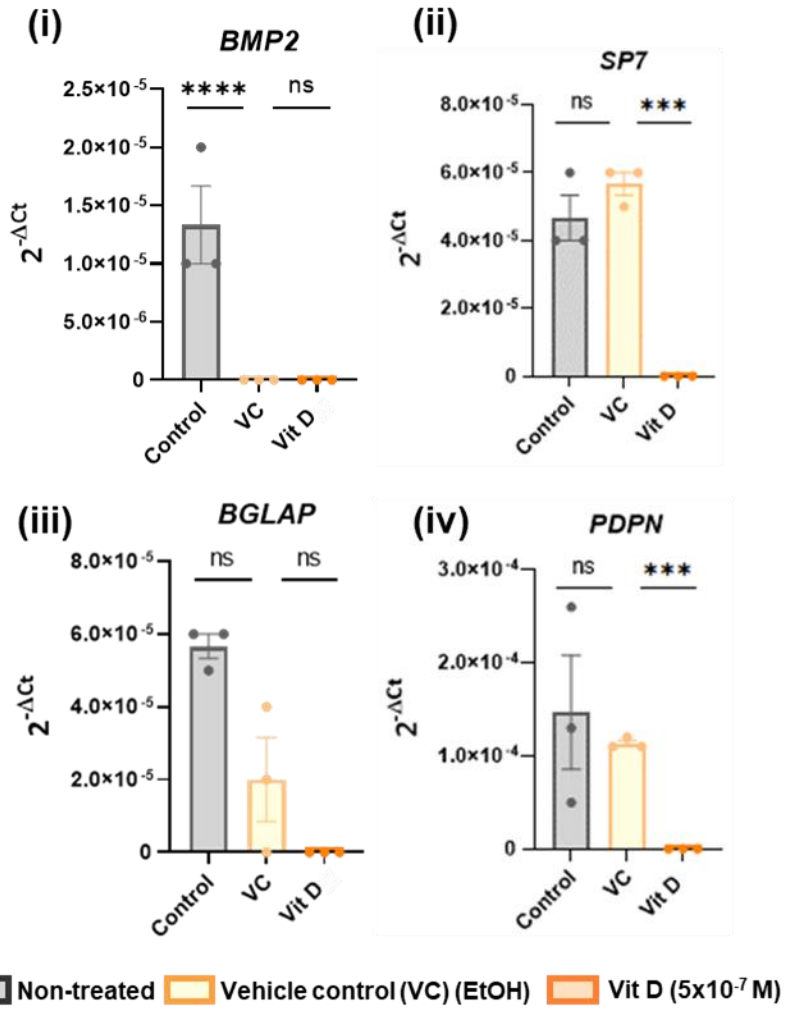


Figure 5.4 - Vit D and VC had an inhibitory effect on the expression of certain osteoblast and osteocyte-specific genes in 2D hFOB 1.19 cells. The expression of genes specific to osteoblasts (i-iii) and osteocytes (iv) was assessed in hFOB 1.19 cells cultured for 1-week with $5x10^{-7}$ M Vit D, vehicle control (VC) (EtOH), and non-treated, which showed an inhibitory effect by Vit D and the VC. Results are mean±SEM (n=3). Raw Ct values analysed using unpaired t-test, with Welch correction if SD ratio = >2. *** = p<0.001; **** = p<0.0001; ns = no significance.

with the VC and Vit D in comparison to non-treated. *SP7* expression was not detectable after Vit D treatment, but not with the VC, which was similar to that of the non-treated cells. Similar was seen with *BGLAP* analysis, which showed a reduced expression in the presence of the vehicle – although not statistically significant to the non-treated cells – and no expression after Vit D treatment. The only osteocyte-specific gene analysed to show expression for non-treated cells, *PDPN*, showed no expression after

Vit D treatment, although was unaffected in the presence in the VC treated cells in comparison to non-treated (non-treat. vs VC: $1.5x10^{-4}$ vs $1.1x10^{-4}$; p=0.93).

5.2.2 SSBM Vit D treatment: qPCR analysis

qPCR was used to analyse gene expression of hFOB 1.19 SSBM constructs after 4-, 8- and 12-weeks of culture under osteogenic conditions, then treated for 1-week with $5x10^{-7}$ M Vit D, which were compared against the data previously attained for hFOB 1.19 SSBM constructs not treated – refer to [Section 4.2]. Refer to [Table 2.3] for gene and TaqMan primer information. B2M was used as the housekeeper gene for the following qPCR analysis.

There were three genes related to matrix formation and mineralisation which showed a significant change in expression after Vit D treatment in comparison to non-treated constructs at one or more analytical time points [Figure 5.5 A]. *ALPL* expression was significantly increased after Vit D treatment for 4-week SSBM cultures (Non-treat. vs Vit D: $6.4x10^{-4}$ vs $19.8x10^{-4}$; p=0.041), however was not significantly affected at any other time point. Similarly, *SPARC* expression was only significantly increased after Vit D treatment with 8-week SSBM constructs (Non-treat. vs Vit D: 0.11 vs 0.33; p=0.01) and was unaffected when SSBM constructs cultured for 4- and 12-weeks previously were treated. BGLAP on the other hand, showed increased expression after Vit D treatment at all analytical time points (4-, 8- and 12-weeks, respectively: $7.1x10^{-6}$ vs $83.3x10^{-6}$; p=0.012. $2.7x10^{-5}$ vs $11.0x10^{-5}$; p=0.052. $5.1x10^{-5}$ vs $30.7x10^{-5}$; p=0.033). Analysis of chondrocyte lineage commitment through SOX9 expression after Vit D treatment [Figure 5.5 B] showed increased expression at all analytical time points, although was only statistically significant for hFOB 1.19 SSBM constructs cultured after 12-weeks (Non-treat. vs Vit D: $1.5x10^{-4}$ vs $13.8x10^{-4}$; p=0.039).

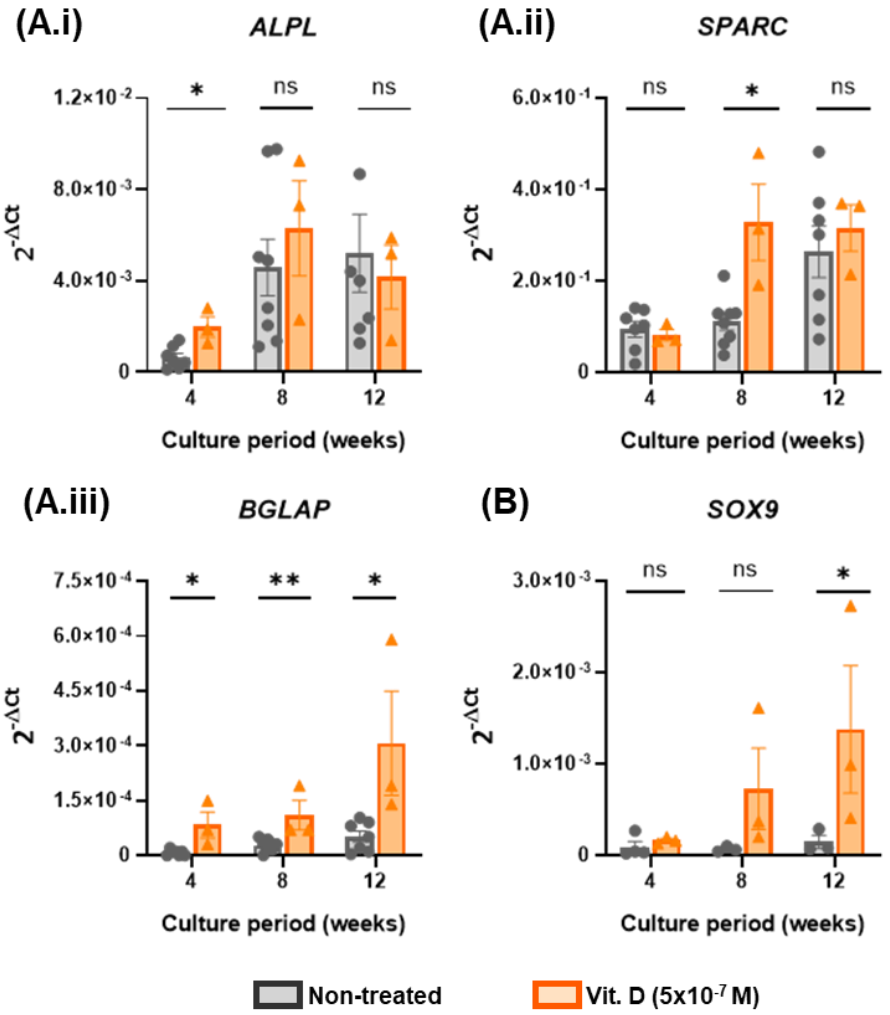


Figure 5.5 - qPCR analysis of matrix and mineralisation, and chondrocyte related gene expression for hFOB 1.19 SSBM construct treatment with Vit D. The expression of genes relating to matrix and mineral formation and maturation **(A)** and chondrocyte lineage commitment **(B)** was assessed in hFOB 1.19 cells cultured in 3D after 4-, 8- and 12-weeks, then treated for 1-week under osteogenic conditions with $5x10^{-7}$ M Vit D and compared against those not treated. Results are mean±SEM (n=3(treatment), 6-8(non-treated)). Raw Ct values analysed using unpaired t-test, with Welch correction if SD ratio = >2. * = p<0.05; ** = p<0.01; ns = no significance.

There were two genes related to osteoblast commitment and differentiation that showed a significant change in expression after Vit D treatment, in comparison to non-treated constructs, at one or more analytical time points [Figure 5.6 A]. *RUNX2* expression was only significantly greater after Vit D treatment for hFOB 1.19 SSBM constructs previously cultured for 8-weeks (non-treat. vs Vit D: $2.2x10^{-3}$ vs $6.9x10^{-3}$;

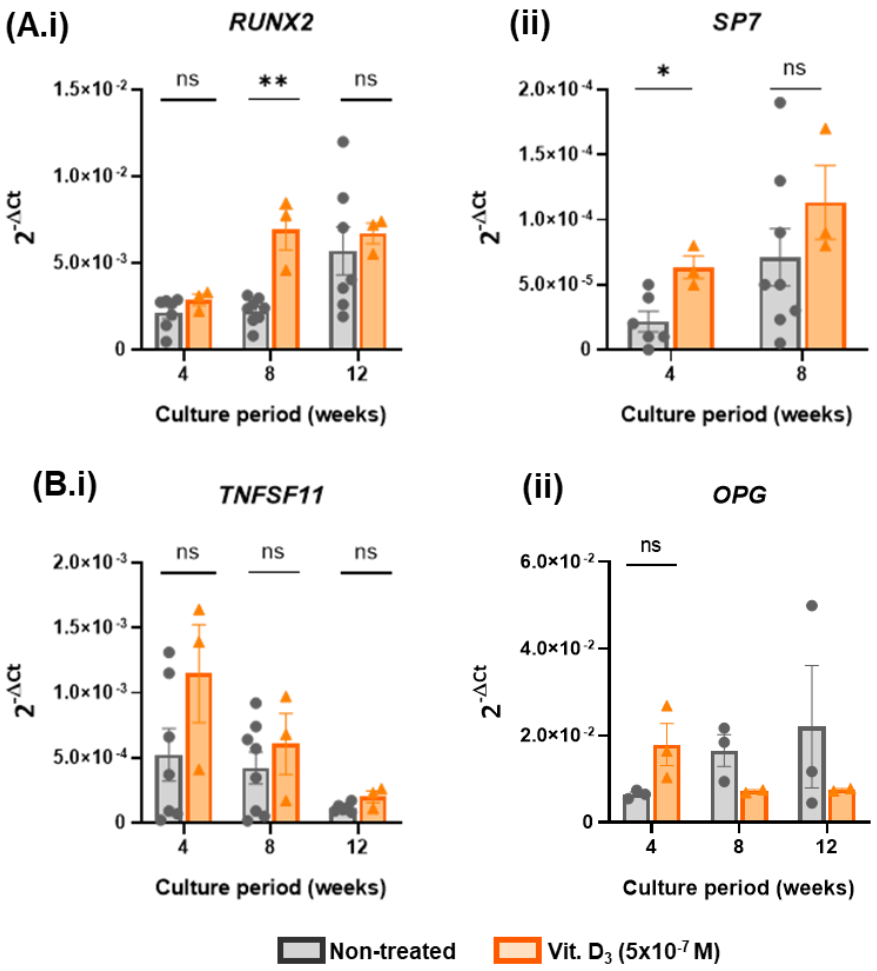


Figure 5.6 - qPCR analysis of osteoblast-specific gene expression for hFOB 1.19 SSBM construct treatment with Vit D. The expression of genes relating to osteoblast differentiation (A) and bone resorption and formation regulation (B) was assessed in hFOB 1.19 cells cultured in 3D after 4-, 8- and 12-weeks, then treated for 1-week under osteogenic conditions with $5x10^{-7}$ M Vit D and compared against those not treated. Results are mean±SEM (n=3(treatment), 6-8(non-treated)). Raw Ct values analysed using unpaired t-test, with Welch correction if SD ratio = >2. * = $p<0.05$; ** = $p<0.01$; ns = no significance. NB no 12-week culture data available for SP7. Also, incomplete analysis for OPG due to n<3.

p=0.006). Similarly, *SP7* expression was only significantly increased for constructs previously cultured for 4-weeks weeks (non-treat. vs Vit D: $2.2x10^{-5}$ vs $6.3x10^{-5}$; p=0.029) and not significantly different at the other analytical time points. Analysis of genes relating to bone remodelling regulation (i.e., *TNFSF11* and *OPG*) [Figure 5.6 B] showed no significant changes in expression after Vit D treatment at any of the analytical time points – please note, statistical analysis of *OPG* for SSBM constructs

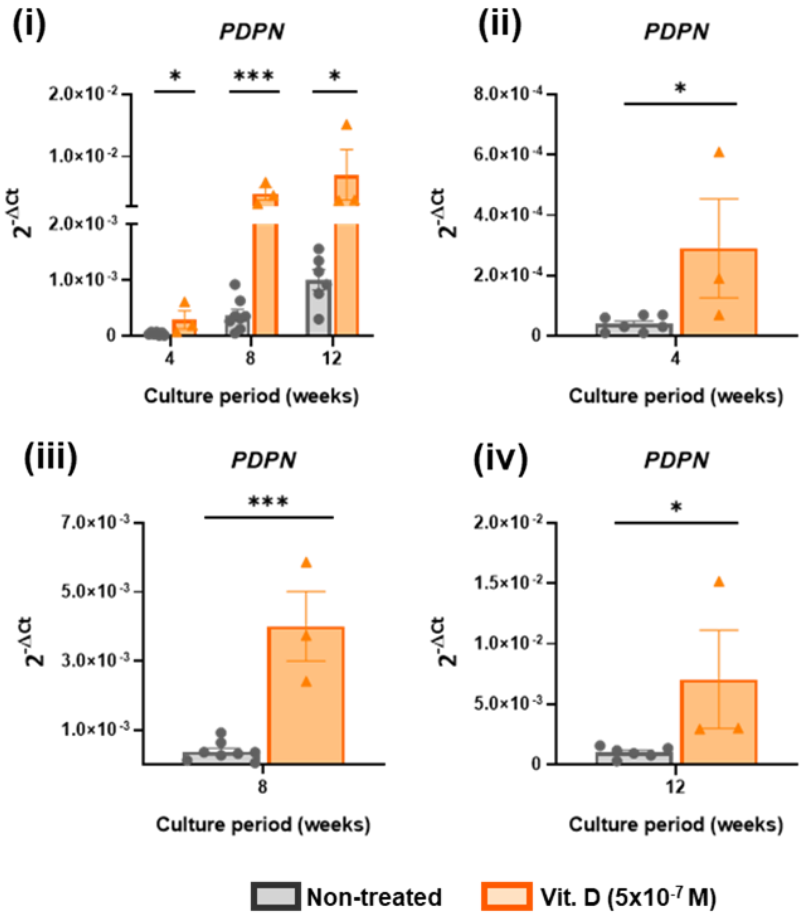


Figure 5.7 - qPCR analysis of podoplanin (PDPN) expression for hFOB 1.19 treatment SSBM construct with Vit D. The expression of PDPN was assessed in hFOB 1.19 cells cultured in 3D after 4-, 8- and 12-weeks, then treated for 1-week under osteogenic conditions with $5x10^{-7}$ M Vit D and compared against those not treated. Results are mean±SEM (n=3(treatment), 6-8(non-treated)). Raw Ct values analysed using unpaired t-test, with Welch correction if SD ratio = >2. * = $p<0.05$; *** = $p<0.001$; ns = no significance.

at 8- and 12-weeks of culture not possible due to low replicate number. The only osteocyte-specific gene analysed to show expression in non-treated hFOB 1.19 SSBM constructs, *PDPN*, [Figure 5.7] showed significantly increased expression after Vit D treatment at all analytical time points (4-, 8- and 12-weeks, respectively: $4.0x10^{-5}$ vs $29.0x10^{-5}$; p=0.018. $3.7x10^{-4}$ vs $40.1x10^{-4}$; p=0.0003. $10.1x10^{-4}$ vs $70.5x10^{-4}$; p=0.0102). For genes not discussed here, results of those genes showed no significant

changes after Vit D treatment in comparison to those not treated at all analytical timepoints. Refer to [Appendix 8.3].

5.2.3 SSBM Vit D treatment: ELISA analysis

Conditioned media was collected from hFOB 1.19 SSBM cultures treated for 1-week with $5x10^{-7}$ M Vit D, after 4-, 8- and 12-weeks of culture under osteogenic conditions – the 1-week treatment period included a 3-day construct isolation period prior to collection [Section 2.3.1]. Media was analysed by enzyme-linked immunosorbent assay (ELISA) to determine OPG concentration and ALP activity [Section 2.3.2].

Results show for both OPG and ALP analyses that Vit D treatment of hFOB 1.19 SSBM constructs only showed a significant difference in protein concentration and activity, respectively, in constructs that had been cultured for 4-weeks prior, and not in those cultured for 8- or 12-weeks prior [Figure 5.8]. Mean OPG concentration increased in response to Vit D treatment, when compared with those not treated (non-treat. vs Vit D: 0.49 ng/mL vs 1.54 ng/mL; p=0.044). However, ALP activity reduced, as shown by a decrease in mean absorbance (i.e., OD at 405 nm) in response to Vit D treatment, when compared with those not treated (non-treat. vs Vit D: 0.79 vs 0.27; p=0.0001).

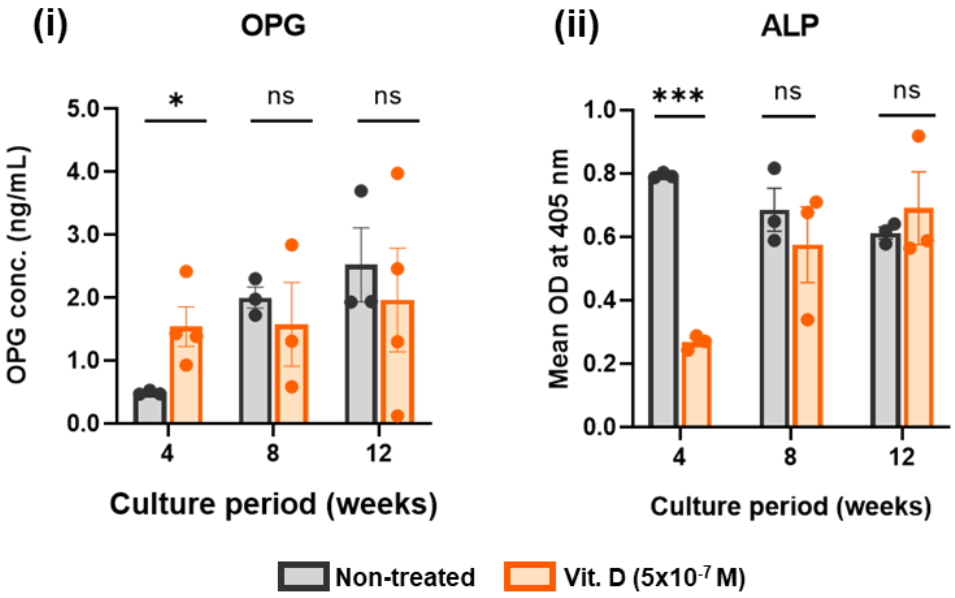


Figure 5.8 - Assessment of hFOB 1.19 SSBM construct conditioned media by ELISA after treatment with Vit D. hFOB 1.19 SSBM constructs cultured for 4-, 8- and 12-weeks post-cell seeding were treated with 5x10-7 M Vit D for 1 week. Conditioned media was collected from constructs isolated 3 days prior and then analysed by ELISA to measure the concentration of OPG **(i)** and examine ALP activity **(ii)** against those non-treated hFOB 1.19 SSBM constructs measured at the same analytical time points. Results are mean±SEM (n=3-4) and analysed using unpaired t-test, with Welch correction if SD ratio = >2. * = p<0.05; *** = p<0.001; ns = no significance.

5.2.4 SSBM Vit D treatment: IF analysis

Following the steps outlined in [Section 2.3.5], high-resolution images and z-stacks of a single hFOB 1.19 SSBM constructs per culture period (4-, 8- and 12-weeks) and treated for 1-week with 5x10^{-7} M Vit D, were obtained to enable visualisation of cell organisation and expression of PDPN at the protein level [Figure 5.9].

In comparison to the non-treated hFOB 1.19 SSBM constructs, a notable increase in the presence of PDPN was detected after treatment with Vit D across all three culture periods. The regions of positive staining were more intense than those not treated and furthermore, there were more areas of the hFOB 1.19 SSBM construct with PDPN staining, whereas with the non-treated constructs, 4- and 8-week SSBM constructs had no to very small discreet areas of staining. However, the areas in which PDPN

staining was observed followed the same pattern as before, with staining at 4-weeks initially seen in areas close to the anchors and over time progressing into the folded edges of the matrix and minimal staining within the central inner surface of the matrix; the latter primarily found in hFOB 1.19 SSBM constructs cultured for 12-weeks prior to treatment.

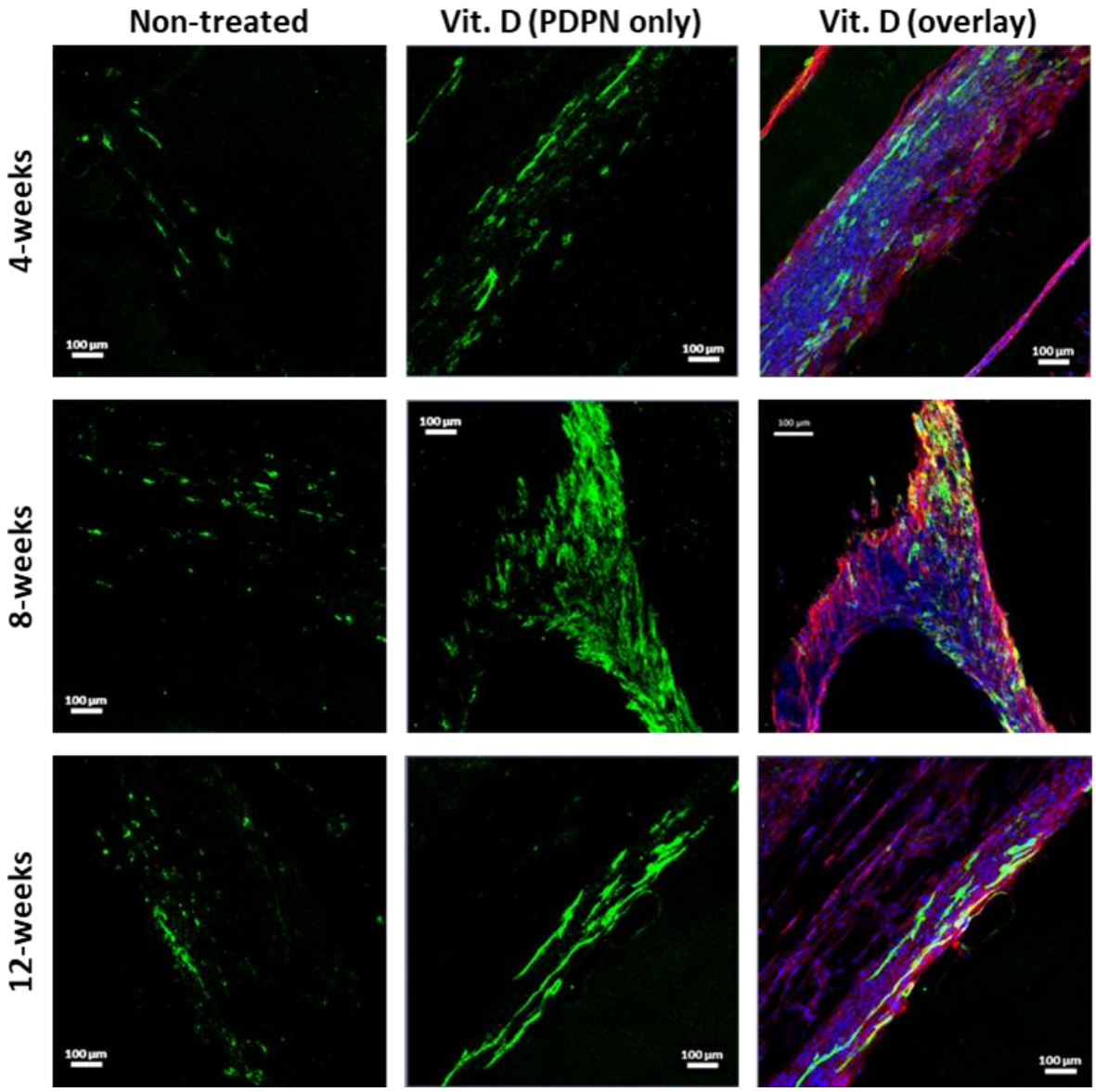


Figure 5.9 - Immunofluorescence (IF) staining detected a notable increase in podoplanin presence after Vit D treatment across all analytical time points. hFOB 1.19 SSBM constructs cultured for 4-, 8- and 12-weeks post-cell seeding were treated with 5x10-7 M Vit D for 1 week. Constructs processed for IF staining and results compared against those non-treated hFOB 1.19 SSBM constructs. Shown were 50 µm sections with an actin (phalloidin; red) and nuclear stain (Hoechst; blue) and an anti-human podoplanin (PDPN) antibody (green). Scale bars = 100 µm. 10x magnification. PDPN images = maximum intensity projection z-stacks (Step size = 2.1 µm). Overlay images = single plane snap shot.

5.3 PTH

5.3.1 2D investigations

Prior to beginning hFOB 1.19 SSBM construct responsivity to PTH treatment concentration and duration was determined by culturing hFOB 1.19 cells to confluence in 2D, then for 7- and 11-days with $1x10^{-8}$ and $1x10^{-7}$ M PTH under osteogenic conditions. These concentrations were selected based on the findings made by Harris *et al*. (375). ALP activity was used as a measure of cellular metabolic response to PTH. In comparison to non-treated hFOB 1.19 cells, 7-days of PTH treatment resulted in a significant increase in ALP activity - shown as an increase in mean absorbance at 405 nm - with both $1x10^{-8}$ (0.27 vs 0.40; p=0.002) and $1x10^{-7}$ M PTH (0.27 vs 0.40; p=0.002) [Figure 5.10 A.i]. However, no significance was seen at this timepoint between the PTH concentrations tested (p=0.89). After 11 days, no significant difference in ALP activity was observed between either of the PTH concentrations and the non-treated cells, or between the two concentrations tested [Figure 5.10 A.ii].

Potential effects by exposure to $1x10^{-7}$ M PTH, or its vehicle, distilled water (d.H_2O) were assessed by monitoring hFOB 1.19 cell proliferation and viability after the 1-week treatment period in 2D, under osteogenic culture conditions. In comparison to non-treated cells, an increase in mean live cell number per well occurred with the VC ($0.42x10^6$ vs $0.61x10^6$ live cells/well; p=0.017), but no further effect with the addition of PTH (VC vs PTH: p=0.7) [Figure 5.10 B]. Assessment of cell viability showed that there was a significant increase in percentage viability with PTH treated cells (149.7% of control; p=0.035), however not with the VC treated cells, nor between the VC and PTH treated cells.

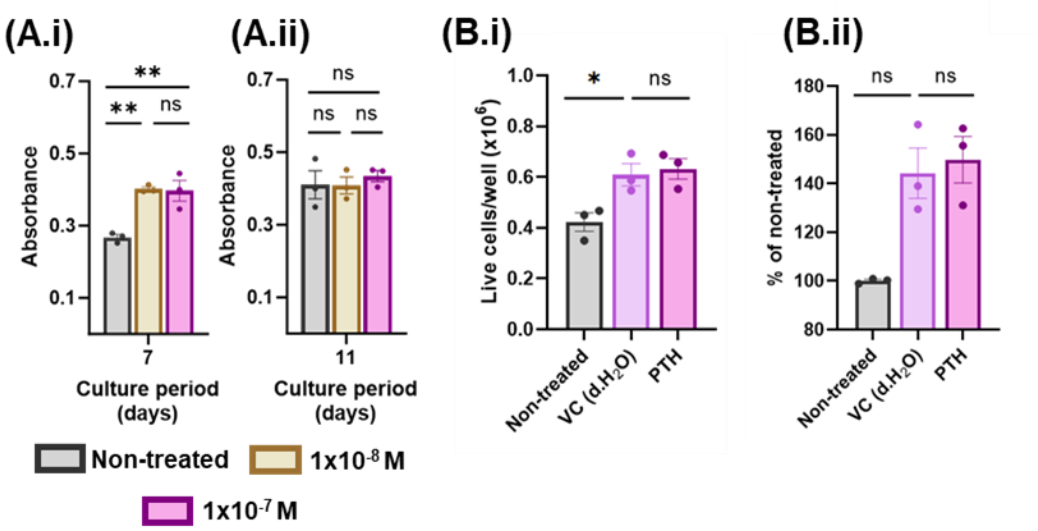


Figure 5.10 -Determining Parathyroid hormone Fragment 1-34 human (PTH) treatment concentration and duration. (A) Based on the results found by Harris *et al.* (375), hFOB 1.19 cells were cultured in 2D and treated with 1x10-8 and $1x10^{-7}$ M PTH, as well as non-treated, for 7 **(i)** and 11 days **(ii)** under osteogenic conditions. Results shown are Mean±SEM (n=3) and analysed using ordinary one way ANOVA with Fisher's LSD, or Brown-Forsythe and Welch ANOVA when SD ratio = >2. Compared against control (i.e., non-treated). **(B)** Live cell counts **(i)** and %viability **(ii)** was assessed for hFOB 1.19 cells cultured with $1x10^{-7}$ M PTH, or vehicle control (VC) (deionised water ($d.H_2O$)), as well as non-treated, for 1 week in 2D. Results are Mean % of non-treated±SD (n=3) and analysed using unpaired t-test, with Welch correction if SD ratio = >2. Multiple comparison results shown. * = p<0.05; ** = p<0.01; ns = no significance.

To gain an insight into if and how hFOB 1.19 cells respond to PTH at the gene expression level, qPCR was used to analyse gene expression of hFOB 1.19 cells treated for 1-week with $1x10^{-7}$ M PTH, or its vehicle, $d.H_2O$, under osteogenic conditions in 2D. B2M was used as the housekeeper gene for the following qPCR analysis.

Results for genes associated with matrix formation, and its subsequent mineralisation [Figure 5.11 A], in this case *ALPL* and *COL1A1*, showed no significant changes in expression in comparison to non-treated cells, when cells were treated with the VC, however expression significantly increased in comparison to the VC after PTH treatment (*ALPL*: $5.8x10^{-3}$ vs $10.2x10^{-3}$; p=0.018. *COL1A1*: 0.17 vs 0.33; p=0.018).

Another matrix gene assessed, *SPARC*, and the gene associated with chondrocyte lineage commitment, *SOX9*, both showed no significant change in expression amongst any of the conditions tested [Figure 5.11 A.iii & B, respectively].

Assessment of osteoblast genes associated with the lineage commitment (i.e., *RUNX2*) and their differentiation (i.e., *PHEX*) [Figure 5.12 A], along with the genes that encode for key regulatory proteins in bone remodelling (i.e., *TNFSF11* and *OPG*) [Figure 5.12 B], showed no significant change in expression between the non-treated cells and VC cells. Nor was there any significant change between the VC and PTH treated cells.

There were four genes analysed which showed expression to completely cease once treated with the VC and PTH [Figure 5.13]. Assessment of matrix gene, *BGLAP*, osteoblast-differentiation gene, *BMP2,* and early osteocyte gene, *PDPN,* showed no expression once treated with the VC and PTH, whereas previously expression was present in non-treated cells. *SP7* expression was not detected after PTH treatment, and noticeably reduced with the VC, in comparison to non-treated cells, although the latter was not statistically different.

5.3.2 SSBM PTH treatment: qPCR analysis

qPCR was used to analyse gene expression of hFOB 1.19 SSBM constructs after 4-, 8- and 12-weeks of culture under osteogenic conditions, then treated for 1-week with $1x10^{-7}$ M PTH, which were compared against the data previously attained for hFOB 1.19 SSBM constructs not treated – refer to [Section 4.2]. Refer to [Table 2.3] for gene

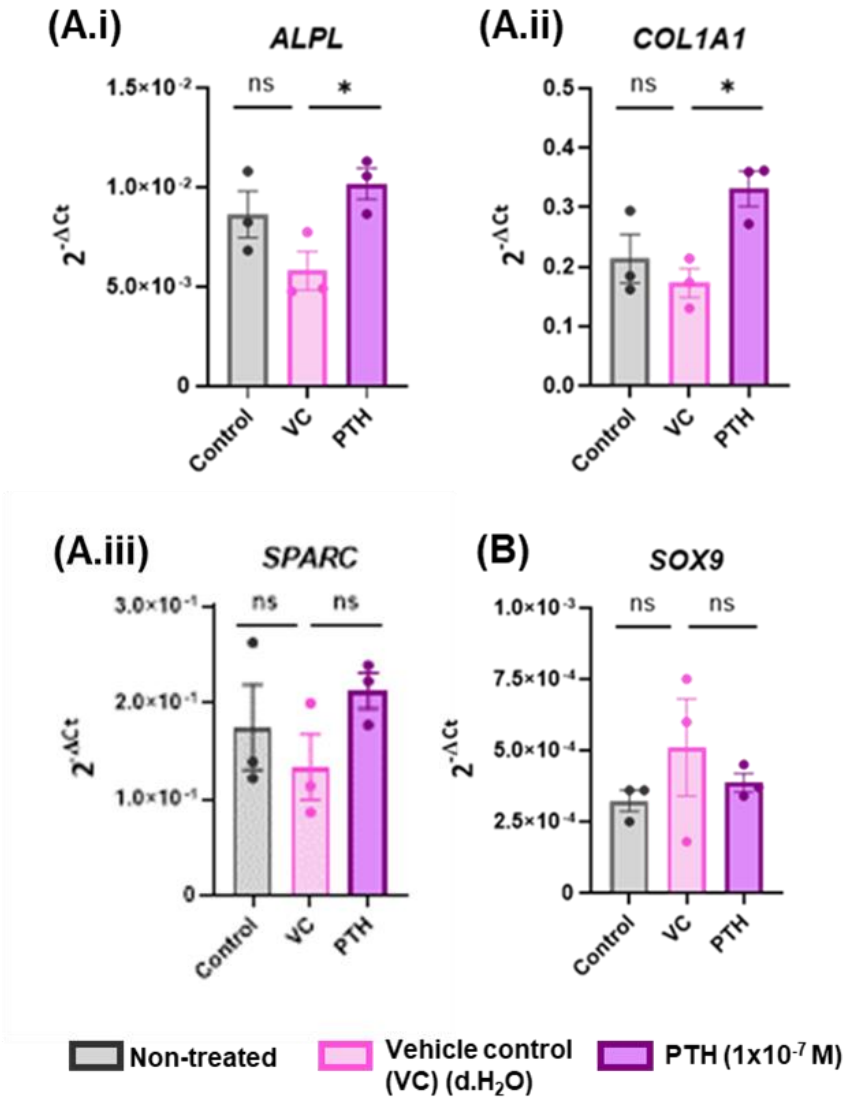


Figure 5.11 - qPCR analysis of matrix and mineralisation, and chondrocyte related gene expression for 2D hFOB 1.19 treatment with PTH. The expression of genes relating to matrix and mineral formation and maturation **(A)** and chondrocyte lineage commitment **(B)** was assessed in hFOB 1.19 cells cultured for 1-week with $1x10^{-7}$ M PTH, vehicle control (VC) ($d.H_2O$), and non-treated. Results are mean±SEM (n=3). Raw Ct values analysed using unpaired t-test, with Welch correction if SD ratio = >2. * = $p<0.05$; ns = no significance.

and TaqMan primer information. B2M was used as the housekeeping gene for the following qPCR analysis.

Two genes relating to matrix formation and maturation showed significant changes in expression in hFOB 1.19 SSBM cultures after PTH treatment [Figure 5.14 A]. In

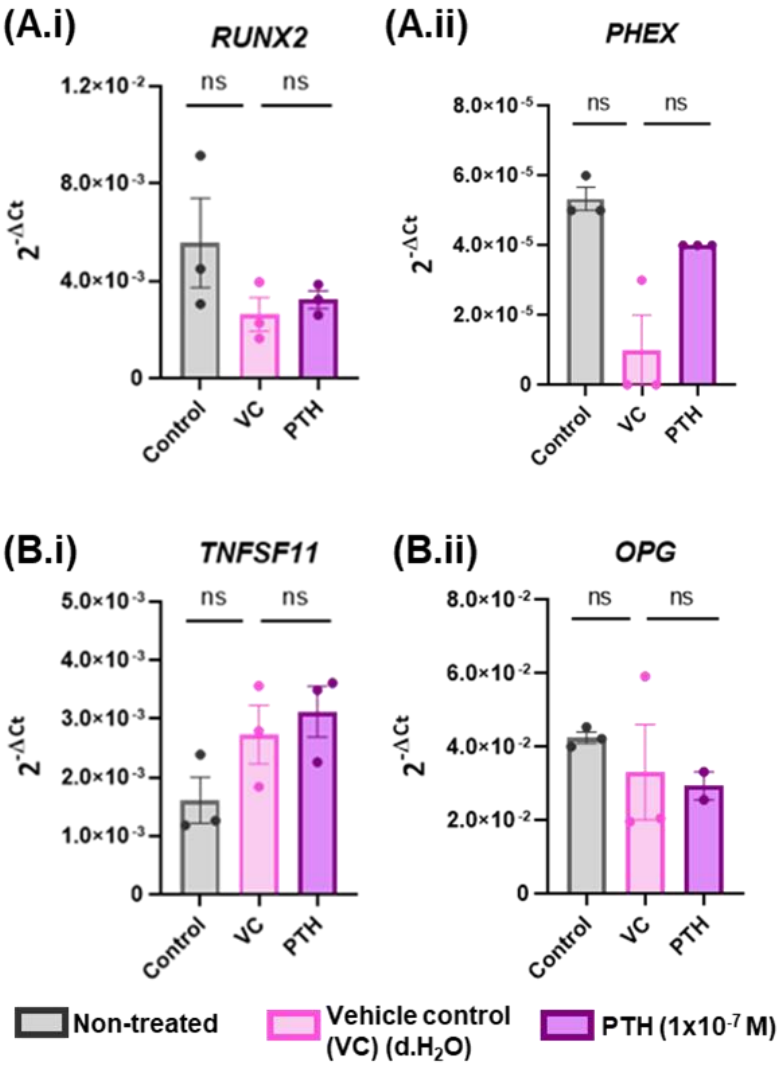


Figure 5.12 - qPCR analysis of osteoblast-specific gene expression for 2D hFOB 1.19 treatment with PTH. The expression of genes relating to osteoblast differentiation **(A)** and bone resorption and formation regulation **(B)** was assessed in hFOB 1.19 cells cultured for 1-week with $1x10^{-7}$ M PTH, vehicle control (VC) ($d.H_2O$), and non-treated. Results are mean±SEM (n=3). Raw Ct values analysed using unpaired t-test, with Welch correction if SD ratio = >2. ns = no significance.

comparison to non-treated SSBM constructs, *BGLAP* showed increased expression after PTH treatment for SSBM constructs with 8-weeks of osteogenic culture only (Non-treat. vs PTH: $2.7x10^{-5}$ vs $7.3x10^{-5}$; p=0.012). Similarly, *SPARC* expression was only significantly increased after PTH treatment in 8-week cultured SSBM constructs (Non-treat. vs PTH: 0.11 vs 0.18; p=0.022) and was unaffected when SSBM constructs

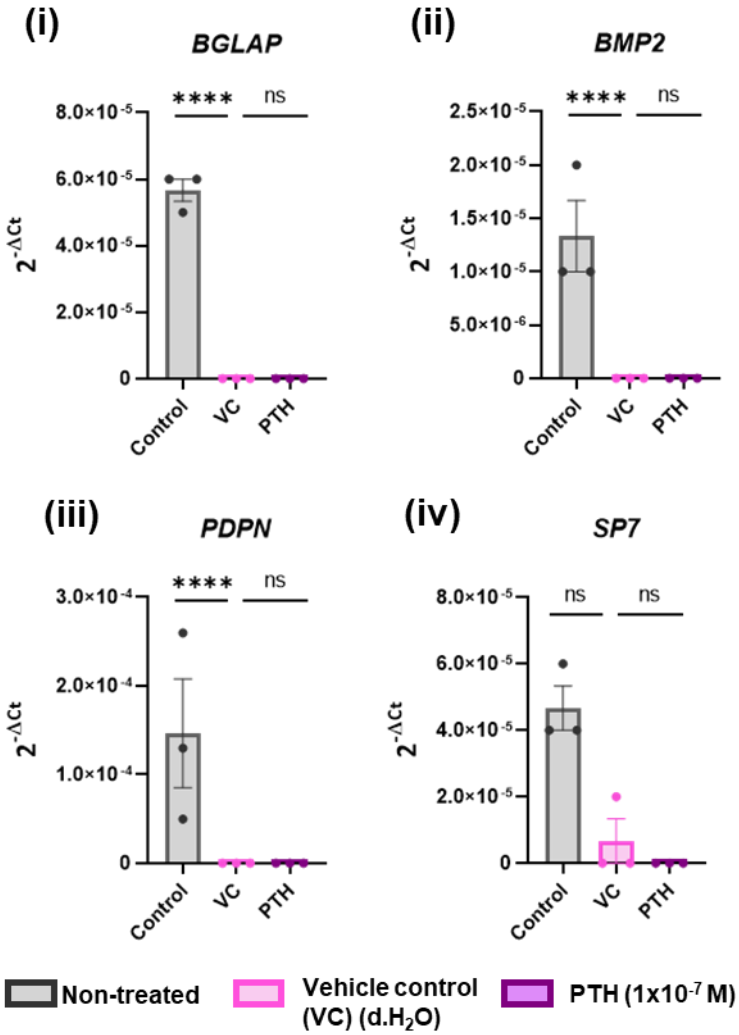


Figure 5.13 - A suggestive inhibitory effect on the expression of certain osteoblast and osteocyte-specific genes in 2D hFOB 1.19 cells by PTH vehicle, d.H_2O. The expression of genes specific to osteoblasts **(i, ii & iv)** and osteocytes **(iii)** was assessed in hFOB 1.19 cells cultured for 1-week with $1x10^{-7}$ M PTH, vehicle control (VC) (d.H_2O), and non-treated, which showed an inhibitory effect by the VC. Results are mean±SEM (n=3). Raw Ct values analysed using unpaired t-test, with Welch correction if SD ratio = >2. **** = p<0.0001; ns = no significance.

cultured for 4- and 12-weeks previously were treated. Only one gene related to osteoblast lineage commitment showed a significant change in expression after PTH treatment in comparison to non-treated constructs at one or more analytical time points [Figure 5.14 B]. *RUNX2* expression was significantly increased after PTH treatment for 8-week SSBM cultures (Non-treat. vs PTH: $4.6x10^{-3}$ vs $5.8x10^{-3}$; p=0.041), however

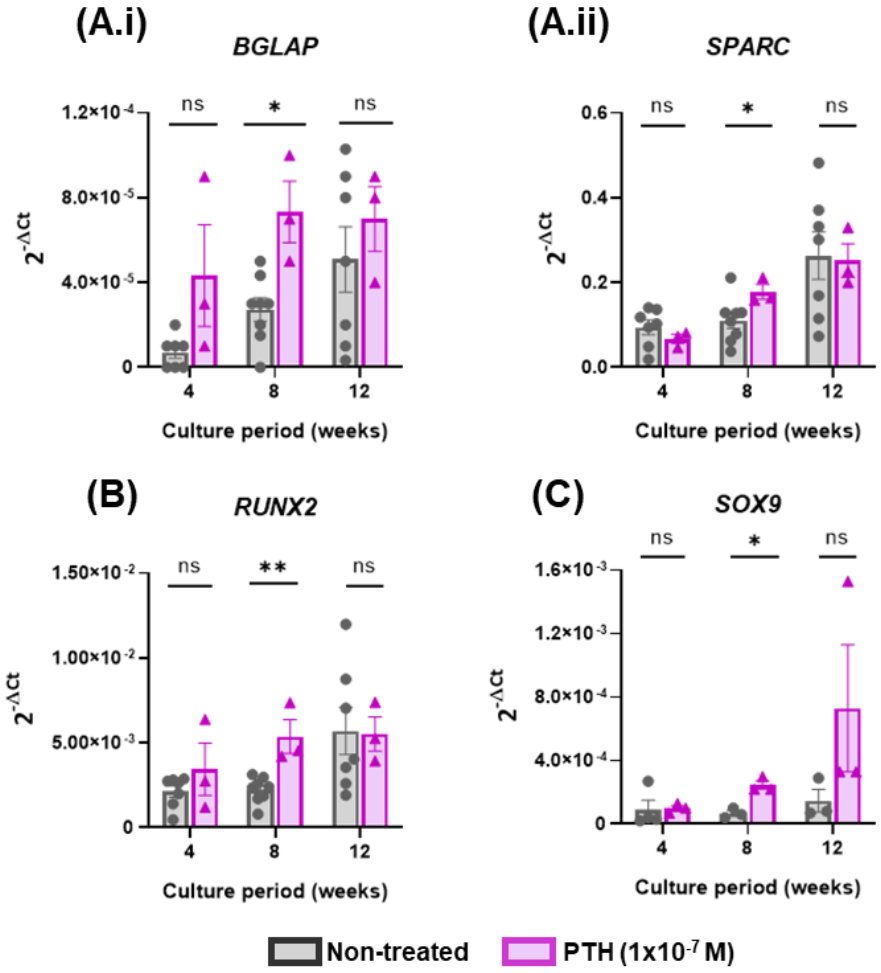


Figure 5.14 - qPCR analysis of matrix and mineralisation, osteoblast lineage commitment, and chondrocyte related gene expression for hFOB 1.19 SSBM construct treatment with PTH. The expression of genes relating to matrix and mineral formation and maturation **(A)**, osteoblast differentiation **(B)** and chondrocyte lineage commitment **(C)** was assessed in hFOB 1.19 cells cultured in 3D after 4-, 8- and 12-weeks, then treated for 1-week under osteogenic conditions with $1x10^{-7}$ M PTH and compared against those not treated. Results are mean±SEM (n=3(treatment), 6-8(non-treated)). Raw Ct values analysed using unpaired t-test, with Welch correction if SD ratio = >2. * = p<0.05; ** = p<0.01; ns = no significance.

was not significantly affected at any other time point. Again, it was only after PTH treatment of SSBM constructs previously cultured for 8-weeks where *SOX9* expression (the gene pertaining to chondrocyte lineage commitment) significantly increased (Non-treat. vsVit D: $6.7x10^{-5}$ vs $24.7x10^{-5}$; p=0.009), whereas there was no significant

change between non-treated and treated hFOB 1.19 SSBM constructs at 4- or 12-weeks of culture [Figure 5.14 C].

When examining the genes involved in regulating bone remodelling, in comparison to non-treated SSBM constructs, PTH treatment significantly increased the expression of the pro-resorptive gene, *TNFSF11*, in hFOB 1.19 SSBM constructs that had been cultured 4- (Non-treat. vs Vit D: $5.2x10^{-4}$ vs $23.6x10^{-4}$; p=0.021) and 12-weeks prior (Non-treat. vs Vit D: $1.1x10^{-4}$ vs $2.7x10^{-4}$; p=0.018), but no significant change was detected in those cultured for 8-weeks prior [Figure 5.15 A]. PTH treatment also showed to significantly increase *OPG* expression in hFOB 1.19 SSBM constructs that had been cultured 4- (Non-treat. vs Vit D: $6.4x10^{-3}$ vs $13.3x10^{-3}$; p=0.009), but at no other analytical time point [Figure 5.15 B].

The early osteocyte gene analysed, *PDPN*, [Figure 5.16] showed significantly increased expression after PTH treatment at all analytical time points (4-, 8- and 12-weeks, respectively: $4.0x10^{-5}$ vs $23.9x10^{-5}$; p=0.034. $3.7x10^{-4}$ vs $26.5x10^{-4}$; p=0.007. $1.0x10^{-3}$ vs $6.5x10^{-3}$; p=0.011).

mRNA expression analysis for other genes was performed but not discussed here, given that these genes showed no significant changes after PTH treatment in comparison to those not treated at all analytical timepoints. Refer to [Appendix 8.3] for a full list.

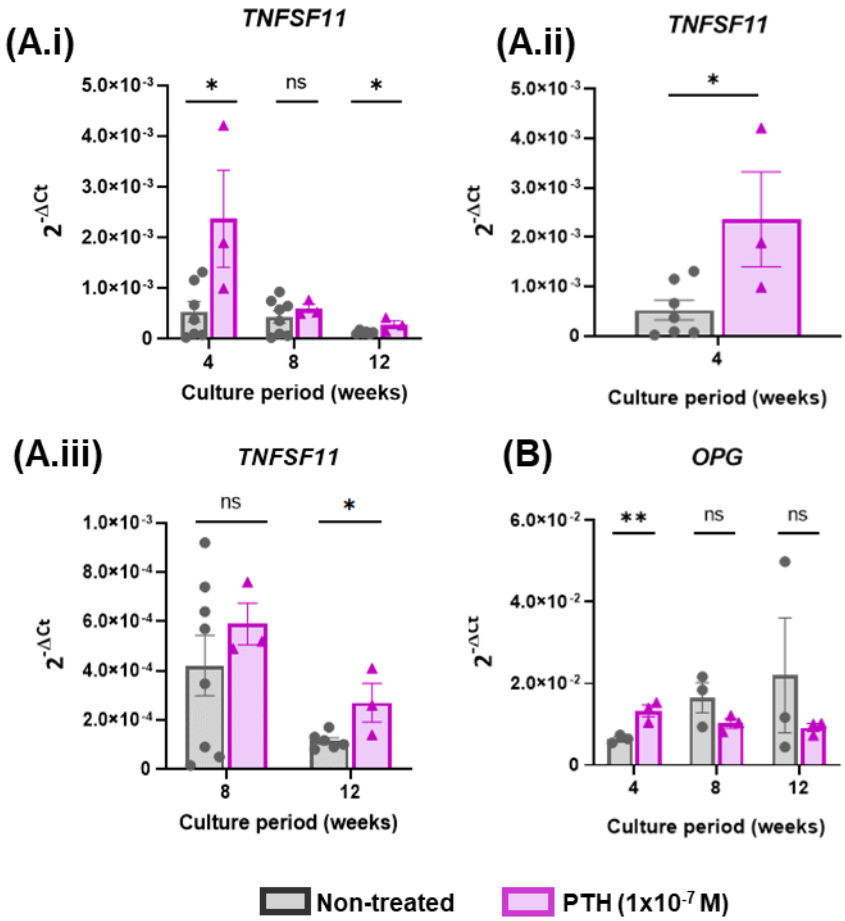


Figure 5.15 - qPCR analysis of formation and resorption regulation related gene expression for hFOB 1.19 SSBM construct treatment with PTH. The expression of genes relating to bone resorption **(A)** and formation regulation **(B)** was assessed in hFOB 1.19 cells cultured in 3D after 4-, 8- and 12-weeks, then treated for 1-week under osteogenic conditions with $1x10^{-7}$ M PTH and compared against those not treated. Results are mean±SEM (n=3(treatment), 6-8(non-treated)). Raw Ct values analysed using unpaired t-test, with Welch correction if SD ratio = >2. * = $p<0.05$; ** = $p<0.01$; ns = no significance.

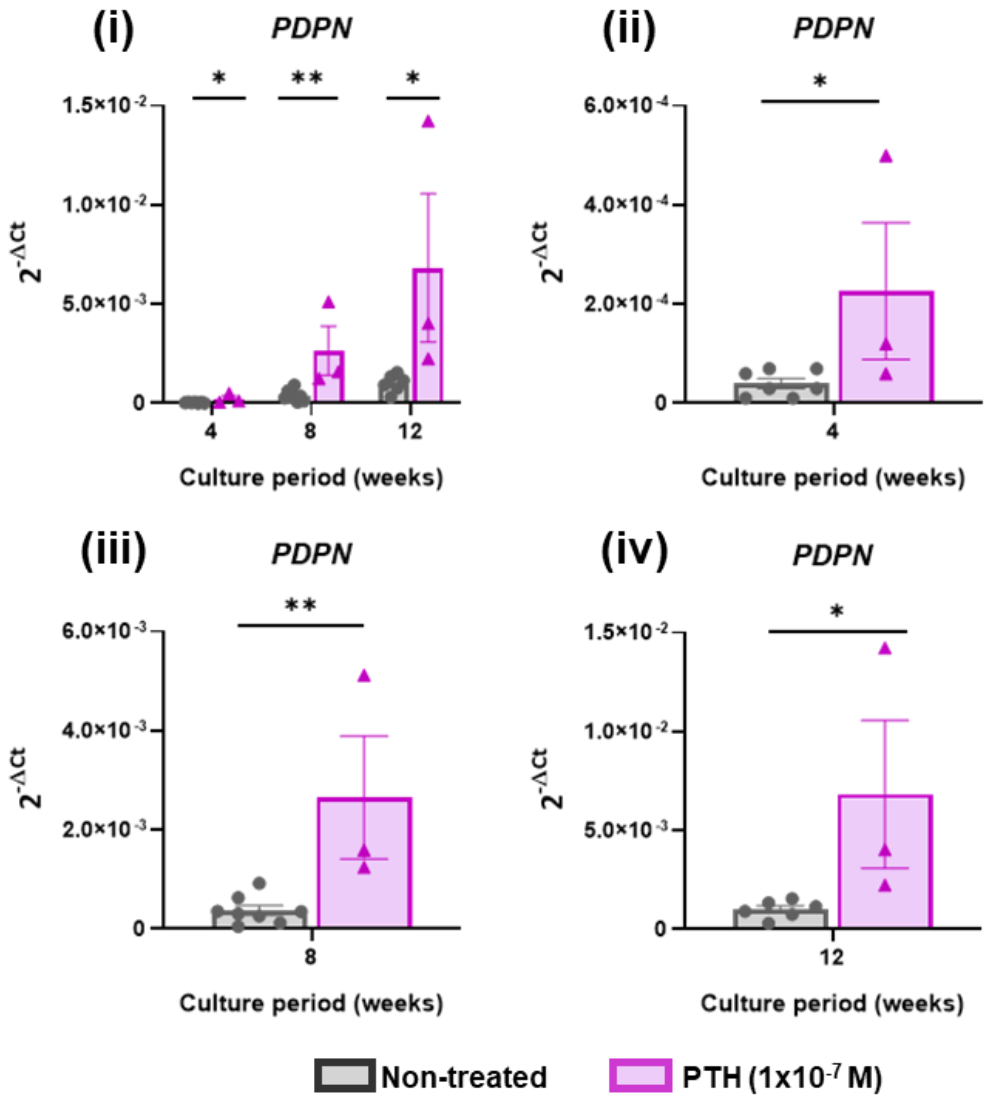


Figure 5.16 - qPCR analysis of podoplanin (PDPN) expression for hFOB 1.19 treatment SSBM construct with PTH. The expression of PDPN was assessed in hFOB 1.19 cells cultured in 3D after 4-, 8- and 12-weeks, then treated for 1-week under osteogenic conditions with $1x10^{-7}$ M PTH and compared against those not treated. Results are mean±SEM (n=3(treatment), 6-8(non-treated)). Raw Ct values analysed using unpaired t-test. * = $p<0.05$; ** = $p<0.01$; ns = no significance.

5.3.3 SSBM PTH treatment: ELISA analysis

Conditioned media was collected from hFOB 1.19 SSBM cultures treated for 1-week with $1x10^{-7}$ M PTH, after 4-, 8- and 12-weeks of culture under osteogenic conditions – the 1-week treatment period included a 3-day construct isolation period prior to

collection [Section 2.3.1]. Media was analysed by ELISA to determine OPG concentration and ALP activity [Section 2.3.2].

Results for OPG ELISA analysis [Figure 5.17 A] showed that after PTH treatment, media collected from hFOB 1.19 SSBM constructs cultured for 4-weeks prior had a significantly greater OPG concentration than conditioned media from non-treated SSBM constructs (non-treat. vs PTH: 0.49 ng/mL vs 3.22 ng/mL; p=0.011). However, results for constructs after 8- and 12-weeks of culture showed no significant change in concentration after treatment. Analysis of ALP activity [Figure 5.17 B] showed a reduction, as shown by a decrease in mean absorbance (i.e., OD at 405 nm) in response to PTH treatment, in conditioned media of SSBM constructs cultured for 4-weeks prior (non-treat. vs PTH: 0.79 vs 0.31; p=0.002). However, for 8-week cultured SSBM constructs, ALP activity was not significantly changed after PTH treatment and for 12-week cultured SSBM constructs, ALP activity was significantly increased after PTH treatment (non-treat. vs PTH: 0.61 vs 1.00; p=<0.0001).

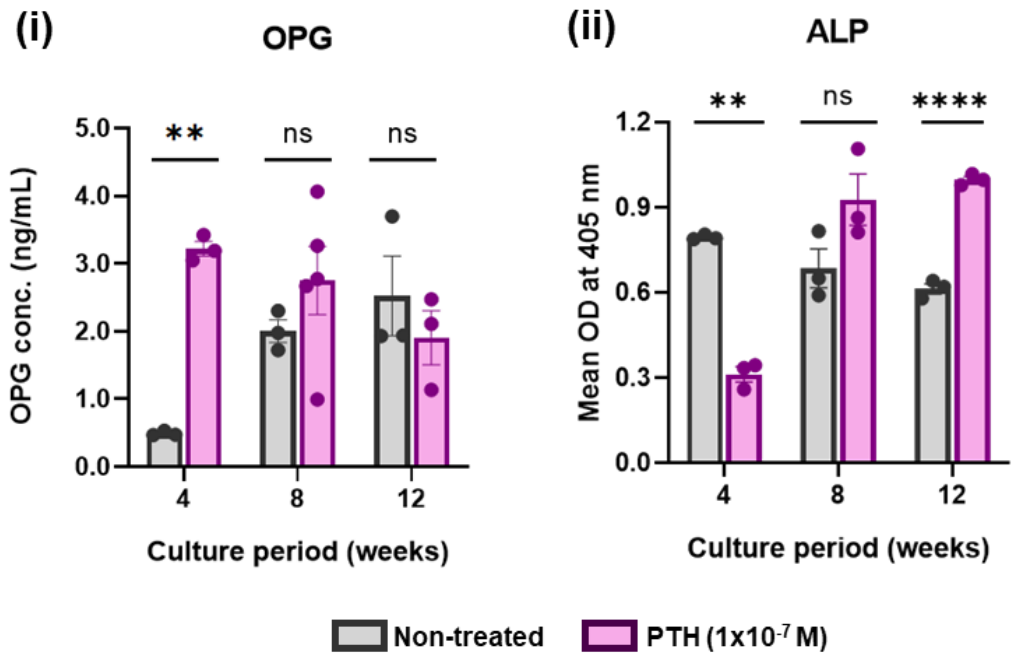


Figure 5.17 - Assessment of hFOB 1.19 SSBM construct conditioned media by ELISA after treatment with PTH. hFOB 1.19 SSBM constructs cultured for 4-, 8- and 12-weeks post-cell seeding were treated with $1x10^{-7}$ M PTH for 1 week. Conditioned media was collected from constructs isolated 3 days prior and then analysed by ELISA to measure the concentration of OPG **(A)** and examine ALP activity **(B)** against those non-treated hFOB 1.19 SSBM constructs measured at the same analytical time points. Results are mean±SEM (n=3) and analysed using unpaired t-test, with Welch correction if SD ratio = >2. * = p<0.05; ** = p<0.01; *** = p<0.001; ns = no significance.

5.3.4 SSBM PTH treatment: IF analysis

Following the steps outlined in [Section 2.3.5], high-resolution images and z-stacks of a single hFOB 1.19 SSBM constructs per culture period (4-, 8- and 12-weeks) and treated for 1-week with $1x10^{-7}$ M PTH, were obtained to enable visualisation of cell organisation and expression of PDPN at the protein level [Figure 5.18].

In comparison to the non-treated hFOB 1.19 SSBM constructs, a notable increase in the presence of PDPN was detected after treatment with PTH across all three culture periods. The regions of positive staining were more intense than those not treated and furthermore, there were also more areas of the hFOB 1.19 SSBM construct with PDPN

staining, whereas with the non-treated constructs, 4- and 8-week SSBM constructs had no to very small discreet areas of staining. However, the areas in which PDPN staining was observed followed the same pattern as before, with staining at 4-weeks initially seen in areas close to the anchors and over time progressing into the folded edges of the matrix and minimal staining within the central inner surface of the matrix; the latter primarily found in hFOB 1.19 SSBM constructs cultured for 12-weeks prior to treatment.

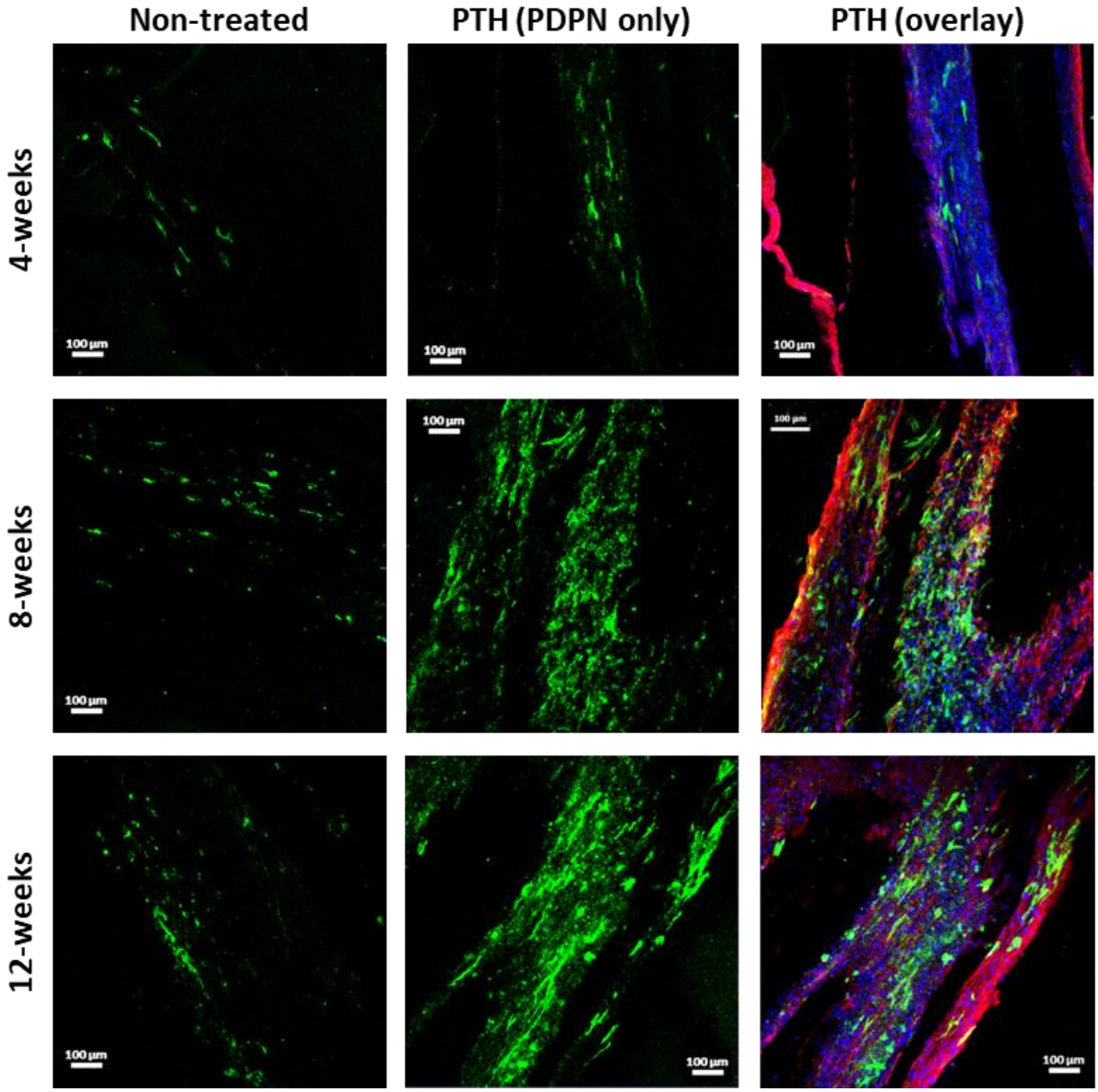


Figure 5.18 - IF staining detected a notable increase in podoplanin presence after PTH treatment across all analytical time points. hFOB 1.19 SSBM constructs cultured for 4-, 8- and 12-weeks post-cell seeding were treated with $1x10^{-7}$ M PTH for 1 week. Constructs processed for IF staining and results compared against those non-treated hFOB 1.19 SSBM constructs. Shown were 50 µm sections with an actin (phalloidin; red) and nuclear stain (Hoechst; blue) and an anti-human podoplanin (PDPN) antibody (green). Scale bars = 100 µm. 10x magnification. PDPN images = maximum intensity projection z-stacks (Step size = 2.1 µm). Overlay images = single plane snap shot.

5.4 Betulin

5.4.1 2D Betulin investigations

Prior to beginning hFOB 1.19 SSBM construct responsivity to Betulin, treatment concentration and duration was determined by culturing hFOB 1.19 cells to confluence in 2D, then for 7- and 11-days with $1x10^{-7}$, $3x10^{-7}$, and $5x10^{-7}$ M Betulin under osteogenic conditions. These concentrations were selected based on the findings made by Mizerska-Kowalska *et al*. (400). ALP activity was used as a measure of cellular metabolic response to PTH. In comparison to non-treated hFOB 1.19 cells, results showed that after 7-days of Betulin treatment [Figure 5.19 A.i], there was a significant increase in ALP activity - shown as an increase in mean absorbance at 405 nm – with $1x10^{-7}$ M (0.27 vs 0.38; p=0.006) and $3x10^{-7}$ M (0.27 vs 0.35; p=0.026). After 11-days of Betulin treatment [Figure 5.19 A.ii], there was no significant difference in ALP activity between the non-treated cells and any of the Betulin concentrations tested, although there was a notable increase in ALP activity for $1x10^{-7}$ M from 7- to 11-days (not statistically due to larger variation in data at 7-days).

Potential effects by exposure to $1x10^{-7}$ M Betulin, or its vehicle, dimethylsulfoxide (DMSO), were assessed by monitoring hFOB 1.19 cell proliferation and viability after the 11-day treatment period in 2D, under osteogenic culture conditions. In comparison to the non-treated cells, neither DMSO alone or Betulin affected hFOB 1.19 proliferation, however the VC had a significant increase in cell viability (22.8±5.0%; p=0.012), with no significance found between the VC and Betulin (p=0.24) [Figure 5.19 B].

To gain an insight into if and how hFOB 1.19 cells respond to Betulin at the gene expression level, qPCR was used to analyse gene expression of hFOB 1.19 cells

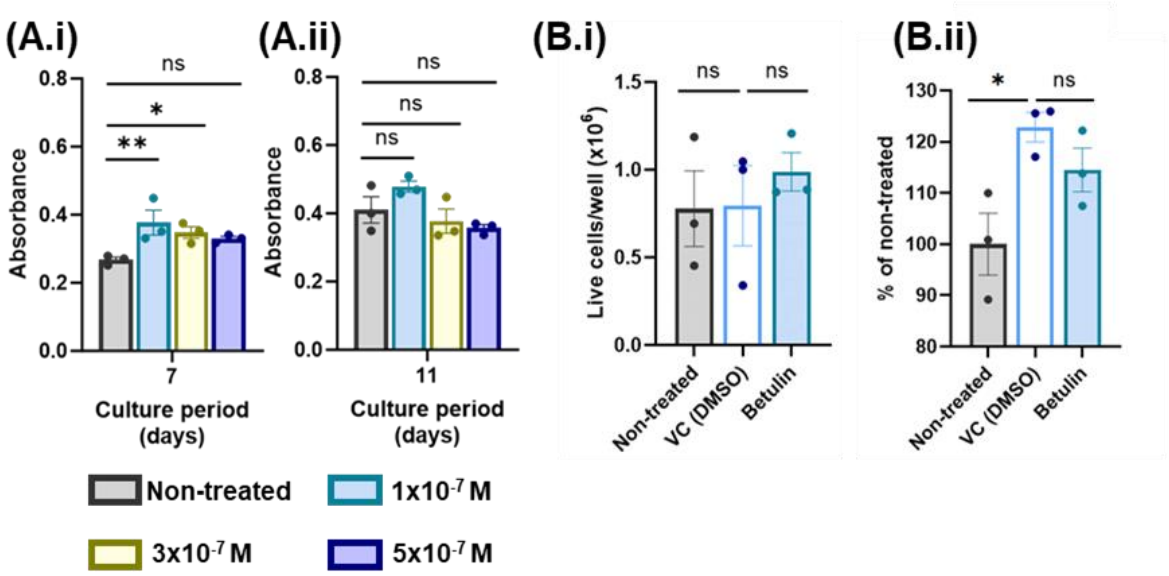


Figure 5.19 - Determining Betulin treatment concentration and duration. (A) Based on the results found by Mizerska-Kowalska *et al.* (400) hFOB 1.19 cells were cultured in 2D and treated with $1x10^{-7}$, $3x10^{-7}$, and $5x10^{-7}$ M Betulin, as well as non-treated, for 7 **(i)** and 11 **(ii)** days under osteogenic conditions. Results shown are Mean±SEM (n=3) and analysed using ordinary one way ANOVA with Fisher's LSD, or Brown-Forsythe and Welch ANOVA when SD ratio = >2. Compared against control (i.e., non-treated). **(B)** Live cell counts **(i)** and %viability **(ii)** was assessed for hFOB 1.19 cells cultured with $1x10^{-7}$ M Betulin, or vehicle control (VC) (DMSO), as well as non-treated, for 1 week in 2D. Results are Mean % of non-treated±SD (n=3) and analysed using unpaired t-test, with Welch correction if SD ratio = >2. Multiple comparison results shown. * = $p<0.05$; ns = no significance.

treated for 11-days with $1x10^{-7}$ M Betulin, or its vehicle, DMSO, under osteogenic conditions in 2D. Refer to [Table 2.3] for gene and TaqMan primer information. B2M was used as the housekeeper gene for the following qPCR analysis. Note, there was no non-treated cell control due to low RNA yields.

Results from analysis of genes associated with matrix formation, and its subsequent mineralisation [Figure 5.20], *ALPL* and *SPARC*, showed no significant changes in expression in comparison to VC-treated cells, when cells were treated with Betulin. However, there was a significantly reduced expression in *BGLAP* and *COL1A1* (*BGLAP*: $7.7x10^{-5}$ vs $1.7x10^{-5}$; p=0.009. *COL1A1*: 0.13 vs 0.08; p=0.036).

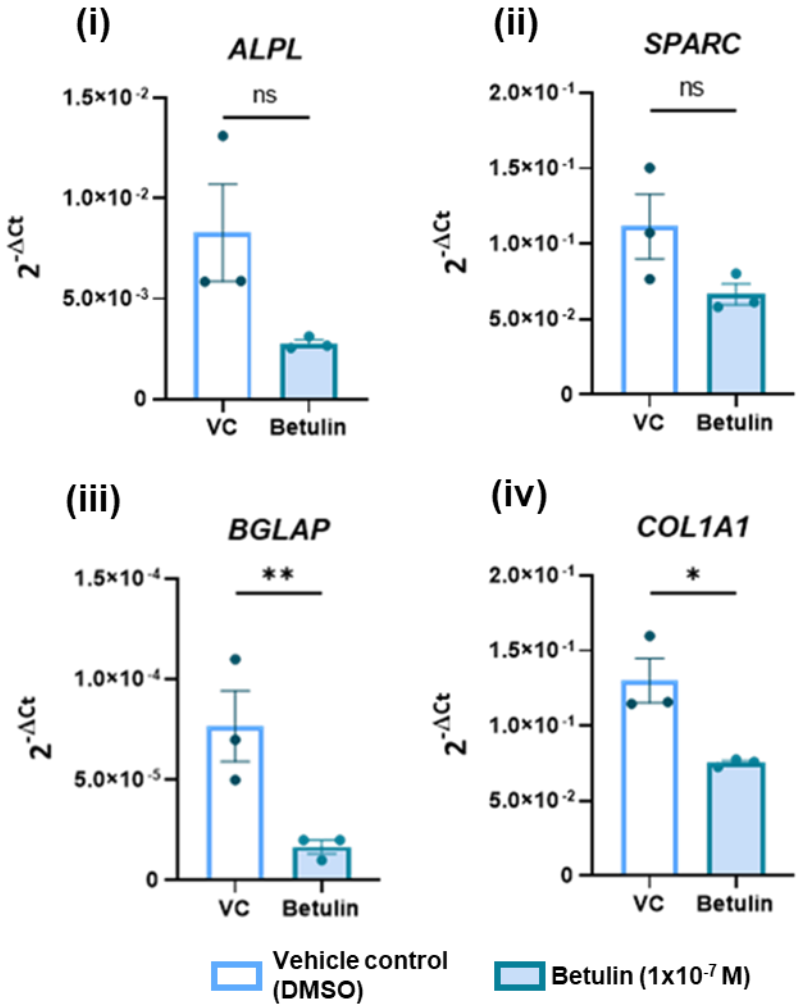


Figure 5.20 - qPCR analysis of matrix and mineralisation, and chondrocyte related gene expression for 2D hFOB 1.19 treatment with Betulin. The expression of genes relating to matrix and mineral formation and maturation was assessed in hFOB 1.19 cells cultured for 11-days with $1x10^{-7}$ M Betulin, or vehicle control (DMSO), and non-treated. Results are mean±SEM (n=3). Raw Ct values analysed using unpaired t-test, with Welch correction if SD ratio = >2. * = $p<0.05$; ** = $p<0.01$; ns = no significance.

In comparison to VC treated cells, assessment of osteoblast genes associated with the lineage commitment and differentiation [Figure 5.21], showed a significantly reduced expression in *RUNX2* ($7.7x10^{-3}$ vs $2.5x10^{-3}$; p=0.027), and *SP7* ($8.3x10^{-5}$ vs $4.0x10^{-5}$; p=0.027). Furthermore, no significant change in expression of *BMP2* and *PHEX* was found, despite an increased and reduced expression seen, respectively.

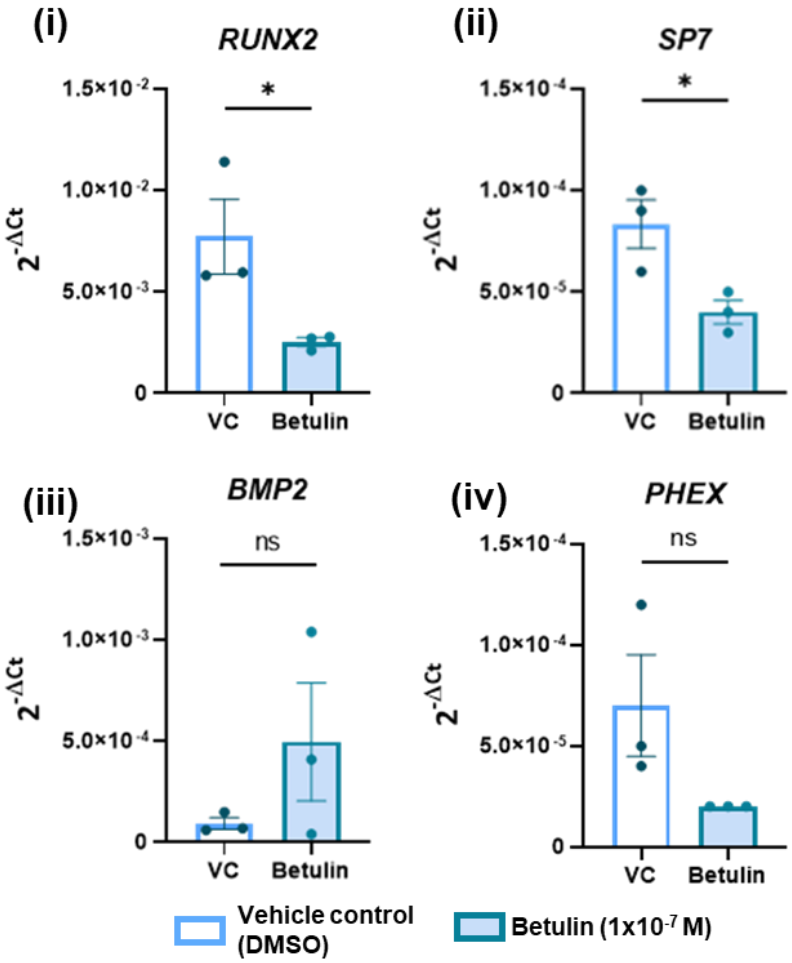


Figure 5.21 - qPCR analysis of osteoblast-specific gene expression for 2D hFOB 1.19 treatment with Betulin. The expression of genes relating to osteoblast differentiation was assessed in hFOB 1.19 cells cultured for 11-days with $1x10^{-7}$ M Betulin, vehicle control (VC) (DMSO), and non-treated. Results are mean±SEM (n=3). Raw Ct values analysed using unpaired t-test, with Welch correction if SD ratio = >2. * = $p<0.05$; ns = no significance.

There was no significant difference in expression found between the VC and Betulin-treated cells for genes associated with bone remodelling regulation, *TNFSF11* and *OPG*, nor was there a significant change in expression of the early osteocyte marker gene, *PDPN* [Figure 5.22 A-B].

However, assessment of chondrocyte lineage commitment gene *SOX9*, showed significantly reduced expression with Betulin treatment ($9.2x10^{-4}$ vs $1.2x10^{-4}$; $p=0.035$) [Figure 5.22 C].

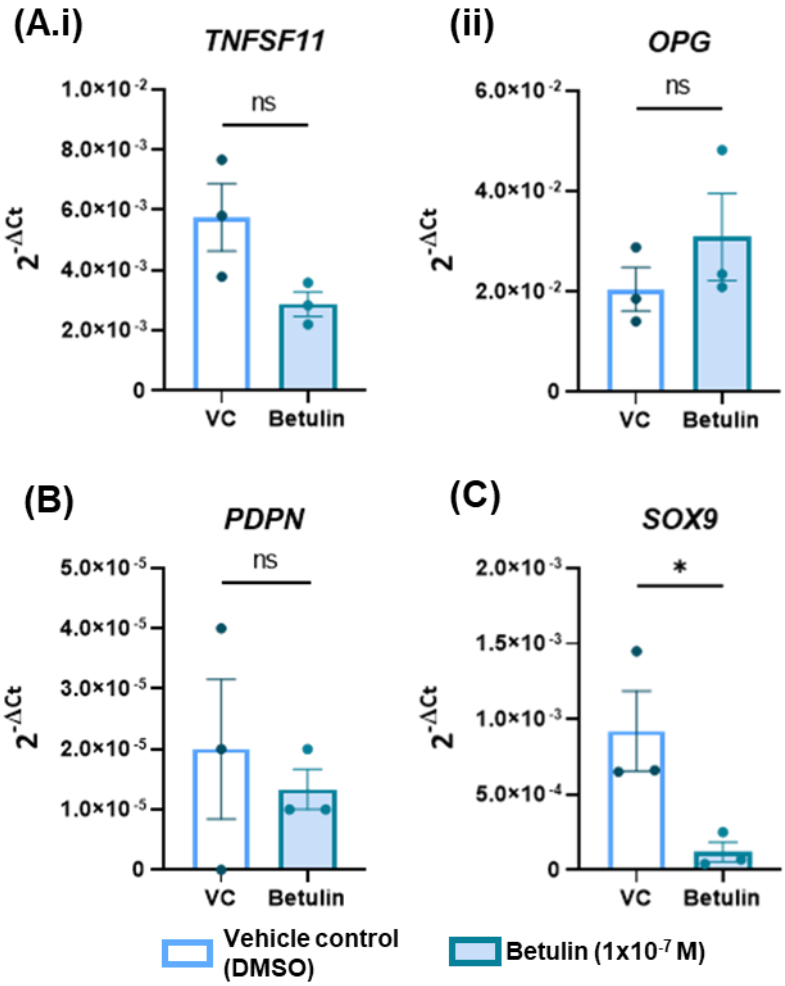


Figure 5.22 - qPCR analysis of resorption and formation regulation, osteocyte and chondrocyte related gene expression for 2D hFOB 1.19 treatment with Betulin. The expression of genes relating to resorption and formation regulation **(A)**, early osteocytogenesis **(B)**, and chondrocyte lineage commitment **(C)** was assessed in hFOB 1.19 cells cultured for 11-days with $1x10^{-7}$ M Betulin, vehicle control (VC) (DMSO), and non-treated. Results are mean±SEM (n=3). Raw Ct values analysed using unpaired t-test, with Welch correction if SD ratio = >2. * = $p<0.05$; ns = no significance.

5.4.2 SSBM Betulin treatment: qPCR analysis

qPCR was used to analyse gene expression of hFOB 1.19 SSBM constructs after 4-, 8- and 12-weeks of culture under osteogenic conditions, then treated for 11-days with $1x10^{-7}$ M Betulin, which were compared against the data previously attained for hFOB 1.19 SSBM constructs not treated – refer to [Section 4.2]. Refer to [Table 2.3] for gene

and TaqMan primer information. B2M was used as the housekeeping gene for the following qPCR analysis.

Four genes relating to matrix formation and maturation showed significant changes in expression in hFOB 1.19 SSBM cultures after Betulin treatment [Figure 5.23]. In comparison to non-treated SSBM constructs, *ALPL* showed increased expression after Betulin treatment for SSBM constructs with 4- and 8-weeks of prior osteogenic culture (4-weeks: $6.4x10^{-4}$ vs $826.7x10^{-4}$; p=<0.0001. 8-weeks: $4.6x10^{-3}$ vs $332.1x10^{-3}$; p=<0.0001). Similarly, *BGLAP* expression was significantly increased after Betulin treatment in 4- and 8-week cultured SSBM constructs (4-weeks: $7.1x10^{-6}$ vs $33.3x10^{-6}$; p=0.006. 8-weeks: $2.7x10^{-5}$ vs $11.0x10^{-5}$; p=<0.0001) and like *ALPL* expression, *BGLAP* expression was unaffected when SSBM constructs cultured for 12-weeks previously were treated. *COL1A1* expression also showed increased expression after Betulin treatment of hFOB 1.19 SSBM constructs previously cultured for 8- and 12-weeks of culture (8-weeks: $91.4x10^{-3}$ vs $332.1x10^{-3}$; p=0.002. 12-weeks: 0.15 vs 0.27; p=0.041). Finally, *SPARC* expression only significantly changed after Betulin treatment of SSBM constructs that were previously cultured for 8-weeks (0.11 vs 0.33; p=0.0008).

Three genes related to osteoblast lineage commitment and differentiation showed a significant change in expression after Betulin treatment in comparison to non-treated constructs [Figure 5.24 A]. In comparison to non-treated hFOB 1.19 SSBM constructs, *PHEX* and *RUNX2* expression both increased in 8-week cultured SSBM constructs (*PHEX*: $3.0x10^{-5}$ vs $10x10^{-5}$; p=0.031. *RUNX2*: $2.2x10^{-3}$ vs $13.6x10^{-3}$; p=<0.0001), but not in those SSBM constructs cultured for 4- or 12-weeks prior to Betulin treatment. *SP7* expression was found to have increased after Betulin treatment for SSBM constructs cultured for 8- and 12-weeks prior (8-weeks: $7.1x10^{-5}$ vs $13.7x10^{-5}$; p=0.049.

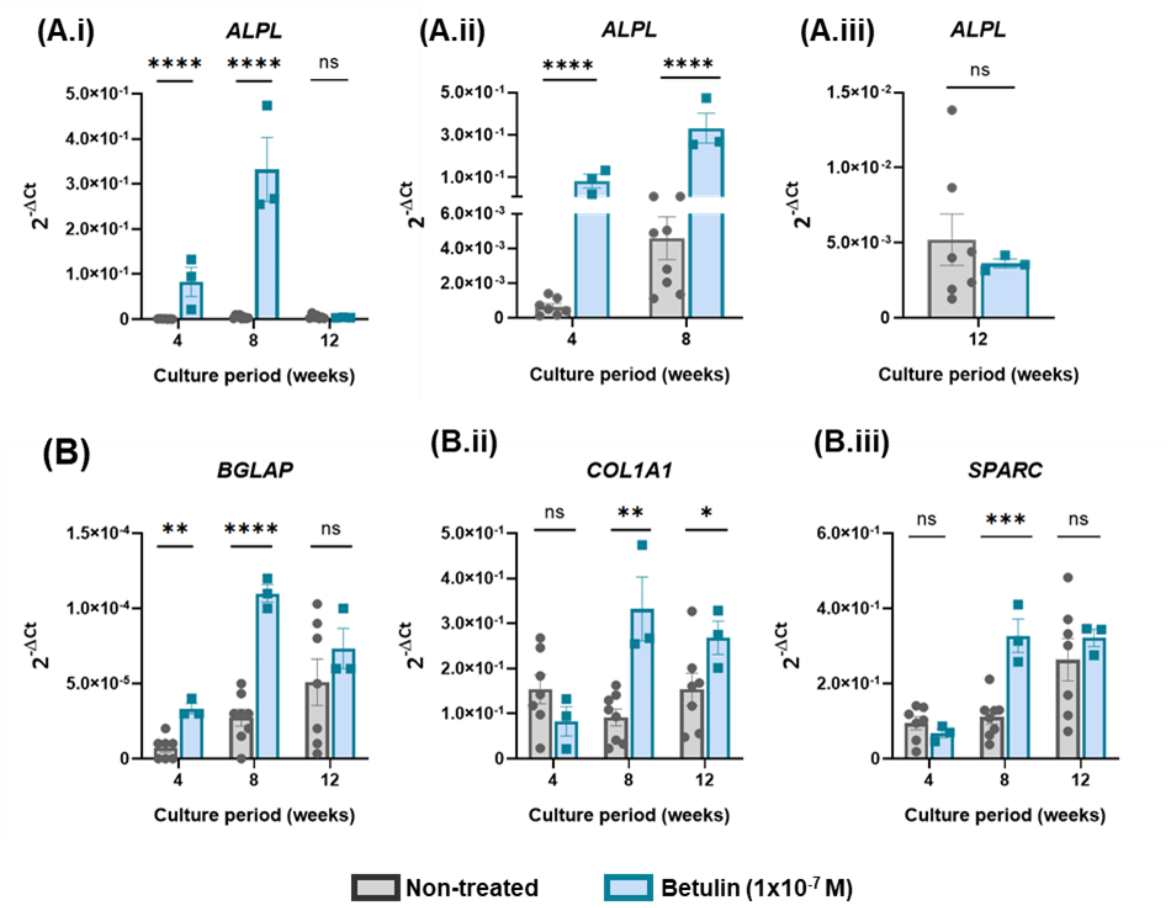


Figure 5.23 - qPCR analysis of matrix and mineralisation related gene expression for hFOB 1.19 SSBM construct treatment with Betulin. The expression of ALPL **(A)** as well as other matrix and mineral formation and maturation genes **(B)** was assessed in hFOB 1.19 cells cultured in 3D after 4-, 8- and 12-weeks, then treated for 1-week under osteogenic conditions with $1x10^{-7}$ M Betulin and compared against those not treated. Results are mean±SEM (n=3(treatment), 6-8(non-treated)). Raw Ct values analysed using unpaired t-test, with Welch correction if SD ratio = >2. * = p<0.05; ** = p<0.01; *** = p<0.001; **** = p<0.0001; ns = no significance.

12-weeks: $5.2x10^{-5}$ vs $10.3x10^{-5}$; p=0.021). Assessment of two genes associated with bone remodelling regulation [Figure 5.24 B] showed that *OPG* expression only significantly increased after Betulin treatment in hFOB 1.19 SSBM constructs cultured for 4-weeks prior ($7.1x10^{-5}$ vs $13.7x10^{-5}$; p=0.049) and not in constructs cultured for 8- or 12- weeks prior; whereas TNFSF11 expression showed to increase significantly after Betulin treatment in 4- and 12- week cultured constructs (4-weeks: $5.2x10^{-4}$ vs

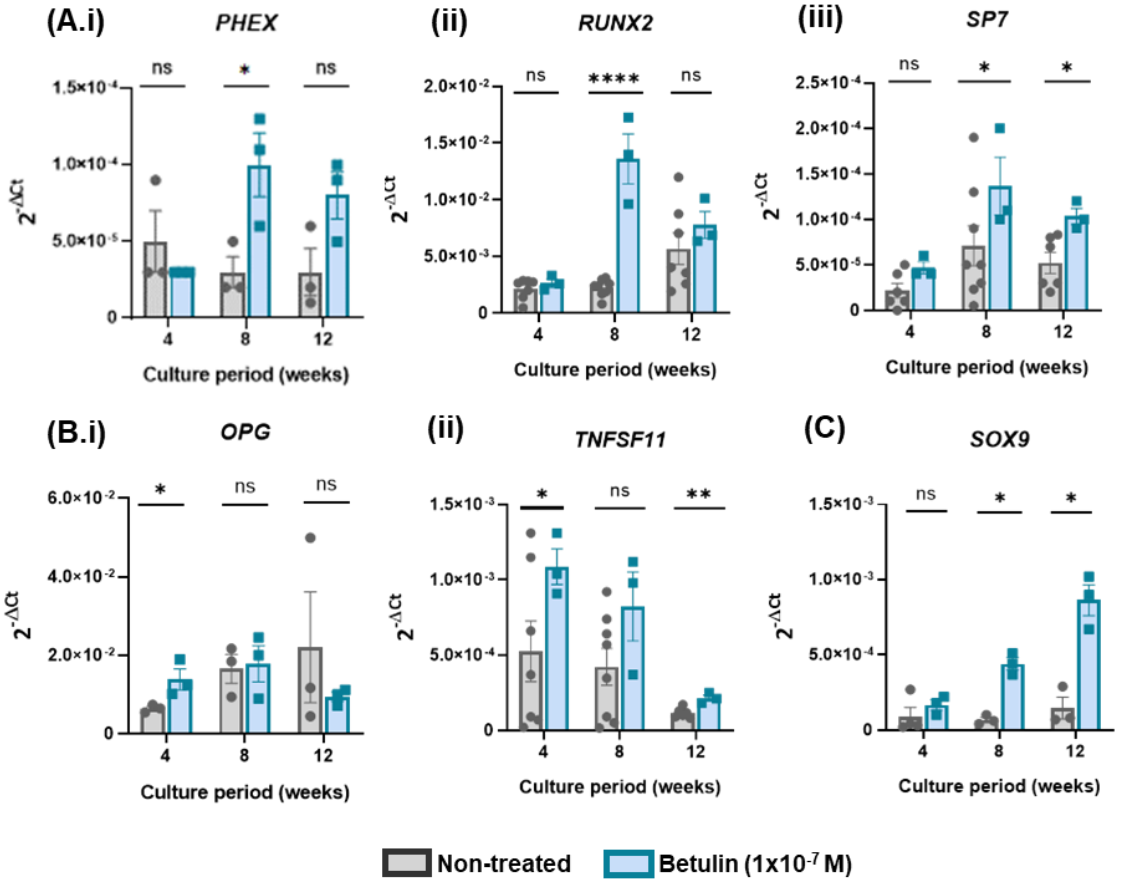


Figure 5.24 - qPCR analysis of osteoblast-specific and chondrocyte related gene expression for hFOB 1.19 SSBM construct treatment with Betulin. The expression of genes relating to osteoblast differentiation and commitment **(A)** formation and resorption **(B)** and chondrocyte lineage commitment **(C)** was assessed in hFOB 1.19 cells cultured in 3D after 4-, 8- and 12-weeks, then treated for 1-week under osteogenic conditions with $1x10^{-7}$ M Betulin and compared against those not treated. Results are mean±SEM (n=3(treatment), 3-8(non-treated)). Raw Ct values analysed using unpaired t-test, with Welch correction if SD ratio = >2. * = p<0.05; ** = p<0.01; **** = p<0.0001; ns = no significance.

$10.9x10^{-4}$; p=0.048. 12-weeks: $1.1x10^{-4}$ vs $2.1x10^{-4}$; p=0.008), despite an increase in expression seen in treated 8-weeks cultured constructs, which was found not to be significantly different. After Betulin treatment in 8- and 12-week cultured constructs, expression of the chondrocyte lineage commitment gene, SOX9, also increased significantly (8-weeks: $6.7x10^{-5}$ vs $44.0x10^{-5}$; p=0.011. 12-weeks: $1.5x10^{-4}$ vs $1.83x10^{-4}$; p=0.041) [Figure 5.24 C].

The only osteocyte-specific gene analysed to also show expression in non-treated hFOB 1.19 SSBM constructs, *PDPN*, [Figure 5.25] showed significantly increased expression after Betulin treatment at all analytical time points (4-, 8- and 12-weeks, respectively: $4.0x10^{-5}$ vs $34.7x10^{-5}$; p=0.036. $3.7x10^{-4}$ vs $38.2x10^{-4}$; p=<0.0001. $1.0x10^{-3}$ vs $5.7x10^{-3}$; p=0.034).

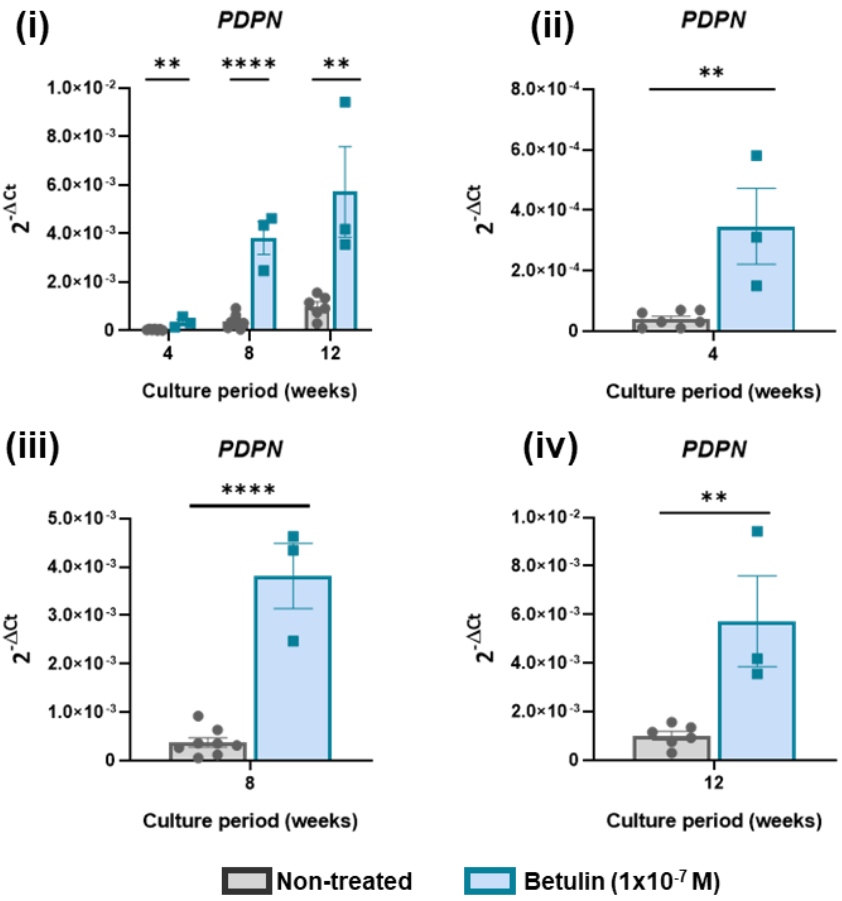


Figure 5.25 - qPCR analysis of podoplanin (PDPN) expression for hFOB 1.19 treatment SSBM construct with Betulin. The expression of PDPN was assessed in hFOB 1.19 cells cultured in 3D after 4-, 8- and 12-weeks, then treated for 1-week under osteogenic conditions with $1x10^{-7}$ M Betulin and compared against those not treated. Results are mean±SEM (n=3(treatment), 6-8(non-treated)). Raw Ct values analysed using unpaired t-test, with Welch correction if SD ratio = >2. ** = p<0.01; **** = p<0.0001; ns = no significance.

For genes not discussed here, results of those genes showed no significant changes after PTH treatment in comparison to those not treated at all analytical timepoints. Refer to [Appendix 8.3] for a full list of genes analysed.

5.4.3 SSBM Betulin treatment: ELISA analysis

Conditioned media was collected from hFOB 1.19 SSBM cultures treated for 11-days with $1x10^{-7}$ M Betulin, after 4-, 8- and 12-weeks of culture under osteogenic conditions – the 11-day treatment period included a 3-day construct isolation period prior to collection [Section 2.3.1]. Media was analysed by ELISA to determine OPG concentration and ALP activity [Section 2.3.2].

Results for OPG ELISA analysis [Figure 5.26 A] showed that after Betulin treatment, media collected from hFOB 1.19 SSBM constructs cultured for 4-weeks prior had a significantly greater OPG concentration than conditioned media from non-treated SSBM constructs (non-treat. vs Betulin: 0.49 ng/mL vs 1.9 ng/mL; p=0.074). However, results for constructs after 8- and 12-weeks of culture showed no significant change in concentration after treatment. Analysis of ALP activity [Figure 5.26 B] showed a reduction, as shown by a decrease in mean absorbance (i.e., OD at 405 nm) in response to Betulin treatment, in conditioned media of SSBM constructs cultured for 4-weeks prior (0.79 vs 0.35; p=<0.0001). However, for 8- and 12-week cultured SSBM constructs, ALP activity was significantly greater after Betulin treatment (8-weeks: 0.68 vs 0.93; p=0.039. 12-weeks: 0.61 vs 1.0; p=0.013).

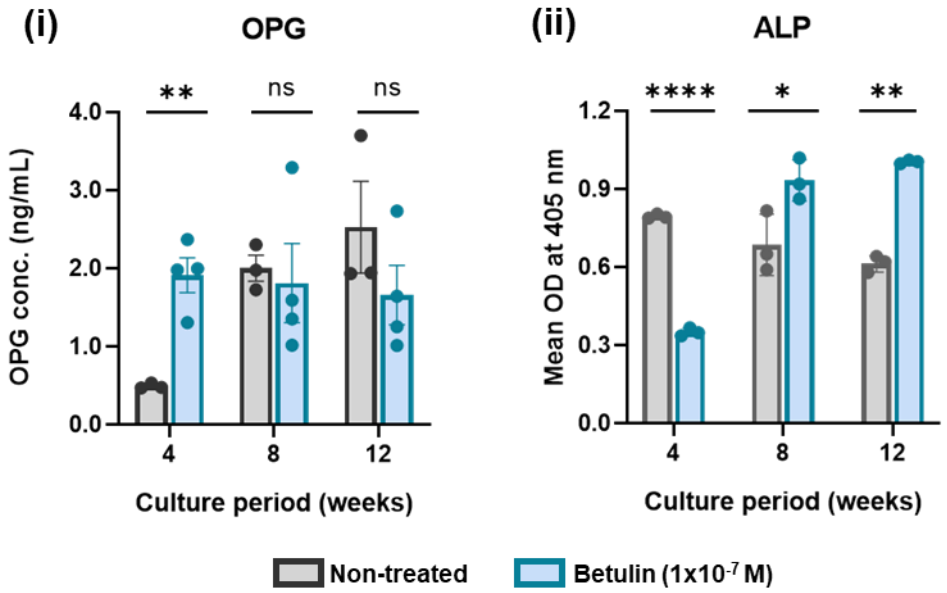


Figure 5.26 - Assessment of hFOB 1.19 SSBM construct conditioned media by ELISA after treatment with Betulin. hFOB 1.19 SSBM constructs cultured for 4-, 8- and 12-weeks post-cell seeding were treated with 1x10-7 M Betulin for 1 week. Conditioned media was collected from constructs isolated 3 days prior and then analysed by ELISA to measure the concentration of OPG **(i)** and examine ALP activity **(ii)** against those non-treated hFOB 1.19 SSBM constructs measured at the same analytical time points. Results are mean±SEM (n=3) and analysed using unpaired t-test, with Welch correction if SD ratio = >2. * = p<0.05; ** = p<0.01; **** = p<0.0001; ns = no significance.

5.4.4 SSBM Betulin treatment: IF analysis

Following the steps outlined in [Section 2.3.5], high-resolution images and z-stacks of a single hFOB 1.19 SSBM construct per culture period (4-, 8- and 12-weeks) and treated for 11-days with $1x10^{-7}$ M Betulin, were obtained to enable visualisation of cell organisation and expression of PDPN at the protein level [Figure 5.27].

In comparison to the non-treated hFOB 1.19 SSBM constructs, a notable increase in the presence of PDPN was detected after treatment with Betulin across all three culture periods. The regions of positive staining were more intense than those not treated and furthermore, there were also more areas of the hFOB 1.19 SSBM construct with PDPN staining, whereas with the non-treated constructs, 4- and 8-week SSBM constructs

had no or only very small, discreet areas of staining. However, the areas in which PDPN staining was observed followed the same pattern as before, with staining at 4-weeks initially seen in areas close to the anchors and over time progressing into the folded edges of the matrix and minimal staining within the central inner surface of the matrix; the latter primarily found in hFOB 1.19 SSBM constructs cultured for 12-weeks prior to treatment.

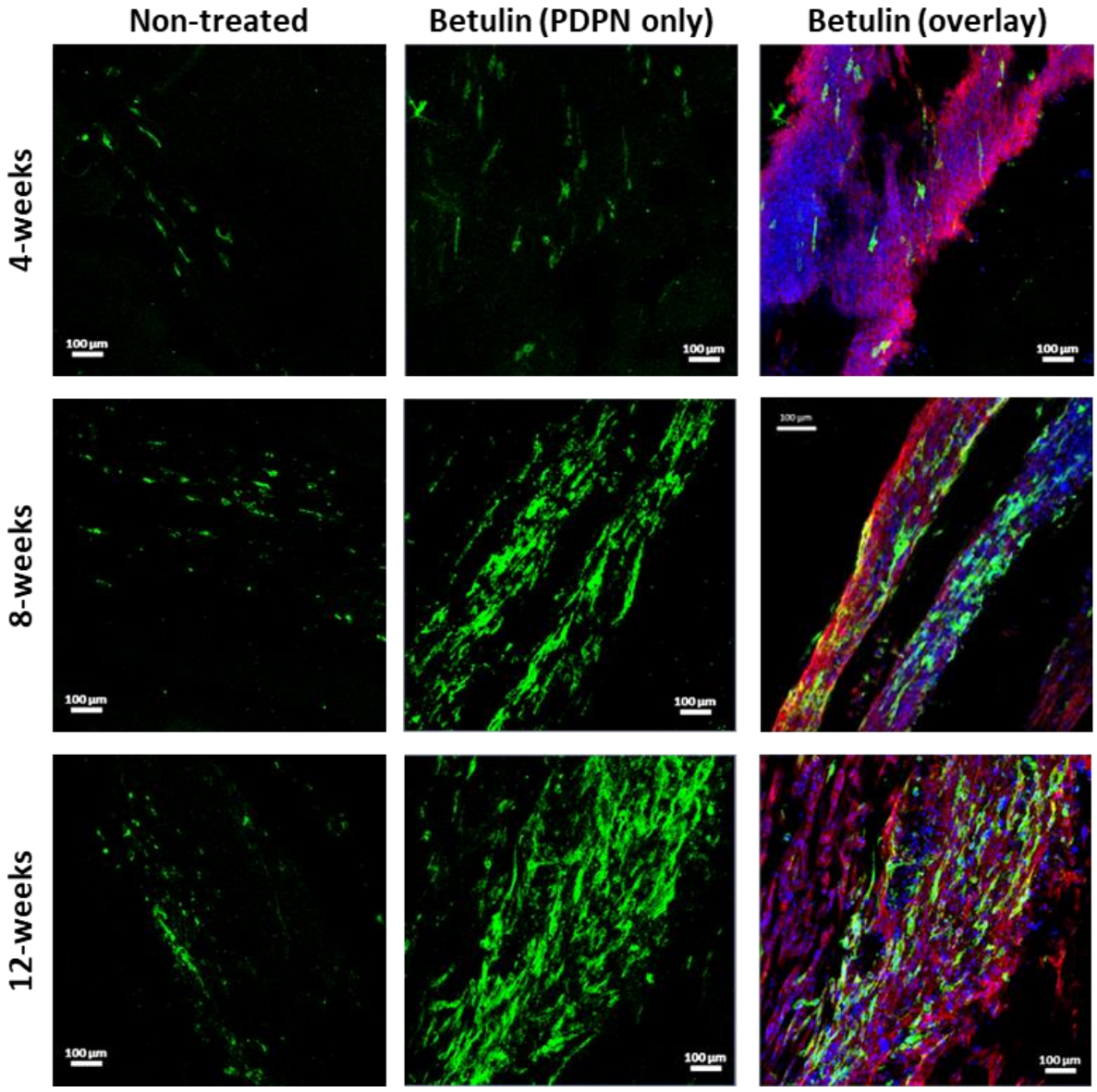


Figure 5.27 - IF staining detected a notable increase in podoplanin presence after Betulin treatment across all analytical time points. hFOB 1.19 SSBM constructs cultured for 4-, 8- and 12-weeks post-cell seeding were treated with $1x10^{-7}$ M PTH for 1 week. Constructs processed for IF staining and results compared against those non-treated hFOB 1.19 SSBM constructs. Shown were 50 µm sections with an actin (phalloidin; red) and nuclear stain (Hoechst; blue) and an anti-human podoplanin (PDPN) antibody (green). Scale bars = 100 µm. 10x magnification. PDPN images = maximum intensity projection z-stacks (Step size = 2.1 µm). Overlay images = single plane snap shot.

5.5 Bioprinting

5.5.1 Bioprinting observations

Bioprinting hFOB 1.19 constructs were prepared and created as outlined in [Section 2.6]. Three constructs were programmed to print in succession and all three were successfully printed, incubated and retrieved from the SLAM solution without breaking [Figure 5.28 A]. It was observed that the first construct printed (1) had a notably larger diameter and wall thickness, of which the latter was also uneven – as seen by the misshaped central canal that are more defined circles in the second (2) and third constructs (3) printed.

Over time, constructs did not contract, unlike the regular SSBM approach. Nor were cells detected outside of the construct e.g., adhered to the tissue culture plastic.

Constructs were prepared and IF stained following the steps outlined in [Section 2.3.5]. During cryosectioning, it was challenging to prevent the sections from rolling and tearing. IF staining showed that the constructs had very low cell numbers and adopted an elongated conformation similar to that seen in low seeding density cultures in 2D [Figure 5.28 B]. However, the cells that were present appeared viable, as indicated by the presence of intact cell nuclei within the positively stained actin.

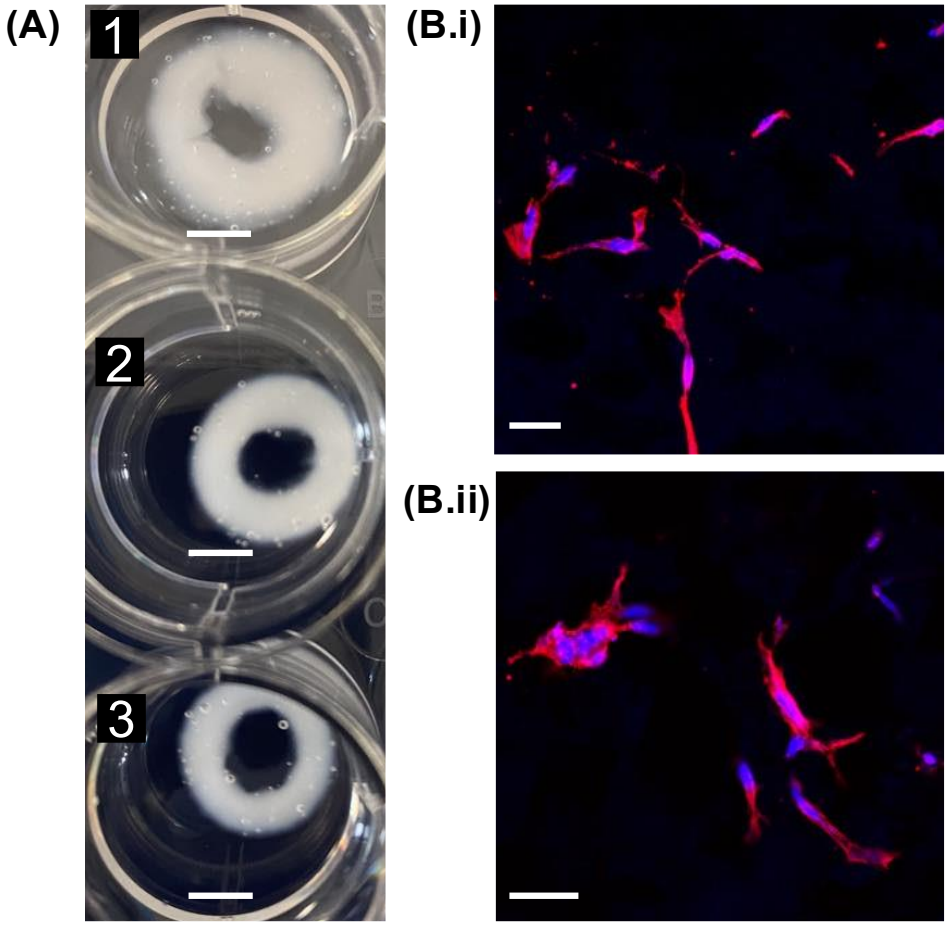


Figure 5.28 - Bioprinting enabled miniaturisation of hFOB 1.19 SSBM constructs. **(A)** Constructs containing hFOB 1.19 cells were printed sequentially (numbered black box) with identical parameters into wells of a 12-well plate and cultured under permissive conditions for up to 2-weeks. Scale bars = 5 mm **(B)** Constructs were processed for IF staining and imaging, revealing the presence of elongated cells (a typical morphology seen in low seeding density cultures) within the bioprinted structures after 2-weeks of culture under permissive conditions. Shown were 50 µm sections with an actin (phalloidin; red) and nuclear stain (Hoechst; blue). 10x magnification. Scale bars = 50 µm.

5.6 Discussion

5.6.1 2D investigations showed hFOB 1.19 were responsive to BFM treatments

Prior to treatment of hFOB 1.19 SSBM constructs with BFMs, 2D hFOB 1.19 cultures were used to establish an appropriate treatment regime, as well as determine if there were any adverse effects on cell proliferation and/or viability upon treatment with the

BFMs or vehicles. As discussed previously, the growth characteristics of hFOB 1.19 cells are unaffected when cultured either under 2D or 3D conditions (429), thus it was assumed the proliferation and viability results in 2D were reflected in 3D SSBM cultures.

Then, gene expression of 2D hFOB 1.19 cell cultures was analysed to ascertain if a detectable response could be measured. This was achieved by comparing qPCR data of VC-treated 2D hFOB 1.19 cells against that of non-treated cells (Control) to ascertain effects caused by the VC and provide a baseline upon which to compare BFM effects (505) which preceded after. A very different set of results were produced for each BFM tested after treatment, which was encouraging on two counts; that the BFMs of choice elicited measurable and significant responses by hFOB 1.19 cells, and that the varied outputs between each BFM showed that these responses were not by chance, and their different mechanisms of action can be detected at the gene expression level. 2D investigations for each BFM will be discussed briefly as follows.

5.6.1.1 2D responsivity: Vitamin D

Vit D treatment regime ($5x10^{-7}$ M Vit D, 1-week) was determined through preliminary investigations using hFOB 1.19 SSBM constructs and selected based on a qPCR finding that showed expression of a later osteocyte marker, *MEPE* [Appendix 8.3] and previous work by Harris *et al*. (375).EtOH showed improved viability signifincantly, with no effect with the inclusion of Vit D [Figure 5.1 B]. Timm *et al.* (561) showed that the ability of cells to tolerate EtOH is dependent on cell type, as well as the extracellular matrix; with notable changes in cell survival and activity influenced by EtOH concentrations as low as 0.01%. Therefore, it is not out of the question that this increased viability was a true response to the 0.001% of EtOH present in the VC and

Vit D media tested. Future work that concerns the use of EtOH and Vit D will investigate the effects EtOH by titring, as well as the possibility of using lower concentrations of the vehicle.

qPCR analysis [Figure 5.2-5.4] showed that VC treatment had no significant effect on the majority of the genes analysed, with the exception of osteoblast differentiation genes *PHEX* and *BMP2*, where EtOH reduced their expression. qPCR analysis of Vit D data compared to VC data for genes relating to bone matrix and mineralisation and chondrocyte lineage commitment showed *ALPL* was the only gene that had significantly increased expression. Although, the mean expression of *COL1A1, SPARC* and *SOX9*, did show an increased trend in expression, this was not statistically significant. Further gene expression analyses of Vit D treatment in 2D hFOB 1.19 cultures revealed an inhibitory action in osteoblast and osteocyte differentiation gene expression (i.e., *RUNX2, SP7* and *PDPN*), as well as a pro-resorptive role through increased expression of *TNFSF11* (i.e., RANKL), and no change in *OPG* expression. Despite not being statistically significant, due to very large variations in the VC data, *BGLAP* expression was undetectable for all replicates upon Vit D treatment.

Focussing on genes relating to osteoblast differentiation (*RUNX2, SP7*) and matrix formation and mineralisation (*ALPL, COL1A1, BGLAP*), Vit D treatment on *in vitro* cell cultures has produced contradicting results amongst published work, showing their expression to be inhibited, stimulated and have no effects at all - reviewed in detail by van de Peppel and van Leeuwen (562). This is primarily due to the variety of different cell types used (i.e., osteosarcoma cell lines, primary MSCs, rodent cell lines, human cells etc.), with Siggelkow *et al.* (563) showing that cell confluence is also a contributing factor to the effects of Vit D. Therefore, it cannot be concluded that the results from this

investigation are a true reflection of what to expect when treating hFOB 1.19 cells with Vit D, and also further highlights the controversial use of 2D cultures to predict *in vivo* responses.

During this investigation, the inactive form of Vit D, cholecalciferol, was used mistakenly, rather than the active form, calcitriol ($1,25(OH)_2D$) and no doubt contributed towards the lack of gene expression changes observed. However, there is published evidence that cholecalciferol does affect osteoblast proliferation and differentiation *in vitro* (564,565). Furthermore, it has been reported previously that osteoblasts are capable of converting inactive forms of Vit D to active calcitriol (566). Therefore, these and subsequent investigations involving Vit D were not omitted from this thesis. However, future investigations will also include assessment of SSBM response to calcitriol, which can be compared against these data obtained for cholecalciferol.

5.6.1.2 2D responsivity: Parathyroid hormone

The PTH treatment regime was determined by detecting changes in ALP activity, which is often used as an indicator of osteoblast metabolism and differentiation (260,400,567). Analysis of hFOB 1.19 cells cultured in 2D showed a significant increase in ALP activity after 7-days of treatment with 1x10-8 M and 1x10-7 M PTH in comparison to those not treated, and with no difference found between the two concentrations. After 11-days of treatment, there were no differences detected amongst the three tested conditions [Figure 5.10 A]. Based on these findings, a PTH treatment duration of 7-days (1-week) was decided upon and then based on the findings by Harris *et al*. (375), showing an increase in hFOB 1.19 metabolism with increasing concentrations of PTH, a treatment concentration of $1x10^{-7}$ M was used. Subsequent analysis of hFOB 1.19 cell cultures in 2D after PTH treatment showed that

the VC (d.H_2O) significantly increased live cell counts in comparison to the non-treated (control) but had no effect on cell viability. Furthermore, live cell count and viability were not affected with the inclusion of PTH, both of which were found to not to be significant in comparison to the VC [Figure 5.10 B].

qPCR analysis [Figure 5.11-5.13] found that gene expression was not significantly affected after treatment with the VC. Although, there was a general (non-significant) reduction in expression seen in genes relating to matrix and mineralisation and osteoblast differentiation, and a non-significant increase in expression of chondrocyte commitment lineage (*SOX9*) and pro-resorptive (*TNFSF11*) genes. However, expression of a number of genes were undetectable entirely upon VC treatment and were not recovered with the addition of PTH. This inhibitory effect shown in [Figure 5.13] was not caused by batch-batch formulation differences, as all qPCR analysis for this investigation was from a single occasion, with each repeat treated with a single preparation of VC and PTH throughout the duration of the investigation and the other genes analysed showed expression like that of non-treated (control) cultures. Nor was this inhibitory effect caused by an innate or batch issue with the cells used, as non-treated cells were acquired from the same cell suspension and as before, gene expression was present for all genes analysed for non-treated cells and the remaining genes for treated cells. The most likely explanation for this inhibitory effect was simply due to user error, where the VC treated cells were mistakenly treated with PTH either during VC preparation, media changes, or plating the cells. This assumption was backed up by the lack of significant changes in gene expression between the VC and PTH treated cells, apart from *ALPL* and *COL1A1,* which show a small significant increase in expression after PTH treatment. If the results here were found to be a true

response to the VC and PTH, it can be concluded that the actions of PTH at the genetic level are limited to that of upregulating matrix production and ALP activity; the latter of which was found at the protein level [Figure 5.10 A].

5.6.1.3 2D responsivity: Betulin

Like PTH, the Betulin treatment regime was determined by detecting changes in ALP activity. Concentrations and incubation times were selected based on the findings by Mizerska-Kowalska *et al.* (400), which showed no cytotoxicity and maintained normal proliferation of 2D hFOB 1.19 cells treated with Betulin at concentrations below $5x10^{-7}$ M as well as significant increases in gene expression of *RUNX2*, *ALPL* and *COL1A1* between 9- and 12-days of culture. ALP activity after 7-days of culture was found to have significantly increased in cells treated with $1x10^{-7}$ and $3x10^{-7}$ M Betulin, however after 11-days of culture, there was no significant difference seen [Figure 5.19 A]. The Betulin concentration that was used for this project ($1x10^{-7}$ M) was chosen based on the most significant increase in ALP activity detectable at 7-days - which also displayed the greatest activity after 11-days (although not statistically significant). The treatment duration (11-days) was selected based on the work carried out by Mizerska-Kowalska *et al.* (400) which showed the most significant increases in gene expression between culture periods of 9 and 11-days, whilst also considering that the results from this investigation showed no detrimental effect on ALP activity after 11-days of Betulin treatment. In comparison to the non-treated cells, live cell numbers of 2D hFOB 1.19 cells was unaffected after 11-days of treatment with $1x10^{-7}$ M Betulin or the VC (DMSO) [Figure 5.19 B.i], which was also found previously (400). However, the viability of the cultures improved significantly in the presence of DMSO, of which was maintained with the addition of Betulin [Figure 5.19 B.ii]. Like EtOH, DMSO can both improve and

reduce cell viability, differentiation and integrity at low concentrations and is dependent on cell type and exposure period (568–571).

qPCR analysis for 2D hFOB 1.19 cells treated with Betulin did not have a non-treated control as a comparator for the VC treated cells due to low total RNA extraction on the first occasion and failure of the housekeeper genes on the second occasion. In comparison to the VC, Betulin showed reduced expression across the majority of the genes analysed, with significant reduction detected for *BGLAP, COL1A1, RUNX2, SP7* and *SOX9* - exceptions to this were the expression of *BMP2* and *OPG*, which both showed non-significant increased expression after Betulin treatment [Figure 5.20-5.22]. These results contradict those found previously (400).

It was difficult to ascertain whether this was erroneous qPCR data or a true response to the VC and Betulin, particularly in the absence of non-treated data. There was no indication of potential errors in regard to RNA extraction, as there were similar concentrations of RNA measured between the VC and Betulin-treated samples, which were both immediately converted to cDNA. Although, qPCR of the VC and Betulin-treated samples were performed on separate occasions, which can introduce variation through errors such as incorrect dilutions, freeze-storage damage. The opinion here was that this was not a true reflection of hFOB 1.19 cells responding to DMSO and was due to errors occurring during the treatment period, or at least one of the qPCR steps. This was based on the unexpected increase in viability with VC treatment – where the majority of cells treated with DMSO report falling viability – as well as understanding the sensitivity of qPCR analysis where repetition of the same samples has produced very different results.

In order to determine whether these data was the result of qPCR errors, the remaining (stored) RNA would be converted to cDNA and qPCR analysis repeated using the new samples. However, due to the lack of non-treated samples, it would be recommended that the investigation of 2D hFOB 1.19 responsivity to Betulin be repeated with to include non-treated samples as well as VC and Betulin-treated samples.

5.6.2 hFOB 1.19 SSBM constructs had measurable responses to BFM treatments

As all three BFMs elicited a detectable response at the level of gene expression on 2D cultured hFOB 1.19 cells, testing these same BFM treatments on 4-, 8- and 12-week cultured hFOB 1.19 SSBM constructs proceeded. In order to carry out all the intended analytical methods with statistical testing, as well as culturing plates for other analyses not involved in responsivity, a large number of plates was set up and cultured at the same time. With limited incubator space, lengthy culture periods (12-weeks) as well as added demands on workload and reagent needs, it was not feasible to culture enough SSBM constructs at the size that they are currently made to treat with the VCs, in addition to the BFMs. Therefore, BFM results were compared against those previously attained from analyses of non-treated hFOB SSBM constructs [Chapter 4 - Biological characterisation of hFOB 1.19 SSBM constructs].

Results showed that hFOB 1.19 SSBM constructs responded to the presence of all three BFMs, which were detected by changes in gene expression (qPCR), protein production (OPG ELISA and IF analysis) and enzyme activity (ALP ELISA). Responses differed in pattern and magnitude for each BFM, as seen during 2D investigations, thus showing that the responses seen were reflective of the different mechanisms by each BFM. Results from each of the three BFMs tested will be discussed separately.

5.6.2.1 hFOB 1.19 SSBM construct responsivity: Vitamin D

As mentioned previously [Section 5.6.1.1], the Vit D used here was the inactive form, cholecalciferol, and therefore it was expected that there would be very little response from the SSBM constructs. Results from Vit D treatment of hFOB 1.19 SSBM constructs provide evidence of greater cholecalciferol activity on matrix production and early osteocytogenesis, with lesser effects on osteoblast differentiation and chondrocyte lineage commitment.

qPCR analysis found that the expression of matrix and mineralisation genes (*ALPL, SPARC, BGLAP*) were most affected after Vit D treatment, as significantly increased expression was detected at every culture period in at least one of these genes [Figure 5.5 A]. The same can be said for the expression of early osteocyte gene marker, *PDPN*, which showed a significant increase in expression at every culture period [Figure 5.7]. Fewer, if any, gene expression changes were seen in those relating to osteoblast differentiation (*RUNX2, SP7*), bone remodelling regulation (*TNFSF11, OPG*) and chondrocytes (*SOX9*) after Vit D treatment. This coincides with the findings of previous studies that also used cholecalciferol, where treatment showed increased matrix production and mineralisation at the structural level (564,565), although no reported effect on osteoblast differentiation, which is increased in the presence of calcitriol. Thus, the findings from the treatment of hFOB 1.19 SSBM constructs provide more evidence that cholecalciferol is not completely inactive and has anabolic effects by stimulatory actions on osteoblasts.

However, findings from SSBM investigations did not align with those found for 2D hFOB 1.19 cultures treated with Vit D, which showed little effect on the expression of the majority of genes analysed. Although, 2D hFOB 1.19 cultures showed a significant

increased effect on the expression of pro-resorptive gene, *TNFSF11*, and despite no significant difference detected, there was a greater expression of this gene in comparison to non-treated at all three timepoints. So, whilst the Vit D here showed an anabolic effect, like most BFMs, there was also some evidence of a catabolic effect. Further investigation into other pro-resorptive genes and protein expression is required to confirm this, similar to that performed by Vu *et al.* (565) who showed cholecalciferol to reduce the size and number of resorptive pits when tested on 3D *in vitro* scaffolds containing active osteoclasts.

ELISA analysis of conditioned media from non-treated and Vit D-treated constructs showed an increase in OPG concentration and an initial decrease in ALP activity in 4-week constructs treated with Vit D, but with no significant difference from non-treated result at the later time points. In comparison to the qPCR data, there was a rise in *OPG* expression after treatment for 4-week constructs, although not significant, and furthermore conclusions cannot be made for 8- and 12-weeks due to insufficient repeats. *ALPL* expression on the other hand had increased expression after treatment with Vit D treatment in 4-week constructs, contradicting the ELISA results. This is further discussed in [Section 5.6.2.4].

5.6.2.2 hFOB 1.19 SSBM construct responsivity: Parathyroid Hormone

hFOB 1.19 SSBM constructs cultured for 4-, 8- and 12-weeks prior showed detectable and significant changes in gene and protein expression and activity in response to PTH treatment. Results revealed a time-dependent action of PTH on hFOB 1.19 cells affecting matrix formation and mineralisation, osteoblast differentiation, chondrocyte lineage commitment and early osteocytogenesis.

qPCR analysis found that gene expression was not significantly affected after PTH treatment for most genes tested; the majority of which displayed a significant difference in comparison to non-treated SSBM constructs at only one analytical time point (*BGLAP, SPARC, RUNX2, SOX9* and *OPG*) - mainly in SSBM constructs cultured for 8-weeks prior, except for OPG (4-weeks) [Figures 5.14-5.15]. Those that showed no significant changes in expression at any time point can be found in [Appendix 8.3]. Previous findings by Isogai *et al.* (572) showed that the effects of PTH on osteoblast differentiation is dependent on osteoblast maturity, with a preference for stimulating immature cells and inhibiting mature cells, and gene expression changes of SSBM constructs at the 8-week timepoint after PTH treatment exemplifies this effect. At this timepoint, hFOB 1.19 SSBM cells had been cultured under osteogenic conditions for four weeks and thus more immature than those present at the 12-week timepoint. Whereas at 4-weeks post-cell seeding, hFOB 1.19 cells had not been under osteogenic conditions and thus were at a pre-osteoblastic stage and not respond to PTH as expected.

PTH treatment showed to significantly increase expression of pro-resorptive gene, *TNFSF11*, in constructs cultured for 4- and 12-weeks prior. In contrast, as mentioned above, pro-anabolic gene, *OPG,* expression is only significantly changed (increased) by PTH at 4-weeks with non-significantly reduced expression in constructs cultured 8- and 12-weeks prior. These results indicate that the SSBM culture system promoted the pro-resorptive actions of PTH which occurs *in vivo* and *in vitro* by upregulation of RANKL (encoded by *TNFSF11*) and downregulation of OPG via gene expression with prolonged PTH exposure (94,541,573). It was also found previously that the pro-

resorptive effect by PTH exposure selectively increased *TNFSF11* expression in mature osteoblasts whilst downregulating *OPG* in early osteoblasts (94).

Overall, where PTH treatment showed to affect expression, it significantly increased expression of genes relating to matrix formation and mineralisation, osteoblast differentiation, chondrocyte lineage commitment and early osteocytogenesis. This contradicts the findings of 2D hFOB 1.19 cultures treated with PTH, which showed very little effect on gene expression, or an inhibitory effect on a range of genes.

ELISA analysis of conditioned media from non-treated and PTH-treated constructs showed a significant increase in OPG concentration after PTH treatment of 4-week mature SSBM constructs, and no significant effect seen at the later time points [Figure 5.17 A]. This aligns with the data obtained from qPCR, where OPG expression significantly increases after PTH treatment only in hFOB 1.19 SSBM constructs cultured for 4-weeks prior [Figure 5.15], thus strengthening the authenticity of this response to PTH treatment by the hFOB 1.19 SSBM constructs. However, whilst ALPL expression is not significantly affected by PTH treatment at any of the analytical time points, ALP activity showed a very significant decline after PTH treatment of 4-week cultured SSBM constructs, whereas 8- and 12-week cultured constructs showed an increase in ALP activity – only found to be significant in 12-week cultures [Figure 5.17]. This is discussed further in [Section 5.6.2.4].

5.6.2.3 hFOB 1.19 SSBM construct responsivity: Betulin

hFOB 1.19 SSBM constructs cultured for 4-, 8- and 12-weeks prior showed detectable and significant changes in gene and protein expression and activity in response to Betulin treatment. Betulin elicited large promoting effects on matrix production,

osteoblast differentiation, chondrocyte lineage commitment and early osteocytogenesis.

qPCR analysis showed increased expression in the majority of the genes analysed, in at least one analytical timepoint, after hFOB 1.19 SSBM constructs were treated with Betulin [Figures 5.24-5.26]. These results opposed those that were found for 2D hFOB 1.19 cultures, where Betulin showed to have no effect or downregulatory effect on gene expression, although this could not be concluded due to the lack of a non-treated control, along with questionable results obtained from the VC-treated constructs. Instead, results from the Betulin-treated hFOB 1.19 SSBM cultures were similar to those found by Mizerska-Kowalska *et al.* (400), which showed significant expression of *ALPL, COL1A1* and *RUNX2* in 2D cultured hFOB 1.19 cells after 12 days of Betulin treatment. Therefore, it is likely an error had occurred during 2D investigations of Betulin.

Apart from *OPG and TNFSF11* – as well as those that showed no significant change in expression in comparison to the non-treated SSBM constructs [Appendix 8.3] - the remaining genes showed significantly increased expression for constructs that had been cultured for 8-weeks prior to Betulin treatment. Again, a similar time-dependent finding also found with Vit D- and PTH-treated SSBM constructs - discussed in further detail in [Section 5.6.2.4].

Expression of genes associated with regulating formation (*OPG*) and bone resorption (*TNFSF11*) [Figure 5.24 B] increased significantly after Betulin treatment in SSBM constructs cultured for 4-weeks prior. Then *TNFSF11* expression significantly increased again in Betulin-treated constructs cultured for 12-weeks prior, whereas

expression of OPG was unaffected after 4-weeks. These results indicate Betulin has a pro-resorptive effect, as well as a pro-anabolic effect, which is normally found with an agent that promotes bone formation due to the negative feedback loop that exists within the bone remodelling process to regulate the balance between bone formation and resorption (574–576).

ELISA analysis of conditioned media from non-treated and Betulin-treated constructs showed a significant increase in OPG concentration after Betulin treatment of 4-week mature SSBM constructs, and no significant effect seen at the later time points [Figure 5.26 A]. This aligns with the data obtained from qPCR, where *OPG* expression significantly increases after Betulin treatment only in hFOB 1.19 SSBM constructs cultured for 4-weeks prior [Figure 5.24 B], thus strengthening the authenticity of this response to Betulin treatment by the hFOB 1.19 SSBM constructs. ALP activity was affected after Betulin treatment at all analytical time points, with significantly increased activity in constructs treated for 8- and 12-weeks prior to treatment. However, the same significant decline after treatment with Vit D [Figure 5.8] and PTH [Figure 5.17] in 4-week cultured SSBM constructs was seen after Betulin treatment. This is discussed further in [Section 5.6.2.4].

5.6.2.4 hFOB 1.19 SSBM construct responsivity: Conclusions

The data obtained from qPCR and ELISA analysis has been discussed for each BFM treatment separately, as they all produced very different data sets and were compared individually (i.e., BFMs weren't compared against each other). However, similar trends and observations within the individual data sets occurred and is discussed here.

One of the most striking observations during qPCR analysis was the significantly increased expression of *PDPN* across all the analytical time points after treatment with any of the three BFMs [Figures 5.7, 5.16 & 5.25]. Furthermore, this increased expression in *PDPN* translated to a visibly significant increase in PDPN using IF staining [Figures 5.9, 5.18 & 5.27]. The pattern of development was the same as that seen in non-treated constructs, which indicates that greater osteoblast maturation primarily occurred within the densely folded/contracted edges of the constructs and within the vicinity of the anchors. Given the lack of vascularisation, the microenvironment within these areas of the constructs is expected to be more hypoxic with a lower pH than the edges. These conditions have been previously found to encourage osteoblast differentiation towards osteocytogenesis (577,578) and do not affect osteocyte viability (579). These results highlight the presence of mature osteoblasts in these regions of the SSBM constructs and treatment by the three BFMs tested here encouraged differentiation of these cells towards an early osteocyte phenotype. As the expression of PDPN was not homogenously distributed throughout the constructs, it was determined that quantification of PDPN using IF staining and imaging analysis was not likely to produce accurate data. Therefore, more accurate methods of quantification, such as western blotting and flow cytometry, should also be developed, optimised and employed to gain a more accurate reflection of the amount of PDPN and PDPN-expressing cells present within SSBM constructs.

Another common trend between each of the BFMs tested was a rise in *OPG* expression (qPCR) and OPG concentration (ELISA) in 4-week cultured hFOB 1.19 SSBM constructs after treatment [Figures 5.8A, 5.17A & 5.26A]. Previously, overexpression of OPG was found to promote osteoblast differentiation (580) and as

the cells within 4-week cultured constructs had been under non-osteogenic culture conditions, it can be assumed that they are pre-early osteoblastic cells. This increase in OPG at the mRNA and protein level indicates that these BFM treatments initiated osteoblast differentiation of preosteoblastic cells.

Yu *et al*. (580) also showed an accompanying increase in ALP activity, which was not seen with the 4-week cultured SSBM constructs, and instead showed a sharp decrease in ALP activity after treatment with any of the three BFMs [Figures 5.8B, 5.17B & 5.26B]. However, ALP activity recovered to either non-treated levels, or greater, after treatment with BFMs in 8- and 12-week constructs. It was likely that these results seen for the 4-week SSBM constructs were contributed by random and/or systematic errors, such as FBS composition where ALP content can vary greatly between batches (581), imprecise pipetting of samples and or pNPP, or inadequate sample storage or processing. Considering the ALP assay performed for analysis of conditioned media samples from SSBM constructs does not include the initial cell lysis steps that are carried out for 2D cell cultures, these results indicate that further optimisation of this method is required, or a new approach must be taken to measure ALP activity.

It can be argued that there was little value to measure the effects of BFMs on hFOB 1.19 SSBM constructs after 4- and 8-weeks of culture when there was a lack of mineralisation, as according to XRF results significant mineralisation of the constructs was not established until after 12-weeks of culture [Section 3.5]. However, this culture system supports the long-term culture of osteoblasts through the early to later phases of differentiation, as indicated by the outcomes of chapter 4, which cannot be reliably achieved under 2D conditions. Therefore, it is beneficial to use these models for drug

testing when the focus of the experiment is looking at drug impact on osteoblasts of different maturity (early, mid to late osteoblasts). For example, the SSBM culture system can be used to determine whether the same differential effects of PTH on early and mature osteoblasts can be demonstrated in 3D in vitro culture as they have been shown previously under 2D conditions (94). Furthermore, where the drug in question focusses on promoting mineralisation, the SSBM culture will provide a platform in which changes in the time for mineralisation to occur can be observed and measured (i.e., structural analysis of SSBM constructs after drug treatment will show the emergence of mineral sooner or later than the 12-week timepoint).

It can be confirmed that hFOB 1.19 SSBM constructs were responsive to Vit D, PTH and Betulin solutions, the responses of which were detected and measured through changes in gene and protein expression. These data showed that the effect of each individual BFM treatment was dependent on the maturity of the cell and/or the matrix composition of the SSBM constructs. Firstly, genes that showed significant changes in expression by BFM treatment were often not seen at all three analytical time points (e.g., SPARC expression in response to any BFMs). Secondly, genes that showed significant expression changes at more than one timepoint had p values (calculated between the non-treated and treated constructs) that varied markedly (e.g., *PDPN* expression in response to any BFM showed lower p values in 4- and 12-week cultured SSBM constructs than those cultured prior for 8-weeks). This osteoblast maturation-dependent effect was exemplified by Isogai *et al.* (572) who showed PTH preferentially stimulated immature cells and inhibited mature cells, and also by Owen *et al.* (267) who showed early osteoblast type I collagen and ALP mRNA expression to be inhibited by Vit D but stimulated in more mature osteoblast cultures. This model therefore

provides a platform for research into elucidating the mechanisms behind cell maturity-dependent effects by BFM.

5.6.2.5 hFOB 1.19 SSBM construct responsivity: Future improvements

Despite the successes achieved from the SSBM responsivity investigations, the lack of time and large workload made an impact on many aspects of the investigation. As such, the following areas of the responsivity investigations need addressing if they were to be repeated, as well as prior to conducting future responsivity work.

- **Determining optimal treatment regimes:** Except for Vit D, 2D cultured hFOB 1.19 cells were treated with BFMs and VCs to determine the treatment regime for the 3D investigations. The selected concentrations and durations were based on previous work that had been performed (375), however, only a small number of concentrations and durations were investigated. Therefore, all BFMs will require more thorough 2D investigations prior to commencing treatment, by testing a broader spectrum of BFM concentrations, as well as the dosing frequencies and duration. Furthermore, the half-life of the BFMs (PTH in particular which is 1 hour (582)) was not considered, and therefore it will be beneficial to determine dosing frequency, as well as duration. Also, further analytical methods to determine the optimal treatment regime for each BFM and respective VC, such as metabolic and viability assays (e.g., MTT and Lactate dehydrogenase assays, respectively) and mineralisation assays (e.g., Alizarin red S) will need to be included.
- **Inclusion of VCs:** Due to the lack of time remaining on the project and the size of the SSBM cultures (i.e., 6-well plate), vehicle controls were not included in the 3D investigations as this will have added to the already demanding

workload, as well as impacted on the limited culture resources and reagent availability. However, for future repetitions and responsivity investigations, it will be necessary to include VC treated SSBM constructs alongside BFM treated constructs. Inclusion of these constructs will make the findings from treated constructs more conclusive, as it cannot be fully concluded whether the responses seen in the current investigations were due to effects by the vehicle and/or the BFM treatment without the VCs present.

- **Refining the investigation for manageable workload:** There were a number of errors made that were a result of having a large workload, including using the inactive form of Vit D, as well as treating 2D hFOB 1.19 cells with PTH only, instead of PTH and its VC. Upon repeating these investigations, it will be considered whether it is necessary to analyse responsivity at all three timepoints, which analytical methods are crucial (which determines how many constructs are required for each treatment and timepoint) and consider investigating each BFM separately, instead of concurrently. These considerations will depend on the research question in mind and whether time is not a limiting factor, although now having hindsight is an added advantage to the decision-making process.
- **Miniaturisation of the SSBM culture system:** As mentioned above, the current size of the SSBM constructs (i.e., 6-well culture plates) is considered to be large and as such limited the available incubation space and required large quantities of hydrogel components and culture reagents. By reducing the size of the constructs from a 6-well culture plate to a single 12-, 24- , 48-well plate, more constructs can be created with the same volume of reagents and

incubation space that would be required. This would enable inclusion of multiple treatment conditions and regimes (e.g., BFM concentrations, durations, and frequencies; VCs; more technical replicates) without impacting on limited resources.

5.6.3 Miniaturisation of hFOB 1.19 SSBM constructs is possible

As discussed in [Section 5.6.2.5], one of the most limiting factors for the responsivity investigation was due to the current size of the hFOB 1.19 SSBM constructs, which meant fewer technical repeats and no VC-treated constructs were present during the SSBM responsivity investigations. Reducing the size of these constructs will enable a more pragmatic and improved investigation by increasing the number of repeats for each condition tested, including vehicle controls, and without adding to the maintenance workload. However, miniaturising these constructs by hand is slow, which affects polymerisation of the hydrogel, as upon addition of thrombin to fibrinogen solution requires incubation no more than 1 minute after, otherwise the integrity of the resultant hydrogel is affected and may fail to support cell cultures. Furthermore, this approach is subjected to systematic error, such as through variations in pipetting-volume and construct size caused by misplacement of anchor distances.

Bioprinting can overcome the issues of miniaturising the SSBM constructs. As an automated system, bioprinting enables more control, precision and accuracy of rapidly and repeatedly creating multiple constructs than is possible to achieve by hand (583). Factors such as extrusion rate, construct shape and size, as well as chamber temperatures can be controlled within bioprinters, thus providing a solution to overcoming the obstacles of miniaturising the SSBM constructs – Bioprinting using

SLAM in particular enables less viscous materials (such as thrombin solution and fibrinogen) to be injected into an inert gel and create a scaffold of fine detail (560,584).

The features offered from bioprinting results in the fabrication of constructs that fulfils the requirements essential for biological platforms within high-throughput assays. In drug discovery, high-throughput assays are designed to test the responsivity of a biological system when treated with compounds – often thousands to millions of compounds at various concentrations per investigation – rapidly and reproducibly (585,586). As such, these systems require scalability and a high degree of intra- and inter-assay precision, which is achieved by the finely tuned and controlled automated features of bioprinting (e.g., incubation conditions, extrusion pressures and rates, construct shape and size). One of the potential avenues of development for the SSBM culture system is to use it as a platform in a high-throughput assay. As shown in the responsivity investigations, responses are measurable when SSBM constructs are treated with BFM solutions, therefore by investigating the ability to print smaller, cell containing SSBM constructs followed by maintenance in culture was the first step to assessing the feasibility of not only creating a more efficient research platform, but also the potential to developing a high-throughput platform.

SLAM-printed structures were printed and cultured successfully for two weeks [Figure 5.28]. It was also noted that the shape of the first construct printed was asymmetrical in comparison to the other two [Figure 5.28 A]. Despite having primed the needle with fibrinogen solution and ensuring air bubbles were removed, the time between priming and commencing printing – although short >1 minute – the higher pressure inside the needle is likely to have caused the fibrinogen to become more viscous, which occurs naturally for fibrinogen at RT and when stored in the fridge at 2-4 °C – and eventually

solidifying after <24 hours and 2-3 days, respectively (unpublished observations from local experts on the SLAM methodology). However, this did not impacted on printing the subsequent constructs, therefore it is advisable for future studies to initially print a separate structure to ensure all subsequent constructs are homogenous.

It was also noted that unlike hand-extruded SSBM constructs, bioprinted SSBM constructs did not contract and they retained their printed shape and size. Despite the absence of CaP anchors, it has been shown that seeded cells were responsible for contraction of the fibrin hydrogel (392,395). IF staining and imaged revealed that the cell population within the SSBM constructs was low and the cells that were present had adopted an elongated morphology which is normally observed in low seeding density cultures (587) [Figure 5.28 B]. This low seeding density is unlikely to have been sufficient to have caused contraction of the matrix. This low seeding density was attributed to an operator error whilst preparing for bioprinting; the fibrinogen solution containing cells was accidentally spilled resulting in a loss of >75% of the total volume prepared.

However, preliminary results show that with further optimisation, miniaturised, fibrin-based, SSBM constructs containing cells can be printed in succession, and then maintained in *in vitro* culture. Thus, providing a feasible solution to creating a more efficient research platform and with scope to building a high-throughput assay platform.

5.6.4 Conclusion

The aims of this chapter were to first address the question of whether hFOB 1.19 SSBM constructs were responsive to known BFMs, and to investigate the use of

bioprinting to miniaturise SSBM constructs. The outcome of which was to determine the possibility of creating an efficient, high-throughput assayable *in vitro* bone platform.

Results indicated that hFOB 1.19 SSBM constructs were responsive after treatment with BFM solutions, detectable at the gene expression and protein levels. This investigation highlighted the cell maturation-dependent effects of each BFM, which was reminiscent of previous findings, and further highlighting the limitations of this type of investigation in 2D *in vitro* culture, due to the necessary prolonged culture periods that are not possible in 2D. Although the presence of mature osteocytic markers were not detected in response to these treatments, early osteocytogenesis was demonstrated with a significant rise in PDPN expression. Bioprinting successfully printed miniaturised SSBM constructs containing cells and demonstrates the feasibility, with further optimisation, of creating an efficient, assayable platform of *in vitro* bone.

Chapter 6

General discussion

6.1 Summary of findings

The work presented here outlines the progress that has been made to develop the Birmingham SSBM method into a humanised *in vitro* bone model with potential as a high-throughput assayable platform. Below are the main aims of this project along with the key findings and outcomes from the respective investigations involved which enabled development of such a model.

1. **Determine the repeatability and adaptability of the Birmingham SSBM culture system.**
    - It was confirmed that the Birmingham SSBM method was repeatable after following the original protocol (398) precisely, using primary rat femoral periosteal cells.
    - The secondary human osteoblast cell line, hFOB 1.19, was determined and selected to be the most appropriate cell line available for humanising the Birmingham SSBM method, as well as introducing homogeneity into the culture system.
    - It was confirmed that the Birmingham SSBM method was adaptable and can accommodate the hFOB 1.19 cell line to create humanised SSBM constructs. The full published method (325) can be found in [Appendix 8.1].
    - Analytical methods were developed and adapted to structurally characterise SSBM constructs. These were alizarin red (AZ) and picrosirius red staining (PSR), x-ray fluorescence (XRF) preparation and scanning.

- Structural analysis demonstrated that long-term culture (up to 12-weeks) of hFOB 1.19 SSBM constructs produced a mineralising collagen-containing matrix reminiscent of *in vivo* bone fracture callus tissue.

2. **Adapt and develop analytical methods for characterisation of SSBM constructs.**
    - Analytical methods were developed and adapted to enable biological characterisation of SSBM constructs. These were RNA extraction and polymerase chain reaction (qPCR), enzyme-linked immunosorbent assay (ELISA), immunofluorescence (IF) preparation and staining, and Invitrogen™ ReadyProbes™ cell viability testing.
    - Biological analysis found that the SSBM culture system supported hFOB 1.19 viability and differentiation long-term (i.e., for at least 12-weeks)
    - Comparison of 2D and 3D cultures of hFOB 1.19 cells confirmed that the traditional 2D culture system does not support long-term cell culture (< 8-weeks) or osteoblast to osteocyte differentiation.
    - Markers relating to matrix formation and mineralisation (ALP and collagen) were detected and measured using biological analytical methods, the results of which corresponded with those measured with structural analytical methods at the same time points.
3. **Assess the responsivity of hFOB 1.19 SSBM constructs after treatment with known bone formation modulators (BFMs).**
    - Characteristics of hFOB 1.19 SSBM cultures at distinct time points (i.e., 4-, 8- and 12-weeks post cell seeding), along with the methods used for characterisation, were able to be used for detecting and measuring

responses of hFOB 1.19 SSBM constructs treated with BFMs, Vit D, PTH and Betulin.

- Treatment of hFOB 1.19 SSBM constructs with BFMs showed that they were responsive and was detectable at the genetic and protein level.
- SSBM construct responses to BFMs were cell-maturity dependent, as found in previous *in vivo* studies. This highlighted the further limitations of long-term 2D culture platforms, given their inability to support osteoblast-osteocyte differentiation.

4. **Determine feasibility of using SSBM constructs to create a high-throughput screening platform.**
    - Miniaturised fibrin hydrogels were successfully printed in succession using SLAM bioprinting.
    - Miniaturised fibrin hydrogels containing hFOB 1.19 cells were successfully printed in succession using SLAM bioprinting and were maintained in culture.

6.2 Cell differentiation in the 3D organotypic microenvironment

One of the most prominent features of this model, which is also central to the successful formation of bone-like material, is the ability to support long-term osteoblast differentiation. Differentiation of hFOB 1.19 cells within the SSBM culture system was assessed after 4-, 8- and 12-weeks of culture using qPCR, ELISA and IF staining [Chapter 4]. Upon comparison to long-term 2D hFOB 1.19 culture, it highlighted the limited culture periods of 2D culture systems, along with differential expression of osteoblast genes and osteoblast activity when cultured under osteogenic conditions,

as well as in response to BFM treatments. As there was a likeness found between the hFOB 1.19 SSBM culture system and *in vivo* bone in terms of its ability to support osteoblast differentiation, this culture system creates an opportunity to alter gene expression through methods such as gene transfection and CRISPR-Cas9. This will enable investigations to elucidate the effects of specific signalling pathways that currently rely on the generation of knock-out mouse strains.

One of the main barriers to making advances in the development of novel bone models is the inability to differentiate and culture osteocytes long-term - isolated primary osteocytes rapidly dedifferentiate and require a 3D culture environment for survival and retaining their phenotype (371). A mineralised matrix under hypoxic conditions has considerable influence on osteocytogenesis (275,372,512,578) and whilst the SSBM culture system provides the necessary mineralised conditions required for osteocyte differentiation and culture, hypoxic incubation conditions would need to be introduced. The expression of podoplanin provided an encouraging indication that the hFOB 1.19 cells within the SSBM constructs reached the onset of osteocytogenesis after 12-weeks of culture as podoplanin is largely considered being the earliest marker of osteocytes (270,276–278,510). However, it is difficult to define the cell phenotype during this stage as osteoblast markers, such as *COL1A1*, *ALPL* and *BGLAP,* and activity are not downregulated until the later stages of osteocyte differentiation (372,578). Therefore, in osteocyte research, more reliance is put upon the upregulated transcription and expression of osteocyte-specific genes, of which there are few, including *FGF23, DMP1*, *MEPE* and *SOST* (270). These osteocyte genes and respective products are essential for osteocyte activity and survival, thus their absence means osteocyte activity is also absent. Therefore, the expression of podoplanin alone

indicates that active, mature osteocytes were not present within the hFOB 1.19 SSBM system after the maximum period of culture investigated (i.e., 12-weeks post-cell seeding).

Furthermore, podoplanin alone cannot be indicative of osteocytes as it is also expressed amongst other cell types in the body such as keratinocytes (588), podocytes (589) and lymphatic endothelial cells (590). Yet, considering hFOB 1.19 cells (i.e., preosteoblasts) were the only cell type within these SSBM constructs, the expression of podoplanin remained a promising result. Due to the presence and rise of this early marker over time, along with the continual expression of osteoblast markers, more cells within the hFOB 1.19 SSBM cultures were entering the very late and very early stages of osteoblast and osteocyte differentiation, respectively, over time, at which point the phenotype of the cell is within a transition period.

With further investigations into optimising the culture conditions of the hFOB 1.19 SSBM culture system, such as the inclusion of hypoxic incubation conditions, the hypothesis is hFOB 1.19 SSBM cultures will contain mature and active osteocytes. Greater assurance of this has been given with the investigations carried out by our collaborator, Dr Corinna Wehmeyer (University Hospital Muenster). Seeding and maintaining the commonly used murine preosteoblast secondary cell line, MC3T3, within the SSBM culture system supported their differentiation to become mature and active osteocytes, detected through the production of sclerostin – a mature osteocyte-specific marker [Appendix 8.4]. Although this conclusion has been made whilst relying on the presence of one marker, these cell cultures contain only a preosteoblast cell line and sclerostin is specific to osteocytes only. These findings and evidence strongly support the capacity for hFOB 1.19 SSBM cultures to differentiate into a more mature

osteocyte, once appropriate adjustments have been made and will be confirmed upon the successful transcription as well as expression of osteocyte-specific markers.

6.3 3Rs Impact

The mission of the NC3Rs is to lead in the application of the 3Rs principles for minimising animal usage and reliance within research, improving animal welfare as well as improving the quality of the science performed (214). The NC3Rs was the funding body for the project that originally developed the Birmingham SSBM culture system (NC/L001403/1) (395,398), and subsequently funded this project (NC/S001646/1) (325). The outcome for these projects, in the long-term, is to replace the use and reduce the reliance on animals within bone research and bone drug candidate testing. However, there were several areas identified within this project where animal usage and reliance can be replaced and reduced immediately.

Much emphasis and discussion has already been made throughout this thesis on the replacement of the primary rat osteoblast cells initially used for the creation of SSBM constructs with a secondary human osteoblast cell line, hFOB 1.19. Previously, legs from three rats were required for each batch of SSBM constructs prepared (398). During this project, this number of rat legs were sufficient for one and three 6-well plates of SSBM constructs on the two occasions when investigating the repeatability of the original protocol. This discrepancy highlighted the reliance on user experience for surgically removing the legs and isolating cells from the fresh tissue, as well as the variability in proliferation rates of the isolated cells.

As of March 2023, the last recorded number of SSBM construct 6-well plates prepared during this project, using secondary cell lines or a non-animal primary cell source was

>120; the equivalent of >720 constructs. If an average of 4 constructs were created per rat, 720 constructs would have required 170 rats in order to have created the same number of constructs made during this project. Thus, using the hFOB 1.19 immediately replaced animal usage and introduced more control for setting up the number of constructs per batch.

Currently, several animal-derived products are required for creating SSBM constructs, and for the continued maintenance of the constructs and cells in culture. These include FBS, aprotinin, thrombin and fibrinogen. The ethical concerns surrounding the production of FBS and its highly variable batch-batch composition have driven research into establishing serum alternatives, such as sericin protein (591), human platelet lysate (592) and celomic fluid (593), as well as serum-free cell lines (594,595).

Unlike FBS, there are fewer alternatives available for aprotinin, thrombin and fibrinogen. Tranexamic acid is a synthetic antifibrinolytic agent and also a medication used to treat heavy bleeding, as well as hereditary angioedema (596), which may be a possible non-animal alternative to aprotinin and has previously been shown to promote mineralisation and cell differentiation in *in vitro* osteoblast cultures (597,598). Thrombin and fibrinogen are the vital blood components that together produce fibrin, and the specific reagents used in the protocol (325) are currently bovine derived. There are human alternatives available, however there has also been a recent publication reporting the synthesis of a “pseudo-fibrin” that possesses similar properties to that of fibrin, using a fibrinogen solution and addition of kosmotropic anions, without the need for enzymes such as thrombin (599,600).

There was a great amount of consideration taken into applying the 3Rs throughout this project in addition to the long-term goal. Although these animal alternatives were not investigated during this project due to a lack of time, it will be made a priority to work towards creating a completely animal-free 3D culture method. Successful implementation of which will have not only reduce and replace the use and reliance on animals, but will also introduce standardisation that will improve reproducibility and reduce variability.

Communication and dissemination are also key tools in promoting uptake of 3Rs applications and practices. As such, there was an active effort throughout this project to attend and present the SSBM culture system at conferences, symposiums and wider laboratory meetings. As such, a number of collaborators have expressed a keen interest and have started using the SSBM culture system for their own research, and as a result, this work is creating a wider positive contribution to the 3Rs. Details of these collaborations can be found in [Appendix 8.4].

6.4 Practical limitations

This project was fully funded by the NC3Rs as a 3-year PhD studentship (NC/S001646/1) beginning October 2019. However, due to the COVID-19 pandemic and a brief period of ill-health, the project was extended by 8-months, to May 2023. It was during this extension period that all the investigations carried out for chapter 5 could be performed and completed.

The unfortunate timing of the COVID-19 pandemic and resultant, prolonged restrictions made carrying out and completing laboratory work challenging. These restrictions included:

- Delayed equipment training
- Time-limited working durations
- Laboratory and office occupancy limits
- Socially distanced workspaces
- Area access restrictions (e.g., LN_2 stores)
- Limited travel for conferences/training/laboratory visits

These COVID-related challenges were further compounded by the long culture periods required for the SSBM constructs, unexpectedly lengthy shipping delays (caused by BREXIT), as well as the expected errors/delays that naturally occur due to the nature of laboratory work (e.g., culture contaminations, equipment faults).

All areas of this project were impacted by the above restrictions and delays, particularly the hFOB 1.19 2D culture and rat SSBM construct investigations shown in Chapter 3. These investigations were stopped prematurely due to the first lockdown and focus was moved to other areas, due to the uncertainties of further lockdowns and of attaining an adequate extension period.

Despite these difficulties and unpredictable climates, a large amount of progress has been made into creating a simple, repeatable and adaptable 3D culture method, along with determining its feasibility as a novel drug screening platform.

6.5 Additional scope and future work

Throughout this thesis and general discussion, areas of adaption, development and optimisation of the SSBM culture system and analytical methods have been identified, as well as the potential applications that would benefit from using the SSBM culture system. Below are those that should take priority for future investigations when using

the culture system, along with further areas of development and use that have not been discussed.

6.5.1 Further method development and optimisations

- **Complete optimisation of analytical methods reported in this thesis***:* The analytical approaches used in the investigations of this project (see chapters 3-5) were developed to an adequate standard for the purposes of this project. Although, these analytical methods can be further optimised, along with the development and optimisation of other analytical approaches to build further confidence in the conclusions made here.
- **Culture methods:** During this project, hFOB 1.19 SSBM cultures were differentiated up to early osteocytogenesis, with evidence of sclerostin-positive cells present in cultures using MC3T3 cells [Appendix 8.4]. This level of differentiation is also expected to be achievable with hFOB 1.19 SSBM cultures with further refinement of the culture conditions (e.g., additional media supplements, greater culture periods, hypoxia), however investigations into this were greatly impacted by COVID-19 [Section 6.4]. Furthermore, as discussed previously [Section 6.3], replacement of cell culture components with animal-free alternatives will have ethical, scientific, and clinical advantages. Therefore, it is imperative these investigations be performed in future investigations.
- **More technical repeats**: Certain investigations during this project had an insufficient number of technical repeats (e.g., 12-week Vitamin D qPCR) and therefore, no statistical analyses could be made and highlights the need for more technical repeats - repetition improves the precision of the data (601). However, the majority of the occasions where repeats were limited was owing

to the size of the constructs, and creating more repeats would have generated additional demands on time and resources which were already limited. As discussed in chapter 5, the use of bioprinting to miniaturise SSBM constructs has the potential to circumvent this issue without adding further time and resource pressures, and preliminary investigations have shown that SSBM constructs containing cells are indeed viable. Therefore, it is essential that developing and optimising the bioprinting protocols of SSBM constructs is made a priority in future investigations.

- **New analytical methods**: Many analytical approaches were trialled and developed during this project with mixed success – refer to [Appendix 8.5] for a detailed account of those methods not reported in the thesis body text. Method development and optimisation is a time-consuming process and as such there were several analytical approaches that were missed, or not fully established. These include methods for structural (e.g., focused ion beam-SEM), RNA (e.g., RNA-sequencing), protein (e.g., Western blotting, further IF imaging) and cellular (e.g., Flow cytometry) analysis. Additional analytical methods will enable a greater understanding of SSBM construct development and characteristics, as well as providing a variety of different analytical readouts for responsivity assays. Developing more analytical methods and improving the current ones is key to fully understanding the versatility and potential applications the SSBM culture method can be used. Although, the findings from the investigations presented here have already revealed a plethora of potential avenues in which the SSBM culture method can be developed further.

6.5.2 Potential applications of the SSBM culture system

- **A foundation for basic bone research and assays**: The results presented here have shown the SSBM culture system as a foundation for creating a novel high-throughput assay platform for bone drug candidate testing. The SSBM system has shown to be a useful research platform into the metabolic processes involved in bone formation, mineralisation and cell differentiation.
- **Personalised medicine and bone disease models**: Collaborative work during this project with Professor Simon Jones' group (University of Birmingham) showed that the culture system can accommodate primary osteoblasts isolated from the bone chips of scoliosis patients. This adaptability to primary human cells adds a further layer to the assay capabilities by opening the possibility of a personalised medicine screening platform. Moreover, the successful adaption of the SSBM culture system using osteoblast cells of a diseased phenotype introduces the capabilities of creating bone disease platforms.
- **Mechanotransduction platform**: Mechanotransduction in response to changing loads and shear stress is vital to the physiological roles of osteocytes, namely those regulating bone remodelling (97,101,268). After establishing the presence of osteocytes, simple methods can be applied to stimulate changes in load or cause shear stress (e.g., moving anchors, plate rocker/vibrating/shakers), thus providing a simple in vitro research model containing osteocytes to assess bone mechanotransduction.
- **Co-culture model**: Bones contain a variety of different cell types in addition to osteoblasts and osteocytes. Adaptions to the culture conditions, regimes and/or the hydrogel composition (e.g., inclusion of collagen) would need to be

investigated prior, in order to establish the SSBM constructs as well as accommodate the other cell types present. The addition of more osteoblasts onto established SSBM constructs would be an interesting investigation to determine if further bone formation will occur, or impact on secondary mineralisation. The production and presence of collagen by osteoblasts, and its subsequent mineralisation, provides promising potential for the introduction of osteoclasts to create a complete *in vitro* remodelling platform. For this to be achieved, further investigations are required into the extent of crosslinked collagen present, which is known to influence osteoclast differentiation and resorption (602). Bone is also a highly vascularised tissue, which is a property SSBM constructs currently lack. Thus, incorporating endothelial cells to SSBM constructs would be a valuable investigation worth pursuing.

6.6 Conclusion

Presented here is the work performed to develop and characterise a 3D humanised *in vitro* model of bone. Using the Birmingham SSBM culture system (395,398) as a foundation, the method was successfully adapted to accommodate a secondary human cell line, hFOB 1.19. Analytical methods regularly used in bone research were adapted and developed specifically for the structural and biological characterisation of the resultant hFOB 1.19 SSBM constructs, as well as assess their responsivity to BFMs, after 4-, 8- and 12-weeks in culture.

The findings from these investigations confirmed the culture system supported long-term osteoblast survival and differentiation towards the point of early osteocytogenesis, as well as production of a new collagen-containing matrix and its subsequent mineralisation. Furthermore, hFOB 1.19 SSBM constructs were found to show cell

maturity-dependent responses after treatment with BFMs. These properties and responses were reminiscent of *in vivo* bone and of the mature fracture callus, which is not possible to achieve using traditional 2D cell culture conditions. These investigations have highlighted the inadequacies of using 2D cell culture in bone research and has provided a new approach that is simple, versatile, adaptable and more physiologically relevant which will circumvent these long-standing limitations.

This developed and characterised SSBM culture system provides the basis for establishing novel bone research platforms and assays, that will reduce and replace the current reliance on animals and animal-derived cells/tissues in the bone research field. What was once a complex and opaque method that required primary cells is now an accessible 3D *in vitro* bone model method with the potential to make a significant impact by enabling bone research.

Chapter 7

Bibliography

1. Steiniche T, Hauge EM. Normal Structure and Function of Bone. In: Handbook of Histology Methods for Bone and Cartilage. Totowa, NJ: Humana Press; 2003. p. 59–72. doi: 10.1007/978-1-59259-417-7_3

2. Oftadeh R, Perez-Viloria M, Villa-Camacho JC, Vaziri A, Nazarian A. Biomechanics and Mechanobiology of Trabecular Bone: A Review. J Biomech Eng. 2015 Jan 1;137(1). doi: 10.1115/1.4029176

3. Osterhoff G, Morgan EF, Shefelbine SJ, Karim L, McNamara LM, Augat P. Bone mechanical properties and changes with osteoporosis. Injury. 2016 Jun 1;47(Suppl 2):S11. [accessed 4 Jul 2023] Available from: /pmc/articles/PMC4955555/

4. Vande Berg BC, Malghem J, Lecouvet FE, Maldague B. Magnetic resonance imaging of normal bone marrow. Eur Radiol. 1998 Sep 24;8(8):1327–34. doi: 10.1007/s003300050547

5. Lee NK, Sowa H, Hinoi E, Ferron M, Ahn JD, Confavreux C, et al. Endocrine Regulation of Energy Metabolism by the Skeleton. Cell. 2007 Aug;130(3):456–69. doi: 10.1016/j.cell.2007.05.047

6. de Jong WF. La Substance Minérale Dans les Os. Recueil des Travaux Chimiques des Pays-Bas. 1926 Sep 3;45(6):445–8. [accessed 17 Mar 2020] Available from: http://doi.wiley.com/10.1002/recl.19260450613

7. Roseberry HH, Hastings AB, Morse JK. X-RAY ANALYSIS OF BONE AND TEETH. [accessed 17 Mar 2020] Available from: http://www.jbc.org/

8. Mitchell HH, Hamilton TS, Steggerda FR, Bean HW. THE CHEMICAL COMPOSITION OF THE ADULT HUMAN BODY AND ITS BEARING ON THE BIOCHEMISTRY OF GROWTH. Journal of Biological Chemistry. 1945 May;158(3):625–37. doi: 10.1016/S0021-9258(19)51339-4

9. Sudhof TC. Calcium Control of Neurotransmitter Release. Cold Spring Harb Perspect Biol. 2012 Jan 1;4(1):a011353–a011353. doi: 10.1101/cshperspect.a011353

10. Singh S, Dodt J, Volkers P, Hethershaw E, Philippou H, Ivaskevicius V, et al. Structure functional insights into calcium binding during the activation of coagulation factor XIII A. Sci Rep. 2019 Aug 5;9(1):11324. doi: 10.1038/s41598-019-47815-z

11. Kohrt WM, Bloomfield SA, Little KD, Nelson ME, Yingling VR. Physical Activity and Bone Health. Med Sci Sports Exerc. 2004 Nov;36(11):1985–96. doi: 10.1249/01.MSS.0000142662.21767.58

12. Rizzoli R, Bianchi ML, Garabédian M, McKay HA, Moreno LA. Maximizing bone mineral mass gain during growth for the prevention of fractures in the

adolescents and the elderly. Bone. 2010 Feb;46(2):294–305. [accessed 5 Jul 2023] Available from: https://pubmed.ncbi.nlm.nih.gov/19840876/

13. Morgan KT. Nutritional Determinants of Bone Health. J Nutr Elder. 2008 Jun 17;27(1–2):3–27. doi: 10.1080/01639360802059670

14. Moyer VA. Vitamin D and calcium supplementation to prevent fractures in adults: U.S. Preventive Services Task Force recommendation statement. Ann Intern Med. 2013 May 7;158(9):691–6. [accessed 5 Jul 2023] Available from: https://pubmed.ncbi.nlm.nih.gov/23440163/

15. Hill TR, Aspray TJ. The role of vitamin D in maintaining bone health in older people. Ther Adv Musculoskelet Dis. 2017 Apr 14;9(4):89–95. doi: 10.1177/1759720X17692502

16. Kenkre JS, Bassett JHD. The bone remodelling cycle. Ann Clin Biochem. 2018;55(3):308–27. Available from: https://doi.org/10.1177/0004563218759371

17. Parfitt AM. Osteonal and hemi-osteonal remodeling: The spatial and temporal framework for signal traffic in adult human bone. J Cell Biochem. 1994;55(3):273–86. doi: 10.1002/jcb.240550303

18. Langdahl B, Ferrari S, Dempster DW. Bone modeling and remodeling: potential as therapeutic targets for the treatment of osteoporosis. Vol. 8, Therapeutic Advances in Musculoskeletal Disease. SAGE Publications Ltd; 2016. p. 225–35. [accessed 2 Nov 2020] Available from: https://pubmed.ncbi.nlm.nih.gov/28255336/

19. Gudde A. A Multi-Scale Approach to Implications of the Preferred Vertebral Trabecular Orientation on Spine Biomechanics. 2018.

20. Manolagas SC. Birth and death of bone cells: Basic regulatory mechanisms and implications for the pathogenesis and treatment of osteoporosis. Endocr Rev. 2000;21(2):115–37. doi: 10.1210/er.21.2.115

21. Jilka RL. Biology of the basic multicellular unit and the pathophysiology of osteoporosis. In: Medical and Pediatric Oncology. John Wiley & Sons, Ltd; 2003. p. 182–5. [accessed 16 Mar 2020] Available from: http://doi.wiley.com/10.1002/mpo.10334

22. Suda T, Takahashi N, Udagawa N, Jimi E, Gillespie MT, Martin TJ. Modulation of osteoclast differentiation and function by the new members of the tumor necrosis factor receptor and ligand families. Vol. 20, Endocrine Reviews. Endocrine Society; 1999. p. 345–57. doi: 10.1210/edrv.20.3.0367

23. Raggatt LJ, Partridge NC. Cellular and molecular mechanisms of bone remodeling. Vol. 285, Journal of Biological Chemistry. American Society for Biochemistry and Molecular Biology; 2010. p. 25103–8. [accessed 21 Oct 2020] Available from: /pmc/articles/PMC2919071/?report=abstract

24. Nakashima T, Hayashi M, Fukunaga T, Kurata K, Oh-Hora M, Feng JQ, et al. Evidence for osteocyte regulation of bone homeostasis through RANKL expression. Nat Med. 2011 Oct 11;17(10):1231–4. [accessed 7 Apr 2020] Available from: http://www.ncbi.nlm.nih.gov/pubmed/21909105

25. Xiong J, Onal M, Jilka RL, Weinstein RS, Manolagas SC, O'Brien CA. Matrix-embedded cells control osteoclast formation. Nat Med. 2011 Oct;17(10):1235–41. [accessed 7 Apr 2020] Available from: http://www.pubmedcentral.nih.gov/articlerender.fcgi?artid=3192296&tool=pmcentrez&rendertype=abstract

26. Mellis DJ, Itzstein C, Helfrich MH, Crockett JC. The skeleton: A multi-functional complex organ. The role of key signalling pathways in osteoclast differentiation and in bone resorption. Vol. 211, Journal of Endocrinology. 2011. p. 131–43. [accessed 19 Mar 2020] Available from: http://www.ncbi.nlm.nih.gov/pubmed/21903860

27. Faulkner B, Astleford K, Mansky KC. Regulation of osteoclast differentiation and skeletal maintenance by histone deacetylases. Vol. 24, Molecules. MDPI AG; 2019. doi: 10.3390/molecules24071355

28. Khosla S. The OPG RANKL RANK system i. Endocrinology. 2001;142(12):5050–5.

29. Rucci N. Molecular Biology of Bone Biology. Clinical Cases in Mineral and Bone Metabolism. 2008;5(1):49–56.

30. Boyle WJ, Simonet WS, Lacey DL. Osteoclast differentiation and activation. Vol. 423, Nature. 2003. p. 337–42. doi: 10.1038/nature01658

31. Faccio R, Novack D V., Zallone A, Ross FP, Teitelbaum SL. Dynamic changes in the osteoclast cytoskeleton in response to growth factors and cell attachment are controlled by β3 integrin. Journal of Cell Biology. 2003 Aug 4;162(3):499–509. [accessed 21 Mar 2020] Available from: https://rupress.org/jcb/article/162/3/499/33460/Dynamic-changes-in-the-osteoclast-cytoskeleton-in

32. Florencio-Silva R, Rodrigues Da G, Sasso S, Sasso-Cerri E, Simões MJ, Cerri PS. Biology of Bone Tissue: Structure, Function, and Factors That Influence Bone Cells. 2015; [accessed 24 Mar 2020] Available from: http://dx.doi.org/10.1155/2015/421746

33. Lakkakorpi PT, Väänänen KH. Kinetics of the osteoclast cytoskeleton during the resorption cycle in vitro. Journal of Bone and Mineral Research. 2009 Dec 3;6(8):817–26. [accessed 21 Mar 2020] Available from: http://doi.wiley.com/10.1002/jbmr.5650060806

34. Reinholt FP, Hultenby K, Oldberg A, Heinegard D. Osteopontin - A possible anchor of osteoclasts to bone. Proc Natl Acad Sci U S A. 1990

Jun;87(12):4473–5. [accessed 8 Apr 2020] Available from: http://www.ncbi.nlm.nih.gov/pubmed/1693772

35. Nakamura H. Morphology, Function, and Differentiation of Bone Cells. J Hard Tissue Biol. 2007;16(1):15–22. [accessed 24 Mar 2020] Available from: http://joi.jlc.jst.go.jp/JST.JSTAGE/jhtb/16.15?from=CrossRef

36. Nakamura I, Duong LT, Rodan SB, Rodan GA. Involvement of αvβ3 integrins in osteoclast function. Vol. 25, Journal of Bone and Mineral Metabolism. Springer; 2007. p. 337–44. doi: 10.1007/s00774-007-0773-9

37. Schlesinger PH, Blair HC, Teitelbaum SL, Edwards JC. Characterization of the Osteoclast Ruffled Border Chloride Channel and Its Role in Bone Resorption*. [accessed 19 Mar 2020] Available from: http://www.jbc.org/

38. Väänänen HK, Laitala-Leinonen T. Osteoclast lineage and function. Vol. 473, Archives of Biochemistry and Biophysics. Academic Press; 2008. p. 132–8. doi: 10.1016/j.abb.2008.03.037

39. Salo J, Lehenkari P, Mulari M, Metsikkö K, Väänänen HK. Removal of osteoclast bone resorption products by transcytosis. Science (1979). 1997 Apr 11;276(5310):270–3. doi: 10.1126/science.276.5310.270

40. Mulari M, Vääräniemi J, Väänänen HK. Intracellular membrane trafficking in bone resorbing osteoclasts. Microsc Res Tech. 2003 Aug 15;61(6):496–503. doi: 10.1002/jemt.10371

41. Hadjidakis DJ, Androulakis II. Bone remodeling. Ann N Y Acad Sci. 2006;1092:385–96. doi: 10.1196/annals.1365.035

42. Andersen TL, Abdelgawad ME, Kristensen HB, Hauge EM, Rolighed L, Bollerslev J, et al. Understanding coupling between bone resorption and formation: Are reversal cells the missing link? American Journal of Pathology. 2013 Jul 1;183(1):235–46. doi: 10.1016/j.ajpath.2013.03.006

43. Everts V, Delaissié JM, Korper W, Jansen DC, Tigchelaar-Gutter W, Saftig P, et al. The bone lining cell: Its role in cleaning Howship's lacunae and initiating bone formation. Journal of Bone and Mineral Research. 2002 Jan;17(1):77–90. [accessed 10 Apr 2020] Available from: http://www.ncbi.nlm.nih.gov/pubmed/11771672

44. Mulari MTK, Qu Q, Härkönen PL, Väänänen HK. Osteoblast-like cells complete osteoclastic bone resorption and form new mineralized bone matrix in vitro. Calcif Tissue Int. 2004 Sep 13;75(3):253–61. doi: 10.1007/s00223-004-0172-3

45. Zhou H, Chernecky R, Davies JE. Deposition of cement at reversal lines in rat femoral bone. Journal of Bone and Mineral Research. 2009 Dec 3;9(3):367–74. [accessed 11 Apr 2020] Available from: http://doi.wiley.com/10.1002/jbmr.5650090311

46. Mckee MD, Nanci A. Osteopontin: An interfacial extracellular matrix protein in mineralized tissues. Connect Tissue Res. 1996;35(1–4):197–205. doi: 10.3109/03008209609029192

47. Zhao C, Irie N, Takada Y, Shimoda K, Miyamoto T, Nishiwaki T, et al. Bidirectional ephrinB2-EphB4 signaling controls bone homeostasis. Cell Metab. 2006;4(2):111–21. doi: 10.1016/j.cmet.2006.05.012

48. Negishi-Koga T, Shinohara M, Komatsu N, Bito H, Kodama T, Friedel RH, et al. Suppression of bone formation by osteoclastic expression of semaphorin 4D. Nature Medicine 2011 17:11. 2011 Oct 23;17(11):1473–80. [accessed 2 Jul 2023] Available from: https://www.nature.com/articles/nm.2489

49. Walker EC, McGregor NE, Poulton IJ, Pompolo S, Allan EH, Quinn JMW, et al. Cardiotrophin-1 is an osteoclast-derived stimulus of bone formation required for normal bone remodeling. Journal of Bone and Mineral Research. 2008 Dec;23(12):2025–32. [accessed 15 Apr 2020] Available from: http://www.ncbi.nlm.nih.gov/pubmed/18665789

50. Pederson L, Ruan M, Westendorf JJ, Khosla S, Oursler MJ. Regulation of bone formation by osteoclasts involves Wnt/BMP signaling and the chemokine sphingosine-1-phosphate. Proc Natl Acad Sci U S A. 2008 Dec 30;105(52):20764–9. doi: 10.1073/pnas.0805133106

51. Lotinun S, Kiviranta R, Matsubara T, Alzate JA, Neff L, Lüth A, et al. Osteoclast-specifc cathepsin K deletion stimulates S1P-dependent bone formation. Journal of Clinical Investigation. 2013 Feb 1;123(2):666–81. doi: 10.1172/JCI64840

52. Howard GA, Bottemiller BL, Turner RT, Rader JI, Baylink DJ. Parathyroid hormone stimulates bone formation and resorption in organ culture: Evidence for a coupling mechanism. Proc Natl Acad Sci U S A. 1981;78(5 I):3204–8. doi: 10.1073/pnas.78.5.3204

53. Tang Y, Wu X, Lei W, Pang L, Wan C, Shi Z, et al. TGF-B1-induced migration of bone mesenchymal stem cells couples bone resorption with formation. Nat Med. 2009 Jul;15(7):757–65. [accessed 22 Oct 2020] Available from: /pmc/articles/PMC2727637/?report=abstract

54. Chen D, Harris MA, Rossini G, Dunstan CR, Dallas SL, Feng JQ, et al. Bone morphogenetic protein 2 (BMP-2) enhances BMP-3, BMP-4, and bone cell differentiation marker gene expression during the induction of mineralized bone matrix formation in cultures of fetal rat calvarial osteoblasts. Calcif Tissue Int. 1997 Mar;60(3):283–90. [accessed 12 May 2023] Available from: https://pubmed.ncbi.nlm.nih.gov/9069167/

55. Komori T, Yagi H, Nomura S, Yamaguchi A, Sasaki K, Deguchi K, et al. Targeted disruption of Cbfa1 results in a complete lack of bone formation

owing to maturational arrest of osteoblasts. Cell. 1997 May 30;89(5):755–64. doi: 10.1016/S0092-8674(00)80258-5

56. Ducy P. Cbfa1: A molecular switch in osteoblast biology. Developmental Dynamics. 2000;219(4):461–71. doi: 10.1002/1097-0177(2000)9999:9999<::AID-DVDY1074>3.0.CO;2-C

57. Akiyama H, Kim JE, Nakashima K, Balmes G, Iwai N, Deng JM, et al. Osteo-chondroprogenitor cells are derived from Sox9 expressing precursors. Proc Natl Acad Sci U S A. 2005 Oct 11;102(41):14665–70. doi: 10.1073/pnas.0504750102

58. Nakashima K, Zhou X, Kunkel G, Zhang Z, Deng JM, Behringer RR, et al. The novel zinc finger-containing transcription factor Osterix is required for osteoblast differentiation and bone formation. Cell. 2002 Jan 11;108(1):17–29. [accessed 12 May 2023] Available from: https://pubmed.ncbi.nlm.nih.gov/11792318/

59. Hill TP, Später D, Taketo MM, Birchmeier W, Hartmann C. Canonical Wnt/β-catenin signaling prevents osteoblasts from differentiating into chondrocytes. Dev Cell. 2005 May 1;8(5):727–38. doi: 10.1016/j.devcel.2005.02.013

60. PRITCHARD JJ. A cytological and histochemical study of bone and cartilage formation in the rat. J Anat. 1952 Jul;86(3):259–77. [accessed 24 Mar 2020] Available from: http://www.ncbi.nlm.nih.gov/pubmed/12980877

61. Dudley RH, Spiro D. The fine structure of bone cells. Journal of Cell Biology. 1961;11(3):627–49. doi: 10.1083/jcb.11.3.627

62. Glenn JD, Whartenby KA. Mesenchymal stem cells: Emerging mechanisms of immunomodulation and therapy. World J Stem Cells. 2014;6(5):526. [accessed 3 Jul 2023] Available from: https://www.wjgnet.com/1948-0210/full/v6/i5/526.htm

63. Vrahnas C, Sims NA. Basic Aspects of Osteoblast Function. Contemporary Endocrinology. 2020;1–16. doi: 10.1007/978-3-319-69287-6_1

64. Herring GM, Ashton BA, Chipperfield AR. The isolation of soluble proteins, glycoproteins, and proteoglycans from bone. Prep Biochem. 1974 Jan 1;4(2):179–200. [accessed 2 Jul 2023] Available from: https://pubmed.ncbi.nlm.nih.gov/4370482/

65. Kini U, Nandeesh BN. Physiology of bone formation, remodeling, and metabolism. In: Radionuclide and Hybrid Bone Imaging. Springer-Verlag Berlin Heidelberg; 2012. p. 29–57. doi: 10.1007/978-3-642-02400-9_2

66. Crane JL, Cao X. Function of matrix IGF-1 in coupling bone resorption and formation. Vol. 92, Journal of Molecular Medicine. NIH Public Access; 2014. p. 107–15. [accessed 23 Oct 2020] Available from: /pmc/articles/PMC3946714/?report=abstract

67. Eriksen EF. Cellular mechanisms of bone remodeling. Vol. 11, Reviews in Endocrine and Metabolic Disorders. Springer; 2010. p. 219–27. [accessed 27 Oct 2020] Available from: https://link.springer.com/article/10.1007/s11154-010-9153-1

68. Jilka RL, Weinstein RS, Bellido T, Parfitt AM, Manolagas SC. Osteoblast Programmed Cell Death (Apoptosis): Modulation by Growth Factors and Cytokines. Journal of Bone and Mineral Research. 1998 May 1;13(5):793–802. [accessed 25 Mar 2020] Available from: http://doi.wiley.com/10.1359/jbmr.1998.13.5.793

69. Rutkovskiy A, Stensløkken K-O, Vaage IJ. Osteoblast Differentiation at a Glance. Med Sci Monit Basic Res. 2016 Sep 26;22:95–106. [accessed 27 Apr 2021] Available from: /pmc/articles/PMC5040224/

70. Boivin G, Meunier PJ. The degree of mineralization of bone tissue measured by computerized quantitative contact microradiography. Calcif Tissue Int. 2002 Jun 1;70(6):503–11. doi: 10.1007/s00223-001-2048-0

71. Ruffoni D, Fratzl P, Roschger P, Klaushofer K, Weinkamer R. The bone mineralization density distribution as a fingerprint of the mineralization process. Bone. 2007 May 1;40(5):1308–19. doi: 10.1016/j.bone.2007.01.012

72. Patterson-Kane JC, Firth EC. Tendon, ligament, bone, and cartilage: Anatomy, physiology, and adaptations to exercise and training. In: The Athletic Horse: Principles and Practice of Equine Sports Medicine: Second Edition. Elsevier Inc.; 2014. p. 202–42. doi: 10.1016/B978-0-7216-0075-8.00022-8

73. Minary-Jolandan M, Yu MF. Nanomechanical heterogeneity in the gap and overlap regions of type I collagen fibrils with implications for bone heterogeneity. Biomacromolecules. 2009 Sep 14;10(9):2565–70. [accessed 23 Oct 2020] Available from: https://pubs.acs.org/sharingguidelines

74. Bala Y, Farlay D, Delmas PD, Meunier PJ, Boivin G. Time sequence of secondary mineralization and microhardness in cortical and cancellous bone from ewes. Bone. 2010 Apr;46(4):1204–12. [accessed 22 Apr 2020] Available from: http://www.ncbi.nlm.nih.gov/pubmed/19969115

75. Akkus O, Polyakova-Akkus A, Adar F, Schaffler MB. Aging of Microstructural Compartments in Human Compact Bone. Journal of Bone and Mineral Research. 2003 Jun 1;18(6):1012–9. [accessed 22 Oct 2020] Available from: https://asbmr.onlinelibrary.wiley.com/doi/full/10.1359/jbmr.2003.18.6.1012

76. Landis WJ, Librizzi JJ, Dunn MG, Silver FH. A study of the relationship between mineral content and mechanical properties of turkey gastrocnemius tendon. Journal of Bone and Mineral Research. 1995;10(6):859–67. [accessed 23 Oct 2020] Available from: https://pubmed.ncbi.nlm.nih.gov/7572309/

77. Landis WJ, Hodgens KJ, Song MJ, Arena J, Kiyonaga S, Marko M, et al. Mineralization of collagen may occur on fibril surfaces: Evidence from conventional and high-voltage electron microscopy and three-dimensional imaging. J Struct Biol. 1996;117(1):24–35. [accessed 23 Oct 2020] Available from: https://pubmed.ncbi.nlm.nih.gov/8776885/

78. Sims NA, Martin TJ. The osteoblast lineage. In: Principles of Bone Biology. Elsevier; 2020. p. 89–110. doi: 10.1016/b978-0-12-814841-9.00004-x

79. Franz-Odendaal TA, Hall BK, Witten PE. Buried alive: How osteoblasts become osteocytes. Developmental Dynamics. 2006 Jan 1;235(1):176–90. [accessed 29 Mar 2020] Available from: http://doi.wiley.com/10.1002/dvdy.20603

80. Buenzli PR, Sims NA. Quantifying the osteocyte network in the human skeleton. Bone. 2015 Jun 1;75:144–50. doi: 10.1016/J.BONE.2015.02.016

81. Schaffler MB, Cheung WY, Majeska R, Kennedy O. Osteocytes: Master orchestrators of bone. Vol. 94, Calcified Tissue International. NIH Public Access; 2014. p. 5–24. [accessed 29 Oct 2020] Available from: /pmc/articles/PMC3947191/?report=abstract

82. Boyce BF, Xing L. Functions of RANKL/RANK/OPG in bone modeling and remodeling. Arch Biochem Biophys. 2008 May 5;473(2):139. [accessed 2 Jul 2023] Available from: /pmc/articles/PMC2413418/

83. Kramer I, Halleux C, Keller H, Pegurri M, Gooi JH, Weber PB, et al. Osteocyte Wnt/β-Catenin Signaling Is Required for Normal Bone Homeostasis. Mol Cell Biol. 2010 Jun 15;30(12):3071–85. [accessed 30 Oct 2020] Available from: https://pubmed.ncbi.nlm.nih.gov/20404086/

84. Li J, Sarosi I, Yan XQ, Morony S, Capparelli C, Tan HL, et al. RANK is the intrinsic hematopoietic cell surface receptor that controls osteoclastogenesis and regulation of bone mass and calcium metabolism. Proc Natl Acad Sci U S A. 2000 Feb 15;97(4):1566–71. [accessed 26 Oct 2020] Available from: /pmc/articles/PMC26475/?report=abstract

85. Walsh JS. Normal bone physiology, remodelling and its hormonal regulation. Vol. 33, Surgery (United Kingdom). Elsevier Ltd; 2015. p. 1–6. doi: 10.1016/j.mpsur.2014.10.010

86. Khosla S, Amin S, Orwoll E. Osteoporosis in men. Vol. 29, Endocrine Reviews. Oxford Academic; 2008. p. 441–64. [accessed 27 Oct 2020] Available from: www.endo-society.org

87. Nakamura T, Imai Y, Matsumoto T, Sato S, Takeuchi K, Igarashi K, et al. Estrogen Prevents Bone Loss via Estrogen Receptor α and Induction of Fas Ligand in Osteoclasts. Cell. 2007 Sep 7;130(5):811–23. doi: 10.1016/j.cell.2007.07.025

88. Shevde NK, Bendixen AC, Dienger KM, Pike JW. Estrogens suppress RANK ligand-induced osteoclast differentiation via a stromal cell independent mechanism involving c-Jun repression. Proceedings of the National Academy of Sciences. 2000 Jul 5;97(14):7829–34. doi: 10.1073/pnas.130200197

89. Hofbauer LC, Khosla S, Dunstan CR, Lacey DL, Spelsberg TC, Riggs BL. Estrogen Stimulates Gene Expression and Protein Production of Osteoprotegerin in Human Osteoblastic Cells*. Endocrinology. 1999 Sep 1;140(9):4367–70. [accessed 27 Oct 2020] Available from: https://academic.oup.com/endo/article/140/9/4367/2991052

90. Khosla S, Oursler MJ, Monroe DG. Estrogen and the skeleton. Vol. 23, Trends in Endocrinology and Metabolism. Elsevier Current Trends; 2012. p. 576–81. doi: 10.1016/j.tem.2012.03.008

91. Goldstein DA. Clinical Methods: The History, Physical, and Laboratory Examinations Chapter 143: Serum Calcium. Vol. 130, THE JOURNAL OF INFECTIOUS DISEASES •. Butterworths; 1990. 677–679 p. [accessed 27 Oct 2020] Available from: https://academic.oup.com/jid/article-abstract/130/5/454/2189293

92. Lee S-K, Lorenzo JA. Parathyroid Hormone Stimulates TRANCE and Inhibits Osteoprotegerin Messenger Ribonucleic Acid Expression in Murine Bone Marrow Cultures: Correlation with Osteoclast-Like Cell Formation*. Endocrinology. 1999 Aug 1;140(8):3552–61. [accessed 27 Oct 2020] Available from: https://academic.oup.com/endo/article/140/8/3552/2990646

93. Bellido T, Ali AA, Plotkin LI, Fu Q, Gubrij I, Roberson PK, et al. Proteasomal degradation of Runx2 shortens parathyroid hormone-induced anti-apoptotic signaling in osteoblasts: A putative explanation for why intermittent administration is needed for bone anabolism. Journal of Biological Chemistry. 2003 Dec 12;278(50):50259–72. [accessed 27 Oct 2020] Available from: http://www.jbc.org/

94. Huang JC, Sakata T, Pfleger LL, Bencsik M, Halloran BP, Bikle DD, et al. PTH differentially regulates expression of RANKL and OPG. J Bone Miner Res. 2004 Feb;19(2):235–44. [accessed 19 Jun 2023] Available from: https://pubmed.ncbi.nlm.nih.gov/14969393/

95. TAM CS, HEERSCHE JNM, MURRAY TM, PARSONS JA. Parathyroid Hormone Stimulates the Bone Apposition Rate Independently of Its Resorptive Action: Differential Effects of Intermittent and Continuous Administration*. Endocrinology. 1982 Feb 1;110(2):506–12. [accessed 27 Oct 2020] Available from: https://academic.oup.com/endo/article-lookup/doi/10.1210/endo-110-2-506

96. Nishida S, Yamaguchi A, Tanizawa T, Endo N, Mashiba T, Uchiyama Y, et al. Increased bone formation by intermittent parathyroid hormone administration is

due to the stimulation of proliferation and differentiation of osteoprogenitor cells in bone marrow. Bone. 1994 Nov 1;15(6):717–23. doi: 10.1016/8756-3282(94)90322-0

97. Frost HM. Bone's Mechanostat: A 2003 Update. Vol. 275, Anatomical Record - Part A Discoveries in Molecular, Cellular, and Evolutionary Biology. Wiley-Liss Inc.; 2003. p. 1081–101. [accessed 30 Oct 2020] Available from: https://anatomypubs.onlinelibrary.wiley.com/doi/full/10.1002/ar.a.10119

98. Sugiyama T, Meakin LB, Browne WJ, Galea GL, Price JS, Lanyon LE. Bones' Adaptive Response to Mechanical Loading Is Essentially Linear Between the Low Strains Associated With Disuse and the High Strains Associated With the Lamellar/Woven Bone Transition. Journal of Bone and Mineral Research. 2012 Aug;27(8):1784. [accessed 3 Jul 2023] Available from: /pmc/articles/PMC3427886/

99. You LD, Weinbaum S, Cowin SC, Schaffler MB. Ultrastructure of the osteocyte process and its pericellular matrix. Anatomical Record - Part A Discoveries in Molecular, Cellular, and Evolutionary Biology. 2004;278(2):505–13. [accessed 29 Oct 2020] Available from: https://pubmed.ncbi.nlm.nih.gov/15164337/

100. McNamara LM, Majeska RJ, Weinbaum S, Friedrich V, Schaffler MB. Attachment of osteocyte cell processes to the bone matrix. Anatomical Record. 2009;292(3):355–63. [accessed 29 Oct 2020] Available from: https://pubmed.ncbi.nlm.nih.gov/19248169/

101. Weinbaum S, Cowin SC, Zeng Y. A model for the excitation of osteocytes by mechanical loading-induced bone fluid shear stresses. J Biomech. 1994 Mar 1;27(3):339–60. doi: 10.1016/0021-9290(94)90010-8

102. Van't Hof RJ, Ralston SH. Nitric oxide and bone. Vol. 103, Immunology. Wiley-Blackwell; 2001. p. 255–61. [accessed 30 Oct 2020] Available from: /pmc/articles/PMC1783253/?report=abstract

103. Li J, Rose E, Frances D, Sun Y, You L. Effect of oscillating fluid flow stimulation on osteocyte mRNA expression. J Biomech. 2012 Jan 10;45(2):247–51. [accessed 3 Jul 2023] Available from: https://pubmed.ncbi.nlm.nih.gov/22119108/

104. Klein-Nulend J, Burger EH, Semeins CM, Raisz LG, Pilbeam CC. Pulsating fluid flow stimulates prostaglandin release and inducible prostaglandin G/H synthase mRNA expression in primary mouse bone cells. Journal of Bone and Mineral Research. 1997 Jan 1;12(1):45–51. [accessed 30 Oct 2020] Available from: https://asbmr.onlinelibrary.wiley.com/doi/full/10.1359/jbmr.1997.12.1.45

105. Bakker AD, Soejima K, Klein-Nulend J, Burger EH. The production of nitric oxide and prostaglandin E2 by primary bone cells is shear stress dependent. J Biomech. 2001;34(5):671–7. [accessed 30 Oct 2020] Available from: https://pubmed.ncbi.nlm.nih.gov/11311708/

106. Robling AG, Niziolek PJ, Baldridge LA, Condon KW, Allen MR, Alam I, et al. Mechanical stimulation of bone in vivo reduces osteocyte expression of Sost/sclerostin. Journal of Biological Chemistry. 2008 Feb 29;283(9):5866–75. doi: 10.1074/jbc.M705092200

107. Gaudio A, Pennisi P, Bratengeier C, Torrisi V, Lindner B, Mangiafico RA, et al. Increased sclerostin serum levels associated with bone formation and resorption markers in patients with immobilization-induced bone loss. J Clin Endocrinol Metab. 2010;95(5):2248–53. [accessed 3 Jul 2023] Available from: https://pubmed.ncbi.nlm.nih.gov/20305005/

108. Moustafa A, Sugiyama T, Prasad J, Zaman G, Gross TS, Lanyon LE, et al. Mechanical loading-related changes in osteocyte sclerostin expression in mice are more closely associated with the subsequent osteogenic response than the peak strains engendered. Osteoporos Int. 2012 Apr;23(4):1225–34. [accessed 3 Jul 2023] Available from: https://pubmed.ncbi.nlm.nih.gov/21573880/

109. Bonewald LF, Johnson ML. Osteocytes, mechanosensing and Wnt signaling. Vol. 42, Bone. NIH Public Access; 2008. p. 606–15. [accessed 30 Oct 2020] Available from: /pmc/articles/PMC2349095/?report=abstract

110. Glass DA, Karsenty G. Molecular bases of the regulation of bone remodeling by the canonical Wnt signaling pathway. Curr Top Dev Biol. 2006;73:43–84. [accessed 3 Jul 2023] Available from: https://pubmed.ncbi.nlm.nih.gov/16782455/

111. Seref-Ferlengez Z, Kennedy OD, Schaffler MB. Bone microdamage, remodeling and bone fragility: how much damage is too much damage? Bonekey Rep. 2015 Mar 18;4:644. [accessed 29 Oct 2020] Available from: /pmc/articles/PMC4371415/?report=abstract

112. Cardoso L, Herman BC, Verborgt O, Laudier D, Majeska RJ, Schaffler MB. Osteocyte Apoptosis Controls Activation of Intracortical Resorption in Response to Bone Fatigue. Journal of Bone and Mineral Research. 2009 Apr;24(4):597–605. [accessed 29 Oct 2020] Available from: https://pubmed.ncbi.nlm.nih.gov/19049324/

113. Kennedy OD, Laudier DM, Majeska RJ, Sun HB, Schaffler MB. Osteocyte apoptosis is required for production of osteoclastogenic signals following bone fatigue in vivo. Bone. 2014;64:132–7. [accessed 29 Oct 2020] Available from: https://pubmed.ncbi.nlm.nih.gov/24709687/

114. Kogianni G, Mann V, Noble BS. Apoptotic bodies convey activity capable of initiating osteoclastogenesis and localized bone destruction. Journal of Bone and Mineral Research. 2008 Jun;23(6):915–27. [accessed 13 Apr 2021] Available from: https://pubmed.ncbi.nlm.nih.gov/18435576/

115. Kovacs CS. The role of vitamin D in pregnancy and lactation: insights from animal models and clinical studies. Annu Rev Nutr. 2012 Aug;32:97–123.

[accessed 2 Mar 2023] Available from: https://pubmed.ncbi.nlm.nih.gov/22483092/

116. Navarro M del C, Saavedra P, Jódar E, Gómez de Tejada MJ, Mirallave A, Sosa M. Osteoporosis and metabolic syndrome according to socio-economic status, contribution of PTH, vitamin D and body weight: The Canarian Osteoporosis Poverty Study (COPS). Clin Endocrinol (Oxf). 2013 May;78(5):681–6. doi: 10.1111/cen.12051

117. Fazeli PK, Klibanski A. Effects of Anorexia Nervosa on Bone Metabolism. Endocr Rev. 2018 Dec 1;39(6):895–910. [accessed 6 Mar 2023] Available from: https://academic.oup.com/edrv/article/39/6/895/5078825

118. Lima CA, Lyra AC, Mendes CMC, Lopes MB, Coqueiro FG, Rocha R, et al. Bone mineral density and inflammatory bowel disease severity. Brazilian Journal of Medical and Biological Research. 2017;50(12). [accessed 6 Mar 2023] Available from: /pmc/articles/PMC5649869/

119. Invernizzi M, Carda S, Viscontini GS, Cisari C. Osteoporosis in Parkinson's disease. Parkinsonism Relat Disord. 2009 Jun;15(5):339–46. [accessed 6 Mar 2023] Available from: https://pubmed.ncbi.nlm.nih.gov/19346153/

120. Egbuna OI, Brown EM. Hypercalcaemic and hypocalcaemic conditions due to calcium-sensing receptor mutations. Best Pract Res Clin Rheumatol. 2008;22(1):129–48. [accessed 9 Jun 2023] Available from: https://pubmed.ncbi.nlm.nih.gov/18328986/

121. Pearson OM, Lieberman DE. The aging of Wolff's 'law': ontogeny and responses to mechanical loading in cortical bone. Am J Phys Anthropol. 2004;Suppl 39:63–99. [accessed 2 Mar 2023] Available from: https://pubmed.ncbi.nlm.nih.gov/15605390/

122. Säämänen AM, Arokoski JPA, Jurvelin JS, Kiviranta I. The structure and regenerative capacity of synovial joint tissues. Regenerative Medicine and Biomaterials for the Repair of Connective Tissues. 2010 Jan 1;1–38. doi: 10.1533/9781845697792.1

123. Robling AG, Hinant FM, Burr DB, Turner CH. Improved bone structure and strength after long-term mechanical loading is greatest if loading is separated into short bouts. J Bone Miner Res. 2002;17(8):1545–54. [accessed 6 Mar 2023] Available from: https://pubmed.ncbi.nlm.nih.gov/12162508/

124. Tucker LA, Strong JE, LeCheminant JD, Bailey BW. Effect of two jumping programs on hip bone mineral density in premenopausal women: a randomized controlled trial. Am J Health Promot. 2015 Jan 1;29(3):158–64. [accessed 6 Mar 2023] Available from: https://pubmed.ncbi.nlm.nih.gov/24460005/

125. Turner CH, Robling AG. Designing exercise regimens to increase bone strength. Exerc Sport Sci Rev. 2003 Jan;31(1):45–50. [accessed 6 Mar 2023] Available from: https://pubmed.ncbi.nlm.nih.gov/12562170/

126. Benedetti MG, Furlini G, Zati A, Mauro GL. The Effectiveness of Physical Exercise on Bone Density in Osteoporotic Patients. Biomed Res Int. 2018;2018. [accessed 6 Mar 2023] Available from: /pmc/articles/PMC6323511/

127. Zerwekh JE, Ruml LA, Gottschalk F, Pak CYC. The Effects of Twelve Weeks of Bed Rest on Bone Histology, Biochemical Markers of Bone Turnover, and Calcium Homeostasis in Eleven Normal Subjects. Journal of Bone and Mineral Research. 1998 Oct 1;13(10):1594–601. [accessed 2 Mar 2023] Available from: https://onlinelibrary.wiley.com/doi/full/10.1359/jbmr.1998.13.10.1594

128. Hargens AR, Vico L. Long-duration bed rest as an analog to microgravity. J Appl Physiol. 2016 Apr 15;120(8):891–903. doi: 10.1152/japplphysiol.00935.2015

129. Baecker N, Tomic A, Mika C, Gotzmann A, Platen P, Gerzer R, et al. Bone resorption is induced on the second day of bed rest: Results of a controlled crossover trial. J Appl Physiol. 2003 Sep 1;95(3):977–82. [accessed 2 Mar 2023] Available from: https://journals.physiology.org/doi/10.1152/japplphysiol.00264.2003

130. Orwoll ES, Adler RA, Amin S, Binkley N, Lewiecki EM, Petak SM, et al. Skeletal health in long-duration astronauts: nature, assessment, and management recommendations from the NASA Bone Summit. J Bone Miner Res. 2013 Jun;28(6):1243–55. [accessed 2 Mar 2023] Available from: https://pubmed.ncbi.nlm.nih.gov/23553962/

131. Feng X, McDonald JM. Disorders of bone remodeling. Annual Review of Pathology: Mechanisms of Disease. 2011 Feb 28;6:121–45. [accessed 5 Nov 2020] Available from: /pmc/articles/PMC3571087/?report=abstract

132. Cao J, Venton L, Sakata T, Halloran BP. Expression of RANKL and OPG correlates with age-related bone loss in male C57BL/6 mice. Journal of Bone and Mineral Research. 2003 Feb 1;18(2):270–7. [accessed 5 Nov 2020] Available from: https://pubmed.ncbi.nlm.nih.gov/12568404/

133. Coipeau P, Rosset P, Langonn A, Gaillard J, Delorme B, Rico A, et al. Impaired differentiation potential of human trabecular bone mesenchymal stromal cells from elderly patients. Cytotherapy. 2009;11(5):584–94. [accessed 2 Nov 2020] Available from: https://pubmed.ncbi.nlm.nih.gov/19626496/

134. Baron R, Kneissel M. WNT signaling in bone homeostasis and disease: from human mutations to treatments. Vol. 19, Nature Medicine. 2013. p. 179–92. doi: 10.1038/nm.3074

135. Ardawi MSM, Al-Kadi HA, Rouzi AA, Qari MH. Determinants of serum sclerostin in healthy pre- and postmenopausal women. Journal of Bone and Mineral Research. 2011 Dec;26(12):2812–22. [accessed 5 Nov 2020] Available from: https://pubmed.ncbi.nlm.nih.gov/21812027/

136. Mosekilde L. Vitamin D and the elderly. Vol. 62, Clinical Endocrinology. John Wiley & Sons, Ltd; 2005. p. 265–81. [accessed 5 Nov 2020] Available from: https://onlinelibrary.wiley.com/doi/full/10.1111/j.1365-2265.2005.02226.x

137. Whitson PA, Pietrzyk RA, Pak CYC. RENAL STONE RISK ASSESSMENT DURING SPACE SHUTTLE FLIGHTS. J Urol. 1997;158(6):2305–10. [accessed 2 Mar 2023] Available from: https://www.auajournals.org/doi/10.1016/S0022-5347%2801%2968240-5

138. Williams D, Kuipers A, Mukai C, Thirsk R. Acclimation during space flight: effects on human physiology. CMAJ : Canadian Medical Association Journal. 2009 Jun 6;180(13):1317. [accessed 2 Mar 2023] Available from: /pmc/articles/PMC2696527/

139. Balemans W, Patel N, Ebeling M, Van Hul E, Wuyts W, Lacza C, et al. Identification of a 52 kb deletion downstream of the SOST gene in patients with van Buchem disease. J Med Genet. 2002;39(2):91–7. [accessed 5 Nov 2020] Available from: https://pubmed.ncbi.nlm.nih.gov/11836356/

140. Balemans W, Ebeling M, Patel N, Van Hul E, Olson P, Dioszegi M, et al. Increased bone density in sclerosteosis is due to the deficiency of a novel secreted protein (SOST). Hum Mol Genet. 2001 Mar 1;10(5):537–43. [accessed 5 Nov 2020] Available from: https://academic.oup.com/hmg/article/10/5/537/2901572

141. Tolar J, Teitelbaum SL, Orchard PJ. Osteopetrosis. N Engl J Med. 2004;351(27). [accessed 4 Jul 2023] Available from: https://pubmed.ncbi.nlm.nih.gov/15625335/

142. Qi Z, Luan J, Zhou X, Cui Y, Han J. Fibrodysplasia ossificans progressiva: Basic understanding and experimental models. Intractable Rare Dis Res. 2017;6(4):242. [accessed 4 Jul 2023] Available from: /pmc/articles/PMC5735276/

143. Alfieri KA, Forsberg JA, Potter BK. Blast injuries and heterotopic ossification. Bone Joint Res. 2012 Aug;1(8):174. [accessed 4 Jul 2023] Available from: /pmc/articles/PMC3626224/

144. Gerrand C, Athanasou N, Brennan B, Grimer R, Judson I, Morland B, et al. UK guidelines for the management of bone sarcomas. Clinical Sarcoma Research 2016 6:1. 2016 May 4;6(1):1–21. [accessed 4 Jul 2023] Available from: https://clinicalsarcomaresearch.biomedcentral.com/articles/10.1186/s13569-016-0047-1

145. Bandeira F, Cusano NE, Silva BC, Cassibba S, Almeida CB, Machado VCC, et al. Bone disease in primary hyperparathyroidism. Arq Bras Endocrinol Metabol. 2014;58(5):553. [accessed 4 Jul 2023] Available from: /pmc/articles/PMC4315357/

146. Rubin MR. Skeletal Manifestations of Hypoparathyroidism. Endocrinol Metab Clin North Am. 2018 Dec 1;47(4):825–37. [accessed 4 Jul 2023] Available from: https://pubmed.ncbi.nlm.nih.gov/30390816/

147. Doolittle ML, Calabrese GM, Mesner LD, Godfrey DA, Maynard RD, Ackert-Bicknell CL, et al. Genetic analysis of osteoblast activity identifies Zbtb40 as a regulator of osteoblast activity and bone mass. Cox GA, editor. PLoS Genet. 2020 Jun 4;16(6):e1008805. [accessed 2 Nov 2020] Available from: https://dx.plos.org/10.1371/journal.pgen.1008805

148. Goodman SB, Jiranek W, Petrow E, Yasko AW. The effects of medications on bone. J Am Acad Orthop Surg. 2007;15(8):450–60. [accessed 4 Jul 2023] Available from: https://pubmed.ncbi.nlm.nih.gov/17664365/

149. Panday K, Gona A, Humphrey MB. Medication-induced osteoporosis: screening and treatment strategies. Ther Adv Musculoskelet Dis. 2014;6(5):185. [accessed 4 Jul 2023] Available from: /pmc/articles/PMC4206646/

150. Dobbs MB, Buckwalter J, Saltzman C. Osteoporosis: The Increasing Role of the Orthopaedist. Iowa Orthop J. 1999;19:43. [accessed 5 Jul 2023] Available from: /pmc/articles/PMC1888612/

151. Zhang L, Wang Y, Gu Y, Hou Y, Chen Z. The need for bone biopsies in the diagnosis of new bone lesions in patients with a known primary malignancy: A comparative review of 117 biopsy cases. J Bone Oncol. 2019 Feb 1;14. [accessed 4 Jul 2023] Available from: /pmc/articles/PMC6329701/

152. Adami G, Fassio A, Rossini M, Caimmi C, Giollo A, Orsolini G, et al. Osteoporosis in Rheumatic Diseases. Int J Mol Sci. 2019 Dec 1;20(23). [accessed 4 Jul 2023] Available from: /pmc/articles/PMC6928928/

153. Sundararaghavan V, Mazur MM, Evans B, Liu J, Ebraheim NA. Diabetes and bone health: latest evidence and clinical implications. Ther Adv Musculoskelet Dis. 2017 Mar 1;9(3):67. [accessed 4 Jul 2023] Available from: /pmc/articles/PMC5349336/

154. Salari N, Darvishi N, Bartina Y, Larti M, Kiaei A, Hemmati M, et al. Global prevalence of osteoporosis among the world older adults: a comprehensive systematic review and meta-analysis. J Orthop Surg Res. 2021 Dec 1;16(1):1–13. [accessed 4 Jul 2023] Available from: https://josr-online.biomedcentral.com/articles/10.1186/s13018-021-02821-8

155. Khosla S. Pathogenesis of age-related bone loss in humans. Journals of Gerontology - Series A Biological Sciences and Medical Sciences. 2013 Oct;68(10):1226–35. [accessed 2 Nov 2020] Available from: /pmc/articles/PMC3826857/?report=abstract

156. Sozen T, Ozisik L, Calik Basaran N. An overview and management of osteoporosis. Eur J Rheumatol. 2017 Mar 1;4(1):46–56. doi: 10.5152/eurjrheum.2016.048

157. Frost HM. Defining osteopenias and osteoporoses: Another view (with insights from a new paradigm). Bone. 1997;20(5):385–91. [accessed 4 Nov 2020] Available from: https://pubmed.ncbi.nlm.nih.gov/9145234/

158. Mirza F, Canalis E. SECONDARY OSTEOPOROSIS: PATHOPHYSIOLOGY AND MANAGEMENT. European journal of endocrinology / European Federation of Endocrine Societies. 2015 Sep 1;173(3):R131. [accessed 5 Jul 2023] Available from: /pmc/articles/PMC4534332/

159. Kanis JA, Melton LJ, Christiansen C, Johnston CC, Khaltaev N. The diagnosis of osteoporosis. J Bone Miner Res. 1994;9(8):1137–41. [accessed 5 Jul 2023] Available from: https://pubmed.ncbi.nlm.nih.gov/7976495/

160. Painter SE, Kleerekoper M, Camacho PM. Secondary osteoporosis: a review of the recent evidence. Endocr Pract. 2006;12(4):436–45. [accessed 5 Jul 2023] Available from: https://pubmed.ncbi.nlm.nih.gov/16901802/

161. Tella SH, Gallagher JC. Prevention and treatment of postmenopausal osteoporosis. Vol. 142, Journal of Steroid Biochemistry and Molecular Biology. Elsevier Ltd; 2014. p. 155–70. [accessed 5 Nov 2020] Available from: /pmc/articles/PMC4187361/?report=abstract

162. Franic D, Verdenik I. Risk factors for osteoporosis in postmenopausal women - from the point of view of primary care gynecologist. Zdr Varst. 2018 Mar 1;57(1):33–8. [accessed 5 Nov 2020] Available from: /pmc/articles/PMC5894367/?report=abstract

163. Golds G, Houdek D, Arnason T. Male Hypogonadism and Osteoporosis: The Effects, Clinical Consequences, and Treatment of Testosterone Deficiency in Bone Health. Vol. 2017, International Journal of Endocrinology. Hindawi Limited; 2017. [accessed 5 Nov 2020] Available from: https://pubmed.ncbi.nlm.nih.gov/28408926/

164. Pazianas M. Anabolic effects of PTH and the ‘anabolic window’. Trends Endocrinol Metab. 2015 Mar 1;26(3):111–3. [accessed 6 Jul 2023] Available from: https://pubmed.ncbi.nlm.nih.gov/25662368/

165. Haas A V., LeBoff MS. Osteoanabolic Agents for Osteoporosis. J Endocr Soc. 2018 Aug 1;2(8):922–32. [accessed 6 Jul 2023] Available from: https://dx.doi.org/10.1210/js.2018-00118

166. Cosman F, de Beur SJ, LeBoff MS, Lewiecki EM, Tanner B, Randall S, et al. Clinician's Guide to Prevention and Treatment of Osteoporosis. Osteoporosis International. 2014 Sep 26;25(10):2359. [accessed 6 Jul 2023] Available from: /pmc/articles/PMC4176573/

167. Drake MT, Clarke BL, Khosla S. Bisphosphonates: Mechanism of action and role in clinical practice. Vol. 83, Mayo Clinic Proceedings. Elsevier Ltd; 2008. p. 1032–45. [accessed 6 Nov 2020] Available from: /pmc/articles/PMC2667901/?report=abstract

168. Gregson CL, Armstrong DJ, Bowden J, Cooper C, Edwards J, Gittoes NJL, et al. UK clinical guideline for the prevention and treatment of osteoporosis. Arch Osteoporos. 2022 Dec 1;17(1):3. [accessed 5 Jul 2023] Available from: /pmc/articles/PMC8979902/

169. Tu KN, Lie JD, Wan CKV, Cameron M, Austel AG, Nguyen JK, et al. Osteoporosis: A Review of Treatment Options. Pharmacy and Therapeutics. 2018 Jan 1;43(2):92. [accessed 5 Jul 2023] Available from: /pmc/articles/PMC5768298/

170. Luckman SP, Hughes DE, Coxon FP, Russell RGG, Rogers MJ. Nitrogen-containing bisphosphonates inhibit the mevalonate pathway and prevent post-translational prenylation of GTP-binding proteins, including Ras. Journal of Bone and Mineral Research. 1998 Apr;13(4):581–9. [accessed 6 Nov 2020] Available from: https://pubmed.ncbi.nlm.nih.gov/9556058/

171. Kennel KA, Drake MT. Adverse Effects of Bisphosphonates: Implications for Osteoporosis Management. Mayo Clin Proc. 2009 Jul;84(7):632. [accessed 5 Jul 2023] Available from: /pmc/articles/PMC2704135/

172. Baron R, Ferrari S, Russell RGG. Denosumab and bisphosphonates: different mechanisms of action and effects. Bone. 2011 Apr 1;48(4):677–92. [accessed 5 Jul 2023] Available from: https://pubmed.ncbi.nlm.nih.gov/21145999/

173. Kendler DL, Cosman F, Stad RK, Ferrari S. Denosumab in the Treatment of Osteoporosis: 10 Years Later: A Narrative Review. Adv Ther. 2022 Jan 1;39(1):58. [accessed 5 Jul 2023] Available from: /pmc/articles/PMC8799550/

174. Zhu Y, Huang Z, Wang Y, Xu W, Chen H, Xu J, et al. The efficacy and safety of denosumab in postmenopausal women with osteoporosis previously treated with bisphosphonates: A review. J Orthop Translat. 2020 May 1;22:7–13. doi: 10.1016/J.JOT.2019.08.004

175. Rauner M, Taipaleenmäki H, Tsourdi E, Winter EM. Osteoporosis Treatment with Anti-Sclerostin Antibodies—Mechanisms of Action and Clinical Application. J Clin Med. 2021 Feb 16;10(4):787. doi: 10.3390/jcm10040787

176. Fabre S, Funck-Brentano T, Cohen-Solal M. Anti-Sclerostin Antibodies in Osteoporosis and Other Bone Diseases. J Clin Med. 2020 Oct 26;9(11):3439. doi: 10.3390/jcm9113439

177. McClung MR. Clinical utility of anti-sclerostin antibodies. Bone. 2017 Mar;96:3–7. doi: 10.1016/j.bone.2016.12.012

178. Bolognese MA. SERMs and SERMs with estrogen for postmenopausal osteoporosis. Vol. 11, Reviews in Endocrine and Metabolic Disorders. Springer; 2010. p. 253–9. [accessed 6 Nov 2020] Available from: https://link.springer.com/article/10.1007/s11154-010-9137-1

179. Morello KC, Wurz GT, DeGregorio MW. Pharmacokinetics of selective estrogen receptor modulators. Clin Pharmacokinet. 2003;42(4):361–72. [accessed 5 Jul 2023] Available from: https://pubmed.ncbi.nlm.nih.gov/12648026/

180. Cummings SR, Eckert S, Krueger KA, Grady D, Powles TJ, Cauley JA, et al. The effect of raloxifene on risk of breast cancer in postmenopausal women: results from the MORE randomized trial. Multiple Outcomes of Raloxifene Evaluation. JAMA. 1999 Jun 16;281(23):2189–97. [accessed 5 Jul 2023] Available from: https://pubmed.ncbi.nlm.nih.gov/10376571/

181. BRIXEN KT, CHRISTENSEN PM, EJERSTED C, LANGDAHL BL. Teriparatide (biosynthetic human parathyroid hormone 1-34): A new paradigm in the treatment of osteoporosis. Basic & clinical pharmacology & toxicology (Print). 2004;94(6).

182. Quattrocchi E, Kourlas H. Teriparatide: A review. Clin Ther. 2004 Jun 1;26(6):841–54. doi: 10.1016/S0149-2918(04)90128-2

183. Sleeman A, Clements JN. Abaloparatide: A new pharmacological option for osteoporosis. American Journal of Health-System Pharmacy. 2019 Jan 25;76(3):130–5. [accessed 5 Jul 2023] Available from: https://dx.doi.org/10.1093/ajhp/zxy022

184. World Health Organization. World health statistics 2023. World Health Organisation; 2023. [accessed 6 Jul 2023] Available from: https://www.who.int/publications/i/item/9789240074323

185. Van Staa TP, Dennison EM, Leufkens HGM, Cooper C. Epidemiology of fractures in England and Wales. Bone. 2001;29(6):517–22. [accessed 5 Jul 2023] Available from: https://pubmed.ncbi.nlm.nih.gov/11728921/

186. Borgström F, Karlsson L, Ortsäter G, Norton N, Halbout P, Cooper C, et al. Fragility fractures in Europe: burden, management and opportunities. Arch Osteoporos. 2020 Dec 1;15(1). [accessed 5 Nov 2020] Available from: /pmc/articles/PMC7166207/?report=abstract

187. Wu AM, Bisignano C, James SL, Abady GG, Abedi A, Abu-Gharbieh E, et al. Global, regional, and national burden of bone fractures in 204 countries and territories, 1990–2019: a systematic analysis from the Global Burden of Disease Study 2019. Lancet Healthy Longev. 2021 Sep 1;2(9):e580–92. [accessed 6 Jul 2023] Available from: http://www.thelancet.com/article/S2666756821001720/fulltext

188. DiMasi JA, Grabowski HG, Hansen RW. Innovation in the pharmaceutical industry: New estimates of R&D costs. J Health Econ. 2016 May 1;47:20–33. doi: 10.1016/j.jhealeco.2016.01.012

189. Lloyd I. Pharma R&D Annual Review 2019. Pharmaprojects. 2019. [accessed 20 Mar 2020] Available from: https://pharmaintelligence.informa.com/~/media/informa-shop-window/pharma/2019/files/whitepapers/pharma-rd-review-2019-whitepaper.pdf

190. Hughes JP, Rees SS, Kalindjian SB, Philpott KL. Principles of early drug discovery. Br J Pharmacol. 2011 Mar;162(6):1239. [accessed 7 Jul 2023] Available from: /pmc/articles/PMC3058157/

191. Sun D, Gao W, Hu H, Zhou S. Why 90% of clinical drug development fails and how to improve it? Acta Pharm Sin B. 2022 Jul 1;12(7):3049. [accessed 7 Jul 2023] Available from: /pmc/articles/PMC9293739/

192. Ehnert S, Rinderknecht H, Aspera-Werz RH, Häussling V, Nussler AK. Use of in vitro bone models to screen for altered bone metabolism, osteopathies, and fracture healing: challenges of complex models. Archives of Toxicology 2020 94:12. 2020 Sep 10;94(12):3937–58. [accessed 9 Jul 2023] Available from: https://link.springer.com/article/10.1007/s00204-020-02906-z

193. Anders HJ, Vielhauer V. Identifying and validating novel targets with in vivo disease models: Guidelines for study design. Drug Discov Today. 2007 Jun 1;12(11–12):446–51. doi: 10.1016/J.DRUDIS.2007.04.001

194. Akhtar A. The Flaws and Human Harms of Animal Experimentation. Cambridge Quarterly of Healthcare Ethics. 2015 Sep 14;24(4):407–19. doi: 10.1017/S0963180115000079

195. van Gaalen SM, Kruyt MC, Geuze RE, de Bruijn JD, Alblas J, Dhert WJA. Use of fluorochrome labels in in vivo bone tissue engineering research. Tissue Eng Part B Rev. 2010;16(2):209–17. [accessed 9 Jul 2023] Available from: https://www.researchgate.net/publication/38036436_Use_of_Fluorochrome_Labels_in_In_Vivo_Bone_Tissue_Engineering_Research

196. Murphy MP, Quarto N, Longaker MT, Wan DC. Calvarial Defects: Cell-Based Reconstructive Strategies in the Murine Model. Tissue Eng Part C Methods. 2017 Dec 12;23(12):971. [accessed 8 Jul 2023] Available from: /pmc/articles/PMC5734144/

197. Samsonraj RM, Dudakovic A, Zan P, Pichurin O, Cool SM, Van Wijnen AJ. A Versatile Protocol for Studying Calvarial Bone Defect Healing in a Mouse Model. Tissue Eng Part C Methods. 2017 Nov 11;23(11):686. [accessed 8 Jul 2023] Available from: /pmc/articles/PMC5689119/

198. Souza VR, Mendes E, Casaro M, Antiorio ATFB, Oliveira FA, Ferreira CM. Description of Ovariectomy Protocol in Mice. Methods Mol Biol. 2019;1916:303–9. [accessed 8 Jul 2023] Available from: https://pubmed.ncbi.nlm.nih.gov/30535707/

199. Khalid AB, Krum SA. Estrogen receptors alpha and beta in bone. Vol. 87, Bone. Elsevier Inc.; 2016. p. 130–5. doi: 10.1016/j.bone.2016.03.016

200. Garcia P, Histing T, Holstein JH, Klein M, Laschke MW, Matthys R, et al. Rodent animal models of delayed bone healing and non-union formation: a comprehensive review. Eur Cell Mater. 2013;26:1–14. [accessed 8 Jul 2023] Available from: https://pubmed.ncbi.nlm.nih.gov/23857280/

201. Lang A, Schulz A, Ellinghaus A, Schmidt-Bleek K. Osteotomy models – The current status on pain scoring and management in small rodents. Lab Anim. 2016 Dec 1;50(6):433–41. [accessed 8 Jul 2023] Available from: https://journals.sagepub.com/doi/full/10.1177/0023677216675007

202. Bonnarens F, Einhorn TA. Production of a standard closed fracture in laboratory animal bone. Journal of Orthopaedic Research. 1984 Jan 1;2(1):97–101. [accessed 8 Jul 2023] Available from: https://onlinelibrary.wiley.com/doi/full/10.1002/jor.1100020115

203. Haffner-Luntzer M, Kovtun A, Rapp AE, Ignatius A. Mouse Models in Bone Fracture Healing Research. Current Molecular Biology Reports 2016 2:2. 2016 Apr 4;2(2):101–11. [accessed 8 Jul 2023] Available from: https://link.springer.com/article/10.1007/s40610-016-0037-3

204. Jilka RL. The Relevance of Mouse Models for Investigating Age-Related Bone Loss in Humans. J Gerontol A Biol Sci Med Sci. 2013 Oct 1;68(10):1209–17. doi: 10.1093/gerona/glt046

205. Rodan GA. Alendronate: preclinical studies. J Clin Rheumatol. 1997 Apr 1;3(2 Suppl):34–6. [accessed 7 Jul 2023] Available from: https://europepmc.org/article/med/19078150

206. Liberman UA, Weiss SR, Bröll J, Minne HW, Quan H, Bell NH, et al. Effect of oral alendronate on bone mineral density and the incidence of fractures in postmenopausal osteoporosis. The Alendronate Phase III Osteoporosis Treatment Study Group. N Engl J Med. 1995 Nov 30;333(22):1437–44. [accessed 7 Jul 2023] Available from: https://pubmed.ncbi.nlm.nih.gov/7477143/

207. Chesnut CH, McClung MR, Ensrud KE, Bell NH, Genant HK, Harris ST, et al. Alendronate treatment of the postmenopausal osteoporotic woman: Effect of multiple dosages on bone mass and bone remodeling. Am J Med. 1995 Aug 1;99(2):144–52. doi: 10.1016/S0002-9343(99)80134-X

208. Burch R, Russell W. The Principles of Humane Experimental Technique by W.M.S. Russell and R.L. Burch. Methuen. 1959. [accessed 20 Mar 2020] Available from: https://caat.jhsph.edu/principles/the-principles-of-humane-experimental-technique

209. Select Committee. House of Lords - Animals In Scientific Procedures - Report. Parliament, London. 2002. [accessed 20 Mar 2020] Available from: https://publications.parliament.uk/pa/ld200102/ldselect/ldanimal/150/15002.htm

210. Hubrecht RC, Carter E. The 3Rs and Humane Experimental Technique: Implementing Change. Animals (Basel). 2019 Oct 1;9(10). [accessed 6 Jul 2023] Available from: /pmc/articles/PMC6826930/

211. MacArthur Clark J. The 3Rs in research: a contemporary approach to replacement, reduction and refinement. British Journal of Nutrition. 2018 Aug 1;120(s1):S1–7. [accessed 6 Jul 2023] Available from: https://www.cambridge.org/core/journals/british-journal-of-nutrition/article/3rs-in-research-a-contemporary-approach-to-replacement-reduction-and-refinement/6ED70F637C9D4D80260B0CEC942C14F2

212. Bombail V, Brown SM, Hammond TJ, Meddle SL, Nielsen BL, Tivey EKL, et al. Crying With Laughter: Adapting the Tickling Protocol to Address Individual Differences Among Rats in Their Response to Playful Handling. Front Vet Sci. 2021 Jun 24;8:677872. doi: 10.3389/FVETS.2021.677872/BIBTEX

213. du Sert NP, Ahluwalia A, Alam S, Avey MT, Baker M, Browne WJ, et al. Reporting animal research: Explanation and elaboration for the ARRIVE guidelines 2.0. PLoS Biol. 2020 Jul 1;18(7):e3000411. [accessed 6 Jul 2023] Available from: https://journals.plos.org/plosbiology/article?id=10.1371/journal.pbio.3000411

214. Burden N, Chapman K, Sewell F, Robinson V. Pioneering Better Science through the 3Rs: An Introduction to the National Centre for the Replacement, Refinement, and Reduction of Animals in Research (NC3Rs). J Am Assoc Lab Anim Sci. 2015 Mar 1;54(2):198. [accessed 25 Jun 2023] Available from: /pmc/articles/PMC4382625/

215. Abubakar AA, Ibrahim SM, Ali AK, Handool KO, Khan MS, Noordin Mustapha M, et al. Postnatal ex vivo rat model for longitudinal bone growth investigations. Animal Model Exp Med. 2019 Mar 1;2(1):34–43. [accessed 9 Jul 2023] Available from: https://onlinelibrary.wiley.com/doi/full/10.1002/ame2.12051

216. Bellido T, Delgado-Calle J. Ex Vivo Organ Cultures as Models to Study Bone Biology. JBMR Plus. 2020 Mar 1;4(3). [accessed 21 Nov 2022] Available from: https://onlinelibrary.wiley.com/doi/full/10.1002/jbm4.10345

217. Abubakar AA, Noordin MM, Azmi TI, Kaka U, Loqman MY. The use of rats and mice as animal models in ex vivo bone growth and development studies. Bone Joint Res. 2016 Dec 1;5(12):610–8. doi: 10.1302/2046-3758.512.BJR-2016-0102.R2/LETTERTOEDITOR

218. Dua R, Jones H, Noble PC. Designing and validation of an automated ex-vivo bioreactor system for long term culture of bone. Bone Rep. 2021 Jun 1;14:101074. [accessed 10 Jul 2023] Available from: /pmc/articles/PMC8102406/

219. Cramer EEA, Ito K, Hofmann S. Ex vivo Bone Models and Their Potential in Preclinical Evaluation. Curr Osteoporos Rep. 2021 Feb 1;19(1):75–87. [accessed 21 Nov 2022] Available from: https://link.springer.com/article/10.1007/s11914-020-00649-5

220. Watson E, Mikos AG. Advances in In Vitro and In Vivo Bioreactor-Based Bone Generation for Craniofacial Tissue Engineering. BME Front. 2023 Jan 31;4. [accessed 10 Jul 2023] Available from: https://spj.science.org/doi/10.34133/bmef.0004

221. Marino S, Staines KA, Brown G, Howard-Jones RA, Adamczyk M. Models of ex vivo explant cultures: applications in bone research. Bonekey Rep. 2016 Jun 29;5. [accessed 10 Jul 2023] Available from: https://napier-repository.worktribe.com/output/462355/models-of-ex-vivo-explant-cultures-applications-in-bone-research

222. Gaspar DA, Gomide V, Monteiro FJ. The role of perfusion bioreactors in bone tissue engineering. Biomatter. 2012 Oct 10;2(4):167. [accessed 10 Jul 2023] Available from: /pmc/articles/PMC3568103/

223. Kazimierczak P, Przekora A. Bioengineered Living Bone Grafts—A Concise Review on Bioreactors and Production Techniques In Vitro. Int J Mol Sci. 2022 Feb 1;23(3). [accessed 10 Jul 2023] Available from: /pmc/articles/PMC8836415/

224. Langer G. Implementation and use of state-of-the-art, cell-based in vitro assays. Handb Exp Pharmacol. 2016 Apr 1;232:171–90. [accessed 10 Jul 2023] Available from: https://link.springer.com/chapter/10.1007/164_2015_18

225. Graudejus O, Ponce Wong R, Varghese N, Wagner S, Morrison B. Bridging the gap between in vivo and in vitro research: Reproducing in vitro the mechanical and electrical environment of cells in vivo. Front Cell Neurosci. 2018;12. doi: 10.3389/CONF.FNCEL.2018.38.00069/EVENT_ABSTRACT

226. Antoni D, Burckel H, Josset E, Noel G. Three-Dimensional Cell Culture: A Breakthrough in Vivo. International Journal of Molecular Sciences 2015, Vol 16, Pages 5517-5527. 2015 Mar 11;16(3):5517–27. [accessed 11 Jul 2023] Available from: https://www.mdpi.com/1422-0067/16/3/5517/htm

227. Sieberath A, Bella E Della, Ferreira AM, Gentile P, Eglin D, Dalgarno K. A comparison of osteoblast and osteoclast in vitro co-culture models and their translation for preclinical drug testing applications. Vol. 21, International Journal of Molecular Sciences. MDPI AG; 2020. doi: 10.3390/ijms21030912

228. Baptista D, Teixeira L, van Blitterswijk C, Giselbrecht S, Truckenmüller R. Overlooked? Underestimated? Effects of Substrate Curvature on Cell Behavior. Trends Biotechnol. 2019 Aug 1;37(8):838–54. [accessed 11 Jul 2023] Available from: https://pubmed.ncbi.nlm.nih.gov/30885388/

229. Hutmacher DW, Loessner D, Rizzi S, Kaplan DL, Mooney DJ, Clements JA. Can tissue engineering concepts advance tumor biology research? Trends Biotechnol. 2010;28(3):125–33. [accessed 11 Jul 2023] Available from: https://pubmed.ncbi.nlm.nih.gov/20056286/

230. Rubin MA, Rubin J, Jasiuk I. SEM and TEM study of the hierarchical structure of C57BL/6J and C3H/HeJ mice trabecular bone. Bone. 2004 Jul;35(1):11–20. [accessed 18 Mar 2020] Available from: http://www.ncbi.nlm.nih.gov/pubmed/15207736

231. Augat P, Schorlemmer S. The role of cortical bone and its microstructure in bone strength. Age Ageing. 2006 Sep 1;35 Suppl 2(SUPPL.2). [accessed 13 Jul 2023] Available from: https://pubmed.ncbi.nlm.nih.gov/16926200/

232. Clarke B. Normal bone anatomy and physiology. Vol. 3 Suppl 3, Clinical journal of the American Society of Nephrology : CJASN. 2008. doi: 10.2215/CJN.04151206

233. Mosekilde L, Ebbesen EN, Tornvig L, Thomsen JS. Trabecular bone structure and strength - remodelling and repair. J Musculoskelet Neuronal Interact. 2000 Sep;1(1):25–30.

234. Ott SM. Cortical or Trabecular Bone: What's the Difference? Am J Nephrol. 2018 Jul 11;47(6):373–5. [accessed 13 Jul 2023] Available from: https://dx.doi.org/10.1159/000489672

235. Nigerian Scholars. Structure of Long Bone | Animal Systems. [accessed 12 Jul 2023] Available from: https://nigerianscholars.com/tutorials/animal-systems-intro/structure-of-long-bone/

236. Gao C, Peng S, Feng P, Shuai C. Bone biomaterials and interactions with stem cells. Bone Research 2017 5:1. 2017 Dec 21;5(1):1–33. [accessed 12 Jul 2023] Available from: https://www.nature.com/articles/boneres201759

237. Chabanon M. Multiscale study of a perfusion bioreactor for bone tissue engineering. Paris: École Centrale Paris; 2015.

238. Brand RA. The classic: The architecture of the trabecular bone (tenth contribution on the mechanics of the human skeletal framework). In: Clinical Orthopaedics and Related Research. Springer New York LLC; 2011. p. 3079–84. doi: 10.1007/s11999-011-2042-4

239. Moreira CA, Dempster DW, Baron R. Anatomy and Ultrastructure of Bone – Histogenesis, Growth and Remodeling. Endotext. 2019 Jun 5; [accessed 19 Feb 2023] Available from: https://www.ncbi.nlm.nih.gov/books/NBK279149/

240. Shapiro F, Wu J. Woven bone overview: structural classification based on its integral role in developmental, repair and pathological bone formation throughout vertebrate groups. Eur Cell Mater. 2019 Oct 1;38:137–67. doi: 10.22203/eCM.v038a11

241. Shapiro F. Cortical bone repair. The relationship of the lacunar-canalicular system and intercellular gap junctions to the repair process. J Bone Joint Surg Am. 1988 Aug;70(7):1067–81.

242. Delmas PD, Malaval L. The Proteins of Bone. In: Physiology and Pharmacology of Bone. Berlin: Springer; 1993. p. 673–724. doi: 10.1007/978-3-642-77991-6_19

243. Naomi R, Ridzuan PM, Bahari H. Current Insights into Collagen Type I. Polymers 2021, Vol 13, Page 2642. 2021 Aug 9;13(16):2642. [accessed 9 Dec 2022] Available from: https://www.mdpi.com/2073-4360/13/16/2642/htm

244. Ricard-Blum S. The Collagen Family. Cold Spring Harb Perspect Biol. 2011 Jan;3(1):1–19. [accessed 23 Oct 2020] Available from: /pmc/articles/PMC3003457/?report=abstract

245. Bou-Gharios G, Abraham D, de Crombrugghe B. Type I collagen structure, synthesis, and regulation. In: Principles of Bone Biology. Elsevier; 2019. p. 295–337. doi: 10.1016/B978-0-12-814841-9.00013-0

246. Kessler E, Takahara K, Biniaminov L, Brusel M, Greenspan DS. Bone morphogenetic protein-1: the type I procollagen C-proteinase. Science. 1996 Jan 19;271(5247):360–2. [accessed 12 Jul 2023] Available from: https://pubmed.ncbi.nlm.nih.gov/8553073/

247. Colige A, Vandenberghe I, Thiry M, Lambert CA, Van Beeumen J, Li S-W, et al. Cloning and Characterization of ADAMTS-14, a Novel ADAMTS Displaying High Homology with ADAMTS-2 and ADAMTS-3. Journal of Biological Chemistry. 2002 Feb;277(8):5756–66. doi: 10.1074/jbc.M105601200

248. Kuo TR, Chen CH. Bone biomarker for the clinical assessment of osteoporosis: recent developments and future perspectives. Biomark Res. 2017;5(1). [accessed 12 Jul 2023] Available from: /pmc/articles/PMC5436437/

249. Henriksen K, Karsdal MA. Type I Collagen. In: Biochemistry of Collagens, Laminins and Elastin: Structure, Function and Biomarkers. Elsevier Inc.; 2016. p. 1–11. doi: 10.1016/B978-0-12-809847-9.00001-5

250. Carvalho MS, Cabral JMS, da Silva CL, Vashishth D. Bone Matrix Non-Collagenous Proteins in Tissue Engineering: Creating New Bone by Mimicking the Extracellular Matrix. Polymers (Basel). 2021 Apr 1;13(7). [accessed 18 May 2023] Available from: /pmc/articles/PMC8036283/

251. Grzesik WJ, Robey PG. Bone matrix RGD glycoproteins: immunolocalization and interaction with human primary osteoblastic bone cells in vitro. J Bone Miner Res. 1994;9(4):487–96. [accessed 14 Jul 2023] Available from: https://pubmed.ncbi.nlm.nih.gov/7518179/

252. Murshed M, Schinke T, McKee MD, Karsenty G. Extracellular matrix mineralization is regulated locally; different roles of two gla-containing proteins. Journal of Cell Biology. 2004 Jun 7;165(5):625–30. doi: 10.1083/jcb.200402046

253. Bi Y, Stuelten CH, Kilts T, Wadhwa S, Iozzo R V., Robey PG, et al. Extracellular Matrix Proteoglycans Control the Fate of Bone Marrow Stromal Cells. Journal of Biological Chemistry. 2005 Aug;280(34):30481–9. doi: 10.1074/jbc.M500573200

254. Hauschka P V., Chen TL, Mavrakos AE. Polypeptide Growth Factors in Bone Matrix. In: Novartis Foundation Symposia. 2007. p. 207–25. doi: 10.1002/9780470513637.ch13

255. Wergedal JE, Mohan S, Lundy M, Baylink DJ. Skeletal growth factor and other growth factors known to be present in bone matrix stimulate proliferation and protein synthesis in human bone cells. J Bone Miner Res. 1990;5(2):179–86. [accessed 14 Jul 2023] Available from: https://pubmed.ncbi.nlm.nih.gov/2156409/

256. Blank M, Sims NA. Cellular Processes by Which Osteoblasts and Osteocytes Control Bone Mineral Deposition and Maturation Revealed by Stage-Specific EphrinB2 Knockdown. Curr Osteoporos Rep. 2019 Oct 10;17(5):270–80. doi: 10.1007/s11914-019-00524-y

257. Gorski JP. Biomineralization of bone: A fresh view of the roles of non-collagenous proteins. Frontiers in Bioscience. 2011 Jun 1;16(7):2598–621. [accessed 23 Oct 2020] Available from: /pmc/articles/PMC4431766/?report=abstract

258. Orriss IR, Arnett TR, Russell RGG. Pyrophosphate: a key inhibitor of mineralisation. Curr Opin Pharmacol. 2016 Jun 1;28:57–68. [accessed 13 Jul 2023] Available from: https://pubmed.ncbi.nlm.nih.gov/27061894/

259. Hessle L, Johnson KA, Anderson HC, Narisawa S, Sali A, Goding JW, et al. Tissue-nonspecific alkaline phosphatase and plasma cell membrane glycoprotein-1 are central antagonistic regulators of bone mineralization. Proc Natl Acad Sci U S A. 2002 Jul 9;99(14):9445–9. [accessed 23 Oct 2020] Available from: www.pnas.orgcgidoi10.1073pnas.142063399

260. Vimalraj S. Alkaline phosphatase: Structure, expression and its function in bone mineralization. Gene. 2020 Sep 5;754. [accessed 13 Jul 2023] Available from: https://pubmed.ncbi.nlm.nih.gov/32522695/

261. Sila-asna M, Bunyaratvej A, Maeda S, Kitaguchi H, Bunyaratavej N. Osteoblast differentiation and bone formation gene expression in strontium-inducing bone marrow mesenchymal stem cell. Kobe J Med Sci. 2007;

262. Termine JD, Kleinman HK, Whitson SW, Conn KM, McGarvey ML, Martin GR. Osteonectin, a bone-specific protein linking mineral to collagen. Cell. 1981;26(1 Pt 1):99–105. [accessed 29 May 2023] Available from: https://pubmed.ncbi.nlm.nih.gov/7034958/

263. Gorski JP, Hankenson KD. Secreted noncollagenous proteins of bone. In: Principles of Bone Biology. Elsevier; 2019. p. 359–78. doi: 10.1016/B978-0-12-814841-9.00015-4

264. Delany AM, Amling M, Priemel M, Howe C, Baron R, Canalis E. Osteopenia and decreased bone formation in osteonectin-deficient mice. Journal of Clinical Investigation. 2000 Apr 1;105(7):915–23. doi: 10.1172/JCI7039

265. Hunter GK, Goldberg HA. Nucleation of hydroxyapatite by bone sialoprotein. Proc Natl Acad Sci U S A. 1993 Sep 15;90(18):8562–5. [accessed 13 Jul 2023] Available from: https://pubmed.ncbi.nlm.nih.gov/8397409/

266. Mizuno M, Imai T, Fujisawa R, Tani H, Kuboki Y. Bone sialoprotein (BSP) is a crucial factor for the expression of osteoblastic phenotypes of bone marrow cells cultured on type I collagen matrix. Calcif Tissue Int. 2000;66(5):388–96. [accessed 13 Jul 2023] Available from: https://pubmed.ncbi.nlm.nih.gov/10773110/

267. Owen TA, Aronow MS, Barone LM, Bettencourt B, Stein GS, Lian JB. Pleiotropic Effects of Vitamin D on Osteoblast Gene Expression Are Related to the Proliferative and Differentiated State of the Bone Cell Phenotype: Dependency upon Basal Levels of Gene Expression, Duration of Exposure, and Bone Matrix Competency in Normal Rat Osteoblast Cultures. Endocrinology. 1991 Mar 1;128(3):1496–504. [accessed 13 Jul 2023] Available from: https://dx.doi.org/10.1210/endo-128-3-1496

268. Bellido T. Osteocyte-driven bone remodeling. Calcif Tissue Int. 2014;94(1):25–34. doi: 10.1007/s00223-013-9774-y

269. Frost HM, STRAATSMA CR. BONE REMODELLING DYNAMICS. Plast Reconstr Surg. 1964; doi: 10.1097/00006534-196402000-00013

270. Bonewald LF. The amazing osteocyte. Journal of Bone and Mineral Research. 2011 Feb 1;26(2):229–38. [accessed 8 Dec 2020] Available from: https://asbmr.onlinelibrary.wiley.com/doi/full/10.1002/jbmr.320

271. Youlten SE, Kemp JP, Logan JG, Ghirardello EJ, Sergio CM, Dack MRG, et al. Osteocyte transcriptome mapping identifies a molecular landscape controlling skeletal homeostasis and susceptibility to skeletal disease. Nat Commun. 2021 May 5;12(1):2444. doi: 10.1038/s41467-021-22517-1

272. Kim W-J, Shin H-L, Kim B-S, Kim H-J, Ryoo H-M. RUNX2-modifying enzymes: therapeutic targets for bone diseases. Exp Mol Med. 2020 Aug 13;52(8):1178–84. doi: 10.1038/s12276-020-0471-4

273. Bone Histology - Embryology. [accessed 8 Dec 2020] Available from: https://embryology.med.unsw.edu.au/embryology/index.php/Bone_Histology#Osteocytes

274. Osteocyte bone cells, SEM - Stock Image - C036/9602 - Science Photo Library. [accessed 23 Jul 2023] Available from: https://www.sciencephoto.com/media/873251/view/osteocyte-bone-cells-sem

275. Prideaux M, Loveridge N, Pitsillides AA, Farquharson C. Extracellular Matrix Mineralization Promotes E11/gp38 Glycoprotein Expression and Drives Osteocytic Differentiation. PLoS One. 2012 May 7;7(5):e36786. doi: 10.1371/journal.pone.0036786

276. Staines KA, Javaheri B, Hohenstein P, Fleming R, Ikpegbu E, Unger E, et al. Hypomorphic conditional deletion of E11/Podoplanin reveals a role in osteocyte dendrite elongation. J Cell Physiol. 2017 Nov 14;232(11):3006–19. doi: 10.1002/jcp.25999

277. Staines KA, Prideaux M, Allen S, Buttle DJ, Pitsillides AA, Farquharson C. E11/Podoplanin Protein Stabilization Through Inhibition of the Proteasome Promotes Osteocyte Differentiation in Murine in Vitro Models. J Cell Physiol. 2016 Jun 28;231(6):1392–404. doi: 10.1002/jcp.25282

278. Staines KA, Hopkinson M, Dillon S, Stephen LA, Fleming R, Sophocleous A, et al. Conditional deletion of E11/Podoplanin in bone protects against ovariectomy-induced increases in osteoclast formation and activity. Biosci Rep. 2020 Jan 31;40(1). doi: 10.1042/BSR20190329

279. Westbroek I, De Rooij KE, Nijweide PJ. Osteocyte-specific monoclonal antibody MAb OB7.3 is directed against Phex protein. Journal of Bone and Mineral Research. 2002 Jan 1;17(5):845–53. [accessed 31 Mar 2020] Available from: http://www.ncbi.nlm.nih.gov/pubmed/12009015

280. Feng JQ, Ward LM, Liu S, Lu Y, Xie Y, Yuan B, et al. Loss of DMP1 causes rickets and osteomalacia and identifies a role for osteocytes in mineral metabolism. Nat Genet. 2006 Nov 23;38(11):1310–5. doi: 10.1038/ng1905

281. Li J, Sarosi I, Cattley RC, Pretorius J, Asuncion F, Grisanti M, et al. Dkk1-mediated inhibition of Wnt signaling in bone results in osteopenia. Bone. 2006 Oct;39(4):754–66. doi: 10.1016/j.bone.2006.03.017

282. BONEWALD LF. Osteocytes as Dynamic Multifunctional Cells. Ann N Y Acad Sci. 2007 Nov 1;1116(1):281–90. [accessed 1 Apr 2020] Available from: http://doi.wiley.com/10.1196/annals.1402.018

283. Poole KES, Van Bezooijen RL, Loveridge N, Hamersma H, Papapoulos SE, Löwik CW, et al. Sclerostin is a delayed secreted product of osteocytes that inhibits bone formation. The FASEB Journal. 2005 Nov 25;19(13):1842–4. doi: 10.1096/fj.05-4221fje

284. Yamaza T, Goto T, Kamiya T, Kobayashi Y, Sakai H, Tanaka T. Study of immunoelectron microscopic localization of cathepsin K in osteoclasts and other bone cells in the mouse femur. Bone. 1998 Dec;23(6):499–509. doi: 10.1016/S8756-3282(98)00138-0

285. Bonnet N, Brun J, Rousseau J-C, Duong LT, Ferrari SL. Cathepsin K Controls Cortical Bone Formation by Degrading Periostin. Journal of Bone and Mineral Research. 2017 Jul;32(7):1432–41. doi: 10.1002/jbmr.3136

286. Bonewald LF. Osteocytes. In: Marcus R, Feldman D, Nelson D, Rosen C, editors. Osteoporosis. 3rd ed. Academic Press; 2008. p. 169–89. doi: 10.1016/B978-0-12-370544-0.50010-0

287. Dallas SL, Prideaux M, Bonewald LF. The Osteocyte: An Endocrine Cell … and More. Endocr Rev. 2013 Oct 1;34(5):658–90. doi: 10.1210/er.2012-1026

288. Zhang K, Barragan-Adjemian C, Ye L, Kotha S, Dallas M, Lu Y, et al. E11/gp38 selective expression in osteocytes: regulation by mechanical strain and role in dendrite elongation. Mol Cell Biol. 2006 Jun 1;26(12):4539–52. [accessed 29 May 2023] Available from: https://pubmed.ncbi.nlm.nih.gov/16738320/

289. Holmbeck K, Bianco P, Pidoux I, Inoue S, Billinghurst RC, Wu W, et al. The metalloproteinase MT1-MMP is required for normal development and maintenance of osteocyte processes in bone. J Cell Sci. 2005 Jan 1;118(1):147–56. doi: 10.1242/jcs.01581

290. Beno T, Yoon Y-J, Cowin SC, Fritton SP. Estimation of bone permeability using accurate microstructural measurements. J Biomech. 2006 Jan;39(13):2378–87. doi: 10.1016/j.jbiomech.2005.08.005

291. Bortel E, Grover LM, Eisenstein N, Seim C, Suhonen H, Pacureanu A, et al. Interconnectivity Explains High Canalicular Network Robustness between

Neighboring Osteocyte Lacunae in Human Bone. Adv Nanobiomed Res. 2022 Apr 29;2(4):2100090. doi: 10.1002/anbr.202100090

292. Sawa N, Fujimoto H, Sawa Y, Yamashita J. Alternating Differentiation and Dedifferentiation between Mature Osteoblasts and Osteocytes. Scientific Reports 2019 9:1. 2019 Sep 25;9(1):1–9. [accessed 20 Jun 2023] Available from: https://www.nature.com/articles/s41598-019-50236-7

293. Torreggiani E, Matthews BG, Pejda S, Matic I, Horowitz MC, Grcevic D, et al. Preosteocytes/Osteocytes Have the Potential to Dedifferentiate Becoming a Source of Osteoblasts. PLoS One. 2013 Sep 6;8(9):e75204. doi: 10.1371/journal.pone.0075204

294. Kato Y, Windle JJ, Koop BA, Mundy GR, Bonewald LF. Establishment of an Osteocyte-like Cell Line, MLO-Y4. Journal of Bone and Mineral Research. 1997;12(12):2014–23. doi: 10.1359/jbmr.1997.12.12.2014

295. Woo SM, Rosser J, Dusevich V, Kalajzic I, Bonewald LF. Cell line IDG-SW3 replicates osteoblast-to-late-osteocyte differentiation in vitro and accelerates bone formation in vivo. Journal of Bone and Mineral Research. 2011 Nov;26(11):2634–46. doi: 10.1002/jbmr.465

296. Bodine PVN, Vernon SK, Komm BS. Establishment and hormonal regulation of a conditionally transformed preosteocytic cell line from adult human bone. Endocrinology. 1996 Nov 1;137(11):4592–604. [accessed 13 Jan 2023] Available from: https://academic.oup.com/endo/article/137/11/4592/3037205

297. Papanicolaou SE, Phipps RJ, Fyhrie DP, Genetos DC. Modulation of sclerostin expression by mechanical loading and bone morphogenetic proteins in osteogenic cells. Biorheology. 2009;46(5):389–99. [accessed 30 Mar 2020] Available from: http://www.ncbi.nlm.nih.gov/pubmed/19940355

298. Brady RT, O'Brien FJ, Hoey DA. The Impact of the Extracellular Matrix Environment on Sost Expression by the MLO-Y4 Osteocyte Cell Line. Bioengineering. 2022 Jan 13;9(1):35. doi: 10.3390/bioengineering9010035

299. Jedrzejczak-Silicka M. History of Cell Culture. In: New Insights into Cell Culture Technology. InTech; 2017. doi: 10.5772/66905

300. Järveläinen H, Sainio A, Koulu M, Wight TN, Penttinen R. Extracellular Matrix Molecules: Potential Targets in Pharmacotherapy. Pharmacol Rev. 2009 Jun;61(2):198–223. doi: 10.1124/pr.109.001289

301. Schmidt S, Friedl P. Interstitial cell migration: integrin-dependent and alternative adhesion mechanisms. Cell Tissue Res. 2010 Jan 17;339(1):83–92. doi: 10.1007/s00441-009-0892-9

302. Sun M, Liu A, Yang X, Gong J, Yu M, Yao X, et al. 3D Cell Culture—Can It Be As Popular as 2D Cell Culture? Adv Nanobiomed Res. 2021 May 22;1(5):2000066. doi: 10.1002/anbr.202000066

303. Jensen C, Teng Y. Is It Time to Start Transitioning From 2D to 3D Cell Culture? Front Mol Biosci. 2020 Mar 6;7. [accessed 26 May 2023] Available from: /pmc/articles/PMC7067892/

304. Kapałczyńska M, Kolenda T, Przybyła W, Zajączkowska M, Teresiak A, Filas V, et al. 2D and 3D cell cultures – a comparison of different types of cancer cell cultures. Arch Med Sci. 2018;14(4):910. [accessed 26 May 2023] Available from: /pmc/articles/PMC6040128/

305. Chen CS, Mrksich M, Huang S, Whitesides GM, Ingber DE. Geometric Control of Cell Life and Death. Science (1979). 1997 May 30;276(5317):1425–8. doi: 10.1126/science.276.5317.1425

306. LEBEYEC J, XU R, LEE S, NELSON C, RIZKI A, ALCARAZ J, et al. Cell shape regulates global histone acetylation in human mammary epithelial cells. Exp Cell Res. 2007 Aug 15;313(14):3066–75. doi: 10.1016/j.yexcr.2007.04.022

307. Szot CS, Buchanan CF, Freeman JW, Rylander MN. 3D in vitro bioengineered tumors based on collagen I hydrogels. Biomaterials. 2011 Nov;32(31):7905–12. doi: 10.1016/j.biomaterials.2011.07.001

308. Maria OM, Maria O, Liu Y, Komarova S V., Tran SD. Matrigel improves functional properties of human submandibular salivary gland cell line. Int J Biochem Cell Biol. 2011 Apr;43(4):622–31. doi: 10.1016/j.biocel.2011.01.001

309. Hongisto V, Jernström S, Fey V, Mpindi J-P, Kleivi Sahlberg K, Kallioniemi O, et al. High-Throughput 3D Screening Reveals Differences in Drug Sensitivities between Culture Models of JIMT1 Breast Cancer Cells. PLoS One. 2013 Oct 23;8(10):e77232. doi: 10.1371/journal.pone.0077232

310. Edmondson R, Broglie JJ, Adcock AF, Yang L. Three-Dimensional Cell Culture Systems and Their Applications in Drug Discovery and Cell-Based Biosensors. Assay Drug Dev Technol. 2014 May;12(4):207–18. doi: 10.1089/adt.2014.573

311. Wetterstrand K. DNA Sequencing Costs: Data from the NHGRI Genome Sequencing Program (GSP). www.genome.gov/sequencingcostsdata. 2023.

312. Mapanao AK, Voliani V. Three-dimensional tumor models: Promoting breakthroughs in nanotheranostics translational research. Appl Mater Today. 2020 Jun;19:100552. doi: 10.1016/j.apmt.2019.100552

313. Abbott A. Biology’s new dimension. Nature. 2003 Aug;424(6951):870–2. doi: 10.1038/424870a

314. Low LA, Mummery C, Berridge BR, Austin CP, Tagle DA. Organs-on-chips: into the next decade. Nat Rev Drug Discov. 2021 May 10;20(5):345–61. doi: 10.1038/s41573-020-0079-3

315. Park SE, Georgescu A, Huh D. Organoids-on-a-chip. Science (1979). 2019 Jun 7;364(6444):960–5. doi: 10.1126/science.aaw7894

316. van Berlo D, Nguyen VVT, Gkouzioti V, Leineweber K, Verhaar MC, van Balkom BWM. Stem cells, organoids, and organ-on-a-chip models for personalized in vitro drug testing. Curr Opin Toxicol. 2021 Dec;28:7–14. doi: 10.1016/j.cotox.2021.08.006

317. Zhu J, Ji L, Chen Y, Li H, Huang M, Dai Z, et al. Organoids and organs-on-chips: insights into predicting the efficacy of systemic treatment in colorectal cancer. Cell Death Discov. 2023 Feb 22;9(1):72. doi: 10.1038/s41420-023-01354-9

318. Bose S, Roy M, Bandyopadhyay A. Recent advances in bone tissue engineering scaffolds. Trends Biotechnol. 2012 Oct;30(10):546–54. doi: 10.1016/j.tibtech.2012.07.005

319. Armentano I, Dottori M, Fortunati E, Mattioli S, Kenny JM. Biodegradable polymer matrix nanocomposites for tissue engineering: A review. In: Polymer Degradation and Stability. Elsevier; 2010. p. 2126–46. doi: 10.1016/j.polymdegradstab.2010.06.007

320. Wagoner Johnson AJ, Herschler BA. A review of the mechanical behavior of CaP and CaP/polymer composites for applications in bone replacement and repair. Vol. 7, Acta Biomaterialia. Elsevier; 2011. p. 16–30. doi: 10.1016/j.actbio.2010.07.012

321. Chen S, Chen X, Geng Z, Su J. The horizon of bone organoid: A perspective on construction and application. Bioact Mater. 2022 Dec;18:15–25. doi: 10.1016/j.bioactmat.2022.01.048

322. Caliari SR, Burdick JA. A practical guide to hydrogels for cell culture. Nat Methods. 2016 May 28;13(5):405–14. doi: 10.1038/nmeth.3839

323. Li Y, Meng H, Liu Y, Lee BP. Fibrin Gel as an Injectable Biodegradable Scaffold and Cell Carrier for Tissue Engineering. The Scientific World Journal. 2015;2015:1–10. doi: 10.1155/2015/685690

324. Akiva A, Melke J, Ansari S, Liv N, Meijden R, Erp M, et al. An Organoid for Woven Bone. Adv Funct Mater. 2021 Apr 9;31(17):2010524. [accessed 3 May 2021] Available from: https://onlinelibrary.wiley.com/doi/10.1002/adfm.202010524

325. Finlay M, Hill LA, Neag G, Patel B, Chipara M, Lamont HC, et al. A detailed methodology for the long-term in vitro culture and analysis of three-dimensional, self-structuring bone models generated from cell lines or primary osteoblastic cell populations. F1000Research 2023 12:357. 2023 Mar 31;12:357. [accessed 4 Jul 2023] Available from: https://f1000research.com/articles/12-357

326. Liu X, Ma PX. Polymeric Scaffolds for Bone Tissue Engineering. Vol. 32, Annals of Biomedical Engineering. 2004.

327. Knowles HJ, Chanalaris A, Koutsikouni A, Cribbs AP, Grover LM, Hulley PA. Mature primary human osteocytes in mini organotypic cultures secrete FGF23 and PTH1-34-regulated sclerostin. Front Endocrinol (Lausanne). 2023 May 8;14:1167734. doi: 10.3389/FENDO.2023.1167734/BIBTEX

328. Kim B-S, Mooney DJ. Development of biocompatible synthetic extracellular matrices for tissue engineering. Trends Biotechnol. 1998 Dec;16(5):224–30. doi: 10.1016/S0167-7799(98)01191-3

329. Kundak H, Bilisik K. Development of Three-Dimensional (3D) Biodegradable Polyglycolic Acid Fiber (PGA) Preforms for Scaffold Applications: Experimental Patterning and Fiber Volume Fraction-Porosity Modeling Study. Polymers (Basel). 2023 Apr 27;15(9):2083. doi: 10.3390/polym15092083

330. Jansen LE, McCarthy TP, Lee MJ, Peyton SR. A synthetic, three-dimensional bone marrow hydrogel. bioRxiv. 2018 Mar 3;275842. [accessed 16 Jul 2023] Available from: https://www.biorxiv.org/content/10.1101/275842v1

331. Sell SA, Wolfe PS, Garg K, McCool JM, Rodriguez IA, Bowlin GL. The Use of Natural Polymers in Tissue Engineering: A Focus on Electrospun Extracellular Matrix Analogues. Polymers (Basel). 2010 Nov 9;2(4):522–53. doi: 10.3390/polym2040522

332. Panzavolta S, Torricelli P, Casolari S, Parrilli A, Fini M, Bigi A. Strontium-Substituted Hydroxyapatite-Gelatin Biomimetic Scaffolds Modulate Bone Cell Response. Macromol Biosci. 2018 Jul;18(7):1800096. doi: 10.1002/mabi.201800096

333. Liu X, Smith LA, Hu J, Ma PX. Biomimetic nanofibrous gelatin/apatite composite scaffolds for bone tissue engineering. Biomaterials. 2009 Apr;30(12):2252–8. doi: 10.1016/j.biomaterials.2008.12.068

334. Roohani-Esfahani SI, Lu ZF, Li JJ, Ellis-Behnke R, Kaplan DL, Zreiqat H. Effect of self-assembled nanofibrous silk/polycaprolactone layer on the osteoconductivity and mechanical properties of biphasic calcium phosphate scaffolds. Acta Biomater. 2012 Jan;8(1):302–12. doi: 10.1016/j.actbio.2011.10.009

335. Okazaki Y. A New Ti–15Zr–4Nb–4Ta alloy for medical applications. Curr Opin Solid State Mater Sci. 2001 Jan;5(1):45–53. doi: 10.1016/S1359-0286(00)00025-5

336. Balla VK, Bodhak S, Bose S, Bandyopadhyay A. Porous tantalum structures for bone implants: Fabrication, mechanical and in vitro biological properties. Acta Biomater. 2010 Aug;6(8):3349–59. doi: 10.1016/j.actbio.2010.01.046

337. Xue W, Krishna BV, Bandyopadhyay A, Bose S. Processing and biocompatibility evaluation of laser processed porous titanium. Acta Biomater. 2007 Nov;3(6):1007–18. doi: 10.1016/j.actbio.2007.05.009

338. Samavedi S, Whittington AR, Goldstein AS. Calcium phosphate ceramics in bone tissue engineering: A review of properties and their influence on cell behavior. Acta Biomater. 2013 Sep;9(9):8037–45. doi: 10.1016/j.actbio.2013.06.014

339. Teixeira S, Fernandes H, Leusink A, van Blitterswijk C, Ferraz MP, Monteiro FJ, et al. In vivo evaluation of highly macroporous ceramic scaffolds for bone tissue engineering. J Biomed Mater Res A. 2009;9999A:NA-NA. doi: 10.1002/jbm.a.32532

340. Ducheyne P, Qiu Q. Bioactive ceramics: the effect of surface reactivity on bone formation and bone cell function. Biomaterials. 1999 Dec;20(23–24):2287–303. doi: 10.1016/S0142-9612(99)00181-7

341. MATSUNO T, HASHIMOTO Y, ADACHI S, OMATA K, YOSHITAKA Y, OZEKI Y, et al. Preparation of injectable 3D-formed .BETA.-tricalcium phosphate bead/alginate composite for bone tissue engineering. Dent Mater J. 2008;27(6):827–34. doi: 10.4012/dmj.27.827

342. Jeong J, Kim JH, Shim JH, Hwang NS, Heo CY. Bioactive calcium phosphate materials and applications in bone regeneration. Biomaterials Research 2019 23:1. 2019 Jan 14;23(1):1–11. [accessed 5 Dec 2021] Available from: https://biomaterialsres.biomedcentral.com/articles/10.1186/s40824-018-0149-3

343. Owen R, Reilly GC. In vitro models of bone remodelling and associated disorders. Vol. 6, Frontiers in Bioengineering and Biotechnology. Frontiers Media S.A.; 2018. p. 134. [accessed 3 Mar 2020] Available from: http://www.ncbi.nlm.nih.gov/pubmed/30364287

344. Bahram M, Mohseni N, Moghtader M. An Introduction to Hydrogels and Some Recent Applications. In: Emerging Concepts in Analysis and Applications of Hydrogels. InTech; 2016. doi: 10.5772/64301

345. Rudzinski WE, Dave AM, Vaishnav UH, Kumbar SG, Kulkarni AR, Aminabhavi TM. Hydrogels as controlled release devices in agriculture. Des Monomers Polym. 2002 Jan 2;5(1):39–65. doi: 10.1163/156855502760151580

346. Mitura S, Sionkowska A, Jaiswal A. Biopolymers for hydrogels in cosmetics: review. J Mater Sci Mater Med. 2020 Jun 25;31(6):50. doi: 10.1007/s10856-020-06390-w

347. Nath PC, Debnath S, Sridhar K, Inbaraj BS, Nayak PK, Sharma M. A Comprehensive Review of Food Hydrogels: Principles, Formation Mechanisms, Microstructure, and Its Applications. Gels. 2022 Dec 20;9(1):1. doi: 10.3390/gels9010001

348. Ho TC, Chang CC, Chan HP, Chung TW, Shu CW, Chuang KP, et al. Hydrogels: Properties and Applications in Biomedicine. Molecules. 2022 May 1;27(9). [accessed 10 May 2023] Available from: /pmc/articles/PMC9104731/

349. Wichterle O, Lím D. Hydrophilic Gels for Biological Use. Nature. 1960;185(4706):117–8. doi: 10.1038/185117a0

350. Kaczmarek B, Nadolna K, Owczarek A. The physical and chemical properties of hydrogels based on natural polymers. In: Hydrogels Based on Natural Polymers. Elsevier; 2020. p. 151–72. doi: 10.1016/B978-0-12-816421-1.00006-9

351. Mengyuan H, Changlin W, Tong X, Ping D, Xiaojun Y, Huaying S, et al. Modification and preparation of four natural hydrogels and their application in biopharmaceutical delivery. Polymer Bulletin. 2023 Jul 11;80(7):7101–44. doi: 10.1007/s00289-022-04412-x

352. Ghassemi T, Shahroodi A, Ebrahimzadeh MH, Mousavian A, Movaffagh J, Moradi A. Current Concepts in Scaffolding for Bone Tissue Engineering. Arch Bone Jt Surg. 2018 Mar;6(2):90–9.

353. Riester O, Borgolte M, Csuk R, Deigner H-P. Challenges in Bone Tissue Regeneration: Stem Cell Therapy, Biofunctionality and Antimicrobial Properties of Novel Materials and Its Evolution. Int J Mol Sci. 2020 Dec 27;22(1):192. doi: 10.3390/ijms22010192

354. Tsiklin IL, Shabunin A V., Kolsanov A V., Volova LT. In Vivo Bone Tissue Engineering Strategies: Advances and Prospects. Polymers (Basel). 2022 Aug 8;14(15):3222. doi: 10.3390/polym14153222

355. Drury JL, Mooney DJ. Hydrogels for tissue engineering: Scaffold design variables and applications. Vol. 24, Biomaterials. Elsevier BV; 2003. p. 4337–51. doi: 10.1016/S0142-9612(03)00340-5

356. Catoira MC, Fusaro L, Di Francesco D, Ramella M, Boccafoschi F. Overview of natural hydrogels for regenerative medicine applications. J Mater Sci Mater Med. 2019 Oct 10;30(10):115. doi: 10.1007/s10856-019-6318-7

357. Furie B, Furie BC. The molecular basis of blood coagulation. Vol. 53, Cell. 1988. p. 505–18. doi: 10.1016/0092-8674(88)90567-3

358. Brummel-Ziedins K, Mann KG. Molecular Basis of Blood Coagulation. Hematology: Basic Principles and Practice. 2018. p. 1885-1905.e8. doi: 10.1016/B978-0-323-35762-3.00126-8

359. Weigandt KM, Pozzo DC, Porcar L. Structure of high density fibrin networks probed with neutron scattering and rheology. Soft Matter. 2009;5(21):4321. doi: 10.1039/b906256d

360. Wang X, Friis T, Glatt V, Crawford R, Xiao Y. Structural properties of fracture haematoma: current status and future clinical implications. J Tissue Eng Regen Med. 2017 Oct;11(10):2864–75. doi: 10.1002/term.2190

361. Catelas I, Sese N, Wu BM, Dunn JCY, Helgerson S, Tawil B. Human Mesenchymal Stem Cell Proliferation and Osteogenic Differentiation in Fibrin Gels *in Vitro*. Tissue Eng. 2006 Aug;12(8):2385–96. doi: 10.1089/ten.2006.12.2385

362. Wang J, Sun Y, Liu Y, Yu J, Sun X, Wang L, et al. Effects of platelet-rich fibrin on osteogenic differentiation of Schneiderian membrane derived mesenchymal stem cells and bone formation in maxillary sinus. Cell Communication and Signaling. 2022 Dec 15;20(1):88. doi: 10.1186/s12964-022-00844-0

363. Colley H, McArthur SL, Stolzing A, Scutt A. Culture on fibrin matrices maintains the colony-forming capacity and osteoblastic differentiation of mesenchymal stem cells. Biomedical Materials. 2012 Aug 1;7(4):045015. doi: 10.1088/1748-6041/7/4/045015

364. Janmey PA, Winer JP, Weisel JW. Fibrin gels and their clinical and bioengineering applications. Vol. 6, Journal of the Royal Society Interface. Royal Society; 2009. p. 1–10. doi: 10.1098/rsif.2008.0327

365. Noori A, Ashrafi SJ, Vaez-Ghaemi R, Hatamian-Zaremi A, Webster TJ. A review of fibrin and fibrin composites for bone tissue engineering. Int J Nanomedicine. 2017 Jul;Volume 12:4937–61. doi: 10.2147/IJN.S124671

366. Zhang D, Wu X, Chen J, Lin K. The development of collagen based composite scaffolds for bone regeneration. Bioact Mater. 2018 Mar;3(1):129–38. doi: 10.1016/j.bioactmat.2017.08.004

367. Oh J-H, Kim H-J, Kim T-I, Woo KM. Comparative evaluation of the biological properties of fibrin for bone regeneration. BMB Rep. 2014 Feb;47(2):110–4. doi: 10.5483/bmbrep.2014.47.2.156

368. Gassling V, Hedderich J, Açil Y, Purcz N, Wiltfang J, Douglas T. Comparison of platelet rich fibrin and collagen as osteoblast-seeded scaffolds for bone tissue engineering applications. Clin Oral Implants Res. 2013 Mar;24(3):320–8. doi: 10.1111/j.1600-0501.2011.02333.x

369. Yang HS, La W-G, Cho Y-M, Shin W, Yeo G-D, Kim B-S. Comparison between heparin-conjugated fibrin and collagen sponge as bone morphogenetic protein-2 carriers for bone regeneration. Exp Mol Med. 2012;44(5):350. doi: 10.3858/emm.2012.44.5.039

370. Boukhechba F, Balaguer T, Michiels J, Ackermann K, Quincey D, Bouler J, et al. Human Primary Osteocyte Differentiation in a 3D Culture System. Journal of Bone and Mineral Research. 2009 Nov 4;24(11):1927–35. doi: 10.1359/jbmr.090517

371. Bernhardt A, Österreich V, Gelinsky M. Three-Dimensional Co-culture of Primary Human Osteocytes and Mature Human Osteoclasts in Collagen Gels.

Tissue Eng Part A. 2020 Jun 1;26(11–12):647–55. [accessed 30 Nov 2021] Available from: https://www.liebertpub.com/doi/abs/10.1089/ten.tea.2019.0085

372. Bernhardt A, Skottke J, von Witzleben M, Gelinsky M. Triple Culture of Primary Human Osteoblasts, Osteoclasts and Osteocytes as an In Vitro Bone Model. Int J Mol Sci. 2021 Jul 2;22(14). [accessed 27 Jun 2023] Available from: https://pubmed.ncbi.nlm.nih.gov/34298935/

373. Nasello G, Alamán-Díez P, Schiavi J, Pérez MÁ, McNamara L, García-Aznar JM. Primary Human Osteoblasts Cultured in a 3D Microenvironment Create a Unique Representative Model of Their Differentiation Into Osteocytes. Front Bioeng Biotechnol. 2020 Apr 24;8. doi: 10.3389/fbioe.2020.00336

374. Munir A, Reseland JE, Tiainen H, Haugen HJ, Sikorski P, Christiansen EF, et al. Osteocyte-Like Cells Differentiated From Primary Osteoblasts in an Artificial Human Bone Tissue Model. JBMR Plus. 2023 Sep 28;7(9). doi: 10.1002/jbm4.10792

375. Harris SA, Enger RJ, Riggs LB, Spelsberg TC. Development and characterization of a conditionally immortalized human fetal osteoblastic cell line. Journal of Bone and Mineral Research. 1995 Feb;10(2):178–86. [accessed 6 Mar 2020] Available from: http://www.ncbi.nlm.nih.gov/pubmed/7754797

376. Einhorn TA. The cell and molecular biology of fracture healing. Clin Orthop Relat Res. 1998;355(355 Suppl). [accessed 16 Feb 2023] Available from: https://pubmed.ncbi.nlm.nih.gov/9917622/

377. Ghiasi MS, Chen J, Vaziri A, Rodriguez EK, Nazarian A. Bone fracture healing in mechanobiological modeling: A review of principles and methods. Bone Rep. 2017 Jun 1;6:87. [accessed 16 Feb 2023] Available from: /pmc/articles/PMC5365304/

378. Cho TJ, Gerstenfeld LC, Einhorn TA. Differential temporal expression of members of the transforming growth factor beta superfamily during murine fracture healing. J Bone Miner Res. 2002;17(3):513–20. [accessed 16 Feb 2023] Available from: https://pubmed.ncbi.nlm.nih.gov/11874242/

379. Bahney CS, Zondervan RL, Allison P, Theologis A, Ashley JW, Ahn J, et al. Cellular Biology of Fracture Healing. J Orthop Res. 2019 Jan 1;37(1):35. [accessed 16 Feb 2023] Available from: /pmc/articles/PMC6542569/

380. Su X, Sun K, Cui FZ, Landis WJ. Organization of apatite crystals in human woven bone. Bone. 2003 Feb 1;32(2):150–62. [accessed 19 Feb 2023] Available from: https://pubmed.ncbi.nlm.nih.gov/12633787/

381. Wang X, Huang J, Huang F, Zong JC, Tang X, Liu Y, et al. Bone morphogenetic protein 9 stimulates callus formation in osteoporotic rats during

fracture healing. Mol Med Rep. 2017;15(5):2537. [accessed 19 Feb 2023] Available from: /pmc/articles/PMC5428899/

382. Faßbender M, Minkwitz S, Strobel C, Schmidmaier G, Wildemann B. Stimulation of bone healing by sustained bone morphogenetic protein 2 (BMP-2) delivery. Int J Mol Sci. 2014 May 14;15(5):8539–52. [accessed 19 Feb 2023] Available from: https://pubmed.ncbi.nlm.nih.gov/24830556/

383. Mackie EJ, Ahmed YA, Tatarczuch L, Chen KS, Mirams M. Endochondral ossification: how cartilage is converted into bone in the developing skeleton. Int J Biochem Cell Biol. 2008;40(1):46–62. [accessed 19 Feb 2023] Available from: https://pubmed.ncbi.nlm.nih.gov/17659995/

384. Shapiro F. Bone development and its relation to fracture repair. The role of mesenchymal osteoblasts and surface osteoblasts. Eur Cell Mater. 2008;15:53–76. doi: 10.22203/ECM.V015A05

385. Barnes GL, Kostenuik PJ, Gerstenfeld LC, Einhorn TA. Growth Factor Regulation of Fracture Repair. Journal of Bone and Mineral Research. 1999 Nov 1;14(11):1805–15. [accessed 16 Feb 2023] Available from: https://onlinelibrary.wiley.com/doi/full/10.1359/jbmr.1999.14.11.1805

386. Oryan A, Monazzah S, Bigham-Sadegh A, Oryan A, Monazzah S, Bigham-Sadegh A. Bone Injury and Fracture Healing Biology. Biomedical and Environmental Sciences, 2015, Vol 28, Issue 1, Pages: 57-71. 2015 Jan 20;28(1):57–71. [accessed 19 Feb 2023] Available from: https://www.besjournal.com/en/article/doi/10.3967/bes2015.006

387. Bahney CS, Hu DP, Miclau T, Marcucio RS. The Multifaceted Role of the Vasculature in Endochondral Fracture Repair. Front Endocrinol (Lausanne). 2015;6(FEB). [accessed 19 Feb 2023] Available from: /pmc/articles/PMC4318416/

388. Schindeler A, McDonald MM, Bokko P, Little DG. Bone remodeling during fracture repair: The cellular picture. Semin Cell Dev Biol. 2008;19(5):459–66. [accessed 19 Feb 2023] Available from: https://pubmed.ncbi.nlm.nih.gov/18692584/

389. Paxton JZ, Grover LM, Baar K. Engineering an in vitro model of a functional ligament from bone to bone. Tissue Eng Part A. 2010 Nov 1;16(11):3515–25. [accessed 20 Feb 2023] Available from: https://pubmed.ncbi.nlm.nih.gov/20593972/

390. Hauser RA. Ligament Injury and Healing: A Review of Current Clinical Diagnostics and Therapeutics. Open Rehabil J. 2013 Jan 24;6(1):1–20. doi: 10.2174/1874943701306010001

391. Paxton JZ, Donnelly K, Keatch RP, Baar K, Grover LM. Factors affecting the longevity and strength in an in vitro model of the bone-ligament interface. Ann

Biomed Eng. 2010 Jun 30;38(6):2155–66. [accessed 20 Feb 2023] Available from: https://link.springer.com/article/10.1007/s10439-010-0044-0

392. Wudebwe UNG, Bannerman A, Goldberg-Oppenheimer P, Paxton JZ, Williams RL, Grover LM. Exploiting cell-mediated contraction and adhesion to structure tissues in vitro. Vol. 370, Philosophical Transactions of the Royal Society B: Biological Sciences. Royal Society of London; 2015. doi: 10.1098/rstb.2014.0200

393. Bayer ML, Yeung CYC, Kadler KE, Qvortrup K, Baar K, Svensson RB, et al. The initiation of embryonic-like collagen fibrillogenesis by adult human tendon fibroblasts when cultured under tension. Biomaterials. 2010 Jun 1;31(18):4889–97. doi: 10.1016/J.BIOMATERIALS.2010.02.062

394. Paxton JZ, Wudebwe UNG, Wang A, Woods D, Grover LM. Monitoring Sinew Contraction During Formation of Tissue-Engineered Fibrin-Based Ligament Constructs. https://home.liebertpub.com/tea. 2012 May 17;18(15–16):1596–607. [accessed 20 Feb 2023] Available from: https://www.liebertpub.com/doi/10.1089/ten.tea.2011.0535

395. Iordachescu A, Amin HD, Rankin SM, Williams RL, Yapp C, Bannerman A, et al. An In Vitro Model for the Development of Mature Bone Containing an Osteocyte Network. Adv Biosyst. 2018;2(2). doi: 10.1002/adbi.201700156

396. Dwek JR. The periosteum: what is it, where is it, and what mimics it in its absence? Skeletal Radiol. 2010 Apr;39(4):319. [accessed 25 Feb 2023] Available from: /pmc/articles/PMC2826636/

397. Iordachescu A. AN IN-VITRO MODEL FOR THE DEVELOPMENT OF MATURE BONE CONTAINING AN OSTEOCYTE NETWORK. Birmingham: University of Birmingham; 2017.

398. Iordachescu A, Williams RL, Hulley PA, Grover LM. Organotypic Culture of Bone-Like Structures Using Composite Ceramic-Fibrin Scaffolds. Curr Protoc Stem Cell Biol. 2019 Feb 1;48(1):e79. [accessed 12 Nov 2020] Available from: http://doi.wiley.com/10.1002/cpsc.79

399. Kusumbe AP, Ramasamy SK, Starsichova A, Adams RH. Sample preparation for high-resolution 3D confocal imaging of mouse skeletal tissue. Nature Protocols 2015 10:12. 2015 Oct 29;10(12):1904–14. [accessed 5 Dec 2021] Available from: https://www.nature.com/articles/nprot.2015.125

400. Mizerska-Kowalska M, Sławinska-Brych A, Kaławaj K, Zurek A, Pawinska B, Rzeski W, et al. Betulin Promotes Differentiation of Human Osteoblasts In Vitro and Exerts an Osteoinductive Effect on the hFOB 1.19 Cell Line Through Activation of JNK, ERK1/2, and mTOR Kinases. Molecules. 2019 Jul 19;24(14). [accessed 16 Jun 2023] Available from: https://pubmed.ncbi.nlm.nih.gov/31331121/

401. Zhang N, Hu L, Cao Z, Liu X, Pan J. Periosteal Skeletal Stem Cells and Their Response to Bone Injury. Front Cell Dev Biol. 2022 Mar 24;10. [accessed 12 Mar 2023] Available from: /pmc/articles/PMC8987235/

402. Zavan B, Giorgi C, Bagnara GP, Vindigni V, Abatangelo G, Cortivo R. Osteogenic and chondrogenic differentiation: comparison of human and rat bone marrow mesenchymal stem cells cultured into polymeric scaffolds. Eur J Histochem. 2007;51 Suppl 1:1–8.

403. Wieczorek G, Steinhoff C, Schulz R, Scheller M, Vingron M, Ropers HH, et al. Gene expression profile of mouse bone marrow stromal cells determined by cDNA microarray analysis. Cell Tissue Res. 2003 Feb 1;311(2):227–37. [accessed 12 Mar 2023] Available from: https://pubmed.ncbi.nlm.nih.gov/12596042/

404. Foudah D, Redaelli S, Donzelli E, Bentivegna A, Miloso M, Dalprà L, et al. Monitoring the genomic stability of in vitro cultured rat bone-marrow-derived mesenchymal stem cells. Chromosome Res. 2009 Dec;17(8):1025–39. [accessed 2 May 2023] Available from: https://pubmed.ncbi.nlm.nih.gov/19957104/

405. Sims NA, White CP, Sunn KL, Thomas GP, Drummond ML, Morrison NA, et al. Human and Murine Osteocalcin Gene Expression: Conserved Tissue Restricted Expression and Divergent Responses to 1,25-Dihydroxyvitamin D3in Vivo. Molecular Endocrinology. 1997 Oct 1;11(11):1695–708. [accessed 2 May 2023] Available from: https://academic.oup.com/mend/article/11/11/1695/2756778

406. Reilly GC, Radin S, Chen AT, Ducheyne P. Differential alkaline phosphatase responses of rat and human bone marrow derived mesenchymal stem cells to 45S5 bioactive glass. Biomaterials. 2007 Oct;28(28):4091–7. [accessed 12 Mar 2023] Available from: https://pubmed.ncbi.nlm.nih.gov/17586040/

407. Rhrissorrakrai K, Belcastro V, Bilal E, Norel R, Poussin C, Mathis C, et al. Understanding the limits of animal models as predictors of human biology: lessons learned from the sbv IMPROVER Species Translation Challenge. Bioinformatics. 2015 Feb 15;31(4):471–83. [accessed 15 Jun 2023] Available from: https://dx.doi.org/10.1093/bioinformatics/btu611

408. Mirabelli P, Coppola L, Salvatore M. Cancer Cell Lines Are Useful Model Systems for Medical Research. Cancers (Basel). 2019 Aug 1;11(8). [accessed 2 May 2023] Available from: /pmc/articles/PMC6721418/

409. ATCC. Primary Cells | ATCC. [accessed 20 Jul 2023] Available from: https://www.atcc.org/cell-products/primary-cells#t=productTab&numberOfResults=24

410. Subramaniam M, Jalal SM, Rickard DJ, Harris SA, Bolander ME, Spelsberg TC. Further characterization of human fetal osteoblastic hFOB 1.19 and

hFOB/ERα cells: Bone formation in vivo and karyotype analysis using multicolor fluorescent in situ hybridization. J Cell Biochem. 2002;87(1):9–15. [accessed 6 Mar 2020] Available from: http://www.ncbi.nlm.nih.gov/pubmed/12210717

411. Rousseau J, Lamoureux F, Picarda G, Gouin F, Trichet V, Rédini F. Animal Models of Malignant Primary Bone Tumors and Novel Therapeutic Approaches. Bone Cancer. 2010 Jan 1;333–46. doi: 10.1016/B978-0-12-374895-9.00028-1

412. Bairoch A. The Cellosaurus, a Cell-Line Knowledge Resource. J Biomol Tech. 2018 Jul 1;29(2):25–38. [accessed 2 May 2023] Available from: https://pubmed.ncbi.nlm.nih.gov/29805321/

413. Winn SR, Randolph G, Uludag H, Wong SC, Hair GA, Hollinger JO. Establishing an Immortalized Human Osteoprecursor Cell Line: OPC1. Journal of Bone and Mineral Research. 1999 Oct 1;14(10):1721–33. [accessed 2 May 2023] Available from: https://onlinelibrary.wiley.com/doi/full/10.1359/jbmr.1999.14.10.1721

414. DeCaprio JA, Ludlow JW, Figge J, Shew JY, Huang CM, Lee WH, et al. SV40 large tumor antigen forms a specific complex with the product of the retinoblastoma susceptibility gene. Cell. 1988 Jul 15;54(2):275–83. [accessed 6 Mar 2020] Available from: http://www.ncbi.nlm.nih.gov/pubmed/2839300

415. Ali SH, DeCaprio JA. Cellular transformation by SV40 large T antigen: Interaction with host proteins. Semin Cancer Biol. 2001 Feb;11(1):15–22. [accessed 6 Mar 2020] Available from: http://www.ncbi.nlm.nih.gov/pubmed/11243895

416. Vélez-Cruz R, Johnson DG. The Retinoblastoma (RB) Tumor Suppressor: Pushing Back against Genome Instability on Multiple Fronts. Int J Mol Sci. 2017 Aug 16;18(8). [accessed 2 May 2023] Available from: /pmc/articles/PMC5578165/

417. Harris SA, Zhang M, Kidder LS, Evans GL, Spelsberg TC, Turner RT. Effects of orbital spaceflight on human osteoblastic cell physiology and gene expression. Bone. 2000 Apr 1;26(4):325–31. doi: 10.1016/S8756-3282(00)00234-9

418. Altvater T, Hendrich C, Noth U, Rader CP, Stach R, Schütze N, et al. Cytotoxicity study of high gold content Degutan surfaces of various degrees of roughness with fibroblasts (BALB 3T3) and osteoblasts (hFOB 1.19). Biomedizinische Technik/Biomedical Engineering. 2000 Jan;45(9):238–42. doi: 10.1515/bmte.2000.45.9.238

419. Brezulier D, Pellen-Mussi P, Tricot-Doleux S, Novella A, Sorel O, Jeanne S. Development of a 3D human osteoblast cell culture model for studying mechanobiology in orthodontics. Eur J Orthod. 2020 Aug 1;42(4):387–95.

[accessed 2 May 2023] Available from: https://pubmed.ncbi.nlm.nih.gov/32144430/

420. Mann V, Grimm D, Corydon TJ, Krüger M, Wehland M, Riwaldt S, et al. Changes in Human Foetal Osteoblasts Exposed to the Random Positioning Machine and Bone Construct Tissue Engineering. Int J Mol Sci. 2019 Mar 2;20(6). [accessed 28 May 2023] Available from: /pmc/articles/PMC6471706/

421. Dozzo A, Chullipalliyalil K, McAuliffe M, O'Driscoll CM, Ryan KB. Nano-Hydroxyapatite/PLGA Mixed Scaffolds as a Tool for Drug Development and to Study Metastatic Prostate Cancer in the Bone. Pharmaceutics. 2023 Jan 1;15(1). [accessed 2 May 2023] Available from: https://pubmed.ncbi.nlm.nih.gov/36678871/

422. Yen M, Chien C-C, Chiu I, Huang H-I, Chen Y-C, Hu H-I, et al. Multilineage differentiation and characterization of the human fetal osteoblastic 1.19 cell line: a possible in vitro model of human mesenchymal progenitors. Stem Cells. 2007 Jan 1;25(1):125–31. [accessed 28 May 2023] Available from: https://pubmed.ncbi.nlm.nih.gov/17204605/

423. Dhurjati R, Liu X, Gay C V., Mastro AM, Vogler EA. Extended-Term Culture of Bone Cells in a Compartmentalized Bioreactor. Tissue Eng. 2006 Nov;12(11):3045–54. doi: 10.1089/ten.2006.12.3045

424. Guo D, Li Q, Lv Q, Wei Q, Cao S, Gu J. MiR-27a Targets sFRP1 in hFOB Cells to Regulate Proliferation, Apoptosis and Differentiation. Zheng SG, editor. PLoS One. 2014 Mar 13;9(3):e91354. [accessed 12 Nov 2020] Available from: https://dx.plos.org/10.1371/journal.pone.0091354

425. Parra-Torres A, Enríquez J, Jiménez-Ortega R, Patiño N, Castillejos-López M, Torres-Espíndola L, et al. Expression profiles of the Wnt/β-catenin signaling-related extracellular antagonists during proliferation and differentiation in human osteoblast-like cells. Exp Ther Med. 2020 Oct 23;20(6):1–1. doi: 10.3892/etm.2020.9384

426. Gruber HE, Ode G, Hoelscher G, Ingram J, Bethea S, Bosse MJ. Osteogenic, stem cell and molecular characterisation of the human induced membrane from extremity bone defects. Bone Joint Res. 2016 Apr;5(4):106–15. doi: 10.1302/2046-3758.54.2000483

427. Ben-David U, Siranosian B, Ha G, Tang H, Oren Y, Hinohara K, et al. Genetic and transcriptional evolution alters cancer cell line drug response. Nature 2018 560:7718. 2018 Aug 8;560(7718):325–30. [accessed 9 May 2023] Available from: https://www.nature.com/articles/s41586-018-0409-3

428. Reading between the lines. Nature. 2018 Aug 1;560(7718):281. doi: 10.1038/D41586-018-05935-Y

429. Marozin S, Simon-Nobbe B, Irausek S, Chung LWK, Lepperdinger G. Kinship of conditionally immortalized cells derived from fetal bone to human bone-derived mesenchymal stroma cells. Scientific Reports 2021 11:1. 2021 May 25;11(1):1–13. [accessed 28 May 2023] Available from: https://www.nature.com/articles/s41598-021-90161-2

430. Mohammadi Farsani T, Motevaseli E, Neyazi N, Khorramizadeh MR, Zafarvahedian E, Ghahremani MH. Effect of Passage Number and Culture Time on the Expression and Activity of Insulin-Degrading Enzyme in Caco-2 Cells. Iran Biomed J. 2018 Jan 1;22(1):70. [accessed 8 May 2023] Available from: /pmc/articles/PMC5712388/

431. Kwist K, Bridges WC, Burg KJL. The effect of cell passage number on osteogenic and adipogenic characteristics of D1 cells. Cytotechnology. 2016 Aug 1;68(4):1661. [accessed 8 May 2023] Available from: /pmc/articles/PMC4960171/

432. Yan XZ, Yang W, Yang F, Kersten-Niessen M, Jansen JA, Both SK. Effects of continuous passaging on mineralization of MC3T3-E1 cells with improved osteogenic culture protocol. Tissue Eng Part C Methods. 2014 Mar 1;20(3):198–204. [accessed 8 May 2023] Available from: https://www.liebertpub.com/doi/10.1089/ten.tec.2012.0412

433. Hughes P, Marshall D, Reid Y, Parkes H, Gelber C. The costs of using unauthenticated, over-passaged cell lines: How much more data do we need? Biotechniques. 2007 May 16;43(5):575–86. [accessed 8 May 2023] Available from: https://www.future-science.com/doi/10.2144/000112598

434. WESTWOOD JC, MACPHERSON IA, TITMUSS DH. Transformation of normal cells in tissue culture: its significance relative to malignancy and virus vaccine production. Br J Exp Pathol. 1957 Apr;38(2):138–54.

435. Drexler HG, Dirks WG, Matsuo Y, MacLeod RAF. False leukemia–lymphoma cell lines: an update on over 500 cell lines. Leukemia 2003 17:2. 2003 Feb 18;17(2):416–26. [accessed 8 May 2023] Available from: https://www.nature.com/articles/2402799

436. Yoshino K, Iimura E, Saijo K, Iwase S, Fukami K, Ohno T, et al. Essential role for gene profiling analysis in the authentication of human cell lines. Human cell : official journal of Human Cell Research Society. 2006;19(1):43–8. [accessed 8 May 2023] Available from: https://link.springer.com/article/10.1111/j.1749-0774.2005.00007.x

437. Stacey GN, Masters JRW, Hay RJ, Drexler HG, MacLeod RAF, Freshney RI. Cell contamination leads to inaccurate data: we must take action now. Nature 2000 403:6768. 2000 Jan 27;403(6768):356–356. [accessed 8 May 2023] Available from: https://www.nature.com/articles/35000394

438. Announcement: Time to tackle cells' mistaken identity. Nature 2015 520:7547. 2015 Apr 15;520(7547):264–264. [accessed 9 May 2023] Available from: https://www.nature.com/articles/520264a

439. Wenger SL, Senft JR, Sargent LM, Bamezai R, Bairwa N, Grant SG. Comparison of established cell lines at different passages by karyotype and comparative genomic hybridization. Biosci Rep. 2004 Dec 12;24(6):631–9. [accessed 8 May 2023] Available from: https://link.springer.com/article/10.1007/s10540-005-2797-5

440. Stacey GN, Bolton BJ, Doyle A. DNA fingerprinting transforms the art of cell authentication. Nature. 1992 May 1;357(6375):261–2. [accessed 8 May 2023] Available from: https://europepmc.org/article/med/1589025

441. Park JB. The effects of dexamethasone, ascorbic acid, and β-glycerophosphate on osteoblastic differentiation by regulating estrogen receptor and osteopontin expression. Journal of Surgical Research. 2012 Mar 1;173(1):99–104. [accessed 12 May 2023] Available from: http://www.journalofsurgicalresearch.com/article/S0022480410007675/fulltext

442. Wang H, Li L, Zhang N, Ma Y. Vitamin K2 Improves Osteogenic Differentiation by Inhibiting STAT1 via the Bcl-6 and IL-6/JAK in C3H10 T1/2 Clone 8 Cells. Nutrients. 2022 Jul 1;14(14). [accessed 12 May 2023] Available from: https://pubmed.ncbi.nlm.nih.gov/35889891/

443. Myneni VD, Mezey E. REGULATION OF BONE REMODELING BY VITAMIN K2. Oral Dis. 2017 Nov 1;23(8):1021. [accessed 12 May 2023] Available from: /pmc/articles/PMC5471136/

444. Cockayne S, Adamson J, Lanham-New S, Shearer MJ, Gilbody S, Torgerson DJ. Vitamin K and the Prevention of Fractures: Systematic Review and Meta-analysis of Randomized Controlled Trials. Arch Intern Med. 2006 Jun 26;166(12):1256–61. [accessed 12 May 2023] Available from: https://jamanetwork.com/journals/jamainternalmedicine/fullarticle/410550

445. Useful Numbers for Cell Culture | Thermo Fisher Scientific - UK. [accessed 12 May 2023] Available from: https://www.thermofisher.com/uk/en/home/references/gibco-cell-culture-basics/cell-culture-protocols/cell-culture-useful-numbers.html

446. Settivari RS, Rowlands JC, Wilson DM, Arnold SM, Spencer PJ. Application of Evolving Computational and Biological Platforms for Chemical Safety Assessment. A Comprehensive Guide to Toxicology in Nonclinical Drug Development. 2017 Jan 1;843–73. doi: 10.1016/B978-0-12-803620-4.00032-3

447. Stich S, Loch A, Park SJ, Häupl T, Ringe J, Sittinger M. Characterization of single cell derived cultures of periosteal progenitor cells to ensure the cell quality for clinical application. PLoS One. 2017 May 1;12(5):e0178560.

[accessed 12 May 2023] Available from: https://journals.plos.org/plosone/article?id=10.1371/journal.pone.0178560

448. Arnsdorf EJ, Jones LM, Carter DR, Jacobs CR. The Periosteum as a Cellular Source for Functional Tissue Engineering. Tissue Eng Part A. 2009;15(9):2637. [accessed 12 May 2023] Available from: /pmc/articles/PMC2792114/

449. Matthews BG, Grcevic D, Wang L, Hagiwara Y, Roguljic H, Joshi P, et al. Analysis of αSMA-labeled progenitor cell commitment identifies notch signaling as an important pathway in fracture healing. J Bone Miner Res. 2014;29(5):1283–94. [accessed 12 May 2023] Available from: https://pubmed.ncbi.nlm.nih.gov/24190076/

450. Bagi CM, Wilkie D, Georgelos K, Williams D, Bertolini D. Morphological and structural characteristics of the proximal femur in human and rat. Bone. 1997 Sep;21(3):261–7. [accessed 12 Nov 2020] Available from: https://pubmed.ncbi.nlm.nih.gov/9276091/

451. Scuteri A, Donzelli E, Foudah D, Caldara C, Redondo J, D'Amico G, et al. Mesengenic differentiation: Comparison of human and rat bone marrow mesenchymal stem cells. Int J Stem Cells. 2014;7(2):127–34. [accessed 8 Dec 2020] Available from: /pmc/articles/PMC4249895/?report=abstract

452. Dapson RW, Fagan C, Kiernan JA, Wickersham TW. Certification procedures for sirius red F3B (CI 35780, Direct red 80). Biotech Histochem. 2011 Jun;86(3):133–9. [accessed 8 May 2023] Available from: https://pubmed.ncbi.nlm.nih.gov/21417582/

453. Junqueira LCU, Bignolas G, Brentani RR. Picrosirius staining plus polarization microscopy, a specific method for collagen detection in tissue sections. Histochem J. 1979 Jul;11(4):447–55. [accessed 8 May 2023] Available from: https://link.springer.com/article/10.1007/BF01002772

454. Chen CZC, Raghunath M. Focus on collagen: In vitro systems to study fibrogenesis and antifibrosis _ state of the art. Fibrogenesis Tissue Repair. 2009 Dec 15;2(1):1–10. [accessed 8 May 2023] Available from: https://fibrogenesis.biomedcentral.com/articles/10.1186/1755-1536-2-7

455. Xu Q, Norman JT, Shrivastav S, Lucio-Cazana J, Kopp JB. In vitro models of TGF-beta-induced fibrosis suitable for high-throughput screening of antifibrotic agents. Am J Physiol Renal Physiol. 2007;293(2). [accessed 8 May 2023] Available from: https://pubmed.ncbi.nlm.nih.gov/17494090/

456. Li X, Yang X, Liu X, He W, Huang Q, Li S, et al. Calcium carbonate nanoparticles promote osteogenesis compared to adipogenesis in human bone-marrow mesenchymal stem cells. Progress in Natural Science: Materials International. 2018 Oct 1;28(5):598–608. doi: 10.1016/J.PNSC.2018.09.004

457. Jones RR, Castelletto V, Connon CJ, Hamley IW. Collagen stimulating effect of peptide amphiphile C16-KTTKS on human fibroblasts. Mol Pharm. 2013 Mar 4;10(3):1063–9. [accessed 8 May 2023] Available from: https://www.researchgate.net/publication/234141020_Collagen_Stimulating_Effect_of_Peptide_Amphiphile_C-16-KTTKS_on_Human_Fibroblasts

458. Sectioning of bone as a specialist histology specimen. [accessed 20 Jul 2023] Available from: https://www.news-medical.net/news/20120709/Sectioning-of-bone-as-a-specialist-histology-specimen.aspx

459. Goldschlager T, Abdelkader A, Kerr J, Boundy I, Jenkin G. Undecalcified bone preparation for histology, histomorphometry and fluorochrome analysis. J Vis Exp. 2010 Jan 8;(35). doi: 10.3791/1707

460. Taqi SA, Sami SA, Sami LB, Zaki SA. A review of artifacts in histopathology. J Oral Maxillofac Pathol. 2018 May 1;22(2):279. [accessed 9 May 2023] Available from: /pmc/articles/PMC6097380/

461. Álvarez-Castillo E, Bengoechea C, Felix M, Guerrero A. Freeze-Drying versus Heat-Drying: Effect on Protein-Based Superabsorbent Material. Processes 2021, Vol 9, Page 1076. 2021 Jun 21;9(6):1076. [accessed 21 Nov 2022] Available from: https://www.mdpi.com/2227-9717/9/6/1076/htm

462. Elavarasan K, Shamasundar BA. Effect of oven drying and freeze drying on the antioxidant and functional properties of protein hydrolysates derived from freshwater fish (Cirrhinus mrigala) using papain enzyme. J Food Sci Technol. 2016 Feb 1;53(2):1303–11. [accessed 21 Nov 2022] Available from: https://pubmed.ncbi.nlm.nih.gov/27162411/

463. Elavarasan K, Shamasundar BA, Badii F, Howell N. Angiotensin I-converting enzyme (ACE) inhibitory activity and structural properties of oven- and freeze-dried protein hydrolysate from fresh water fish (Cirrhinus mrigala). Food Chem. 2016 Sep;206:210–6. doi: 10.1016/j.foodchem.2016.03.047

464. Tan M, Mei J, Xie J. The Formation and Control of Ice Crystal and Its Impact on the Quality of Frozen Aquatic Products: A Review. Crystals 2021, Vol 11, Page 68. 2021 Jan 15;11(1):68. [accessed 11 May 2023] Available from: https://www.mdpi.com/2073-4352/11/1/68/htm

465. Steu S, Baucamp M, Von Dach G, Bawohl M, Dettwiler S, Storz M, et al. A procedure for tissue freezing and processing applicable to both intra-operative frozen section diagnosis and tissue banking in surgical pathology. Virchows Arch. 2008 Mar;452(3):305–12. [accessed 11 May 2023] Available from: https://pubmed.ncbi.nlm.nih.gov/18253747/

466. Janssens K, Vittiglio G, Deraedt I, Aerts A, Vekemans B, Vincze L, et al. Use of Microscopic XRF for Non-destructive Analysis in Art and Archaeometry. X-Ray Spectrometry. 2000;29(1):73–91. doi: 10.1002/(SICI)1097-4539(200001/02)29:1<73::AID-XRS416>3.0.CO;2-M

467. Anitha A, Brasoveanu A, Duarte M, Hughes S, Daubechies I, Dik J, et al. Restoration of X-ray fluorescence images of hidden paintings. Signal Processing. 2013 Mar 1;93(3):592–604. doi: 10.1016/J.SIGPRO.2012.09.027

468. Stockmann U, Cattle SR, Minasny B, McBratney AB. Utilizing portable X-ray fluorescence spectrometry for in-field investigation of pedogenesis. Catena (Amst). 2016 Apr 1;139:220–31. doi: 10.1016/J.CATENA.2016.01.007

469. Cheung TW, Law AWL, Ahmed R, Mak CY, Lau C. Assessment of bone calcium and phosphorus content using micro X-ray fluorescence spectrometry (μ-EDXRF): effects of long-term cadmium poisoning. X-Ray Spectrometry. 2016 Nov;45(6):339–43. doi: 10.1002/xrs.2710

470. Yue B. Biology of the extracellular matrix: an overview. J Glaucoma. 2014 Dec 10;23(8 Suppl 1):S20–3. [accessed 26 May 2023] Available from: https://pubmed.ncbi.nlm.nih.gov/25275899/

471. Kim SH, Turnbull J, Guimond S. Extracellular matrix and cell signalling: the dynamic cooperation of integrin, proteoglycan and growth factor receptor. Journal of Endocrinology. 2011 May 1;209(2):139–51. [accessed 26 May 2023] Available from: https://joe.bioscientifica.com/view/journals/joe/209/2/139.xml

472. Gattazzo F, Urciuolo A, Bonaldo P. Extracellular matrix: A dynamic microenvironment for stem cell niche. Biochim Biophys Acta. 2014;1840(8):2506. [accessed 26 May 2023] Available from: /pmc/articles/PMC4081568/

473. Wong ML, Medrano JF. Real-time PCR for mRNA quantitation. Biotechniques. 2005 May 30;39(1):75–85. [accessed 26 May 2023] Available from: https://www.future-science.com/doi/10.2144/05391RV01

474. Taylor SC, Nadeau K, Abbasi M, Lachance C, Nguyen M, Fenrich J. The Ultimate qPCR Experiment: Producing Publication Quality, Reproducible Data the First Time. Trends Biotechnol. 2019 Jul 1;37(7):761–74. doi: 10.1016/J.TIBTECH.2018.12.002

475. Löfström C, Josefsen MH, Hansen T, SØndergaard MSR, Hoorfar J. Fluorescence-based real-time quantitative polymerase chain reaction (qPCR) technologies for high throughput screening of pathogens. High Throughput Screening for Food Safety Assessment: Biosensor Technologies, Hyperspectral Imaging and Practical Applications. 2015 Jan 1;219–48. doi: 10.1016/B978-0-85709-801-6.00009-5

476. Kralik P, Ricchi M. A basic guide to real time PCR in microbial diagnostics: Definitions, parameters, and everything. Front Microbiol. 2017 Feb 2;8(FEB):108. doi: 10.3389/FMICB.2017.00108/BIBTEX

477. Livak KJ, Schmittgen TD. Analysis of Relative Gene Expression Data Using Real-Time Quantitative PCR and the 2−ΔΔCT Method. Methods. 2001 Dec 1;25(4):402–8. doi: 10.1006/METH.2001.1262

478. Bustin SA, Nolan T. Pitfalls of Quantitative Real-Time Reverse-Transcription Polymerase Chain Reaction. J Biomol Tech. 2004 Sep;15(3):155. [accessed 25 May 2023] Available from: /pmc/articles/PMC2291693/

479. Goldenthal KL, Hedman K, Chen JW, August JT, Willingham MC. Postfixation detergent treatment for immunofluorescence suppresses localization of some integral membrane proteins. http://dx.doi.org/101177/3383894499. 1985 Aug 1;33(8):813–20. [accessed 25 May 2023] Available from: https://journals.sagepub.com/doi/10.1177/33.8.3894499

480. Im K, Mareninov S, Diaz MFP, Yong WH. An introduction to Performing Immunofluorescence Staining. Methods Mol Biol. 2019;1897:299. [accessed 25 May 2023] Available from: /pmc/articles/PMC6918834/

481. Thomson H. 6 Ways to Improve the Quality of Quantitative Histopathology Data. 2018. [accessed 25 May 2023] Available from: https://oraclebio.com/histopathology-data-quality-blog/

482. Yang M, Li CJ, Xiao Y, Guo Q, Huang Y, Su T, et al. Ophiopogonin D promotes bone regeneration by stimulating CD31hiEMCNhi vessel formation. Cell Prolif. 2020 Mar 1;53(3). [accessed 3 May 2021] Available from: https://pubmed.ncbi.nlm.nih.gov/32080957/

483. Hosoya A, Hoshi K, Sahara N, Ninomiya T, Akahane S, Kawamoto T, et al. Effects of fixation and decalcification on the immunohistochemical localization of bone matrix proteins in fresh-frozen bone sections. Histochem Cell Biol. 2005 Jul 7;123(6):639–46. [accessed 25 May 2023] Available from: https://link.springer.com/article/10.1007/s00418-005-0791-4

484. Tang JYH. Detection of Microbiological Hazards. Food Safety Management. 2023 Jan 1;835–50. [accessed 26 May 2023] Available from: https://linkinghub.elsevier.com/retrieve/pii/B9780128200131000024

485. Bustin SA, Nolan T. RT-qPCR Testing of SARS-CoV-2: A Primer. Int J Mol Sci. 2020 Apr 2;21(8). [accessed 26 May 2023] Available from: /pmc/articles/PMC7215906/

486. Organization WH. Laboratory testing for 2019 novel coronavirus (2019-nCoV) in suspected human cases: Interim guidance. 2020;7–7. [accessed 26 May 2023] Available from: https://apps.who.int/iris/rest/bitstreams/1272454/retrieve

487. Dutta D, Naiyer S, Mansuri S, Soni N, Singh V, Bhat KH, et al. COVID-19 Diagnosis: A Comprehensive Review of the RT-qPCR Method for Detection of SARS-CoV-2. Diagnostics. 2022 Jun 1;12(6). [accessed 26 May 2023] Available from: /pmc/articles/PMC9221722/

488. Rio DC, Ares M, Hannon GJ, Nilsen TW. Purification of RNA Using TRIzol (TRI Reagent). Cold Spring Harb Protoc. 2010 Jun 1;2010(6):pdb.prot5439. [accessed 26 May 2023] Available from: http://cshprotocols.cshlp.org/content/2010/6/pdb.prot5439.full

489. Ali SA, Alman B. RNA extraction from human articular cartilage by chondrocyte isolation. Anal Biochem. 2012 Oct;429(1):39–41. doi: 10.1016/j.ab.2012.06.028

490. Reimann E, Abram K, Kõks S, Kingo K, Fazeli A. Identification of an optimal method for extracting RNA from human skin biopsy, using domestic pig as a model system. Sci Rep. 2019 Dec 27;9(1):20111. doi: 10.1038/s41598-019-56579-5

491. Schmittgen TD, Zakrajsek BA. Effect of experimental treatment on housekeeping gene expression: validation by real-time, quantitative RT-PCR. J Biochem Biophys Methods. 2000 Nov 20;46(1–2):69–81. doi: 10.1016/S0165-022X(00)00129-9

492. Nygard AB, Jørgensen CB, Cirera S, Fredholm M. Selection of reference genes for gene expression studies in pig tissues using SYBR green qPCR. BMC Mol Biol. 2007 Aug 15;8. [accessed 27 May 2023] Available from: https://pubmed.ncbi.nlm.nih.gov/17697375/

493. Panina Y, Germond A, Masui S, Watanabe TM. Validation of Common Housekeeping Genes as Reference for qPCR Gene Expression Analysis During iPS Reprogramming Process. Scientific Reports 2018 8:1. 2018 Jun 7;8(1):1–8. [accessed 27 May 2023] Available from: https://www.nature.com/articles/s41598-018-26707-8

494. Sullivan-Gunn M, Hinch E, Vaughan V, Lewandowski P. Choosing a stable housekeeping gene and protein is essential in generating valid gene and protein expression results. Br J Cancer. 2011 Mar 1;104(6):1055–1055. doi: 10.1038/bjc.2011.35

495. Stephens AS, Stephens SR, Morrison NA. Internal control genes for quantitative RT-PCR expression analysis in mouse osteoblasts, osteoclasts and macrophages. BMC Res Notes. 2011;4:410. [accessed 27 May 2023] Available from: /pmc/articles/PMC3204251/

496. Yang X, Hatfield JT, Hinze SJ, Mu X, Anderson PJ, Powell BC. Bone to pick: the importance of evaluating reference genes for RT-qPCR quantification of gene expression in craniosynostosis and bone-related tissues and cells. BMC Res Notes. 2012;5:222. [accessed 27 May 2023] Available from: /pmc/articles/PMC3476976/

497. Okamura K, Inagaki Y, Matsui TK, Matsubayashi M, Komeda T, Ogawa M, et al. RT-qPCR analyses on the osteogenic differentiation from human iPS cells: an investigation of reference genes. Scientific Reports 2020 10:1. 2020 Jul

16;10(1):1–11. [accessed 27 May 2023] Available from: https://www.nature.com/articles/s41598-020-68752-2

498. Valente V, Teixeira SA, Neder L, Okamoto OK, Oba-Shinjo SM, Marie SKN, et al. Selection of suitable housekeeping genes for expression analysis in glioblastoma using quantitative RT-PCR. Ann Neurosci. 2014;21(2):62. [accessed 27 May 2023] Available from: /pmc/articles/PMC4117159/

499. Jemiolo B, Trappe S. Single muscle fiber gene expression in human skeletal muscle: Validation of internal control with exercise. Biochem Biophys Res Commun. 2004 Jul 30;320(3):1043–50. [accessed 27 May 2023] Available from: https://pubmed.ncbi.nlm.nih.gov/15240153/

500. Zhao H, Chen Q, Alam A, Cui J, Suen KC, Soo AP, et al. The role of osteopontin in the progression of solid organ tumour. Cell Death & Disease 2018 9:3. 2018 Mar 2;9(3):1–15. [accessed 29 May 2023] Available from: https://www.nature.com/articles/s41419-018-0391-6

501. Si J, Wang C, Zhang D, Wang B, Hou W, Zhou Y. Osteopontin in Bone Metabolism and Bone Diseases. Med Sci Monit. 2020 Jan 30;26:e919159-1. [accessed 29 May 2023] Available from: /pmc/articles/PMC7003659/

502. Morinobu M, Ishijima M, Rittling SR, Tsuji K, Yamamoto H, Nifuji A, et al. Osteopontin Expression in Osteoblasts and Osteocytes During Bone Formation Under Mechanical Stress in the Calvarial Suture In Vivo. Journal of Bone and Mineral Research. 2003 Sep 1;18(9):1706–15. doi: 10.1359/jbmr.2003.18.9.1706

503. Kannan S, Ghosh J, Dhara SK. Osteogenic differentiation potential of porcine bone marrow mesenchymal stem cell subpopulations selected in different basal media. Biol Open. 2020 Oct 10;9(10). [accessed 18 May 2023] Available from: /pmc/articles/PMC7595700/

504. Kaneto CM, Lima PSP, Zanette DL, Oliveira TYK, de Assis Pereira F, Lorenzi JCC, et al. Osteoblastic differentiation of bone marrow mesenchymal stromal cells in Bruck Syndrome. BMC Med Genet. 2016 May 4;17(1):1–9. [accessed 18 May 2023] Available from: https://bmcmedgenet.biomedcentral.com/articles/10.1186/s12881-016-0301-7

505. Moser SC, van der Eerden BCJ. Osteocalcin — A versatile bone-derived hormone. Front Endocrinol (Lausanne). 2019 Jan 10;10(JAN):794. doi: 10.3389/FENDO.2018.00794/BIBTEX

506. Rosset EM, Bradshaw AD. SPARC/Osteonectin in Mineralized Tissue. Matrix Biol. 2016 May 1;52–54:78. [accessed 28 May 2023] Available from: /pmc/articles/PMC5327628/

507. Hrubi E, Imre L, Robaszkiewicz A, Virág L, Kerényi F, Nagy K, et al. Diverse effect of BMP-2 homodimer on mesenchymal progenitors of different origin.

Hum Cell. 2018 Apr 1;31(2):139–48. [accessed 29 May 2023] Available from: https://link.springer.com/article/10.1007/s13577-018-0202-5

508. Barros NMT, Hoac B, Neves RL, Addison WN, Assis DM, Murshed M, et al. Proteolytic processing of osteopontin by PHEX and accumulation of osteopontin fragments in Hyp mouse bone, the murine model of X-linked hypophosphatemia. J Bone Miner Res. 2013 Mar;28(3):688–99. [accessed 29 May 2023] Available from: https://pubmed.ncbi.nlm.nih.gov/22991293/

509. Atkins GJ, Rowe PS, Lim HP, Welldon KJ, Ormsby R, Wijenayaka AR, et al. Sclerostin Is a Locally Acting Regulator of Late-Osteoblast/Preosteocyte Differentiation and Regulates Mineralization Through a MEPE-ASARM-Dependent Mechanism. Journal of Bone and Mineral Research. 2011 Jul;26(7):1425. [accessed 29 May 2023] Available from: /pmc/articles/PMC3358926/

510. Bonewald LF. Generation and function of osteocyte dendritic processes. J Musculoskelet Neuronal Interact. 2005;5(4):321–4.

511. Yang L, Tsang KY, Tang HC, Chan D, Cheah KSE. Hypertrophic chondrocytes can become osteoblasts and osteocytes in endochondral bone formation. Proc Natl Acad Sci U S A. 2014 Aug 19;111(33):12097–102. doi: 10.1073/pnas.1302703111

512. Capulli M, Paone R, Rucci N. Osteoblast and osteocyte: Games without frontiers. Arch Biochem Biophys. 2014 Nov 1;561:3–12. doi: 10.1016/J.ABB.2014.05.003

513. Alhajj M, Farhana A. Enzyme Linked Immunosorbent Assay. StatPearls. 2023 Jan 30; [accessed 27 May 2023] Available from: https://www.ncbi.nlm.nih.gov/books/NBK555922/

514. Drijvers JM, Awan IM, Perugino CA, Rosenberg IM, Pillai S. The Enzyme-Linked Immunosorbent Assay: The Application of ELISA in Clinical Research. Basic Science Methods for Clinical Researchers. 2017 Jan 1;119–33. doi: 10.1016/B978-0-12-803077-6.00007-2

515. Sakamoto S, Putalun W, Vimolmangkang S, Phoolcharoen W, Shoyama Y, Tanaka H, et al. Enzyme-linked immunosorbent assay for the quantitative/qualitative analysis of plant secondary metabolites. J Nat Med. 2018 Jan 21;72(1):32–42. doi: 10.1007/s11418-017-1144-z

516. Crowther JR. ELISA. 1995 May 3;42. [accessed 28 May 2023] Available from: http://link.springer.com/10.1385/0896032795

517. Minic R, Zivkovic I, Minic R, Zivkovic I. Optimization, Validation and Standardization of ELISA. Norovirus. 2020 Dec 3; [accessed 28 May 2023] Available from: https://www.intechopen.com/chapters/74297

518. Azizipour N, Avazpour R, Sawan M, Rosenzweig DH, Ajji A. Uniformity of spheroid-on-chip by surface treatment of PDMS microfluidic platforms. bioRxiv. 2022 Feb 19;2022.02.15.480543. [accessed 27 May 2023] Available from: https://www.biorxiv.org/content/10.1101/2022.02.15.480543v1

519. Shetty S, Kapoor N, Bondu J, Thomas N, Paul T. Bone turnover markers: Emerging tool in the management of osteoporosis. Indian J Endocrinol Metab. 2016 Nov 1;20(6):846. [accessed 30 May 2023] Available from: /pmc/articles/PMC5105571/

520. Gillett MJ, Vasikaran SD, Inderjeeth CA. The Role of PINP in Diagnosis and Management of Metabolic Bone Disease. Clin Biochem Rev. 2021;42(1):3. [accessed 30 May 2023] Available from: /pmc/articles/PMC8252919/

521. Brandt J, Krogh TN, Jensen CH, Frederiksen JK, Teisner B. Thermal Instability of the Trimeric Structure of the N-terminal Propeptide of Human Procollagen Type I in Relation to Assay Technology. Clin Chem. 1999 Jan 1;45(1):47–53. [accessed 30 May 2023] Available from: https://academic.oup.com/clinchem/article/45/1/47/5642737

522. Flynn A, Jones D, Man E, Shipman S, Tung S. The effects of pH on Type VII-NA Bovine Intestinal Mucosal Alkaline Phosphatase Activity. Journal of Experimental Microbiology and Immunology (JEMI). 2002;2:50–6.

523. Coleman JE. Structure and mechanism of alkaline phosphatase. Annu Rev Biophys Biomol Struct. 1992;21:441–83. [accessed 30 May 2023] Available from: https://pubmed.ncbi.nlm.nih.gov/1525473/

524. Riss TL, Moravec RA, Niles AL, Duellman S, Benink HA, Worzella TJ, et al. Cell Viability Assays. Assay Guidance Manual. 2016 Jul 1; [accessed 30 May 2023] Available from: https://www.ncbi.nlm.nih.gov/books/NBK144065/

525. Jonsson B, Liminga G, Csoka K, Fridborg H, Dhar S, Nygren P, et al. Cytotoxic activity of calcein acetoxymethyl ester (calcein/AM) on primary cultures of human haematological and solid tumours. Eur J Cancer. 1996 May;32(5):883–7. doi: 10.1016/0959-8049(96)00015-9

526. Eilenberger C, Kratz SRA, Rothbauer M, Ehmoser EK, Ertl P, Küpcü S. Optimized alamarBlue assay protocol for drug dose-response determination of 3D tumor spheroids. MethodsX. 2018 Jan 1;5:781. [accessed 30 May 2023] Available from: /pmc/articles/PMC6072978/

527. Edmondson R, Broglie JJ, Adcock AF, Yang L. Three-Dimensional Cell Culture Systems and Their Applications in Drug Discovery and Cell-Based Biosensors. Assay Drug Dev Technol. 2014 May 5;12(4):207. [accessed 30 May 2023] Available from: /pmc/articles/PMC4026212/

528. Holick MF. Sunlight and vitamin D for bone health and prevention of autoimmune diseases, cancers, and cardiovascular disease. Am J Clin Nutr.

2004;80(6 Suppl). [accessed 8 Jun 2023] Available from: https://pubmed.ncbi.nlm.nih.gov/15585788/

529. Bellavia D, Costa V, de Luca A, Maglio M, Pagani S, Fini M, et al. Vitamin D Level Between Calcium-Phosphorus Homeostasis and Immune System: New Perspective in Osteoporosis. Current Osteoporosis Reports 2016. 2016 Oct 13;1–12. [accessed 8 Jun 2023] Available from: https://link.springer.com/article/10.1007/s11914-016-0331-2

530. Jones G, Strugnell SA, DeLuca HF. Current understanding of the molecular actions of vitamin D. Physiol Rev. 1998;78(4):1193–231. [accessed 8 Jun 2023] Available from: https://journals.physiology.org/doi/10.1152/physrev.1998.78.4.1193

531. Martin A, David V, Darryl Quarles L. Regulation and function of the FGF23/klotho endocrine pathways. Physiol Rev. 2012 Jan;92(1):131–55. [accessed 8 Jun 2023] Available from: https://pubmed.ncbi.nlm.nih.gov/22298654/

532. Shimada T, Kakitani M, Yamazaki Y, Hasegawa H, Takeuchi Y, Fujita T, et al. Targeted ablation of Fgf23 demonstrates an essential physiological role of FGF23 in phosphate and vitamin D metabolism. J Clin Invest. 2004 Feb 15;113(4):561–8. [accessed 8 Jun 2023] Available from: https://pubmed.ncbi.nlm.nih.gov/14966565/

533. Tripkovic L, Lambert H, Hart K, Smith CP, Bucca G, Penson S, et al. Comparison of vitamin D2 and vitamin D3 supplementation in raising serum 25-hydroxyvitamin D status: a systematic review and meta-analysis. Am J Clin Nutr. 2012 Jun 1;95(6):1357. [accessed 8 Jun 2023] Available from: /pmc/articles/PMC3349454/

534. Albarri EMA, Alnuaimi AS, Abdelghani D. Effectiveness of vitamin D2 compared with vitamin D3 replacement therapy in a primary healthcare setting: a retrospective cohort study. Qatar Med J. 2022;2022(3). [accessed 8 Jun 2023] Available from: /pmc/articles/PMC9372493/

535. Heaney RP, Recker RR, Grote J, Horst RL, Armas LAG. Vitamin D3 Is More Potent Than Vitamin D2 in Humans. J Clin Endocrinol Metab. 2011 Mar 1;96(3):E447–52. [accessed 8 Jun 2023] Available from: https://dx.doi.org/10.1210/jc.2010-2230

536. Chesney RW. Theobald palm and his remarkable observation: how the sunshine vitamin came to be recognized. Nutrients. 2012;4(1):42–51. [accessed 8 Jun 2023] Available from: https://pubmed.ncbi.nlm.nih.gov/22347617/

537. Jones G. 100 YEARS OF VITAMIN D: Historical aspects of vitamin D. Endocr Connect. 2022 Apr 4;11(4). [accessed 8 Jun 2023] Available from: /pmc/articles/PMC9066576/

538. Woeckel VJ, Alves RDAM, Swagemakers SMA, Eijken M, Chiba H, Van Der Eerden BCJ, et al. 1Alpha,25-(OH)2D3 acts in the early phase of osteoblast differentiation to enhance mineralization via accelerated production of mature matrix vesicles. J Cell Physiol. 2010 Nov;225(2):593–600. [accessed 8 Jun 2023] Available from: https://pubmed.ncbi.nlm.nih.gov/20506116/

539. DeLuca HF. Evolution of our understanding of vitamin D. Nutr Rev. 2008 Oct 1;66(suppl_2):S73–87. [accessed 8 Jun 2023] Available from: https://dx.doi.org/10.1111/j.1753-4887.2008.00105.x

540. Silva BC, Bilezikian JP. Parathyroid hormone: anabolic and catabolic actions on the skeleton. Curr Opin Pharmacol. 2015;22:41. [accessed 9 Jun 2023] Available from: /pmc/articles/PMC5407089/

541. Ma YL, Cain RL, Halladay DL, Yang X, Zeng Q, Miles RR, et al. Catabolic effects of continuous human PTH (1--38) in vivo is associated with sustained stimulation of RANKL and inhibition of osteoprotegerin and gene-associated bone formation. Endocrinology. 2001;142(9):4047–54. [accessed 19 Jun 2023] Available from: https://pubmed.ncbi.nlm.nih.gov/11517184/

542. Xia H, Tian Y, Lin Y, Huang Q, Xue Y. Evaluating Osteogenic Differentiation of Osteoblastic Precursors Upon Intermittent Administration of PTH/IGFBP7. Front Pharmacol. 2022 Apr 6;13:839035. doi: 10.3389/FPHAR.2022.839035/BIBTEX

543. Jilka RL, Weinstein RS, Bellido T, Roberson P, Parfitt AM, Manolagas SC. Increased bone formation by prevention of osteoblast apoptosis with parathyroid hormone. J Clin Invest. 1999 Aug 15;104(4):439–46. doi: 10.1172/JCI6610

544. Neer RM, Arnaud CD, Zanchetta JR, Prince R, Gaich GA, Reginster J-Y, et al. Effect of parathyroid hormone (1-34) on fractures and bone mineral density in postmenopausal women with osteoporosis. N Engl J Med. 2001 May 10;344(19):1434–41. [accessed 9 Jun 2023] Available from: https://pubmed.ncbi.nlm.nih.gov/11346808/

545. Hodsman AB, Bauer DC, Dempster DW, Dian L, Hanley DA, Harris ST, et al. Parathyroid Hormone and Teriparatide for the Treatment of Osteoporosis: A Review of the Evidence and Suggested Guidelines for Its Use. Endocr Rev. 2005 Aug 1;26(5):688–703. [accessed 9 Jun 2023] Available from: https://dx.doi.org/10.1210/er.2004-0006

546. Sikon A, Batur P. Profile of teriparatide in the management of postmenopausal osteoporosis. Int J Womens Health. 2010;2(1):37. [accessed 9 Jun 2023] Available from: /pmc/articles/PMC2971740/

547. Vahle JL, Sato M, Long GG, Young JK, Francis PC, Engelhardt JA, et al. Skeletal changes in rats given daily subcutaneous injections of recombinant human parathyroid hormone (1-34) for 2 years and relevance to human safety.

Toxicol Pathol. 2002;30(3):312–21. [accessed 9 Jun 2023] Available from: https://pubmed.ncbi.nlm.nih.gov/12051548/

548. Tashjian AH, Chabner BA. Commentary on clinical safety of recombinant human parathyroid hormone 1-34 in the treatment of osteoporosis in men and postmenopausal women. J Bone Miner Res. 2002;17(7):1151–61. [accessed 9 Jun 2023] Available from: https://pubmed.ncbi.nlm.nih.gov/12096828/

549. Hordyjewska A, Ostapiuk A, Horecka A, Kurzepa J. Betulin and betulinic acid: triterpenoids derivatives with a powerful biological potential. Phytochemistry Reviews 2019 18:3. 2019 Jul 25;18(3):929–51. [accessed 10 Jun 2023] Available from: https://link.springer.com/article/10.1007/s11101-019-09623-1

550. Laszczyk MN. Pentacyclic triterpenes of the lupane, oleanane and ursane group as tools in cancer therapy. Planta Med. 2009;75(15):1549–60. [accessed 10 Jun 2023] Available from: http://www.thieme-connect.de/products/ejournals/html/10.1055/s-0029-1186102

551. Król SK, Kiełbus M, Rivero-Müller A, Stepulak A. Comprehensive review on betulin as a potent anticancer agent. Biomed Res Int. 2015;2015. doi: 10.1155/2015/584189

552. Oliveira-Costa JF, Meira CS, Neves MVG das, Dos Reis BPZC, Soares MBP. Anti-Inflammatory Activities of Betulinic Acid: A Review. Front Pharmacol. 2022 May 23;13. [accessed 10 Jun 2023] Available from: /pmc/articles/PMC9168372/

553. Pavlova NI, Savinova O V., Nikolaeva SN, Boreko EI, Flekhter OB. Antiviral activity of betulin, betulinic and betulonic acids against some enveloped and non-enveloped viruses. Fitoterapia. 2003;74(5):489–92. [accessed 10 Jun 2023] Available from: https://pubmed.ncbi.nlm.nih.gov/12837369/

554. Song TJ, Park CH, In KR, Kim JB, Kim JH, Kim M, et al. Antidiabetic effects of betulinic acid mediated by the activation of the AMP-activated protein kinase pathway. PLoS One. 2021 Apr 1;16(4). [accessed 10 Jun 2023] Available from: /pmc/articles/PMC8021171/

555. Frew Q, Rennekampff HO, Dziewulski P, Moiemen N, Zahn T, Hartmann B. Betulin wound gel accelerated healing of superficial partial thickness burns: Results of a randomized, intra-individually controlled, phase III trial with 12-months follow-up. Burns. 2019 Jun 1;45(4):876–90. [accessed 10 Jun 2023] Available from: https://pubmed.ncbi.nlm.nih.gov/30559054/

556. Kim KJ, Lee Y, Hwang HG, Sung SH, Lee M, Son YJ. Betulin Suppresses Osteoclast Formation via Down-Regulating NFATc1. J Clin Med. 2018 Jun 15;7(6). [accessed 10 Jun 2023] Available from: /pmc/articles/PMC6025465/

557. Jeong DH, Kwak SC, Lee MS, Yoon KH, Kim JY, Lee CH. Betulinic Acid Inhibits RANKL-Induced Osteoclastogenesis via Attenuating Akt, NF-κB, and

PLCγ2-Ca2+ Signaling and Prevents Inflammatory Bone Loss. J Nat Prod. 2020;2020. [accessed 10 Jun 2023] Available from: https://pubs.acs.org/doi/full/10.1021/acs.jnatprod.9b01212

558. Wei J, Li Y, Liu Q, Lan Y, Wei C, Tian K, et al. Betulinic Acid Protects From Bone Loss in Ovariectomized Mice and Suppresses RANKL-Associated Osteoclastogenesis by Inhibiting the MAPK and NFATc1 Pathways. Front Pharmacol. 2020 Jul 7;11:532112. doi: 10.3389/FPHAR.2020.01025/BIBTEX

559. Cao X, Maharjan S, Ashfaq R, Shin J, Zhang YS. Bioprinting of Small-Diameter Blood Vessels. Engineering. 2021 Jun 1;7(6):832–44. doi: 10.1016/J.ENG.2020.03.019

560. Moxon SR, Cooke ME, Cox SC, Snow M, Jeys L, Jones SW, et al. Suspended Manufacture of Biological Structures. Advanced Materials. 2017 Apr 1;29(13):1605594. [accessed 11 Jun 2023] Available from: https://onlinelibrary.wiley.com/doi/full/10.1002/adma.201605594

561. Timm M, Saaby L, Moesby L, Hansen EW. Considerations regarding use of solvents in in vitro cell based assays. Cytotechnology. 2013 Oct;65(5):887. [accessed 15 Jun 2023] Available from: /pmc/articles/PMC3967611/

562. van de Peppel J, van Leeuwen JPTM. Vitamin D and gene networks in human osteoblasts. Front Physiol. 2014;5. [accessed 4 Mar 2023] Available from: /pmc/articles/PMC3988399/

563. Siggelkow H, Schulz H, Kaesler S, Benzler K, Atkinson MJ, Hüfner M. 1,25 dihydroxyvitamin-D3 attenuates the confluence-dependent differences in the osteoblast characteristic proteins alkaline phosphatase, procollagen I peptide, and osteocalcin. Calcif Tissue Int. 1999;64(5):414–21. [accessed 15 Jun 2023] Available from: https://pubmed.ncbi.nlm.nih.gov/10203418/

564. Sumathra M, Munusamy MA, Alarfaj AA, Rajan M. Osteoblast response to Vitamin D3 loaded cellulose enriched hydroxyapatite Mesoporous silica nanoparticles composite. Biomedicine & Pharmacotherapy. 2018 Jul 1;103:858–68. doi: 10.1016/J.BIOPHA.2018.04.078

565. Vu AA, Bose S. Effects of vitamin D 3 release from 3D printed calcium phosphate scaffolds on osteoblast and osteoclast cell proliferation for bone tissue engineering. RSC Adv. 2019 Oct 29;9(60):34847–53. [accessed 15 Jun 2023] Available from: https://pubs.rsc.org/en/content/articlehtml/2019/ra/c9ra06630f

566. Driel M, Koedam M, Buurman CJ, Hewison M, Chiba H, Uitterlinden AG, et al. Evidence for auto/paracrine actions of vitamin D in bone: 1alpha-hydroxylase expression and activity in human bone cells. FASEB J. 2006 Nov;20(13):2417–9. [accessed 8 Jun 2023] Available from: https://pubmed.ncbi.nlm.nih.gov/17023519/

567. Sabokbar A, Millett PJ, Myer B, Rushton N. A rapid, quantitative assay for measuring alkaline phosphatase activity in osteoblastic cells in vitro. Bone Miner. 1994;27(1):57–67. [accessed 15 Jun 2023] Available from: https://pubmed.ncbi.nlm.nih.gov/7849547/

568. Sangweni NF, Dludla P V., Chellan N, Mabasa L, Sharma JR, Johnson R. The Implication of Low Dose Dimethyl Sulfoxide on Mitochondrial Function and Oxidative Damage in Cultured Cardiac and Cancer Cells. Molecules 2021, Vol 26, Page 7305. 2021 Dec 1;26(23):7305. [accessed 16 Jun 2023] Available from: https://www.mdpi.com/1420-3049/26/23/7305/htm

569. Hajighasemi F, Tajic S. Assessment of Cytotoxicity of Dimethyl Sulfoxide in Human Hematopoietic Tumor Cell Lines. Iranian Journal of Blood and Cancer. 2017;9(2):48–53. [accessed 16 Jun 2023] Available from: http://ijbc.ir/article-1-719-en.html

570. Ho N G , Yo N G C H S, Wang AO. Apoptosis of human leukemic HL-60 cells induced to differentiate by treatment with RA or DMSO. Cell Research 1995 5:2. 1995 Dec;5(2):181–6. [accessed 16 Jun 2023] Available from: https://www.nature.com/articles/cr199517

571. Rodríguez-Burford C, Oelschlager DK, Talley LI, Barnes MN, Partridge EE, Grizzle WE. The use of dimethylsulfoxide as a vehicle in cell culture experiments using ovarian carcinoma cell lines. Biotech Histochem. 2003;78(1):17–21. [accessed 16 Jun 2023] Available from: https://pubmed.ncbi.nlm.nih.gov/12713137/

572. Isogai Y, Akatsu T, Ishizuya T, Yamaguchi A, Hori M, Takahashi N, et al. Parathyroid hormone regulates osteoblast differentiation positively or negatively depending on the differentiation stages. Journal of Bone and Mineral Research. 1996 Oct 1;11(10):1384–93. [accessed 17 Jun 2023] Available from: https://onlinelibrary.wiley.com/doi/full/10.1002/jbmr.5650111003

573. Kondo H, Guo J, Bringhurst FR. Cyclic adenosine monophosphate/protein kinase A mediates parathyroid hormone/parathyroid hormone-related protein receptor regulation of osteoclastogenesis and expression of RANKL and osteoprotegerin mRNAs by marrow stromal cells. J Bone Miner Res. 2002;17(9):1667–79. [accessed 19 Jun 2023] Available from: https://pubmed.ncbi.nlm.nih.gov/12211438/

574. Kular J, Tickner J, Chim SM, Xu J. An overview of the regulation of bone remodelling at the cellular level. Clin Biochem. 2012 Aug 1;45(12):863–73. doi: 10.1016/J.CLINBIOCHEM.2012.03.021

575. Rodan GA, Martin TJ. Therapeutic approaches to bone diseases. Science (1979). 2000 Sep 1;289(5484):1508–14. [accessed 20 Jun 2023] Available from: https://www.science.org

576. Martin TJ, Sims NA. Osteoclast-derived activity in the coupling of bone formation to resorption. Trends Mol Med. 2005 Feb 1;11(2):76–81. doi: 10.1016/J.MOLMED.2004.12.004

577. Zelmer AR, Starczak Y, Solomon LB, Richter K, Yang D, Atkins GJ. Culture of Saos-2 cells under hypoxic conditions stimulates rapid differentiation to an osteocyte-like stage. bioRxiv. 2023 May 2;2023.04.23.537998. [accessed 20 Jun 2023] Available from: https://www.biorxiv.org/content/10.1101/2023.04.23.537998v2

578. Chen X, Wang L, Zhao K, Wang H. Osteocytogenesis: Roles of Physicochemical Factors, Collagen Cleavage, and Exogenous Molecules. Tissue Eng Part B Rev. 2018 Jun 6;24(3):215. [accessed 20 Jun 2023] Available from: /pmc/articles/PMC5994157/

579. Jähn K, Kelkar S, Zhao H, Xie Y, Tiede-Lewis LAM, Dusevich V, et al. Osteocytes Acidify Their Microenvironment in Response to PTHrP In Vitro and in Lactating Mice In Vivo. Journal of Bone and Mineral Research. 2017 Aug 1;32(8):1761–72. [accessed 20 Jun 2023] Available from: https://onlinelibrary.wiley.com/doi/full/10.1002/jbmr.3167

580. Yu H, de Vos P, Ren Y. Overexpression of osteoprotegerin promotes preosteoblast differentiation to mature osteoblasts. Angle Orthod. 2011;81(1):100–6. [accessed 20 Jun 2023] Available from: https://pubmed.ncbi.nlm.nih.gov/20936961/

581. Ansari S, Ito K, Hofmann S. Alkaline Phosphatase Activity of Serum Affects Osteogenic Differentiation Cultures. ACS Omega. 2022 Apr 19;7(15):12724–33. [accessed 18 Jun 2023] Available from: https://pubs.acs.org/doi/full/10.1021/acsomega.1c07225

582. Satterwhite J, Heathman M, Miller PD, Marín F, Glass E V., Dobnig H. Pharmacokinetics of Teriparatide (rhPTH[1–34]) and Calcium Pharmacodynamics in Postmenopausal Women with Osteoporosis. Calcif Tissue Int. 2010 Dec 16;87(6):485–92. doi: 10.1007/s00223-010-9424-6

583. Agarwal S, Saha S, Balla VK, Pal A, Barui A, Bodhak S. Current Developments in 3D Bioprinting for Tissue and Organ Regeneration–A Review. Front Mech Eng. 2020 Oct 30;6. doi: 10.3389/fmech.2020.589171

584. Senior JJ, Cooke ME, Grover LM, Smith AM. Fabrication of Complex Hydrogel Structures Using Suspended Layer Additive Manufacturing (SLAM). Adv Funct Mater. 2019 Dec 27;29(49). doi: 10.1002/adfm.201904845

585. Attene-Ramos MS, Austin CP, Xia M. High Throughput Screening. In: Encyclopedia of Toxicology. Elsevier; 2014. p. 916–7. doi: 10.1016/B978-0-12-386454-3.00209-8

586. Avery VM, Camp D, Carroll AR, Jenkins ID, Quinn RJ. The Identification of Bioactive Natural Products by High Throughput Screening (HTS). In: Comprehensive Natural Products II. Elsevier; 2010. p. 177–203. doi: 10.1016/B978-008045382-8.00062-9

587. Kim SN, Choi B, Lee CJ, Moon JH, Kim MK, Chung E, et al. Culturing at Low Cell Density Delays Cellular Senescence of Human Bone Marrow-Derived Mesenchymal Stem Cells in Long-Term Cultures. Int J Stem Cells. 2021;14(1):103. [accessed 20 Jun 2023] Available from: /pmc/articles/PMC7904528/

588. Scholl FG, Gamallo C, Vilaró S, Quintanilla M. Identification of PA2.26 antigen as a novel cell-surface mucin-type glycoprotein that induces plasma membrane extensions and increased motility in keratinocytes. J Cell Sci. 1999 Dec 15;112(24):4601–13. doi: 10.1242/jcs.112.24.4601

589. Breiteneder-Geleff S, Matsui K, Soleiman A, Meraner P, Poczewski H, Kalt R, et al. Podoplanin, novel 43-kd membrane protein of glomerular epithelial cells, is down-regulated in puromycin nephrosis. Am J Pathol. 1997 Oct;151(4):1141–52.

590. Schacht V, Dadras SS, Johnson LA, Jackson DG, Hong Y-K, Detmar M. Up-Regulation of the Lymphatic Marker Podoplanin, a Mucin-Type Transmembrane Glycoprotein, in Human Squamous Cell Carcinomas and Germ Cell Tumors. Am J Pathol. 2005 Mar;166(3):913–21. doi: 10.1016/S0002-9440(10)62311-5

591. Terada S, Nishimura T, Sasaki M, Yamada H, Miki M. Sericin, a protein derived from silkworms, accelerates the proliferation of several mammalian cell lines including a hybridoma. Cytotechnology. 2002 Nov 1;40(1–3):3–12. [accessed 25 Jun 2023] Available from: https://pubmed.ncbi.nlm.nih.gov/19003099/

592. Johansson L, Klinth J, Holmqvist O, Ohlson S. Platelet lysate: a replacement for fetal bovine serum in animal cell culture? Cytotechnology. 2003;42(2):67–74. [accessed 25 Jun 2023] Available from: https://pubmed.ncbi.nlm.nih.gov/19002929/

593. Chellathurai Vasantha N, Rajagopalan K, Selvan Christyraj JD, Subbiahanadar Chelladurai K, Ganesan M, Azhagesan A, et al. Heat-inactivated coelomic fluid of the earthworm Perionyx excavatus is a possible alternative source for fetal bovine serum in animal cell culture. Biotechnol Prog. 2019 Jul 1;35(4). [accessed 25 Jun 2023] Available from: https://pubmed.ncbi.nlm.nih.gov/30972965/

594. UKHSA. Culture Collections. [accessed 25 Jun 2023] Available from: https://www.culturecollections.org.uk/products/celllines/generalcell/serumfreecelllines.jsp

595. FCS-Free. Fetal Calf Free Serum Database - Fetal Calf Serum Free Database. [accessed 25 Jun 2023] Available from: https://fcs-free.org/fcs-database

596. Rang H, Dale M, Ritter J, Flower R. Rang and Dale's Pharmacology. 6th ed. Edinburgh: Churchill Livingstone; 2007. 344–345 p.

597. Keller J, Appelt J, Tseneva K, Jahn D, Jiang S, Frosch K-H, et al. Tranexamic acid promotes matrix mineralization in osteoblasts and inhibits osteoclastogenesis in vitro. Z Orthop Unfall. 2020 Nov;158(S 01):DKOU20-516. [accessed 25 Jun 2023] Available from: http://www.thieme-connect.com/products/ejournals/html/10.1055/s-0040-1717432

598. Baranowsky A, Appelt J, Tseneva K, Jiang S, Jahn D, Tsitsilonis S, et al. Tranexamic Acid Promotes Murine Bone Marrow-Derived Osteoblast Proliferation and Inhibits Osteoclast Formation In Vitro. Int J Mol Sci. 2021 Jan 1;22(1):1–13. [accessed 25 Jun 2023] Available from: /pmc/articles/PMC7795046/

599. Hense D, Strube OI. Fibrillogenesis and Hydrogel Formation from Fibrinogen Induced by Calcium Salts. Gels. 2023 Feb 22;9(3):175. [accessed 21 Jun 2023] Available from: https://pubmed.ncbi.nlm.nih.gov/36975624/

600. Hense D, Büngeler A, Kollmann F, Hanke M, Orive A, Keller A, et al. Self-Assembled Fibrinogen Hydro- and Aerogels with Fibrin-like 3D Structures. Biomacromolecules. 2021 Oct 11;22(10):4084–94. [accessed 25 Jun 2023] Available from: https://pubmed.ncbi.nlm.nih.gov/34410695/

601. Kroll EB, Rieger J, Vogt B. How does repetition of signals increase precision of numerical judgment? Lecture Notes in Computer Science (including subseries Lecture Notes in Artificial Intelligence and Lecture Notes in Bioinformatics). 2010;6334 LNAI:200–11. [accessed 26 Jun 2023] Available from: https://link.springer.com/chapter/10.1007/978-3-642-15314-3_19

602. Ida T, Kaku M, Kitami M, Terajima M, Rocabado JMR, Akiba Y, et al. Extracellular matrix with defective collagen cross-linking affects the differentiation of bone cells. PLoS One. 2018 Sep 1;13(9):e0204306. [accessed 27 Jun 2023] Available from: https://journals.plos.org/plosone/article?id=10.1371/journal.pone.0204306

603. Chimen M, McGettrick HM, Apta B, Kuravi SJ, Yates CM, Kennedy A, et al. Homeostatic regulation of T cell trafficking by a B cell derived peptide is impaired in autoimmune and chronic inflammatory disease. Nat Med. 2015 May 1;21(5):467. [accessed 29 Jun 2023] Available from: /pmc/articles/PMC4425550/

604. Peterson WJ, Tachiki KH, Yamaguchi DT. Serial passage of MC3T3-E1 cells down-regulates proliferation during osteogenesis in vitro. Cell Prolif. 2004 Oct;37(5):325. [accessed 29 Jun 2023] Available from: /pmc/articles/PMC6495877/

605. Sapir-Koren R, Livshits G. Osteocyte control of bone remodeling: is sclerostin a key molecular coordinator of the balanced bone resorption-formation cycles? Osteoporos Int. 2014 Dec 1;25(12):2685–700. [accessed 29 Jun 2023] Available from: https://pubmed.ncbi.nlm.nih.gov/25030653/

606. Fukuda N, Tsuru K, Mori Y, Ishikawa K. Fabrication of self-setting β-tricalcium phosphate granular cement. J Biomed Mater Res B Appl Biomater. 2018 Feb;106(2):800–7. doi: 10.1002/jbm.b.33891

607. Campbell GM, Sophocleous A. Quantitative analysis of bone and soft tissue by micro-computed tomography: applications to ex vivo and in vivo studies. Bonekey Rep. 2014 Aug 20;3:564. [accessed 23 Jun 2023] Available from: /pmc/articles/PMC4140449/

608. Obata Y, Bale HA, Barnard HS, Parkinson DY, Alliston T, Acevedo C. Quantitative and qualitative bone imaging: A review of synchrotron radiation microtomography analysis in bone research. J Mech Behav Biomed Mater. 2020 Oct 1;110. [accessed 23 Jun 2023] Available from: https://escholarship.org/uc/item/476191vw

609. Hou Y, Carne A, McConnell M, Mros S, Vasileva EA, Mishchenko NP, et al. PHNQ from Evechinus chloroticus Sea Urchin Supplemented with Calcium Promotes Mineralization in Saos-2 Human Bone Cell Line. Mar Drugs. 2020 Jul 19;18(7). [accessed 5 Dec 2021] Available from: /pmc/articles/PMC7404214/

610. Wang YH, Liu Y, Maye P, Rowe DW. Examination of Mineralized Nodule Formation in Living Osteoblastic Cultures Using Fluorescent Dyes. Biotechnol Prog. 2006 Nov;22(6):1697. [accessed 9 May 2023] Available from: /pmc/articles/PMC2538552/

611. Bonewald LF, Harris SE, Rosser J, Dallas MR, Dallas SL, Camacho NP, et al. Von Kossa staining alone is not sufficient to confirm that mineralization in vitro represents bone formation. Calcif Tissue Int. 2003 May 1;72(5):537–47. [accessed 9 May 2023] Available from: https://link.springer.com/article/10.1007/s00223-002-1057-y

612. Schneider MR. Von Kossa and his staining technique. Histochem Cell Biol. 2021 Dec 1;156(6):523. [accessed 9 May 2023] Available from: /pmc/articles/PMC8695535/

Chapter 8

Appendix

8.1 Published method

F1000Research F1000Research 2023, 12:357 Last updated: 31 MAR 2023

Check for updates

METHOD ARTICLE

A detailed methodology for the long-term *in vitro* culture and analysis of three-dimensional, self-structuring bone models generated from cell lines or primary osteoblastic cell populations [version 1; peer review: awaiting peer review]

Melissa Finlay[1,2], Laurence A Hill[1,2], Georgiana Neag[1], Binal Patel[1], Miruna Chipara[1,2], Hannah C Lamont[2], Kathryn Frost[1], Kieran Patrick[1], Jonathan W Lewis[1], Thomas Nicholson[1], James Edwards[3], Simon W Jones[1], Liam M Grover[2], Amy J Naylor[1]

[1]Institute of Inflammation and Ageing, University of Birmingham, Birmingham, West Midlands, B15 2TT, UK
[2]Healthcare Technologies Institute, University of Birmingham, Birmingham, West Midlands, B15 2TT, UK
[3]NDORMS, University of Oxford, Oxford, Oxfordshire, OX3 7HE, UK

v1 **First published:** 31 Mar 2023, **12**:357
https://doi.org/10.12688/f1000research.130779.1
Latest published: 31 Mar 2023, **12**:357
https://doi.org/10.12688/f1000research.130779.1

Abstract

Background: There are insufficient *in vitro* bone models that accommodate long-term culture of osteoblasts and support their differentiation to osteocytes. The increased demand for effective therapies for bone diseases, and the ethical requirement to replace animals in research, warrants the development of such models. Here we present an in-depth protocol to prepare, create and maintain three-dimensional, *in vitro*, self-structuring bone models that support osteocytogenesis and long-term osteoblast survival (>1 year).
Methods: Osteoblastic cells are seeded on a fibrin hydrogel, cast between two beta-tricalcium phosphate anchors. Analytical methods optimised for these self-structuring bone model (SSBM) constructs, including qPCR, immunofluorescence staining and XRF, are described in detail.
Results: Over time, the cells restructure and replace the initial matrix with a collagen-rich, mineralising one; and demonstrate differentiation towards osteocytes within 12 weeks of culture.
Conclusions: Whilst optimised using a secondary human cell line (hFOB 1.19), this protocol readily accommodates osteoblasts from other species (rat and mouse) and origins (primary and secondary). This simple, straightforward method creates reproducible *in vitro* bone models that are responsive to exogenous stimuli, offering a versatile platform for conducting preclinical translatable research studies.

Open Peer Review

Approval Status *AWAITING PEER REVIEW*

Any reports and responses or comments on the article can be found at the end of the article.

Keywords
Osteocyte, bone, animal reduction, 3D model, in vitro culture

This article is included in the NC3Rs gateway.

Corresponding author: Amy J Naylor (a.naylor@bham.ac.uk)

Author roles: Finlay M: Data Curation, Formal Analysis, Investigation, Methodology, Writing – Original Draft Preparation, Writing – Review & Editing; **Hill LA**: Investigation, Methodology; **Neag G**: Investigation, Methodology; **Patel B**: Investigation; **Chipara M**: Investigation; **Lamont HC**: Investigation, Methodology; **Frost K**: Investigation; **Patrick K**: Investigation; **Lewis JW**: Investigation; **Nicholson T**: Investigation; **Edwards J**: Resources; **Jones SW**: Supervision; **Grover LM**: Conceptualization, Funding Acquisition, Methodology, Resources, Supervision, Writing – Original Draft Preparation, Writing – Review & Editing; **Naylor AJ**: Conceptualization, Funding Acquisition, Investigation, Methodology, Supervision, Writing – Original Draft Preparation, Writing – Review & Editing

Competing interests: No competing interests were disclosed.

Grant information: MF was supported by the National Centre for the Replacement, Refinement and Reduction of Animals in Research (NC3Rs NC/S001646/1). AJN was funded by a Career Development Fellowship from Versus Arthritis (#21743).

Copyright: © 2023 Finlay M *et al*. This is an open access article distributed under the terms of the Creative Commons Attribution License, which permits unrestricted use, distribution, and reproduction in any medium, provided the original work is properly cited.

How to cite this article: Finlay M, Hill LA, Neag G *et al.* **A detailed methodology for the long-term *in vitro* culture and analysis of three-dimensional, self-structuring bone models generated from cell lines or primary osteoblastic cell populations [version 1; peer review: awaiting peer review]** F1000Research 2023, **12**:357 https://doi.org/10.12688/f1000research.130779.1

First published: 31 Mar 2023, **12**:357 https://doi.org/10.12688/f1000research.130779.1

Research highlights

Scientific benefits

Allows:

- Study of osteoblast activity in long-term culture (>8 weeks).
- Study of osteoblast to osteocyte differentiation.
- Study of mineralisation and extracellular matrix production by osteoblasts.
- Study of osteoblasts and osteocytes in a 3D, organotypic environment.

3Rs benefits

- Reduces the need for osteoblast and osteocyte isolation from vertebrates in skeletal research by supporting long-term culture of primary osteoblasts and secondary cell lines.
- Provides a platform for osteocyte research *in vitro*, reducing the requirement for vertebrate *in vivo* experimentation.

Practical benefits

- Inexpensive, uses commonly available equipment and reagents.
- Readily adaptable - can use cells of different origin and species.
- Organotypic - 3D environment and matrix production and mineralisation performed by the osteoblasts.

Current applications

- Suitable for comparing phenotypes of osteoblasts isolated from genetically modified vertebrates or from patient samples.
- Suitable for studying osteoblast and osteocyte function and for screening their response to therapeutic candidate compounds.
- Suitable for long-term 3D culture of human osteoblast cell lines, such as hFOB, and for assessment and manipulation of their differentiation towards osteocytes.

Potential applications

Offers a platform for:

- Studying osteoblast/osteocyte interactions with other cell types e.g. osteoclasts.
- Screening of compound libraries to identify therapeutic candidate compounds.
- Assessing efficacy of drugs and therapeutics under relevant conditions.

Introduction

Bone is a dynamic tissue that continually adapts throughout life to ensure maintenance of strength and integrity and to fulfil its many other functions, which include: adaptation to loading, preservation of mineral homeostasis (particularly calcium and phosphorous) and conservation of energy balance.[1] These roles are made possible by the tightly controlled intercellular process called bone remodelling. Bone remodelling is a cyclical process that begins with tissue breakdown by bone resorbing osteoclasts, to release stored mineral and osteogenic factors such as bone morphogenic proteins and fibroblast growth factors.[2] Resorption is followed by the formation of new bone tissue by osteoblasts. The balance between bone formation and bone resorption activity is critical for maintenance of tissue integrity. Likewise, this remodelling process allows bone to be repaired when damaged and to adapt rapidly to changes in physical demand, for example increased weight-bearing sports training or, oppositely, unloading through bed rest after injury and illness[3] as well as from prolonged zero gravity experienced during space exploration.[4]

The precise coupling of osteoblast and osteoclast activity is tightly regulated by osteocytes (reviewed in Ref. 5). Up to 20% of osteoblasts differentiate into osteocytes[6,7] which become entombed within newly deposited, immature bone tissue. Upon differentiation, they undergo a profound morphological change from a polygonal structure to a highly dendritic form. Entombed within individual lacunae, osteocyte dendrites extend through canaliculi to connect with other osteocytes, osteoblasts, osteoclasts, neurons, and the vasculature, creating a highly interconnected osteocyte-canalicular network. This distinguishing feature of osteocytes is a stipulation for their role as the main regulatory unit in bone metabolism and as orchestrators of bone cell activity.[7,8]

Dysregulation of bone remodelling is caused by multiple factors, the most notable of which is aging, which results in osteoporosis. As the global population ages, osteoporosis-induced fragility fractures are predicted to increase markedly – estimates made from six of the largest countries in Europe put the rise at 23.3% by 2030 compared to 2017.[9] These figures give heightened urgency and a major push in research efforts to meet, or better yet curb, the impending demands for effective bone therapeutics.

Currently, bone researchers employ a range of platforms within *in vivo*, *ex vivo* and *in vitro* systems, all with their own advantages and disadvantages - detailed reviews of these platforms have been reported recently.[10,11] *In vivo* bone models provide a complete and vascularised osseous system used to investigate bone metabolism, disease, healing, and development, as well as drug candidate efficacy and safety. However, these studies often require large sample numbers for moderate to severe procedures such as bone healing and ovariectomy-induced osteoporosis. Although *ex vivo* bone models, such as calvarial and femoral head culture, can be employed to investigate some of the same research questions as *in vivo* studies, the high running costs and intrinsic interspecies differences that exist when using animal tissue to study human disease limit their utility. Osteoblast and osteoclast *in vitro* cultures are widely employed, with multiple activity assessment assays and complex co-culture systems developed. However, they have been limited by the minimal success of osteocyte culture within these systems, and by the challenges of recapitulating the composition of inorganic mineral amalgamated to a complex hierarchy of collagen fibres that characterises native bone tissue in an *in vitro* system.[12]

To obtain a complete reflection of bone metabolic activity, the presence of interconnected osteocytes within any bone model is fundamental, however, isolation of primary osteocytes followed by cell culture under standard conditions is not successful and results in dedifferentiation to osteoblasts.[13] Some immortalised osteocyte cell lines have been developed,

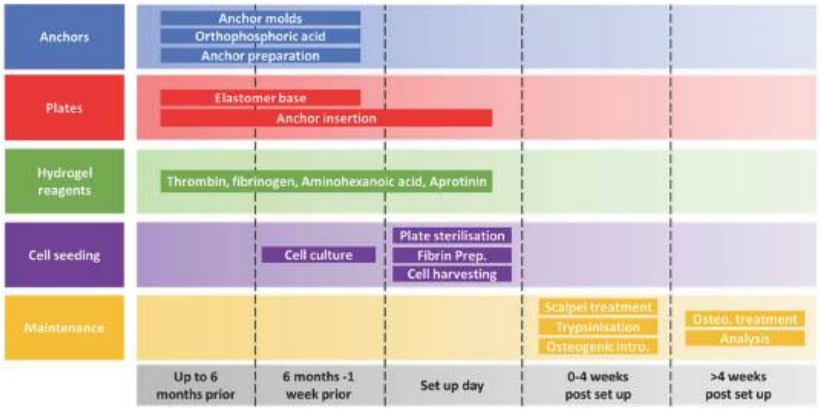


Figure 1. Schematic of the self-structuring bone model (SSBM) method planning and maintenance time scales. The SSBM method is divided into 5 separate aspects (anchors, plates, hydrogel reagents, cell seeding and maintenance) each with their own steps for preparing, setting up and maintaining SSBM constructs. The minimum amount of preparation time required for setting up SSBM cultures is one week, providing all materials are available. However, many of the steps can be carried out up to six months in advance; this is recommended for stock preparation. Depending on the cell lines/types to be used for SSBM set up, preparing cells for cell seeding can vary and may take less than one week (i.e. faster proliferation rates). Cell seeding procedures on set up day will take 1-2 hours to complete. Maintenance steps within the first four weeks post SSBM set-up are performed on defined days after cell seeding but may vary depending on the cell type chosen. Analytical timepoints are selected at the researchers' discretion, and dependent on the research question, with four weeks post SSBM set-up (i.e. just prior to introducing and maintaining osteogenic treatment) typically being the minimum analytical timepoint.

which retain osteocyte morphology during 2D culture, for example the murine MLO-Y4[14] and the human HOB-01-C1[15] osteocytic cell lines. The challenges of *in vitro* osteocyte culture have led researchers to conduct a significant amount of bone research *in vivo*, with murine models being preferred due to lower running costs, simpler husbandry and genetic manipulability,[16,17] as well as their rapid rate of bone turnover.[18] In recent years, the movement towards replacing and reducing reliance on laboratory animals, and the requirement for *in vitro* systems for compound screening in drug development pipelines that are translatable, have renewed interest in the development of humanised *in vitro* bone assays capable of supporting osteocytes. Here we describe a three-dimensional, self-structuring bone model (SSBM) culture system that uses a biocompatible scaffold to support the differentiation of osteoblasts to osteocytes and the production of a complex collagen-rich mineralised matrix, that resembles native bone. We provide a detailed and descriptive protocol for preparing, setting up and maintaining SSBM constructs [Figure 1] and the analytical methods that have been developed specifically for their analysis.

Methods

Choice of cell source

This method (originally described in Ref. 19) relies on osteoblast-mediated contraction of a biocompatible scaffold (fibrin hydrogel) around a source of calcium and phosphate ions in the form of two cement anchors consisting of a combination of brushite ($CaHPO_4.2H_2O$) and B-TCP ($Ca_3(PO_4)_2$). Contraction provides a 3D environment within which the osteoblasts, over time, replace the original fibrin matrix with organotypic collagen and facilitate its calcium phosphate mineralisation.

The original method[19,20] utilised primary rat periosteal cells. The figures included here were generated using the human osteoblastic cell line, hFOB 1.19 (RRID: CVCL_3708) – selected based on their homogenous human origin, as well their stable karyotype,[21] but the SSBM method can be readily adapted to accommodate osteoblasts derived from a number of different species, from primary osteoblasts isolated from vertebrate bone samples or from cell lines. We have used primary human osteoblasts and the human osteoblast cell line, hFOB 1.19,[22] with similar success (data not shown). We note that primary cells have high levels of batch-batch variation in cell type populations and metabolic rates, as has been previously observed[23] and that there are intrinsic differences in the proliferation rates of cell lines therefore, seeding densities and culture media composition should be adapted and validated on a case-by-case basis.

The following preparation, set up and maintenance methods have been separated into 5 distinct aspects, summarised in Figure 1.

1. Anchor preparation

Note – Sections 1.1-1.3 are prepared under non-sterile conditions

1.1 Anchor mould preparation

Required:

- Fused deposition modelling 3D Printer
- Fusion 360 computer-aided design software (V.2.0) (Supplier: Autodesk, USA), or similar
- 1.75 mm polylactic acid plastic filament (cat no.: 55318; supplier: Verbatim, Germany)
- Perfection Plus Impress-E putty (Soft) (cat no.: 238-0084; supplier: Dental Sky Wholesaler Ltd., Kent (UK only))

Steps:

1. 3D print a positive frame of 1.75 mm polylactic acid plastic for the anchor moulds with the dimensions shown [Figure 2.A]. *3D Object (.3mf) and GCODE files are available as extended data.*[39]
2. Prepare the impression putty, as per the supplier's instructions, and press the putty into the positive frame, ensuring the frame is completely filled.
3. Allow the impress material to set for at least 24 hours at room temperature before removing from the mould. Make at least two. These are the anchor moulds for use in section 1.3.

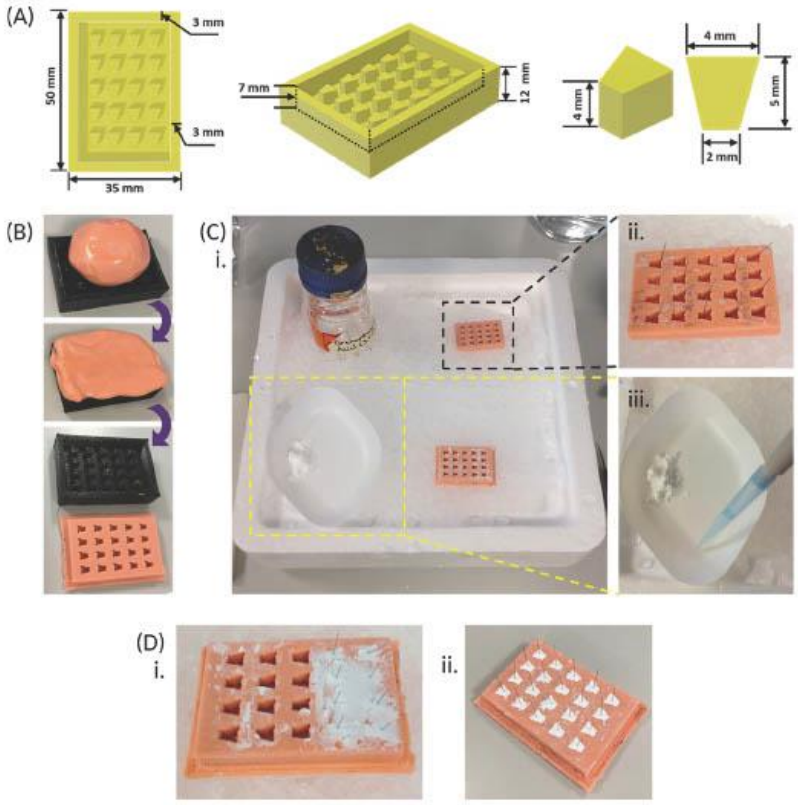


Figure 2. Preparing and using a mould for creating beta-tricalcium phosphate (β-TCP) cement anchors. (A) A 3D sketch of a positive frame for the anchor mould, containing twenty equally spaced pegs, is drawn up with the dimensions provided above, using computer-aided design software, and a reusable frame is 3D printed with polylactic acid. (B) Dental impression material is pressed into the positive frame, ensuring the whole frame is filled, after which the mould is peeled out once completely set. (C) The recommended set up when preparing the β-TCP cement anchors. An ice tray is prepared with a spare anchor mould containing a single insect pin in each well placed in a top corner (black dotted box) and an empty mould in the adjacent bottom corner; as well as the orthophosphoric acid (3.5 M) in the vacant top corner. The β-TCP is weighed out and kept to one side of the weighing boat and placed in the vacant bottom corner of the ice tray (yellow dotted box) at a slight forward angle. The orthophosphoric acid is added to the same weighing boat as the β-TCP but kept separate prior to mixing. (D) When mixed, the resultant cement created, using the weight and volumes outlined [Section 1.3] is sufficient to fill 2-3 rows of the empty anchor mould, and pins from the spare anchor mould (C, black dotted box) are inserted immediately, prior to hardening (i). After repeating cement preparation, the cement is left to completely set within the anchor mould for approximately 3 days (ii).

1.2 Orthophosphoric acid (3.5 M) preparation

Required:

- Orthophosphoric acid (85-90% purity) (cat no.: 20624.262; supplier: VWR Chemicals, Leicestershire, UK)
- Distilled water (d.H_2O)

Steps:

1. Assuming 87.5% purity; for every 100 mL of Orthophosphoric acid:

76.8 mL d.H_2O + 23.2 mL Orthophosphoric acid

CRITICAL - Add the acid to water, never water to acid

2. Store at 2-4 °C for up to 6 months.

1.3 Calcium phosphate anchor preparation

Required:

- Beta-tricalcium phosphate (β-TCP) (<125 μm particle size) (Plasma Biotal Limited., Tideswell, UK)
- Orthophosphoric acid (3.5 M), prepared as described above [Section 1.2]
- Austerlitz insect pins (stainless steel, 0.200 mm ø.) (cat no.: 26002-20; supplier: InterFocus Ltd., Linton, UK)
- Anchor moulds (at least 2) [Section 1.1]
- Fine metal tweezers
- Metal Chattaway or flat-headed spatulas (~10 mm width)
- Large weighing boats (100 mL) (cat no.: 611-9189; supplier: VWR)
- Tray/bucket of ice
- Paper towels

Note - The recommended workspace set-up is shown [Figure 2.C.i] to ensure required equipment is within reach during anchor preparation.

Steps:

1. Using tweezers, add a single pin to each well of one of the spare anchor moulds [Figure 2.C.ii].
2. Weigh out 1.25 ± 0.005 g of β-TCP into a large weighing boat (keep the powder to one side of the weighing boat [Figure 2.C.iii] then place the weighing boat on top of the ice tray.
3. Add 500 μL orthophosphoric acid to the same weighing boat, but away from the powder [Figure 2.C.iii].
   - *Tip - Point the weighing boat at a small angle down towards you.*
4. Mix the powder and acid together using the metal spatula, keeping the weighing boat on the ice, until the liquid mixture becomes a runny paste.
   - ***Note – there are batch-batch differences with β-TCP powder. Weigh out the mass stated above in [step 1] and adjust the volume of orthophosphoric acid by 100 μL increments/reductions until achieving the desired consistency (e.g. condensed milk).***
5. Quickly scrape and apply the paste onto 2-3 rows of the empty mould using the spatula, then submerge the spatula into the ice, followed by quickly transferring a single pin from the spare mould to each filled well. This must be completed before the cement hardens, which will take about 30 s [Figure 2.D.i].
   - ***Note – there will be an excess of cement on top of the mould during application, try to scrape off as much as possible, but a slight excess is permissible.***

- *Tip – plunging the spatula into the ice helps with subsequent cleaning with a paper towel. If the excess cement is not readily removed with wiping, use hot soapy water.*

6. Clean the spatula (as above), then repeat steps 2-5 [Section 1.3] with the remaining wells in the mould, using a new weighing boat each time.

7. Allow the anchors to set in the mould at room temperature for up to 3 days [Figure 2.D.ii], then remove from the mould and store in a sealed container at room temperature for up to 6 months.

2. Plate preparation

Note – Plates may be prepared under non-sterile conditions, as they are sterilised just prior to hydrogel preparation.

Required:

- 6-well plate(s) (Cat no.: CLS3516; supplier: Corning, Flintshire, UK) – *Tissue culture-treated plates are recommended, but not essential*
- Sylgard 184 silicone elastomer kit (Cat no.: 634165S; supplier: VWR)
- Calcium phosphate anchors (12 per plate) prepared as described above [Section 1.3]
- Large weighing boats
- BD Emerald disposable syringe (10 mL) (Cat no.: 15205093; supplier: Fisher Scientific, Loughborough, UK)
- BD PlastiPak disposable syringes (1.0 & 50 mL) (Cat nos.: 15489199 & 12651406; supplier: Fisher Scientific)
- Tweezers

Steps:

1. Weigh out 10 ± 0.1 g of the base component of the elastomer kit into a weighing boat using a 50 mL syringe [Figure 3.A].

2. Weigh out 1.0 ± 0.1 g of the curing component of the elastomer kit into the same weighing boat as the base component using a 1.0 mL syringe [Figure 3.A].

3. Mix the base and curing components and slowly take up the mixture using a 10 mL syringe [Figure 3.A].

   - *Tip – Use the end of the 10 mL syringe to mix the components.*
   - *Tip – Hold the weighing boat at an angle when taking up to allow the mixture to collect.*
   - *Tip – Continue mixing the components at regular intervals whilst taking it up.*

4. Add 1.5 mL of the mixture to each well of the plate [Figure 3.A].

   - *Tip – If preparing more than one plate, weighing boats and syringes can be reused.*

5. Return the lids onto the plates and allow elastomer to set at room temperature for 7 days.

   - ***Note - Plates can be stored at room temperature after elastomer has set (no expiration has been found for using these plates).***

6. Once the elastomer has set, mark two anchor points on the underside of the plates, approximately 15 mm apart on each well [Figure 3.B.i].

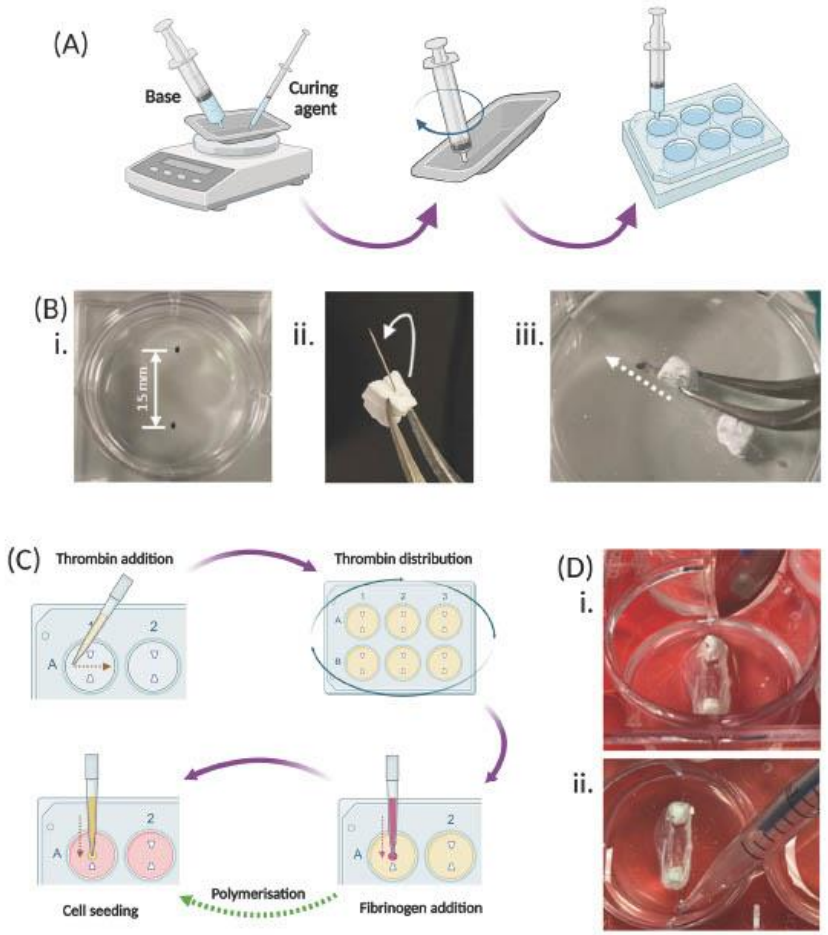


Figure 3. Plate and hydrogel preparation, cell seeding and construct maintenance. (A) The elastomer base, followed by the curing agent, are weighed at a 10:1 ratio into the same weighing boat, and then thoroughly mixed with the end of an empty syringe. The mixture is then transferred to an empty 6-well culture plate using this same syringe and left to set for 7 days. (B) Once the elastomer has set, 2 β-TCP cement anchors are inserted into each well of the 6-well plate. Firstly, 2 marks are made 15 mm apart on the underside of the plate for each well (i). The pins within the β-TCP anchors are bent at a slight angle, towards the long edge of the trapezoidal base using tweezers (ii), then the pins are inserted at an angle into the elastomer (white arrows), using the measured points as guide, so that the base of the anchors sit on the top surface of the elastomer (white dotted line) (iii). (C) SSBM set up involves preparing the hydrogel by addition of the thrombin across each well of the plate, and ensuring the whole surface is covered by gently mixing and tapping the sides of the plate. Addition of fibrinogen straight into the centre of each well begins polymerisation and creation of the hydrogel. Cells are seeded directly on top of the polymerised hydrogel and cultured under normal culture conditions. (D) 3 days post-cell seeding, a scalpel is run around the walls of each well to detach any fibrin from the edge of the culture well. (i). When pipetting from the well, such as during media renewal, the plate is tilted forward to pool the liquid at the bottom to ensure that the fibrin matrix is not disturbed (ii). Created with Biorender.com.

7. Bend the inserted pins towards the longer edge of the calcium phosphate anchor [Figure 3.B.ii] and insert into the elastomer at the marked point so that the bottom of the anchor sits on the top surface of the elastomer [Figure 3.B.iii].

    - ***Note – Plates with inserted anchors can be stored at room temperature and must be used within 6 months.***

3. Reagent preparation for the fibrin hydrogel

3.1 Phosphate buffered saline (PBS) solution

Required:

- Gibco Phosphate buffered saline (PBS) tablets (1X) (cat no.: 18912014; supplier: Fisher Scientific,)
- Distilled water (d.H_2O)

Steps:

1. Dissolve PBS tablets in d.H_2O at a ratio of 1 tablet per 500 mL d.H_2O.
2. Store at room temperature.

3.2 Fibrinogen solution (20 mg/mL)

Required:

- Fibrinogen (cat no.: F8630; supplier: Sigma-Aldrich, Gillingham, UK)
- Ham's F-12K (Kaighn's) Medium (F-12K medium) (cat no.: 21127-022; supplier: Fisher Scientific)
- BD Emerald disposable syringe (10 mL) (Cat no.: 15205093; supplier: Fisher Scientific)
- 0.22-μm PES (Sterile) syringe filters (cat no.: E4780-1226; supplier: Starlab, Milton Keynes, UK)
    - ***Note – Several PES filters might be required***

Steps:

1. Place F-12K medium in 37 °C water bath for at least 20 mins.
2. Weigh out at least 100 mg of fibrinogen (X) and use the following calculation to determine volume of media (Y) required:

$$X\,\text{mg fibrinogen}/20 = Y\,\text{mL of F}-12\text{K}$$

3. In a cell culture hood, dilute fibrinogen in calculated volume of F-12K medium - do not vortex.
4. Place in a 37°C water bath for 1 to 2 hr, gently agitating every 30 min.
5. In a cell culture hood, filter through 0.22-μm filters with the syringe, then store at -20 °C if not using straight away.

3.3 Aprotinin (10 mg/mL)

Required:

- Aprotinin (cat no.: A4529-10mg; supplier: Sigma-Aldrich)
- PBS solution [Section 3.1]

- BD Emerald disposable syringe (2.0 mL) (Cat no.: 15285083; supplier: Fisher Scientific)
- 0.22-µm PES (sterile) syringe filters (cat no.: E4780-1226; supplier: Star Lab)

Steps:

1. Reconstitute entire contents of aprotinin vial using PBS solution at a ratio of 10 mg aprotinin to 1 mL PBS solution
    - ***Note – the above is for a 10 mg aprotinin vial. If purchased a different size, adjust resuspension volume accordingly to acquire 10 mg/mL***
    - *Tip – If acquired a 10 mg aprotinin vial, add 1 mL PBS solution directly into the aprotinin vial.*
2. Under sterile conditions, filter through 0.22-µm syringe filter with the syringe and prepare into 30 µL aliquots. Store at -20 °C.
    - ***Note - 1x 30 µL aliquots prepares 4x six-well plates. Avoid freeze-thaw cycles.***

3.4 Aminohexanoic acid (200 mM)

Required:

- Aminohexanoic acid (cat no.: 07260-10g; supplier: Sigma-Aldrich)
- PBS solution [Section 3.1]
- BD Emerald disposable syringe (5.0 mL) (Cat no.: 15295083; supplier: Fisher Scientific)
- 0.22-µm PES (sterile) syringe filters (cat no.: E4780-1226; supplier: Star Lab)

Steps:

1. Weigh out at least 50 mg aminohexanoic acid (*X*) and use the following calculation to determine volume of PBS required (*Y*):

$$X \text{ mg aminohexanoic acid} / 26.2 = Y \text{ mL of PBS}$$

2. In a cell culture hood, resuspend in determined volume of PBS. Vortex until completely dissolved.
3. In a cell culture hood, filter through 0.22-µm filter with the syringe and prepare into 30 µL aliquots. Store at -20 °C.
    - ***Note - 1x 30 µL aliquots prepares 4x six-well plates. Avoid freeze-thaw cycles.***

3.5 Thrombin (200 U/mL)

Required:

- Thrombin, bovine (cat no.: 605157 – 1KU; supplier: Sigma-Aldrich)
- Bovine serum albumin (BSA) (cat no.: A8806-5g; supplier: Sigma-Aldrich)
- Ham's F-12K (Kaighn's) Medium (cat no.: 21127-022; supplier: Fisher Scientific)
- 21G disposable needle (cat no.: SYR6232; supplier: SLS Scientific, Wilford, UK)

- BD Emerald disposable syringe (2.0 mL) (Cat no.: 15285083; supplier: Fisher Scientific)
- 0.22-µm PES (sterile) syringe filters (cat no.: E4780-1226; supplier: Star Lab)
    - ***Note – The steps for thrombin preparation below is for a single 1 KU vial. Adjust accordingly if using a different quantity.***

Steps:

1. Prepare 0.1% BSA solution by weighing out at least 6 mg BSA and use the following calculation to determine volume of F-12K medium required:

$$X\ \text{mg of BSA} = X\ \text{mL of F} - 12\text{K medium}$$

2. Using the needle and syringe, pierce through the rubber stopper to reconstitute the entire content of the thrombin vial in 500 µL of 0.1% BSA solution
3. Remove the syringe and invert the vial until the thrombin is completely dissolved, then remove the rubber stopper and reconstitute entire contents of vial in a single 4.5mL aliquot of 0.1% BSA solution.
4. In a cell culture hood, filter the reconstituted thrombin through a 0.22-µm filter with the syringe and prepare 700 µL aliquots. Store the aliquots at -20 °C.
    - ***Note - A 700 µL aliquot is sufficient to prepare 4x six-well plates. Avoid freeze-thaw cycles.***

4. Preparing the fibrin hydrogel and construct set up

Required:

- Thrombin (200 U/mL)
- Aminohexanoic acid (200 mM)
- Aprotinin (10 mg/mL)
- Cell media (Non-osteogenic; refer to your cell supplier guidelines)
- Fibrinogen solution (20 mg/mL)
- Anchored plates

Steps:

1. Prior to cell seeding, spray the inside and outside of the plates with 70% ethanol and leave to dry in a sterile cell culture hood with the lids off
2. Determine the number of 6-well plates to be prepared. See Table 1 to determine volumes required for thrombin solution preparation, based on the number of 6-well plates to be prepared.
3. Thaw the appropriate number of aliquots of each of the above reagents and the fibrinogen solution and warm the media in a 37 °C water bath.
4. Once thawed, in a cell culture hood, mix the thrombin solution reagents [Table 1] in their required quantities, based on the number of plates to be prepared and the volumes given in Table 1 below.

Table 1. Thrombin solution preparation. Reagents and volumes required per 6-well plate to be prepared *(Note - Volumes below account for an excess).*

Reagent	Volume (µL)
Thrombin	162.5
Aminohexanoic acid	6.5
Aprotinin	6.5
Media	3074.5

Table 2. Seeding density guide. Seeding density required for construct set up depends on the cell type being used. *(Note - When using a new cell type, trial different seeding densities – in general, the faster the proliferation rate, the lower the seeding density required).*

Cell line	Seeding density (cells/mL)
Primary rat periosteal/mouse calvarial	0.1×10^6
MC3T3-E1	0.04×10^6
Primary human	$0.1\text{-}0.3 \times 10^6$ **
hFOB 1.19	$0.1\text{-}0.2 \times 10^6$

**High variation between individuals.

5. Add 500 µL of thrombin solution across the elastomer surface between the two anchors of each well of the plate(s) - do not add onto the side of the wells. Ensure the culture surface of the well is completely covered [Figure 3.C].

    - *Tip – Swirl and tap the sides of the plate to encourage even coverage, which can be challenging due to the hydrophobic nature of the elastomer.*

6. Add 200 µL of fibrinogen solution directly onto the thrombin solution between the two anchors of each well of the plate(s) - do not add onto the side of the wells. Immediately and gently, swirl the plate to ensure complete mixing of the fibrinogen and thrombin solutions [Figure 3.C].

7. Incubate the plates at 37 °C in an incubator for 20-30 min to allow for polymerisation. If the intention is to use the plates immediately, during this polymerisation step, isolate the cells to be used and achieve the appropriate seeding density [Table 2].

    - ***Note - after polymerisation, plates can be stored at 2-8°C for up to a week. Preheat in an incubator at 37 °C for 30 mins prior to cell seeding.***

8. Seed 3.5 mL of cell suspension at the appropriate seeding density [Table 2] directly onto the fibrin hydrogel between the two anchors of each well of the plate(s) - do not add onto the side of the wells. Briefly swirl the plate and incubate under normal cell culture conditions.

5. Maintenance of constructs

Required:

- Disposable sterile scalpel (cat no.: 0511; supplier: Swann-Morton, Sheffield, UK)
    - *No specific blade size required – blade No. 24 used here*
- PBS solution [Section 3.1] – Autoclave sterilised
- Trypsin-EDTA (2X) (cat no.: SLCC7608; supplier: Sigma-Aldrich)
    - ***Note – Diluted from 10X stock conc. to 2X conc. using sterile PBS solution***

- Non-osteogenic cell culture media – refer to your cell supplier guidance
- Osteogenic cell culture media – refer to your cell supplier guidance

Steps:

3-days post cell seeding – fibrin detachment

This step aids fibrin contraction by detaching any fibrin that may have adhered to the well walls

1. Slowly run a scalpel around the edges of the wells at the top surface of the elastomer [Figure 3.D.i] to detach any fibrin that has not successfully retracted.
    - *Tip – Run the scalpel from the 12 o'clock to the 6 o'clock points in the clockwise and anti-clockwise directions – do not run the scalpel around the whole well in one direction as this risks dislodging the fibrin from the anchors*
2. Remove 1.5 mL of media/well and replace with 1.5 mL of non-osteogenic cell culture media [Figure 3.D.ii]
3. Continue to renew media every 3-4 days by removing and replacing 1.5 mL media/well. Ensure each well contains a minimum media volume of 3.5 mL

At 1 and 2 weeks post cell seeding – trypsin wash

This step is to prevent cell adherence and matrix formation outside of the fibrin construct

1. Remove all media from each well and wash with 1.0 mL PBS. Discard the PBS.
2. Add 0.5 mL of 2X Trypsin-EDTA to each well and incubate at 37 °C for 3 mins. Gently tap the sides of the plate and add 1.0 mL cell culture media.
3. Remove entire volume of Trypsin-EDTA/media solution and replace with 3 mL non-osteogenic cell culture media.

2-4 weeks post cell seeding – osteogenic incubation

Osteogenic incubation can begin at the discretion of the user; commonly at 4 weeks post-cell seeding, or earlier if fibrin matrix width becomes < 3 mm

1. Remove entire media volume from each cell culture well and replace with osteogenic media. Continue the normal media renewal regime using osteogenic media (refer to "*3 days post-cell seeding – fibrin detachment": Step 3*).

Results and analytical methods

Expected results post-cell seeding

The first significant observation is contraction of the fibrin matrix around the anchors [Figure 4.A.] which, depending on the cell source used, can occur in as little as 24 hours or up to 7 days post cell seeding. Cell-matrix interactions between the cell-bound integrins and Arg-Gly-Asp (RGD)-containing moieties, such as vitronectin, found within the extracellular matrix (ECM),[24] are essential to cell behaviour, phenotype and survival. 2D culture platforms typically adhere cells through weak electrostatic forces on one side of the cell, which encourages an unnatural flattened conformation. By seeding cells in a 3D, naturally occurring matrix, the strong affinity between these integrins and ECM components on all surfaces of the cells results in complete enrobing of the cells in the matrix, which is observed as matrix contraction.[25] Furthermore, with the presence of the two anchors in the well, the matrix contraction is controlled and forced into a cylindrical-like structure, whereas a disorganised spheroid will form in their absence.[25] Because of the cylindrical matrix, the cells themselves are organised into a parallel and striated conformation [Figure 4B], which provides an in-built strain that further encourages cell differentiation and bone formation.

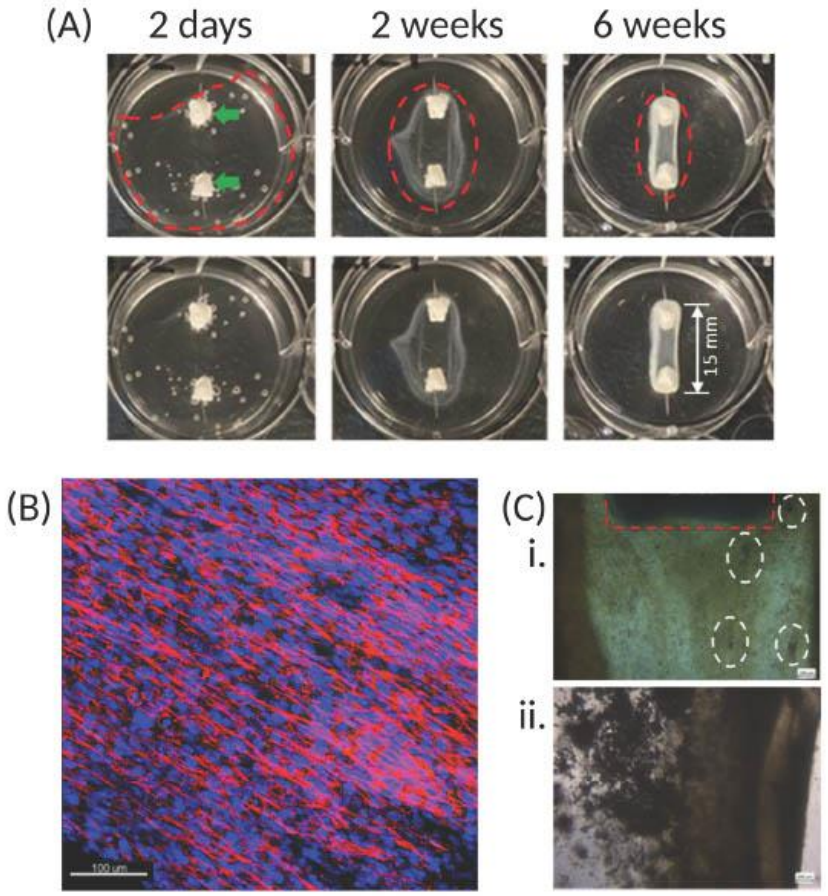


Figure 4. Matrix and cell organisation over time. (A) Once cells are seeded onto the fibrin hydrogel, contraction of the matrix around the two calcium phosphate anchors (green arrows) occurs. Upper and lower panels are the same images, with construct outline (dotted red line) excluded in the lower panel for clarity. Over time, the cells progressively form an organised and coordinated construct (as indicated by the narrowing of the red dotted rings). The resulting structure has a defined border-due to fibrin accumulation – which becomes stiffer and increasingly opaque following introduction of osteogenic conditions at 4 weeks. (B) Immunofluorescence staining of the cell nuclei (blue) and actin (red) shows that the cells present within the fibrin matrix align longitudinally between the two anchors, resulting in a striated configuration. This Z-stack maximum intensity projection image is of a construct cultured for 4-weeks. 20x magnification, scale bar is 100 µm. Stains: Hoechst (cat no.: 62249; supplier: Fisher Scientific) for nuclei (blue), phalloidin-488 (cat no.: A12379; supplier: Fisher Scientific) for actin (red). (C) Initially, mineral deposits are observed as dark specks (white dotted rings) of varying size within the matrix of the SSBM constructs (i). Following introduction of osteogenic media at 4 weeks, these become denser and more apparent (ii). Calcium phosphate anchor within red dotted ring. Images taken with light microscope; 4x magnification. Scale bars are 200 µm.

Over time, the fibrin matrix contracts into a more defined structure, which then becomes increasingly opaque upon culturing under osteogenic conditions. This opacity is due to the occurrence of osteoid deposition by the cells and its subsequent mineralisation on the matrix [Figure 4.C].

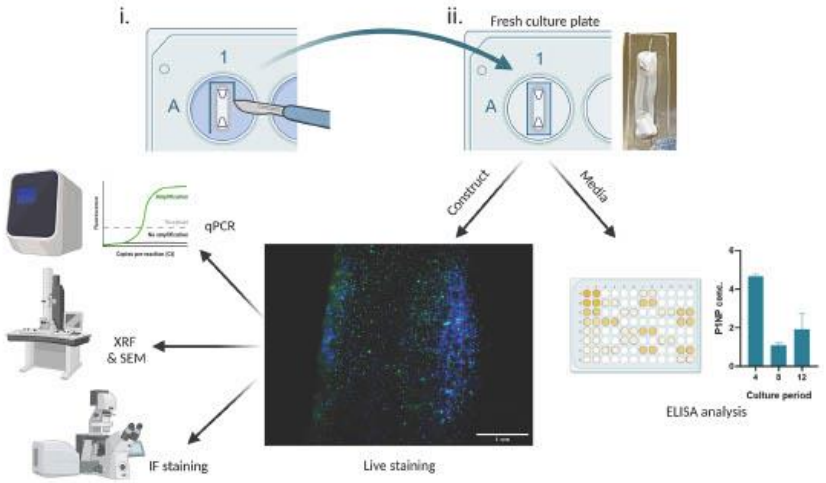


Figure 5. Achieving efficient analysis of SSBM cultures. (i) For analysis of exposed SSBM construct media, 3-4 days prior to the chosen analytical timepoint, intact SSBM constructs are isolated from their culture plates by cutting a strip of elastomer surrounding it, (ii) then incubated it in a fresh culture plate. At the timepoint, media can be collected and used for analysis, such as enzyme-linked immunosorbent assay (ELISA). The remaining construct can also be used for further analysis, such as live-dead imaging with ReadyProbes™ (cat no.: R37609; supplier: Invitrogen). Greater analytical efficiency can be achieved by using live-dead imaged constructs for other analytical approaches. To date, methods that have been optimised, and are under development, for SSBM construct analysis include quantitative polymerase chain reaction (qPCR), x-ray fluorescence (XRF), scanning electron microscopy (SEM) and immunofluorescent (IF) staining. Created with Biorender.com.

Analytical efficiency

With the correct planning, many analytical approaches can be carried out using a single construct, which demonstrates the analytical efficiency of the SSBM construct method; for example, Figure 5 shows the journey of a single construct through five separate analytical techniques. First the construct is stained intact using non-toxic ReadyProbes™ (cat no.: R37609; supplier: Invitrogen, Hertford, UK) for live-dead imaging. Subsequently, it is subjected to X-ray fluorescence (XRF) and then scanning electron microscopy (SEM). Meanwhile, the media collected from these constructs can be analysed by enzyme-linked immunosorbent assays (ELISA) at multiple timepoints throughout the construct culture period. Constructs stained with the ReadyProbes™ are also in an acceptable condition to be used for other analytical techniques, such as qPCR and immunofluorescence (IF) staining.

SSBM isolation

The protocol above details the measures used to ensure cells attach to and remain within the fibrin matrix, and prevent cell adherence and proliferation occurring outside of the fibrin matrix – i.e. using hydrophobic Sylgard 184 silicone elastomer and regularly treating the wells with trypsin-EDTA. Although hydrophobic surfaces won't completely prevent cell attachment (as previously demonstrated by the murine osteoblastic cell line, MC3T3), they can reduce cellular proliferation rate.[26] Furthermore, trypsin-EDTA is a calcium chelator,[27] which could affect the development of calcium-phosphate mineral, therefore it is used sparingly throughout the culture period. Given this, two separate cell populations exist within the culture dish - one outside and the other inside the SSBM construct. This is problematic for methods that involve analysing exposed media, (e.g. ELISA) as the results will reflect the activity of both cell populations, rather than just those within the SSBM construct. To overcome this problem, prior to media analysis, SSBM constructs must be isolated from their original culture plates and transferred into fresh plates. This can be achieved whilst retaining their shape integrity, and viability, by dissecting the elastomer as close as possible to the SSBM construct, with the anchors still attached, and placing it into a new 6-well dish [Figure 5]. Following culture in the appropriate media (i.e. complete or osteogenic media) for 3-4 days, the media is collected and used for analysis immediately, or stored for analysis at a later date (refer to manufacturer's guidance for any specific preparation steps or storage requirements for cell supernatant, prior to beginning analysis or storing) – long-term storage at -80 °C is adequate for most analysis.

Biological analysis

Live-dead imaging

There are many approaches that can be used to determine cell viability based on their enzymatic and metabolic activity (e.g. MTT tetrazolium reduction, resazurin reduction and protease activity assays), or their membrane integrity (e.g. trypan blue exclusion and DNA binding dyes). However, these methods are often destructive, irreversible or cause long-term cytotoxicity. ReadyProbes™ penetrate the SSBM construct matrix and enable simple, as well as fast viability testing, without causing cell damage or cytotoxicity. Following manufacturer guidance, constructs still attached to their anchors and a strip of elastomer (as indicated above [Figure 5]) are resuspended and incubated for 30 min (33.5°C or 37 °C, 5% CO_2) in 3.5 mL media with 2 drops/mL of NucBlue® Live and NucGreen® Dead reagents added directly, then imaged using a fluorescence microscope with standard DAPI (excitation/emission: 360/460 nm) and FITC/GFP filters (excitation/emission: 504/523 nm).

RNA extraction for qPCR

Quantitative polymerase chain reaction (qPCR) is a widely used technique that enables gene expression analysis in cells and tissue samples. During osteoblast differentiation, from progenitor cells through to osteocytogenesis, there are notable and patterned changes in the expression of specific genes, which have been reviewed extensively.[28–30] Data from qPCR can be used as an indicator of osteoblast cell maturity within the SSBM construct, as well as to provide insights into how cells are responding to particular stimuli (e.g. bone formation modulators) and culture environment etc.

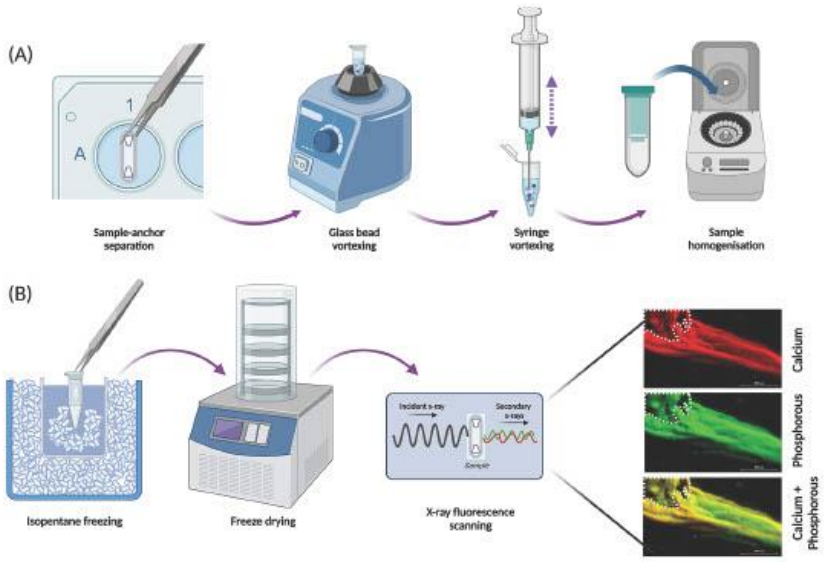


Figure 6. Optimised approaches for structural analysis of SSBM constructs. (A) SSBM constructs are disrupted and homogenised prior to extraction of RNA for qPCR analysis, by following a process optimised for these constructs. Disruption involves vortexing samples, without the anchors, with glass beads, then by repeated aspiration using a syringe and needles. Disrupted samples are homogenised using QIAShredders (cat no.: 79656; supplier: QIAGEN), with the resultant sample ready for RNA extraction. (B) The elemental composition of the mineral present on SSBM constructs can be analysed using x-ray fluorescence (XRF). Whole constructs are first snap frozen in a dry ice bath using isopentane, immediately followed by dry freezing. XRF produces elemental map read-outs and energy spectra which can be used to locate and determine mineral distribution and maturity. The elemental maps shown here reveal co-localisation of calcium (red) and phosphorous (green), resulting in a yellow colouration, suggesting presence of a calcium phosphorous compound (yellow) i.e. bone-like mineral. β-TCP anchors within white dotted outline. Scale bar is 2.0 mm. Created with Biorender.com.

Table 3. Range of RNA yield following extraction from hFOB 1.19 SSBM constructs. *Note - resultant yields will vary considerably with the culture period time and culture conditions, the cell type used to create the SSBM constructs and user experience. Values are the range obtained from successful RNA extractions performed previously (sample number, n, given for each timepoint).*

Culture period post-cell seeding (post-osteogenic introduction)	RNA Concentration (ng/μL)	n
4 (0) weeks	211.8–802.7	6
8 (4) weeks	145.0–1022.8	8
12 (8) weeks	69.2–409.9	11

Analysis by qPCR (or RNA sequencing) relies on extraction of RNA of satisfactory quantity and quality, which is greatly influenced by the first steps in the extraction method; disruption and homogenisation of the cells and/or tissue lysates. This method has been developed and optimised for extracting good quality RNA from the SSBM constructs [Figure 6A], using the QIAGEN Mini RNEasy® Kit (cat no.: 74104; supplier: QIAGEN, Manchester, UK).

First, the SSBM construct must be unhooked from the anchors, then placed it in a 2.0 mL eppendorf tube containing 10-15 3 mm diameter glass beads (cat no.: Z143928-1EA; supplier: Sigma-Aldrich) and 600 μL of buffer RLT containing 10% β-mercaptoethanol (v/v) (cat no.: M6250; supplier: Sigma-Aldrich). Each sample is vortexed (bench top vortex) for 1-2 minutes, followed by shredding by repeated aspiration with a syringe first using a 16G (cat no.: 11532445; supplier: Fisher Scientific) needle, then a 19G needle (cat no.: 15341537; supplier: Fisher scientific), the construct and the buffer RLT mixture is repetitively aspirated with the syringe until the construct is a fine powder in suspension. Care is needed as a vacuum is created in the presence of large pieces of construct. To reduce RNA loss, the same syringe is used between needles for the same sample; but to prevent cross contamination, a new syringe and set of needles are used for each individual SSBM construct. The resultant lysate is transfered to a QIAshredder spin column (cat no.: 79654; supplier: QIAGEN) and centrifuged (2 min; max speed in a microcentrifuge), followed by a repeat centrifugation of the resultant supernatant, with the shredder removed and collection tube capped. The supematant is transferred by careful pipetting - to ensure no pelleted debris is taken up - to a new 1.5 mL Eppendorf and then used for RNA extraction following the steps outlined by the QIAGEN RNEasy® Mini handbook, beginning with addition of 70% ethanol to the supernatant (section "Protocol: Purification of Total RNA from Animal Tissues", pages 51-52, as of October 2019). Typical RNA yields for hFOB 1.19 are shown in Table 3, with the purity of the RNA extracted deemed acceptable when the ratio of absorbance at 260 and 280 nm is 2.0 ± 0.15.

Structural analysis

Fixation

The structure of SSBM constructs must be preserved at the elected timepoints to obtain an accurate snapshot of structural development and changes. Like bone, SSBM constructs are composite "tissues", containing an organic and an inorganic phase, which require different methods of preservation. SSBM constructs that are to be used for structural analysis (for either the organic or inorganic phase) must first be fixed, whilst remaining attached to the anchors (as indicated above [Figure 5]). This begins with an incubation of 4.0 mL/construct 4% formaldehyde (cat no.: HT501128; supplier: Sigma-Aldrich) for 4 hours on a shaker plate at 4.0 °C; followed by three washes with 4.0 mL/construct PBS. Constructs can then be stored in PBS at 4.0 °C for up to 2 weeks. Fixation of SSBM constructs by paraformaldehyde preserves the organic phase whilst retaining the inorganic mineral phase.

Freeze-drying

For structural analysis that particularly concerns the inorganic phase of the SSBM constructs, moisture must be removed from samples. Freeze-drying (lyophilisation) is the preferred method to remove water from SSBM constructs, as it maintains sample structure (both microscopically and chemically) better than alternative approaches such as oven-drying.[31,32]

SSBM constructs must first be frozen rapidly, as slow freezing can cause crystallisation of the ice, which will distort and damage the samples. This can be achieved using liquid nitrogen immersion, however, with the SSBM constructs, this can be too vigorous and can result in damage to the fragile constructs. A more successful alternative is to freeze in an isopentane bath [Figure 6.B]. Place a glass beaker, half-filled with isopentane and a small amount of dry ice, into a container of dry ice, ensuring the beaker is surrounded completely. SSBM constructs attached to their anchors and a strip of elastomer (as indicated above [Figure 5]) are placed in an Eppendorf tube and submerged in the isopentane beaker for

5 minutes. Ensure that the Eppendorf is completely submerged and add additional dry ice pellets to the isopentane if the bubbling begins to slow/stop. The submersion time can be increased if the construct is not completely frozen after 5 minutes. Once frozen, constructs are stored at -80 °C, or immediately freeze-dried (Lablyo mini, York, UK) at -50 °C for at least 4 hours. Freeze-dried constructs can be stored in a sealed container at room temperature, away from moisture, for up to 6 months.

X-ray fluorescence

X-ray fluorescence (XRF) is an inexpensive, non-destructive and rapid analytical approach to investigate the elemental composition of samples.[33–36] In this case, the location and extent of calcium and phosphorous within the SSBM constructs can be assessed. Constructs are placed in an XRF (M4 Tornado, Bruker Nano Gmbh, Germany) under a 20 mBar vacuum. After adjusting the focus on the construct, the region of interest (ROI) is outlined and then scanned with the X-ray (50 kV, 400 uA) at 1000 spots/10 mm (spot size = 25 μm), 5 ms/pixel exposure time.

By overlaying the calcium and phosphorous elemental maps [Figure 6.B], the resultant yellow colouration indicates co-localisation of the two elements, which strongly suggests the presence of calcium-phosphate mineral compounds. The resultant maps and spectra provide further information regarding the distribution and maturity of the mineral present through the varying degrees of colour intensity visualised on the maps, which are determined by the size of each element's unique energy signal. Regarding the SSBM constructs, mineral distribution and maturation appears heterogeneous as found in *in vivo* bone tissue.[37]

Immunofluorescent staining

Immunofluorescence (IF) staining techniques offer the capability to visualise the structural and biological characteristics of samples with high resolution and accuracy. The ability to section samples [Figure 7.A.i] and the vast range of fluorescent secondary antibodies available means a single sample can be analysed for numerous structural and biological markers of interest, thus furthering analytical efficiency. Furthermore, SSBM constructs can also be IF stained intact, enabling a gross overview of the cellular orientation, as well as the expression of markers of interest in relation to their location within the construct within the construct [Figure 4.B, Figure 7.A.ii].

Prior to staining, constructs must be fixed and then unhooked from their anchors – the constructs tend to retain their shape after unhooking once they have been fixed, as well as with increasing maturity (i.e. older constructs are stiffer).

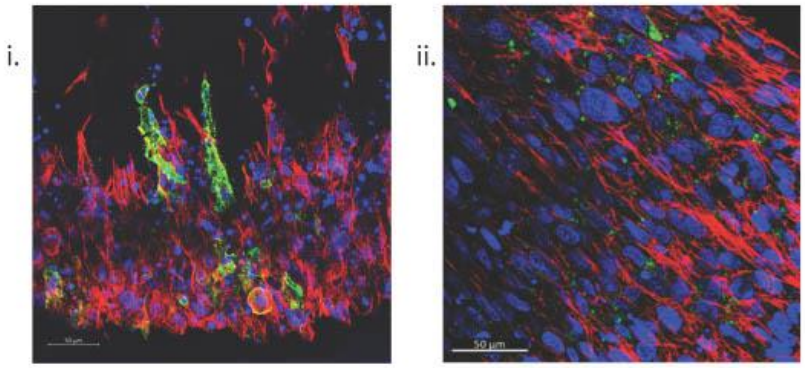


Figure 7. Immunofluorescent staining of SSBM constructs is achievable once sectioned or whole. Following adapted protocols for an established gelatin-based embedding, sectioning, and immunofluorescent staining protocol[37] (i) and one general protocol optimised for sectioned collagen-based matrices (ii), respectively, resultant 50 μm sections (i) and whole intact (ii) SSBM constructs are used to examine specific bone cell markers e.g., podoplanin (green), within the SSBM constructs, as well as an overview of cell presence and conformation. Left to right: Images above are z-stack maximum intensity projections of cultured SSBM constructs, using phalloidin for actin staining (red) and hoechst nuclei staining (blue). Scale bars are 50 μm.

IF Staining: Sectioned constructs

The method developed by Kusumbe *et al.*, 2015[38] reliably allows the preparation of bone tissue for high-resolution IF images without compromising tissue structure or proteins. Due to the delicate and bone-like nature of the SSBM constructs, this method is also ideal for their IF staining.

The method begins with sample fixation steps, which have been adapted and described above for the SSBM constructs (refer to *'structural analysis' above*), followed by decalcification and cryoprotection steps in preparation for embedding. Unlike traditional methods of embedding (e.g. paraffin embedding), this method uses gelatin-based embedding, with polyvinylpyrrolidone (PVP) and sucrose cryoprotection, as it has been found to prevent bone disintegration and allows for thicker sectioning. However, due to the fragility of the SSBM constructs in comparison to bone (i.e. a thinner composite tissue containing collagen and fibrin), the incubation conditions required for embedding are altered from 45 mins at 60 °C, to 90 mins at 45 °C. Once embedded and frozen, the protocol[38] outlines the steps for sectioning the resultant tissue blocks. In the case of the SSBM constructs, 50 µm sections are recommended [Figure 7.A.i]. Finally, the method outlines the IF staining procedure. Antibody incubation durations, dilutions, and fluorophore panels are subject to the researcher's discretion. Figure 7.A.i shows SSBM constructs stained for podoplanin using an anti-human podoplanin rabbit monoclonal antibody (1:200) (cat no.: D9D7; supplier: Cell Signaling Technology, USA), followed by an Alexa Fluor® 647 AffiniPure donkey anti-rabbit IgG secondary (1:200) (cat no.: 711-605-152; supplier: Jackson ImmunoResearch, Ely, UK). Along with hoechst (1:400) (cat no.: 62249; supplier: Fisher Scientific) for nuclei and phalloidin-488 (1:100) (cat no.: A12379; supplier: Fisher Scientific) for actin. Once stained, the SSBM construct sections are treated with ProLong™ Diamond Antifade Mountant (cat no.: P36961; supplier: Fisher Scientific) then coverslipped.

IF Staining: Whole constructs

A general IF staining protocol developed for collagen-based matrices, that have been paraffin-embedded and sectioned, has been developed in our laboratories and forms the basis of the method that is used for staining SSBM constructs whole and intact [Figure 7.A.ii].

SSBM constructs that have been unhooked from their anchors, are decalcified and cryoprotected as described by Kusumbe *et al.*, 2015.[38] In a fresh 6-well plate, SSBM constructs are treated with blocking buffer [Table 4] for 1 hour at room temperature (RT) – ensuring the constructs are completely submerged (>3.0 mL solution per construct) – then washed twice with PBS. Primary antibody is diluted accordingly using antibody buffer [Table 4] and >3.0 mL solution per construct added to each well, then incubated for 2 hours at RT. Constructs are washed 3 times with PBS and treated with the secondary antibody, as well as hoechst (1:400) and phalloidin (1:100), diluted accordingly in antibody buffer [Table 4], at >3.0 mL solution per construct for 2 hours at RT and covered. Finally, the SSBM constructs are washed 3 times with PBS and are immediately imaged on a confocal microscope, not in solution, on a glass-bottomed (170±5 µm thickness) imaging dish (cat no.: 80137; supplier: Ibidi, Germany).

Table 4. Reagent recipes required for whole construct IF staining.

Reagent	Final concentration	Cat no.	Supplier
Blocking buffer			
PBS	Diluent	18912014	Fisher Scientific
Triton X	0.1%	X100 5ML	Sigma-Aldrich
BSA	30 mg/mL	A8806-5g	Sigma-Aldrich
Antibody buffer			
PBS	Diluent	18912014	Fisher Scientific
Tween 20	0.5%	P1379 25ML	Sigma-Aldrich
BSA	30 mg/mL	A8806-5g	Sigma-Aldrich

Troubleshooting

Table 5. Troubleshooting table.

Problem	Possible reasons	Solutions
Fibrin not contracting	- Cell seeding density too low - Cell viability too low - Fibrinogen batch-batch variation	Discard constructs that have not contracted and attempt the following solutions for subsequent set ups: - Increase cell seeding density – varies between species and origin - Ensure cell viability is >85% prior to seeding - Order new fibrinogen with a different lot number (available on fibrinogen vial)
RNA too low	- Construct not completely disrupted - Construct viability/ metabolic activity too low	- Carry out cDNA reverse transcriptase with low RNA sample, followed by cDNA amplification - Vortex and aspirate subsequent constructs for longer during disruption and aspiration steps of RNA extraction
Dry freezing snapping constructs	- Constructs not completely frozen prior to freeze drying	- Submerge subsequent constructs in isopentane bath for >5 min - Try a different snap freezing method (e.g. liquid nitrogen) - Try oven drying methods
Cement hardening too quickly	- Orthophosphoric acid/ equipment not cold enough - Equipment contains traces of solidified cement - Volume of orthophosphoric acid too low	- Ensure acid is stored at 4 °C and is kept cool - Set up workstation [Figure 2.C.I] at least 30 mins prior to beginning - Ensure all equipment being used is clean (i.e. fresh weighing boats, clean spatulas etc.) - Adjust acid volume by increments/reductions of 100 µL until obtaining the desired consistency

Conclusion

This detailed step-by-step protocol for the preparation, production, and maintenance of a novel 3D *in vitro* bone model, and the adapted analytical methods described, can accommodate various osteoblastic cell sources and species. Importantly, we have now demonstrated the utility of this model using hFOB 1.19 cells (as shown here), and previously with primary rodent osteoblasts,[19,20] as well as with primary human osteoblasts (data not shown). This inherent flexibility in cell source, and the minimal requirement for specialist equipment/reagents (beyond those available in most well-resourced molecular biology laboratories) widens the potential applications and accessibility for this model. The use of cell lines or, where available, primary human cells rather than primary cells from other vertebrate species, should be used to reduce the requirement for animals as the osteoblast source.

The humanisation of the method using the hFOB cell line has reduced our requirement for *ex vivo* samples considerably. We estimate that the work conducted over the past two years in our laboratory (during which time, a total of >280 hFOB-containing constructs have been produced) would have required tissue from >140 rats using the previous *ex vivo* iteration of the method.[19] Within the UK, there are at least 6 research groups working on bone modelling currently using animal-derived primary tissue models. Considering a similar level of animal use to our laboratory, we estimate that the development of our humanised *in vitro* model for the long-term study of bone has the potential to replace over 840 rodents per year for similar research across the UK alone. With the development potential and adaptability of the model to study normal development, as well as bone diseases and novel therapies, the replacement potential for this *in vitro* model is significant.

We anticipate that this assay could be readily adapted to incorporate mixed cell populations to study cell-cell interactions. For example, co-culture with osteoclasts to study bone remodelling or with malignant cells to study bone metastasis. Assessment of the effects of candidate therapeutic compounds on construct mineralisation rate and osteocyte differentiation and function will allow screening for efficacy prior to *in vivo* studies. Such uptake of this method at the discovery stage of research, particularly with the capacity to utilise human and patient cells, will lead to a reduced requirement for *in vivo* and *ex vivo* platforms, therefore further replacing the use of laboratory animals, and improve the translatability of preclinical studies.

Data availability

Underlying data

Zenodo: A detailed methodology for the long-term in vitro culture and analysis of three-dimensional, self-structuring bone models generated from cell lines or primary osteoblastic cell populations. https://doi.org/10.5281/zenodo.7620806[39]

This project contains the RNA yields data and original image files.

Extended data

Zenodo: A detailed methodology for the long-term in vitro culture and analysis of three-dimensional, self-structuring bone models generated from cell lines or primary osteoblastic cell populations. https://doi.org/10.5281/zenodo.7620806[39]

This project contains the following extended data:

- 6-well 20 x anchors Mold Frame.gcode
- 6-well 20 x anchors.3mf

Data are available under the terms of the Creative Commons Attribution 4.0 International license (CC-BY 4.0).

Acknowledgements

The authors would like to give their appreciation and gratitude to the NC3Rs for funding and supporting the research needed for the development of this protocol. Dr Triin Major (Birmingham Tissue Analytics, University of Birmingham) and Miss Julia Manning (Institute of inflammation and Ageing, University of Birmingham) for immunofluorescence staining and imaging support. Dr Erik Hughes and Mr Adam McGuinness (School of Chemical Engineering, University of Birmingham) for x-ray fluorescence support.

References

1. Confavreux CB: Bone: from a reservoir of minerals to a regulator of energy metabolism. *Kidney Int. Suppl.* 2011 Apr [cited 2022 Nov 9]; 79(S121): S14–S19.
PubMed Abstract | Publisher Full Text | Free Full Text

2. Rucci N: Molecular Biology of Bone Biology. *Clin. Cases Miner. Bone Metab.* 2008; 5(1): 49–56.
PubMed Abstract

3. Rittweger J, Frost HM, Schiessl H, *et al.*: Muscle atrophy and bone loss after 90 days' bed rest and the effects of flywheel resistive exercise and pamidronate: results from the LTBR study. *Bone.* 2005 Jun [cited 2022 Nov 21]; 36(6): 1019–1029.
Publisher Full Text | Reference Source

4. Stavnichuk M, Mikolajewicz N, Corlett T, *et al.*: A systematic review and meta-analysis of bone loss in space travelers. *npj Microgravity.* 2020 May 5 [cited 2023 Jan 13]; 6(1): 1–9.
Publisher Full Text | Reference Source

5. Bonewald LF: The amazing osteocyte. *J. Bone Miner. Res.* 2011 Feb 1 [cited 2020 Dec 8]; 26(2): 229–238.
PubMed Abstract | Publisher Full Text | Free Full Text

6. Franz-Odendaal TA, Hall BK, Witten PE: Buried alive: How osteoblasts become osteocytes. *Dev. Dyn.* 2006 Jan 1 [cited 2020 Mar 29]; 235(1): 176–190.
PubMed Abstract | Publisher Full Text

7. Bellido T: Osteocyte-driven bone remodeling. *Calcif. Tissue Int.* 2014; 94(1): 25–34.
PubMed Abstract | Publisher Full Text | Free Full Text

8. Bonewald LF: Generation and function of osteocyte dendritic processes. *J. Musculoskelet. Neuronal Interact.* 2005; 5(4): 321–324.

9. Borgström F, Karlsson L, Ortsäter G, *et al.*: Fragility fractures in Europe: burden, management and opportunities. *Arch. Osteoporos.* 2020 Dec 1 [cited 2020 Nov 5]; 15(1): 59.
PubMed Abstract | Publisher Full Text | Free Full Text

10. Ehnert S, Rinderknecht H, Aspera-Werz RH, *et al.*: Use of in vitro bone models to screen for altered bone metabolism, osteopathies, and fracture healing: challenges of complex models. *Arch. Toxicol.* 2020 Dec 1 [cited 2021 Nov 30]; 94(12): 3937–3958.
PubMed Abstract | Publisher Full Text | Free Full Text

11. Bellido T, Delgado-Calle J: Ex Vivo Organ Cultures as Models to Study Bone Biology. *JBMR Plus.* 2020 Mar 1 [cited 2022 Nov 21]; 4(3).
PubMed Abstract | Publisher Full Text | Free Full Text

12. Park Y, Cheong E, Kwak JG, *et al.*: Trabecular bone organoid model for studying the regulation of localized bone remodeling. *Sci. Adv.* 2021 Jan 20 [cited 2022 Nov 21]; 7(4).
PubMed Abstract | Publisher Full Text | Free Full Text

13. Bernhardt A, Österreich V, Gelinsky M: Three-Dimensional Co-culture of Primary Human Osteocytes and Mature Human Osteoclasts in Collagen Gels. *Tissue Eng. - Part A.* 2020 Jun 1 [cited 2021 Nov 30]; 26(11–12): 647–655.
PubMed Abstract | Publisher Full Text

14. Papanicolaou SE, Phipps RJ, Fyhrie DP, *et al.*: Modulation of sclerostin expression by mechanical loading and bone morphogenetic proteins in osteogenic cells. *Biorheology.* 2009 [cited 2020 Mar 30]; 46(5): 389–99.
PubMed Abstract | Publisher Full Text

15. Bodine PVN, Vernon SK, Komm BS: Establishment and hormonal regulation of a conditionally transformed preosteocytic cell line from adult human bone. *Endocrinology.* 1996 Nov 1 [cited 2023 Jan 13]; 137(11): 4592–4604.
PubMed Abstract | Publisher Full Text | Reference Source

16. Lelovas PP, Xanthos TT, Thoma SE, *et al.*: The Laboratory Rat as an Animal Model for Osteoporosis Research. *Comp. Med.* 2008 Oct [cited 2022 Nov 21]; 58(5): 424.
Free Full Text

17. Turner AS: Animal models of osteoporosis--necessity and limitations. *Eur. Cell. Mater.* 2001 [cited 2022 Nov 21]; 1: 66–81.
PubMed Abstract | Publisher Full Text

18. Takakura A, Takao-Kawabata R, Isogai Y, *et al.*: Differences in vertebral, tibial, and iliac cancellous bone metabolism in ovariectomized rats. *J. Bone Miner. Metab.* 2016 May 1 [cited 2021 Dec 5]; 34(3): 291–302.
PubMed Abstract | Publisher Full Text

19. Iordachescu A, Williams RL, Hulley PA, *et al.*: Organotypic Culture of Bone-Like Structures Using Composite Ceramic-Fibrin Scaffolds. *Curr. Protoc. Stem Cell Biol.* 2019 Feb 1 [cited 2020 Nov 12]; 48(1): e79.
PubMed Abstract | Publisher Full Text

20. Iordachescu A, Amin HD, Rankin SM, *et al.*: An In vitro Model for the Development of Mature Bone Containing an Osteocyte Network. *Adv. Biosyst.* 2018; 2(2).
Publisher Full Text

21. Subramaniam M, Jalal SM, Rickard DJ, *et al.*: Further characterization of human fetal osteoblastic hFOB 1.19 and hFOB/ERα cells: Bone formation in vivo and karyotype analysis using multicolor fluorescent in situ hybridization. *J. Cell. Biochem.* 2002 [cited 2020 Mar 6]; 87(1): 9–15.
PubMed Abstract | Publisher Full Text

22. Harris SA, Enger RJ, Riggs LB, *et al.*: Development and characterization of a conditionally immortalized human fetal osteoblastic cell line. *J. Bone Miner. Res.* 1995 Feb [cited 2020 Mar 6]; 10(2): 178–186.
PubMed Abstract | Publisher Full Text

23. Kaur G, Dufour JM: Cell lines: Valuable tools or useless artifacts. *Spermatogenesis.* 2012 Jan [cited 2022 Nov 21]; 2(1): 1–5.
PubMed Abstract | Publisher Full Text | Free Full Text

24. van der Flier A, Sonnenberg A: Function and interactions of integrins. *Cell Tissue Res.* 2001 [cited 2022 Nov 21]; 305(3): 285–298.
Publisher Full Text

25. Wudebwe UNG, Bannerman A, Goldberg-Oppenheimer P, *et al.*: Exploiting cell-mediated contraction and adhesion to structure tissues in vitro. *Philos. Trans. R. Soc. Lond. B Biol. Sci.* 2015; 370: 20140200.
PubMed Abstract | Publisher Full Text | Free Full Text

26. Lourenço BN, Marchioli G, Song W, *et al.*: Wettability influences cell behavior on superhydrophobic surfaces with different topographies. *Biointerphases.* 2012 Jul 26 [cited 2022 Nov 21]; 7(1–4): 1–11.
PubMed Abstract | Publisher Full Text

27. Lai TY, Cao J, Ou-Yang P, *et al.*: Different methods of detaching adherent cells and their effects on the cell surface expression of Fas receptor and Fas ligand. *Sci. Reports.* 2022 Apr 5 [cited 2022 Nov 21]; 12(1): 1–8.
Publisher Full Text | Reference Source

28. Chen X, Wang L, Zhao K, *et al.*: Osteocytogenesis: Roles of Physicochemical Factors, Collagen Cleavage, and Exogenous Molecules. *Tissue Eng. Part B Rev.* 2018 Jun 6 [cited 2022 Nov 21]; 24(3): 215–225.
PubMed Abstract | Publisher Full Text | Free Full Text

29. Bonewald LF: Osteocytes. Marcus R, Feldman D, Nelson D, *et al.*, editors. *Osteoporosis.* 3rd ed. Academic Press; 2008; pp. 169–89.

30. Dallas SL, Bonewald LF: Dynamics of the Transition from Osteoblast to Osteocyte. *Ann. N. Y. Acad. Sci.* 2010 [cited 2022 Nov 21]; 1192: 437–443.
PubMed Abstract | Publisher Full Text | Free Full Text

31. Álvarez-Castillo E, Bengoechea C, Felix M, *et al.*: Freeze-Drying versus Heat-Drying: Effect on Protein-Based Superabsorbent Material. *Process.* 2021 Jun 21 [cited 2022 Nov 21]; 9(6): 1076.
Publisher Full Text | Reference Source

32. Elavarasan K, Shamasundar BA: Effect of oven drying and freeze drying on the antioxidant and functional properties of protein hydrolysates derived from freshwater fish (Cirrhinus mrigala) using papain enzyme. *J. Food Sci. Technol.* 2016 Feb 1 [cited 2022 Nov 21]; 53(2): 1303–1311.
PubMed Abstract | Publisher Full Text | Free Full Text

33. Janssens K, Vittiglio G, Deraedt I, *et al.*: Use of Microscopic XRF for Non-destructive Analysis in Art and Archaeometry. *X-Ray Spectrom.* 2000; 29(1): 73–91.
Publisher Full Text

34. Anitha A, Brasoveanu A, Duarte M, *et al.*: Restoration of X-ray fluorescence images of hidden paintings. *Signal Process.* 2013 Mar 1; 93(3): 592–604.
Publisher Full Text

35. Stockmann U, Cattle SR, Minasny B, *et al.*: Utilizing portable X-ray fluorescence spectrometry for in-field investigation of pedogenesis. *Catena.* 2016 Apr 1; 139: 220–231.
Publisher Full Text

36. Specht AJ, Lin Y, Weisskopf M, *et al.*: XRF-measured bone lead (Pb) as a biomarker for Pb exposure and toxicity among children diagnosed with Pb poisoning. *Biomarkers.* 2016 May 18 [cited 2022 Nov 21]; 21(4): 347–352.
PubMed Abstract | Publisher Full Text | Free Full Text

37. Salbach-Hirsch J, Rauner M, Hofbauer C, *et al.*: New insights into the role of glycosaminoglycans in the endosteal bone microenvironment. *Biol. Chem.* 2021 Oct 1 [cited 2022 Nov 21]; 402(11): 1415–1425.
PubMed Abstract | Publisher Full Text

38. Kusumbe AP, Ramasamy SK, Starsichova A, *et al.*: Sample preparation for high-resolution 3D confocal imaging of mouse skeletal tissue. *Nat. Protoc.* 2015 Oct 29 [cited 2021 Dec 5]; 10(12): 1904–1914.
PubMed Abstract | Publisher Full Text | Reference Source

39. Finlay M, Hill L, Neag G, *et al.*: A detailed methodology for the long-term in vitro culture and analysis of three-dimensional, self-structuring bone models generated from cell lines or primary osteoblastic cell populations. *Zenodo.* 2023.
Publisher Full Text

The benefits of publishing with F1000Research:

- Your article is published within days, with no editorial bias
- You can publish traditional articles, null/negative results, case reports, data notes and more
- The peer review process is transparent and collaborative
- Your article is indexed in PubMed after passing peer review
- Dedicated customer support at every stage

For pre-submission enquiries, contact research@f1000.com

F1000Research

8.2 Chapter 3 & 4 appendix

Table 8.1 – Extracted RNA yields for hFOB 1.19 SSBM cultures.

Culture period	Sample_ replicate	Culture temp. (°C)	RNA yeild (ng/µL)	260/280	Date RNA measured	RNA Extraction method
4	090221_1	33.5	38.1	-	01/06/2021	LN2
4	090221_2	33.5	565.5	-	06/09/2021	Needle
4	100921_1	33.5	284.6	2.11	07/10/2021	Needle
4	210921_1	33.5	802.7	2.13	15/03/2022	Needle
4	180222_1	33.5	211.8	2.08	21/03/2022	Needle
4	110322_1	33.5	323.2	2.08	06/07/2022	Needle
4	170522_1	33.5	278.2	2.07	06/07/2022	Needle
4	050722_1**	33.5	15.7	1.89	30/08/2022	Needle
4	050722_1**	33.5	98.4	2.00	30/08/2022	Needle
4	140722_1	33.5	442.5	2.13	21/09/2022	Needle
4	310522_1	33.5	748.3	2.11	21/09/2022	Needle
8	090221_1	37	18.6	-	08/06/2021	LN2
8	070621_1	37	78.2	-	06/09/2021	Needle
8	090221_2	37	153.0	-	06/09/2021	Needle
8	090221_2	37	155.2	2.11	22/02/2022	Needle
8	070621_1	37	144.9	2.07	06/10/2021	Needle
8	100921_1	37	459.8	2.10	22/02/2022	Needle
8	100921_1	37	455.9	2.09	28/02/2022	Needle
8	070621_2	37	148.3	2.06	15/03/2022	Needle
8	010222_1	37	509.9	2.09	01/04/2022	Needle
8	010222_1	37	502.6	2.06	06/07/2022	Needle
8	140722_1	37	1022.8	2.17	21/09/2022	Needle
8	170522_1	37	674.1	2.11	21/09/2022	Needle
12	111220_1	33.5	33.8	2.09	20/05/2021	LN2
12	111220_1	33.5	30.1	2.01	06/10/2021	LN2
12	111220_1	37	2.0	-	08/06/2021	LN2
12	111220_1	37	1.8	1.39	06/10/2021	LN2
12	171220_1	37	1.0	-	08/06/2021	LN2
12	171220_1	37	0.6	1.27	06/10/2021	LN2
12	310521_1	33.5	316.1	2.09	25/08/2021	Needle
12	220421_1	37	1.4	-	06/09/2021	Needle
12	220421_1	37	1.5	2.94	06/10/2021	Needle
12	111220_1	33.5	38.7	2.09	01/10/2021	Needle
12	070621_1	33.5	144.5	2.09	01/10/2021	Needle
12	210921_2	37	102.8	2.08	26/01/2022	Needle
12	210921_2	37	98.5	2.09	11/02/2022	Needle
12	240921_1	37	69.2	2.08	26/01/2022	Needle
12	210921_4	37	130.0	1.83	11/02/2022	Trizol
12	100921_1	37	132.6	2.08	28/02/2022	Needle
12	100921_1	37	132.4	2.08	22/02/2022	Needle

12	220421_2	37	1.1	-	22/02/2022	Needle
12	240921_2	37	6.5	1.71	15/03/2022	Needle
12	070621_1	33.5	87.4	2.05	15/03/2022	Needle
12	171220_2	37	37.4	2.06	15/03/2022	Needle
12	310521_1	37	210.3	2.06	15/03/2022	Needle
12	310521_2	37	198.1	2.07	21/03/2022	Needle
12	010222_1	37	174.4	2.07	06/07/2022	Needle
12	010222_1	33.5	354.9	2.07	06/07/2022	Needle
12	180222_1	37	116.0	2.07	06/07/2022	Needle
12	180222_2	37	409.9	2.06	06/07/2022	Needle

** = *technical repeats. hFOB 1.19 Batch testing.*
Yellow highlight = repeat measurement of one replicate

Table 8.2 – Extracted RNA yields for hFOB 1.19 SSBM cultures after bone formation modulator (BFM) treatment.

Culture period	Sample_ replicate	BFM	BFM Concentration (x 10^{-7} M)	RNA yeild (ng/µL)	260/280	Date RNA measured
4	261122_1	PTH	1	802.4	2.08	04/01/2022
4	181122_1	Vit D	5	331.5	2.11	04/01/2022
4	261122_1	Betulin	1	725.8	2.07	04/01/2022
4	291122_1	Vit D	5	630.5	2.06	11/01/2023
4	291122_1	Betulin	1	792.1	2.09	11/01/2023
4	021222_1	Vit D	5	896.4	2.09	11/01/2023
4	021222_1	PTH	1	902.9	2.06	11/01/2023
4	061222_1	PTH	1	414.6	2.12	13/01/2023
4	061222_1	Betulin	1	775.6	2.11	13/01/2023
8	181122_1	Vit D	5	321.4	2.11	10/02/2023
8	291122_1	Vit D	5	663.3	2.10	10/02/2023
8	021222_1	Vit D	5	462.2	2.12	10/02/2023
8	261122_1	PTH	1	319.0	2.12	10/02/2023
8	021222_1	PTH	1	451.3	2.12	10/02/2023
8	061222_1	PTH	1	150.0	2.10	10/02/2023
8	261122_1	Betulin	1	759.5	2.09	10/02/2023
8	291122_1	Betulin	1	131.5	2.08	10/02/2023
8	061222_1	Betulin	1	186.7	2.09	10/02/2023
12	181122_1	Vit D	5	42.5	2.09	07/03/2023
12	291122_1	Vit D	5	263.3	2.10	07/03/2023
12	021222_1	Vit D	5	266.1	2.08	07/03/2023
12	261122_1	PTH	1	737.5	2.07	13/03/2023
12	021222_1	PTH	1	346.3	2.10	07/03/2023
12	061222_1	PTH	1	166.1	2.10	07/03/2023
12	261122_1	Betulin	1	412.4	2.11	13/03/2023
12	291122_1	Betulin	1	458.3	2.10	13/03/2023
12	061222_1	Betulin	1	264.7	2.10	13/03/2023

Yellow highlight = RNA yield low – not analysed

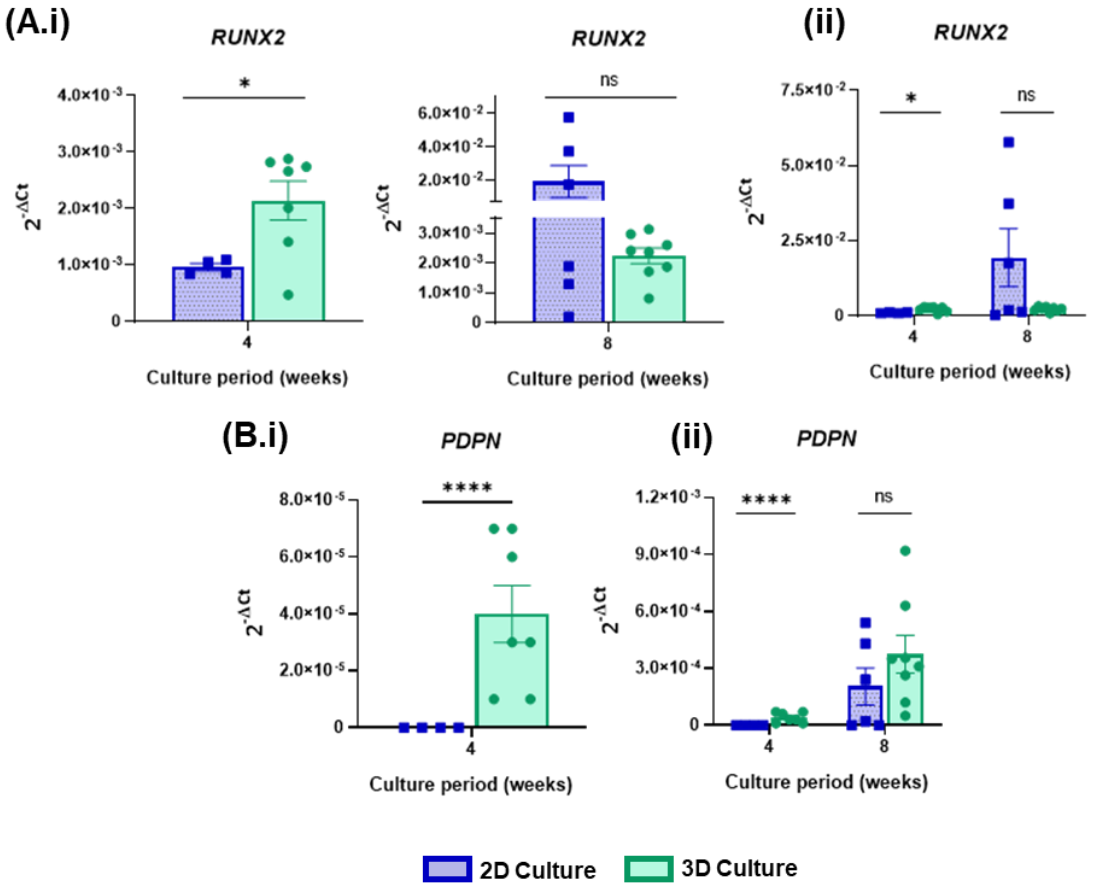


Figure 8.1 – Comparison of gene expression between hFOB 1.19 cells cultured in 2D or 3D and showed no significant difference long-term (Part 1). qPCR analysis of *RUNX2* **(A)** and *PDPN* **(B)** expression in hFOB 1.19 cells cultured in 2D (n=3-4) or 3D (n=7-8) for 4- and 8-weeks post cell seeding were compared between the two culture conditions. Despite an initial significant difference in expression after 4-weeks of culture, expression was not significantly different by 8-weeks. Compared to housekeeper gene B2M. Results are mean±SEM. Raw Ct values analysed using unpaired t-test, with Welch correction if SD ratio = >2. * = $p<0.05$; **** = $p<0.0001$; ns= no significance.

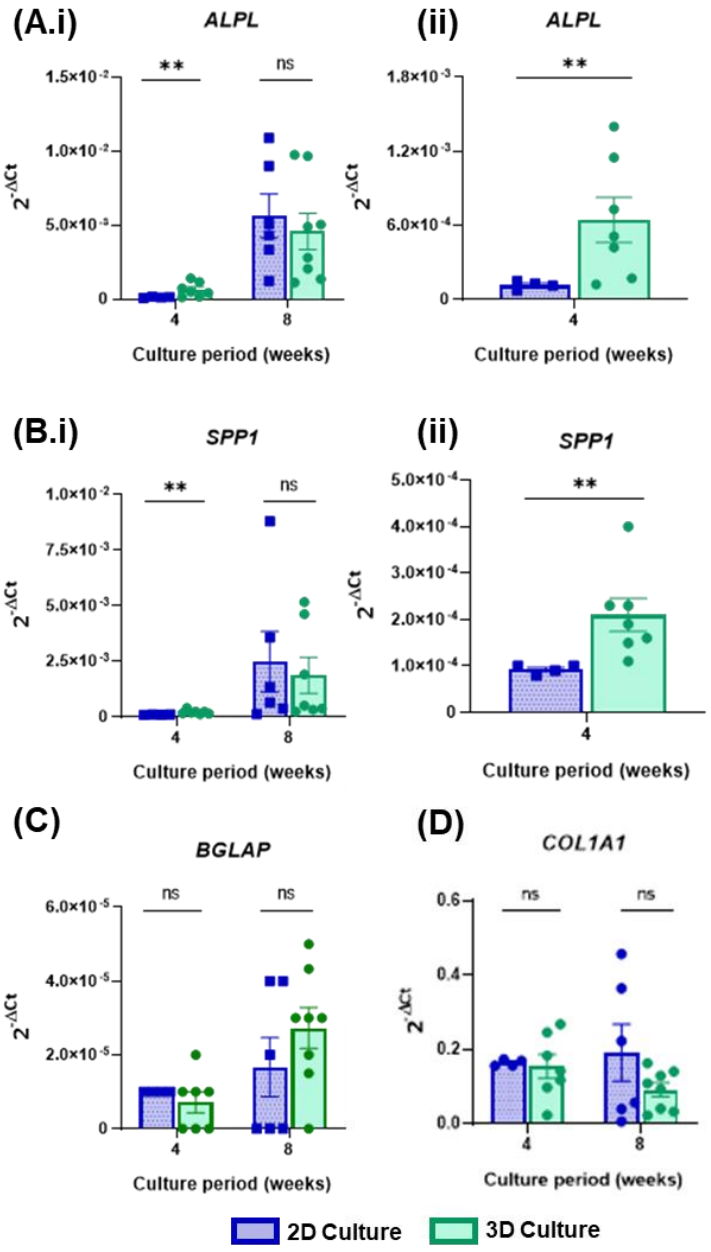


Figure 8.2 – Comparison of gene expression between hFOB 1.19 cells cultured in 2D or 3D and showed no significant difference long-term (Part 2). qPCR analysis between 2D and 3D hFOB 1.19 culture showed an initial significant difference in gene expression after 4-weeks of culture for *ALPL* **(A)** and *SPP1* **(B),** but they were not significantly different by 8-weeks. *BGLAP* **(C)** and *COL1A1* **(D)** expression however was not significantly different between the two culture conditions across the total culture period. Compared to housekeeper gene B2M. Results are mean±SEM (2D (n=3-4); 3D (n=7-8)) Raw Ct values analysed using unpaired t-test, with Welch correction if SD ratio = >2. ** = $p<0.01$; ns= no significance.

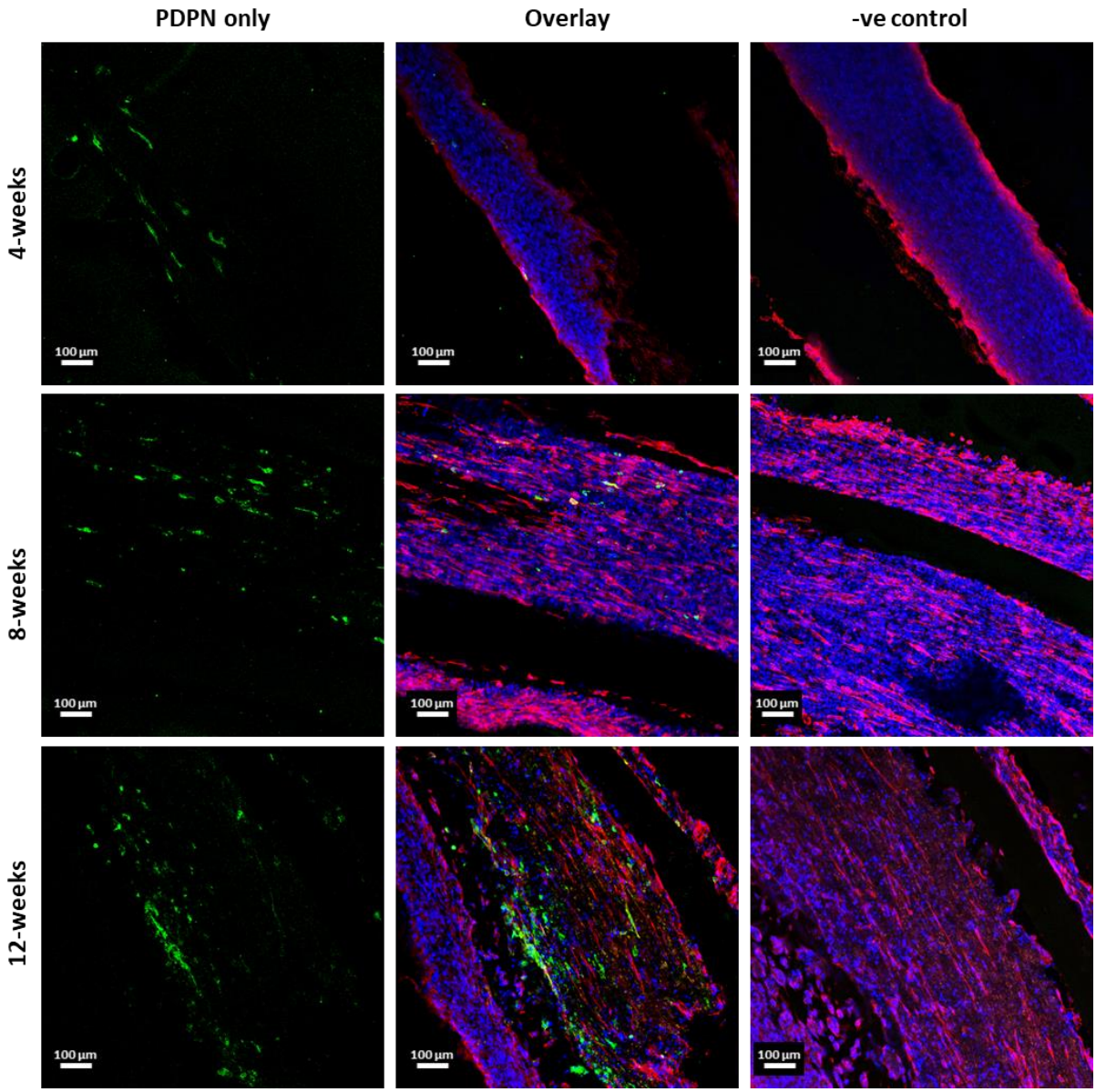


Figure 8.3 – Negative (-ve) control images for IF staining and imaging of podoplanin. Shown were 50 µm sections with an actin (phalloidin; red) and nuclear stain (Hoechst; blue) and an anti-human podoplanin (PDPN) antibody (green). Scale bars = 100 µm. 10x magnification. PDPN images = maximum intensity projection z-stacks (Step size = 2.1 µm). Overlay and –ve control images = single plane snap shot.

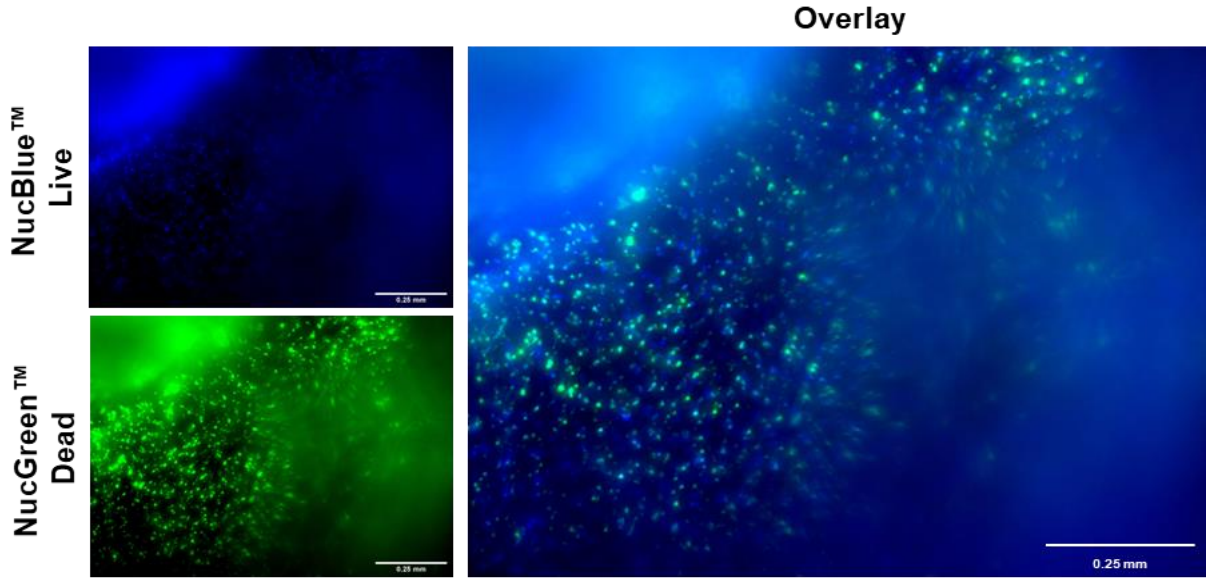


Figure 8.4 – Mineral presence interferes with determining cell viability in 12-week hFOB 1.19 SSBM samples. The Invitrogen™ ReadyProbes™ Cell Viability Imaging kit [Section 2.3.3] was used to stain all cells (blue) and dead cells (green) within whole, intact constructs, by adding and incubating the ready-to-use probes to the culture media. However, the presence of mineral interferes with optimising image quality and fluorescence intensity. Scale bar = 1 mm.

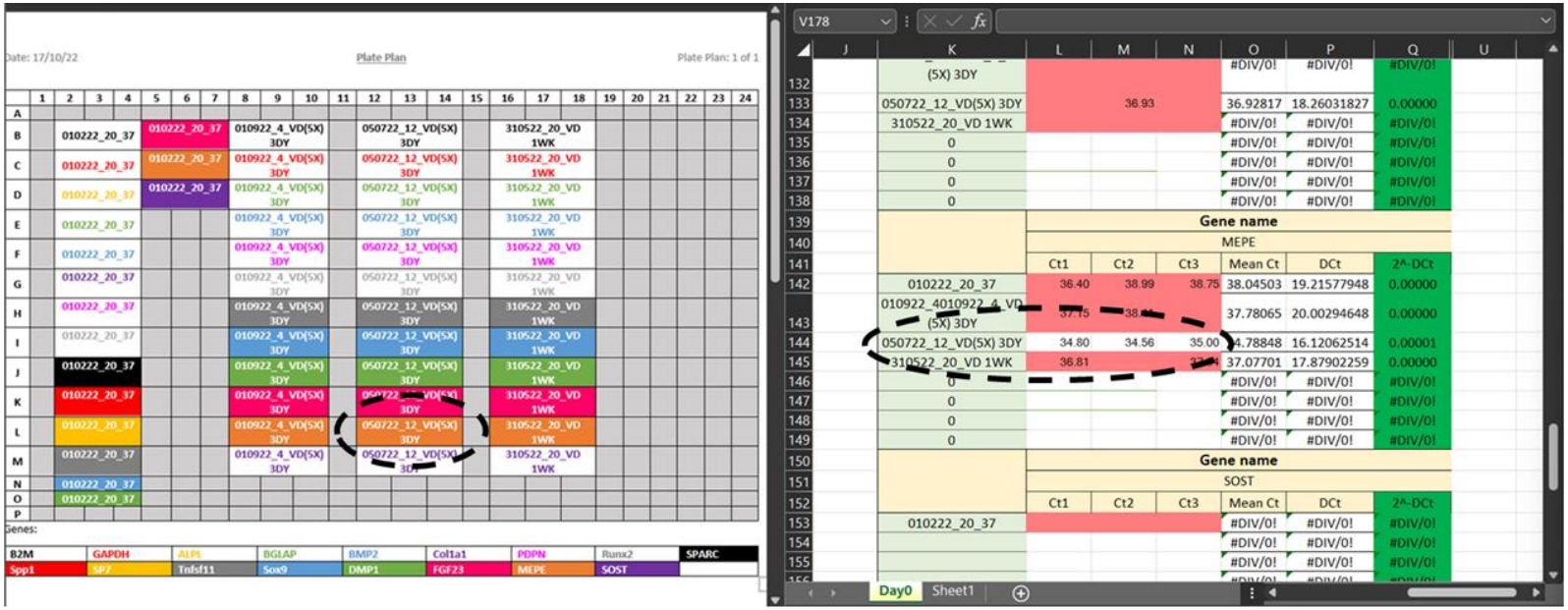


Figure 8.5 – Preliminary qPCR investigations found positive expression of osteocyte gene, *MEPE*, after treatment with Vit D_3. This was the first time a second osteocyte gene was expressed in the hFOB 1.19 SSBM constructs and therefore decided that a concentration of $5x10^{-7}$ M Vit D_3 was to be used during responsivity investigations. Shown is the plate plan of the qPCR plate prepared and the resultant individual Ct values of the wells (black dotted circle).

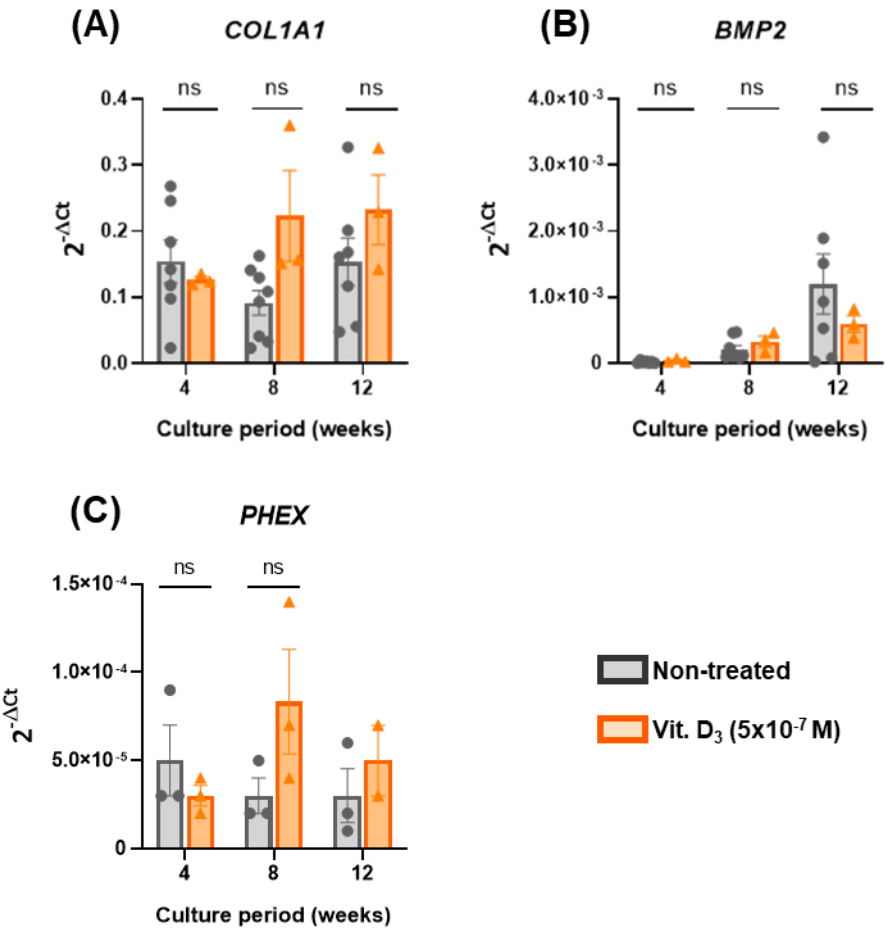


Figure 8.6 - qPCR analysis of hFOB 1.19 SSBM construct treatment with Vit D where there was no significant change in gene expression. The expression of *COL1A1* **(A)**, *BMP2* **(B)** and *PHEX* **(C)** did not change in response to Vit D treatment in SSBM constructs cultured for 4-, 8- and 12-weeks prior. Results are mean±SEM (n=3(treatment), 3-8(non-treated)). Raw Ct values analysed using unpaired t-test, with Welch's correction if SD ratio = >2. ns = no significance. N.B. No statistical test for 12-week *PHEX* due to n=<3 (treated).

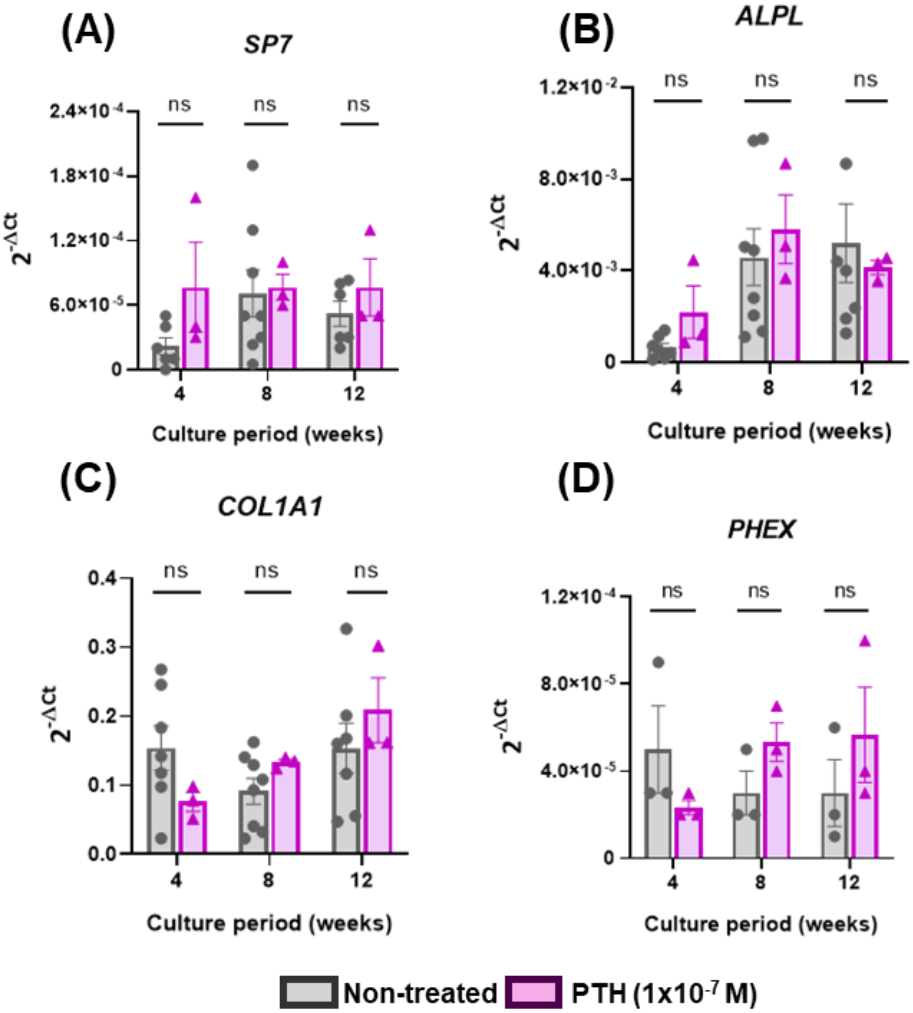


Figure 8.7 - qPCR analysis of hFOB 1.19 SSBM construct treatment with PTH where there was no significant change in gene expression. The expression of *SP7* **(A)**, *ALPL* **(B)**, *COL1A1* **(C)** and *PHEX* **(D)** did not change in response to PTH treatment in SSBM constructs cultured for 4-, 8- and 12-weeks prior. Results are mean±SEM (n=3(treatment), 3-8(non-treated)). Raw Ct values analysed using unpaired t-test, with Welch's correction if SD ratio = >2. ns = no significance.

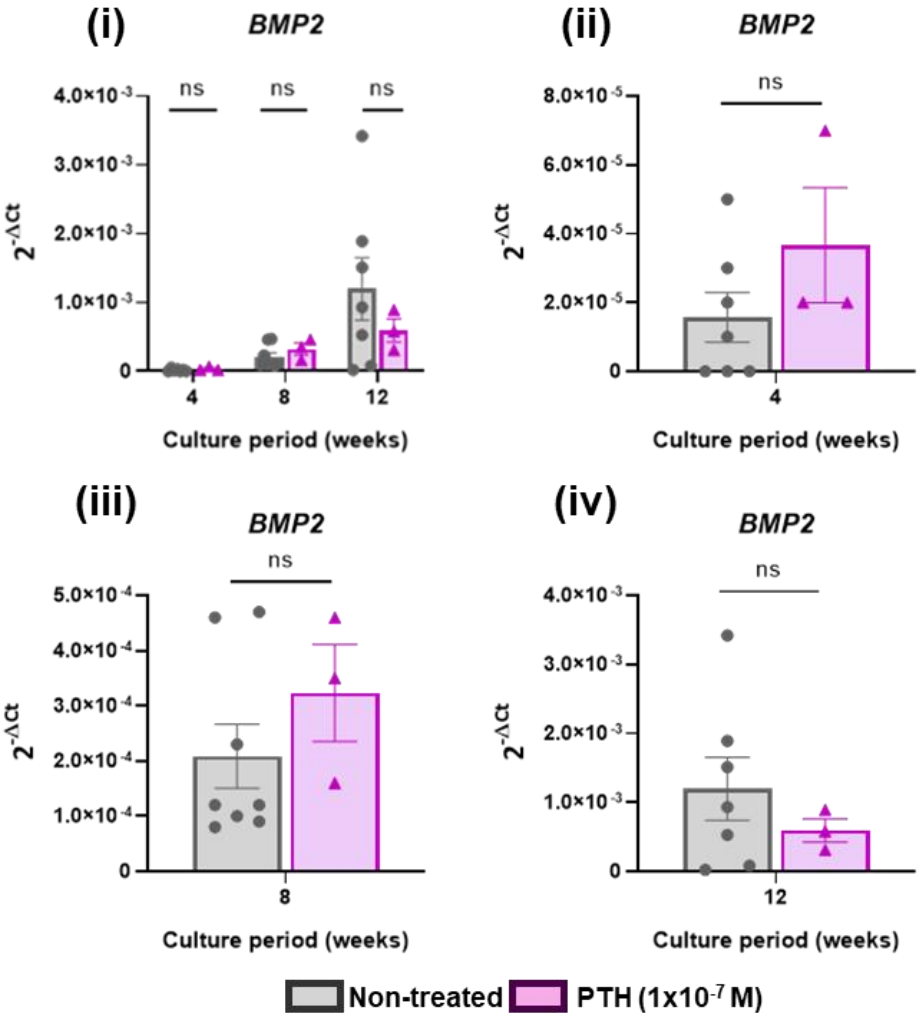


Figure 8.8 - qPCR analysis of *BMP2* expression in hFOB 1.19 SSBM construct treated with PTH. Individual timepoints for analysis of *BMP2* expression showed no change in response to PTH treatment in hFOB 1.19 SSBM constructs cultured for 4- **(ii)**, 8- **(iii)** and 12-weeks prior **(iv)**. Results are mean±SEM (n=3(treatment), 7-8(non-treated)). Raw Ct values analysed using unpaired t-test, with Welch's correction if SD ratio = >2. ns = no significance.

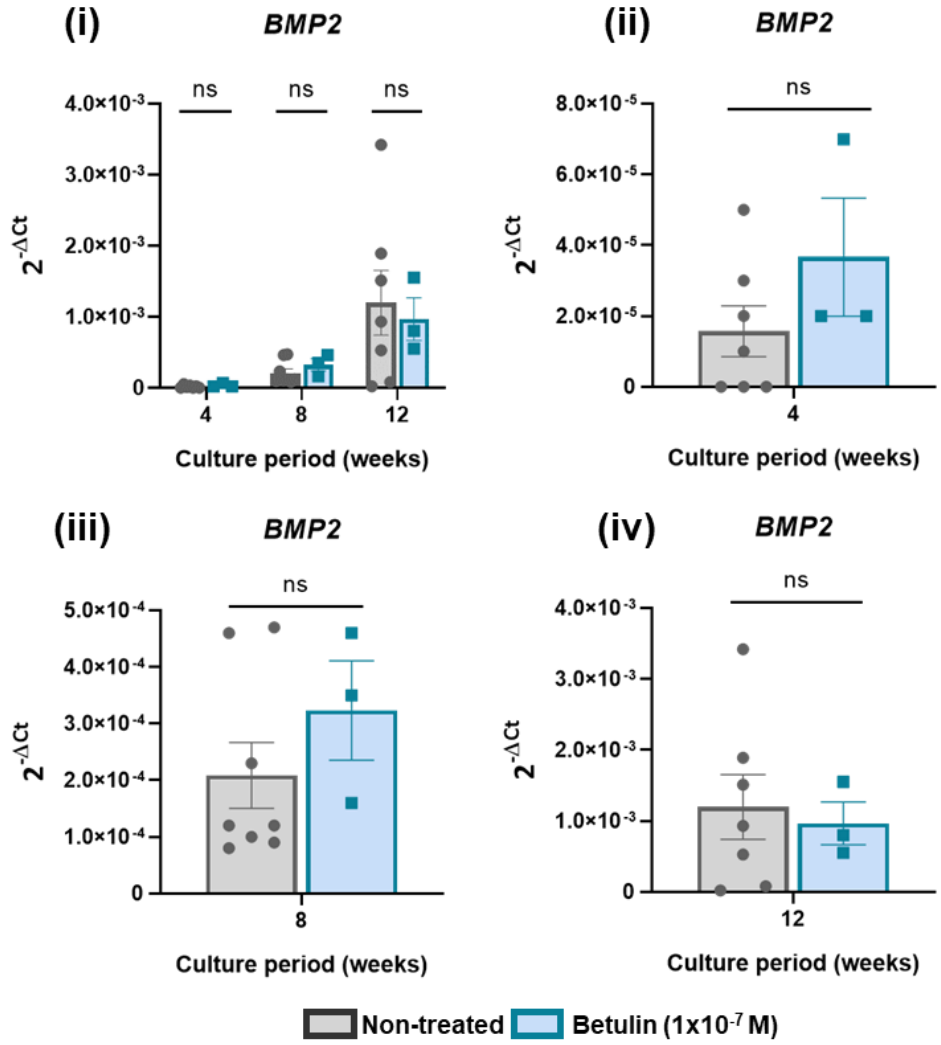


Figure 8.9 - qPCR analysis of *BMP2* expression in hFOB 1.19 SSBM construct treated with Betulin. Individual timepoints for analysis of *BMP2* expression showed no change in response to Betulin treatment in hFOB 1.19 SSBM constructs cultured for 4- **(ii)**, 8- **(iii)** and 12-weeks prior **(iv)**. Results are mean±SEM (n=3(treatment), 7-8(non-treated)). Raw Ct values analysed using unpaired t-test, with Welch's correction if SD ratio = >2. ns = no significance.

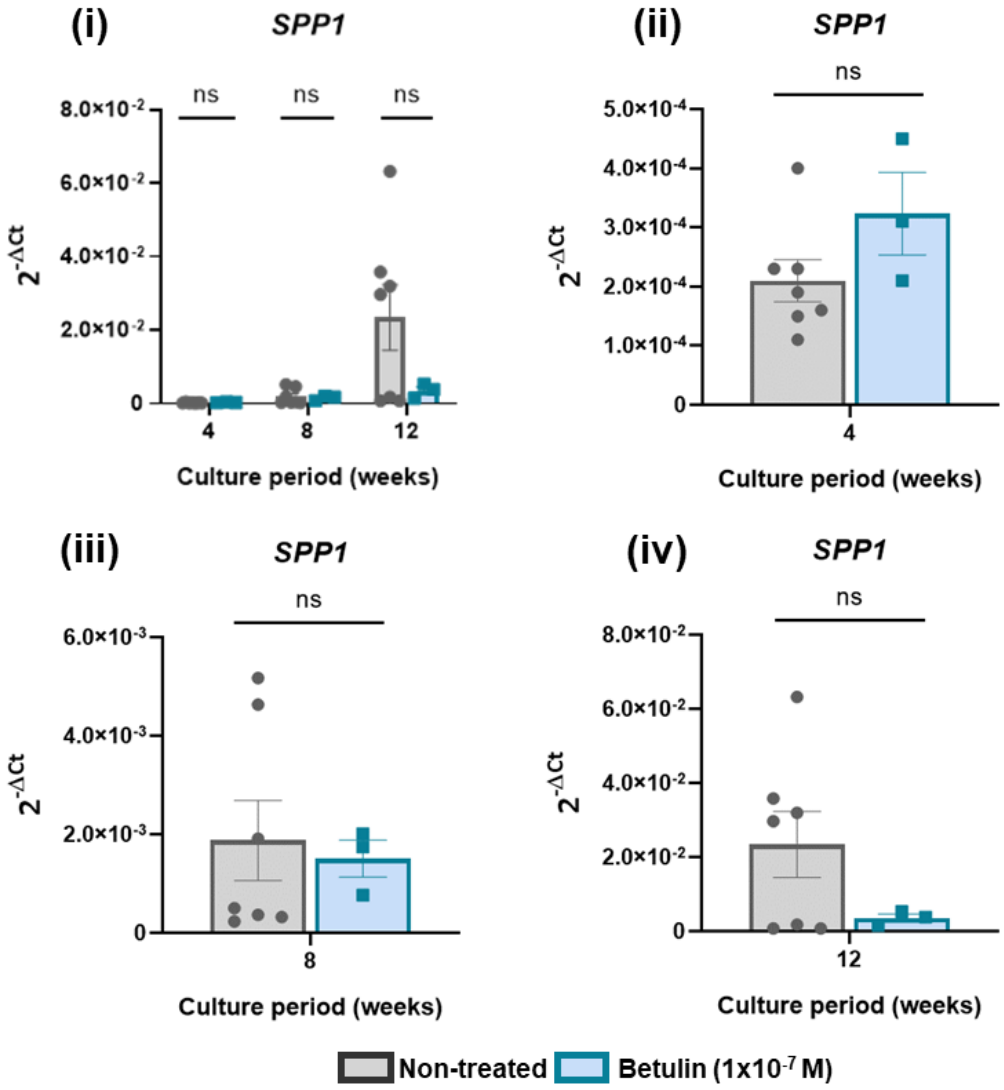


Figure 8.10 - qPCR analysis of *SPP1* expression in hFOB 1.19 SSBM construct treated with Betulin. Individual timepoints for analysis of *SPP1* expression showed no change in response to Betulin treatment in hFOB 1.19 SSBM constructs cultured for 4- **(ii)**, 8- **(iii)** and 12-weeks prior **(iv)**. Results are mean±SEM (n=3(treatment), 6-7(non-treated)). Raw Ct values analysed using unpaired t-test, with Welch's correction if SD ratio = >2. ns = no significance.

8.4 Adaptability – Dissemination and Collaborations

The funding for this project was from the NC3Rs. One of the key aims of this funding was to disseminate the methodology and ensure its uptake in other laboratories to have a wider impact on reducing and replacing animal reliance and usage in bone research. This was achieved by presenting the SSBM method, and its updates, at several conferences and symposiums, as well as through online social media platforms – See [Research dissemination] for a list of conferences attended. As a result, collaborations have been made throughout the duration of this project, which has been advantageous in revealing further capabilities of the SSBM method.

After adapting the Birmingham SSBM method using hFOB 1.19 cells, a collaboration with Professor Simon Jones' group within the Institute of inflammation and ageing aimed to adapt the method again to accommodate primary osteoblasts isolated from bone chips from the curved side of scoliosis spinal samples. The same adaptions made as previously (i.e., substitute the media and alter culture conditions) and samples from four patients were seeded onto individual SSBM plates at $0.25x10^6$ cells/well. Two patient samples successfully formed SSBM constructs which were maintained in culture for up to 9-months, at which point they were used for qPCR analysis. The remaining two patient samples unfortunately failed to create an SSBM construct. However, after a second attempt (one patient sample only) at a higher seeding density ($0.75x10^6$ cells/well), SSBM constructs were successfully formed, although highlighted the variability that exists with using primary cultures. The work performed here confirmed the feasibility of culturing primary human samples in 3D, which formed one of the main aims of a current PhD project identifying candidate pathways and

pharmacological drugs that mediate pathological skeletal remodelling in spinal osteoblasts.

The hFOB 1.19 SSBM cultures was tested with another BFM currently under investigation in our laboratories; peptide inhibitor of trans-endothelial migration (PEPITEM) (603). PEPITEM has shown to increase bone formation *in vivo* (using an ovariectomised mouse model) and 2D osteoblast *in vitro* cultures. However, after treatment of hFOB 1.19 SSBM cultures with PEPITEM, initial results showed no effect on the expression of the genes analysed in response. The exact mechanism(s) of action of PEPITEM is unknown and are still under investigation. These results indicate that the mechanism is not at the level of transcription, or higher up the signalling cascade that leads to changes in gene expression.

Three collaborators (Dr Scott Dillon, University of Cambridge; Dr Corinna Wehmeyer, University Hospital Munster; Mr Adam McGuinness; University of Birmingham) wanted to use the SSBM method with the commonly used murine secondary osteoblast cell line, MC3T3 (RVID:). The MC3T3 cell line has rapid proliferation rates (604) and was causing the fibrin hydrogel to degrade faster than the production of the new bone matrix. However, a seeding density of $40x10^3$ cells/construct was found to be successfully create SSBM constructs that could be cultured for up to 12-weeks. At this point, the presence of sclerostin-positive cells were present [Figure 8.11]; a protein specifically produced by mature osteocytes found to be one of the main protein regulators of bone remodelling (605). These results prove that the SSBM culture system is indeed supportive of mature osteocytogenesis, thus providing scope of achieving the same using other cell types with prolonged and optimised culture.

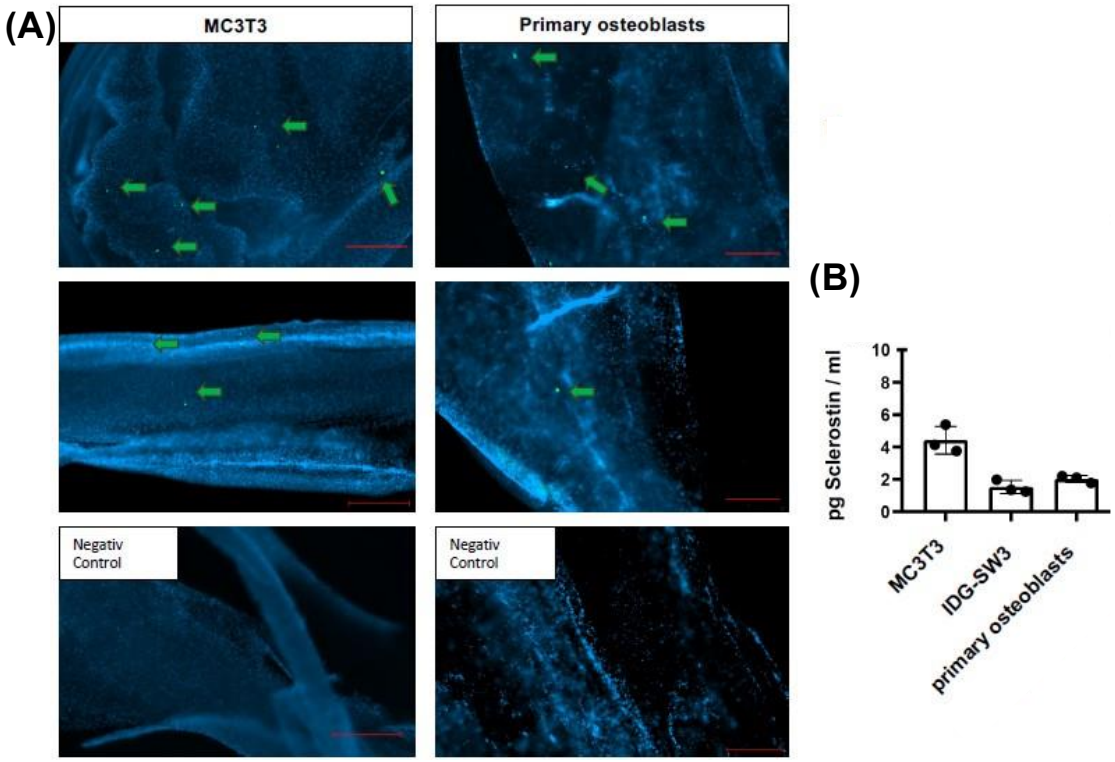


Figure 8.11 – Data obtained and provided by Dr Corinna Wehmeyer (University Hospital Munster): Sclerostin expression in 12-week SSBM constructs. Cells were seeded at 40,000 cells/well (MC3T3), 100,000 cells/well (IDGSW3) and 220,000 cells/well (primary osteoblasts) and cultured for 12-weeks. **(A)** Immunofluorescence staining for sclerostin (green). Nuclei were stained with DAPI (blue). Scale bar= 500 µm. **(B)** Sclerostin expression in supernatants of SSBM constructs by ELISA (n=3). All data are means ±SEM.

The collaborations made during this project using the Birmingham SSBM culture system has made a positive impact to those involved. It has also highlighted the extensive adaptability of the culture system to other osteoblast cell lines, which removes the limitations of future users who want to use a specific cell line. Furthermore, increased uptake of the method will subsequently increase its dissemination further and have positive impacts on the 3Rs movement within bone research.

8.5 Analytical method development

An SSBM construct is a novel composite material, which contains fibrin, collagen and mineral; the ratios of which changes with prolonged culture. Due to the novelty and dynamic nature of this material, methods currently used for analysing bone tissue and 2D cell cultures had to be adapted and developed specifically for SSBM constructs. This enabled structural and biological characterisation of hFOB 1.19 SSBM constructs cultured for up to a period of 12 weeks, as well as providing read outs when investigating their responsivity in the presence of BFMs.

Many of the analytical approaches used in this project were selected based on their ease of use and adaptability. Furthermore, methods were performed and prioritised as such to expand the analytical potential of SSBM constructs. In other words, acquire as much data possible from a single SSBM construct using many and different analytical approaches, without impacting on their structural or biological integrity (refer to [Section 8.1]). Presented in the previous chapters were the analytical methods that successfully and repeatedly produced outputs with few or no outlying data points. However, many other methods were considered and trialled, and as such required a large portion of time during this project. These are discussed briefly.

8.5.1 Delaying CaP cement setting

To prevent rapid solidification of the β-TCP with orthophosphoric acid when creating the CaP anchor cement, an ice bath set up was devised; shown in [Section 8.1]. Prior to this, attempts were made to slow this reaction with the addition of citric acid diluted to final concentrations of 0.01 and 0.1 M in orthophosphoric acid (3.5 M), which has previously shown to slow the setting of a similar β-TCP cement (606). This measure did delay the setting of the cement anchors – providing more time to fill all wells in the

mould with wet cement and insert the insect pins – and furthermore did not impact on the structure, shape or fragility of the set cement. However, once used in culture reduced cell viability and reduced fibrin contraction, most likely due to an increased acidity within the culture. As the reaction between the β-TCP and orthophosphoric acid is exothermic, the ice bath set up was designed to slow the reaction by ensuring all reagents and consumables involved were below RT as well as ensuring optimal time efficiency and simplicity.

8.5.2 Micro-computed tomography and Scanning electron microscopy

Micro-computed tomography (μCT) is a routinely used imaging technique that uses a series of x-rays to create a 3D reconstruction of the scanned sample and enable structural analysis in fine detail. In bone research, μCT is used to study and observe changes in bone microarchitecture, both qualitatively and quantitatively, in *in vitro*, *ex vivo* and *in vivo* (machine dependent) (607,608). Here, μCT analysis was intended to be used as an approach to quantify mineral content of the hFOB 1.19 SSBM constructs over time, as well as follow its progression and distribution. However, processing the reconstruction of the acquired scans failed in the absence of mineral, which meant constructs prior to the 12-week culture period were unable to be analysed using μCT. One successful reconstruction of a 12-week cultured SSBM construct can be found in [Figure 8.12]. It was decided that an adequate amount of data could be acquired from XRF analysis of the constructs, which does not exclude less mature constructs.

Scanning electron microscopy (SEM) is another imaging technique used for topographical analysis of sample surfaces. This technique was intended to investigate the surface characteristics of the SSBM constructs and look for the presence of osteocytes, as previously shown by Iordachescu *et al.* (395). Although successful in

obtaining high-resolution images [Figure 8.13], the analysis was limited to the surface of the construct, thus neglecting the internal system where it was predicted the majority of the cells were located. Despite not being destructive to the sample architecture, the preparatory steps involved (i.e., dry freezing followed by sputter coating with gold) meant the constructs were no longer fit for further analysis and thus limiting the amount of analytical data that could be obtained from a single construct. Since, a collaborator, Dr Scott Dillon (University of Cambridge), has kindly agreed to analyse SSBM constructs using focused ion beam-SEM, a highly precise imaging technique that simultaneously slices and scans samples to enable reconstruction of a whole sample (externally and internally). As these samples are yet to be processed, results are not shown here.

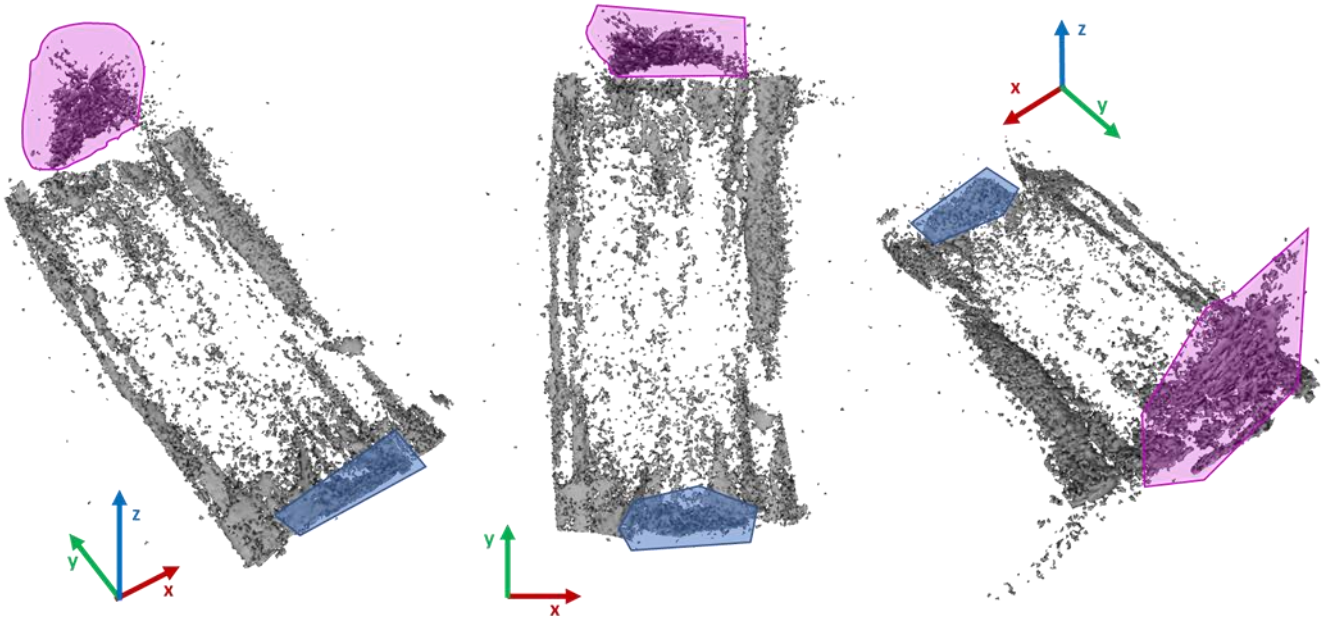


Figure 8.12 – hFOB 1.19 construct mineral localisation, distribution and accumulation visualised by micro-computed tomography (µCT). A reconstruction of a single hFOB 1.19 construct 84 days post-cell seeding shown at 3 different angles (xyz axes provided for position reference. Mineral within the purple and blue regions are that of the anchors). The reconstruction shows mineral deposition is more condensed in regions adjacent to and proximal to the anchors, as well as around the edges of the construct where the matrix was highly condensed. The mineral present within the construct boundaries appears as small nodules of mineral that became sparser when nearing the most central point between the two anchors present.

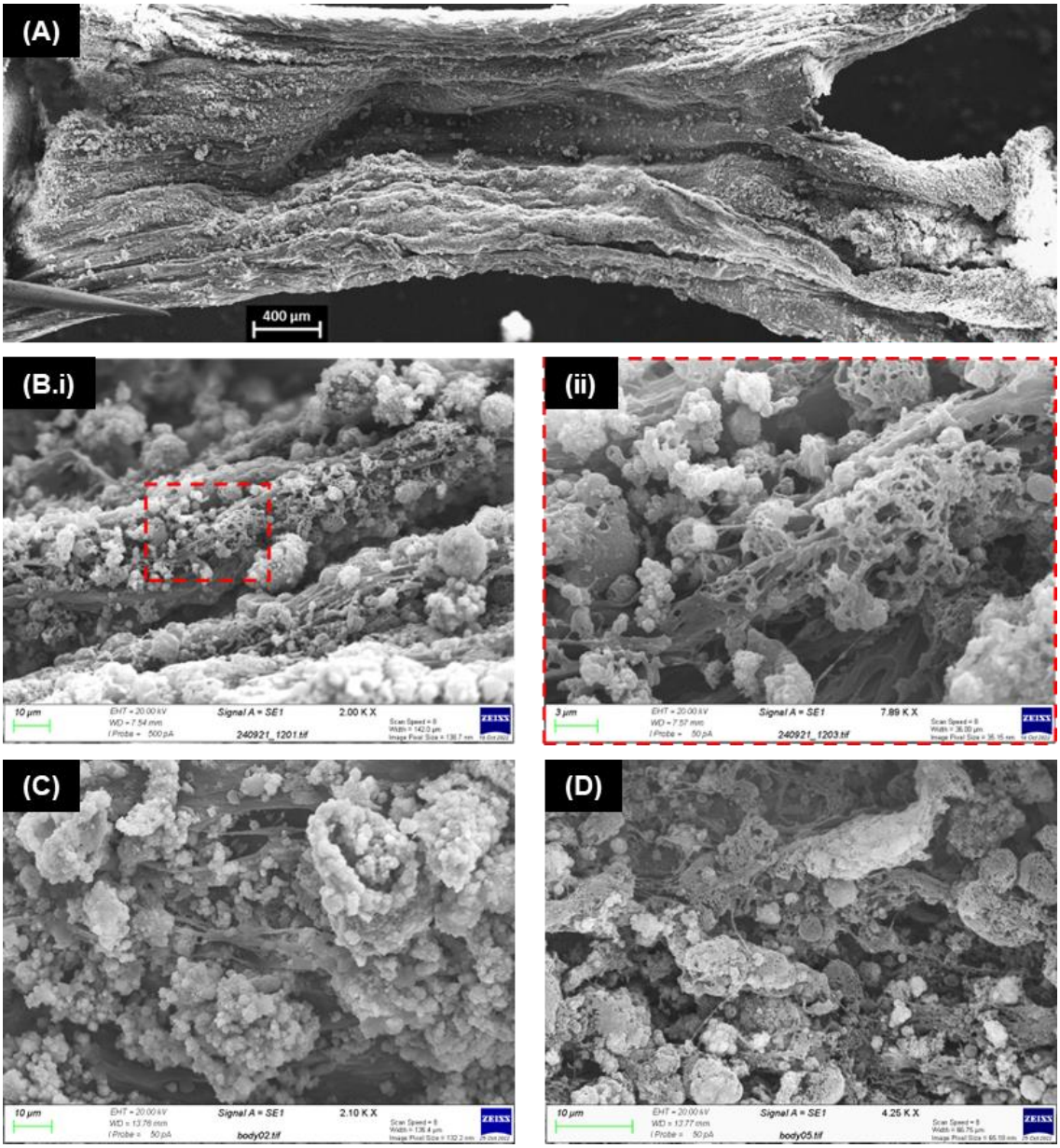


Figure 8.13 – Scanning electron microscopy (SEM) images of 12-week hFOB 1.19 SSBM construct. SEM produces high- resolution images at magnifications over a large range; from the macroscopic level (i.e., a whole SSBM construct **(A)**) and magnifications from x2000 **(B.i)** to x7890 **(B.ii)**. This enables detailed topographical observation and analyses of hFOB 1.19 SSBM construct surface, including visual evidence of possible early osteocytes and osteocytic dendrite presence **(C-D)**. Coated in gold using a sputter coater. Red dotted square **(B.i)** indicates area magnified and imaged **(B.ii)**.

8.5.3 Mineral staining

Staining approaches to study mineralisation of cultures and tissues provides relatively inexpensive and readily available options, particularly where other methods requiring specialised equipment (e.g., electron microscopy electron diffraction analysis) is not so easily accessible. There are a number of stains routinely used in bone research to stain for the presence of mineral, however they often require fixation and are irreversible, and again impacts on the analytical potential of the SSBM constructs. Therefore, non-cytotoxic mineral stains were investigated, such as xylenol orange (XO).

XO is a fluorescent, non-cytotoxic stain previously used for staining mineral in 2D *in vitro* osteoblast cultures (609,610). It does not require a fixation step, thus SSBM construct can be used for subsequent analyses, such as qPCR. Upon imaging, XO had successfully stained the mineral present on the SSBM constructs, confirmed upon comparison with the successfully stained excess β-TCP residue after anchors were removed [Figure 8.14], which was treated as a positive control. However, background/auto-fluorescence increased with prolonged culture, which interfered with resultant images and any attempts to quantify the mineral present would likely be inaccurate. Therefore, focus was moved to more established staining methods.

The two most common staining methods used in mineralisation studies is von Kossa and AZ. von Kossa staining has lower specificity to mineral and can only be quantified through image analysis, and as such is not recommended to be used as a sole measure of mineralisation (611,612). As imaging is limited to a 2D plane, for a 3D construct this will require multiple sections of unmineralised tissue, which involves expensive specialised equipment. Therefore, AZ staining was selected for quantifying

mineral AZ staining, as it can be quantified through images, as well as through its extraction

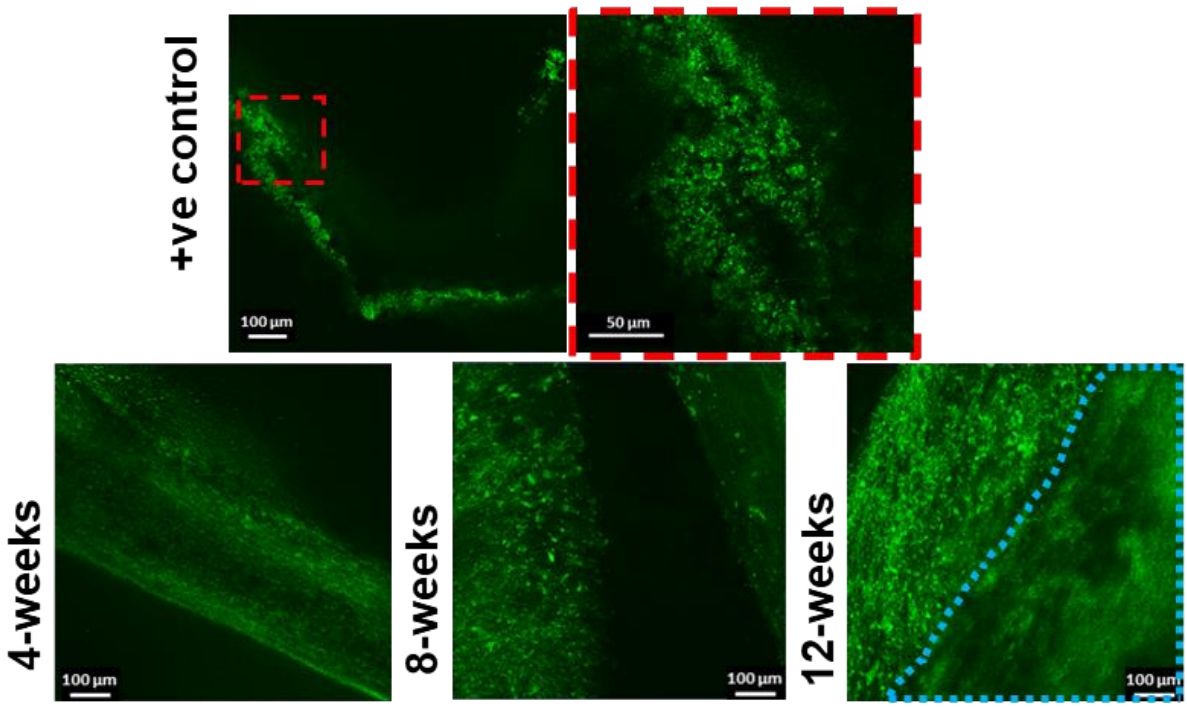


Figure 8.14 – Xylenol orange (XO) whole mount staining of SSBM constructs is not an efficient approach for visualising mineral deposition. hFOB 1.19 SSBM constructs incubated in 100µM XO for 24 hours were imaged and z-stacks obtained shown. Excess mineral from the CaP anchors that remained on the SSBM constructs were used as a positive control. Visually, mineral appears "speckled", however autofluoresence (within dotted blue area) was seen and will cause interference when assessing "true" staining. Scale bars = 100 µm (Red bordered image = 50 µm).

8.5.4 Conclusions

A great amount of consideration was given to developing analytical methods that were simple to follow and repeat with reliable outcomes; that were efficient with time, resources and finances; and furthermore were performed in an order that capatilised on the amount of data that could be attained from a single construct. Overall, the analytical methods performed and presented in the previous chapters were believed to have been adequately developed and optimised for sufficient biological and structural characterisation of hFOB 1.19 SSBM constructs with prolonged culture.